به نام خدا

مرکز دانلود رایگان
مهندسی متالورژی و مواد

---

www.Iran-mavad.com

COMPREHENSIVE MATERIALS PROCESSING

EDITOR-IN-CHIEF

Saleem Hashmi

Dublin City University, Dublin, Ireland

ASSOCIATE EDITORS-IN-CHIEF

Gilmar Ferreira Batalha

University of São Paulo, São Paulo, Brazil

Chester J. Van Tyne

Colorado School of Mines, Golden, CO, USA

Bekir Yilbas

King Fahd University of Petroleum and Minerals, Dhahran, Saudi Arabia

VOLUME 6

WELDING AND BONDING TECHNOLOGIES

VOLUME EDITOR

Emin Bayraktar

School of Mechanical and Manufacturing Engineering, France

ELSEVIER

AMSTERDAM • BOSTON • HEIDELBERG • LONDON • NEW YORK • OXFORD
PARIS • SAN DIEGO • SAN FRANCISCO • SINGAPORE • SYDNEY • TOKYO

www.iran-mavad.com
مرجع مهندسی مواد و متالورژی

Elsevier
Radarweg 29, PO Box 211, 1000 AE Amsterdam, Netherlands
The Boulevard, Langford Lane, Kidlington, Oxford OX5 1GB, UK
225 Wyman Street, Waltham, MA 02451, USA

Copyright © 2014 Elsevier, Ltd. unless otherwise stated. All rights reserved.

No part of this publication may be reproduced, stored in a retrieval system or transmitted in any form or by any means electronic, mechanical, photocopying, recording or otherwise without the prior written permission of the publisher.

Permissions may be sought from Elsevier's Science & Technology Rights department in Oxford, UK: phone (+44) (0) 1865 843830; fax (+44) (0) 1865 853333; email: permissions@elsevier.com. Alternatively you can submit your request online by visiting the Elsevier website at http://elsevier.com/locate/permissions and selecting *Obtaining permission to use Elsevier material*.

Website links cited in the Encyclopedia were accepted as accurate when first submitted to the publisher, however, the Publisher is unable to ensure that they will continue to remain so.

Notice
No responsibility is assumed by the publisher for any injury and/or damage to persons or property as a matter of products liability, negligence or otherwise, or from any use or operation of any methods, products, instructions or ideas contained in the material herein, Because of rapid advances in the medical sciences, in particular, independent verification of diagnoses and drug dosages should be made

British Library Cataloguing in Publication Data
A catalogue record for this book is available from the British Library

Library of Congress Cataloging-in-Publication Data
A catalog record for this book is available from the Library of Congress

ISBN: 978-0-08-096532-1

For information on all Elsevier publications
visit our website at store.elsevier.com

Printed and bound in Italy
14 15 16 17 18 19 10 9 8 7 6 5 4 3 2 1

Project Manager: Gemma Tomalin
Associate Project Manager: Joanne Williams

www.iran-mavad.com
مرجع مهندسی مواد و متالورژی

EDITOR-IN-CHIEF

Saleem Hashmi graduated from East Pakistan University of Engineering and Technology in 1967, and in 1972 he completed his master's and PhD degrees from the University of Manchester. He was appointed as a postdoctoral fellow with UMIST, Manchester, in January 1973, and in October 1973, he joined Sheffield Hallam University as a lecturer. In 1976, he was promoted to senior lecturer, then to principal lecturer in 1977, and to reader in 1984.

In January 1987, Professor Hashmi founded the School of Mechanical & Manufacturing Engineering at Dublin City University. While in the process of establishing this school, he attracted substantial external research funding to set up the Material Processing Research Centre (MPRC), a research center of excellence in the field of material processing. To this day, he continues his affiliation with Dublin City University as an emeritus professor in the school he founded 27 years ago.

In 1990, Professor Hashmi established Advances in Materials and Processing Technologies (AMPT), a much needed international conference in materials processing. He continues to be the Chairperson of the Steering Committee for this series of conferences. In 1998, he was appointed as editor-in-chief of Elsevier *Journal of Material Processing Technology* and continued in this role until 2008.

In 1995, Professor Hashmi was awarded the higher doctorate degree of DSc, by the University of Manchester, the highest academic degree any university in the United Kingdom can award.

Professor Hashmi has supervised or co-supervised 110 PhD and 55 MEng research students to successful completion. Over the years, he has also acted as an external examiner and expert assessor for PhD candidates and engineering departments with universities in Ireland, the United Kingdom, India, Pakistan, Bangladesh, Hong Kong, Canada, Australia, and Malaysia. He is a Chartered Engineer (CEng), a Fellow of the Institution of Mechanical Engineers, UK (FIMechE) and also a Fellow of the Institution of Engineers of Ireland (FIEI). He has published over 430 papers and 12 books and is still publishing.

www.iran-mavad.com
مرجع مهندسی مواد و متالورژی

This page intentionally left blank

www.iran-mavad.com
مرجع مهندسی مواد و متالورژی

EDITORIAL BOARD

Chester J. Van Tyne is the FIERF (Forging Industry Education and Research Foundation) professor at Colorado School of Mines (CSM) in Golden, Colorado. He received his undergraduate and graduate degrees from Lehigh University and worked for Bethlehem Steel as a research engineer for a short period before joining Lafayette College in the Metallurgical Engineering Department as a professor in 1980. In 1988, he joined the Metallurgical and Materials Engineering Department at CSM. He is actively engaged in the research operations of the Advanced Steel Processing and Products Research Center at CSM. His research interests are in metal deformation processes especially forging, sheet stamping, and friction during metalworking operations.

Gilmar F. Batalha graduated as a mechanical engineer from the University of Brasilia in 1982. He completed his MSc in Mechanical Engineering at the Federal University of Santa Catarina (1987), his PhD in Mechanical Engineering (1995) and habilitation/livre-docencia in manufacturing processes (2010) at the Department of Mechatronics and Mechanical Systems, Polytechnic School of Engineering, University of Sao Paulo, where he has been a tenured professor since 1989. He has had postdoctoral research experience at the Friedrich Alexander University Erlangen–Nuremberg, Germany (1997–98). He was a visiting professor at Ecole Centrale de Lille, France (2004–06), and at the Faculty of Mechanical Engineering of the Silesian University of Technology, Gliwice, Poland (2012–13). He served as an adjunct professor at the Faculty of Engineering, UDESC, Joinville, Brazil (1984–89). He has been an advisor on several PhD theses and master's dissertations, coordinator of the Laboratory of Manufacturing Engineering of the EPUSP, and is responsible for several international and national cooperation agreements for exchange of students and researchers as well as for consultancy with the industry. He is the volume editor for the *Materials Modeling and Characterization* volume in Elsevier's *Comprehensive Materials Processing series*.

Sergio T. Button received his PhD in Mechanical Engineering from School of Mechanical Engineering, University of Campinas, Brazil, in 1990. He is currently full professor of Manufacturing Processes at the University of Campinas. His main research fields include metal forming and numerical simulation. Currently, his research is focused on cross wedge rolling and hot stamping. He is the coauthor of 2 books and more than 100 papers in international journals and conferences. He is the editor and reviewer of many international journals, and participates in the organization of three national and international scientific conferences.

www.iran-mavad.com
مرجع مهندسی مواد و متالورژی

David Cameron is currently scientific advisor to Miktech Oy, Finland, and adjunct professor in Dublin City University, Ireland. From 2003 to 2013, he was professor of Material Technology in Lappeenranta University of Technology, Finland, where he established the Advanced Surface Technology Research Laboratory (ASTRaL). He obtained his doctorate from the University of Glasgow in 1980 and has spent his research career working on thin-film technology. He was a senior research fellow at the Royal Signals and Radar Establishment in the United Kingdom until 1982 when he joined the School of Electronic Engineering at Dublin City University, becoming associate professor. His research focus is on atomic layer deposition and its industrialization.

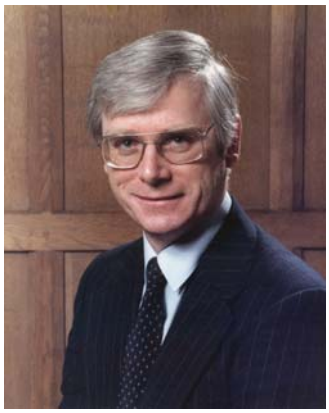

Joseph A. McGeough is an honorary professorial fellow in the School of Engineering at the University of Edinburgh. He is a graduate from the universities of Glasgow (BSc and PhD) and Aberdeen (DSc). He held research appointments at the universities of Leicester, Queensland, and Strathclyde. As a student he gained numerous county, university, and national championship athletic awards. His industrial training began as an undergraduate vacation apprentice for a firm of electrical contractors based at ICI ltd Nobel Division, and he subsequently undertook postgraduate experience at International Research and Development, Newcastle upon Tyne, before returning to university service. He was successively a lecturer, senior lecturer, and reader in Engineering at Aberdeen University, and then moved to Edinburgh University to take up its Regius Chair of Engineering. His research work has dealt mainly with manufacturing processes for which he has been awarded Institution of Mechanical Engineers and the Society for Underwater Technology prizes. He has been the recipient of a Royal Society/SERC (Science and Engineering (now Engineering and Physical Sciences) Research Council) Industrial Fellowship in order to transfer the results of his research to industry. His publications include *Principles of Electrochemical Machining*, *Advanced Methods of Machining*, and *Micromachining of Engineering Materials* (editor). His latest book is *The Engineering of Human Joint Replacements* (2013), which contains details of the materials and manufacturing processes used in this field. He is a fellow of the Institution of Mechanical Engineers, International Academy for Production Engineering, Royal Society of Edinburgh, and Royal Academy of Engineering.

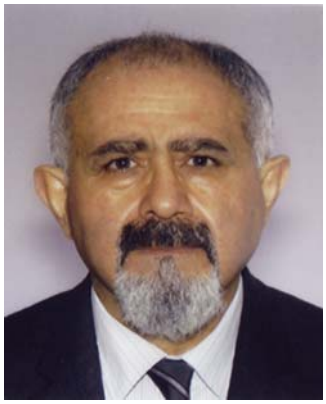

Emin Bayraktar is a full university professor and research director at Supmeca/Paris, School of Mechanical and Manufacturing Engineering, Paris, France. He was awarded a PhD degree in Mechanical Engineering by IST/OSU and a second PhD degree in Materials Science and Engineering in Paris. Subsequently, Professor Bayraktar was awarded a higher doctorate degree of habilitation (DSc) in Mechanics of Materials in recognition of his research contributions at Paris 6, University Marie-Curie. His teaching and research expertise lies on the processing and manufacturing of the composite materials and damage analysis. Recently he has been appointed as an adjunct professor in UNICAMP-Campinas, Brazil, on the new design of composites for the application in aeronautical engineering. He is on the editorial board of a number of scientific journals. He is also a member of the Steering Committee for the International Conference Series on Advances in Materials and Processing Technologies (AMPT).

www.iran-mavad.com
مرجع مهندسی مواد و متالورژی

Bekir S. Yilbas received his PhD degree in Mechanical Engineering from Birmingham University. He was awarded the Doctor of Engineering degree in 2005 by Birmingham University due to his significant contribution to his field of study. He has published 375 journal papers in reputable international journals and presented over 60 papers at international conferences. He has served as an editorial board member of international journals, including *International Journal of Machine Tool and Manufacture Design, Research and Application, International Journal of Subsurface Sensing Technologies and Applications, Journal of Materials Processing Technology, Journal of Achievements in Materials and Manufacturing Engineering, International Journal of Nanomanufacturing, and Archives of Materials Science and Engineering*. He has received numerous awards in recognition of his research work.

Nabil Bassim was born and raised in Cairo, Egypt. Dr. Bassim received a BSc in Chemical Engineering from Cairo University in 1965. He went to the University of Virginia, United States, where he received his MSc in Chemical Engineering (Nuclear Engineering option), and a PhD in Materials Science in 1973. He moved to Canada where he is now professor of Materials Science and Engineering at the University of Manitoba. He served for years as associate dean of research at the Faculty of Engineering and was director of International Programs for the faculty. His areas of research interest include mechanisms and mechanics of plastic deformation, dislocation theory, fracture and fatigue, and nondestructive evaluations. He has patents on the use of acoustic emission for monitoring of structures. He also has an interest in studying the behavior of materials at high strain rates and large strains as they affect processes such as metal forming and machining. He has published over 120 papers and supervised numerous MSc and PhD theses.

Syed H. Masood is professor of Mechanical and Manufacturing Engineering at Swinburne University of Technology in Melbourne, Australia, where he is also the program coordinator of the master's program in advanced manufacturing technology. He obtained his PhD from the University of Queensland, Australia; MEng from the University of New Brunswick, Canada; PG Dip from IIT Delhi; and BSc Eng Hons from Aligarh Muslim University, India. Professor Masood has worked previously at Central Queensland University, Rockhampton, and PNG University of Technology, Papua New Guinea. He has published over 275 technical articles in international journals, books, and conferences in different areas of advanced manufacturing. His current research interests include additive manufacturing technologies, especially fused deposition modeling and direct metal deposition, plastics manufacturing processes, material development, and material characterization.

www.iran-mavad.com
مرجع مهندسی مواد و متالورژی

Mustafizur Rahman is currently a professor at the Department of Mechanical Engineering at National University of Singapore (NUS), and has been with NUS since 1982. He obtained his BSc in Engineering from Bangladesh University of Engineering and Technology (BUET), MEng and PhD from Tokyo Institute of Technology, Japan. His research interests include micro-/nanomachining, design and development of miniature machine tools and devices for micro-/nanomachining, and high-speed machining of difficult-to-machine materials. He has received Outstanding Achievement Awards from the Singapore Institute of Engineers and the Japan Society of Mechanical Engineers in 2003 and 2005, respectively.

George Krauss is currently university emeritus professor at the Colorado School of Mines and a metallurgical consultant specializing in steel microstructural systems. Dr. Krauss received the BSc in Metallurgical Engineering from Lehigh University in 1955 and the MSc and ScD degrees in Metallurgy from the Massachusetts Institute of Technology in 1958 and 1961, respectively, after working at the Superior Tube Company as a development engineer in 1956. In 1962–63, he was an NSF postdoctoral fellow at the Max Planck Institut für Eisenforschung in Düsseldorf, Germany. He served at Lehigh University as assistant professor, associate professor, and professor of Metallurgy and Materials Science from 1963 to 1975, and in 1975 joined the faculty of the Colorado School of Mines as the AMAX Foundation professor in Physical Metallurgy. He was the John Henry Moore professor of Metallurgical and Materials Engineering at the time of his retirement from the Colorado School of Mines in 1997.

In 1984, Dr. Krauss was a principal in the establishment of the Advanced Steel Processing and Products Research Center, an NSF Industry-University cooperative research center at the Colorado School of Mines, and served as its first director until 1993. He has authored the book *Steels: Processing, Structure, and Performance*, (ASM International, 2005), coauthored the book *Tool Steels*, fifth edition, (ASM International, 1998), and edited or coedited conference volumes on tempering of steel, carburizing, zinc-based coatings on steel, and microalloyed forging steels. He has published over 330 papers and lectured widely in technical conferences, universities, corporations, and ASM International chapters, presenting a number of keynote, invited, and honorary lectures. He presented the Edward DeMille Campbell Memorial Lecture of ASM International in 2000, the Howe Memorial Lecture of ISS in 2003, and the Adolf Martens Memorial Steel Lecture of AIST in 2010.

Dr. Krauss has served as the president of the International Federation of Heat Treatment and Surface Engineering (IFHTSE), 1989–91, and as President of ASM International, 1996–97. He is a fellow of ASM International, TMS, and IFHTSE. He has been awarded the Adolf Martens Medal of the German Society for Heat Treatment and Materials, the Charles S. Barrett Silver Medal of the Rocky Mountain Chapter of ASM, the George Brown Gold Medal of the Colorado School of Mines, and several other professional and teaching awards, including the ASM Albert Easton White Distinguished Teacher Award in 1999. He is an honorary member of the Iron and Steel Institute of Japan, a distinguished member of the Iron and Steel Society, an honorary member of ASM International, and an honorary member of the Japan Institute of Metals.

www.iran-mavad.com
مرجع مهندسی مواد و متالورژی

CONTRIBUTORS TO VOLUME 6

Q. Ahsan
Universiti Teknikal Malaysia Melaka (UTeM), Melaka, Malaysia

A. Alaswad
Dublin City University, Dublin, Ireland

E. Bayraktar
School of Mechanical and Manufacturing Engineering, France

K.Y. Benyounis
Dublin City University, Dublin, Ireland

J.L. Caron
Haynes International, Inc., Kokomo, IN, USA

G. Casalino
DMMM — Politecnico di Bari, Bari, Italy

S.Y. Chang
Universiti Teknikal Malaysia Melaka (UTeM), Melaka, Malaysia

S. Emamian
Universiti Putra Malaysia, Selangor, Malaysia

M. Ghobakhloo
Universiti Putra Malaysia, Selangor, Malaysia

A.S.M.A. Haseeb
University of Malaya, Kuala Lumpur, Malaysia

S.M. Homayouni
Lenjan Branch, Islamic Azad University, Isfahan, Iran

T.S. Hong
Universiti Putra Malaysia, Selangor, Malaysia

M.F. Jamaluddin
University of Malaya, Kuala Lumpur, Malaysia

W. Khaksar
University Tenaga Nasional, Selangor, Malaysia

R.L. Lorza
University of La Rioja, Spain

R. Lostado
University of La Rioja, Spain

A.G. Olabi
University of the West of Scotland, Paisley, Renfrewshire, UK

J.W. Sowards
National Institute of Standards and Technology, Boulder, CO, USA

S. Sulaiman
Universiti Putra Malaysia, Selangor, Malaysia

N.I. Syahriah Binti Hussein
Universiti Teknikal Malaysia Melaka (UTeM), Melaka, Malaysia

M.R. Vasili
Lenjan Branch, Islamic Azad University, Isfahan, Iran

M. Vural
Istanbul Technical University, Istanbul, Turkey

M.A. Wahab
Louisiana State University, Baton Rouge, LA, USA

F. Yusof
University of Malaya, Kuala Lumpur, Malaysia

www.iran-mavad.com
مرجع مهندسی مواد و متالورژی

This page intentionally left blank

www.iran-mavad.com
مرجع مهندسی مواد و متالورژی

CONTENTS OF VOLUME 6

Editor-in-Chief v

Editorial Board vii

Contributors to Volume 6 xi

Preface xv

6.01 Introduction to Welding and Bonding Technologies 1
E Bayraktar

6.02 Welding Processes and Technologies 3
M Vural

6.03 Manual Metal Arc Welding and Gas Metal Arc Welding 49
M A Wahab

6.04 Robotic Welding Technology 77
T S Hong, M Ghobakhloo and *W Khaksar*

6.05 Mathematical Modeling of Weld Phenomena, Part 1: Finite-Element Modeling 101
A G Olabi and *G Casalino*

6.06 Mathematical Modeling of Weld Phenomena, Part 2: Design of Experiments and Optimization 111
A G Olabi, A Alaswad and *K Y Benyounis*

6.07 Welding Defects and Implications on Welded Assemblies 125
F Yusof and *M F Jamaluddin*

6.08 9% Nickel Steels and Their Welding Behavior 135
Q Ahsan, A S M A Haseeb, N I Syahriah Binti Hussein and *S Y Chang*

6.09 Weldability of Nickel-Base Alloys 151
J L Caron and *J W Sowards*

6.10 Review of Microstructures, Mechanical Properties, and Residual Stresses of Ferritic and Martensitic Stainless-Steel Welded Joints 181
A G Olabi, R Lostado and *K Y Benyounis*

6.11 Quality Control in Welding Process 193
A G Olabi, R L Lorza and *K Y Benyounis*

6.12 Safety and Security Conditions in Welding Processes 213
T S Hong and *M Ghobakhloo*

6.13 Optimum Speed of Friction Stir Welding on 304L Stainless Steel by Finite Element Method 227
S Sulaiman and *S Emamian*

6.14 Bonding Technologies in Manufacturing Engineering 237
S M Homayouni, M R Vasili and *T S Hong*

www.iran-mavad.com
مرجع مهندسی مواد و متالورژی

This page intentionally left blank

www.iran-mavad.com
مرجع مهندسی مواد و متالورژی

PREFACE

In recent years considerable advances have taken place in materials and their processing technologies, the pace of which is progressing at an accelerated rate. It is therefore vitally important that researchers, academics, design engineers, and manufacturing technologists be up to date with these new developments. Such developments open up excellent opportunities to improve effective utilization of material resources, improve efficiency, reliability, durability, and cost effectiveness of the products. This comprehensive series will serve researchers all over the world in keeping them fully abreast of such new developments.

Comprehensive Materials Processing is a one-stop resource consolidating and enhancing the literature of the materials processing and manufacturing universe. The work addresses recent progress in materials technologies and science as well as covering recent developments in specific manufacturing processes involved with materials for applications in engineering, biomedical, environmental protection, health and safety, and sensor materials and technologies. The authoritative analysis of these processes will assist scientists and engineers in the selection, design, and usage of materials, whether required in the lab or in action across industry.

As the editor-in-chief of this comprehensive series, a truly collaborative work, I am greatly indebted to the volume editors, internationally renowned experts in their fields, for guiding and selecting the topics for their respective volumes, commissioning authors, and reviewing the content so meticulously. Their true dedication to the scientific community is reflected in the time and energy they have given to this project. My sincere thanks are also due to all of the authors—researchers and materials practitioners who have contributed extensive coverage of literature review as well as recent works of research to this huge project. Their insight and specialist knowledge in their respective fields is reflected in the high quality of this work.

Myself, the three associate editors-in-chief, and all of the volume editors are greatly appreciative of all the hard work undertaken to turn this idea into a publishable work. Our special thanks go to Gemma Tomalin, the project manager, along with Joanne Williams, and the rest of the team at Elsevier who served successively to keep the project on track through friendly nudges in order to ensure timely completion. We are also hugely grateful to Mohamed Imrankhan for his dutiful coordination of the proofs.

The extensive academic discussion of core theories and applications, supplemented by applied case studies and advanced multimedia features has drawn together numerous areas of research and I sincerely hope that this work will prove to be of great help to both the young and experienced members of the international research community, academics, and industrial practitioners for many years to come.

Saleem Hashmi
Editor-in-Chief

www.iran-mavad.com
مرجع مهندسی مواد و متالورژی

This page intentionally left blank

www.iran-mavad.com
مرجع مهندسی مواد و متالورژی

6.01 Introduction to Welding and Bonding Technologies

E Bayraktar, School of Mechanical and Manufacturing Engineering, France

© 2014 Elsevier Ltd. All rights reserved.

6.01.1 Concluding Remarks and Acknowledgments 2

The research and progress in welding and joining technologies and their applications in advanced manufacturing engineering systems are still growing and ongoing.

In fact, welding and joining processes are fundamental to the development of manufacturing engineering applications. Welding is an interdisciplinary scientific activity that touches upon different scientific domains (such as physics, chemistry, electronics, computer science, materials science, etc.). Therefore, we have tried to present detailed work that can be used as a comprehensive reference by everyone, requiring materials science and manufacturing interrelated to welding and joining information. It is imperative that the manufacturing engineers work with the designers for the product design to guarantee that well-matched materials, methods, and properties are selected for the final assembly stage. If the design can be created carefully and the parts can be produced correctly, the welding process becomes much easier and inexpensive, and both the quality and reliability of the product can be improved.

For a welding-product engineer, broad experience and scientific knowledge are vital requirements to combine these different scientific domains and to apply them effectively to a variety of processes. There are very different scientific problems and theoretical approaches to be resolved, which both require final and precise solutions. For example, in the case of fusion welding, the professional experience of a welding engineer is a critical prerequisite. As fusion welding always produces thermal stress, deformation, and residual stress in products, the mechanism of production of stress and deformation and their influences upon the performance of welded structures are matters of acute concern for welding engineers. The theory of welding mechanics presents the theoretical framework for understanding these consequences.

In classic welding procedures, theories are based on an empirical formula and using simplified models. Nevertheless, in recent times, thermal elastic–plastic analysis by the finite element method (FEM) has become popular and has been applied to simulate the general behavior of metal parts during welding. In practice, general structures are fabricated by a series of production processes. The welding procedure belongs to the first and basic manufacturing domain, called fusion welding, that is, to fasten together components by melting a very small fraction of the metal (it can be imagined as a local and special foundry operation between two pieces). The energy sources for melting metal are very different such as gas, arc, plasma, electron beam, laser, etc. These sources are chosen contingent upon the type of structure and the efficiency of the manufacturing system. For example, manufacturing of a simple pressure vessel requires an efficient heat source such as electron-beam welding. However, for the structure of a ship or bridge or a petroleum platform, etc., arc welding is extensively used because of its type of usage. Usually, fusion welding is carried out by a mobile heat source along the weld line. The welding process by a type of fusion welding is more or less the same and includes the heating process, melting process, and solidification process.

For this reason, arc welding is selected as an example, and the basic model of computational welding procedures is also presented in this volume. As for the computational welding procedure, it should supply a significant practice for modeling the welding processes. Welding simulations are input used in developing the design and control of welding processes and the performance of welded parts or structures. Computational welding can be used to model experiences such as heat generation, thermal stresses, and bulk plastic deformations of components or structures. In addition, it has extensive applications in modeling thermomechanical and microstructural incidents in metals. In other words, the computational welding procedure is a standard work for welding engineers and all those researching welding processes and wider thermomechanical and microstructural phenomena in metals.

Volume 6 of the *Comprehensive Materials Processing* (the 'work') edited by Professor Saleem Hashmi (the 'Editor-in-Chief') represents a dense work for this series, and it was arranged for the needs of the materials science and manufacturing communities.

There are 14 chapters that address general information and basic methods of welding and bonding technologies as an essential scientific area and are outlined as follows:

Chapter 1 (6.01) presents a general introduction of this volume and demonstrates an overview of welding and bonding technologies. The chapter also outlines future developments and potential impacts of welding and bonding technologies on manufacturing systems.

Chapter 2 (6.02) presents a detailed overview of the research undertaken with welding processes and technologies in several key areas including process improvements and applications.

Chapter 3 (6.03) presents a very dense study on manual metal arc welding and on gas metal arc welding.

Chapter 4 (6.04) provides a detailed study on robotic welding technology.

Chapter 5 (6.05) presents mathematical modeling of weld phenomena in two parts: FEM is first given in detail followed by experimental design and optimization (in (6.06)).

Chapter 7 (6.07) provides details of research and development on welding defects and advanced implications on welded assemblies.

Chapter 8 (6.08) reviews weldability of 9% Ni steels.

www.iran-mavad.com
مرجع مهندسی مواد و متالورژی

Chapter 9 (6.09) reviews the weldability of nickel-based alloys.
Chapter 10 (6.10) provides a detailed overview on microstructure, mechanical properties, and residual stresses of ferritic and martensitic stainless steel welded joints.
Chapter 11 (6.11) provides a comprehensive overview of research regarding quality control in welding processes.
Chapter 12 (6.12) presents an overview on safety and security conditions in welding processes.
Chapter 13 (6.13) provides an overview of research to ascertain the optimum speed in friction stir welding.
Chapter 14 (6.14) provides general research on bonding technologies in manufacturing engineering.

6.01.1 Concluding Remarks and Acknowledgments

This volume presents a collection of chapters related to aspects of the general information and methods of welding and joining technologies. Aggregating a volume of successful work of this scale is a skillful attempt and could not have been achieved without the contributed and hard-working efforts of the authors of the chapters of this volume. The editor conveys his deep admiration to all the authors and coauthors of the actual chapters of this volume for all their strong and highly qualified efforts that have been devoted to preparing their individual chapters. Their contributions are gratefully acknowledged.

And finally, my deep and sincere acknowledgments to Professor Saleem Hashmi, the Editor-in-Chief of *Comprehensive Materials Processing* for his role as a driving force of this hard work to edit, which helped us finish each volume. Special thanks are also due to the coordinating staff members of Elsevier and their editorial staff for this massive work.

www.iran-mavad.com
مرجع مهندسی مواد و متالورژی

6.02 Welding Processes and Technologies

M Vural, Istanbul Technical University, Istanbul, Turkey

© 2014 Elsevier Ltd. All rights reserved.

6.02.1	**General Introduction**	4
6.02.2	**Fusion Welding Processes**	7
6.02.2.1	Oxyfuel Gas Welding	8
6.02.2.1.1	Fuel Gases	9
6.02.2.1.2	Oxygen	9
6.02.2.1.3	Welding Torch	9
6.02.2.1.4	Welding Flame	10
6.02.2.1.5	Welding Consumables	11
6.02.2.1.6	Irregularities in Gas Welding	11
6.02.2.2	Metal Arc Welding	13
6.02.2.2.1	The Processes in the Arc	13
6.02.2.2.2	Welding Power Sources	16
6.02.2.2.3	Power Source Characteristics	16
6.02.2.2.4	Types of Welding Power Sources	18
6.02.2.2.5	Duty Cycle	21
6.02.2.3	The Manual Metal Arc Welding	21
6.02.2.3.1	Electrodes	22
6.02.2.3.2	Types of Electrode Coating	23
6.02.2.3.3	Designation of the Electrodes	23
6.02.2.3.4	Covered Electrodes for Welding Carbon and Carbon Manganese Steels	23
6.02.2.3.5	Low Alloy Electrodes	23
6.02.2.3.6	Electrodes for Alloy and Stainless Steels	25
6.02.2.3.7	Technology of Welding	25
6.02.2.3.8	Irregularities in Manual Metal Arc Welding	26
6.02.2.4	Submerged Arc Welding	27
6.02.2.4.1	Electrodes	27
6.02.2.4.2	Welding Flux	27
6.02.2.4.3	Welding Equipment	28
6.02.2.4.4	Weld Irregularities	28
6.02.2.5	Gas Shielded Arc Welding	29
6.02.2.6	Gas Tungsten Arc Welding	30
6.02.2.6.1	Welding Technique	31
6.02.2.6.2	Irregularities in TIG Welding	32
6.02.2.7	Plasma Welding	32
6.02.2.7.1	Plasma Arc	32
6.02.2.7.2	Weld Irregularities in Plasma Welding	34
6.02.2.8	Electron Beam Welding	34
6.02.2.9	LASER Welding	36
6.02.2.9.1	Beam Formation	36
6.02.2.9.2	Welding with the Laser	37
6.02.2.10	Resistance Welding	38
6.02.2.10.1	Spot Welding	38
6.02.2.10.2	Welding Power Sources	38
6.02.2.10.3	Weldability of Materials	38
6.02.2.10.4	Welding Parameters	39
6.02.2.10.5	Welding Electrodes	41
6.02.2.10.6	Resistance Projection Welding	41
6.02.2.10.7	Resistance Seam Welding	42
6.02.2.10.8	Resistance Butt and Flash Welding	43
6.02.2.11	Stud Welding	43
6.02.3	**Solid-State Welding Processes**	44
6.02.3.1	Diffusion Bonding	45
6.02.3.2	Friction Welding	46
6.02.3.3	Ultrasonic Welding	47
References		48

www.iran-mavad.com
مرجع مهندسی مواد و متالورژی

6.02.1 General Introduction

Welding is the joining of materials in the welding zone with the use of heat and/or force, with or without filler metal. It can be facilitated with the help of, for example, shielding gases, welding powders, or pastes. The energy required for welding is supplied from the outside.

The history of welding began very early. In 4000 BC, the Sumerians were already welding metals together. They welded gold with gold. It then took a very long time until the next major step in the field of welding technology was achieved. In 2700 BC, the Egyptians constructed copper lines by fire welding. The tubes were then sealed as water pipes for urban water supply. Fire welding was also used for making jewelry. In the following centuries, many important discoveries were made in the field of welding technology, such as the electrical machine of Guerick, the electric sparks of Leibniz, or the capacitor of EC von Kleist in 1745. The big breakthrough, however, came only during 1880–87. During this period the Russian Nikolai Nikolaijewitsch Bernados developed what today is known as the arc welding process. He managed to join for the first time two metal parts using electric arc. The first presentation of his case was made in 1881 in Paris, where he created an arc between a workpiece and a carbon electrode. In the following years, this process became a very common method used for joining steel. Resistance welding is due to E. Thomson (1886). Batteries were used as power sources first. With the availability of acetylene as fuel gas, the oxyacetylene welding process was introduced in 1900. Further developments in welding technology are basically improvements of this method. For example, in Sweden Oskar Kjellberg developed coated electrodes in 1908. This improved immensely the quality of the welds produced. A further increase in quality in the field of arc welding was achieved by Roberts and Nuys, as they used inert gases for the first time during the welding process. Today, the most widely used partially and fully mechanical methods are all significantly newer:

- Submerged arc welding, 1936
- Tungsten inert gas (TIG) welding, 1936
- Metal inert gas (MIG) welding, 1948
- Metal active gas (MAG) welding, 1953
- Plasma welding from 1960
- Laser welding from 1970

Welding is one of the most systematic joining techniques. The processes of joining are divided into four groups, shown in Figure 1, as joining by forming, welding, brazing, and adhesive bonding.

All processes given here are among the non-separables. Each method can be defined as follows:

Joining by forming comprises the processes in which the parts to be joined or the auxiliary joining parts are formed locally, so that the joining is secured by positive engagement against unintentional loosening.

Welding is the joining of base metals under application of heat or pressure, or both, with or without using a filler.

Brazing is the joining of metal workpieces with the aid of a molten filler metal, whose melting temperature is below that of the base materials joined. The base materials are not melted, but only wetted; if necessary, they are worked with a flux.

Adhesive bonding is the joining of two parts by using an adhesive, i.e., a non-metallic material, the parts to be joined by surface bonding (adhesion), and between and within the molecular adhesive forces (cohesion).

Welding is a materials joining process in which two or more parts are coalesced at their contacting surfaces by a suitable application of heat or pressure or both. Many welding processes are accomplished by heat alone, with no pressure applied; others by a combination of heat and pressure; and still others by pressure alone, with no external heat supplied.

In some welding processes, a filler material is added to facilitate coalescence. The assemblage of parts that are joined by welding is called a weldment. Welding is most commonly associated with metal parts, but the process is also used for joining plastics.

Depending on the nature of the base material to be joined, the purpose of the welding process, or the type of production, other systematic subdivisions are made. Figure 1 gives an overview of the performance and efficiency of key processes.

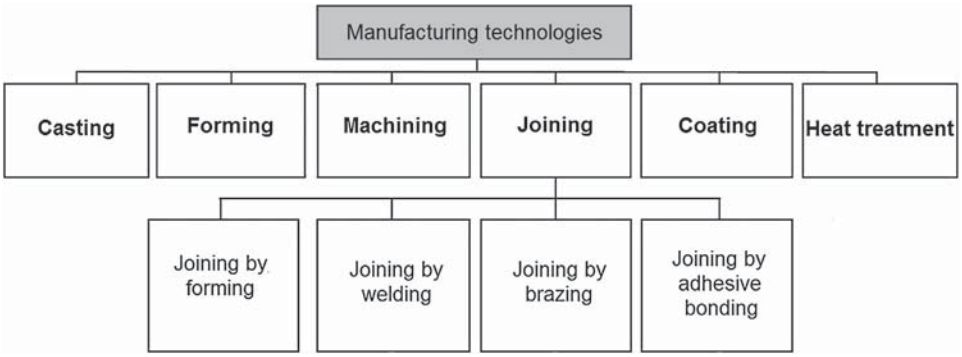

Figure 1 Classification of the joining methods among the manufacturing technologies.

www.iran-mavad.com
مرجع مهندسی مواد و متالورژی

By welding, joinings can be created, in which the welded metals have the same properties as those of the base material. One exception is still the fatigue strength, with lower values in all cases for the weld. For steels, in most cases the suitable welding methods are available, the classic casting materials can be reliably welded today in many cases except for alloys with special properties; welding of nonferrous metals is also largely dominated.

The material is affected during welding by the applied heat. The fact that this may change the performance characteristics requires special consideration. When welding steels, for example, one must pay attention to the aging, hardening, and formation of brittle fracture; it still continues to influence segregation behavior and anisotropy properties.

A 'safe' weldment is when the weld joints in the construction remains functional under the action of the load without brittle or break or crack formation. Welding safety is thus defined as a variable that is influenced by the material and the construction.

The advantages and disadvantages of the welding can be summarized as follows:

- Welding provides a permanent joint. The welded parts become a single entity.
- The welded joint can be stronger than the parent materials if a filler metal is used that has strength properties superior to those of the parents, and if proper welding techniques are used.
- Welding is usually the most economical way to join components in terms of material usage and fabrication costs. Alternative mechanical methods of assembly require more complex shape alterations (e.g., drilling of holes) and addition of fasteners (e.g., rivets or bolts). The resulting mechanical assembly is usually heavier than a corresponding weldment.
- Welding is not restricted to the factory environment. It can be accomplished 'in the field.'

Although welding has the advantages indicated, it also has certain limitations and drawbacks (or potential drawbacks):

- Most welding operations are performed manually and are expensive in terms of labor cost. Many welding operations are considered skilled trades, and the labor to perform these operations may be scarce.
- Most welding processes are inherently dangerous because they involve the use of high energy.
- Since welding accomplishes a permanent bond between the components, it does not allow for convenient disassembly. If the product must occasionally be disassembled (e.g., for repair or maintenance), then welding should not be used as the assembly method.
- The welded joint can suffer from certain quality defects that are difficult to detect.
- The defects can reduce the strength of the joint.

The standard numbers of welding and allied processes are given in **Table 1** according to ISO 4063, Welding and allied processes – Nomenclature of processes and reference numbers (*1–7*).

Table 1 Standard numbers of welding and allied processes according to ISO 4063

1 Arc welding
101 Metal arc welding
11 Metal arc welding without gas protection
111 Manual metal arc welding (metal arc welding with covered electrode); shielded metal arc welding/USA/
112 Gravity (arc) welding with covered electrode; gravity feed welding/USA/
114 Self-shielded tubular-cored arc welding
12 Submerged arc welding 12 Soudage à l'arc sous flux (en poudre); soudage à l'arc submergé/B/
121 Submerged arc welding with one wire electrode
122 Submerged arc welding with strip electrode
*123 Submerged arc welding with multiple wire electrodes
124 Submerged arc welding with metallic powder addition
125 Submerged arc welding with tubular cored electrode
13 Gas-shielded metal arc welding; gas metal arc welding/USA/
131 Metal inert gas welding; MIG welding; gas metal arc welding/USA/
135 Metal active gas welding; MAG welding; gas metal arc welding/USA/
136 Tubular cored metal arc welding with active gas shield; flux cored arc welding/USA/
137 Tubular cored metal arc welding with inert gas shield; flux cored arc welding/USA/
14 Gas-shielded welding with nonconsumable electrode
141 Tungsten inert gas welding; TIG welding; gas tungsten arc welding/USA/
15 Plasma arc welding 15 Soudage plasma 15 Plasmaschweißen
151 Plasma MIG welding
152 Powder plasma arc welding
18 Other arc welding processes
185 Magnetically impelled arc butt welding
2 Resistance welding 2 Soudage par résistance 2 Widerstandsschweißen
21 Spot welding; resistance spot welding/USA/
*211 Indirect spot welding; indirect welding/USA/

(*Continued*)

www.iran-mavad.com
مرجع مهندسی مواد و متالورژی

Table 1 Standard numbers of welding and allied processes according to ISO 4063—Cont'd

*212 Direct spot welding
22 Seam welding; resistance seam welding/USA/
221 Lap seam welding
222 Mash seam welding
225 Foil butt-seam welding
226 Seam welding with strip
23 Projection welding
*231 Indirect projection welding
*232 Direct projection welding
24 Flash welding
*241 Flash welding with preheating
*242 Flash welding without preheating
25 Resistance butt welding; upset welding/USA/
29 Other resistance welding processes
291 HF resistance welding (high frequency resistance welding); high frequency upset welding/USA/

3 Gas welding; oxyfuel gas welding/USA/
31 Oxy-fuel gas welding; oxyfuel gas welding/USA/
311 Oxy-acetylene welding; oxyacetylene welding/USA/
312 Oxy-propane welding
313 Oxy-hydrogen welding; oxy-hydrogen welding/USA/

4 Welding with pressure
41 Ultrasonic welding
42 Friction welding
44 Welding by high mechanical energy
441 Explosive welding; explosion welding/USA/
45 Diffusion welding
47 Oxy-fuel gas pressure welding; pressure gas welding/USA/
48 Cold pressure welding; cold welding/USA/
*1) 5 Beam welding
*1) 51 Electron beam welding
*1) 511 Electron beam welding in vacuum
*1) 512 Electron beam welding in atmosphere
*1) 52 Laser welding; laser beam welding/USA/
*1) 521 Solid state laser welding
*1) 522 Gas laser welding

7 Other welding processes
71 Aluminothermic welding; thermite welding/USA/
72 Electroslag welding
73 Electrogas welding
74 Induction welding
*741 Induction butt welding; induction upset welding/USA/
*742 Induction seam welding
75 Light radiation welding
753 Infrared welding
77 Percussion welding
78 Stud welding
782 Resistance stud welding
*783 Drawn arc stud welding with ceramic ferrule or shielding gas; arc stud welding/USA/
*784 Short-cycle drawn arc stud welding; arc stud welding/USA/
*785 Capacitor discharge drawn arc stud welding; arc stud welding/USA/
*786 Capacitor discharge stud welding with tip ignition; arc stud welding
*787 Drawn arc stud welding with fusible collar
*788 Friction stud welding

*8 Cutting and gouging
*81 Flame cutting; oxygen cutting/USA/
*82 Arc cutting
*821 Air arc cutting; air carbon arc cutting/USA/
*822 Oxygen arc cutting

www.iran-mavad.com
مرجع مهندسی مواد و متالورژی

Table 1 Standard numbers of welding and allied processes according to ISO 4063—Cont'd

*83 Plasma cutting; plasma arc cutting/USA/
*84 Laser cutting; laser beam cutting/USA/
*86 Flame gouging; thermal gouging/USA/
*87 Arc gouging
*871 Air arc gouging; air carbon arc cutting/USA/
*872 Oxygen arc gouging; oxygen gouging/USA/
*88 Plasma gouging

9 Brazing, soldering, and braze welding
91 Brazing
911 Infrared brazing
912 Flame brazing; torch brazing/USA/
913 Furnace brazing
914 Dip brazing
915 Salt-bath brazing; dip brazing/USA/
916 Induction brazing
918 Resistance brazing
919 Diffusion brazing
924 Vacuum brazing
93 Other brazing processes
94 Soldering
941 Infrared soldering
942 Flame soldering; torch soldering/USA/
943 Furnace soldering
944 Dip soldering
945 Salt-bath soldering
946 Induction soldering
947 Ultrasonic soldering
948 Resistance soldering
949 Diffusion soldering
951 Wave soldering
952 Soldering with soldering iron
954 Vacuum soldering
956 Drag soldering
96 Other soldering processes
97 Braze welding
971 Gas braze welding
972 Arc braze welding

113 Bare wire metal arc welding; bare metal arc welding/USA/
115 Coated wire metal arc welding
118 Firecracker welding
149 Atomic-hydrogen welding
181 Carbon-arc welding
32 Air-fuel gas welding
321 Air-acetylene welding; air acetylene welding/USA/
322 Air-propane welding
43 Forge welding
752 Arc image welding
2) 781 Arc stud welding
917 Ultrasonic brazing
923 Friction brazing
953 Abrasion soldering

6.02.2 Fusion Welding Processes

Fusion welding processes use heat to melt the base metals without applying an external force. In many fusion welding operations, a filler metal is added to the molten pool to facilitate the process and provide bulk and strength to the welded joint. A fusion welding operation in which no filler metal is added is referred to as an autogenous weld. The fusion category includes the most widely used welding processes, which can be organized into several general groups.

An overview of the methods belonging to this group of processes is given in **Figure 2**.

www.iran-mavad.com
مرجع مهندسی مواد و متالورژی

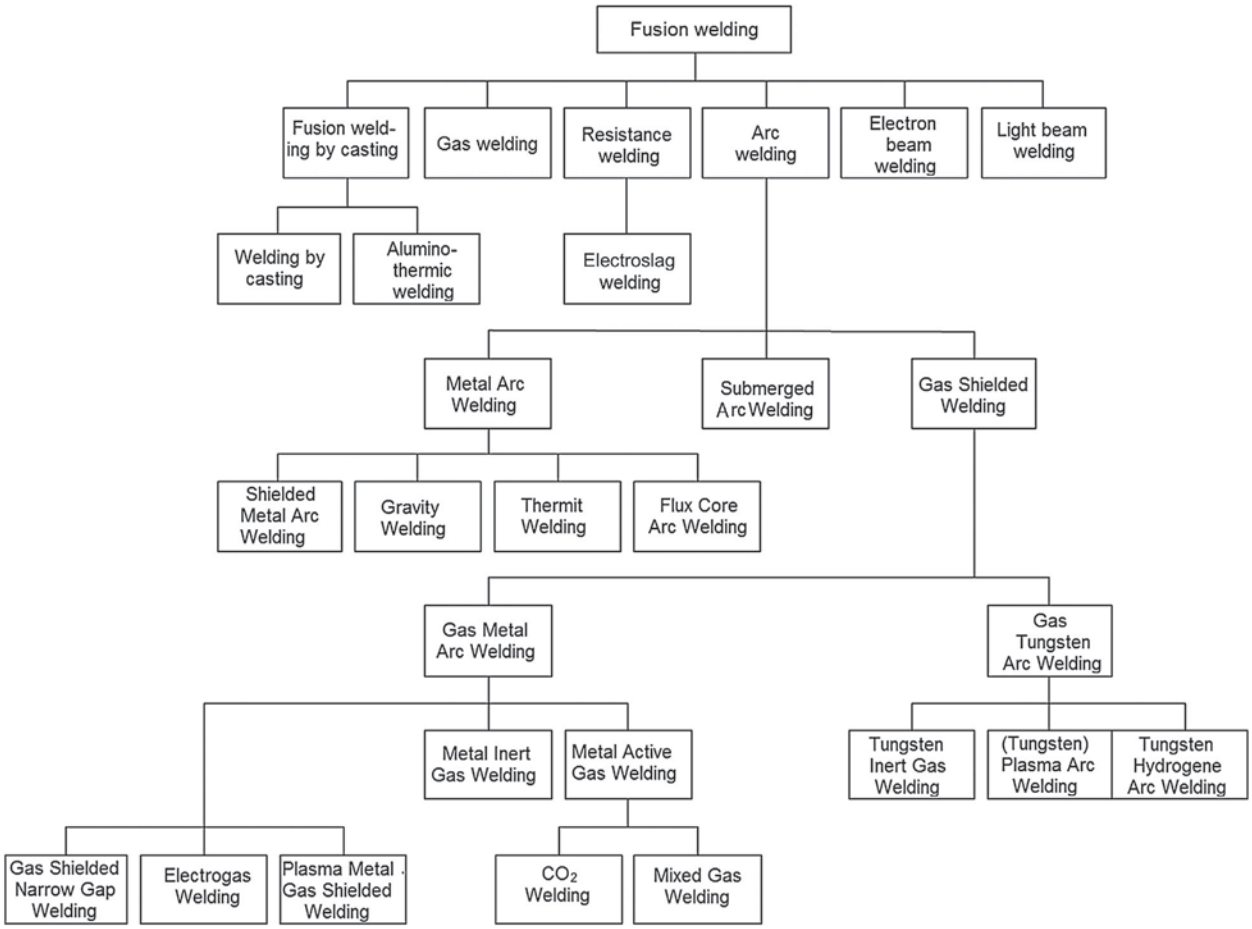

Figure 2 Classification of fusion welding processes. Reproduced from Fachkundeschweiβtechnik, CD-ROM, DVS-Media, 2000.

6.02.2.1 Oxyfuel Gas Welding

Oxyfuel gas welding is the term used to describe the group of fusion welding operations that burn various fuels mixed with oxygen to perform welding. The oxyfuel gas welding processes employ several types of gases, which is the primary distinction among the members of this group. Oxyfuel gas is also commonly used in cutting torches to cut and separate metal plates and other parts. The most important oxyfuel gas welding process is oxyacetylene welding.

In oxyfuel gas welding, also called autogenous welding, the melt flow is caused by a direct, localized exposure to a fuel gas–oxygen flame. The heat and filler metal, if used, are supplied separately, see **Figure 3**.

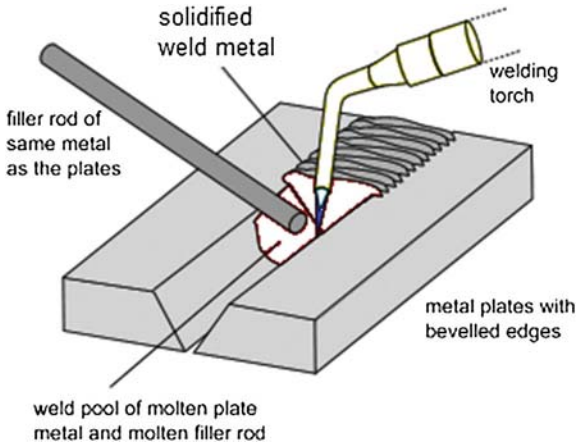

Figure 3 Gas welding equipment. Reproduced from Fachkundeschweiβtechnik, CD-ROM, DVS-Media, 2000.

www.iran-mavad.com
مرجع مهندسی مواد و متالورژی

Table 2 Properties of fuel gases for gas welding

Fuel gas	*Density*[a] *kg m*$^{-3}$	*Calorific value* H_u *kJ m*$^{-3}$	*Max. flame temperature with* O_2 *°C*	*Ignition temperature in air °C*	*Explosion limit in air Vol.%*	*Consumption value m s*$^{-1}$	*Flame power kW cm*$^{-2}$
Hydrogen (H_2)	0.09	10.800	2.100	585	4 bis 74	8.9	13.98
Acetylene (C_2H_2)	1.1	57.000	3.160	335	3.4 bis 80	13.5	42.74
Propane (C_3H_8)	1.88	93.000	2.750	510	2.0 bis 9.5	3.7	10.27
Methane (CH_4)	0.67	36.000	2.770	645	4 bis 17	3.3	8.51

[a]At 15 °C and 1 bar.

6.02.2.1.1 Fuel Gases

The gases listed in Table 2 can be considered fuel gases.

For the assessment of the suitability for welding in addition to the flame temperature achieved and the combustion speed, the flame power is of importance. As the most appropriate gas arises from the fact that with acetylene (this gas also meets several other important conditions for the application: it is not poisonous), there is with proper burner adjustment no combustion residue in the seam and provides in reduced flame to a good protection of the molten bath.

This points to acetylene gas, which also meets several other important conditions for the application: it is not poisonous, and with proper burner adjustment, there is no combustion residue in the seam and it provides reduced flame, leading to good protection of the molten bath.

The explosion limits are still of importance which are mixture of oxygen/acetylene from 2.4 to 93% acetylene.

Acetylene (ethyne, C_2H_2) is a hydrocarbon with the structural formula HC≡CH. Acetylene is generally obtained from the reaction of calcium carbide and water:

$$CaC_2 + 2H_2O \rightarrow C_2H_2 + Ca(OH)_2 + \text{heat}.$$

There are also thermal manufacturing processes that emanate from hydrocarbons. Acetylene is now ready to be put in steel cylinders in the trade, and the use of own acetylene generators in operation is no longer common.

Due to the triple bond, acetylene is unstable at pressures above 3.5 bar or higher temperature. In contrast to other gases, it cannot therefore be stored under high pressure. The steel tanks used for storage today are filled with a highly porous monolithic mass of calcium silicates or plastic pellets, in which they are charged with acetylene acetone intercalates. Thus, a uniform distribution of the acetone is achieved in the storage chamber and simultaneously prevents the solvent's being entrained in the gas removal. This measure involves raising the tank pressure up to 19 bar allowed.

6.02.2.1.2 Oxygen

The oxygen required for combustion is obtained industrially by liquefaction and subsequent rectification of the atmospheric air. It comes in steel cylinders with a pressure of 200 bar or 300 bar in trade. For larger consumers, it is favorable to apply the liquid oxygen in tanks and in cold carburetors in place to transform the consumption state. Based on the gas law (Boyle's law), one 50 l bottle at 200 bar equals 10 m^3 of oxygen at 1 bar.

The color code for an oxygen cylinder is white (formerly blue). The connection of the regulator to the tank via a 3/4 right thread. All parts that come into contact with oxygen must be kept absolutely free of grease and oil.

6.02.2.1.3 Welding Torch

In the torch, fuel gas and oxygen are mixed in an adjustable ratio to one another. It is important that this is done in a simple and reproducible manner so that during welding constant operating conditions are met. The burner designs are distinguished by constant pressure and injector (suction). At constant pressure burner, as is common in the United States, the two gases are supplied under the same pressure. In contrast, in Europe it is conventional for the injector type torch, see Figure 4, in which the oxygen is at a pressure of about 2.5, while the acetylene is fed at a pressure of about 0.2. The oxygen flows at a higher speed of the pressure nozzle in the injector. Due to the negative pressure produced, acetylene is sucked and mixed with the oxygen, which is substantially in the mixing nozzle and the mixing tube. After ignition of the gas mixture, the welding flame is then formed.

The injector is not adjustable and is part of the burner insert. When starting the burner therefore first the oxygen valve is opened and then by regulating the acetylene pressure a combustible gas mixture is produced; conversely, after completing the welding work, the acetylene valve is first closed and then the oxygen valve. The reverse order would result in the destruction of the burner.

The gas consumption is based on the use of welding that is appropriate for the thickness of the sheet to be welded.

A benchmark for neutral flame setting is a guideline of 100 l of oxygen and acetylene per millimeter of thickness and burning hour.

www.iran-mavad.com
مرجع مهندسی مواد و متالورژی

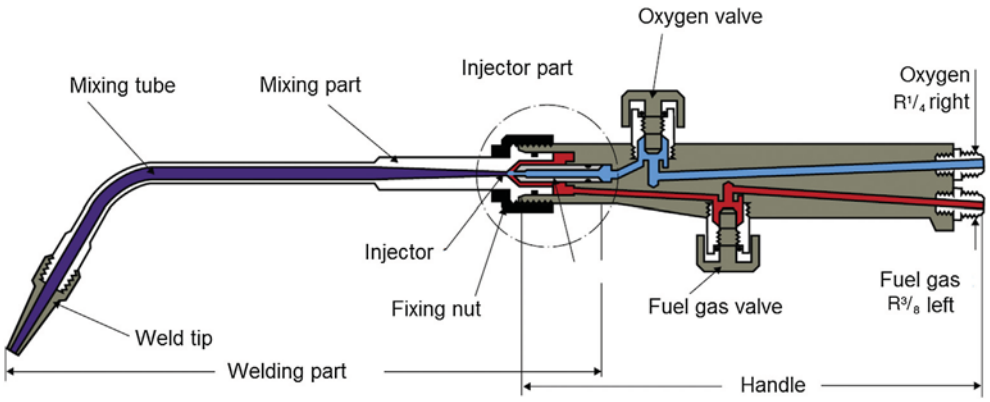

Figure 4 Sectional drawing of a torch using the injector. Reproduced from Fachkundeschweiβtechnik, CD-ROM, DVS-Media, 2000.

6.02.2.1.4 Welding Flame

For the welding of steel, the oxy-acetylene flame may be adjusted so that with a mixing ratio of about 1:1 to 1:1.2, a neutral flame is used. In this setting, the maximum flame temperature is about 3200 °C, and the flame has a reducing effect on the work area. Figure 5 schematically shows a neutral flame. It is divided into the first combustion stage with the flame cone and its glowing coat and the second combustion stage with a spreading flame.

In the combustion stage, the acetylene is decomposed in the heat. With the admixture of oxygen at neutral flame, the following reaction takes place:

$$2C_2H_2 + 2O_2 + 2H_2 \rightarrow 4CO$$

Carbon monoxide and hydrogen, the products of incomplete combustion of the first stage, burned with oxygen, which is withdrawn from the area in the second combustion stage:

$$4CO + 2H_2 + 3O_2 \rightarrow 4CO_2 + 2H_2O$$

This complete combustion takes place in a range from about 2–4 mm from the flame cone. Here there is the highest flame temperature. Optionally, this flame protects the weld pool from surrounding oxygen and nitrogen. The welding has to be made in this area.

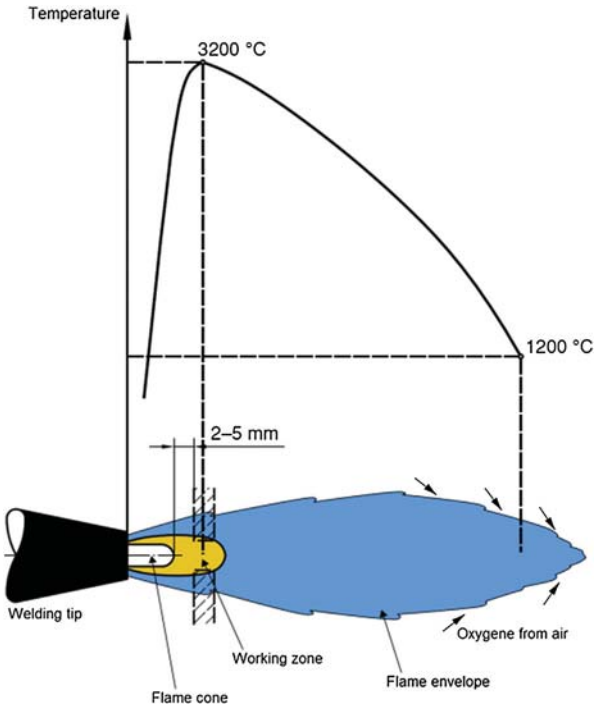

Figure 5 Zones and temperatures in a neutral set oxy-acetylene flame. Reproduced from Fachkundeschweiβtechnik, CD-ROM, DVS-Media, 2000.

www.iran-mavad.com
مرجع مهندسی مواد و متالورژی

Working with a higher oxygen content, the result is a short, hard flame of bluish-purple and a pointed cone of flame. Here complete combustion occurs in the first combustion stage.

$$\text{First level}: 4O_2 + 2C_2H_2 \rightarrow 4CO_2 + 2H_2$$

$$\text{Second level}: 4CO_2 + 2H_2 + O_2 \rightarrow 4CO_2 + 2H_2O$$

Thus, there is temperature-reducing and temperature-increasing effects of the combustion of the CO. Characteristics of this flame setting when welding steel are a rough weld surface and slag inclusions in the weld. Use of this flame setting may still work for welding brass, since thereby the evaporation of the zinc is decreased.

A large, soft flame with bright red, bright appearance and wide, blurred flame cone is obtained when working with acetylene. Here in the first combustion stage elemental carbon occurs, which also in the second stage cannot be completely burned.

$$\text{First level}: 2C_2H_2 + O_2 \rightarrow 2CO + 2H_2 + 2C$$

$$\text{Second level}: 2CO + 2H_2 + 2C + 2O_2 \rightarrow 2CO_2 + 2H_2O + 2C$$

This free carbon charges in the steel melt, causing it to reach thin fluidity. The weld surface is smooth, the seam itself is slack and tough. When welding cast iron, aluminum, and repair welds, this flame with more acetylene has advantages.

6.02.2.1.5 Welding Consumables

The welding of steels serving gas welding rods are divided into six classes, designated I–VI, as shown in Table 3.

In practice, mostly the pressure levels of classes III and IV are used. The individual classes differ in chemical composition and in the resulting weld behavior. Table 3 gives an overview of the alloy composition of gas welding rods, from the behavior during welding.

Gas weldings are of two types: forehand and backhand welding. The names are drawn from the series of weld pool, weld wire, and weld flame.

Forehand welding, shown in Figure 6, is used only for sheet thicknesses up to 3 mm. The reason for this limitation is the low heat input through the sequence 'pool-flame-wire' in the direction of welding. The welding torch in this technique is guided rectilinearly, with a progression to left. The flame cone faces the quiet out, dabbing wire, thereby simultaneously running the pool into the joint. The outer envelope of the flame warms the weld preparation but sufficient only for thin sheets.

Above a sheet thickness of 3 mm, backhand welding is applied, which is characterized by the sequence 'pool-wire-flame,' as shown in Figure 7. Here the burner is operated without oscillating movement in the welding direction to the right. The welding rod is to be run in semicircular stirring movements in the pool, taking the rod immersed in the pool. The flame cone is directed to the rod and the melt, whereupon a keyhole is achieved that ensures the penetration welding of the root. The spreading flame keeps the already finished joint warm, ensuring a good degassing.

In addition to higher welding speed, the turnright welding against the turnleft welding has other advantages, such as the spreading flame acting like a protective veil of gas to the molten bath. The lowered hottest zone of the flame is directed to the edge of the groove and the tip of the flame cone into the gap.

6.02.2.1.6 Irregularities in Gas Welding

Besides defects arising from the incorrect setting of the flames in gas welding, some defects are observed, which are mainly due to an incorrect execution of the weld. These are

- Sagging or excess weld
- Pores
- Lack of fusion
- Root defect

Table 3 Chemical compositions and the weld behavior of oxyfuel gas weld rods (Acc. EN 12536)

	Chemical composition						*Behavior*		
Welding rod class	*C %*	*Si %*	*Mn %*	*P %*	*S %*	*Other %*	*Fluidity*	*Spatter*	*Tendency to porosity*
I	0.03–0.12	<0.20	0.35–0.65	<0.030	<0.025		Thin	More	Yes
II	0.03–0.20	0.05–0.25	0.50–1.20	<0.025	<0.025		Less thin	Less	Yes
III	0.05–0.15	0.05–0.25	0.95–1.25	<0.020	<0.020	Ni 0.35–0.80	Dense	No	Yes
IV	0.08–0.15	0.10–0.15	0.90–1.20	<0.020	<0.020	Mo 0.45–0.65			
V	0.10–0.15	0.10–0.25	0.80–1.20	<0.020	<0.020	Mo 0.45–0.65 Cr 0.80–1.20			
VI	0.03–0.10	0.10–0.25	0.40–0.70	<0.020	<0.020	Mo 0.90–1.20 Cr 2.00–2.20			

Mo < 0.3%; Ni < 0.3%; Cr < 0.15%; Cu < 0.35% (includes coating); V < 0.03%.

www.iran-mavad.com
مرجع مهندسی مواد و متالورژی

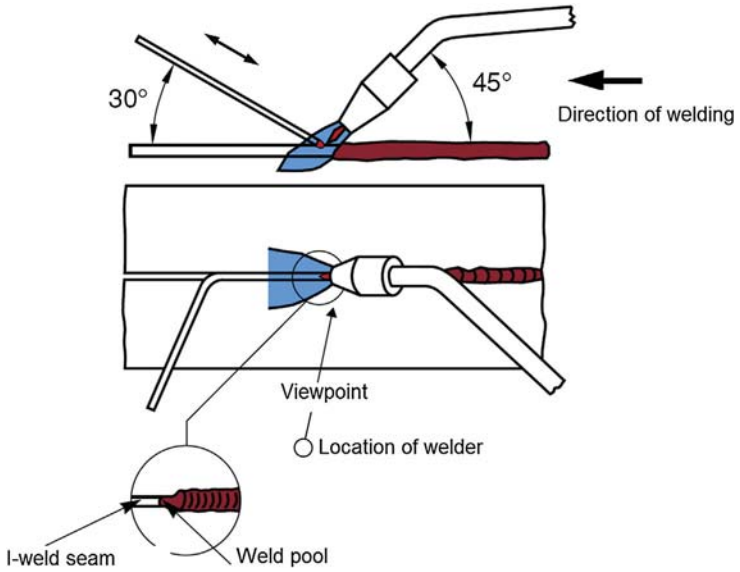

Figure 6 Forehand welding. Reproduced from Fachkundeschweiβtechnik, CD-ROM, DVS-Media, 2000.

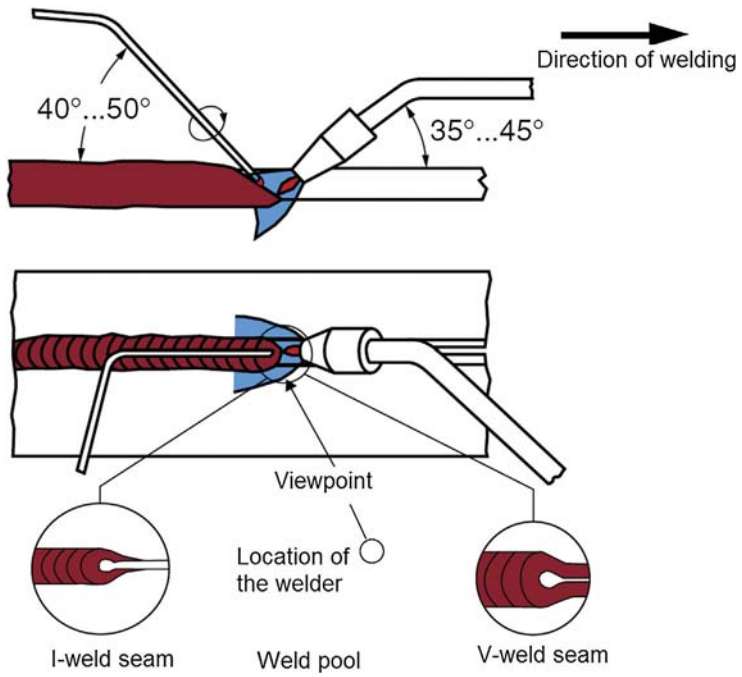

Figure 7 Backhand welding.

The described weld defects occur at too low welding speed. If too little weld metal is used, the weld seam would be sagging; on the contrary, if too much weld metal is used, the result will be an excessive seam. A flaky appearance of the weld seam points to an uneven welding speed.

The formation of pores can result from a contaminated surface with rust and grease at the joint edges. Also, an incorrect guidance of the torch and the welding rod can be the cause of this defect. Fusion defects occur in the fusion line, i.e., in the transition from weld seam to the base metal. The reason for its existence can be too low heat or improper welding technique; one-sided heating or too great a distance from the flame result (*1,6–9*)

www.iran-mavad.com
مرجع مهندسی مواد و متالورژی

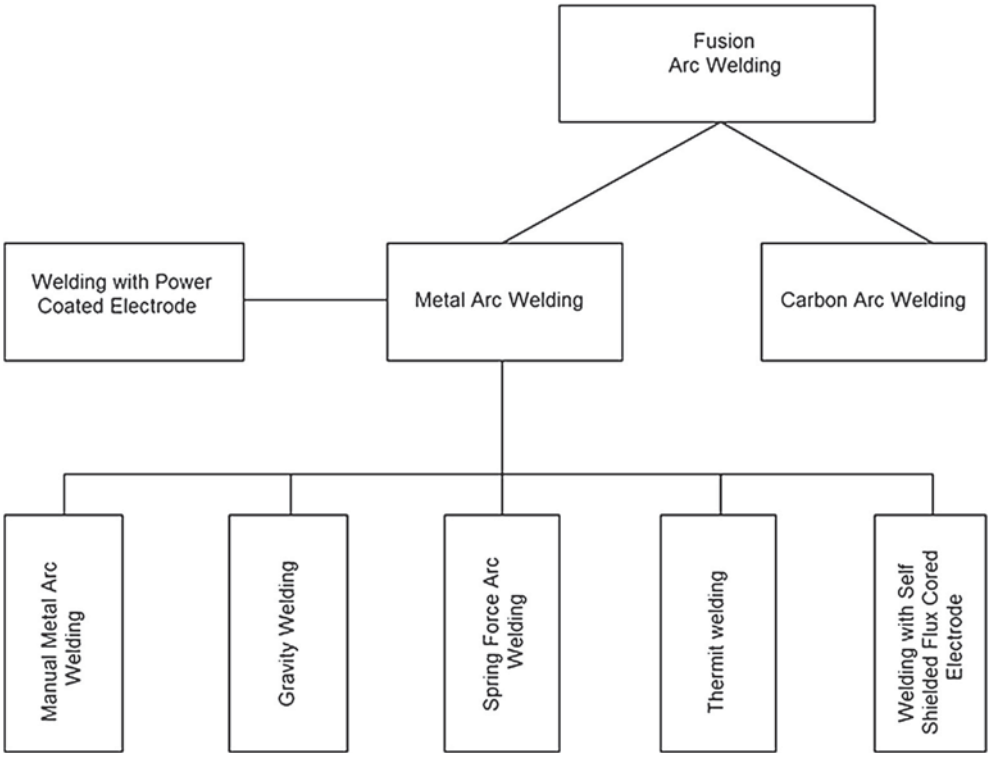

Figure 8 The process of metal arc welding. Reproduced from Fachkundeschweiβtechnik, CD-ROM, DVS-Media, 2000.

6.02.2.2 Metal Arc Welding

Metal arc welding method includes several groups, as shown in Figure 8. ISO 857-1 defines these processes as follows: the arc between a consumable electrode and the material in the atmosphere only by slags or inert gas protection, derived from the electrode coating or a powder. Common to all these processes is the use of the arc as an energy source.

6.02.2.2.1 The Processes in the Arc

An electric arc is a discharge of electric current across a gap in a circuit. It is sustained by the presence of a thermally ionized column of gas (called a plasma) through which current flows. In general, atmospheric air is a poor conductor of electric current. The distance between the electrodes, however, is small, and the applied voltage is high, so that a gas discharge, i.e., the formation of an arc, may occur.

In the build-up between the oppositely polarized electrodes, an electric field electrically accelerates the charged particles toward the opposite pole. It is important in this context that the electrons that are accelerated as nearly massless negatively charged particles are very strong and therefore able to transport energy. After their arrival to the anode they meet with high energy gas molecules and split into their constituent atoms. These can be re-ionized. The positive ions move to the cathode, and the negatively charged ions were knocked out of the atomic shell electrons according to the anode. On their way to the anode, the electrons can impact processes to again ionize gas molecules, so that the number of charge carriers grows exponentially. So by ionization to the electrical conductor which has become gas is also known as plasma.

As shown in Figure 9, in the arc thus formed, charges are transported in both directions. This operation, the impact ionization, is important for the formation of the arc. For maintaining the arc, more physical processes are required. In essence, it is the field emission and thermionic emission. The field emission is defined as the emission of electrons from the metal due to an applied electric field. The field without the thin surface electrons occupying when applying a field removes and accelerates toward the anode, which emerge from the new metal electrons. The number of the electrons thus emitted is dependent on the level of the applied voltage.

In front of the cathode as well as the anode, a thin layer oppositely polarized particles is generated. Between these carriers and the surfaces of the electrodes, a potential gradient is formed with a large gradient, which is referred to as the cathode and anode drops. The majority of the voltage drop is attributable to these two areas. The drop in the arc plasma itself is linear and is in relation to the cathode and anode case low. From the voltage waveform in the arc column it can be deduced that the length of the arc and the arc voltage increase. The arc is thus a movable part of the welding circuit; it follows accordingly physical laws that applies to a current-carrying conductor.

For the description of the arc, the arc behavior characteristic is of importance, which reflects the relationship between the arc voltage and arc current. In Figure 10, two areas are clearly visible. For the welding the voltage drop at low current levels, the so-called

www.iran-mavad.com
مرجع مهندسی مواد و متالورژی

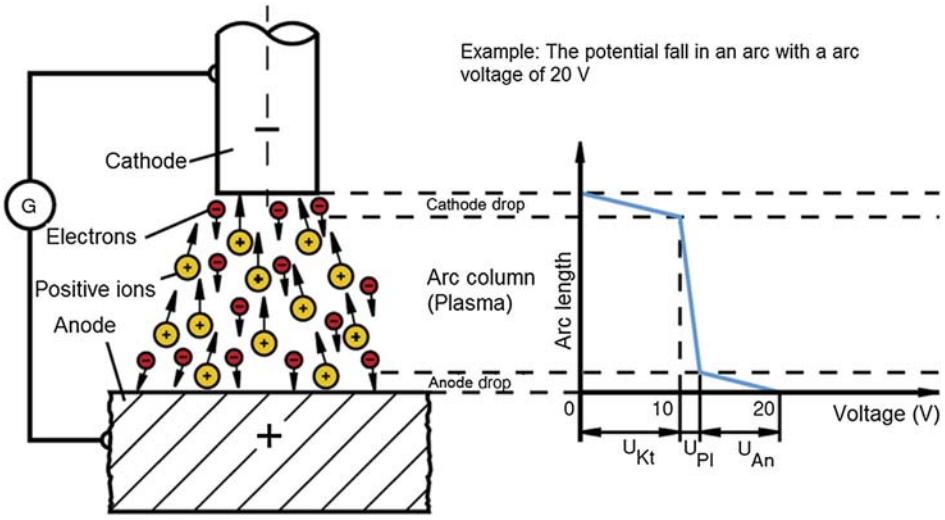

Figure 9 The flow of current in the direct current arc and the voltage gradient in the arc when welding with direct current. Reproduced from Fachkundeschweiβtechnik, CD-ROM, DVS-Media, 2000.

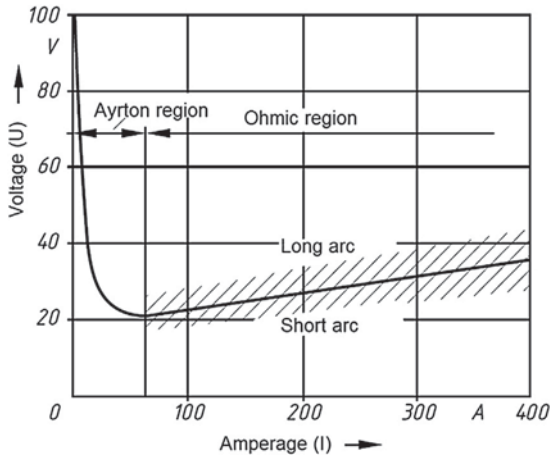

Figure 10 The arc characteristics. Reproduced from Fachkundeschweiβtechnik, CD-ROM, DVS-Media, 2000.

Ayrton region is of minor importance. For welding, a linear increase in voltage with increasing current resistive region is used. As already mentioned, the voltage in the arc is different depending on the length of the arc. At constant current, different arc voltages are obtained. From the figure it can be seen that a long arc with the same current strength has a higher voltage than a short arc. The temperature distribution in the arc is not uniform: it is also dependent on the type of the sheet and the nature of the plasma. Plasma even occur when welding with metal electrodes on temperatures around 5000 K, in TIG welding over 10 000 K. The higher temperature is measured at the anode, since the impingement of high energy electrons creates an additional warming. Arc welding can generally be done with direct current or alternating current. The best solution is to weld with direct current. By the constant voltage without changing polarity, the arc burns for a long time, thus creating favorable conditions for the formation of the charge carriers and the ionization given for all methods.

An important point when working with direct current is that of the magnetic arc blow. Each current-carrying electrical conductor is surrounded by a circular magnetic field. During welding, the arc is a highly movable conductor, which allows the current transfer between the electrode and the base material. As **Figure 11** shows, it is due to the more or less strong deflection of the magnetic field at the base of the arc to a compaction of the field on the one hand, to a weakening on the other side. Due to this compression, the arc of a movable head is relegated to the direction of the weak magnetic field. This phenomenon is called magnetic arc blow and observed in both magnetic and non-magnetic metals. In magnetic materials, a second effect is superimposed that is due to the different magnetic conductance of air and metals. The arc is deflected toward these masses at high current-carrying materials. It is possible that the magnetic blow effect is completely abolished. The blow can possibly lead to the extinction of the arc; therefore, appropriate measures must be taken to counteract it. This can be done by an appropriate slope of the electrode and the laying of the connection of the ground cable. The use of alternating current also solves the problem. If this is not possible, by storing larger pieces of steel at certain points, the arc can be deflected in the desired direction. In many cases, however, an inclination of the electrode also brings relief, see **Figure 12**.

www.iran-mavad.com
مرجع مهندسی مواد و متالورژی

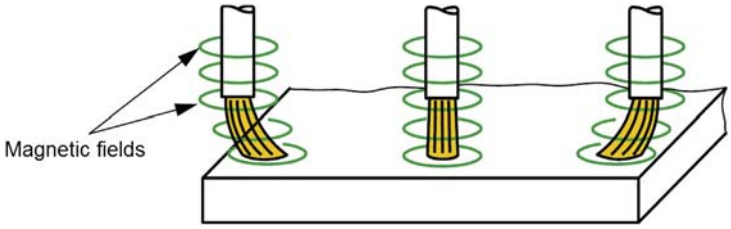

Figure 11 The magnetic arc blow when welding with direct current is due to the deflection of the magnetic field. Reproduced from Fachkundeschweiβtechnik, CD-ROM, DVS-Media, 2000.

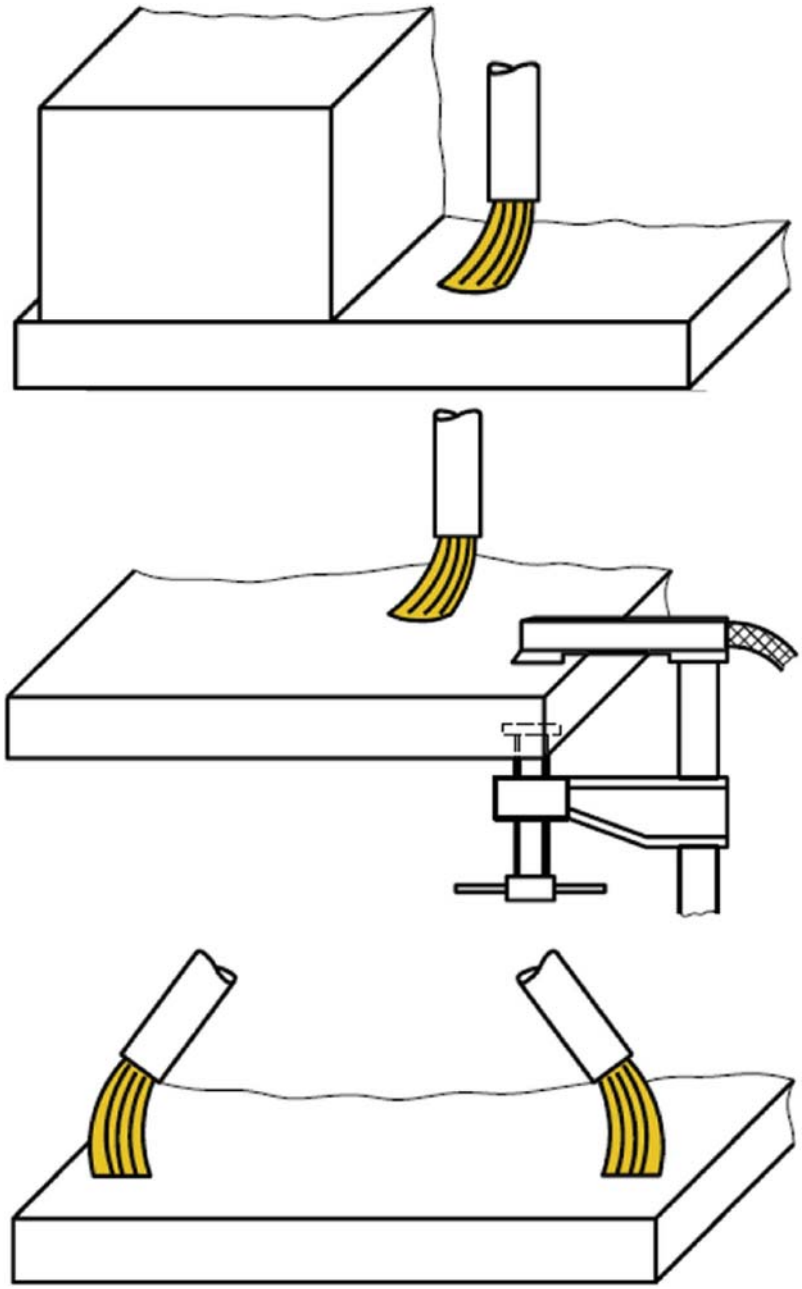

Figure 12 Methods to prevent arc blow. Reproduced from Olson, D. L.; Siewert, T. A.; Liu, S.; Edwards, G. R. *ASM Handbook: Welding, Brazing and Soldering*, 1993; Vol. 6.

www.iran-mavad.com
مرجع مهندسی مواد و متالورژی

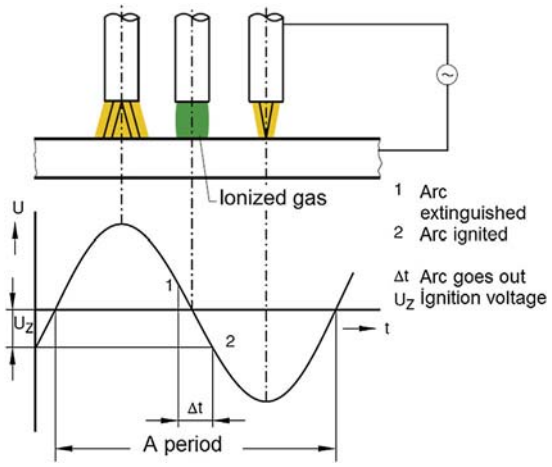

Figure 13 Alternating current welding the arc goes out periodically and must be reignited. Reproduced from Olson, D. L.; Siewert, T. A.; Liu, S.; Edwards, G. R. *ASM Handbook: Welding, Brazing and Soldering*, 1993; Vol. 6.

In alternating current welding, the polarity changes in the number of frequency. During a period the arc is extinguished twice when changing the polarity and must be reignited each time. **Figure 10** illustrates how with decreasing voltage and amperage, the arc is extinguished and after the zero crossing with altered polarity must again be reignited. **Figure 13** illustrates how with decreasing voltage and amperage the arc is extinguished and after the zero crossing with altered polarity must be again ignited. This presupposes that there are enough charge carriers in the area between the electrode and workpiece. A higher frequency, a higher open circuit voltage of the power source, the use of ignition aids, and welding with coated electrodes facilitate this. Also, it is advantageous to use welding power sources with square-wave; the current–time curve is not sinusoidal but rectangular.

Metal arc welding and gas metal arc welding are carried out with a consumable electrode; this type of electrode, therefore, both supports the arc medium and the welding filler metal. The material transfer takes place independent of the polarity of the electrode to always work in the form of drops. The electrode liquefies because of the high temperature at the base of the arc. The melted material shapes itself to drop, and the shape and size will be the properties of the metal but also influenced by the prevailing forces in the arc. The constriction of the drop at the end of liquefied electrodes is due to the pinch effect, which can be explained by the Lorentz force.

6.02.2.2.2 Welding Power Sources

Various reasons prohibit the required welding current to be taken directly from the public network. The high voltages pose a lethal threat to the welder, and erratic fluctuations occur during welding in the strong current, which would weigh heavily on the network. Generally, the welding power sources must be expected to meet the following requirements:

1. The open circuit voltage must not jeopardize the welder, but it must ensure a good ignition. This requirement is met by limiting the maximum voltage at the DC to 113 V and AC to 80 V (rms). For welding with increased electrical hazard, e.g., in steel and boiler constructions, are required or AC 48 V open circuit voltage (rms).
2. The short circuit current must not exceed a maximum value. This maximum current depends on the type of power source and must ensure that their winding insulation and do not heat up too high.
3. The voltage must be governed by the short circuit instantaneously adjust to the labor value. This requirement shall be made in respect of a quiet burning arc (dynamic properties).
4. The power source must provide a process-specific current–voltage characteristic.

6.02.2.2.3 Power Source Characteristics

For identification of the behavior of welding power sources under load, the static characteristics are considered. They describe the relationship between welding current and arc voltage with a slow change in the load. Significant variables here are the load voltage U0 and the short-circuit current IK. Each current source has a plurality of curves, whereby each of the lowest operating point can be adjusted.

There are two different characteristic curves: the power source with a negative slope and the power source with constant voltage characteristic. As a third possibility, the current source is to be mentioned with a constant current characteristic for the sake of completeness.

- Power source with a negative slope.

Figure 14 shows the static characteristic of a welding power source with drooping characteristic.

www.iran-mavad.com
مرجع مهندسی مواد و متالورژی

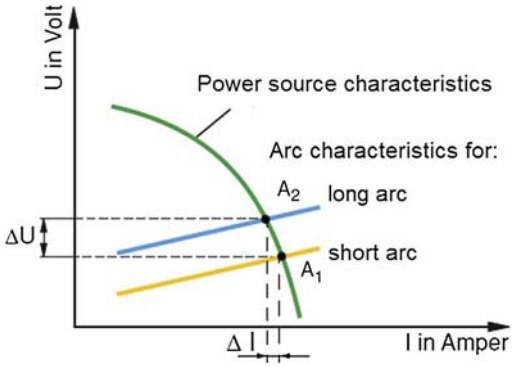

Figure 14 Static characteristic of a welding power source with drooping characteristics. Reproduced from Olson, D. L.; Siewert, T. A.; Liu, S.; Edwards, G. R. *ASM Handbook: Welding, Brazing and Soldering*, 1993; Vol. 6.

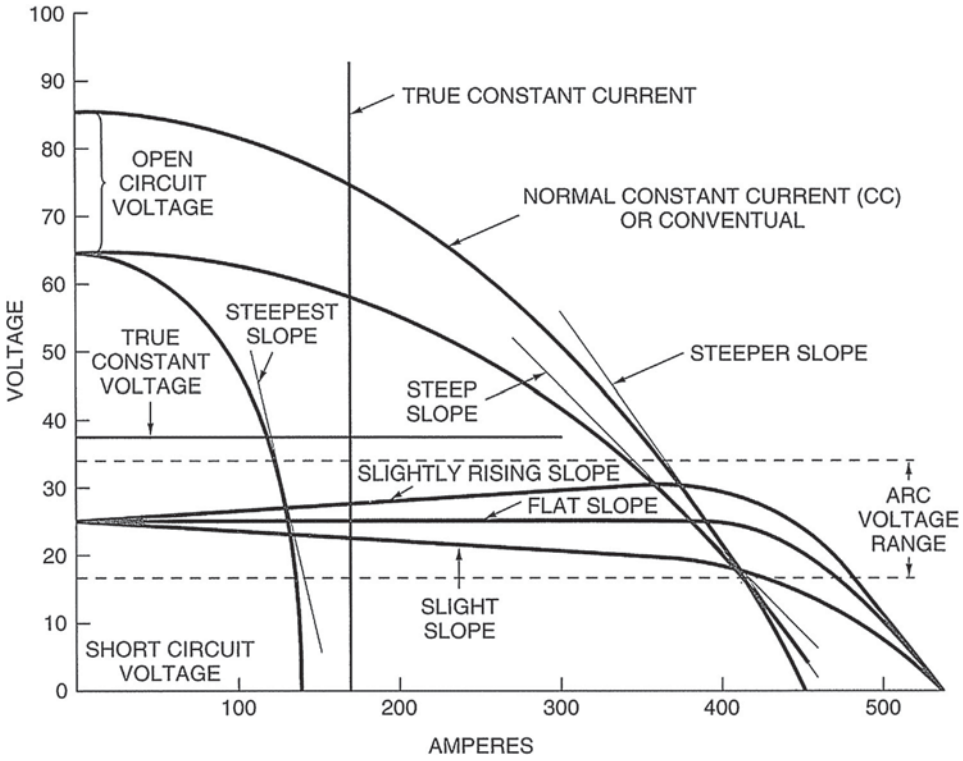

Figure 15 Static characteristic of a welding power source with constant voltage characteristic (compared with drooping characteristics). Reproduced from Fachkundeschweiβtechnik, CD-ROM, DVS-Media, 2000.

For power sources with these characteristics, the arc length is controlled by an external intervention (external regulation, Δ*U* control). In manual arc welding, for example, this is done by the welder, which corrects the length of the arc itself.

A change in the arc length is expressed in a significant change of voltage, due to the steep gradient of the curve, so that only a small change in the current is connected power sources with these characteristics are particularly suitable for manual arc welding, TIG welding and submerged arc welding with a large wire diameter (>3 mm).

- Power source with a constant voltage characteristic.

Figure 15 shows how to link a small change in the length of the arc, that is, a slight change in the arc voltage. At this characteristic, with a large change in the current strength, the voltage drop is between 2 and 8 V 100 A. For example, the arc is shorter, with the reduced voltage, the current strength increases sharply. This causes a greater melting of the electrode and thereby an extension of the arc. In this 'inside control' or Δ*i* control, then, is a 'self-adjusting,' who makes these power sources ideal for all procedures with automatic feeding of the filler, especially the MIG-/MAG welding but also submerged arc welding with thin wire electrodes (<3 mm) (Figure 16).

www.iran-mavad.com
مرجع مهندسی مواد و متالورژی

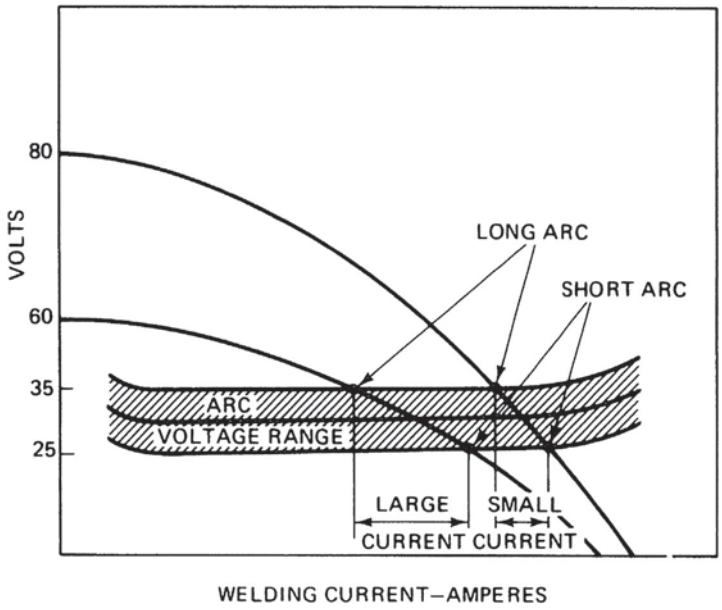

Figure 16 The course of the current and voltage during the ignition of the welding arc. Reproduced from Fachkundeschweiβtechnik, CD-ROM, DVS-Media, 2000.

6.02.2.2.4 Types of Welding Power Sources

According to the electrical principles for arc welding, the following types can be distinguished:

- Welding transformer
- Welding rectifier
- Welding generator
- Power sources with power electronics

6.02.2.2.4.1 Welding transformers

The transformer consists, in principle, of two separate windings on a common iron core. Network side is a coil with many turns. It forms a time-varying magnetic field that covers the iron core. This magnetic field changes with the frequency of the alternating current to its size and direction, whereby in the secondary coil with fewer turns, an alternating voltage of the same frequency but lower voltage is induced. Figure 17 shows the basic structure of a welding transformer. The voltage U2 in the secondary circuit, the welding circuit, is calculated from the ratio of turns N of the primary and secondary coils U1:U2 = N1:N2. The associated currents behave in lossless operation of U1:U2 = I2:I1.

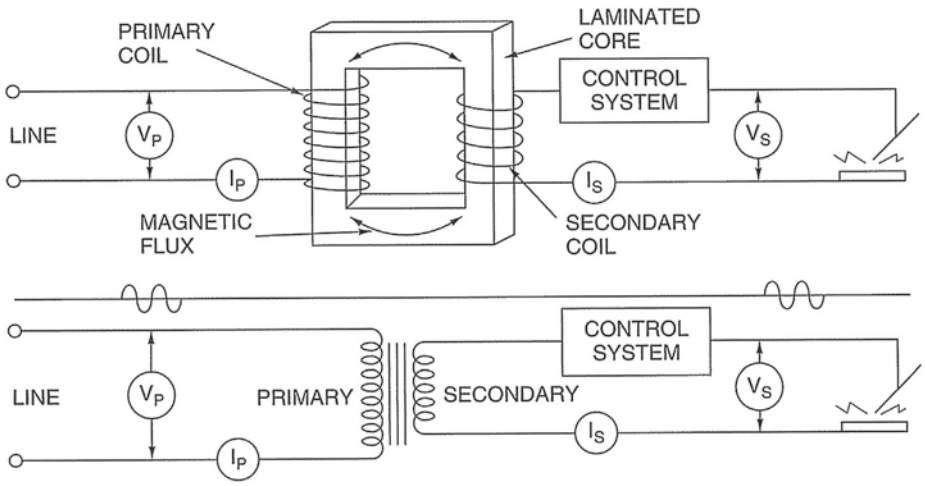

Figure 17 Basic structure of a transformer. Reproduced from Fachkundeschweiβtechnik, CD-ROM, DVS-Media, 2000.

www.iran-mavad.com
مرجع مهندسی مواد و متالورژی

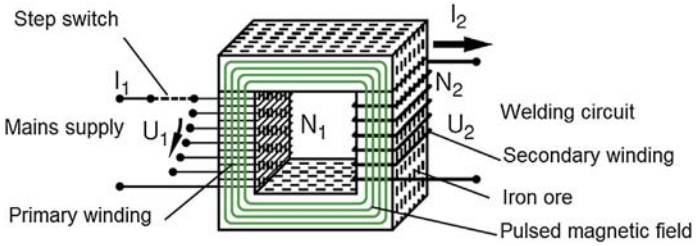

Figure 18 Control in welding transformers. Regulation by tapping of the primary or secondary coil. Reproduced from Fachkundeschweiβtechnik, CD-ROM, DVS-Media, 2000.

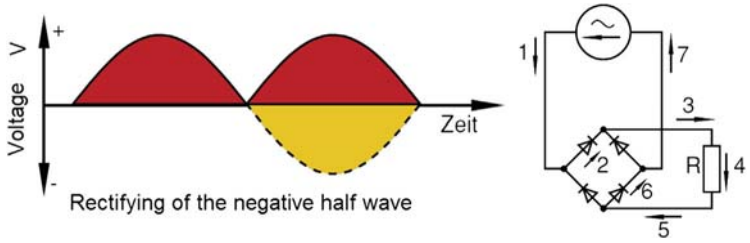

Figure 19 Basic circuit of a single-phase rectifier. Reproduced from Fachkundeschweiβtechnik, CD-ROM, DVS-Media, 2000.

Smaller welding transformers to about 4 kVA power are operated on AC power, so it will be necessary to work with AC. In general, welding transformers have a drooping characteristic. For adaptation to the respective welding tasks, current and voltage can be adjusted by changing the characteristic curve (**Figure 18**).

6.02.2.2.4.2 Welding rectifiers

The welding rectifier has the task of alternating high voltage, as it is removed from the network, converting it to direct current low voltage. Structurally, it consists of a transformer for the transformation of the network alternating current and a downstream rectifier, see **Figure 19**. Rectifiers are now almost exclusively semiconductor components, preferably used silicon diodes. Diodes can pass through the electric current only in one direction, which act in the opposite direction, however, as an insulator. If one arranges the secondary circuit at only a single diode, it would only let through a half-wave, while the second half-cycle would be suppressed. It would result in a voltage waveform shown in **Figure 20**, which is not suitable for welding.

6.02.2.2.4.3 Welding converter

The welding converter is the oldest welding power source. It generates the required welding power from mechanical energy. Then there is the motor-generator set of a drive motor and a person sitting on the same shaft generator. It is used mainly on construction sites where no main power is available. Second, as a drive, an AC motor, usually an asynchronous motor, can be used. The focus is here, however, the generation of direct current through a 'mechanical rectification.'

6.02.2.2.4.4 Power sources with power electronics

The above-described conventional power sources to meet the demands for weld quality, repeatability of the welding parameters, and to control or regulate the operations in the arc have been inadequate. Especially, for the arc welding processes therefore primarily power sources used are ones with power electronics. These devices have a transistorized power section, consisting of transformer and rectifier, which is equal for all welding processes. The electronic control leads to then

- Analog transistorized welding power sources (**Figure 21**)
- Secondary-pulsed welding power sources (chopper)
- Primary-switched power sources (inverter)

Besides the potential for conventional power source arc types, thus the welding with a pulsed arc is possible. The pulse frequency and the pulse shape are adjusted as desired.

The clock frequency is used by semiconductor-dependent type and lies between 30 and 200 kHz. Building on this principle is development of the secondary-pulsed power source, whose block diagram is shown in **Figure 22**.

In the fully digitized welding power sources, the analog process controllers are replaced by digital signal processors. The arc characteristic here is no longer determined by almost invariable components but mapped by software. With current sources of this kind, there is the possibility that characteristics of the power source are in accordance with the program requirements of each production task. In MAG welding with short arc, for example, the following parameters are taken into consideration:

1. Wire material, diameter, feed rate
2. Gas mixture, flow rate per unit of time
3. Open circuit voltage power source, inclination of the power source characteristic curve, constants of current drop rate, and constants of the current drop

www.iran-mavad.com
مرجع مهندسی مواد و متالورژی

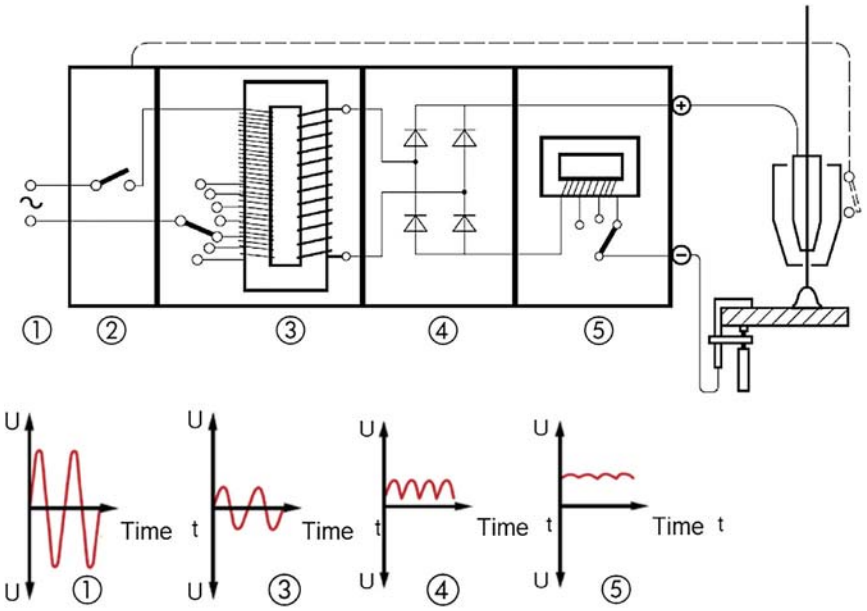

① Mains supply
② On/Off switch for mains supply
③ Transformer with step switch
Function: The mains voltage is decreased to welding voltage
The mains amperage is increased to welding amperage
④ Rectifier
Function: Alternating current is converted to direct current
⑤ Shock coil
Function: Current fluctuations in the welding current circuit are eliminated

Figure 20 Block diagram of a conventional power source. Reproduced from Fachkundeschweiβtechnik, CD-ROM, DVS-Media, 2000.

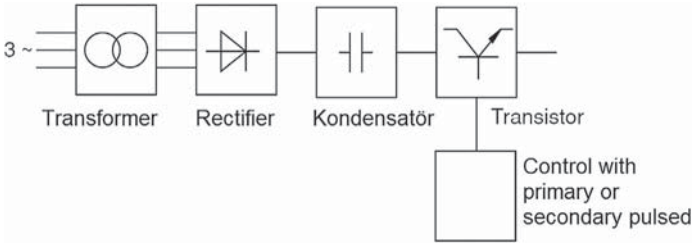

Figure 21 Block diagram of a welding power source analog transistorized.

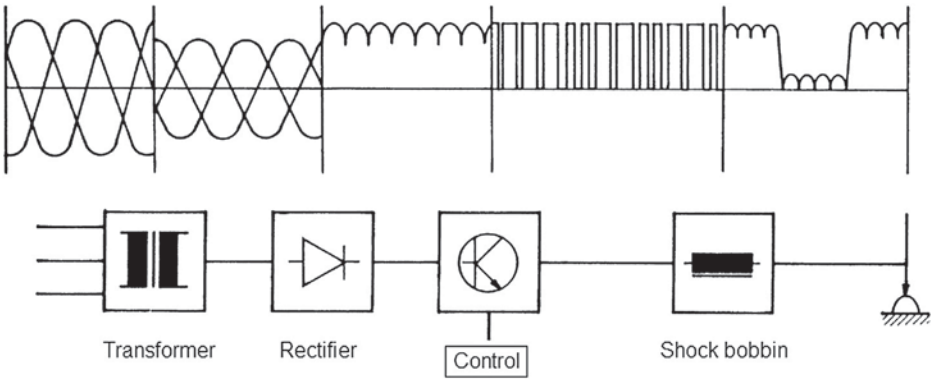

Figure 22 Block diagram of a secondary-pulsed welding power source.

www.iran-mavad.com
مرجع مهندسی مواد و متالورژی

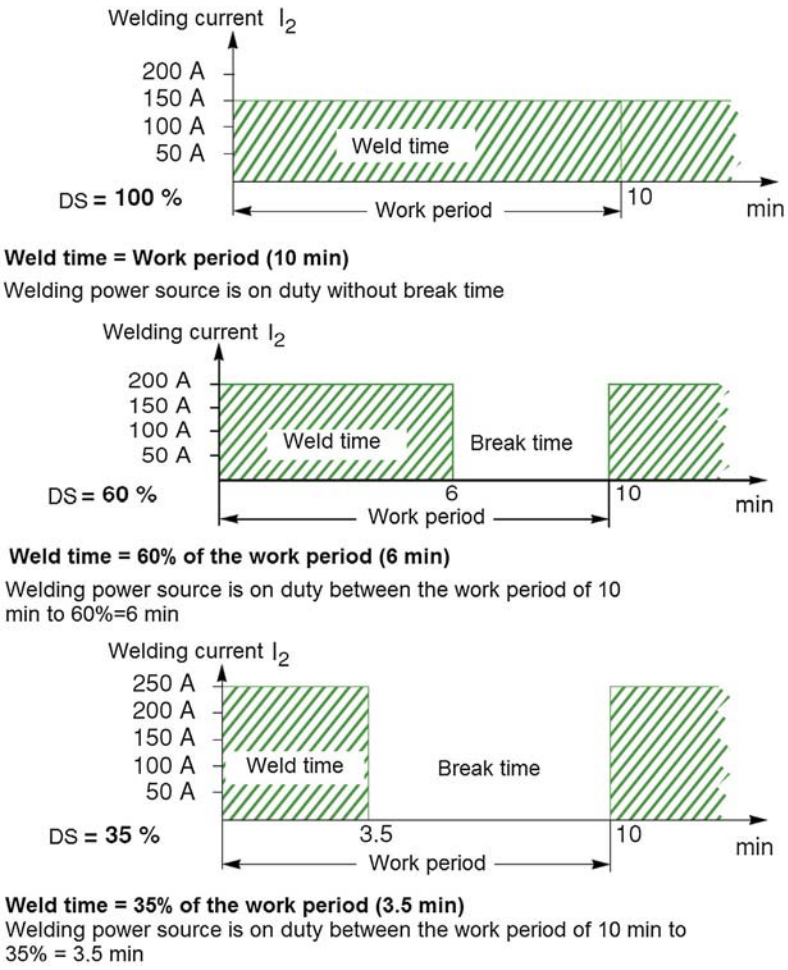

Figure 23 Duty cycle. Reproduced from Larry Jeffus, *Metal Fabrication Technology for Agriculture*; Cengage Learning, 2011.

Today quality assurance and monitoring the data of the welding process is important, possibly associated with a statistical analysis. In the simplest case, such a monitoring system is for the metrological detection of the data, the filtering and storage, for example, in a computer. Depending on the welding process, a large number of different parameters are evaluated and processed. Since all parameters are randomly distributed, only statistical evaluation methods are suitable. The result of the analysis can then be displayed from different points of view and documented.

6.02.2.2.5 Duty Cycle

The thermal capacity of a welding power source is also dependent on how long the arc burns. In addition to the current, therefore, the so-called duty factor is an important parameter for the assessment of a welding power source. Duty cycle is defined as the ratio of the operating time under load to the total time for a given time, it deals with a playing time of 10 min (5 min earlier) and is given in percent. A duty cycle of 60% therefore means that load time = welding time of 6 min, and a period of 4 min follows, see Figure 23 (*1,6–10*).

6.02.2.3 The Manual Metal Arc Welding

The manual metal arc welding is a process group of metal arc welding. The arc burns between a consumable, manually operated rod electrode and the workpiece. Arc and weld pool are shielded against the effects of the atmosphere by gases and slags derived from the electrode covering. The basic arrangement of the process image is shown in Figure 24. With the manual metal arc welding, steels and castings are welded; aluminum, copper, nickel, and their alloys may also be welded.

Under certain conditions, the welding of the various grades of cast iron is possible. Restrictions on the weldable sheet thicknesses do not exist, and the smallest possible thickness is about 1.5 mm.

www.iran-mavad.com
مرجع مهندسی مواد و متالورژی

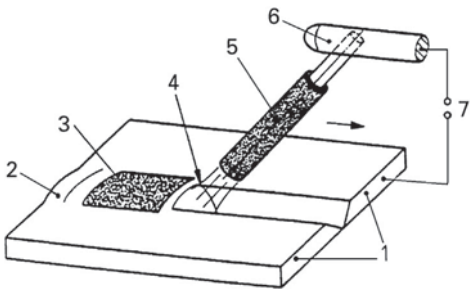

1 Workpiece
2 Weld
3 Slag
4 Arc
5 Covered electrode
6 Electrode holder
7 Power source

Figure 24 Basic procedural order in manual metal arc welding. From ISO 857-1. Reproduced from Larry Jeffus, *Metal Fabrication Technology for Agriculture*; Cengage Learning, 2011.

6.02.2.3.1 Electrodes

Under current-carrying welding, filler metal means the consumable welding rods. In manual arc welding, it is stick electrodes, i.e., cut bar of cold drawn wire with a covering. Depending on the thickness of the cover "D", they are wrapped as thin ($D \leq 1.2\ d$), ($1.2\ d \leq D \leq 1.6\ d$), or very thick coated ($D \geq 1.6\ d$) of medium thickness. Electrodes without covering are no longer common. The stick electrodes are standardized today by material-related aspects:

- Non-alloy and fine-grain steels (Re $\leq$ 500 N mm^{-2}) ISO 2560 (since 2005)
- High-strength steels to 757
- Stainless and heat-resistant steels EN 1600
- Hardfacing alloys EN 14700
- Nickel materials EN ISO 14172
- Heat-resistant steels to EN 1599

The core wire diameters are from about 2 to 6 mm, the bar lengths are between 200 and 450 mm.
The covering has several requirements:

1. It should stabilize the arc. This is achieved by the addition of substances, which low energy input can ionize. This also makes it possible to weld with alternating current.
2. It should surround the arc with a protective gas shielding. For this purpose the organic substances such as cellulose, which release corresponding gaseous combustion products when burned, are added. Inorganic compounds such as calcium carbonate, $CaCO_3$, are also suitable. In the extinguishing of the arc, it produces the gaseous CO_2 in addition to CaO, which serves as a protective gas.
3. It is intended to form a slag. In order to prevent rapid cooling of the melted weld, and thus also hardening, heat insulation of the bead is desired. This is achieved by the formation of a slag over the weld metal. This simultaneously protects the molten weld metal slag from the influences of the surrounding atmosphere. The slag has to meet, not least, a metallurgical task. It should remove from the weld metal any impurities, such as sulfur or phosphorus, and thus improve the quality of the weld metal. Since metal and covering melt simultaneously, already the forming and passing over the arc drop is covered by the minerals of the envelope and protected. For the droplet size, the oxygen content of the covering is important, because the surface tension is influenced by the supply of oxygen.
4. It should alloy the weld metal. At high temperatures in the arc, some elements such as carbon, silicon, and manganese in the wire are incinerated. This erosion can be compensated by the ferroalloys in the covering. This act also has to deoxidize.

The stick electrodes are classified by the chemical nature of the covering into the following types:
A = acid coated
C = cellulose coated
R = rutile coated (medium thickness)
RR = rutile coated (thick)
RC = rutile cellulose – mixed
RA = rutile acid – mixed
RB = rutile basic – mixed
B = basic coated

www.iran-mavad.com
مرجع مهندسی مواد و متالورژی

6.02.2.3.2 Types of Electrode Coating

There are three main classes of electrode coating;

The first, '**Cellulosic**,' contains a large proportion, up to about 35%, of the organic compound cellulose $(C_6H_{10}O_5)_n$, together with slag-forming items, principally rutile, a mineral form of titanium dioxide, TiO_2. Cellulose is a naturally occurring constituent of wood, which at high temperatures will dissociate into oxides of carbon and water. In ferrous welding, the latter will react with iron to produce metallic oxide and the gas hydrogen, which to some extent will be absorbed into the weld. Such coatings will produce a limited amount of slag, and they tend to be restricted to smaller diameters and may be used for work in all positions.

In the second type of coating, '**Basic**,' a protective gas is produced by the dissociation of basic carbonates, mainly $CaCO_3$, which at high temperature is converted to CaO and CO_2. These coatings usually include some calcium fluoride or fluorspar, CaF_2, to give fluidity to the slag; and they have the advantage that only small amounts of hydrogen are generated provided the coating is dry, thus reducing the absorption of hydrogen by the weld metal. This type of electrode is generally used where low hydrogen contents need to be guaranteed.

The third coating type, '**Rutile**,' is one consisting mainly of titanium dioxide plus various mineral constituents, and a small proportion of cellulose, up to about 15%. Protection of the metal as it is passed across the arc is provided by the dissociation of the cellulose and the production of large quantities of slag which will coat the metal droplets as they are transferred.

Metal powders (e.g., iron) may be included in the flux coating to raise the efficiency of the process and both basic and rutile coating variations of this type are available. The heavier rutile coatings contain only about 5% cellulose and as both varieties produce large quantities of molten metal and slag they are usually restricted to flat (downhand) and horizontal–vertical fillet welds. Other types of coating are available, such as acid rutile, acid, and oxidizing, but these are, however, little used. Although there may be considerable differences in the compositions of the electrode cores depending on the properties desired in the weld, the technique of modifying composition by including alloying elements in the coating can be of great importance.

Electrode coatings are summarized in Table 4.

Constituents of the coatings may also include various clays; silica; oxides and carbonates of iron, manganese, and calcium; aluminum and magnesium silicates; calcium fluoride or fluorspar; carbonates and silicates of sodium and potassium; and ferromanganese as a deoxidizer.

Coating compositions are described in general terms only, the proportions of the different ingredients and even the total number present being the manufacturer's prerogative and his secret. The quality of the product is determined in the judgment of the purchaser, and although there are undoubtedly differences between suppliers, equally, there are variations in the opinions and tastes of individual welders and their employers.

It should be apparent that the coating on the electrode not only has an important influence on the properties of the resulting weld metal, but also will be the principal influence on the welding characteristics themselves, especially affecting such aspects as welding positions.

The functions of the individual constituents in a coating are listed in Table 4.

6.02.2.3.3 Designation of the Electrodes

Electrode specifications are usually prefixed with E followed by several digits and/or letters and/or chemical symbols.

6.02.2.3.4 Covered Electrodes for Welding Carbon and Carbon Manganese Steels

The European system (i.e., EN standards) is principally concerned with the mechanical properties of deposited weld metal, namely yield and tensile strengths and impact toughness. Additional information is included in the classification that relates to the weld metal composition, type of coating, recommended welding positions, welding current requirements, deposition efficiency, and hydrogen control (e.g., E4631NiB54H5).

In the American system, electrodes are classified under the American Welding Society (AWS) specification A 5.1, which is less complicated then the European system. Essentially, it is a four-digit number with the prefix E designating an electrode. The first two digits define the nominal minimum tensile strength of the deposited metal in thousands of pounds per square inch (kpsi); for mild steel, these will be 60 or 70. The third digit indicates the recommended positions (i.e., the digit 1 signifies suitability for all welding positions, 2 for flat or horizontal fillet welds, and 3 for the flat position only). The fourth digit determines the electrical power requirements. The last two digits together refer to the type of electrode coating as stipulated in the specification (e.g., E7018).

6.02.2.3.5 Low Alloy Electrodes

Most of the low alloy steel electrode classifications are based on the low hydrogen or basic type of covering. The composition of the basic covering makes it possible to add a number of alloying elements to produce a range of weld metal analyses and strengths. The increased strength of the weld metal is obtained by the addition of alloying elements, which may be achieved either through the core wire or via the coating.

The European classifications include the chemical symbols such as Mn, Ni, Cr, when they are present as alloying additions, together with an indication of the carbon content, the type of covering, and the hydrogen control if required. Appropriate mechanical properties are specified, including tensile strength, proof stress, elongation, and if required impact tests at various temperatures (e.g., ECrMo1LB).

The AWS specification for these electrodes is A5.5 and is very similar to that for carbon steels described above. The first two, or sometimes three, digits of the classification reflect the tensile strength of the weld deposit (e.g., 80, 110). For example, the covering

www.iran-mavad.com
مرجع مهندسی مواد و متالورژی

Table 4 Electrode coating characteristics and normal applications

Class	*Composition of covering*	*Characteristics*	*Uses*
Cellulosic (C)	Organic material containing cellulose with some titanium oxide. Hydrogen releasing.	Thin, easily removable slag. Rather high splatter loss. Considerable envelope of shielding gas. Coarse ripple on weld surface, deeply penetrating arc with rapid burn-off rate.	All classes of mild steel welding in all positions: AC or DC electrode positive.
Basic (B)	Calcium or other basic carbonates and fluorspar bonded with sodium or potassium silicates. Medium coating. Coating compounds contain little hydrogen. CO_2 releasing.	Brown slag easy to remove. Medium ripple on weld metal, medium penetration. Fillet profile flat or convex. Deposited metal has high resistance to cold cracking because there is a low hydrogen content in the weld. Electrodes must be stored under warm dry conditions and dried before use.	Suitable for dc (electrode positive) or AC with OCV of 70 V. Used for mild, low-alloy, high tensile, and structural steels, particularly for conditions of high restraint. For flat, vertical, and overhead positions, the latter having a flat deposit.
Basic high efficiency (BB)	Similar to basic electrode covering but have additional metallic materials (e.g., iron powder) in the covering which raise the efficiency to 130% and more.	These electrodes are suitable for welding in the flat and horizontal/vertical positions with a greatly increased rate of metal deposition. Their high-efficiency covering makes them unsuitable for welding in the vertical and overhead positions. They can be used either AC or DC generally with electrode +ve. Efficiency is indicated by a three digit figure beginning the additional coding.	
Rutile (R)	Titanium dioxide (rutile) and other hydrated minerals and/or organic cellulose materials. Coating thickness less than 50% of the core wire diameter.	Easy to use, with smooth weld finish and medium penetration. High level of hydrogen in the weld metal limits their use in thick sections or restrained joints. Suitable for AC or DC; the fast freezing of weld metal and fluid slag makes them suitable for vertical and overhead weldings.	
Rutile heavy coating (RR)	Similar covering to the previous rutile electrode but containing in addition metallic substances (e.g., iron powder), which raises the efficiency to 130% or more. Coating thickness at least 50% greater than the core wire diameter.	Similar characteristics to rutile electrodes but generally unsuitable for vertical and overhead weldings because of increased slag. Increased rate of metal deposition. Efficiency is indicated by a three digit figure beginning the additional coding.	
Acid (A)	Oxides and carbonates of iron and manganese, with deoxidizers such as ferro-manganese.	Generally, a thick coating that produces a fluid slag of large volume and solidifies in a 'puffed-up' manner, is full of holes and easily detached. Smooth weld finish with small ripples. Good penetration. Weld liable to solidification cracking if plate weldability is not good.	Usually in the flat position only but can be used in other positions; AC or DC.
Acid rutile (AR)	Generally, a thick coating containing up to 35% rutile. Ilmenite (iron oxide) and titanium oxide are also used.	A fluid slag with other characteristics similar to the acid type of covering.	Similar to the acid type of coating.
Oxidizing (O)	Iron oxide with or without manganese oxide and silicates.	Oxidizing slag so that the weld metal has a low carbon and manganese content referred to as 'dead soft.' Reduction of area and impact values are lower than for other types of electrodes. Core wire melts up inside coating forming a cup so that the electrode can be used for 'touch-welding.' Low penetration; solid slag often self-deslagging, with weld of neat appearance.	DC or AC supply with OCV as low as 45 V.
Any other type (S)	This category is for any electrode coverings not included in the foregoing list. Iron powder electrodes do not come into this category but should be indicated by their efficiency with a three-digit figure.		

www.iran-mavad.com
مرجع مهندسی مواد و متالورژی

of E9016 will be similar to an E7016 electrode although the tensile strength will be 90 kpsi and the covering will generally contain the alloying elements (e.g., E9016-C2).

6.02.2.3.6 Electrodes for Alloy and Stainless Steels

The trend for these electrodes is for the weld metal to be at least as high in alloy content as the base material, and in some instances it may be considerably higher.

The European standard refers to electrodes for chromium and chromium–nickel steels, and the classification is indicated by the major alloying elements of the weld deposit. The first three character sets indicate the nominal chromium, nickel, and molybdenum contents, respectively. The letter L or H is then added for low or high carbon content, respectively. Other chemical symbols such as Mn, Cu, and Nb follow if required. Finally, appropriate electrode coating symbols such as B for basic and R for rutile appear (e.g., 19.12.3.Nb.R).

The AWS specification for these electrodes is A5.4. As before, they are denoted by the prefix E followed by a specification number for the weld metal deposit. These specification numbers are the same as those of the AISI series for stainless and alloy steels (e.g., E316L).

It will be appreciated that the foregoing descriptions relate only to their barest essentials. It cannot be emphasized too strongly that when dealing with standard specifications, it is important that they are studied in their official form and their requirements fully understood.

6.02.2.3.7 Technology of Welding

The electrode is to lead the welder, so that a uniform formation of the weld pool is created in the welding direction. The electrode connected is dependent on the following variables:

1. Type of electrode
2. Base material
3. Type of current
4. Welding position (Figure 25)
5. Weld shape
6. Seam construction

Any irregularity in the electrode guide promotes the occurrence of defects such as cold spots, slag inclusions, or pores. Welding a butt weld in a horizontal position, for example, the electrode must be directed precisely to the center of the weld joint. Figure 33 shows how it is located in a plane that is perpendicular to the plane of the sheet, and in this plane is inclined at an angle of approximately 45° in the direction of welding. The arc length is approximately equal to the core wire diameter.

The welder performs this slowly with the welding electrode from different movements. He pulls the electrode in a sliding motion toward the weld pool. At the same time he pulls the electrode toward the end of the seam. The result is a stringer bead. Thicker sheets can require a construction of the seam by a weaving welding (Figure 26). The welder pulls the electrode tip

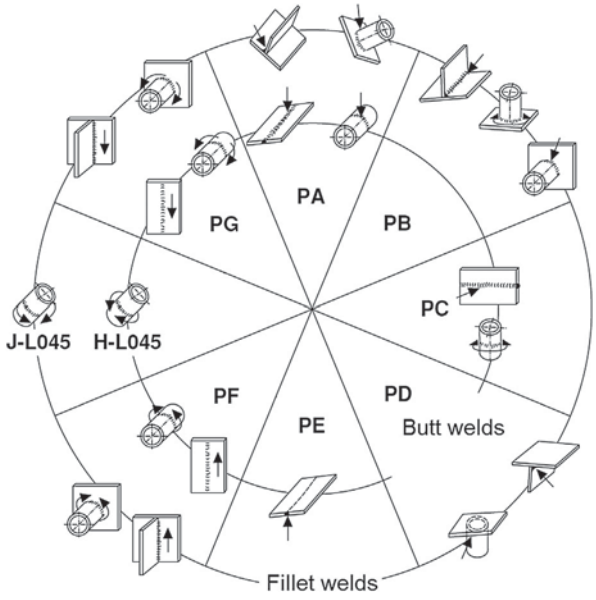

Figure 25 Welding positions.

www.iran-mavad.com
مرجع مهندسی مواد و متالورژی

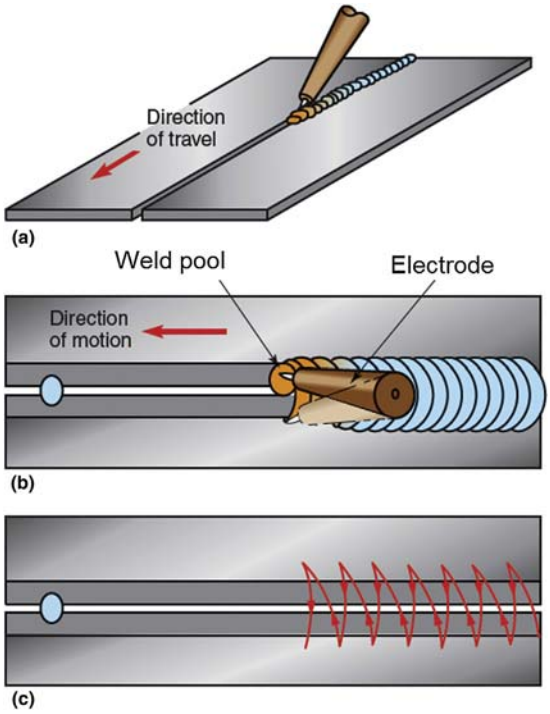

Figure 26 Guide the electrode positions during arc welding. (a) Pull the electrode to the end of the weld (reproduced from Olson, D. L.; Siewert, T. A.; Liu, S.; Edwards, G. R. *ASM Handbook: Welding, Brazing and Soldering*, 1993; Vol. 6), (b) motion of the electrode tip, and (c) pendulum of the electrode tip.

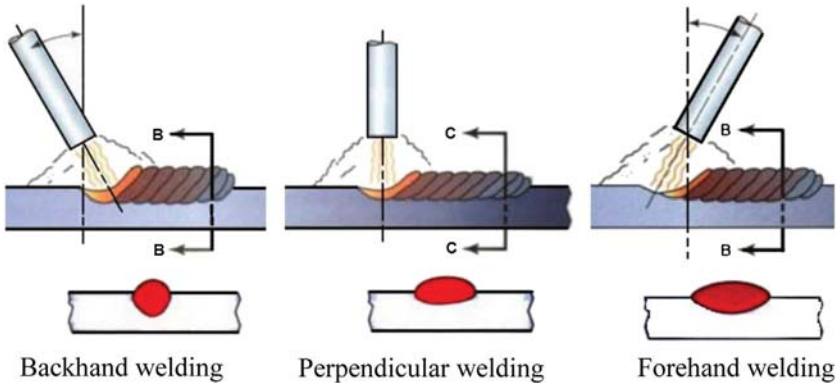

Figure 27 Execution of the welding.

additionally in a crescent-shaped pendulum motion. Other possibilities are the backhand welding and forehand welding (Figure 27).

6.02.2.3.8 Irregularities in Manual Metal Arc Welding

The formation of pores in weld metal is mainly due to a solution of carbon monoxide and hydrogen in the melt and their outgassing during solidification. Carbon monoxide is produced when high levels of carbon and oxygen come together. A greater supply of oxygen can be found especially in acid electrodes. The oxygen required for the formation of gas can penetrate into the weld when segregation zones are melted. Recommended, therefore, is the use of potted calms steels or basic electrodes.

Hydrogen porosity can be found, especially in basic and cellulosic electrodes. This should be dried prior to welding as specified by the manufacturer. Usually, this is done at temperatures between 250 and 350 °C with holding times from 30 min to 2 h. It once played a role in the hygroscopic ingredients, but much more important are the degassing conditions that are unfavorable for these electrodes as a result of the tough slag (*1,6–9,11,12*).

www.iran-mavad.com
مرجع مهندسی مواد و متالورژی

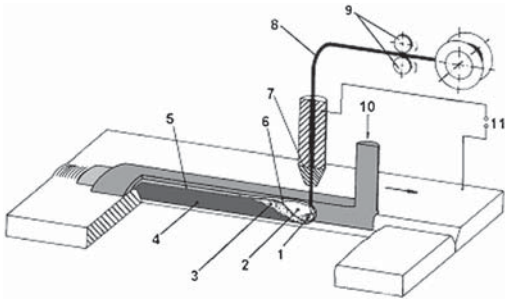

Figure 28 Basic process configuration during submerged arc welding with a wire electrode. From ISO 857-1.

In multipass welding the slag is removed carefully prior to placing the next layer. Failure to remove slag residue remains in the weld metal leads to lack of fusion. These act as internal notches and thus reduce the strength in the region of the weld. Undercuts occur preferentially in welding electrodes of thick coverings. They are observed on both sides of fill and cover layers for butt welds or at the top of fillet welds. By reducing the current here can be remedied.

6.02.2.4 Submerged Arc Welding

Submerged arc welding is characterized by the use of a bare wire electrode that is fed mechanically and a powder that meets the object of the sheath at the electrodes. Figure 28 shows the basic process flow.

The electrode is immersed in the force applied by a corresponding device before the welding head powder charge. The arc burns between the end of the wire electrode and the workpiece. In the vicinity of the arc, the powder is melted, thereby forming a cavity with ionized gases, in which the arc burns and the material transfer takes place in a teardrop. It is formed from a molten bath with a pronounced direction of flow opposite to the direction of welding. The molten powder due to its lower density rises up to the surface of the molten bath and forms beneath the bed of powder a liquid slag in which the bath solidifies the weld bead. Due to the complete shielding of the arc and the weld from the atmosphere and the reactions between the slag bath and mechanical and metallurgical properties of the weld metal are very possible.

In submerged arc welding, the welding current is fed just before the end of the consumable wire electrode. The low-current-carrying wire length allows for currents from 100 to 3600 A at voltages of 20–50 V, which leads to high deposition rates. Together with the high thermal efficiency of about 68%, this causes a relatively large molten bath with a high proportion of base material (up to 60%). The welding speed in the submerged arc welding – depending on the process variant – may be up to 800 mm min^{-1}.

Submerged arc welding is suitable for welding of all weldable steels. Favorable as long welds in PA or PB positions (see Figure 25). The welding process is not observable in submerged arc welding, making the welding root pass is difficult. One remedy is the use of backings in the form of metal rails. For the same reason, careful preparation of the joint must be done. Another disadvantage is the columnar grains may occur in the weld metal, combined with the tendency to hot cracking and segregation.

6.02.2.4.1 Electrodes

It is common to use wire-shaped electrodes, which are supplied in diameters from 1.2 to 12 mm. The main focus diameters 2.4–4 mm are used. The wires are coated with copper to protect against corrosion and to improve the current transition.

The marking of wire electrodes for submerged arc welding of non-alloy and fine-grain steels is done by an 'S,' which follows a code that – divided by a factor 2 – the average manganese content in percent, e.g., S2 EN 756. If other elements contain an increased proportion, they are added in the usual abbreviation.

In addition to wire electrodes, especially for surfacing and cladding, band-shaped electrodes are also used. They are 0.5–1 mm thick and 30–60 mm wide. Both for the joining and also for repair weldings, flux-cored wires are also available.

6.02.2.4.2 Welding Flux

The powder used for submerged arc welding has to fulfill the same function as the envelope of the bar-shaped electrodes. It is a granular, fusible product from minerals and metals, prepared according to various methods. It can be distinguished according to DIN EN as melted 760 (F), agglomerated (A) powder, and mixed powder (M). According to the mineralogical main components, the flux can be divided into 10 types of powders.

www.iran-mavad.com
مرجع مهندسی مواد و متالورژی

In addition to the classification according to the main components, a difference based on the degree of alkalinity is possible. This is the ratio of basicity B from metallurgy for themselves basic behaving components (CaO, MgO, etc.) back to the first acidic behaving (SiO_2, Al_2O_3, etc.). This results in the following assignments:

- $B < 1$ acid flux
- $B > 1$ basic welding flux
- $B = 1$ neutral flux

Another feature is the powder grade, indicating for which basic materials the welding powders are also suitable.

The weld substantially affected the behavior of the melt, the current carrying capacity, and the composition of the melt. Great importance therefore must be given to the combination of the submerged arc welding wire and flux. EN 756 contains information on the minimum yield strength, tensile strength, elongation, and impact strength of the weld metal as a function of the wire-flux combination.

The choice of wire and flux combination is based on the material properties of the welded steels and the metallurgical behavior. In the weld pool, there is reaction between the liquid metal and the slag and the gases dissolved in the melt. It results, depending on temperature and concentration of the elements involved, in both burning up and accumulating certain elements. Carbon burns up from all powders. Silicon accumulates usually in the melt, while manganese can both burn and accumulate. The focus for the ratio of the supply of manganese and silicon from the wire to the electrode is derived from the powder.

The mechanical properties of the weld joint can be influenced by the wire–flux combination. The toughness values are obtained for unalloyed steels when low-sulfur and phosphorus contents, the ratio of manganese/silicon, is greater than 2:1. This is achieved through the use of powders that act basic to high basic. This is due to the low oxygen content of the weld metal. EN 760, containing the information about combustion behavior and mechanical properties, states that chemical composition and mechanical properties of the weld metal are interdependent.

6.02.2.4.3 Welding Equipment

Welding equipment used for submerged arc welding systems consist of three components: the powder feeder, the wire feeder, and the welding power source. Depending on degree of mechanization, there is also the means for the movement of the welding head and the welding portion. The welding powder is fed from a reservoir via pipes and hoses to the fusion point where the welding head is in the powder bed. Unused powder lies loosely on the solid slag layer and can be extracted with a trailer, and returned to the circulation. The wire feed consists of the wire feed motor and the two feed rollers, between which the wire passes. One of the rollers is located on the motor shaft and causes the removal of the wire from the reel. The second roll acts as a counter-pressure roller. The speed at which the wire is fed must be controlled so that the length of the arc to the desired welding current results. When submerged arc welding is dependent on the welding flux used with both DC and AC, working with AC, so will the power sources have a falling characteristic. Welding rectifiers for submerged arc welding have a strong decline to constant static characteristics. The static characteristic of the welding power source used is strongly affected by the type of control. When submerged arc welding is preferably carried out with the so-called external control (ΔU control), the arc voltage controls the speed of the wire feed motor. The current needs to fit through a corresponding change so the characteristic curve can be selected. The control is affected, depending on the voltage over the wire feed, by which is connected to the change in the arc length control voltage change of the wire feed speed ΔU. The single-wire – a wire electrode and a power source – may be used as partial or fully mechanized procedures. To increase the deposition rate, a number of variants for submerged arc welding were developed. In double wire submerged arc welding, also occasionally referred to as a parallel-wire welding, two wires are melted together or one after the other in the welding joint. Both electrodes are located on a power source, and are fed together and burning in an arc (**Figure 29**). The advantages are a higher deposition rate compared to the single wire, and a better degassing of the melt, due to the fact that the bath is greater, and thus more slowly, and solidifies at a higher welding speed.

The tandem welding electrodes are arranged in succession in the welding direction. They each have their own power source with its own rules (**Figure 36**). By the separate control, it is possible to achieve a deep penetration with the first electrode at high amperage, so that while operating at a plurality of electrodes with the final electrode with a higher voltage, a good weld surface is produced. The tandem system has been extended to multi-wire systems with up to four electrodes. Another variation is hot wire welding. In addition to the arc melting electrode, a second wire is supplied with its own power source and its own control. This wire is directly next to the arc contact with the workpiece, and this area is heated by resistance heating to red heat. Reached the so heated wire portion of the arc, it is sealed there. The advantage of this arrangement is that with a relatively small electrical power, a high deposition rate can be achieved.

The economics of the UP process can also be enhanced by so-called narrow gap welding. This is done in this process variant where the volume to be filled to the seam is reduced. Also advantageous is the reduction of heat input to the base material. Special attention is given to the removability of the slag, so that as a rule, gap widths of at least 35 mm are required.

6.02.2.4.4 Weld Irregularities

During submerged arc welding, three typical errors occur:

- Pores
- Lack of fusion
- Solidification cracking

www.iran-mavad.com
مرجع مهندسی مواد و متالورژی

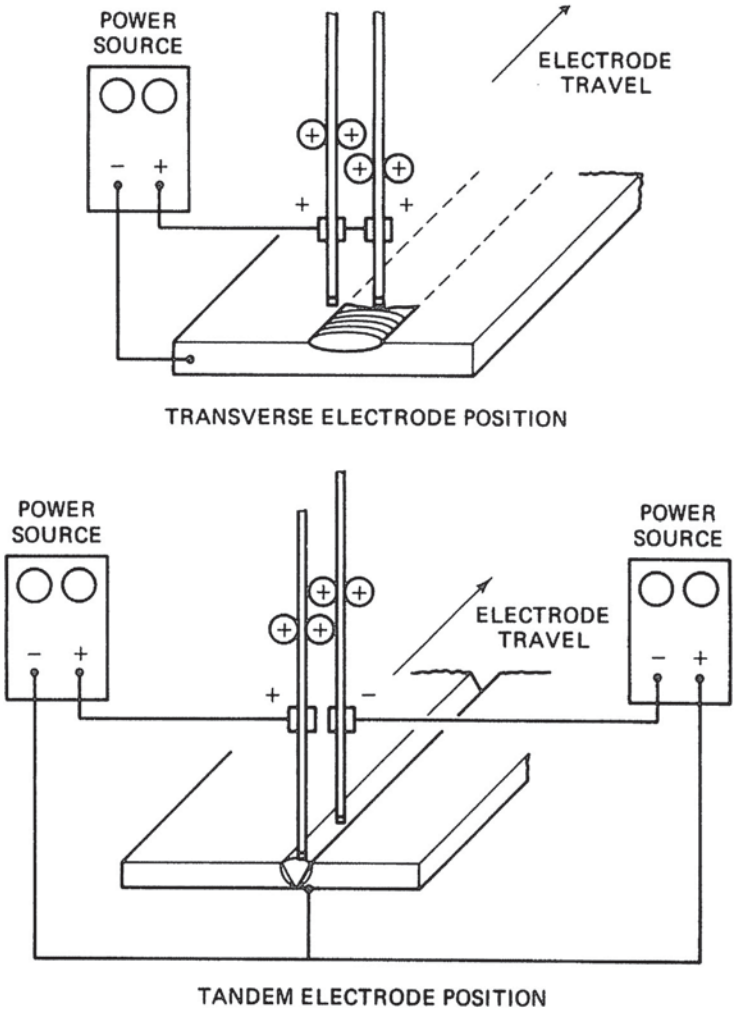

Figure 29 Submerged arc double wire welding and tandem welding.

The formation of carbon monoxide in the submerged arc welding can result in the formation of pores. They are arranged in the center of the beaded joint. This is due to an increase in the oxygen content in the weld pool, caused by the melting of segregation zones or the penetration of oxides from rust or scale. By the use of wires with a high Si content and powders high in MnO content, this can be remedied. The formation of pores may also be attributed to the evolution of hydrogen in the use of wet powder. Resulting pores can be recognized because they extend to the bead surface and are arranged in a nest shape. Binding errors occur during submerged arc welding mostly in the form of non-welded bars. It can cause an insufficient penetration (too thick electrode, false welding speed), its magnetic arc blow due to incorrect position of the ground terminal or a false guide the electrode. During welding, melting phases occur, so there may be depending on the nature of the crystallization to segregation in the weld. Particularly in steels and weld metal with a high carbon content or austenitic stainless steels, this has to be expected. In the worst case of solidification, in deep, narrow seams, the low-melting phases are pushed into the core of the weld cross-section, where they solidify last. This can lead to shrinkage, but also to the formation of hot cracks that run intercrystalline. This problem can be resolved by a change in the weld geometry, i.e., a broadening seam. (*1,6–9*)

6.02.2.5 Gas Shielded Arc Welding

In arc welding, the weld pool is formed by the action of an arc. This burns visibly between an electrode and the workpiece or between two electrodes. Electrode, arc, and weld pool are shielded from the atmosphere through a specially fed inert or active shielding gas.

The electrode processes are divided into two groups:

- Gas tungsten arc welding
- Metal inert gas welding

Even within the groups, a further subdivision is made due to the arc and the type of shielding gas (**Figure 30**).

www.iran-mavad.com
مرجع مهندسی مواد و متالورژی

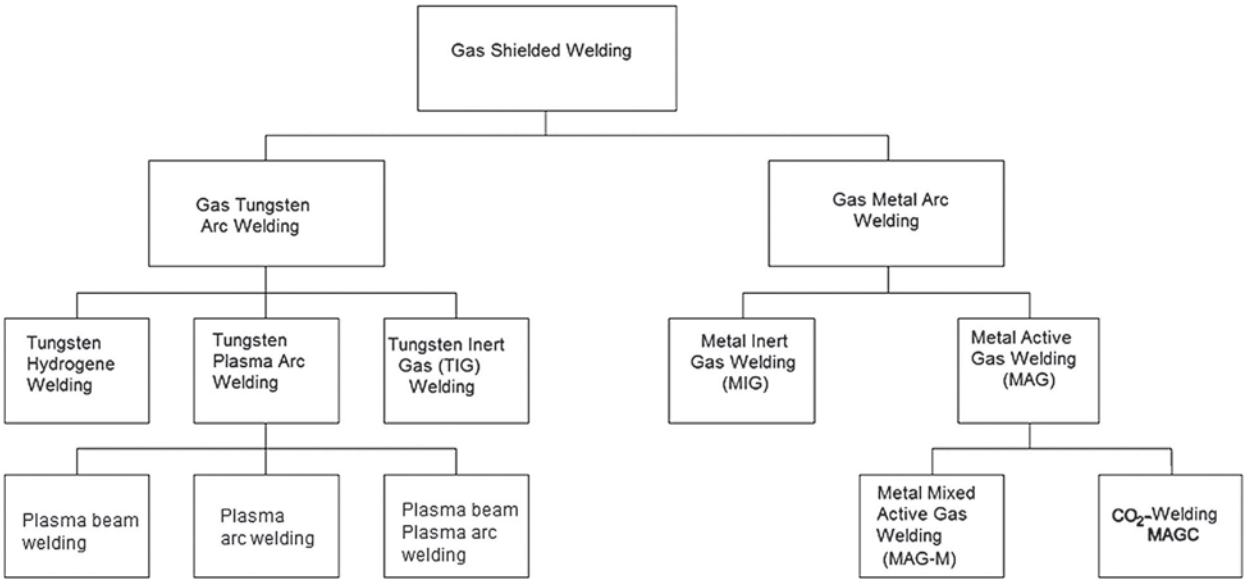

Figure 30 The process group 'gas shielded arc welding.'

6.02.2.6 Gas Tungsten Arc Welding

In TIG welding, the arc burns between a tungsten electrode and the workpiece. The protective gas is inert in the rule. As **Figure 31** shows, in TIG welding, a pole is located on the non-consumable tungsten electrode and the other on the workpiece. Between the two poles, the arc burns. Material must be added, which is done by hand using mechanized welding rods or on a specific wire feeder wire. The tungsten electrode, which is arranged concentrically through one nozzle, emanates the shielding gas and shielding electrode, arc, and weld pool from the atmosphere.

The method is characterized by

- A very high quality of the weld
- A concentrated stable arc
- A smooth and flat seam
- Lack of spatter
- Lack of slag

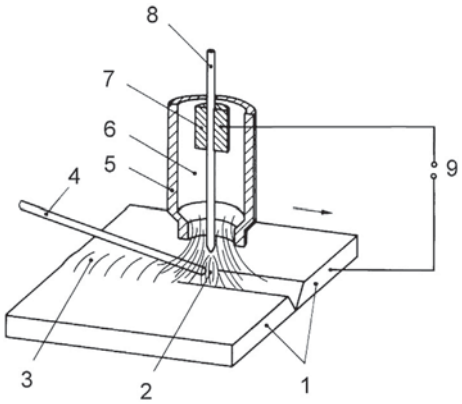

1 Workpiece
2 Arc
3 Weld
4 Filler metal
5 Nozzle
6 Shielding gas
7 Electrical contact
8 Tungsten electrode
9 Power source

Figure 31 Tungsten inert gas welding. From ISO 857-1.

www.iran-mavad.com
مرجع مهندسی مواد و متالورژی

In Europa, argon is usually used as protective gas. This must have a purity of 99.5%, since otherwise there may be an oxidation of the tungsten electrode. Commercially, argon for steel bottles of 10 m^3 is at a pressure of 200 bar (50 l bottles). Besides a pressure reducing valve, a gas flowmeter is required, so that the amount of gas can be adjusted reliably. These flowmeters must be calibrated to the type of gas. Depending on the material to be welded, argon-based mixed gases with helium, hydrogen, and nitrogen are used at different levels. Here increased welding speed and a better penetration are achieved.

During TIG welding, it is important to have good protection of the weld using a suitable material for the inert gases. The quantity must be large enough that the air surrounding the fusion zone is not affected. On the other hand, it must not be too large, otherwise it may lead to the introduction of air turbulence.

The TIG process can be used to weld all major metals, steel, aluminum, copper, nickel, titanium, and their alloys, and zirconium can be welded.

However, disadvantages are the low deposition rate and the required dexterity, so for economic reasons are often preferred over other methods. Up to 4 mm thickness, it is, however, highly capable. An increase in the deposition rate can be achieved by application of hot wire TIG welding, or the combination of TIG welding with a plasma.

The method is ideally suited for one-sided welding root passes through, which is why often the root welded with the TIG process, which will fill and cap layers but performed by other methods.

Power sources with a negative slope are suitable for welding, but are even more suitable sources with constant-current characteristic. Welding is usually direct current, to avoid thermal overloading of the electrode that is located at the negative pole.

6.02.2.6.1 Welding Technique

Aluminum and magnesium and their alloys are often welded with alternating current due to the stable oxide films. Because of the positive polarity of the electrode, the oxides are destroyed by high energy gas ions with local fast-changing arc starting points of high heat concentration. Conveniently, there is a rectangular alternating current with the opportunity to change the relationship between negative and positive half-cycles (balance), to work with different frequencies. Advantageously, the rectangular current waveform is also for the re-ignition, which must otherwise be supported by a high voltage pulse superimposition. The ignition behavior is also influenced by the inert gas used, and pure argon at the positive polarity electrode ensures particularly good results. More recently, in TIG welding, pulse technology has found its way. Here a low background current has superimposed current pulses with an adjustable low frequency. Under the effect of the momentum, the material is melted, and during the time of the base current it solidifies again. This creates a seam like scales overlapping welds. This technique makes it possible to weld even greater thicknesses than butt and dominate the weld in confined spaces and better for thin sheets.

The use of pure tungsten electrodes for TIG welding is possible; however, alloyed electrodes offer advantages in terms of carrying capacity, arc stability, and electron emission. Currently preferred as alloying additives oxides of rare-earth elements such as zirconium, lanthanum, and cerium, the former practice of using thorium oxide is no longer used because of the potential health impact of the welder. The electrode materials are standardized in EN 26848. Tungsten electrodes are sensitive to oxygen and polluted atmosphere as can, for example, occur when welding galvanized or oily metal sheets.

The diameter of the electrodes is determined by the welding current during welding occurring starch, the standard diameter is between 1.0 and 4.8 mm with a length of 150 and 175 mm. The shape of the electrode tip is essentially determined by the current type. Shape and roughness, however, will negatively affect the ignition and welding properties and the geometry of the weld. When working with DC a conical tip is used (1:3 or 30° cone tip angle). If welding with alternating current, usual cylindrical electrode ends are truncated.

The ignition of the arc should protect the tungsten electrode from possible contact. Therefore, in TIG ignition, aids are used, which allow for this. One possibility is the superposition of a high-frequency high voltage. This must be so high that a spark can jump between the poles, which ionizes the air between the electrode and the workpiece, thus allowing the formation of an arc without shorting. The disadvantage here, however, is the disruption of radio and television receivers for the high frequency. Therefore, the high voltage pulse ignitors have advantages. These devices work in the field of power frequency, but produce voltage pulses of several thousand volts, so the same effect is achieved without disturbing impact on the outside.

The use of ignition aids is particularly important in welding with alternating current, as it needs to be re-ignited after each zero passage of the arc. When using electronic power sources, it is possible to apply the so-called Liftarc ignition. This is a non-contact, electronic controlled ignition with the advantage of higher reliability and protection of the electrode. Also, it does not cause disruption of the function of computers and computer numerically controlled (CNC) controls.

With a special burner, it is possible to execute punctiform welding (TIG spot welding). The electrode here is in the nozzle, back slightly, so that the electrode holder is connected to directly to the gas discharge nozzle, and overlapping sheets can be attached. With the TIG arc, it is possible for the tubular members to perform so-called orbital welding. At larger diameters, for example, a TIG welding head runs to the stationary member, wherein the welding head is moved by a motor along a guide band.

Welding is mostly with pulsating direct current, and an average of a welding speed of 150 mm min^{-1} can be achieved. The consumables used for TIG welding are dependent on standardized materials.

www.iran-mavad.com
مرجع مهندسی مواد و متالورژی

Unalloyed and fine-grain steels acc. EN 1668
Creep resistant steels acc. EN ISO 21952
Stainless and heat-resisting steels acc. EN ISO 14343
Aluminum based materials acc. EN ISO 18273
Nickel-based materials acc. EN ISO 18274

6.02.2.6.2 Irregularities in TIG Welding

The following may be possible irregularities:

- Pores
- Lack of fusion
- Tungsten inclusions
- Oxide inclusions

When welding carbon steels and aluminum the formation of pores must be expected. As with the manual metal arc welding already described, when welding steels pores are a result of carbon monoxide formation. TIG welding when it is, however, also observed in Al- or Si-killed steel, even if the residual Si content in the steel is less than 0.1%.

During the TIG welding of aluminum, pores are observed on the solution of hydrogen in the weld pool. This come from the humidity of the air due to the incomplete protection, but mostly it comes from the moisture content of hygroscopic oxide films of the base material and the filler wire.

Fusion defects can occur as sidewall fusion and situation as lack of fusion. They arise due to inadequate penetration, i.e., due to incomplete sealing of the land. This error can be a false guide to the burner or a blunt electrode tip. When igniting the tungsten electrode to the weld area or when welding a touch of welding electrode to the weld pool edge, parts of the electrode may pass into the weld. By overloading the electrode due to an excessive current tungsten parts can get into the bath. If it is small, widely scattered particles can remain safely in the seam. Local accumulations of tungsten, however, must be removed by grinding. Oxide inclusions are found primarily at seams by using filler wire TIG-welded aluminum materials. This is due to the oxidation of the droplet at the tip of welding wire, if that is not melted in the shielding gas.

6.02.2.7 Plasma Welding

Plasma is known as the fourth state of matter that can occupy the matter. Plasma consists of electrons, ions, molecules, and atoms, which are, due to the high temperature, in a very strong, disordered motion. For the same reason, the molecules can be dissociated and ionize the atoms partially. If these particles reach the colder surface of the workpiece, they are recombined and enter it from the previously absorbed energy to the workpiece. As already indicated, there is every arc of pure plasma. By special measures, such as cooling of the plasma, it is possible to achieve a narrowing of the arc, and thus an increase in the power density.

This increases the temperature of the arc at the same amperage. Systematically include the plasma welding, for gas tungsten arc welding. In ISO 857-1, the process is characterized as follows: The arc is constricted. It burns at the plasma jet welding between the tungsten electrode and the inner wall of the plasma (non-transferred arc) or the plasma arc welding between the tungsten electrode and the workpiece (transferred arc). The shielding gas is inert, such as argon or helium, or active, such as hydrogen, or a mixture of inert and active gases. Plasma jet plasma arc welding is a variant of plasma welding, and is carried out at with non-transferred arc. **Figures 32** and **33** show the general arrangement of the described processes. In plasma jet welding, the tungsten electrode is concentrically surrounded by two nozzles, said inner and outer shield plasma. The tungsten electrode is located at the negative terminal of the DC power source, and the positive pole to the water-cooled copper nozzle, which also represents the plasma. The arc between the tungsten electrode and the plasma gas nozzle is heated while passing the plasma gas. This then enters like a flame from off the burner (non-transferred arc).

In plasma arc welding, however, the positive pole is at the workpiece, so that the arc is here between the electrode and workpiece. In contrast to the 'flame' of the plasma beam welding expires this transferred arc when the torch is lifted from the workpiece.

A combination of both processes is plasma jet plasma arc welding. The process therefore represents two welding power sources. The arc is not transferred as a rule, used as a so-called pilot or auxiliary arc, the ignition of a light the main arc allowed.

6.02.2.7.1 Plasma Arc

One of the characteristics of the plasma arc is the constriction of the arc (**Figure 34**). This is again achieved by the cooled plasma, on the other hand by the cold inert gas (argon). The plasma gas is argon, and due to its low ionization energy it reaches a high ionization. For the welding of stainless steels, a small fraction of hydrogen is mixed with the argon. This improves the thermal conductivity and increases the penetration and the welding speed as a result of the higher energy of the beam. When welding steels, inert gas argon–hydrogen gas mixtures are used, and argon–CO_2 – or argon–O_2 mixtures apply. Aluminum, titanium, and zirconium can be welded, preferably with argon–helium mixtures. If the plasma welding is used for joining, a division into plasma welding and plasma welding thick sheets is made according to the thickness of the parts.

Micro plasma welding is used for films and sheets to about 1 mm thickness.

www.iran-mavad.com
مرجع مهندسی مواد و متالورژی

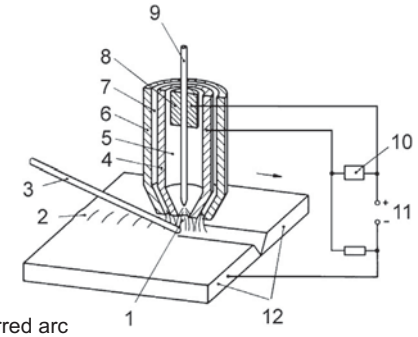

1 Transferred arc
2 Weld
3 Filler metal
4 Plasma gas nozzle
5 Plasma gas
6 Shielding gas nozzle
7 Shielding gas
8 Electrical contact
9 Tungsten electrode
10 Ignition device
11 Power source
12 Workpiece

Figure 32 Plasma arc welding (ISO 857-1).

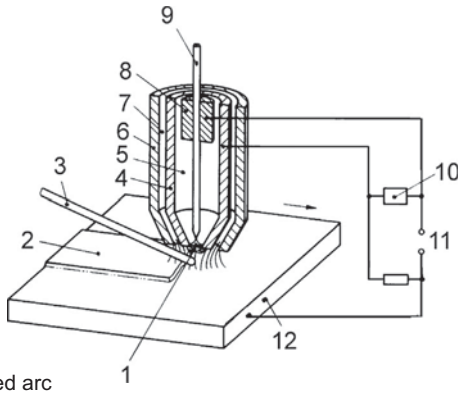

1 Semi-transferred arc
2 Build-up welding
3 Filler metal
4 Plasma gas nozzle
5 Plasma gas
6 Nozzle
7 Shielding gas
8 Electrical contact
9 Tungsten electrode
10 Ignition device
11 Power source
12 Workpiece

Figure 33 Plasma jet plasma arc welding (ISO 857-1). Reproduced from Killing, R., Killing, U. *Kompendium der Schweiβtechnik Band 1: Verfahren der Schweiβtechnik, Fachbuchreihe Schweiβtechnik Band 128/1*; DVS-Media, 2002.

Accordingly, the range of the current thickness is between 0.05 and 50 A. In the area of small currents of 1 A, the constricted arc of plasma welding has particular advantages over the TIG process: it also in this area is calm and steady burning. The thick sheet welding comprises the area between 1 and 10 mm thickness and 12 mm in the case of steel aluminum materials corresponding amperages 40–350 A.

The plasma fusion welding is preferably carried out without filler metal in flat position. The I-butt welds are made with no gap between the parts. The technology of welding depends on the sheet thickness. With thin sheets, the energy is supplied in a concentrated form of the surface, from where it flows into the deeper layers. The result is that the molten bath is also formed from the surface. The arc pushes toward the root, creating a root reinforcement. This type of welding is called a push-through technique.

www.iran-mavad.com
مرجع مهندسی مواد و متالورژی

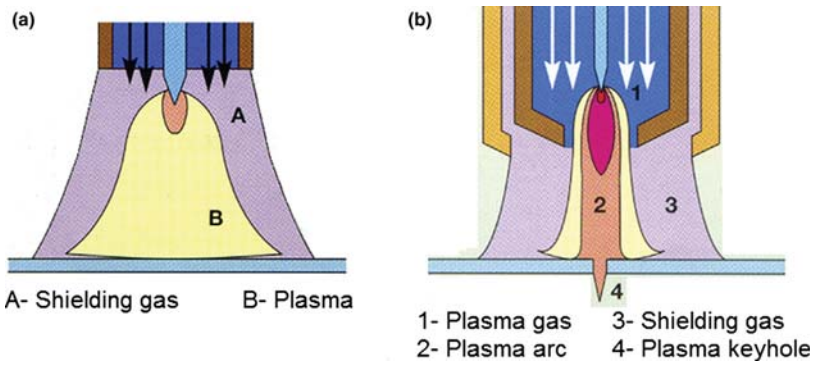

Figure 34 Normal plasma torch (left) and a focusing plasma torch (right).

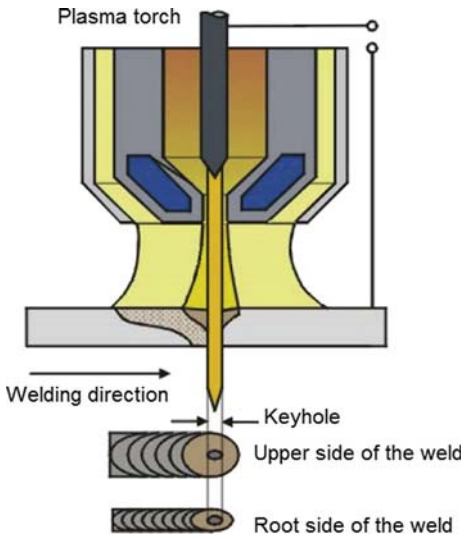

Figure 35 Formation of the weld pool during keyhole welding.

The other technique, applied from about 2.5 to 12 mm thickness, is the keyhole technique. The plasma beam penetrates the entire thickness here. It pushes the formed melt to the side so that a tubular loop is formed. A flow of the meltdown is prevented by the surface tension, and at the same time forms a tangential flow, which leads to a confluence of the melt downstream of the tap-hole, where the weld solidifies. The needle hole at the end of the welding process must be closed again, to which current and gas pressure can be reduced slowly. Since a tap-hole forms only at constant welding speed, this method is used only with a mechanically guided burner Figure 35.

6.02.2.7.2 Weld Irregularities in Plasma Welding

Essentially four irregularities can occur:

- Sunken bead surface
- Errors in the crater
- Pore formation
- Lack of fusion

As shown, the pressure of the plasma gas for the formation of the weld is of great importance; the seam surface will be affected. If the pressure of the plasma gas is too high or the amount is too large, the surface is pressed and the root sags.

As in TIG welding, special attention is devoting to the crater. In plasma welding, cavities and pores can occur at this point. This is prevented by a gradual closing of the needle hole. Carbon monoxide can lead also to form pores in plasma welding of unalloyed and low-alloy steels. The carbon monoxide originates from the reaction of oxygen with the carbon of the steel.

On stainless steels, with the use of mixed gases as the plasma gas, the hydrogen content does not exceed 5% by volume. It is the only way to prevent that in the hydrogen-sensitive steels pore formation occurs by hydrogen. When welding aluminum and its alloys, as well as the welding of titanium and zirconium, no hydrogen-containing plasma and shielding gases are used (*1,6–9*).

6.02.2.8 Electron Beam Welding

In electron beam welding, the high energy of accelerated electrons is used for heating and melting the material. The generation of radiation serving as a carrier of energy releases free electrons under vacuum from a thermionic cathode. The cathode of a high-heated

www.iran-mavad.com
مرجع مهندسی مواد و متالورژی

tungsten wire is at a high negative potential, so that the emitted electrons are accelerated in an electric field toward the anode. The acceleration voltage is 30–150 kV, and capacities of up to 120 kW can be achieved. The thermionic cathode is known as a Wehnelt cylinder. By a special shape and also a negative polarity through it a focusing of the electron beam is achieved, whereby the jet is emitted as a narrow beam from the anode aperture.

By a system of electromagnetic lenses, the beam is focused on its way to the workpiece. Together with a deflection system, which allows a static or dynamic deflection of the beam, the cathode and electromagnetic systems are housed in a so-called gun, which is arranged on the actual working chamber (Figure 36).

The electron beam gun and working chamber are evacuated, since the electrons are deflected in the atmosphere which contained much heavier molecules. In the working chamber, the parts to be welded are placed on appropriate devices and moved relative to the beam.

The impingement of the high-energy electrons, which have a power density of up to 107 W cm^{-2}, to the material is penetrated them in the boundary layer, but they are braked there quickly. Here, the kinetic energy converts into heat, and even in a small part to radiation. The heat causes the material to melt and evaporate. Due to the high vapor pressure of the melt, a gas channel is formed in the center, and a rotation of the melt takes place. This gas channel, also referred to as a vapor cavern, allows the deep welding effect, which it is possible in a single pass of sheet steel up to 200 mm. Thick sheets of aluminum materials are welded to 350 mm in thickness, although the penetration depth of the electrons is less than an order of magnitude (Figure 37).

In accordance with the welding progress the cavern moves along the weld groove, where the melt flows along behind it and solidifies there. The result is a weld, characterized by a narrow cross section, low melt volume, and slightly wedge-shaped edges. Electron beam welding usually works without filler, and the joint is formed as a butt joint. It is necessary to center the parts to be

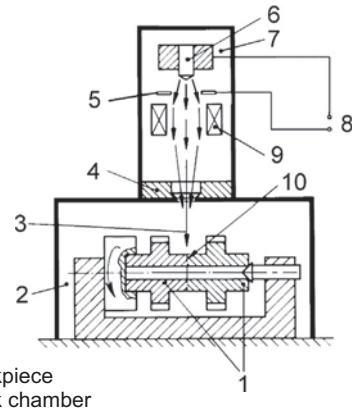

1 Workpiece
2 Work chamber
3 Electron beam
4 Deflector coil
5 Anode
6 Cathode
7 Vacuum chamber
8 Power source
9 Focusing coil
10 Weld

Figure 36 Process principle of electron beam welding (ISO 857-1).

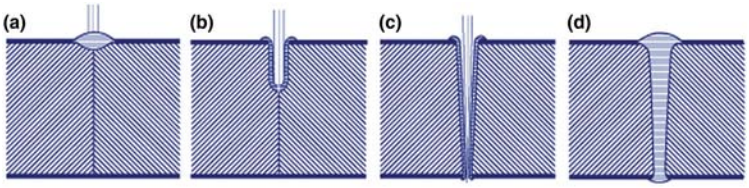

(a) Due to the high energy density in the beam the material starts to meld

(b) The material evaporates at the center.

(c) The occurred vapour capillary pushes the beam deeper in the part

(d) As the part moves forth, the molten metal flows to the back site due to the capillary effect and the back part solidifies.

Figure 37 The melting process in electron beam welding.

www.iran-mavad.com
مرجع مهندسی مواد و متالورژی

joined and the margins in a device for securing the position of the shock. The shape of the suture is dependent on whether it is completely welded through – with a drop in the root forms – or whether one weld backing is present, which prevents the beam weld and escape on the root side. If it will be welded completely, the top of the seam must be considered. When welding with weld pool restriction, a seam curvature occurs, called a nail head (humping effect) on which is observed so-called root-spiking in the root zone. It is melt, which penetrates into the root gap and there solidifies icicle-like prematurely. The result is formation of pores and separation of materials, which leads to a reduction in fatigue strength.

Before electron beam welding, apparatus and parts to be welded had to be demagnetized, since residual field strength of more than 1.5 Oe at the surface deflects the beam.

With the electron beam, almost all metals can be welded. A particular advantage of the method is that refractory or gas-sensitive metals and alloys are welded. When welding steels, pore formation may occur when the contents of sulfur and phosphorus are too high. With too high C content may result from the high cooling involve material hardness increases, the corresponding degraded by heat treatment immediately after welding must be done.

The forged titanium materials have good weldability, but the cast types have limitations. Heat-resistant metals such as molybdenum, tungsten, tantalum, niobium, and zirconium can be welded. The process has been proven for the welding of aluminum alloys; even the hardenable Al alloys AlCuMg and AlZnMgCu can be welded. However, Ni, Ni–Fe, or Co-based precipitation hardenable materials cause difficulties. The advantages in electron beam welding are the high welding performance and the low heat transfer to the base material.

A disadvantage is that the required vacuum chamber due to the size of the components had restrictions imposed. For the welding of large components, devices with a local vacuum to the welding point can be used. Here, the beam generator moves the beam during welding in a stationary-sealed region.

6.02.2.9 LASER Welding

The artificial word LASER is an acronym for Light Amplification by Stimulated Emission of Radiation (LASER). The laser is a generator and amplifier of electromagnetic waves having frequencies in the visible spectrum and adjacent. The laser can be viewed as a radiation source that emits a narrow collimated beam, depending on the type of laser has a characteristic wavelength for this, which is monochromatic and coherent.

Each laser has three main components: the laser medium, the pump source, and the resonator (Figure 38).

6.02.2.9.1 Beam Formation

If nuclear energy is supplied from the outside, the atom is in the excited state and in the shell electrons are raised to higher energy levels. This excited state is not stable; after a certain residence, the electrons fall back completely irregular in the basic level. The prerecorded absorbed energy is emitted as visible or invisible radiation. There is a spontaneous emission of light that is incoherent and not monochromatic.

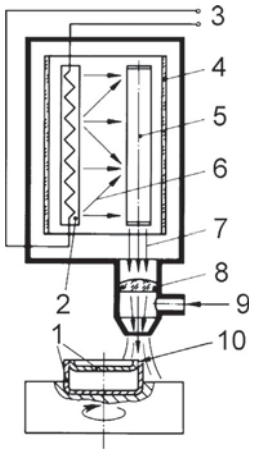

1 Workpiece
2 Light source
3 Power source
4 Elliptical mirror
5 Laser rod or gas filled tube
6 Light beam
7 Laser beam
8 Lense
9 Shielding gas
10 Weld

Figure 38 Schematic structure of the laser. Reproduced from SFI-Aktuell 2011, DVS-Media, 2011.

www.iran-mavad.com
مرجع مهندسی مواد و متالورژی

The emission of radiation in the laser is achieved by the fact that energy is injected into a laser-active material usually in the form of light characterized whose atoms or molecules are excited to pass (lower laser level) from a low level of energy to a higher energy level (upper laser level). The condition for the occurrence of the laser effect is that many more particles must be in the upper laser level than in the lower one. This is called population inversion. If such a condition is achieved by the pump, then the laser-active material leaves the coupled energy in the form of a radiation of a certain frequency, and the propagation direction again. There occurs an induced emission. Here the atoms or molecules fall back into the lower laser level and the ground state.

In the typical laser-active media, the reinforcing effect is low initially, since only after passing through a longer distance, the ratio of spontaneous to stimulated emission in favor the latter changes. This route consists of one to several hundred meters. Optical paths of this length can be realized in the so-called resonator. This resonator basically consists of two parallel plane mirrors, one of which is semi-permeable. The laser material is placed between the mirrors. After each pass through the laser-active material, the light is reflected back onto this and thus strengthened continuously by further stimulated emission. The mirrors also ensure that the resonator only light waves are parallel to the axis, are obliquely running rays flipped out. After a series of runs only stimulated emission occurs along the resonator, the laser light is produced and can be coupled out through the semi-transparent mirror.

6.02.2.9.2 Welding with the Laser

The laser offers a number of advantages for welding:

- High-energy density
- Workpieces are welded without contact at high speed
- Narrow weld geometry at large depth/width ratio
- Only low distortion
- Low heat input, very small heat-affected zone, low thermal load on the workpiece
- Welds executed even in hard-to-reach areas of the workpiece
- Low spatter, good weld surface
- High degree of automation

For welding with the laser, mainly the CO_2 laser and the Nd:YAG or diode lasers are used. CO_2 lasers are used with power between 700 W and approximately 12 kW in cw (continuous wave) mode.

Solid-state lasers are used in both pulse and continuous-wave operation. Nd:YAG laser pulse is used in pulse mode power up to 25 kW. Another advantage is the possibility of beam delivery via fiber optic cable and the low values for the absorption.

Typically, the laser welding is stationary with a high degree of mechanization. The development of hand-held laser welding equipment extends the scope of the process considerably. It is important to pay attention to the hazards caused by the laser radiation. Laser welding is distinguished by two methods: heat conduction welding and deep penetration welding (**Figure 39**).

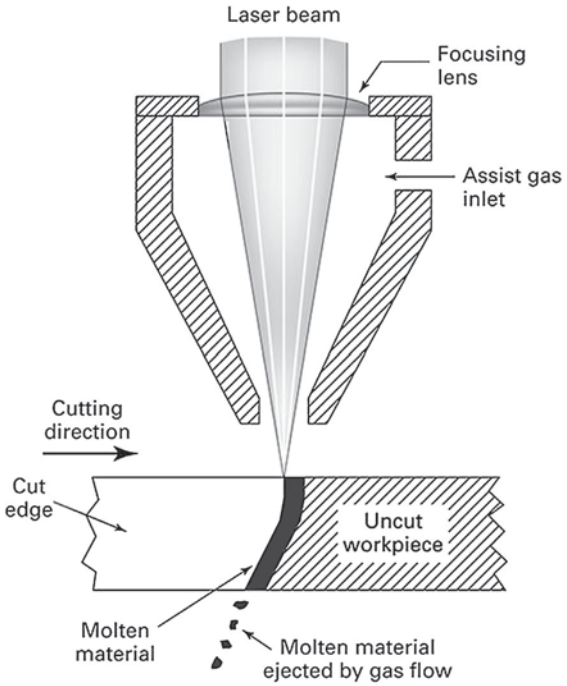

Figure 39 Welding process (after stocking); left: heat conduction welding, right: deep penetration welding.

www.iran-mavad.com
مرجع مهندسی مواد و متالورژی

The characteristic for heat conduction welding is that the material is melted by the laser beam only to a depth of about 0.5 mm. The beam power is sufficient for this method, but to melt, but not to evaporate, the material.

In this process, a pulsed Nd:YAG laser is preferred. If the energy density of the laser beam is above a critical threshold of about 106 W cm^{-2}, the material is heated so high that it vaporizes at the impingement of the beam.

Processes produce a deep penetration into the workpiece vapor channel. It thus achieves electron beam welding of known deep welding effect. The metal vapor is ionized owing to the absorption of part of the beam energy, whereby a plasma is generated. The advantage in the case of the CO_2 laser is that the absorbance of the plasma for the wavelength of this laser is higher than that of the melt. Thus, the energy of the laser beam with the assistance of the plasma is brought almost completely into the workpiece. The CO_2 laser and Nd:YAG laser in continuous wave mode are used for deep penetration welding.

Welding with the CO_2 laser requires the use of a so-called working gas. It has influence on the object, density, and size of the developing of the metal vapor plasma so that this does not detach from the workpiece, and thus shields against the laser beam. Helium is particularly suitable for this task. However, argon, nitrogen, and carbon dioxide can also be used as a working gas. The melt and the bead during cooling are protected by inert gases. Also for this purpose, helium is preferably used. Depending on the material to be welded, however, other gases are used.

The special requirements are as follows:

- The reflectance of the material should be low, i.e., the absorption capacity to be large.
- For steel, the C content must not be too high, otherwise there is the risk of hardening and embrittlement of the weld.
- Consistent quality of the weld can be achieved only by a constant quality of the material.
- A grease-free and oil-free surface is a prerequisite for a good non-porous weld seam.

6.02.2.10 Resistance Welding

This group include the processes:

- Spot welding
- Projection welding
- Seam welding

as well as

- Butt welding
- Flash butt welding

As the characteristics of all the above processes, the heat required for welding is generated by a resistance heating, and so heated parts are welded under pressure.

The processes differ in terms of

- The shape of electrode
- The workpiece design
- The control of the welding process

6.02.2.10.1 Spot Welding

As Figure 40 shows, two pin-shaped electrodes press the parts to each other to be assembled. A joining point at the impulse heat-sealing temperature (Figure 41), is generated by the mechanical pressure, a welded joint, and the welding point.

6.02.2.10.2 Welding Power Sources

The energy required for welding is generated in particular welding power sources. In general, these are transformers that take the required three-phase power to the public. At higher welding currents at a frequency of 50 Hz, the transformers are more elaborate. It therefore makes sense to work with DC voltage.

This voltage is in a transformer placed on welding amperage and rectified secondary. Due to the higher frequency, the transformers are light weight, allowing their integration into a robot, or a hand-operated welding gun. In addition to this, it allows the direct current generated in the secondary stage to also use pliers with great projections, since the inductive resistance is eliminated from the secondary stage. Another possibility is welding with capacitor-pulsed current, a method that is currently used in particular in the welding of small parts made of non-ferrous metals.

Figure 42 shows a spot welder in conventional construction. A hand-operated spot welding gun is shown in Figure 43.

6.02.2.10.3 Weldability of Materials

Wires, sheets, and foils can be welded. For steel, the total thickness is a maximum of 2 × 20 mm, and for aluminum and brass the total thickness is a maximum of 2 × 5 mm. The weldability of the materials is mainly determined by their

- Physical properties
- The surface finish
- The metallurgical and chemical characteristics

www.iran-mavad.com
مرجع مهندسی مواد و متالورژی

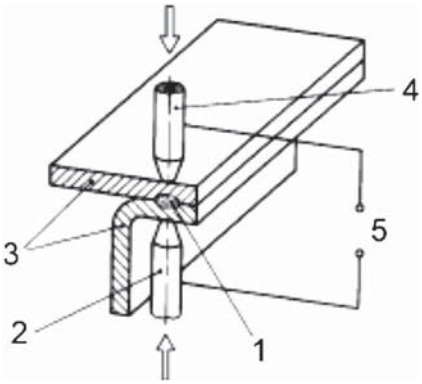

1 Weld spot
2 Spot-welding electrode
3 Workpiece
4 Spot-welding electrode
5 Power source

Figure 40 Schematic diagram of two-sided spot welding (ISO 857-1).

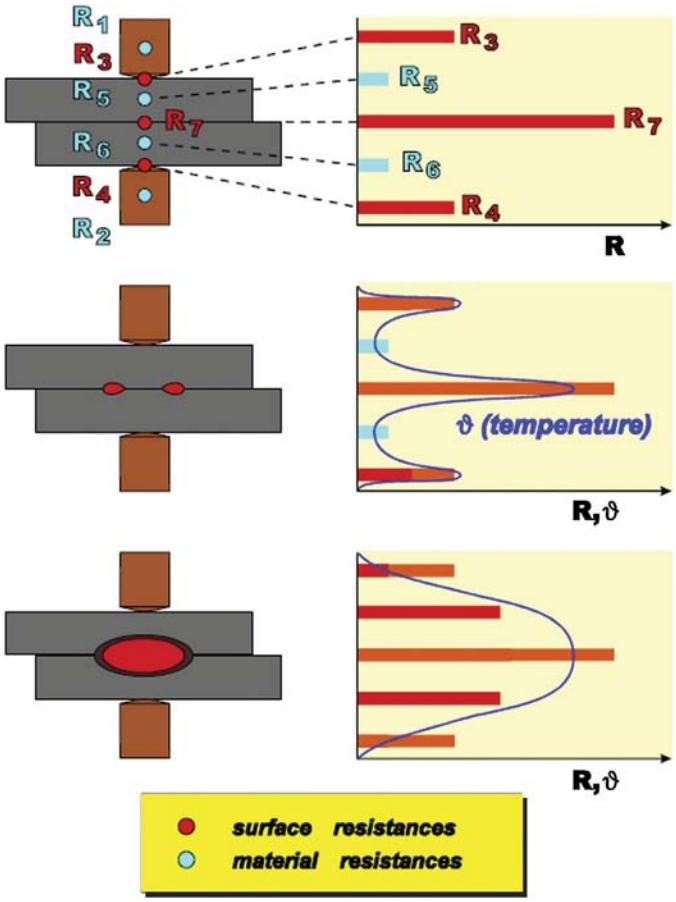

Figure 41 Change of resistance and temperature during resistance spot welding.

6.02.2.10.4 Welding Parameters

The amount of heat generated in the workpiece Q is calculated from Joule's law

$$Q = I^2 \cdot R \cdot T$$

where I denotes the effective value of the welding current in amperes, R is the resistance between the electrodes in ohms, and the time T, while the current flows, is in seconds. For economic and technical reasons, short welding times are required, so as to

www.iran-mavad.com
مرجع مهندسی مواد و متالورژی

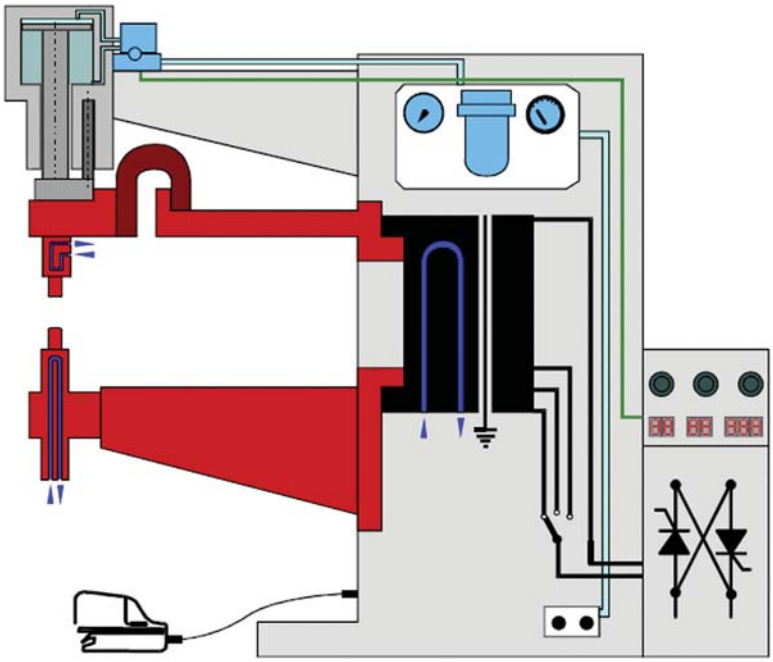

Figure 42 Spot welding machine with pneumatic actuator.

Figure 43 Hand-operated spot welding gun.

prevent a greater flow of heat and the material thermally not to burden too high. The required amount of heat is therefore generated by relatively high current intensities. The current is limited at the top by the contact resistance between the electrode and plate, whereby the maximum possible current density is given. If this limit is exceeded, the result at the welds splashes that cause high electrode wear and ultimately useless welds. Spatter limit current is absorbed by water-cooled electrodes, usually without problems.

The depth in the calculation of the amount of heat resistance is composed of two parts: the material resistance and the contact resistance. Resistance of the material is a material-specific parameter is influenced by the temperature and the formation of the current path between the electrodes. This allows the material resistance by the diameter and shape of the electrode to be somewhat influenced. The contact resistances occur once between electrodes and the adhered surfaces, on the other at the contact point of the parts to be welded. The electrode-sheet resistance should be as small as possible, which can be achieved by a high electrical conductivity of the electrodes, a clean surface of the sheets, an adequate contact force, and the shape and size of the contact surface. For welding, a large influence is – especially at the beginning of the welding process – the contact resistance between the joined parts, because at this point in the formation of the weld nugget, the largest thermal energy is required. Here in addition to the pressing force, the current density in particular, the properties of the boundary layers, roughness and conductivity are also important.

www.iran-mavad.com
مرجع مهندسی مواد و متالورژی

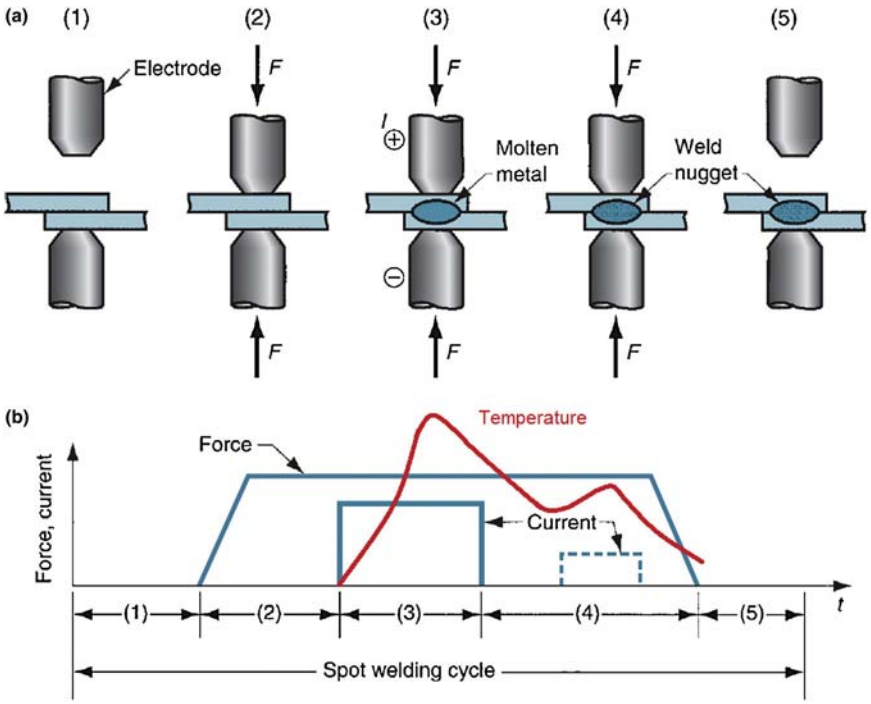

Figure 44 Extending from force, welding current and temperature as a function of time for spot welding (schematically).

A special role is played by the welding time. Because in practice it is not possible to detect the temperature at the connection point, and thus to control the fusion process, the most favorable for the welding temperature at the connecting point is preferably on the time during which current flows (current time) is controlled. Figure 44 shows the chronological course of the most important parameters in the manufacture of a spot weld without a control program of power and current.

By compressed air, oil, or hydraulic leverage, the parts to be welded are pressed together between the electrodes. This type of power generation, however, has the disadvantage that the electrodes during opening and closing must always pass through the entire stroke, which extends the cycle times significantly. The movement of the electrodes is therefore for new machines by actuators in micro-welding equipment by actuators. The force depends on the material to be joined depending on their thickness. When the required power is reached, the welding current is switched on. The duty cycle is from about 4–15 cycles, if a frequency of 50 Hz is a basis. They must be chosen so that the pressure required for the welding temperature is reached. The force acts during the 'cooling time' after switching off the welding current on, so that the solidification of the weld takes place under pressure.

Today for the control of welding machine diagrams to help spot diameter, minimum tensile, and shear plate thickness of the welding current adjustment variables, current time, and electrode force can be determined.

6.02.2.10.5 Welding Electrodes

The electrodes for spot welding is of great importance. They require the following:

- A large electrical and thermal conductivity
- High strength and hardness (heat hardening)
- A high softening and recrystallization
- A slight tendency for alloying

The electrode materials are standardized in ISO 5182. There, the materials are classified into two groups. Group A contains the copper-based materials, alloyed with Cd, Cr, and Zr (Type 1, not heat), Co and Be (Type 2, higher hardness than type 1), Ni, Si, and P (type 3, hardened alloys), and Ag, Al, and Fe (type 4, with special features). In Group B, the sintered metals are summarized on the basis of Cu/W, Cu/WC, Mo, W, and Ag/W. This standard is supplemented by information on the range of individual materials (Figure 45).

6.02.2.10.6 Resistance Projection Welding

Projection welding allows one to generate a plurality of welding points with a pair of electrodes at the same time (Figure 46). The current density and the surface pressure decrease is due to the increased contact surface electrodes, which increases the life of the electrode.

www.iran-mavad.com
مرجع مهندسی مواد و متالورژی

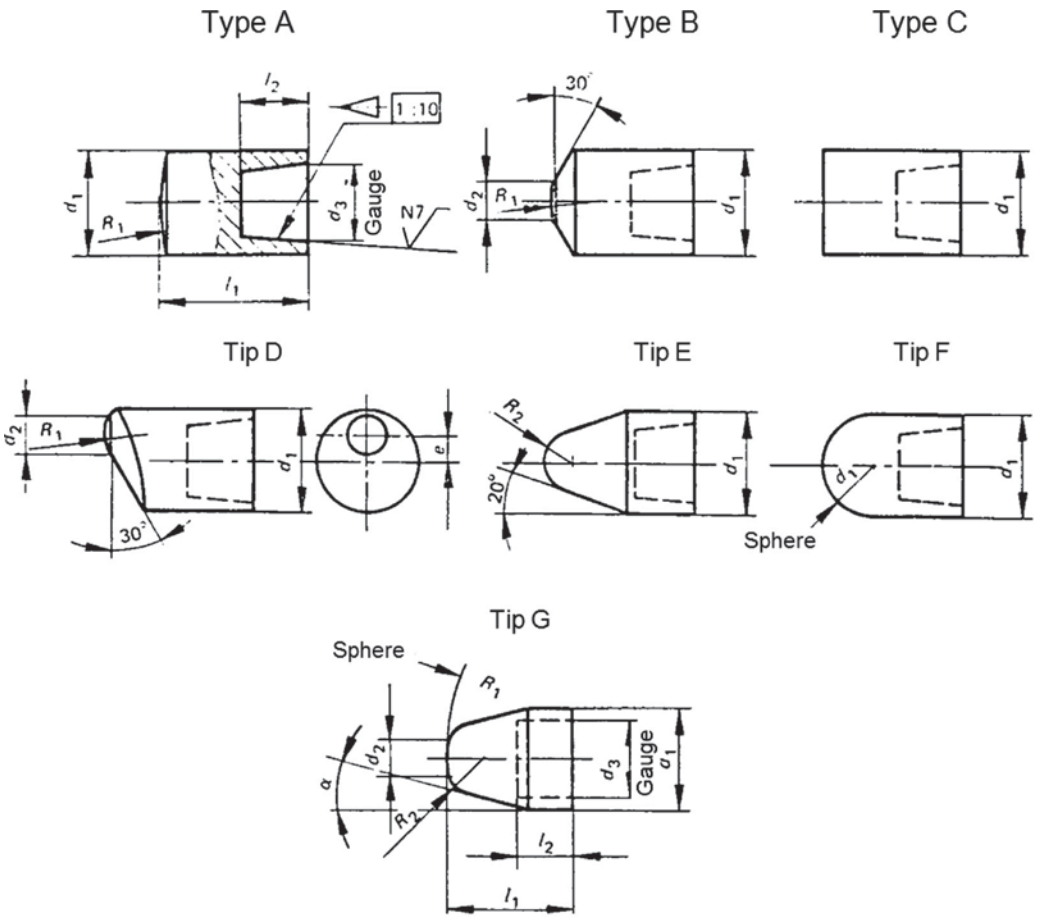

d_1 h11	d_2	d_3 [1)]	l_1	l_2 +0.5 0	e	R_1	R_2	α	electrode force F_{max} [2)] kN
13	5	10	18	8	3	32	5	--	2.5
16	6	12	20	9.5	4	40	6	15°	4
20	8	15	22	11.5	5	50	8	22.5	6.3

1) corresponds to the corse diameter on the plane of reference of the gauge
2) for information only

Figure 45 Electrode shapes for the spot welding (in accordance with ISO 5821).

6.02.2.10.7 Resistance Seam Welding

For producing a force-transmitting point sequence, or for the production gas or fluid-tight seams, the seam welding is used (Figure 47). When seam welding in certain distances from each, arranged spot welds are made. The roll-shaped rotating electrode, and by a pulse-type power supply, the welding points are generated at equal intervals. The current in short successive pulses, i.e., supplied almost continuously, then creating overlapping weld points, leading to a liquid- or gas-tight seam. It is advantageous that the rotation of the electrode, the current transition always at a different location, is creating a life extension. There is, however, a considerable portion of the stream running through the already formed seam, forming a shunt. In relation to the spot welding, therefore, much higher currents are required. This makes it necessary to cool the rollers with water.

In principle, the resistance spot welding works without any additional material. With the introduction of high-strength steel grades in body but there were the technological limits of the classical method achieved. This led to the development of resistance pressure welding with filler material. In this variant, before the joining, a ring-or line-shaped element out of the filler material is fixed between the joint parts and the flow passage with melted. Welding consumables such as type S2 or CuSi also come into consideration. Advantageous of all is the possible reduction in the number of spot welds (large weld area, greater strength). On the other hand, in this, the surface of the joining parts is not damaged in the area of the joints.

www.iran-mavad.com
مرجع مهندسی مواد و متالورژی

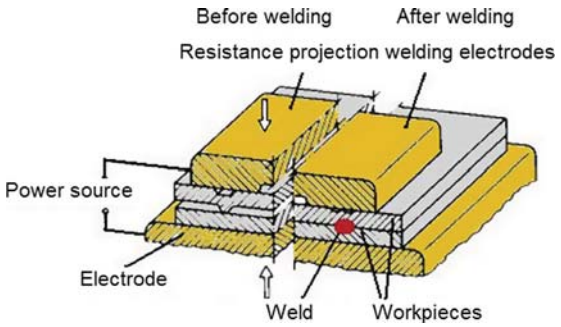

Figure 46 Two-sided projection welding (ISO 857-1). Reproduced from Groover, M.K. *Fundamentals of Modern Manufacturing*, 3rd ed.; Wiley, 2010.

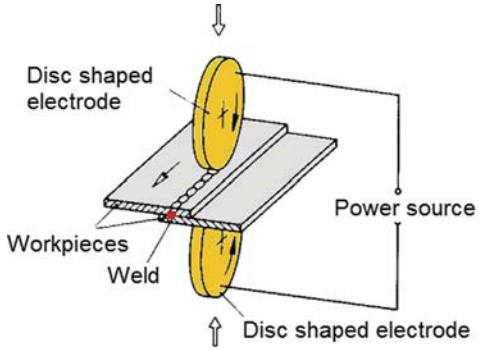

Figure 47 Seam welding (according to ISO 857-1).

6.02.2.10.8 Resistance Butt and Flash Welding

Both processes have in common that waves, profiles, tubes, and the like may be welded to the front side parts together. The required heat is generated during the passage of electric current through the junction of the parts by means of resistance heating, wherein the flash-butt welding can occur in a molten phase, which is pressed during the compression of the joint zone. When butt welding the parts to be clamped into water-cooled jaws, the front sides are pressed against each other and energized. Here, the plan worked contact point is heated by the high-contact resistance up to welding temperature. If this is reached, the current is switched off and simultaneously increases the compressive force. While the plasticized material to the weld bead will be immersed (**Figures 48** and **49**). The method is suitable for cross sections up to about 500 mm^2 in area. It can be applied to components made of steel, copper, and aluminum.

6.02.2.11 Stud Welding

The most important process of this group is arc stud welding (stud welding), which is used for securing bolt-shaped components such as screws, pins, or the like, on panels or tubes. Stud welding has significant cost advantages over clinching and blind rivet. According to the applied firing, three main variants are as follows:

- Drawn arc stud welding with ceramic ferrule or shielding gas
- Short-term drawn arc stud welding
- Capacitor discharge welding with tip ignition

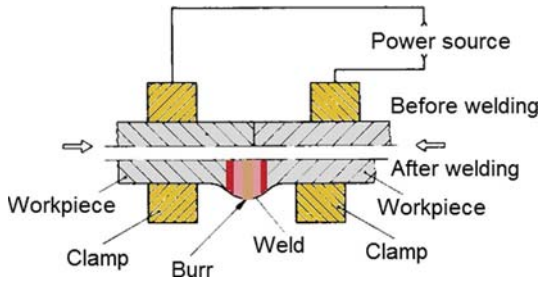

Figure 48 Resistance butt welding (ISO 857-1).

www.iran-mavad.com
مرجع مهندسی مواد و متالورژی

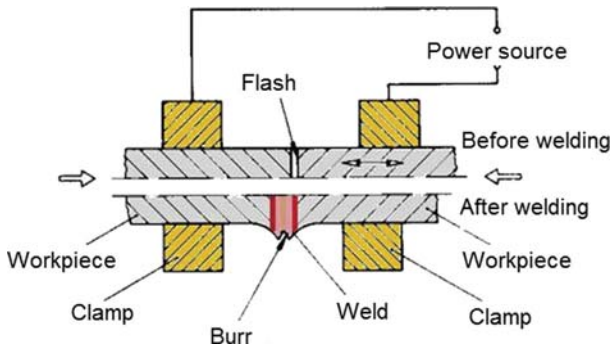

Figure 49 Flash welding (according to ISO 857-1). Reproduced from Groover, M.K. *Fundamentals of Modern Manufacturing*, 3rd ed.; Wiley, 2010.

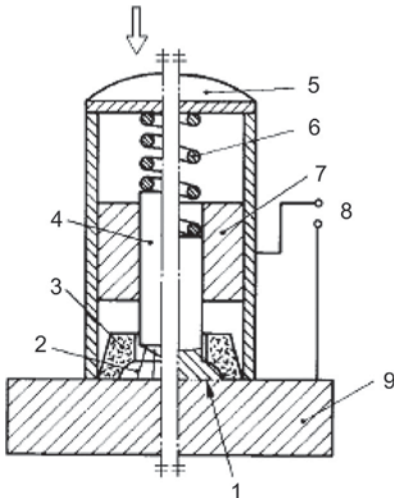

1 Weld
2 Arc
3 Ceramic ferrule
4 Stud (workpiece)
5 Welding gun
6 Spring
7 Lifting magnet
8 Power source
9 Workpiece

Figure 50 Arc drawn arc stud welding (ISO 857-1).

In the drawn arc method, the bolt is inserted into a special welding gun or stationary bolt setting device. The bolt is to be welded at the end of beveled blunt and with a coating (flux, metal) provided to facilitate the ionization of the arc gap and effect in the molten bath is also metallurgical reactions. Furthermore, the bolt bears on this end a ceramic ring that forms the weld pool, it protects against the ingress of the atmosphere, and it will after welding be repulsed. Figure 50 shows the process principle. This end of the pin is placed on the workpiece. Just pressing a button on the gun turns on the power as well as removing the bolts magnetically so that an arc between the stud and work piece is formed. It melts the bolts and base material locally. After a pre-selected time with power off, the bolt is pushed into the melt; it is welded there to the base material.

6.02.3 Solid-State Welding Processes

Solid-state welding refers to joining processes in which coalescence results from application of pressure alone or a combination of heat and pressure. If heat is used, the temperature in the process is below the melting point of the metals being welded. No filler metal is utilized. Representative welding processes in this group include the following:

- Diffusion welding: Two surfaces are held together under pressure at an elevated temperature and the parts coalesce by solid-state diffusion.
- Friction welding: Coalescence is achieved by the heat of friction between two surfaces.

www.iran-mavad.com
مرجع مهندسی مواد و متالورژی

- Ultrasonic welding: Moderate pressure is applied between the two parts and an oscillating motion at ultrasonic frequencies is used in a direction parallel to the contacting surfaces. The combination of normal and vibratory forces results in shear stresses that remove surface films and achieves atomic bonding of the surfaces.

In solid-state welding, coalescence of the part surfaces is achieved by (1) pressure alone, or (2) heat and pressure. For some solid-state processes, time is also a factor. If both heat and pressure are used, the amount of heat by itself is not sufficient to cause melting of the work surfaces. In other words, fusion of the parts would not occur using only the heat that is externally applied in these processes. In some cases, the combination of heat and pressure, or the particular manner in which pressure alone is applied, generates sufficient energy to cause localized melting of the faying surfaces. Filler metal is not added in solid-state welding.

In most of the solid-state processes, a metallurgical bond is created with little or no melting of the base metals. To metallurgically bond two similar or dissimilar metals, the two metals must be brought into intimate contact so that their cohesive atomic forces attract each other. In normal physical contact between two surfaces, such intimate contact is prohibited by the presence of chemical films, gases, oils, and so on. In order for atomic bonding to succeed, these films and other substances must be removed. In fusion welding (as well as other joining processes such as brazing and soldering), the films are dissolved or burned away by high temperatures, and atomic bonding is established by the melting and solidification of the metals. But in solid-state welding, the films and other contaminants must be removed by other means to allow metallurgical bonding to take place.

In some cases, a thorough cleaning of the surfaces is done just before the welding process; while in other cases, the cleaning action is accomplished as an integral part of bringing the part surfaces together. To summarize, the essential ingredients for a successful solid-state weld are that the two surfaces must be very clean, and they must be brought into very close physical contact with each other to permit atomic bonding.

Welding processes that do not involve melting have several advantages over fusion welding processes. If no melting occurs, then there is no heat-affected zone, and so the metal surrounding the joint retains its original properties. Many of these processes produce welded joints that comprise the entire contact interface between the two parts, rather than at distinct spots or seams, as in most fusion-welding operations. Also, some of these processes are quite applicable to bonding dissimilar metals, without concerns about relative thermal expansions, conductivities, and other problems that usually arise when dissimilar metals are melted and then solidified during joining.

6.02.3.1 Diffusion Bonding

The workpieces are placed at the abutting surfaces, or by cross in vacuum, under an inert gas or in a liquid, and heated using a continuous force preferably welded without filler. The compound is formed by diffusion of atoms on the abutment surfaces of time. In the region of the weld joint there is only slight plastic deformation (**Figure 51**).

The diffusion of metals is a process in which atoms are caused to move by differences in concentration. There is a tendency to compensate for these differences in concentration. Diffusion in solids requires a longer time. By increasing the temperature, the diffusion rate can be greatly increased. It still depends on the diffusion mechanism, which may consist of the substitution of atoms on adjacent seats and the migration of atoms on interstitial sites or in the diffusion of vacancies. The sequence of compound formation is divided into three phases:

- Preparation of the metal contact by a plastic deformation of the contact surface,
- Enlargement of the interface by flowing
- Connection of the interfaces by surface diffusion with a migration of atoms on the contact surfaces and formation of a new structure by grain growth of the interfaces and grain boundaries

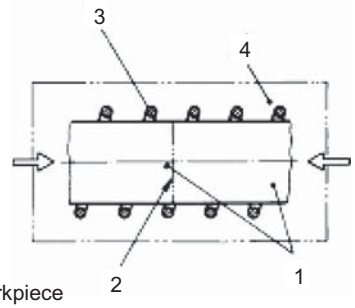

1 Workpiece
2 Weld
3 Induction heating
4 Work chamber

Figure 51 Diffusion welding (ISO 857-1).

www.iran-mavad.com
مرجع مهندسی مواد و متالورژی

The procedure is largely determined by four variables:

- The welding temperature
- The welding pressure
- The welding time
- The pressure of the protective gas and the height of the vacuum

The welding temperature is in the range of Ts = (0.5–0.7 K). The material is still in the solid state, but it is deformed in the interfaces easily plastically, which leads to a good contact between the joining parts. This also promotes the diffusion temperature of the atoms. Together with the increased temperature, this causes welding of the welding pressure, which is about 10 N mm^{-2}, a flattening of the protrusions, and thus increases in the contact area.

It is also favorable that by the increased pressure and the deformation caused by the recrystallization, temperature is lowered. The strength of the weld is diffusion time, i.e., the weld time, dependent. Depending on the material or combination of materials, the welding times are between 1 min and 4 h. The surface of the parts to be joined – placed on the high standards for the rest of parallelism – must be absolutely clean, and oxide films must first be removed by pickling. To prevent the formation of oxide films during the welding at the prevailing high temperatures, the diffusion bonding must be done in a vacuum or carried out under protective gas. At best, the work in vacuum is at 10^{-3} up 10^{-6} mm Hg, as the absorption layers of gases and vapors are largely removed. The vacuum has the disadvantage that a long pumping time is required, and a sealed vacuum chamber must be provided.

6.02.3.2 Friction Welding

During friction welding, the workpieces are moved to the abutting surfaces of each other and, in this case, utilizing the resulting friction and heat deformation under application of force without filler welded.

It is especially suitable for connecting symmetrical shapes with each other or with other moldings, one part is clamped in the chuck of the welding machine, and the other part into the chuck of the spindle. The spindle is set in rotary motion, with the contacting end faces of the parts rubbing against each other and heated by the heat of friction (Figure 52). In the first phase, the friction phase, the temperature increases in the friction surface and a thin surface layer of the two parts on forging temperature. When the plasticity required for welding of the material is reached, the rotation is braked and the pressure is increased. In this second phase, the compression phase, the parts are connected together. Through the upsetting process, plasticized material is extruded in the form of a weld bead, making the parts to be axially shortened somewhat. Figure 53 shows schematically the course of speed, torque, thrust, and upsetting in friction welding.

The process is characterized by a simple operation, and the parameters – speed, pressure, distance – are easy to monitor. For carbon steels (S355), for example, at a speed of $n = 1000$ min^{-1}, a friction pressure of 50 N mm^{-2}, and a compression pressure of 150 N mm^{-2}, within 30 s perfect weld is obtained. Here, the compression is about 5 mm. Another advantage is the low-temperature regime and the pressing of impurities from the weld zone. This proves to be particularly favorable, the possibility to combine parts of various materials together. The compound is formed during the friction in the solid-state diffusion processes across interfaces.

The following are the advantages of friction welding:

- Short welding time
- No additional material required
- High level of accuracy achievable
- Material combinations are possible
- Fully automated procedure
- Good reproducibility
- Good quality of the welding

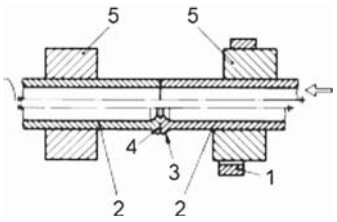

1 Brake
2 Workpiece
3 Flash
4 Weld
5 Clamp

Figure 52 Examples of friction-welded parts of machinery and transport equipment.

www.iran-mavad.com
مرجع مهندسی مواد و متالورژی

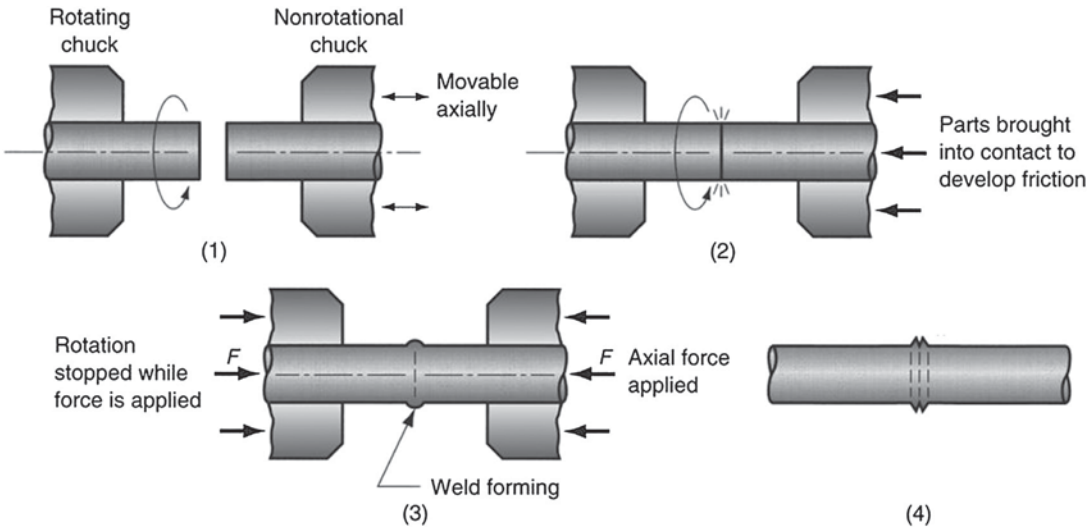

Figure 53 Principle of friction welding process.

The following are the disadvantages of friction welding:

- The occurrence of a weld bead
- Higher investment costs
- It must be admitted to the material balance of the weld bead

6.02.3.3 Ultrasonic Welding

The workpieces are on the abutting surfaces by the action of ultrasound with or without simultaneous heat supply by the use of force preferably welded without filler. Vibrating direction of the ultrasound and the direction of force extend perpendicular to each other whereby the abutting faces the workpieces rub together (Figure 54).

Ultrasonic welding can be considered as a combination of friction and cold pressure welding. The two overlapping parts to be joined are pressed together locally between a fixed anvil and the called sonotrode vibrating tool. By the friction, existing foreign layers are destroyed and surface roughness leveled. Simultaneously, the surface layer of both parts to be joined is heated up to a small depth, so that under the pressure of the contact pressure, the parts are welded together. The welding is preferably carried out in the solid phase by adhesion. The temperature increase, however, is negligible in total, so that an oxidation of the welded material does not occur. The adhesion is supported by diffusion processes and recrystallization. A post-treatment is not required because the material does not distort and leaves no residual stresses.

Ultrasonic welding is used primarily for connecting nonferrous metals; combinations of materials such as Al–Cu, Au–Al, or Al–glass are possible. The main application is the joining of thin films or bands as well as the production of electrically conductive terminals in semiconductor technology (*1,6–12*).

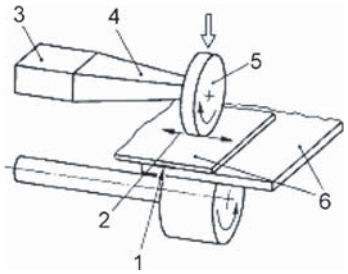

1 Weld
2 Ultrasonic vibration
3 Transducer
4 Sonotrode
5 Vibrating tool

Figure 54 Ultrasonic welding (ISO 857-1).

www.iran-mavad.com
مرجع مهندسی مواد و متالورژی

The joining of thinnest films with thicker parts is also possible. Note, however, that the strength of compounds which were prepared by means of ultrasonic welding cannot be overestimated. The electrical conductivity of these compounds is very good because no recrystallization occurs during welding. Ultrasonic welding is also suitable for welding as well as roll-clad porous metal foams.

See also: Manual Metal Arc Welding and Gas Metal Arc Welding; Robotic Welding Technology; Welding Defects and Implications on Welded Assemblies.

References

1. Fahrenwaldt, H. J.; Schuler, V. *Praxiswissen Schweisstechnik;* Springer Verlag: Kapfenberg, Austria, 2006.
2. ISO Standards, sales@iso.org.
3. Groover, M. K. *Fundamentals of Modern Manufacturing,* 3rd ed.; Wiley, 2010.
4. Cary, H. B. *Modern Welding Technology,* 2nd ed.; Prentice Hall, 1989.
5. Anik, S. Gedik Welding Education Foundation, Istanbul, Turkey, Private Communication, 2012.
6. Killing, R. *Handbuch der Schweißverfahren Teil I: Lichtbogenschweißverfahren* In: *Fachbuchreihe Schweißtechnik,* **Band 76/I**; DVS-Media, 1999.
7. Böhme, D.; Hermann, F. D. *Handbuch der Schweißverfahren Teil II: Autogentechnik, Thermisches Schneiden, Elektronen-/Laserstrahlschweißen, Reib-, Ultraschall- und Diffusionsschweißen.* In: *Fachbuchreihe Schweißtechnik,* **Band 76/II**; DVS-Media, 1992.
8. Anik, S.; Dorn, L. *Schweißeignung metallischer Werkstoffe.* In: *Fachbuchreihe Schweißtechnik,* **Band 122**; DVS-Media, 1995.
9. Killing, R.; Killing, U. *Fachbuchreihe Schweißtechnik.* In: *Kompendium der Schweißtechnik Band 1: Verfahren der Schweißtechnik,* **Band 128/1**; DVS-Media, 2002.
10. Singh, R. *Applied Welding Engineering,* 1st ed.; Elsevier Store, 2011.
11. Olson, D. L.; Siewert, T. A.; Liu, S.; Edwards, G. R. *ASM Handbook; Welding, Brazing and Soldering*, 1993*;* Vol. 6.
12. Anik, S.; Vural, M. *Welding Processes and Equipments;* GEV Publishing: Istanbul, Turkey, 2013.

www.iran-mavad.com
مرجع مهندسی مواد و متالورژی

6.03 Manual Metal Arc Welding and Gas Metal Arc Welding

MA Wahab, Louisiana State University, Baton Rouge, LA, USA

© 2014 Elsevier Ltd. All rights reserved.

6.03.1	**Introduction and General Problem Definition in Welding**	50
6.03.2	**Manual Metal Arc Welding Also Known as Shielded Metal Arc Welding**	51
6.03.2.1	Introduction	51
6.03.2.2	Design Benefits of Welding	51
6.03.2.3	Manual Metal Arc Welding Electrode	51
6.03.2.4	Identification of Electrode Type according to AWS	53
6.03.2.5	Arc Power Source in MMAW	54
6.03.2.5.1	Ion Theory of Arc Column in MMAW	54
6.03.2.5.2	Electron Theory Arc Column of MMAW	54
6.03.2.6	MMAW Welding Circuit	55
6.03.2.7	Power Sources for MMAW	56
6.03.2.8	CC Characteristics	57
6.03.2.9	The Principle of the MMAW Process	58
6.03.2.10	High-Quality Weld Procedures	58
6.03.2.10.1	Essentials for High-Quality Welding	58
6.03.2.11	The Operation Principle	59
6.03.2.12	Applications of MMAW	60
6.03.2.13	The Advantages of MMAW	60
6.03.2.14	The Limitations of MMAW	61
6.03.2.15	MMA Weld Quality	61
6.03.2.16	Safety in MMAW	61
6.03.2.17	Conclusions	62
6.03.3	**Gas Metal Arc Welding Also Known as Metal Inert Gas Welding**	62
6.03.3.1	Introduction	62
6.03.3.2	GMAW Process	63
6.03.3.3	Basic Operation Principle of GMAW	63
6.03.3.4	The Relationships between Current, Wire Feed, and Deposition Rate	64
6.03.3.5	Basic Equipment	65
6.03.3.6	Relationships of Arc Voltage and Arc Length	65
6.03.3.7	The Driving Forces during the Gas Metal Arc Welding Process	67
6.03.3.8	Equipment for GMAW	67
6.03.3.8.1	Welding Power Supplies	67
6.03.3.9	Metal Deposition Rate	68
6.03.3.10	Process Variables	68
6.03.3.11	Control Parameters	68
6.03.3.11.1	Electrode Extension	68
6.03.3.11.2	Electrode Diameter	69
6.03.3.11.3	Arc Voltage	69
6.03.3.11.4	Welding Current	69
6.03.3.12	Shielding Gases	69
6.03.3.13	Important Observations for Shielding Gas	71
6.03.3.14	Metal-Transfer Mechanisms in Gas Metal Arc Welding	71
6.03.3.14.1	Free Flight Transfer	71
6.03.3.14.2	Bridging Transfer	71
6.03.3.14.3	Short-Circuiting Transfer	71
6.03.3.14.4	Globular Transfer	72
6.03.3.14.5	Spray-Arc Transfer	73
6.03.3.14.6	Rotating-Arc Transfer	74
6.03.3.15	Effect of Operating Variables on the Weld Quality	74
6.03.3.15.1	Gas Metal Arc DCEP Welding	74
6.03.3.15.2	Gas Metal Arc DCEN Welding	74
6.03.3.15.3	Use of Alternating Current in GMAW	75
6.03.3.16	Advantages and Limitations	75
6.03.3.16.1	Advantages in GMAW	75

www.iran-mavad.com
مرجع مهندسی مواد و متالورژی

6.03.3.16.2 Limitations in GMAW 75
6.03.3.17 Special Process Features 75
Acknowledgments 75
References 76

6.03.1 Introduction and General Problem Definition in Welding

Welding is a joining process that is being applied to an everwidening range of fabrication activities, from inland, underground, underwater to outerspace in transportation, manufacturing, construction and mining, marine and ship building, oil and gas pipelines, offshore structures, and nuclear structures, etc. In pipeline construction and offshore structures, welding is essential. Welding is a complex process with successful outcomes dependent on a range of input parameters. Often the physical properties of welded joints are critical to structural integrity. Thermal problems, which are associated with welding, are intrinsic and they include induced postweld residual stress and distortion; and altered microstructural properties, which stem from the intense localized nonuniform heating and cooling, applied to the materials during the welding process. Traditionally, management of welding processes has been achieved by experimental, trial and error approaches but, increasingly, computer simulation tools have been applied. Refined numerical tools are the ideal way to test process variations such as weld procedure or preheat conditions; and these may ultimately become the 'virtual' welding machine. Mathematical simulation of welding and related phenomena is termed *computational weld mechanics* (CWM) which is, now, an established and growing field of research endeavor; and one that is significant in international welding research.

Forecasting the thermal cycle during welding is a key step to the prediction of microstructural changes or to the prediction of postweld distortion and locked-in residual stresses. Thermal analysis seeks to calculate the changing temperatures during welding, which is the key input for computational weld mechanics. Thermal modeling may calculate the full thermal field as it varies with time, during welding, as direct output. Then, by using the thermal results as input, further calculations can be used to calculate microstructural changes, induced thermal stresses, and postweld distortions. There exist strong links among the following three segments: thermal response, microstructures, and stress and deformation as indicated in **Figure 1** (*1*).

The inherent complexities must be understood with the various welding processes so that when the welding processes are studied, associated problems must be understood and special attention to details must be placed to alleviate them. To understand fully the inherent complexities in any welding process, the following important aspects must be kept in mind:

1. **Thermal-field prediction**: Weld bead width and weld penetration (depth) from the fusion isotherm. Also, the peak temperature at any point in the workpiece can be observed, as this is often a design constraint.
2. **Postweld properties:** ***Microstructure prediction*** – The microstructure of some metal has important implications on structural failure, creep, and fatigue crack initiation. It also influences material strength and toughness. Thermal history cycle information enables prediction of microstructural changes during welding. Microstructural predictions can be used to determine suitable weld materials, electrode materials, and preheat treatment and postheat-treatment of welded parts.
3. **Hardness prediction**: In steel, the thermal cycle combined with composition determines the heat-affected-zone (HAZ) hardness values, which are influenced by microstructural changes within the HAZ region, a property that strongly affects toughness and weld integrity (*2*).
4. **Postweld distortion prediction**: Thermally induced distortion can happen both during and within postweld conditions. This is particularly relevant when welding large structures such as submarines, offshore structures, and ship-building industries. Modeling is perfectly suited for the investigation of different weld sequences which can be used to minimize the distortion.

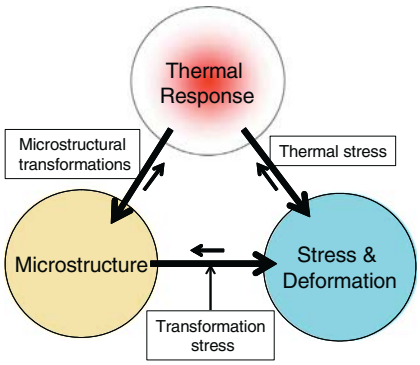

Figure 1 Flow diagram for weld thermal response as primary input into CWM. Reproduced from Karlsson, L. Thermal Stresses in Welding. In Hetnarski, R. B., Ed.; Elsevier Science Publishers, 1986; Vol. 1.

www.iran-mavad.com
مرجع مهندسی مواد و متالورژی

5. **Postweld residual stress (locked-in) prediction**: Peak values can be monitored; also, the level of prestress that will negate the welding residual stress can be calculated. Modeling the welding process has further value in which insight can be gained into the process and driving forces within the arc and the weld pool, which ultimately determines the quality and strength of the weld. The models give a glimpse of the vigorous flow field within the molten weld pool, which is currently difficult to visualize.

In this particular chapter on the manual metal arc welding (MMAW) and gas metal arc welding (GMAW), a general introduction to these two basic welding processes is included; but the intrinsic problems associated with these welding processes must be kept in mind to understand them.

6.03.2 Manual Metal Arc Welding Also Known as Shielded Metal Arc Welding

6.03.2.1 Introduction

At the beginning of the nineteenth century, the electric arc was first discovered by Sir Humphrey Davy in 1801 while he was concerned primarily with the possibilities of the use of the arc for illumination. By 1809, he had demonstrated that it was possible to maintain a high voltage arc for varying periods of time. By the middle of the nineteenth century, workable electrical generating devices were invented and developed on a practical basis and, fortunately, these inventions were the forerunner of the present-day arc welding processes such as MMAW, which is also known as shielded metal arc welding (SMAW) and the second one is gas metal arc welding (GMAW). The first documented evidence of fusion welding was established by Auguste de Meritens in 1881. The bare-metal electrode welding GMAW was introduced in 1888 by N.G. Slavianoff, a Russian. His discovery was first recognized in Western Europe in 1892. In general, welding processes can be classified into three main groups: fusion welding, electrical resistance welding, and solid-phase or cold welding; and among them, fusion welding parts are heated by an electric arc until they melt together without the needed application of additional/external pressure. Both MMAW and GMAW fall into these categories.

6.03.2.2 Design Benefits of Welding

The main objective of welding is to produce a joint in which the valuable properties of the materials being welded are properly utilized for structural integrity of the joint. Many methods of joining two metals have been developed, and the ease and cost of making of the joint and the characteristics and capabilities of the completed joints vary widely. Major advantage of welding is that it has given us the flexibility in design as well as, it produces continuous load path from one member to another with less severe stress-concentration effects and, eventually, enhances the in-service performance under alternating and impact loads. This also gives us freedom from crevices, gaps, and cracks which promote corrosion; and, above all, welding utilizes only a minimum of excess metal.

MMAW is the most widely used welding process in the fabrication industry today and it is also known as SMAW, but commonly called Stick Electrode or Covered Electrode welding, as well.

This is performed manually, hence called manual arc (**Figure 2**) welding process; in this, the heat for welding is generated by an electric arc established between flux-covered consumables, metal rod (electrode), and the workpiece (the two metal components to be joined or welded).

The concept behind fusion welding consists of three basic steps: (1) the members to be joined are prepared and the faying surfaces are placed close together; (2) the joint faces are fused and the space between the faying surfaces is filled with molten metal; and (3) the solidification of the metal joins the members (*3*).

Due to its flexibility to operate in all-welding positions (horizontal, flat, vertical, and overhead), reasonable high weld-deposition rate and with minimal capital cost requirement, this process has been used widely in all sectors. This process is also known as SMAW, as it involves the use of a welding electrode consisting of metal core wire covered with a flux coating outside the metal core. The flux coating is used primarily for shielding the weld-pool area and the electrode from oxygen, nitrogen, hydrogen, and other atmospheric contaminants. For many years, the accepted method of putting large structures together was by arc welding and called stick-electrode welding in the trade. The term stickwelding was used because the coated welding rod was a stick of wire about 12 inches (305 mm) long, covered with flux to provide strong and defect-free welds.

6.03.2.3 Manual Metal Arc Welding Electrode

The welding electrode in MMAW is typically 9 in. to 18 in. (225 mm to 450 mm) long and 1/16 in. to 3/8 in. (1.6 mm to 9.5 mm) in diameter; the shorter lengths are associated with the smaller-diameter electrodes. A bare, uncoated end of the electrode (the grip end) is provided for making electrical contact in the electrode holder. The electrodes used in the MMAW process have many different compositions of core wire and a wide variety of flux-covering types, and weights have been used. The filler metal used in the rod must be compatible with the base metal (workpiece) to be welded, the composition usually being very close to that of the base metal to be welded. The electrode is usually a piece of steel, stainless steel, or aluminum rod that is coated with a flux of a claylike mixture of fluorides, carbonates, oxides, metal alloys, and binders to provide a gas shield for the weld puddle. The coatings outside the welding electrode may consist of powdered cellulose (i.e., cotton and wood powders) mixed with oxides, carbonates, and other

www.iran-mavad.com
مرجع مهندسی مواد و متالورژی

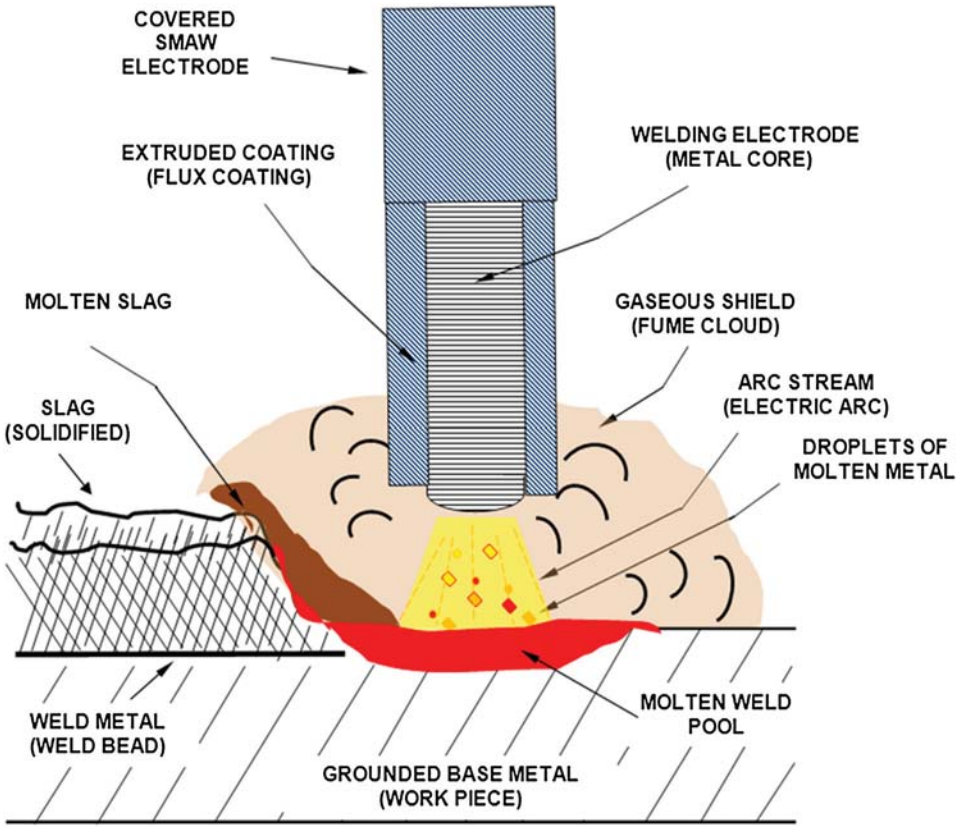

Figure 2 Schematic of manual metal arc welding. Reproduced from Welding Handbook, Vol. 2, Part-1, 9th ed., Welding Processes, American Welding Society (AWS), 2001; Welding Handbook, Vol. 1, 9th ed., Welding Science and Technology, American Welding Society (AWS), 2001.

ingredients held together by a silicate binder. The heat of the welding process melts the coating to provide a protective atmosphere and slag for the welding operation. It also helps to stabilize the welding arc and regulate the rate at which the electrode melts. Metal powders are also sometimes included in the coating to increase the amount of filler metal and to add alloying elements. Most of the nuclear power plants in the United States were welded with low hydrogen electrodes with arc welding machines. Low hydrogen electrodes are important to produce high-quality welds to avoid hydrogen-assisted cracking of the weld joints, which has been a very difficult problem. When the rod is used in welding, the coatings outside the electrode cleans and provides a protective cover for the hot weld bead to protect it from atmospheric contaminations. Oxygen and nitrogen are the main gases which must be kept away from the weld zone. If these gases are kept out of the weld zone, the chances are high that the deposited metal will contain properties that are comparable to those of the base metal and sound weld will be produced. The coating on the electrode burns as the electrode-wire melts from the intense heat of the arc. As the electrode wire melts, the electrode covering or the flux provides a gaseous shield round the arc, preventing contamination.

The arc is generally initiated by momentarily touching or scratching the electrode on the surface of the base metal and the resulting arc melts both the base metal and the tip of the electrode. The molten electrode metal and flux is transferred across the arc by the arc forces to the base metal weld pool, where it becomes the weld deposit covered by the protective, less dense slag from the electrode covering (**Figure 3**). Because of the many possible variations in the composition of the electrode covering and the large selection of core-wire chemistry the process can produce an extensive range of weld metal deposits with desirable mechanical and physical properties, while providing for a smooth arc, and uniform metal transfer characteristics.

The arc welding processes could create several types of weld defects, and weld failures could originate from these locations. Therefore, the welding process must follow the established weld procedures. The MMAW process could be responsible for producing the following general types of weld defects and these are:

Uniformly scattered porosity (poor welding technique or faulty materials), clustered porosity (improper starting or stopping techniques), linear porosity (contamination within the joint, roots, interbead boundaries), piping porosity or wormhole porosity (contamination at the root or gas escaping from the weld pool at the same rate as the pool is solidifying), jagged or irregularly shaped inclusions of nonmetallic materials, slags, oxides etc., inadequate joint-penetration (weld depth is less than that needed to fuse through the plate), incomplete fusion, arc strikes, rollover or overlap, undercut, crater or star cracks, and lamellar tearing, etc. (*4*,*5*).

www.iran-mavad.com
مرجع مهندسی مواد و متالورژی

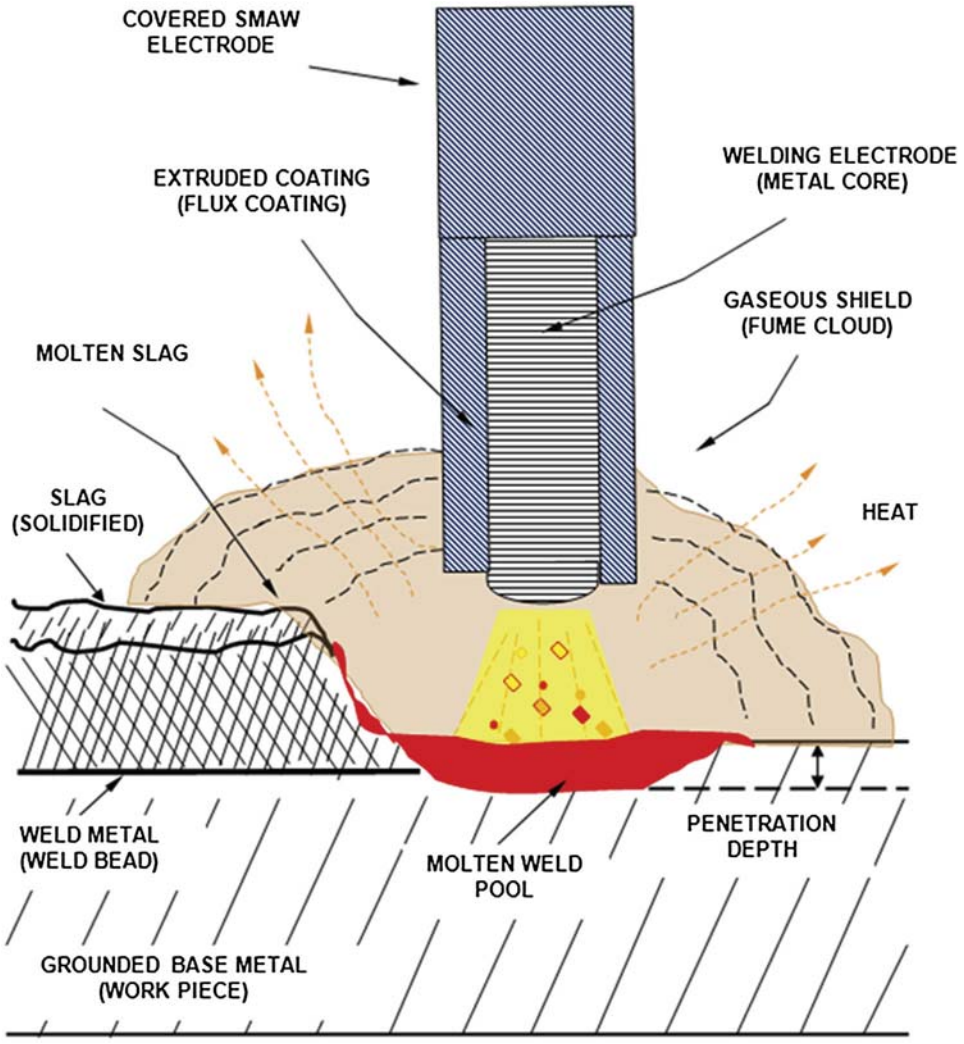

Figure 3 Molten pool in MMAW. Reproduced from Welding Handbook, Vol. 2, Part-1, 9th ed., Welding Processes, American Welding Society (AWS), 2001; Welding Handbook, Vol. 1, 9th ed., Welding Science and Technology, American Welding Society (AWS), 2001.

The MMAW has the advantages of less heat loss and less oxidation than that of the oxyacetylene flame welding. It is one of the simplest welding processes and continues to be widely used. The fluxcoating on the electrode provides the following functions:

- Produces normal carbon dioxide gas from the decomposition of certain coating ingredients to shield the arc and weld zone from the atmosphere;
- Used as deoxidizers for scavenging and purifying the deposited weld metal;
- Used as slag formers, which protects the deposited weld metal from atmospheric oxidation and helps shape the weld bead;
- Used as ionizing elements to make the arc more stable and operate with alternating current (AC);
- Used as alloying elements which provides special characteristics to the weld deposit; and
- Used as iron powder, in certain electrodes, to increase the productivity for welding ferrous metals.

6.03.2.4 Identification of Electrode Type according to AWS

In the United States of America, the American Welding Society has established a system for classifying different types of welding electrodes. All MMAW electrodes have the prefix of letter '**E**' to indicate 'welding electrode.' The symbols that follow the prefix are based on criteria that best describe the welding capabilities of the electrode metal (6). These criteria include: (1) chemical composition of the deposited weld metal, (2) weld-metal mechanical properties, (3) certain process parameters, or combinations of all factors. For mild and low-alloy steel covered-electrodes, the prefix used to identify these electrodes is followed by a number series that indicates minimum strength level, position capability, and type of covering and welding current. In AWS, A5.1, the specification for carbon steel electrodes and AWS, A5.5, the specification for low-alloy steel electrodes for MMAW are described. The first two digits after the E in the E**60**10 electrode designate a tensile strength of at least 62 ksi (430 MPa) for the deposited metal in the

www.iran-mavad.com
مرجع مهندسی مواد و متالورژی

as-welded condition. The third digit (E60**1**0) indicates the position in which satisfactory welds can be made with the electrode. Thus, the '**1**' in E60**1**0, for example, means that the electrode is satisfactory for use in all positions (flat, vertical, horizontal, and overhead). The '**2**' in E60**2**0 indicates that the electrode is suitable for the flat position and horizontal fillets. The last digit or last two digits (E60**10**), taken together, indicate the applicable current type to be used and the type of covering on the electrode.

6.03.2.5 Arc Power Source in MMAW

Two theories have been considered to describe the arc column for MMAW and they are (1) ion theory and (2) electron theory (*7*).

6.03.2.5.1 Ion Theory of Arc Column in MMAW

The arc column is generated between an **anode**, the positive pole of a DC power supply, and the **cathode**, the negative pole shown in Figure 4 to the left. The electrical theory of the arc column is that the ions pass from the positive pole to the negative pole because metal ions are positively charged so they are attracted to the negative pole. The cathode and anode are touched together, and an air-gap is established after they are drawn apart. Ions pass through this air-gap because of their attraction to the negative cathode. They are seeking a negative charge by which to balance the atomic structure disrupted by electricity. As they travel through this air-gap, the ions collide with gas molecules in the atmosphere which produces a thermal ionization layer. This ionized gas column acts as a high-resistance conductor that enables more ions to flow from the anode to the cathode. Heat is generated as the ions strike the cathode.

6.03.2.5.2 Electron Theory Arc Column of MMAW

However, the ion theory mentioned above does not completely explain the arc column; whereas the electron theory of the arc column explains in a better way what happens within the arc column more fully (Figure 5).

Basically, electrons have a small mass (9.1×10^{-28} g) and they are easily disassociated from the metal at the negative pole, or the cathode.

This small amount of negatively charged mass is accelerated away from the cathode to the positive pole, or the anode, striking it at a highly accelerated velocity. This path of the negatively charged mass is generally in the interior of the arc column which is the hotter portion of the arc column. The electrons carry an electrostatic charge, 4.8×10^{-10}. This electrostatic or small current-carrying capacity is multiplied thousands of times, causing part of the heat of the arc column. Another part of the heat liberated by the arc column is directly related to kinetic energy (kinetic energy $= (1/2)mv^2$, where, $m =$ mass of each electron and $v =$ velocity). The electrons accelerate to a high velocity. Their masses are extremely small but there still is a very high amount of energy stored within them. As they strike the anode, heat energy is released. Intermingling with the negatively charged electrons, ions that are positively charged are returning from the anode to the cathode and producing the ionized gas layer which further protects the electrons and the electrostatic unit within the electron. The electrostatic unit is induced into the anode causing in the anode an electromotive (e.m.f.) force, which is directly transferred into the heat energy. The energy or kilowatt hour rating of the arc column is easy to predict because there is a direct relationship between the energy supplied to the arc column and the heat that will be liberated by the arc column.

Because of the characteristics of the electrons and ions in the arc column, three areas of heat are liberated in the arc stream: the cathode area, the plasma area, and the anode area (Figures 4 and 5 above). Of these three areas, the anode area is the high-heat area where approximately 10 000 °F to 11 000 °F of heat is liberated. The liberation of the heat results from the combination of the impingement of the electrons upon the anode anvil and the current-carrying capacity of the electrons. The plasma area is heated mainly as a result of the atomic collision of the few electrons and the many ions that are passing through the ionized gas column. The cathode or the negative pole is subject mainly to ionic bombardment, which produces the state of medium heat in the arc

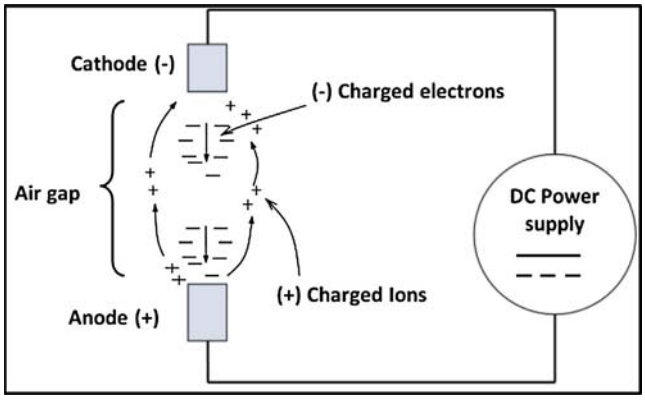

Figure 4 The ion theory of arc column in MMAW. Reproduced from Little, Richard. *Welding and Welding Technology*, McGraw-Hill, 1973.

www.iran-mavad.com
مرجع مهندسی مواد و متالورژی

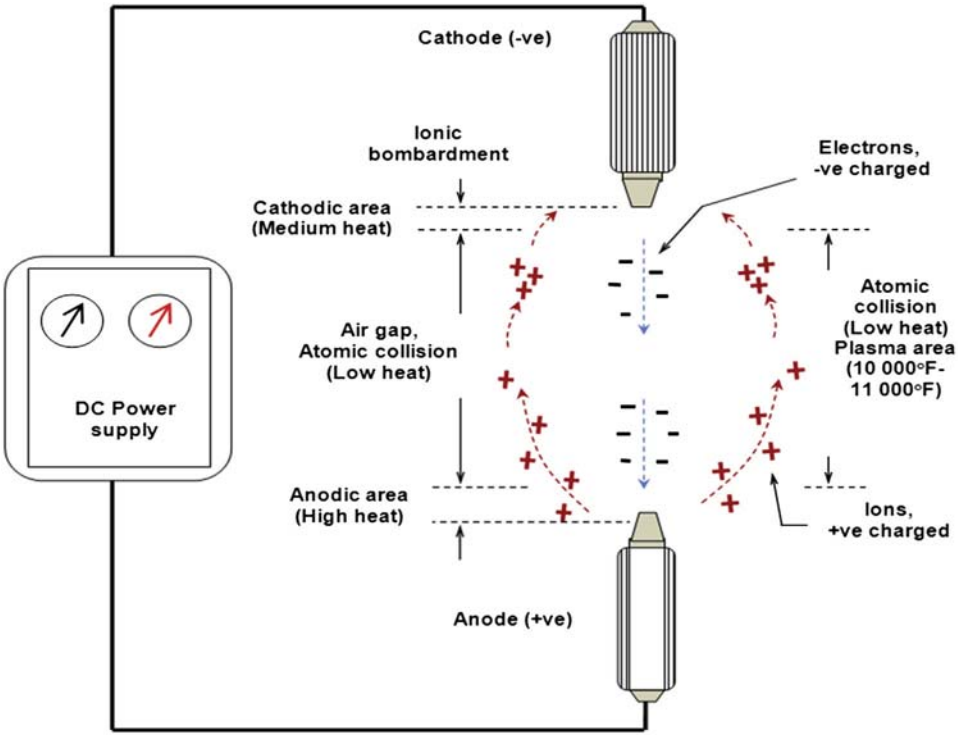

Figure 5 Electron theory arc column in MMAW. Reproduced from Little, Richard. *Welding and Welding Technology*; McGraw-Hill, 1973.

column. The arc is one of the most efficient means for producing heat. Approximately 50% of the electrical energy put into the arc system comes out in the form of heat energy. The major point to remember in the selection of the heat zone is that approximately two-thirds of the energy released in the arc column system is always at the anode, i.e., at the positive pole. This is true in all DC systems.

Another type of arc power source used in MMAW is AC. When an AC power supply is used, the heat in the arc column is generally equalized between the anode and the cathode areas so that the area of medium heat is then in the plasma area (Figure 5).

In welding, electrons are forced from the end of an electrode onto a base metal by an electrical charge. Theoretically, the electrical charge disrupts the flow of the electron in its orbit causing it to fly off at a tangent from its orbital path to seek another positive nucleus to which it will reassociate itself automatically. Metals characteristically release electrons readily, especially when the temperature of the metal is increased. This characteristic is called thermoionic emission. When an atom loses its characteristic electrical balance by the addition or subtraction of electrons from their orbits, it is considered an 'ion.' An atom in an ionized state will seek to rebalance itself to the neutral state by associating with an electron. These reactions result in the flow of electrons and ions in the arc column during welding.

6.03.2.6 MMAW Welding Circuit

The welding circuit consists of a power source; two cables, the electrode cable, and the ground cable; the ground clamp; the electrode holder; the stinger; and the electrodes or rods (Figure 6). The two basic types of power supplies for arc welding are the DC generator rectifier and the AC transformer. Each of these two power supplies has distinct advantages. In DC welding, the electron flow is in one direction; in AC welding, the electron flow is in both directions.

In DC welding, the direction can be changed by simply reversing the cables at the terminals located on the generator. The different settings on the terminals indicate that the electron flow will be either from the electrode to the work, which is the positive ground, or from the work to the electrode, which is the negative ground.

Two-thirds of the heat is developed near the positive pole, while the remaining one-third is developed near the negative pole. As a result, a welding electrode that is connected to the positive pole will burn away at a pace approximately 50% faster than the one that is connected to the negative pole. This is helpful in obtaining the desired penetration of the base metal. If the positive ground is used, the penetration will be greater because of the amount of heat energy supplied by the electrode force to the workpiece. At the same time, the electrode will burn away slowly. If the poles are reversed and there is a negative ground, two-thirds of the heat will remain in the tip of the electrode.

For this reason, the penetration of the heat zone in the base metal will be shallow when compared to the penetration depth of the positive ground arc column. AC combines the characteristics of both the deep penetration and the shallow penetration, yielding

www.iran-mavad.com
مرجع مهندسی مواد و متالورژی

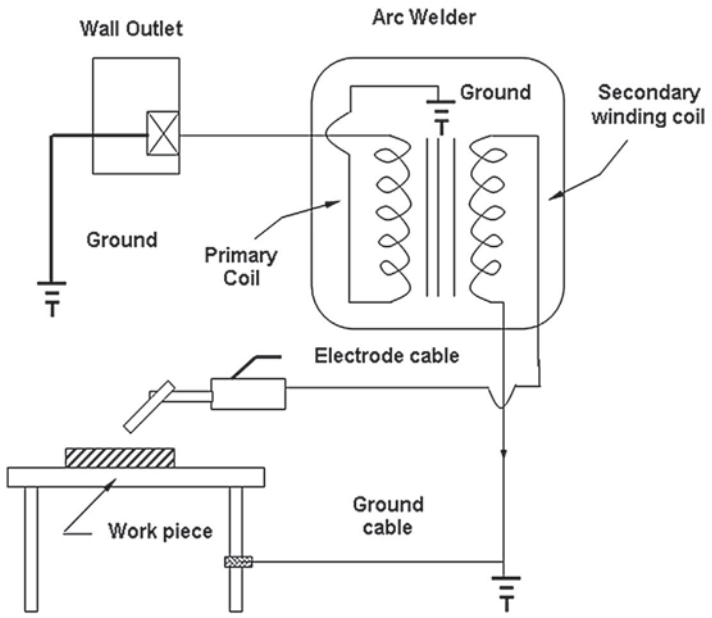

Figure 6 Welding circuit. Reproduced from Little, Richard. *Welding and Welding Technology*; McGraw-Hill, 1973.

a penetration depth that is approximately halfway between that achieved by the DC positive ground and negative ground. The electron flow switches grounds every time the AC cycle changes, yielding a bead penetration depth approximately between the two DC types.

In **straight polarity**, the electrode is negative (DCEN) and the workpiece is positive (Figure 7(a)). The electron flow goes from the electrode into the work piece. When the electrode is positive (DCEP) and the work piece is negative, the electron flow is from the work piece to the anode, which is called **reverse polarity** (Figure 7(b)). When reverse polarity is used, the work piece remains cooler than when straight polarity is used. In both the AC and DC power sources, the arc serves the same purpose.

The welding machine, or power source, is the main equipment of the MMAW process. Its primary purpose is to provide electrical power of the proper current and voltage to maintain a controllable and stable welding arc. Its output characteristics must be of the constant current (CC) type. MMAW electrodes operate within the range from 25 to 500 A, and the operating arc voltage (AV) varies between 15 and 35 V.

6.03.2.7 Power Sources for MMAW

Power sources deliver output current and voltage with the electrical characteristics that make arc welding possible. Two types of power sources are used for MMAW: (1) static machines that convert the energy supplied by electrical power companies and (2) motor generators that combust fuel (chemical energy). The arc welding process requires enough electric current (*Amperage*) to produce melting of the work piece and the metal electrode and the proper voltage (*Volts*) to maintain the arc. Depending on their

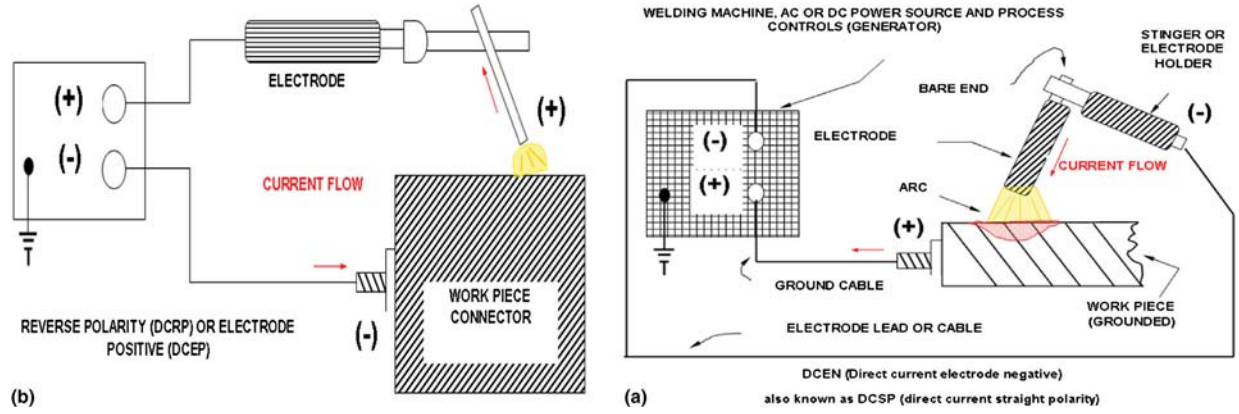

Figure 7 (a) and (b) Circuit diagram for MMAW showing welding circuit and current flow. Reproduced from Bohnart, Edward R. *Welding – Principles and Practices*, 4th ed.; McGraw Hill, 2012.

www.iran-mavad.com
مرجع مهندسی مواد و متالورژی

size and type, electrodes require 15 to 45 V and approximately 30 to 500 A. The current can be alternating or direct, but it must be provided through a source that can be controlled to meet the many conditions encountered on the job. Welding power sources also known as power supplies and welding machines. All machines may be classified by: (1) Output slope, whether CC or constant voltage (CV); and (2) Power source type, such as transformers, transformer-rectifier, inverter, or generator. The preferred power source for MMAW is a CC type with at least 60% duty cycle at the maximum application current. CV power sources are not used with MMAW because the output electrical characteristics require the weld to maintain a constant arc length, which is nearly impossible.

6.03.2.8 CC Characteristics

Open circuit voltage (OCV) and AV: OCV is the voltage generated by the welding machine when no welding is being done. The machine is running idle. AV is the voltage generated between the molten tip of the electrode and the surface of the molten weld pool during welding. It is also referred to as **arc length**. Load voltage is the voltage at the output terminals of the welding machine when an arc is going. Load voltage is the combination of the AV plus the voltage drop in the welding circuit. OCV generally runs between 50 and 100 volts. AV runs between 18 and 36 V. The two OCVs expressed in Figure 8 are approximately 90 V and slightly below 50 V. The AVs range from 32 (long arc) to 22 V (short arc) (*8*,*9*).

OCV drops to AV when the arc is struck, and the welding load is on the machine. AV is determined by the arc length held by the welder and the type of electrode used. When the arc is lengthened, the AV increases and the current decreases. For shortened arc, the AV decreases and the current increases. Note that in Figure 8 there is a difference of 40 A between the long arc and the short arc. Just how much change takes place depends on the OCV setting. Although the total current range between the long arc and the short arc in Figure 8 is 40 A, the range that the two OCVs have in common is only 15 A. The minimum OCV produces a much wider current range than the maximum CV.

OCV on CC machines is higher (about 80 V) than on most CV machines (about 50 V). AV depends on the physical arc length at the point of welding and is controlled by the welder in SMAW.

AV is much lower than OCV: normally about 20 to 30 V for SMAW. There is no voltage adjustment dial on CC welding machines. However, OCV can be adjusted with the fine current adjustment dial on welding machines having dual control. In SMAW, the welder cannot hold the arc length truly constant; rather wide changes in arc length and, therefore, a voltage change will occur. Relatively small changes in current (amperage) result from changes in arc length with a CC machine. Thus the welding heat and burn-off rate of the electrode are influenced very little, and the welder is able to maintain good control of the weld pool and the welding operation.

For applications that involve high welding currents with large-diameter electrodes, a steeper volt–ampere curve is desirable. When more precise control of the size of the weld pool is required – for example, for out-of-position welds and root-passes of joints with varying fit-up configurations – a flatter volt–ampere curve is desirable. The flatter response enables the welder to substantially change the welding current within a specific range simply by changing the arc length. A flat response gives the welder greater control

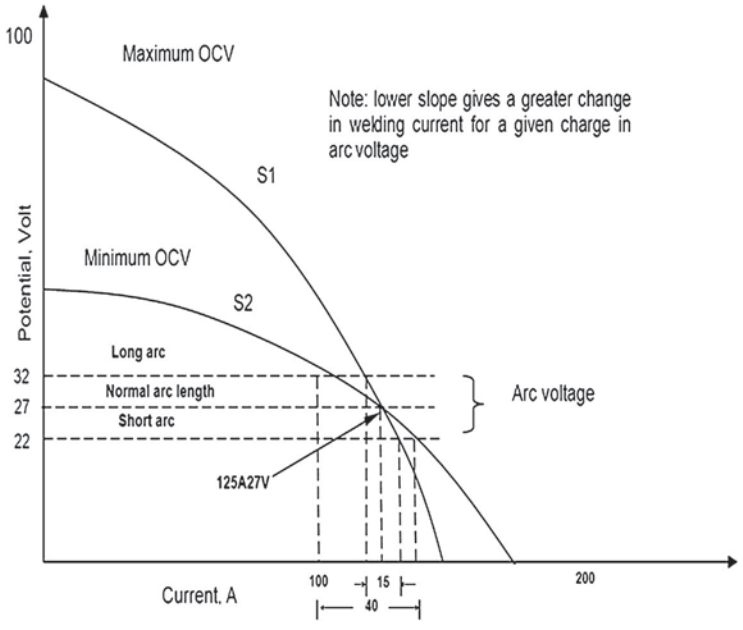

Figure 8 Two possible output slopes for a constant current welding power source. Reproduced from Welding Handbook, Vol. 2, Part-1, 9th ed., Welding Processes, American Welding Society (AWS), 2001; Welding Handbook, Vol. 1, 9th ed., Welding Science and Technology, American Welding Society (AWS), 2001.

www.iran-mavad.com
مرجع مهندسی مواد و متالورژی

over the amount of filler metal that is being deposited. Figure 8 portrays these different volt–ampere curves for a typical welding power source. Even though there are substantial differences in the slope of the various curves, the power source is still considered a CC power source. The changes shown in the volt–ampere curve are accomplished by adjusting both the OCV and the current settings on the power source.

The steep slope (from maximum OCV curve) gives minimum current variation. The flatter slope (from minimum OCV curve) indicates the variation in current by changing the length of the arc. Note that changing the OCV changes the slope of the curve.

6.03.2.9 The Principle of the MMAW Process

The process involves combustion and decomposition of the electrode (covered with fluxcoating), which creates gaseous shields that protect the arc, the electrode-tip, weld puddle or weld pool area, and the highly heated and melted work piece from atmospheric contamination. The decomposition of the flux covering not only generates a shielding gas but also provides fluxing elements (molten slugs), which protect the molten weld-metal droplets and the weld pool. The slug must be completely removed and the weld area cleaned from oxides, residues, etc., before a second weld pass is deposited for multi-pass welding operations. The flux coating also allows several alloy additions to the molten weld metal to improve the weld metal composition and its mechanical properties. There is a wide range of electrode coatings that are available and can be used depending upon the specific application.

For the MMAW, the welding energy sources could be generator, transformer, or transformer-rectifier; the mechanics involved is the stick electrode with flux covering; the molten pool and weld metal shielding is done from the gases and slag from flux coating. High temperature is generated (6000 °F to 10 000 °F) or (3320 °C to 5540 °C) by an electric arc between the electrode-tip and the work piece. The core temperature of the welding arcs varies widely depending on the physical characteristics of the elements in the arc zone. The temperature distribution in the arc varies both radially and longitudinally and the radial temperature gradients depend upon the thermal conductivity of the arc atmosphere leading to different power densities at similar overall power levels. The flux coating on the welding electrode is heated to a gas and liquid, which shield the molten puddle from the atmosphere. The shield prevents the molten puddle from chemically reacting with or being contaminated by atmospheric gases, which can cause hydrogen embrittlement, porosity, and other weld defects. As the weld puddle solidifies the flux also solidifies, forming a coating on the weld bead and protecting it from the atmosphere as it cools down. This resolidified flux, called slag is glass-like, and can then be chipped-off to reveal the weld bead. The arc welding rod sprays molten metal into the molten puddle on the base metal.

Gaseous fluids become electrically conducive at reasonable voltage levels under the following conditions; at ambient pressures the initial resistance must be broken down, usually by high voltage or thermal excitement, and thereafter current can be passed at reasonably low voltages, typically 10 to 20 V. In this situation, which is most applicable to welding arcs, commonly operate within the ranges 20 to 40 V, 10 to 1000 A. The power density of welding arcs is quite high (50 to 100 W mm^{-2}) compared to that of oxyfuel welding. This is a vital characteristic of arc welding processes without which fusion of the metals, with their high thermal conductivity, would be possible only for those with low melting points. The arc itself is a complex mixture of molecules, atoms, and electrons derived from the material of the electrodes and the surrounding atmosphere. The proportions of these species depend on such factors as the degree of dissociation of molecules and of ionization of atoms, both of which are temperature dependent. The term plasma is used to describe this complex fluid which extends between the two electrodes. Metal is transferred to the molten pool from the electrode by the formation of a spray of small droplets. The process may use either AC or direct current (DC) with the electrode connecting to cathode or anode. The current may range from 5 to 500 A and the voltage from 12 to 40 V.

6.03.2.10 High-Quality Weld Procedures

The relationships among the welding parameters such as welding current, electrodes sizes, and the welding position must be understood for correct welding procedures. These parameters must be selected to ensure that the welder has the molten weld pool under complete control at all times during the welding. When weld pool becomes too large, it could become difficult to manage; perhaps allowing molten metal to run out, particularly during out-of-position welding, which would be an option. The steady frying and crackling sound that comes with the use of correct procedures should be maintained during the welding operation. The shape of the molten pool and the movement of the molten metal at the rear of the pool both serve as guides in checking weld quality. The ripples produced on the bead should be uniform and have good side tie-in with no undercut or excessive reinforcement.

6.03.2.10.1 Essentials for High-Quality Welding

The following factors described below are essential for maintaining high-quality welding (5):

1. ***Electrode type*** – Select proper electrode for each job based on the type of base metal, expected service, and mechanical properties required.
2. ***Electrode size*** – Electrode size should depend on the electrode type, welding position, joint preparation, base metal thickness, and skill of the welder.
3. ***Welding current*** – Electrode melts too fast if the current is too high and the molten pool becomes large, irregular, and difficult to control; on the other hand, too, low current will not provide enough heat to melt the base metal, causing the molten pool to be sluggish, with a high, irregular, rope-like weld bead. Generally, electrode has inherent current limits and if the current is too

www.iran-mavad.com
مرجع مهندسی مواد و متالورژی

high, then the core wire overheats and the coating cracks. For current that is too low, there is insufficient heat to maintain the arc and form the protective gas shield.

4. ***Arc length*** – If an arc length is too long, the metal melts off the electrode in large globules that shift from side to side, resulting in a wide and irregular weld bead with considerable spatter, and porosity may form and degradation of the mechanical property may occur. If the arc is too short, then it has insufficient heat to melt the base metal and electrode, which often results in the electrode sticking to the work.
5. ***Travel speed*** – If the welding speed is too fast, that may allow the weld pool to freeze before impurities and gases can escape, and the bead will be narrow and inadequate in size, whereas for speeds that are too slow the metal piles up and the bead is larger than required.
6. ***Electrode angle*** – In fillet welding and deep groove welding, the electrode angle is important. When making a fillet weld the electrode should be held so that it equally divides the angle between the plates and is perpendicular to the line of the weld so that heat is distributed uniformly to both weld areas. When undercut occurs in the vertical member, the angle should be lowered and the arc directed toward the vertical member.
7. ***Arc manipulation*** – When weaving is expected, the width of the weave and the pause at the ends of the weave become important. The welder must pause at each end of the weave to allow adequate fill buildup and fusion to occur. The welder should also quickly move across the center of the weld, because heating is more concentrated in the center than at the edges.
8. ***Breaking the arc*** – Before an arc is broken, it is important to know whether it will be reestablished with the next electrode and the weld continued or whether it is the end of a weld pass. For continuation of welding the crater should remain and the arc quickly broken off; but if it is the end of a weld pass, the arc should not be broken off until the crater has filled.
9. ***Interbead cleaning*** – Proper interbead cleaning for deslagging is essential for the production of high-quality welds which prevents slag inclusions, lack-of-fusion defects, and porosity (**Figure 9**).

6.03.2.11 The Operation Principle

In the past, most electrodes were bare/wire and with these bare electrodes, the arc was difficult to control and cooled too quickly; as a result, the weld bead absorbed oxygen and nitrogen from the atmosphere, which turned into oxides and nitrides producing a brittle, weak weld.

The force of the arc column striking the work piece digs a crater in the base metal which fills with molten metal (**Figure 9**). As the flux melts, part of it mixes with the impurities in the molten pool causing them to float to the top of the weld. When this mixture of impurities and flux cools, it forms slag, which also does its part to improve the weld. It protects the bead from the atmosphere and causes the bead to cool more uniformly. The slag also helps to design the contour of the weld bead, itself, by acting as an insulator. By insulating the HAZ, located in the parent metal or the base metal and completely surrounding the weld bead, the slag allows an even rather than erratic heat loss from this HAZ, thus helping to control the crystal or grain size of the metal. The arc column reaches temperatures generally of 5000 to 7000 °F, which have a harsh effect on the parent metal. The molten pool, which must maintain a temperature of approximately 2800 °F, radiates heat outward and changes the crystals surrounding the weld bead. Many times, after welding, the part must be heat-treated to change the size of the grains in the weld bead and the surrounding area. The heating of the base metal by the arc stream and the resultant molten weld puddle or crater generally extend deep into the base metal. The extent of the HAZ can be observed by studying the crystalline structure of the base metal in this zone. It is generally represented by a large grain. The grains in the unaffected areas of the metal are smaller. Because of the protection of the flux, the weld bead itself has medium-sized grains that extend to large grains at deeper penetration. It is not necessary to heat-treat mild steel; but, with many metals, this heating will result in locked-in residual stresses that must be relieved either through peening or further heat treatment of the entire piece of metal.

During the operation of the bare metal end of the welding electrode (opposite the welding tip) is clamped in an electrode holder that is connected to the power source. The holder has an insulated handle so that it can be held and manipulated by a human welder. Currents typically used in MMAW range between 30 and 500 A at voltages from 15 to 45 V. Selection of the proper power parameters depends on the metals being welded, electrode type and length, and depth of weld penetration required.

The arc is an electrical discharge or spark sustained in a gap in the electrical circuit. The resistance of the air or gas in the gap to the passage of the current transforms the electrical energy into heat at extremely high temperatures. Electrical power consists of amperage and the voltage. The amount of energy available is the product of amperage and voltage flowing through the circuit and is measured in watts and kilowatts. The energy used is affected by such variables as the constituents electrode coatings, the type of current (AC or DC), the direction of current flow, and many other factors.

In the modern arc welding process, the arc is shielded to control the complex arc phenomenon and to improve the physical properties of the weld deposit. This shielding is accomplished through various techniques: a chemical coating on the electrode wire, inert gases, granular flux compounds, and metallic salts placed in the core of the electrode. Arc shielding varies with the type of arc welding process; such as in MMAW welding, a consumables covered electrode is used. In all cases, the shielding is intended to (1) protect the molten metal from the air either with gas, vapor, or slag; (2) to add alloying or fluxing ingredients; and (3) to control the melting of the rod for more effective use of the arc energy. The arc welding process requires a continuous supply of electric current sufficient in amperage and voltage to maintain an arc – this current may be either AC or DC; but it must be provided through a source which can be controlled to satisfy the variables of the welding process: amperage and voltage.

www.iran-mavad.com
مرجع مهندسی مواد و متالورژی

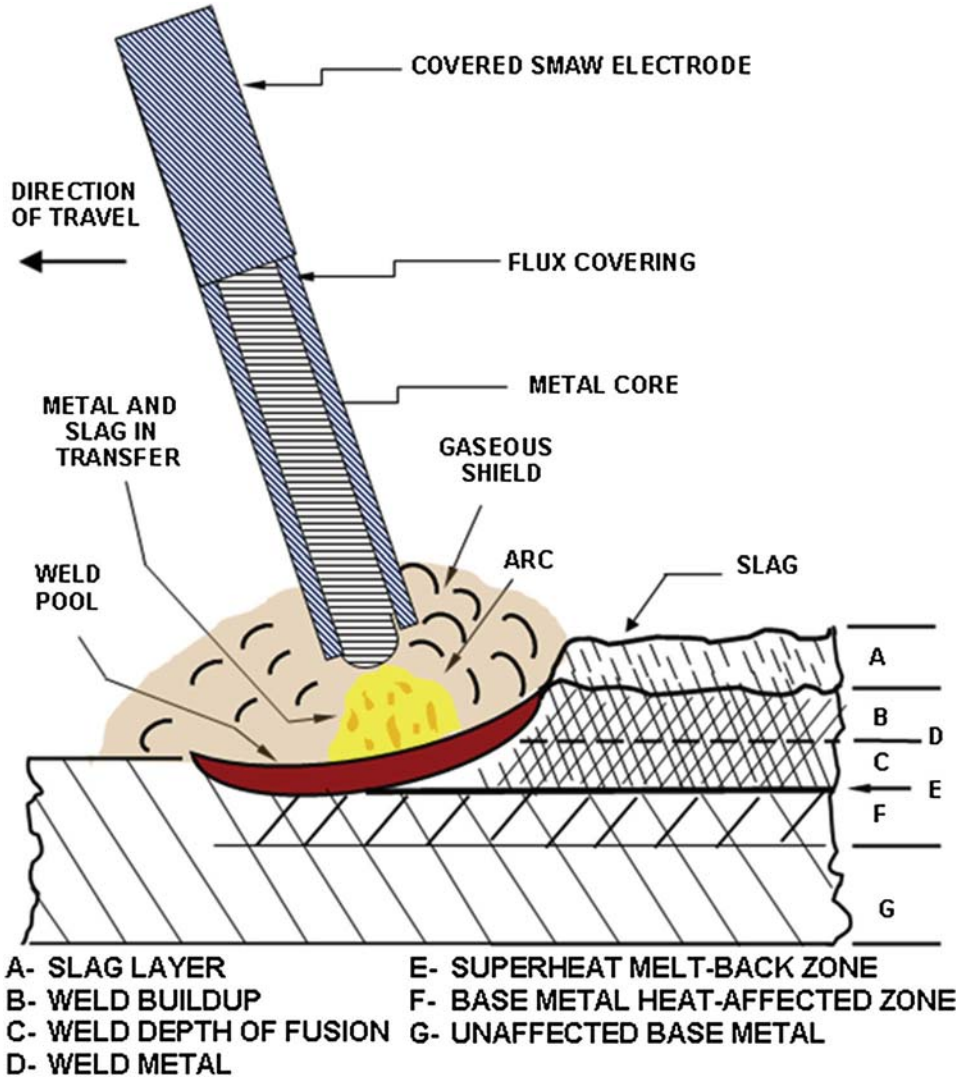

Figure 9 Schematic of MMAW. Reproduced from Welding Handbook, Vol. 2, Part-1, 9th ed., Welding Processes, American Welding Society (AWS), 2001; Welding Handbook, Vol. 1, 9th ed., Welding Science and Technology, American Welding Society (AWS), 2001.

6.03.2.12 Applications of MMAW

The MMAW is performed manually. The common applications include construction, pipelines, machinery structures, shipbuilding, fabrication job shops, and repair work. It is preferred over oxy-fuel gas welding for thicker sections above 3/16 in. (5 mm) because of higher power density (PD = (Voltage × Welding current)/Weld area) available in this process. The equipment is portable and of low cost, making MMAW highly versatile and probably the most widely used arc welding processes. Base metals used include steels, stainless steel, cast irons, and certain nonferrous alloys. The MMAW process is used for welding virtually all steel types and many nonferrous alloys, but it is primarily used to join steels which include low carbon or mild steels, low-alloy steels, high-strength steels, quenched and tempered steels, high-alloy steels, stainless steels, and many of the cast irons. This process is also used to join nickel and its alloys, and to a lesser degree, copper and titanium and its alloys. It can be, but rarely, used for welding aluminum. In addition to joining metals, this process is frequently used for the protective surfacing of base metals for the purpose of corrosion control or wear resistance (hardsurfacing).

6.03.2.13 The Advantages of MMAW

- Simple in terms of equipment requirements and low capital cost, the equipment is portable, and the process has reasonably high weld-deposition rates;
- High flexibility in the operation that is not restricted by component geometry and welding positions;
- Welding electrodes are available for virtually all manufacturing, constructions, and maintenance applications;

www.iran-mavad.com
مرجع مهندسی مواد و متالورژی

- The process has innumerable applications because of the availability of the wide variety of electrodes;
- The process can be employed for hardfacing and overlay/metal deposition to reclaim parts or to develop other characteristics like wear resistance, etc.;
- Good metallurgical control of weld metal compositions; and
- Joints that are difficult to reach and have limited accessibility to weld by automatic welding machines are easily accomplished by his process. It has the flexibility of all the welding processes, because it can be used in all welding positions (flat, vertical, horizontal, and overhead), with a wide range of base-metal thicknesses, 1/16 in. (1.6 mm and greater).

6.03.2.14 The Limitations of MMAW

- Each weld run must be thoroughly deslagged before a subsequent pass is made; the deslagging process may include chipping, wire brushing, and electrode replacement, etc., which reduces the **duty cycle** (operator factor by the welder = (arc time/total time)). This electrode replacement and cleaning operation occurs many times during the work day (about every 2 min, or the time it generally takes to consume an electrode of certain length).
- Electrode baking and storage procedures are necessary to avoid hydrogen cracking in hardenable materials.
- The success of good weld quality depends on the welder's skill – this is basically a manual process and the skill level of the welder is important in producing an acceptable weld.
- Because of the limited length of each electrode and brittle flux coating on it, mechanization is difficult.
- Because of the limited length of the electrode, when one electrode finishes, the process has to be stopped and restart again with another new electrode; and special care must be taken to make the weld run continuously and defect free. As the electrodes are used up, they must periodically be changed. This reduces the arctime with this welding process.
- Because of the flux coated electrodes, the chances of slag entrapment and other related defects are higher as compared to other similar processes such as GMAW.
- Another limitation is the current level that can be used, because the electrode length varies during the operation and this electrode length affects the resistance heating of the electrode; and current levels must be maintained within a safe range otherwise the coating will overheat and melt prematurely when starting a new welding stick.

6.03.2.15 MMA Weld Quality

The quality of the weld depends on the joint design and accessibility of the joint, as well as, on the electrode, the technique, and the skill of the welder. If the joint details vary greatly from the established joint-design details, then a lower-quality weld can result. Other factors that also could reduce quality are improper interbead cleaning, poor location of individual weld beads within the joint, and various problems with individual electrodes, including partially missing flux, and core wires that are not centered within the flux covering. Generally, weld quality depends on the skill of the welder and the technique used by the welder.

The base-metal thicknesses that can be welded using the MMAW process generally range from 1/16 in (1.6 mm) to a large unlimited thickness. The thinner materials require a skill welder, tight fit-up, and the proper small-diameter welding electrode. Welding position also is important when determining the minimum plate thicknesses that can be welded. Flat-position butt welds and horizontal fillet welds are generally considered the easiest to weld, but out-of-position welding such as vertical and overhead welding requires greater skill.

6.03.2.16 Safety in MMAW

The MMAW process has a number of potential hazards. All MMAW electrode containers must carry a warning label to alert welders of the safety concern that identifies the three most common safety hazards in the following terms:

- *Electric shock* can be dangerous and it could also be fatal. Accordingly, electrically live-parts or electrodes must not be allowed to come in contact with human skin or wet clothing and wet gloves. The welder must insulate himself/herself from the work piece and the ground.
- *Fumes and gases* can be dangerous to health and these must be kept away from the breathing zone and general areas through proper ventilations or with safety equipment. The welder's head must be out of the fume areas and enough ventilation or exhaust at the arc, or both, must be provided.
- *Arc rays* can injure eyes and burn skin and the welder must wear correct eye, ear, and body protection. Even though the major portion of the arc column is shielded and the flux covers the solidifying portion of the weld, the light that is given off from the arc column is harmful to the eyes. Therefore, head shields are used to protect the welder from radiation. Lenses for eye protection are extremely important because large quantities of infrared and ultraviolet radiation are given off by the arc. This radiation can burn the retina and even cause third-degree burns on the skin. All good welding lenses generally stop 99.5% of the infrared and ultraviolet rays. Although the visible light given off by the arc does not contain harmful rays, it is uncomfortable to the eye and will cause blurred vision.

In addition to the general warnings on the container, further detailed information relating to safety is contained in ANSI/AWS Z49.1, *Safety in Welding and Cutting*.

www.iran-mavad.com
مرجع مهندسی مواد و متالورژی

6.03.2.17 Conclusions

This long established MMAW is widely available and has been used heavily in many operations and a wide range of consumables are also available to suit individual applications using this process. Although the process has an inherently low duty cycle (indicates the proportion of the operating time during which welding is actually being done), and needs a fairly high degree of skill from the welder to produce high-quality and defect-free welds; but in many circumstances it still proves to be the chosen method, especially at some critical locations where automatic machines cannot reach. However, the tremendous pressures for high productivity are steadily reducing the proportion of the work done with flux-covered MMAW. The duty cycle in MMAW operations varies widely with the type of application and operating conditions. In most welding shops using MMAW as the principal welding process, duty cycles below 30% are common. Where conditions allow the use of electrodes with flux formulations to give good slag detachability, interrun deslag, and cleaning times can be reduced such that even a 50% duty cycle can be achieved. However, incentive must exist for welders to achieve and maintain this high welding rate. Where welding requires intermittent chipping of adhered slag and grinding between weld runs, the duty cycle may fall even below 10%. Much has been done to assist welders to increase their duty cycle, electrode formulations to give spatter-free welds, and self-detaching slags being one such example.

6.03.3 Gas Metal Arc Welding Also Known as Metal Inert Gas Welding

6.03.3.1 Introduction

GMAW is a welding process which joins metals by heating the metals to their melting point with an electric arc and the arc is struck between a continuous, consumable bare (not covered) electrode wire and the work piece; whereas the arc is shielded from atmospheric contaminants by a shielding gas. The shielding is accomplished by flooding the arc, melted end of the metal-electrode, and weldpool area with a shielding gas. The bare wire is fed continuously and automatically from a spool through the welding gun, Figure 10 illustrates the schematic representation of the GMAW process.

The basic concept of GMAW was introduced in the 1920s; however, the process did not become commercially available until 1948; implemented as a high-current-density, small-diameter, 'bare-metal-electrode' process using an inert gas for arc-shielding.

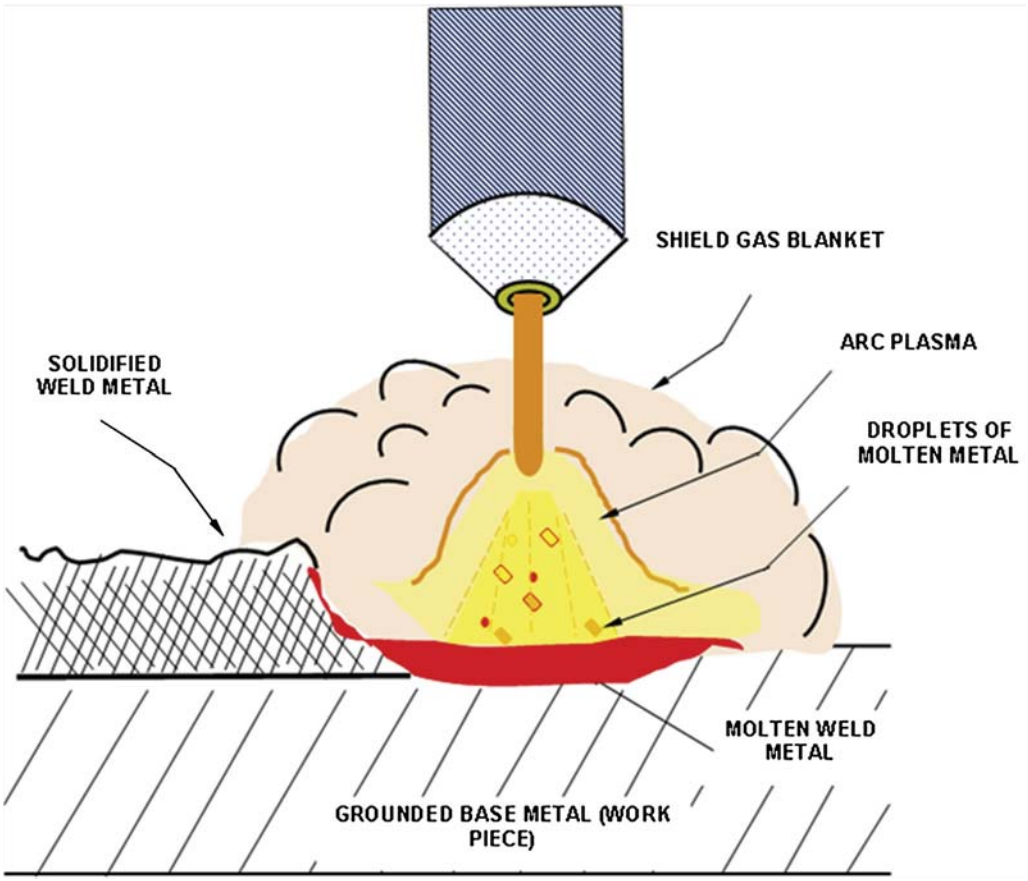

Figure 10 Schematic of GMAW. Reproduced from Jeffus, Larry. *Welding Principles and Applications*; Delmar Publisher, Inc., 1993.

www.iran-mavad.com
مرجع مهندسی مواد و متالورژی

As a result, the process was called metal inert gas welding. The GMAW was primarily used for welding aluminum, but subsequent process developments included operation at low current densities and pulsed current, application to a broader range of materials, and the use of reactive gases (particularly, CO_2) and other combination of gas mixtures.

The process uses both inert and reactive gases as shielding gases. The various metals on which GMAW is used and the variations of the process itself have given rise to a variety of names for GMAW. When this same welding process was applied to steel, it was found that inert gases (argon and helium) were expensive and a reactive gas, CO_2, was used as a substitute; hence the term **CO_2 welding** was applied. Refinements in GMAW for steel welding have led to the use of gas mixtures, including CO and argon, and even oxygen and argon. Small quantities of oxygen (up to 5%) are sometimes mixed with argon. Properly blended mixtures result in smoother arc performance, less spatter, and enhanced wetting (i.e., spreading and adhering) of the weld to the base metal. Some mixtures have been standardized and are commercially available in cylinders. Selection of gases (and mixtures of gases) depends on the metal being welded, as well as other factors. Inert gases are used for welding aluminum alloys and stainless steels, while CO_2 or a mixture of argon/carbon dioxide is commonly used for welding low and medium carbon steels. The combination of bare electrode wire and the shielding gases eliminates the slag covering on the weld bead and thus precludes the need for manual grinding and cleaning of the slag from the deposited weld zone. The GMAW process is, therefore, ideal for making multiple weld-passes on the same joint, and a much higher production rate is achievable.

GMAW is used for a wide variety of applications in the fields of industrial manufacturing, agriculture, construction industry, shipbuilding, marine and ground vehicle industries, and mining. The process is used in building construction weld pipe, pressure vessels, structural steel components, furniture, automotive components, and numerous other products. All commercially important metals including carbon steel, high-strength low-alloy steel, stainless steel, aluminum, copper, titanium, and nickel alloys can be welded in all positions with GMAW process by choosing the appropriate combination of shielding gas, electrodes, and welding variables.

GMAW can be achieved in three different ways:

1. Semiautomatic welding – equipment controls only the electrode wire feeding. Movement of welding gun is controlled by hand. This may be called hand-held welding.
2. Machine welding – uses a gun that is connected to a manipulator of some kind (not handheld). An operator has to constantly set and adjust controls that move the manipulator.
3. Automatic welding – uses equipment which welds without the constant adjusting of controls by a welder or operator. On some equipment, automatic sensing devices control the correct gun alignment in a weld joint.

6.03.3.2 GMAW Process

When the atoms at the edge of one piece of metal come close enough to the atoms at the edge of another piece of metal, interatomic attraction develops and the two pieces become one through the welding process. Although the principle concept is quite simple, the reality is quite difficult to achieve since surface roughness, impurities, fitting imperfections, and the varied properties of the materials being joined complicate the joining process. Welding processes and procedures have been developed to overcome these difficulties by incorporating the use of significant heat or pressure, or both. In GMAW, only the significant heat is being used to achieve the process of joining two materials. This heat becomes a means to bring the atoms at the edge of one piece of material close enough to the atoms of another piece for inter-atomic attraction.

However, this heat is detrimental to the microstructure of the materials being joined, as hot metal tends to oxidize. Therefore, sufficient protection from oxidation must be provided by the welding process to prevent this detrimental reaction with ambient oxygen. Some metals are far more sensitive than others, in which case, protection from oxidation becomes more demanding. Thus, for each welding process, the process by which the heat is produced must be considered and the means by which sufficient protection against oxidation is provided by the process should then be identified. This must be strictly followed through for GMAW process.

In GMAW, an electric arc is used as the source of heat. The creation of a weld between metals using the GMAW process does not involve pressure but utilizes a consumables continuous filler metal electrode. The arc is struck between the work piece and the electrode tip while the intense heat produced by the arc, quickly melts a portion of the base metal and the electrode, resulting in the formation of a weld. The arc welding process may be moved along the joint to produce the weld or the arc is held stationary, while the work piece is moved under the process.

6.03.3.3 Basic Operation Principle of GMAW

The GMAW process utilizes the automated feeding of a continuous, bare, consumable electrode that is shielded by an externally supplied shielding gas. The process is shown schematically in **Figure 11**. After the initial settings on the welding machine, the equipment provides for automatic self-regulation of the electrical characteristics of the arc. The only actions controlled by the welder for semiautomatic operations are the travel speed, weld direction, and the gun positioning. Given the proper equipment and settings the AV and the wire-feed speed (current) are automatically maintained.

During welding, all materials experience high elevated temperatures and react with oxygen and nitrogen, and exclusion of air from the weld zone by a stream of compatible gas (shielding gas), which forms the basis of this GMAW processes. In this process the

www.iran-mavad.com
مرجع مهندسی مواد و متالورژی

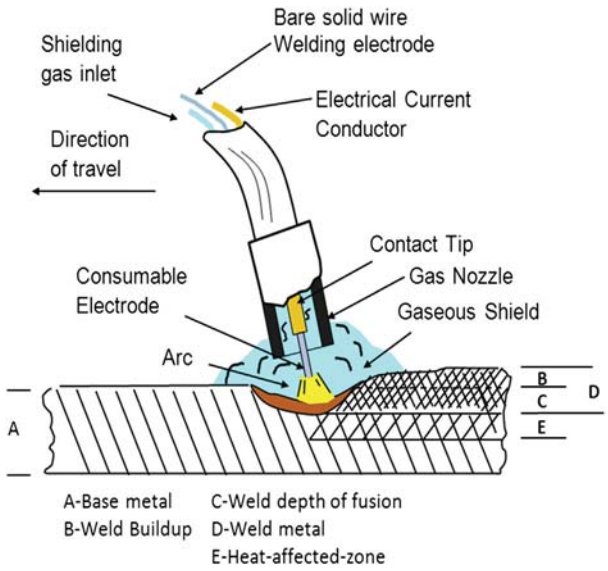

Figure 11 GMAW process. Reproduced from Welding Handbook, Vol. 2, Part-1, 9th ed., Welding Processes, American Welding Society (AWS), 2001; Welding Handbook, Vol. 1, 9th ed., Welding Science and Technology, American Welding Society (AWS), 2001.

electrode from which the arc is struck by contacting or scratching the work piece is consumed during welding. Electrode wire diameters ranging from 1/32 in. to 1/4 in. (0.8 mm to 6.5 mm) are commonly used in GMAW, the size depending on the thickness of the parts being joined and the desired weld metal deposition rate. The gun guides the consumable electrode, conducts the electrical current, and directs shielding gas to the work piece.

This provides the means to establish and maintain the arc, melt the electrode, and provide the needed protection from the ambient atmosphere. One of two combinations of electrode feed units and power sources may be used to achieve the desirable self-regulation of arc length. Most commonly, a constant-voltage power source is used in conjunction with a constant-speed electrode feed unit to regulate arc length. Conversely, a constant-current power source is coupled with an electrode feed unit that is arc-voltage controlled.

With the constant-voltage, constant wire-feed combination, changes in the gun position causing a change in the welding current due to a change in the electrode extension. For example, when the gun-to-work piece distance is suddenly increased, the arc length momentarily becomes longer. The longer arc length causes a reduction in current, momentarily reducing the electrode melt-off rate. Since the feed rate remains the same, the arc length decreases and the current increases until the melt-off rate again equals the feed rate. The final current at the longer extension is lower than that resulting from the shorter extension with a slightly longer arc length. In effect, the resistance heating (I^2R) of the electrode extension has increased and arc heating at the electrode-tip has decreased. Consequently, the arc heating of the work piece, as well as weld penetration, is decreased. The opposite occurs if the gun-to-work piece distance is suddenly decreased.

The constant-current, arc-voltage control wire-feed combination results in self-regulation: AV fluctuations readjust the control circuits of the wire feeder, which appropriately adjusts the wire-feed speed. For welding aluminum, it may be preferable to deviate from these standard combinations and couple a constant-current power source with a constant-speed electrode feed unit. This combination provides only a small degree of automatic self-regulation and, therefore, requires more operator skill in semiautomatic welding.

With the various choices of arc modes, the wide range of electrode sizes, and the various shielding gas mixtures available, the GMAW process can be used to weld many ferrous and nonferrous metals. These metals can range in size from 0.020 in (0.5 mm) thin-gauge sections to any desired plate or pipe section thickness. With the proper procedure, welding can be performed in all positions. If the variables are properly balanced, less skill is required for the GMAW than for the arc welding processes.

GMAW employs either a solid electrode wire or an electrode with a core of powdered metal. A variety of ferrous and nonferrous alloys are available. It is economically advisable to use the largest-sized electrode wire wound on the largest-sized spool, coil, or drum practical for the application.

6.03.3.4 The Relationships between Current, Wire Feed, and Deposition Rate

A significant variable in this GMAW wire-fed process is the distance the electrode protrudes past the end of the contact-tip to the work piece, termed electrode extension. The electrode is a small conductor and, therefore, has high electrical resistance. If the extension of the electrode increases even a fraction of an inch in a constant-voltage system, the current decreases rapidly because more current is used to preheat the electrode. The current is a function of wire-feed speed and electrode-extension. The current varies

www.iran-mavad.com
مرجع مهندسی مواد و متالورژی

directly with wire-feed speed but inversely with electrode-extension. The deposition rate on the other hand is a function of the wire-feed speed only; therefore, if the wire-feed is constant, the deposition rate is constant even though the current changes as the electrode-extension changes.

6.03.3.5 Basic Equipment

The basic equipment and accessories used in GMAW are mentioned below. In semi-mechanized welding the operator holds the welding gun, controlling its attitude, extension, and travel speed along the joint. Alternatively, the gun can be mounted on a carriage with an adjustable speed control and moved along the joint at the desired travel speed.

The basic equipment for a typical GMAW semiautomatic setup includes the following:

1. Welding power source – provides welding power;
2. Electrode – wire feeders (constant speed and voltage-sensing) – controls supply of wire to welding gun.
   (a) Constant speed feeder – Use only with a CV power source. This type of feeder has a control cable that will connect to the power source. The control cable supplies power to the feeder and allows the capability of remote voltage control with certain power source/feeder combinations. The wire feed speed (WFS) is set on the feeder and will always be constant for a given preset value.
   (b) Voltage-sensing feeder – Can be used with either a CV, CC, or DC power source. This type of feeder is powered-off of the AV and does not have a control cord. When set to CV, the feeder is similar to a constant speed feeder. When set to CC, the WFS depends on the voltage present. The feeder changes the WFS as the voltage changes. A voltage sensing feeder does not have the capability of remote voltage control.
3. Supply of electrode wire.
4. Welding gun – delivers electrode wire and shielding gas to the weld puddle. This could be air or water-cooled.
5. Shielding gas cylinder – provides a supply of shielding gas to the arc.
6. Miscellaneous items include welding control unit, cables and hoses, water circulation system, etc.

Figure 12 above shows the molten droplets from the electrode tip to the weldpool depicting how the molten droplets add to the weldpool.

6.03.3.6 Relationships of Arc Voltage and Arc Length

The terms 'arc voltage' and 'arc length' are often used interchangeably. However, these terms have different connotations even though they are directly related. With GMAW, the arc length is a critical variable that must be carefully controlled. For example, in the spray-arc metal transfer mode (discussed below) with argon shielding, too short-arc experiences momentary short-circuit. These short-circuits cause pressure fluctuations, pumping air into the arc stream, producing porosity or embrittlement due to absorbed nitrogen. For too short-arc the electrode-tip short-circuits the weld pool, causing instability.

For too long arc, it tends to fluctuates and wander; affecting both the penetration and the surface bead profiles and disrupts the gas-shield. In the case of a buried-arc with a carbon-dioxide shield, a long-arc results in an unburied condition and produces excessive spatter and porosity.

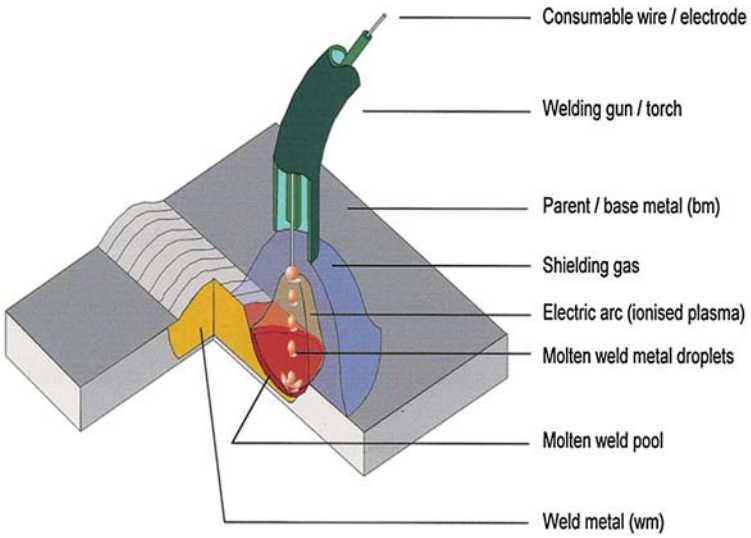

Figure 12 Shows the molten droplets from the electrode tip to the weldpool.

www.iran-mavad.com
مرجع مهندسی مواد و متالورژی

AV depends on the arc length, the electrode composition and dimensions, the shielding gas, the welding technique, electrode extension, and even the length of the welding cable, since AV often is measured at the power source, as well as many other variables. As shown in Figure 13, AV is an approximate means of stating the physical arc length in electrical terms even though the measured AV also includes the voltage drop in the electrode extension beyond the contact tip. With all variables held constant, AV is directly related to arc length. Even though the arc length is the variable and should be controlled, the voltage is more easily monitored. The requirement being that the AV be specified in the welding procedure, the term AV is commonly used.

AV settings vary depending on the material, shielding gas, and transfer mode. Trial runs are necessary to adjust the AV to produce the most favorable arc characteristics and weld-bead appearance. Trials are essential because the optimum AV is dependent upon metal thickness, the type of joint, welding position, electrode size, shielding gas composition, the type of weld as well as several other factors. From any specific value of AV, a voltage increase tends to flatten the weld-bead and increase the width of the fusion zone. Excessively high voltage may cause porosity, spatter, and undercut. A reduction in voltage results in a narrower weld bead with a higher crown and deeper penetration. Excessively low voltage may cause the ***stubbing*** of the electrode, a condition in which the electrode dips into the weld pool and then solidifies into place due to the lack of a short-circuit current. From any specific value of AV, an increase tends to flatten the weld bead and increase the width of the fusion zone. Excessively high voltage can cause porosity, spatter, and undercut. A reduction in voltage results in a narrower weld bead with a higher crown.

GMAW is widely used in fabrication operations in factories for welding a variety of ferrous and nonferrous metals. Because it uses continuous filler weld wire rather than welding sticks, it has a significant advantage over MMAW in terms of arc-time when performed manually. For the same reason, it also lends itself to automation of arc welding. The electrode stubs remaining after stick welding also become waste filler metal, so the utilization of electrode material is higher with GMAW. Other features of GMAW include no elimination of slag removal required (since no flux is used in GMAW), therefore higher deposition rates than SMAW with good versatility can be achieved.

The electric arc is formed in a shielding gas between a continuously fed metal wire electrode and the work piece, current being applied to the electrode as it passes through a copper contact tube. The details of the torch and arc region for GMAW are shown in Figure 13. In the GMAW process, the electrode diameters are significantly smaller than in MMAW, so that the arc energy is very concentrated near the axis, giving a deep-penetrating characteristic. It can be used as either a manual or mechanized technique in a number of applications depending on material type, thickness, and welding positions. Generally, high deposition rates can be achieved by a mechanized operation at which the consumable electrode is fed continuously into the welding arc. Shielding gas composition has a significant effect upon process characteristics, weld-bead shapes, spatter, and weld-metal mechanical properties. GMAW with CO_2 shielding gas is widely used for welding mild steels for general applications where the good surface appearance, improved tolerance to welding-parameter variation, and good toughness properties are required. When mixtures of Ar/CO_2 or $Ar/CO_2/O_2$ mixtures are used, the increase in the cost is compensated for by the improved weld appearance.

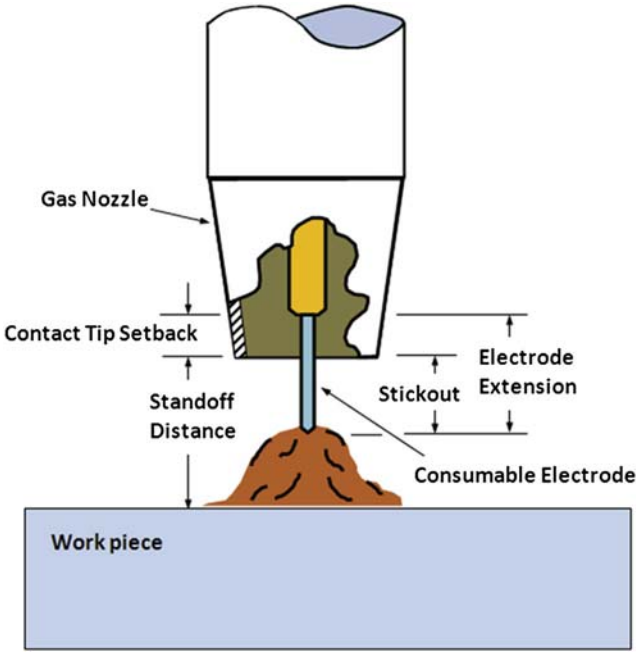

Figure 13 Arc welding gun nomenclature. Reproduced from Welding Handbook, Vol. 2, Part-1, 9th ed., Welding Processes, American Welding Society (AWS), 2001.

www.iran-mavad.com
مرجع مهندسی مواد و متالورژی

6.03.3.7 The Driving Forces during the Gas Metal Arc Welding Process

A schematic representation of the driving forces in the GMAW process is shown in Figure 14 (*10*). The electric potential established between the electrode and the work piece causes current flow, which generates thermal energy in the partially ionized gas. The current also creates the surrounding magnetic field, which interacts with the diverging current field to induce an electromagnetic force which accelerates the plasma, generating a flow toward and across the work piece surface. Intense heat generation and high plasma velocities are created, with a rapid transfer of heat into the molten weld pool. In the GMAW process, heat is generated both by resistive heating and by heat transfer from the arc current. The tip of the electrode wire is melted and molten droplets are formed and driven into and through the plasma jet into the weldpool. A detailed description of the physical process is given by Lancaster (*4*).

6.03.3.8 Equipment for GMAW

For GMAW, DC power sources with constant potential types are used, whereby constant wire-feed speed changes the arc length. Sufficient change in current restores the desired arc length. This characteristic describes the self-adjusting arc. The filler wire is fed via motor driven rollers through a conduit to the contact tube in the welding gun, around which a nozzle conveys the shielding gas to the weld zone. For currents over about 150 A, the welding gun gets hot and is often water-cooled. By supplying water along the main power cable to the gun, the size of the cable and, hence, its weight can be somewhat reduced. The equipment needed for GMAW is somewhat complicated mainly because of the inclusion of a wire-feed unit for the consumable electrode filler wire.

Appropriate timing circuits and relays are used in GMAW to ensure that the water flow, gas flow, wire feed, and welding current can all be started and stopped by a single switch at appropriate time intervals. The level of welding current is controlled by the wire feed speed, and the arc length by the OCV setting of the power source. Some power sources contain provision for changing the Voltage/Ampere characteristics (slope control) and the dynamic response (inductance) for improved process control in special applications.

6.03.3.8.1 Welding Power Supplies

Until the introduction of the GMAW process, power supplies for metal arc welding were designed with drooping volt–ampere output characteristics; that is, the voltage of the arc decreased as the current increased. This characteristic was essential for welding with covered electrodes since they were guided manually. The electrode- to-work piece distance then is an unavoidable variable that changes the arc length and the AV. Providing relatively CC output, the penetration also remains constant. When striking an arc, the short circuit is limited to a reasonable surge of 2–3 times the machine's rated current (Figure 15). A surge of this proportion is enough to help establish an arc and clear short circuits caused by large drops, but not enough to damage the machine. The high open circuit associated with the drooping characteristic also helps maintain a stable arc (*11*).

The welding power source provides suitable electrical power (generally 20 V to 80 V) that is delivered to the electrode and work piece to produce the arc. Because the vast majority of GMAW applications utilize DCEP, the positive lead is connected to the gun and the negative lead, to the work piece. The power source can be the 'static' type in which incoming utility power (120 to 480 V) is reduced to welding voltage by a transformer or solid-state inverter. The static type is normally used in shops where there is an available source of power. Power sources can be designed and built to provide either a CC or constant potential (CP) output, the latter of which is the most common by far. On newer power sources, this CP output can be pulsed at either a constant or variable frequency. When used in conjunction with a constant-speed wire feeder, the CV power source compensates for the variations in the contact-tip-work-distance that can occur during normal welding operations. It does this

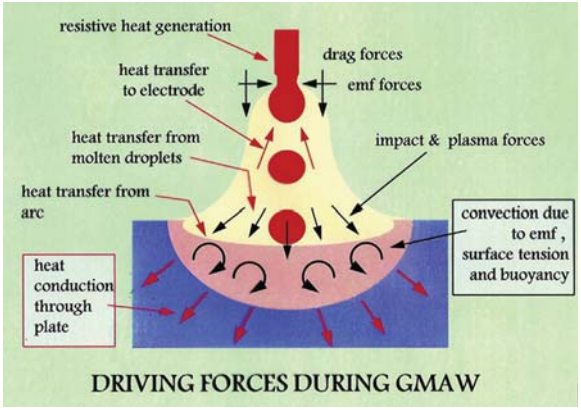

Figure 14 Schematic representation of the driving forces in the GMAW process. Reproduced from Wahab, M. A.; Painter, M. J.; Davies, M. H. The Prediction of Temperature Distribution and Weldpool Geometry in the Gas Metal Arc Welding Process. *J. Mater. Process. Technol.* **1998,** *77*, 233–239.

www.iran-mavad.com
مرجع مهندسی مواد و متالورژی

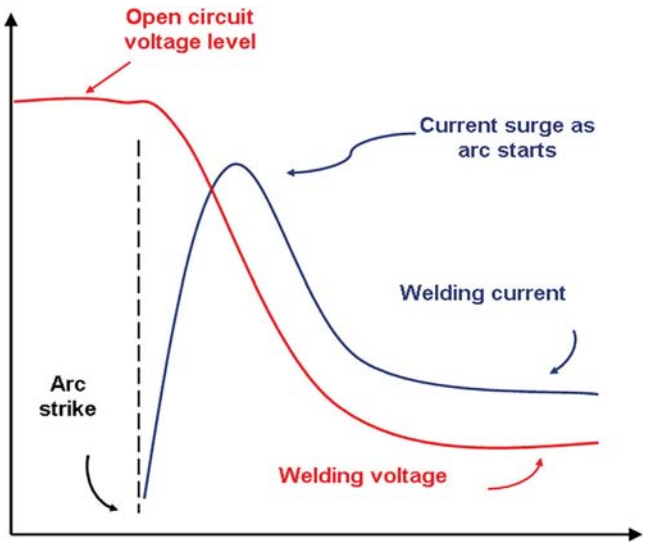

Figure 15 Current surge at arc-strike. Reproduced from Jeffus, Larry. *Welding Principles and Applications*; Delmar Publisher, Inc., 1993.

by instantaneously increasing or decreasing welding current to increase or decrease the electrode burn-off rate. The initial arc length is established by adjusting the voltage at the power source. Once this is set, no other changes are required during welding. The wire-feed speed, which is also the current control, is then set by the operator and adjusted as necessary. In addition to this self-regulating feature of the CP power source, control over slope and inductance is included on those machines intended for short-circuiting transfer.

6.03.3.9 Metal Deposition Rate

The GMAW process is usually operated on DC electrode positive (DCEP) and the wire melt-off rate is not significantly affected by the arc atmosphere (i.e. the type of shielding gas). For a wire of given chemical composition, the melting rate depends primarily on the current and on the stick-out length (length of wire protruding beyond the end of the contact tube). For aluminum, the deposition rate is about one-half of that required for steel. For fine wires of high electrical resistivity, I^2R heating can be a useful way of increasing metal deposition rate, although the consequent voltage drop along the wire stick-out must be compensated for by increased OCV setting to avoid unsuitably short arc lengths.

6.03.3.10 Process Variables

The important variables of the GMAW process that affect weld penetration, bead geometry, and overall weld quality includes (1) welding current (electrode feed-speed), (2) polarity, (3) AV (arc length), (4) travel speed, (5) electrode extension, (6) electrode orientation (gun angle), and (7) electrode diameter.

6.03.3.11 Control Parameters

A brief description of the major four control parameters are included in the following.

6.03.3.11.1 Electrode Extension

Electrode extension (stick-out length) is the length of the filler wire that extends past the contact tube. This is the area where preheating of the filler wire occurs. It controls the dimensions of the weld bead since the length of the filler wire extension affects the burn-off rate. Electrode extension exerts an influence on penetration through its effect on the welding current. As the extension length is increased, the preheating of the wire increases and the current is reduced. The current reduction in turn, decreases the amount of penetration into the work piece. Stick-out distance may vary from 1/8 to 1/4 in. (3.175 mm to 6.35 mm). Short electrode extensions (1/8–1/2 in. (3.175–12.7 mm)) are used for the short-circuit mode of transfer generally with the smaller diameter electrodes (0.023–0.045 in. (0.58–1.14 mm)). For stainless steel, the shorter electrode extension is used because of its higher resistivity (1/8–1/4 in. (3.175–6.35 mm)). The longer electrode extensions are used for spray-arcs transfer mode (1/2 in.). These are generally done with the larger diameter electrodes. Excessively long arcs with active gases reduce the mechanical properties in the weld, because of various alloys being burned out as the metal is transferred across the longer arc. The relationship that exists between electrode extension and current, and electrode extension and penetration should be understood to achieve sound quality weld.

www.iran-mavad.com
مرجع مهندسی مواد و متالورژی

6.03.3.11.2 Electrode Diameter

The electrode diameter influences the size of the weld bead, the depth of penetration, and the speed of welding. As a general rule, for the same current (wire-feed speed setting needs to be increased) the arc becomes more penetrating as the electrode diameter decreases. At the same time, the speed of the welding is also affected because the deposition (burn-off) rate also increases. When welding with wires below 0.045 in. (1.14 mm), the smaller wire operating at a given current density burns-off faster than the larger wire. To get the maximum deposition rate at a given current density, use the smallest wire possible that is consistent with an acceptable weld profile. With wires 0.045 in. (1.14 mm) and larger for a given welding current, the next size larger wire provides a lower deposition rate. This is because the effects of preheating the larger wires are less. Large wires deposit wider beads than small wires do under identical conditions.

6.03.3.11.3 Arc Voltage

In the GMAW process, the welder generally sets the voltage constant and the burn-off rate of the metal filler electrode remains constant at a given voltage setting. The AV has an effect on surface heating, and on the weld profile namely on the bead height and bead width. The function of the voltage is to stabilize the welding arc and to provide a smooth, spatter-free weld bead. For any given welding current, there is a particular optimum voltage that will provide the smoothest possible arc and good quality weld profile with little or no spatter or undercut. A higher or lower than this optimum AV causes the arc to become unstable and affects the surface heating. Higher AV produces a wider, and a flatter bead. Excessive voltage also increases the possibility of porosity in the weld metal and the spatter. In fillet welds, it increases undercut and produces a concave fillet subject to cracking. Lower voltage causes the bead to be high and narrow. Extremely low voltage causes the wire to stub on the plate. Therefore, changes in voltage have serious effects on bead height and bead width. As the AV increases, bead height decreases and bead width increases. This does not change the overall size of the bead, as in the case of welding current and travel speed, but it only changes the profile of the bead.

6.03.3.11.4 Welding Current

The wire-feed speed control setting determines the amount of current that is delivered at the arc. The term current is often related to current density (i.e., amperage per square inch of cross-sectional area of the electrode). Thus, at a given amperage the current density of an electrode 0.035 in. (0.89 mm) in diameter is higher than that of an electrode 0.045 in. (1.14 mm) in diameter. Each type and size of the electrode has a minimum and maximum current density, and the best working range lies between them.

The depth of penetration, bead formation, filler wire burn-off, speed of travel, and the size and appearance of the weld profile are all affected by the amount of welding current. There is a direct relationship between the welding current and penetration. In general, for any change in welding current, there is a corresponding change in penetration. As the welding current increases, the penetration increases, and as the welding current decreases, the penetration decreases.

Increasing the current also increases the wire melt-off rate and the rate of deposition. If the current is too low for a given electrode size, metal transfer is sluggish and poor penetration and poor fusion result, and the bead becomes rough and excessively convex. If the current is too high, penetration may become too deep and excessive penetration causes burn-through and undercut. The weld bead then has a poor profile. Undercut is a particular problem in making fillet welds with current settings that are too high. Each filler wire size and type has a minimum and maximum current range that gives the best results.

Knowledge and control of these variables are essential to consistently produce welds of satisfactory quality. Because they are not completely independent of one another, changing one variable generally requires changing one or more of the others to produce the desired results. Considerable skill and experience are necessary to select the optimal combination for each application. This selection is further complicated by the fact that the optimal settings for the above mentioned variables are also affected by the type of the base metal, the electrode composition, the welding position, quality requirements, and the number of completed weldments required. Thus, no single set of parameters provides optimal results in every case and, therefore, establishment of welding process variables may becomes a complex task.

6.03.3.12 Shielding Gases

The major shielding gases used for GMAW process are oxygen, argon, carbon dioxide, and helium or a combination of these four gases. The gases that are used in the shielding gas systems can be classified either as inert gases, which are those gases that have their outer electron sub-shells completely full and are stable; and the chemically reactive gases, such as carbon dioxide; and oxygen, which do not have their outer electron shells filled, making it possible for the bare electrons to combine with other elements in the welding zone to create impurities.

The two inert gases that are generally used for shielding gases are argon and helium. Helium is a less dense gas than argon which means that when helium is used, more cubic feet per hour are required than with argon. Lower voltages can be used with argon than with helium because it has a lower electrical resistance. The lower voltages required in the short-arc process lend themselves well to the electrical characteristics of argon. Since argon permits the operation of lower voltages at any amperage setting, it is better suited for the welding of thin metals. Also, argon does not greatly affect the heat during a manual operation in which the arc length varies as the weld operator manipulates the inert-gas arc torch.

Helium can be operated at much higher voltages. It is used often in the consumable electrode gas arc welding processes and is often used in the automatic GMAW welding process. Because a greater flow of cubic feet per hour is required with helium, greater

www.iran-mavad.com
مرجع مهندسی مواد و متالورژی

weld speeds are possible. It is possible to weld approximately 35 to 40% faster with helium than when using argon for the shielding gas.

Differences in penetration are caused by the intermingling of the inert-gas molecules in the ionization column of the arc stream, creating an ionized gas, which offers more resistance to the arc column in certain locations of the weld bead (**Figure 16**).

Welding speed is increased and a required penetration pattern is maintained many times by mixing argon and helium, capitalizing on the characteristics of each of the inert gases. In this way, the speed permitted by helium can be used with the penetration patterns that result from the use of argon.

A combination that is used many times is a mixture of 25% argon and 75% helium or 20% argon and an 80% helium mixture for the welding of aluminum. Most nonferrous metals can be welded with either argon or helium or a mixture of argon and helium. All ferrous metals can be welded with these gases.

Carbon dioxide (CO_2) is a gas that is used only for welding ferrous metals because it is less expensive than many inert gases. Carbon dioxide costs approximately one-tenth as much as argon or helium and is capable of producing a high-quality weld when used as a shielding gas. The penetration characteristics of carbon dioxide are similar to the penetration characteristics of helium because of the similarities in the weights of the gases. The carbon dioxide that is used for welding must be free of all moisture because moisture releases hydrogen which will in turn produce porosity in the weld metal. Because carbon dioxide has greater electrical resistant qualities, the current setting must be 20 to 30% higher than those used with argon or helium. One small negative characteristic in the use of carbon dioxide as a shielding gas in a welding process is the formation of a small amount of oxygen in the metal, resulting from the heat in the arc column.

This small amount of oxygen can reduce the nominal test strength of the metal. When oxygen molecule is released from CO_2, the gas that is formed in the outer shielding portion of the shielding gas is carbon monoxide, a toxic gas. Another major disadvantage of CO_2 is its extreme resistance to current. Because of this resistance, the arc length is sensitive. When the arc length is too great, it will extinguish more readily than when an inert gas such as argon or helium is used.

Other inert gases used for gas shielding are nitrogen, oxygen, and hydrogen. Nitrogen is used for a mixing or carrier gas with a very small percentage of nitrogen used. Up to 10% of oxygen can be used. Oxygen used above this will yield porosity in the weld bead. Mixtures of (oxygen and CO_2), or mixtures of (oxygen, CO_2, and argon), are generally used for the welding of mild steel. Mixtures of nitrogen and argon, or hydrogen and argon, are used for the welding of stainless steels. The nitrogen content for the nitrogen and argon mixture can be as high as 20% and the hydrogen in the hydrogen and argon mixture can be as high as 15%. Many times the mixtures that contain nitrogen or hydrogen are used as backup gases for the far side of the weld, which protect the root of the weld bead.

The inert gas, argon, has many desirable characteristics for GMAW of most metals; a degree of specialty can be adopted whereby other pure gases or mixtures can be more appropriate in specialized applications. For welding thick sections of steel, aluminum, and copper, additional heat input and improved penetration accrue from the use of CO_2, helium, and nitrogen respectively. However, there is an increase in spatter and the process parameters must be adjusted more critically to avoid sputtering and therefore, Argon-based mixtures have been favored.

Many different combinations (mixtures) of shielding gases have been developed over the years. They consists the mixtures of argon plus 1% to 5% O_2, argon plus 8% to 50% CO_2, pure CO_2, and helium, argon plus helium and tri-mix of (90% helium + 7.5% Argon + 2.5% CO_2).

The metal transfer mode is generally affected by the chemical activity of the shielding gas. At higher CO_2 contents, and particularly with pure CO_2, the drop at the electrode-tip is large and irregular in form and is repelled by the arc. Eventually, it detaches in an upward or sideways direction. To obtain effective transfer to the weld pool with CO_2 shielding at low currents it is necessary to use short-circuiting transfer, which is discussed later.

For welding structural steels, CO_2 is widely applied usually in the short-circuiting mode. A number of other gas mixtures based on Ar/CO_2 or Ar/O_2 are being used for alloy steels and stainless steels, and these are finding increasing application for work where low spatter is beneficial. For aluminum, pure argon is still favored on economic grounds, but the use of helium, especially on thicker work, is favored particularly since the hotter weld pool allows more opportunity to avoid porosity.

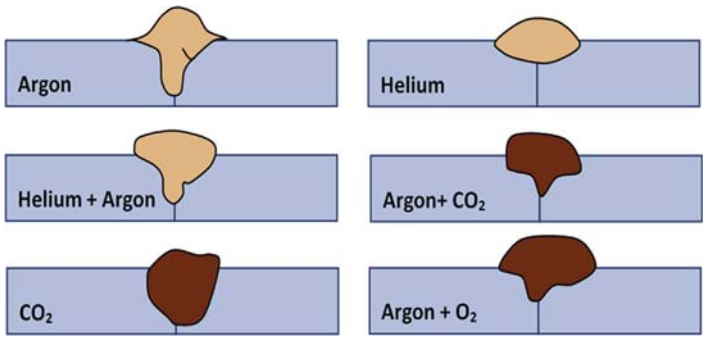

Figure 16 Weld penetration comparisons in weld cross-sections made with several shielding gases. Reproduced from Bohnart, Edward R. *Welding – Principles and Practices*, 4th ed.; McGraw Hill, 2012.

www.iran-mavad.com
مرجع مهندسی مواد و متالورژی

6.03.3.13 Important Observations for Shielding Gas

Argon and helium still continue to be the basic shielding gases that are used in GMAW. Argon is used more than helium on ferrous metals to keep low-spattering. Since argon is heavier than air, it gives better weld coverage. Oxygen or CO_2 is added to the pure gases to improve arc stability, minimize undercut, reduce porosity, and improve the appearance of the weld. Helium may be added to argon to increase penetration with relatively little effect on metal transfer characteristics. Hydrogen and nitrogen are used for only a limited number of special applications in which their presence will not cause porosity or embrittlement of the weld metal.

Carbon dioxide is popular as a shielding medium, and it has several advantages such as low cost, high density, resulting in low flow rates, and less burn-back problems because of its shorter arc characteristics. The following recommendations concerning mostly-used metals are helpful:

1. **Aluminum alloys**: Argon. With DCEP, argon removes surface oxide.
2. **Magnesium and aluminum alloys**: 75% helium, 25% argon. Correct heat input reduces the tendency toward porosity and removes surface oxide.
3. **Stainless steels**: argon plus oxygen. When DCEP is used, 2% oxygen improves arc stability.
4. **Low alloy steel**: argon, plus 2% oxygen. Oxygen eliminates undercutting tendencies and removes oxidation.
5. **Mild steel**: 15% argon, 25% CO_2 (dip transfer); 100% CO_2 may also be used with deoxidized wire. They promote high quality. It is suitable for low current, out-of-position welding. There is little spatter.

It is essential to ensure that the flow rate is appropriate for particular nozzle diameter, and that the gas system has no leaks which could allow air to be entrained. When welding at higher currents and travel speeds, auxiliary shielding gases are needed to shield the rear end of the weld pool, and also the reverse side of the joint. For GMAW of butt joints, the torch is normally set to a 10–15° forehand angle; though this may be increased at high travel speeds so that the gas coverage is efficiently maintained. The torch position also has an effect on the depth of penetration and the weld-bead contour. Careful selection of the appropriate gas mixture for a particular application and proper torch-positioning is necessary for both in weld quality and overall economy of GMAW.

6.03.3.14 Metal-Transfer Mechanisms in Gas Metal Arc Welding

The characteristics of the GMAW process are best described by reviewing the three basic means by which metal is transferred from the electrode to the work piece: short-circuiting transfer, globular transfer, and spray transfer. The type of transfer is determined by a number of factors, the most influential of which are (1) magnitude and type of welding current, (2) electrode diameter, (3) electrode composition, (4) electrode extension beyond the contact tip or tube, (5) shielding gas, and (6) power supply output.

The drops of molten metal from the electrode are transferred across the arc and flow to the weld pool. The metal-transfer mode depends on the above welding parameters and also the chemical behavior of the shielding gas. International Institute of Welding has made general classification in the modes of metal transfer but this classification is phenomenological, and makes no attempt to define the mechanisms of the various transfer modes. There are various modes of weld metal transfers in GMAW that are classified as follows.

6.03.3.14.1 Free Flight Transfer

Globular: (1) droplet (for low current), (2) repelled (CO_2 shielded GMAW), spray: (1) projected (intermediate-current), (2) streaming (medium-current), and (3) rotating (high-current).

6.03.3.14.2 Bridging Transfer

(1) short-circuiting (short-arc), (2) bridging without interruption (with filler wire addition).

A schematic illustration of the various modes of weld metal-transfer in GMAW is shown in **Figure 17**.

Several types of metal transfer variations can be used in GMAW depending on a number of factors which include the globular, spray, short-circuiting, and rotating-arc metal transfer modes. Figure below summarizes these arc modes as a function of current density, illustrating their respective positions in relation to one another.

The GMAW process can be operated in four main modes of metal transfer to the weldpool.

6.03.3.14.3 Short-Circuiting Transfer

Short circuit transfer refers to the welding wire actually 'short circuiting' (touching) the base metal between 90–200 times per second. With short circuit transfer, wire feed speeds, voltages, and deposition, rates are usually lower than with other types of metal transfer such as spray transfer. This makes short circuit transfer very versatile allowing the welder to weld on thin or thick metals in any position. Limitations of short circuit transfer are (1) a relatively low deposition rate, (2) lack of fusion on thicker metals, and (3) generally more spatter. Short circuit transfer usually has a crackling (bacon frying) sound when a good condition exists, i.e., it has a characteristic buzzing sound, which is obtained at the lowest range of current densities and can be applied in all welding positions. The shielding gas mixture used in this mode is typically rich in argon. It produces small, quickly solidifying welds suited to joining thin materials or bridging root openings. In the bridging root-opening case, this mode provides full penetration and fusion to both members on the reverse side of an open-root butt joint.

www.iran-mavad.com
مرجع مهندسی مواد و متالورژی

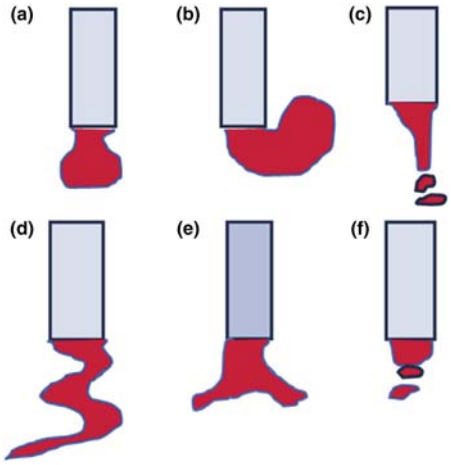

Figure 17 Metal transfer in GMAW: (a) droplet, (b) repelled, (c) streaming, (d) rotating, (e) short-circuiting, and (f) projected. Reproduced from Lancaster, J. F. *The Physics of Welding*; Pergamon Press, (IIW), 1984; Nguyen, N. T. *Thermal Analysis of Welds*; WIT Press, 2000.

At low currents (less than 200 A) and low AVs around 20 V, which cannot sustain a continuous arc, another change in metal transfer mode occurs. Under these conditions, a short-circuiting process occurs in which the arc length shortens, the wire-tip touches the weld pool and the rapid rise in current due to the short circuit rapidly melts the wire which is drawn into the weld pool by surface tension. An arc is re-established and the cycle repeats itself at a rapid rate depending on the current, wire diameter, and the OCV. The molten droplet formed at the electrode end is regularly in contact with the weld pool and the metal transfer is achieved by means of surface tension and electromagnetic forces. This mode of operation can be operated quite stably with optimized welding parameters.

For the short-circuiting metal transfer cycle, first a globule is formed on the electrode tip just before being freed and then the globule short-circuits to the weld pool, extinguishing the arc for an instant. Although this is not perceptible to the unaided eye, high-speed film has proven that the arc does indeed extinguish. Because of the short circuit, the globule is then pinched off as the current peaks, and then the arc is restored again. This cycle can occur up to 200 times per second, depending on the electrical current and gas parameters used. The following sequences may take place in short-circuit metal transfer mode: (1) Electrode is short circuited to base metal. No arc and current is flowing through electrode wire and base metal. (2) Resistance increases in electrode wire causing it to heat, melt, and 'neck down.' (3) Electrode wire separates from weld puddle, creating an arc. Small portion of electrode wire is deposited which forms a weld puddle. (4) Arc length and load voltage are at maximum. Heat of arc is flattening the puddle and increasing the diameter tip of electrode. (5) Wire feed speed overcomes heat of arc and wire approaches base metal again. (6) Arc is off and the short circuit cycle starts again. An important precaution must be observed when implementing the short-circuiting arc mode; sufficient power must be used to obtain thorough fusion as soon as the mass of the base metal becomes critical.

6.03.3.14.4 Globular Transfer

This type of transfer refers to the state of transfer between short-circuiting and spray-arc transfer modes. Large globules of wire are expelled off the end of the electrode wire and enter the weld puddle. Globular transfer can result when welding parameters such as voltage, amperage, and wire feed speed are somewhat higher than the settings for short-circuit transfer. Limitations of globular transfer includes (1) presence of spatter, (2) less desirable weld appearance than spray arc transfer, (3) welding is limited to flat positions and horizontally fillet welds, and (4) welding is limited to metal 1/8 in. (3 mm) or thicker. The type of shielding gas used also affects the metal transfer modes. For example, when using CO_2 the resulting metal transfer is characteristically globular even at high current density. The larger the electrode used, the higher the current required for a given current density.

Globular transfer mode is obtained when the current density is just below the transition current density level. The metal droplets formed at the end of electrode are larger in diameter than the electrode, itself. With a solid electrode, wire globular mode produces a rather erratic arc. In this case, the metal globules are propelled from randomly varying positions with respect to the center of the electrode tip. Substantial spatter results producing a weld deposit, which can be applied in all welding positions.

Below the critical current, the droplets are transferred across the arc as large globules, mainly due to the effects of gravity. This mode of transfer, known as globular transfer, sometimes results in the globules landing outside the weld pool itself. If the deposition rate is increased as a result of the increased current density (approximately, from 200 to 250 A) and wire feed rate, the process operates under the globular transfer mode, in which the end of the electrode no longer touches the weld pool. Large droplets or globules are detached by gravity and electro-magnetic forces at irregular intervals. In this current range, the process is operated in the pulsed spray transfer mode (at frequencies of approximately 50 Hz) and controlled by means of the current waveform. As a result, spatter is minimized and a smooth weld bead is achieved. Weld spatter is less in this mode but it is sensitive to variations in joint fit-up and pulse parameters. This mode is accompanied by a number of additional parameters. Therefore, careful optimization is required to obtain a stable arc-length condition.

www.iran-mavad.com
مرجع مهندسی مواد و متالورژی

These two modes of transfer are collectively described as free-flight transfer and shown in Figure 17. The change in droplet transfer mode is attributed to the development of a strong plasma jet stream in argon above the critical current density, and this becomes particularly important in positional welding. In the spray transfer mode, all-positional welding is possible, whereas, in the globular mode welding is restricted to the downhand (i.e., flat) position.

6.03.3.14.5 Spray-Arc Transfer

Spray-arc transfer 'sprays' a stream of tiny molten droplets across the arc, from the electrode wire to the base metal. Spray-arc transfer uses relatively high voltage, wire-feed speed, and amperage values compared to short-circuit transfer. To achieve a true spray transfer, an argon-rich shielding gas must be used. When proper parameters are used, the spray arc transfer produces a characteristic humming or buzzing sound. Advantages of spray arc transfer includes (1) high deposition rates, (2) good fusion and penetration, (3) good weld bead appearance, (4) capability of using larger diameter electrode wires, and (5) presence of very little spatter. The limitations of spray-arc transfer are (1) used only on material 1/8 in. (3 mm) and thicker (handheld) and (2) limited to flat and horizontal fillet weld position (except for some spray-transfer on aluminum). Good fit-up is always required as there is no open-root capability.

Spray transfer mode is activated when the current density level rises above the transition current density level. The transition current density is defined as the current density level above which spray transfer occurs. In spray transfer mode, the electrode metal is transferred as tiny droplets across a stiff stable arc. The stable arc is rather quiet and produces very little spatter (*11*).

The shielding gas mixture should be argon rich. Because this mode produces a high volume of molten metal at a high rate of speed, spray transfer is considered suitable for the flat and horizontal positions only.

The utility of GMAW depends on the manner in which the filler metal is transferred to the weld pool. This affects several important characteristics such as, the degree of spatter, porosity, and the weld penetration profile. As the current is increased for a given wire size, the droplet size decreases, at first gradually, but over a critical current range, the droplet size decreases markedly and transfer becomes a stream of fine droplets having diameters less than that of the wire, which is known as spray transfer.

Above the critical current for a given wire chemistry, this type of transfer depends on wire diameter and electrical stick-out length, and the droplets that are projected along the arc axis. If the current is increased above 220–250 A, the metal transfer mode becomes the spray transfer mode in which fine droplets with a diameter less than that of the electrode are propelled from the electrode toward the weld pool at a high speed across the open arc. This mode requires the use of a mixture of Ar/CO_2 and relies on high currents (higher than around 250 A) to detach metal droplets and transfer them across the arc to the work piece. Only a narrow current range is applicable and a compromise of conditions is required to prevent excessive arc forces at high currents. The constant metal transfer results in a smooth weld bead but high current (high heat input) results in a relatively wide weld-bead. Due to the highly liquid weld pool, the positional capability of this mode is limited to the horizontal down-hand position only.

This spray transfer process requires three conditions: argon shielding (or argon-rich shielding gas mixtures), DCEP polarity, and a current level above a critical amount called the transition current. Figure 18 illustrates how the rate of drops transferred changes in relationship to the welding current (*11*). At low currents, drops are large and are transferred at rates below 10 per second.

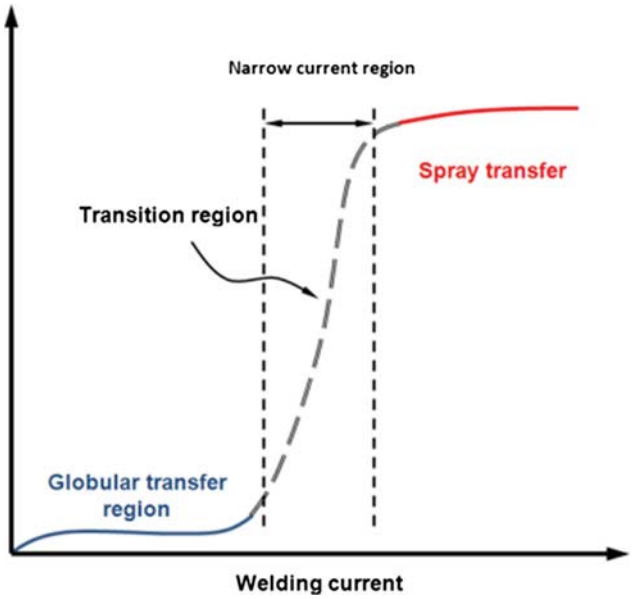

Figure 18 Desirable spray transfer showing drops per second versus welding current. Reproduced from Jeffus, Larry. *Welding Principles and Applications*; Delmar Publisher, Inc., 1993.

www.iran-mavad.com
مرجع مهندسی مواد و متالورژی

These drops move slowly, falling from the electrode-tip as gravity pulls them down. They tend to bridge the gap between the electrode tip end and molten weld pool. This produces a momentary short circuit that throws off spatter. However, the mode of transfer changes very abruptly above the critical current, producing the desirable spray. This change in the rate of transfer related to current is shown schematically in Figure 18.

The transition current depends on the alloy being welded. It also is proportional to the wire diameter, meaning that higher currents are needed with larger diameter wires. The need for high current density imposes some restrictions on the process. The high current hinders welding sheet metal because the high heat cuts through sheet metal. High current also limits its use to the flat, vertical down, and horizontal welding positions. Weld control, in the vertical up or overhead positions, is very difficult to impossible.

6.03.3.14.6 Rotating-Arc Transfer

At very high currents (above 500 A), a rotating arc transfer can be achieved. Kink instability of the molten electrode taper is created under this condition and it is perpetuated by a longitudinal magnetic field. At the same time, the tiny droplets are expelled from the electrode-end toward the weld pool. The main characteristics of this mode are very high deposition rates, higher spatter, and irregular weld bead quality. It is, therefore, rarely used in practice. This mode requires a moderately high level of optimization of welding parameters and manual welding skill.

In an attempt to overcome some of the problems impeding the widespread acceptance of Gas Tungsten Arc welding, flux-cored GMAW wire consumables were developed. Subsequent development has aimed to increase further weld deposition rates and to improve weld-metal mechanical properties. Weld-pool control for positional welding has also been benefited since readily ionizable elements in the flux-cored wire contribute to a stable arc and weld pool shape. Introduction of self-shielded flux-cored consumables has led to a great improvement in the GMAW process where shielding is provided by CO_2 generated by breakdown of carbonates. The formation of metal vapor from elements such as Li and Mg contained in the flux give additional shielding protection for the arc and weld metal. However, this may cause problems of toxic welding fume, necessitating good extraction equipment for workshops.

In the GMAW process, the mode of metal transfer changes with increasing current. The distinction between globular and spray-transfer mode corresponds roughly with initial acceleration. For a 1.2-mm diameter electrode, at above 200 A, the metal drop forms at the tip of the conical region of the electrode. The cone is in a quasi-stationary condition, i.e. the liquid metal flows into the base of the cone and flows out of the cone tip. Conical-drop formation is typical of steel welding but not of aluminum welding as the conical drop is considered to be associated with the relatively low thermal conductivity steel. At higher current, there is a transition to streaming transfer where a column of liquid metal flows from the solid/liquid interface and in line with the electrode and eventually this column disperse into drops. At still higher current (>500 A), a kink instability develops and the axial cylinder becomes a rotating spiral. In both streaming and rotating, the metal liquid column breaks up into drops.

6.03.3.15 Effect of Operating Variables on the Weld Quality

Welding variables are the factors that affect the operation of the arc and the weld deposit. Good appearance and sound weld results are achieved when the variables are in balance. Each welding process also has its own characteristics.

6.03.3.15.1 Gas Metal Arc DCEP Welding

Electrode wire positive, work piece negative: In this process electrons flow from the −ve work piece to the +ve electrode and the gas ions flow from the +ve electrode to the −ve work piece. The DCEP is generally used for gas metal arc weld since it provides maximum heat input into the work piece, whereby resulting in relatively deep penetration. It also assists in the removal of oxides from the plate, which contributes to a clean weld deposit of high quality. Low current values produce globular transfer of metal from the electrode. A gradual increase in the current increases the electrode melting rate so that at relatively high current values the spray transfer of metal is produced. To achieve a spray transfer along with high current requirement, we also need correct proportion of shielding gas and voltage. On carbon steel, the shielding gas must contain a minimum of 80% argon. The voltage level must be high enough to keep the electrode from dipping into the weld pool. The welding of ferrous metals with DCEP, solid or metal-cored electrode, and pure argon causes the arc to be unstable and introduces porosity into the weld metal. This condition may be corrected by the addition of 2% to 5% oxygen to the gas mixture.

6.03.3.15.2 Gas Metal Arc DCEN Welding

Electrode wire is negative and the work piece is positive: In this case, the electrons flow from electrode to the work piece and the gas ions flow from the work piece to the electrode and the resulting bead has the lower penetration than DCEP. The DCEN has a limited use in the welding of thin gauge materials. The greatest amount of heat occurs at the electrode tip. The wire melt-off rate is a great deal faster than with DCEP. The arc is not stable at the end of the filler wire, and it becomes very difficult to direct the transfer of weld metal where it is desired. The erratic arc results in poor fusion and a considerable amount of spatter. The unstable arc can be corrected to a considerable extent by the use of a shielding gas mixture of approximately 5% oxygen added to argon. The normally high electrode melt-off rate, however, is reduced substantially when oxygen is added so that any advantage of DCEN is canceled out.

www.iran-mavad.com
مرجع مهندسی مواد و متالورژی

6.03.3.15.3 Use of Alternating Current in GMAW

AC is rarely used in GMAW. The arc becomes unstable as the current and voltage both passes through the zero point many times each second as the current reverses. Since AC is a combination of DCEN and DCEP polarity, the rate of metal transfer and the depth of penetration fall between those of both polarities. It has found some use for the welding of aluminum.

6.03.3.16 Advantages and Limitations

6.03.3.16.1 Advantages in GMAW

The GMAW is versatile and has wider acceptance as the mostly-used welding process in industrial manufacturing sector and in robotic welding. These increased usages can be attributed to its many advantages, which include the following:

- It can be operated in a manual or a mechanized manner and can be used in all welding positions.
- It is an efficient, flexible consumable-electrode process with high filler metal weld-deposition rates that can be used to weld all commercial metals and alloys.
- A modified flux-cored consumables are available to improve weld-pool shielding.
- Modified process of pulsed GMAW offers the potential for easier control of the entire welding operation.
- It overcomes the restriction of limited electrode length encountered with MMAW (stick electrode welding).
- Because the electrode (wire-feed) is continuous, welding speeds are higher than those attained with MMAW and long welds can be deposited without intermediate stops and starts.
- When spray-arc transfer is used deeper penetration is possible than with MMAW.
- Minimal post-weld cleaning is required due to the absence of heavy slag.
- It is a low-hydrogen process, making it a good choice for welding materials that are susceptible to hydrogen-embrittlement.
- Process skills are readily taught and acquired.

6.03.3.16.2 Limitations in GMAW

The major limitations of GMAW welding include the following:

- The welding equipment required for GMAW is more complex, more costly, and less portable than that for MMAW.
- GMAW is difficult to use in hard-to-reach places because the welding gun is larger than a MMAW arc electrode holder and the welding gun must be close to the joint, (i.e., between 10 and 19 mm (3/8 and 3/4 in.) to ensure that the weld metal is properly shielded.
- The welding arc must be protected against air drafts in excess of 5 miles per hour, which may disperse the shielding gas and this limits outdoor applications unless protective shields are placed around the welding area.
- Another limitation involves the relatively high levels of radiated heat and arc intensity, which can contribute to resistance on the part of operators to accept the process.
- The process has been prone to several types of defects such as lack of sidewall fusion, spatter and porosity.
- Precise control of welding parameters through good equipment design is necessary and capital costs are higher in comparison with MMAW.
- Flux-cored self-shielded welding can give rise to toxic welding fume that must be extracted from confined workshop spaces.
- Comparably high cost of production for argon-based gas compared to carbon dioxide (CO_2) based gas.
- CO_2 process does not exhibit a spray transfer mode and the weld bead has poorer appearance, poor arc stability, and high spatter.

6.03.3.17 Special Process Features

The GMAW process is capable of a wide range of applications on all metals from sheet dimensions to almost unlimited thickness, and in all positions. Even in manual operation, high productivity is possible and the system is very amenable to automation in production line situations. The automatically fed filler wire means that the operator is responsible only for guiding the welding gun whilst maintaining the contact-tip at an appropriate distance from the work.

The absence of fluxes means that low hydrogen process quality is more readily achieved, provided that the work itself is free from contamination. This makes the GMAW process most attractive for welding of highly hardenable steels.

The process embraces many procedural variables and, for optimum results, demands a high degree of expertise in obtaining the best settings for each application. Likewise, proper attention must be paid to operator training, despite the high degree of automation inherent in the process, itself. At the present time, the ranges of filler wire sizes and types are somewhat restricted outside Europe and the United States, although a good range of shielding gas mixtures is available in many countries.

Acknowledgments

The author gratefully acknowledges the help received from Ms. Annette O'Brien, Senior Editor of the American Welding Society (AWS) Handbooks for granting permission to use several figures from AWS Handbooks (Vol. 9). The author also acknowledges

www.iran-mavad.com
مرجع مهندسی مواد و متالورژی

the generous help received from his student, from Dr Jiandong Liang, for computer graphics and drawings of many figures used in this chapter.

See also: Oxyacetylene Gas welding; Thermit Welding; Gas Tungsten Arc Welding; GTAW; Submerged Arc; Resistance Spot; Plasma Arc Welding; Electron-Beam Welding; Laser-Beam Welding; Electro slag Welding; Electro gas Welding; Solid State (Low and high Temperature) Welding; Diffusion Welding

References

1. Karlsson, L. Thermal stresses in welding. In *Thermal Stresses;* Hetnarski, R. B., Ed.; Elsevier Science Publishers: Amsterdam, 1986; Vol. 1.
2. Goldak, John A.; Akhlagi, Mehdi. *Computational Welding Mechanics;* Springer: New York, 2005.
3. Yeomans, S. R., Ed. *Welding in Structural Engineering: Steels and Aluminum Alloys;* University of New South Wales: Canberra, Australia, April 1996.
4. Lancaster, J. F. *The Physics of Welding;* Pergamon Press, (IIW): Oxford, 1984.
5. Nguyen, N. T. *Thermal Analysis of Welds;* WIT Press, 2000.
6. Bohnart, Edward R. *Welding – Principles and Practices*, 4th ed.; McGraw Hill: New York, 2012.
7. Little, Richard. *Welding and Welding Technology;* McGraw-Hill: New York, 1973.
8. Welding Handbook, Vol. 2, Part-1, 9th ed., Welding Processes, American Welding Society (AWS), 2001.
9. Welding Handbook, Vol. 1, 9th ed., Welding Science and Technology, American Welding Society (AWS), 2001.
10. Wahab, M. A.; Painter, M. J.; Davies, M. H. The Prediction of Temperature Distribution and Weldpool Geometry in the Gas Metal Arc Welding Process. *J. Mater. Process. Technol.* **1998,** *77,* 233–239.
11. Jeffus, Larry. *Welding Principles and Applications;* Delmar Publisher, Inc., 1993.

www.iran-mavad.com
مرجع مهندسی مواد و متالورژی

6.04 Robotic Welding Technology

TS Hong and M Ghobakhloo, Universiti Putra Malaysia, Selangor, Malaysia
W Khaksar, University Tenaga Nasional, Selangor, Malaysia

© 2014 Elsevier Ltd. All rights reserved.

6.04.1	**Introduction**	77
6.04.1.1	History of Welding	77
6.04.1.2	Industrial Automation	78
6.04.1.3	Welding Robots	79
6.04.2	**Robotics in Welding**	80
6.04.2.1	Motivations	80
6.04.2.2	Disadvantages of Welding Robots	81
6.04.2.3	Automated Welding	81
6.04.2.4	Examples of Welding Robots	82
6.04.3	**Robotics in Different Welding Techniques**	84
6.04.3.1	Spot Welding	84
6.04.3.2	Arc Welding	86
6.04.3.3	Friction Stir Welding	89
6.04.4	**Current Research Topics in Robotic Welding**	92
6.04.4.1	Path/Motion Planning	92
6.04.4.2	Image Processing	94
6.04.4.3	Artificial Intelligence	94
6.04.5	**Conclusions**	96
References		96

6.04.1 Introduction

Probably no other technique has been and is more important to the durability, easement, and development of humankind than welding. It is an essential process in building our world in different aspects, including agriculture through the manufacture of tillers, tractors, and combines; food processing through production of crushers, cookers, and conveyors; mining through manufacture of drills, excavators, and trams; transportation through the production of trucks, trains, ships, cars, buses, and planes; security maintenance by manufacture of tanks, missiles, and submarines; power generation and transmission; information communication; and hundreds of other applications (*1*).

Welding is a technology that provides the fastest, strongest, and most economical method of joining metals. The field of welding has moved from coal-fired furnaces and hammers used for forging iron to modern methods such as the concentrated accelerated free electrons of the electron beam process and the advantages of robots and lasers. Welding had its ancient origins in the fires of blacksmiths, who could forge two white-hot pieces of metal together with hammer blows and patience (*2*).

Preliminarily, the simple definition of welding was "joining metals through heating them to a molten state and fusing them together." With increasing progress in welding processes and techniques, the definition has changed. It is quite true to say that the weld is stronger than the base metal. Beside the classic application areas of welding such as shipbuilding, automobile manufacturing, building construction, and pipelines, currently welding techniques are being used in more complex application fields, including aircraft, space vehicles, and nuclear reactors.

Conventionally, arc welding and oxyacetylene fuel welding were two main welding techniques, but currently more modern technologies are being used, such as pulsed gas tungsten arc welding (GTAW), plasma welding and cutting, submerged arc, pulsed gas metal gas welding (GMAW), and electron beam and laser welding. Basically, there are two types of welding, namely fusion and non-fusion. The former is the most common and involves the actual melting of the parent metals being joined. Non-fusion welding is most commonly represented by soldering and brazing where the parent metal is heated, but not melted, and a second or 'filler' metal is melted between them, forming a strong bond when all are cooled (*3*).

6.04.1.1 History of Welding

The earliest evidence of welding can be traced back to the Bronze Age. The earliest examples of welding are welded gold boxes belonging to the Bronze Age. The Egyptians also learned the art of welding. Several of their iron tools were made by welding. During the Middle Ages, a set of specialized workmen called blacksmiths came to the fore. Blacksmiths of the Middle Ages welded various types of iron tools by hammering. The welding methods remained more or less unchanged until the dawn of the nineteenth century. In the nineteenth century, major breakthroughs in welding were made. The use of open flames (acetylene) was an important milestone in the history of welding since open flames allowed the manufacture of intricate metal tools and equipment. Englishman

www.iran-mavad.com
مرجع مهندسی مواد و متالورژی

Edmund Davy discovered acetylene in 1836, and acetylene was soon utilized by the welding industry. In 1800, Sir Humphrey Davy invented a battery-operated tool that could produce an arc between carbon electrodes. This tool was extensively used in welding metals. In 1881, French scientist Auguste De Meritens succeeded in fusing lead plates using the heat generated from an arc. Later, Russian scientist Nikolai N. Benardos and his compatriot Stanislaus Olszewski developed an electrode holder for which they secured US and British patents.

During the 1890s, one of the most popular welding methods was carbon arc welding. Around the same time, American C.L. Coffin secured a US patent for metal electrode arc welding. N.G. Slavianoff of Russia used the same principle for casting metals in molds. A coated metal electrode was first introduced in 1900 by Strohmenger. A coating of lime helped the arc be much more stable. A number of other welding processes were developed during this period. Some of them included seam welding, spot welding, flash butt welding, and projection welding. Stick electrodes became a popular welding tool around this time as well.

After the end of World War I, the American Welding Society was established by Comfort Avery Adams. The aim of the society was the advancement of welding processes. C.J. Holstag also invented the alternating current in 1919. However, alternating current was first commercially utilized by the welding industry only in the 1930s. Automatic welding was first introduced in 1920. Invented by P.O. Nobel, automatic welding integrated the use of arc voltage and bare electrode wires. It was used for repairing and molding metals. Several types of electrodes were also developed during this decade.

The New York Navy Yard developed stud welding. Stud welding was increasingly used for the construction industry and also for shipbuilding. It was during this time that the National Tube Company developed a welding process called smothered arc welding. In the sector of shipbuilding, the stud welding process was replaced by the more advanced submerged arc welding. A new type of welding for seamlessly welding aluminum and magnesium was developed in 1941 by Meredith. This patented process came to be known as Heliarc® welding. Gas-shielded metal arc welding, or GTAW, was another significant milestone in the history of welding; it was developed at Battelle Memorial Institute in 1948. The CO_2 welding process popularized by Lyubavskii and Novoshilov in 1953 a first choice for welding steels, because it was comparatively economical. Soon, electrode wires of smaller diameter made welding of thin materials more convenient. There were several advancements in the welding industry during the 1960s: dual shield and inner shield welding and electroslag welding were some of the important welding developments of the decade. Plasma arc welding was also invented by Gage during this time. It was used for metal spraying. The French also developed electron beam welding, which is still used by the aircraft manufacturing industries of the United States.

Some of the recent developments in the welding industry include the friction welding process developed in Russia, and laser welding. Laser was originally developed in Bell Telephone Laboratories, but it is now being used for various kinds of welding work. Because of the tremendous concentration of energy in a small space, it proved to be a powerful heat source. This is due to the inherent capacity of lasers in rendering precision to all kinds of welding jobs. Friction welding, which uses rotational speed and upset pressure to provide friction heat, was developed in the Soviet Union. It is a specialized process and has applications only where a sufficient volume of similar parts is to be welded because of the initial expense for equipment and tooling. This process is called inertia welding.

Recently, magnetic pulse welding was introduced by Pulsar Ltd. of Israel using capacitive power as a solid-state welding process. Discharging 2 million amps in less than 100 μs, this process can create a metallurgical, a non-metallurgical, or a mechanical lock, depending on the substrate involved. No heat-affected zone (HAZ) is created since a rise of only 30 °C occurs.

There have been more innovations in welding during the last 50 years, and with the invention of the laser, using a laser beam to do welding has become popular in automated plants. There have also been many safety improvements as well, and the tools, equipment, and protective clothing now make welding a very safe activity (*4*).

6.04.1.2 Industrial Automation

In today's global marketplace, manufacturing organizations are facing national as well as international competition, forcing them to further improve their performances. To this effect, the concept of *computer integrated manufacturing* (CIM) has been introduced in various production environments with different purposes, including human productivity improvement, product quality improvement, capital resource productivity improvement, and provision of rapid response to market demands. The CIM strategy is to integrate the information bases of the various units of automation within the conventional framework of manufacturing. In this respect, CIM can be viewed as a closed loop control system where a typical input is the order for a product and the corresponding output is the delivery of the finished product (*5*).

Automation of the physical production processes on the shop floor is a key component of the CIM strategy for improving productivity. In this context, robots have played an important role in the automation of various operations. Robots have been successful in automating simple and repetitive operations while simultaneously enhancing the quality of manufactured products in many production areas. The use of robots is also highly desirable in hazardous manufacturing operations such as spray painting, and welding that pose known health risks to human operators.

Industrial robots are essential components of today's factory, and even more of the factory of the future. The demand for the use of robots stems from the potential for flexible, intelligent machines that can perform tasks in a repetitive manner at acceptable cost and quality levels. The most active industry in the application of robots is the automobile industry, and there is great interest in applying robots to weld and assembly operations, and to material handling. Typical applications of robots include welding, painting, assembly, pick and place (such as packaging, palletizing, and surface mount technology), product inspection, and testing; all accomplished with high endurance, speed, and precision.

www.iran-mavad.com
مرجع مهندسی مواد و متالورژی

The most commonly used robot configurations are articulated robots, SCARA robots, Delta robots, and Cartesian coordinate robots (also known as gantry robots or x-y-z robots). In the context of general robotics, most types of robots would fall into the category of robotic arms (inherent in the use of the word manipulator in the previously mentioned ISO standard). Robots exhibit varying degrees of autonomy:

- Some robots are programmed to carry out specific actions over and over again (repetitive actions) without variation and with a high degree of accuracy. These actions are determined by programmed routines that specify the direction, acceleration, velocity, deceleration, and distance of a series of coordinated motions.
- Other robots are much more flexible as to the orientation of the object on which they are operating or even the task that has to be performed on the object itself, which the robot may even need to identify. For example, for more precise guidance, robots often contain machine vision sub-systems acting as their 'eyes,' linked to powerful computers or controllers. Artificial intelligence, or what passes for it, is becoming an increasingly important factor in the modern industrial robot.

George Devol applied for the first robotics patents in 1954 (granted in 1961). The first company to produce a robot was Unimation, founded by Devol and Joseph F. Engelberger in 1956, and was based on Devol's original patents. Unimation robots were also called programmable transfer machines because their main use at first was to transfer objects from one point to another, less than a dozen feet or so apart. They used hydraulic actuators and were programmed in joint coordinates; i.e., the angles of the various joints were stored during a teaching phase and replayed in operation. They were accurate to within 1/10 000 of an inch (*5*) (note: although accuracy is not an appropriate measure for robots, usually evaluated in terms of repeatability). Unimation later licensed their technology to Kawasaki Heavy Industries and GKN, manufacturing Unimates in Japan and England, respectively. For some time Unimation's only competitor was Cincinnati Milacron Inc. of Ohio. This changed radically in the late 1970s when several big Japanese conglomerates began producing similar industrial robots (*6*).

In 1969 Victor Scheinman at Stanford University invented the Stanford arm, an all-electric, six-axis articulated robot designed to permit an arm solution. This allowed it accurately to follow arbitrary paths in space and widened the potential use of the robot to more sophisticated applications such as assembly and welding. Scheinman then designed a second arm for the MITAI Lab, called the 'MIT arm.' Scheinman, after receiving a fellowship from Unimation to develop his designs, sold those designs to Unimation who further developed them with support from General Motors and later marketed it as the Programmable Universal Machine for Assembly (PUMA).

Industrial robotics took off quite quickly in Europe, with both ABB Robotics and KUKA Robotics bringing robots to the market in 1973. ABB Robotics (formerly ASEA) introduced IRB 6, among the world's first commercially available all electric microprocessor-controlled robot. The first two IRB 6 robots were sold to Magnusson in Sweden for grinding and polishing pipe bends and were installed in production in January 1974. Also in 1973, KUKA Robotics built its first robot, known as FAMULUS, also one of the first articulated robots to have six electromechanically driven axes.

Interest in robotics increased in the late 1970s, and many US companies entered the field, including large firms like General Electric, and General Motors (which formed joint venture FANUC Robotics with FANUC LTD of Japan). US startup companies included Automatics and Adept Technology, Inc. At the height of the robot boom in 1984, Unimation was acquired by Westinghouse Electric Corporation for $US 107 million. Westinghouse sold Unimation to Stäubli Faverges SCA of France in 1988, which is still making articulated robots for general industrial and cleanroom applications and even bought the robotic division of Bosch in late 2004.

Only a few non-Japanese companies ultimately managed to survive in this market, the major ones being Adept Technology, Stäubli-Unimation, the Swedish-Swiss company ABB Asea Brown Boveri, the German company KUKA Robotics, and the Italian company Comau.

6.04.1.3 Welding Robots

What makes robotics so interesting is that it is a science of ingenious devices, constructed with precision, powered by a permanent power source, and flexible from the programming point of view. That does not mean necessarily open source, but instead the availability of powerful advanced programming interfaces, and de facto standards both for hardware and software, enabling access to system potentialities without limitations. This is particularly necessary in research environments, where good access to resources is needed to implement and test new ideas. If that is available, then a system integrator (or even a researcher) will not require open source software, at least for the conventional fields of robotics (industrial robot manipulators and mobile robots). In fact, that could also be very difficult to achieve since those fields of robotics have decades of engineering efforts, achieving very good results and reliable machines, which are not easy to match. That open source issue is nevertheless very important for the emerging robotics research (like humanoid robotics, space robotics, robots for medical use) as a way to spread and accelerate development.

Industrial robotic welding is by far the most popular application of robotics worldwide (*7*). In fact, there are a huge number of products that require welding operations in their assembly processes. The car industry is probably the most important example, with the spot and MIG/MAG welding operations in the body workshops of the assembly lines. Nevertheless, an increasing number of smaller businesses, client oriented, are manufacturing small series or unique products designed for each client. These users require a good and highly automated welding process to respond to client needs in time and with high quality. It is for these companies that the concept of agile production (*8,9*) applies the most, obviously supported by flexible manufacturing setups (**Figure 1**). Despite all this interest, industrial robotic welding has evolved just a bit and is far from being a solved technological process, at least in a general

www.iran-mavad.com
مرجع مهندسی مواد و متالورژی

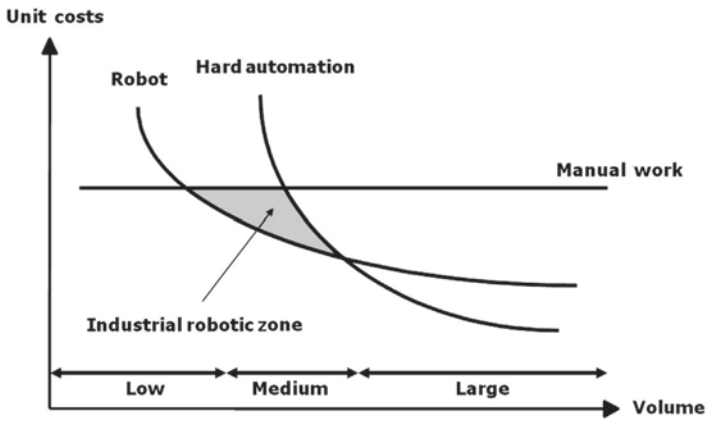

Figure 1 Industrial robot zone. Reproduced from Pires, N.; Loureiro, A.; Bölmsjo, G. *Welding Robots, Technology, System Issues and Applications*; Springer-Verlag: London, 2006.

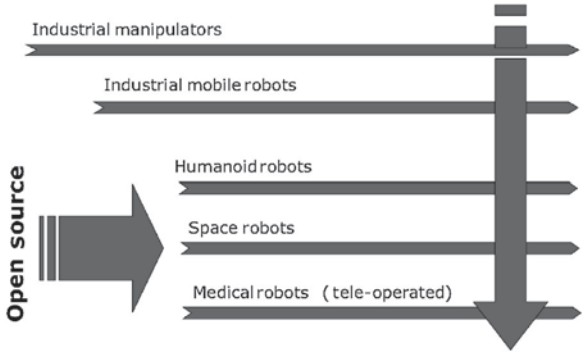

Figure 2 Conventional and modern fields in robotics research. Reproduced from Pires, N.; Loureiro, A.; Bölmsjo, G. *Welding Robots, Technology, System Issues and Applications*; Springer-Verlag: London, 2006.

way. The welding process is complex, difficult to parameterize and to effectively monitor and control (*10–14*). In fact, most of the welding techniques are not fully understood, namely the effects on the welding joints, and are used based on empirical models obtained by experience under specific conditions. The effects of the welding process on the welded surfaces are currently not fully known. Welding can in most cases (i.e., MIG/MAG welding) impose extremely high temperatures concentrated in small zones. Physically, that makes the material experience extremely high and localized thermal expansion and contraction cycles, which introduce changes in the materials that may affect its mechanical behavior along with plastic deformation (*15–17*).

Those changes must be well known in order to minimize the effects. Using robots with welding tasks is not straightforward and has been a subject of various R&D efforts (*18–22*). And that is so because the modern world produces a huge variety of products that use welding to assemble some of their parts (**Figure 2**). If the percentage of welding connections incorporated in the product is great enough, then some kind of automation should be used to perform the welding task. This should lead to cheaper products since productivity and quality can be increased, and production costs and manpower can be decreased (*23*). Nevertheless, when a robot is added to a welding setup, the problems increase in number and in complexity. Robots are still difficult to use and program by regular operators, have limited remote facilities and programming environments, and are controlled using closed systems and limited software interfaces (*24–28*).

6.04.2 Robotics in Welding

6.04.2.1 Motivations

Automated welding is no longer just for long-run, large-lot applications. New digital technology that links welding equipment and robotics to create easily programmable cells is enhancing its appeal for ever-smaller and more specialized applications. When robotics and welding operations come together on the shop floor, the results can include dramatic improvements in quality, better repeatability, faster production cycles, less downtime, and, with all of this, an increase in profits. New options in welding automation are broadening its application and its economic value as a production tool. More flexible programming and finely tuned digital communications between welding power sources, robotic arms, and positioning equipment make it possible to create a system that is economically justifiable and productive for manufacturing operations of almost any size.

www.iran-mavad.com
مرجع مهندسی مواد و متالورژی

The conventional wisdom has been that automated welding made sense only for longer runs of repetitive parts. Historically, the costs of fixturing and special work stations tended to create these limitations. New systems that combine easier programming, more flexible work holding, and cells that provide closer coordination between weld control, robotic motion, and work-piece positioning promise to make all but the smallest jobs candidates for automation. A company running different batches of 50 or 100 weldments now can gain many of the same benefits as one that is producing hundreds or even thousands of identical assemblies. Larger firms too can benefit by automating their shorter run or more specialized production welding using a 'packaged' pre-engineered system that is easily programmed to their changing needs. With strategic alliances between manufacturers of welding equipment, robotics, and positioners, even custom cells are often within reach for small-lot applications.

In the past, manufacturers often looked at only their most complex parts as candidates for automation and concluded the investment was not economically justifiable. Today, more flexible systems minimize the need for dedicated fixturing and make it easy to switch production from one part to another. The 80/20 rule frequently applies, as 80% of a company's production typically represents only 20% of its part sizes. The new robotic welding cells make it easier to automate more of these simple, often repetitive jobs and to switch quickly from one to another. The biggest reason to automate is that it makes economic sense. Robotic systems for short-to-medium run applications are now more affordable than ever. With a lower investment and greater productivity improvements, the return on investment (ROI) is greater than with larger, individually designed welding lines (3).

Consistent quality is another reason to automate. The fewer uncontrolled variables in the process, the higher the quality of the welds and the more uniform they will be. Improved quality levels and faster turnaround times also help create greater customer satisfaction. In contrast to custom fixtures, the flexible fixturing or work holding incorporated into the newest robotic cells makes it easy to switch back and forth between a variety of different products with little change over time. This also increases productivity and improves ROI. As with many skilled trades, there is a severe shortage of trained welding operators. This situation creates an 'automation imperative' in which it makes sense to transfer the skills to the machine and automate as many repetitive tasks as possible. Even when an operator is involved, labor content is lower. In a robotic welding cell, handling and welding occur simultaneously in two zones. While the operator loads and unloads in one zone, the robot welds in the other. Connectivity between the system's components is what makes welding automation different today from just a few years ago. New industrial communication networks now create a continuous loop for feedback and control of the entire process, from office computer to factory floor and back. Digital communications make these systems much faster than analog controls. They provide more throughputs and are more flexible as well. Moreover, it is easy to add parameters without adding more wires. Real-time process evaluation and connectivity to the Internet make it possible to monitor the process without hardwiring the components together, not only on the factory floor but also remotely, in a control room or even at a totally different location.

Equipment manufacturers that previously functioned independently are forming more strategic relationships. By pooling their individual knowledge, they are able to design products that work together effectively as systems. A company with welding expertise that joins with a leading robotics manufacturer and a supplier of innovative positioning systems can offer automated welding solutions that are more effective than if a user tried to assemble a work cell independently. Moreover, the manufacturers of complementary equipment are blurring the lines between their individual firms and creating a new synergy as they cooperate on re-engineering each other's products to work together.

Most robotics manufacturers do their major product development internationally, which sometimes makes it more difficult to coordinate the design of a system in which all components communicate effectively with each other. To facilitate this exchange, at least one robotics firm has centered its development of products for the North American market in the United States while also maintaining its international resources. This 'best of both worlds' approach allows the company to respond more quickly and effectively to local market needs.

6.04.2.2 Disadvantages of Welding Robots

Despite the advantages of using a robotic welder, they also present a few concerns. Robotic welders are expensive to purchase, which means that an average business cannot afford one. They require trained personnel to man and program and can often break down or need repair. Other concerns are that the limited movement of a robotic arm might not allow the robot to weld all necessary places. This means that a human welder will still have to go in and finish the job. If the object needing to be welded has been placed incorrectly, the welding robot will still weld in exactly the same programmed places, so that the welds are 'off' or located in the wrong place. Poor programming can also produce inaccurate results. Robots are also limited to only a few types of welding, and many of these take longer to cool or can even weaken metal if not used properly (4).

6.04.2.3 Automated Welding

Rectilinear robots move in line in any of three axes (X, Y, and Z). In addition to linear movement of the robot along axes, there is a wrist attached to the robot to allow rotational movement. This creates a robotic working zone that is box shaped. Articulating robots utilize arms and rotating joints. These robots move like a human arm with a revolving wrist at the end. This creates an irregularly shaped robotic working zone known as the work arc.

www.iran-mavad.com
مرجع مهندسی مواد و متالورژی

There are many factors that need to be considered when setting up a robotic welding facility. Robotic welding needs to be engineered differently than manual welding. Some of the considerations for a robotic welding facility are listed here.

The selected welding programs include start/stop, gas pre-flushing, electrode feed, and nozzle flushing. Robots have been used for about 15 years to weld complete automotive body assembly and subassembly components. In general, equipment for automatic arc welding is designed differently from that used for manual arc welding. Automatic arc welding normally involves high duty cycles, and the welding equipment must be able to operate under those conditions. In addition, the equipment components must have the necessary features and controls to interface with the control system. The number of items of any one type to be welded must be large enough to justify automating the process. If the joints are to be welded on a work piece are few, straight, and easily accessible, a rack automatic GMAW gun or GTAW torch may be suitable for key welds.

An automatics gun also can be used in a fixed position or on a curved track for a curved or circular weld such as joining two pieces of pipes or welding a flat base to a cylindrical shape – a task in which a work piece can be rotated past the gun. If parts normally need adjustment to fit together correctly, or if joints are to be welded, or if they are too wide or different positions from piece to piece, automating the procedure will be difficult or impossible. The tabletop size robot is used to maximum effect: welding a work piece is one side of a revolving jig. Each side of jig also can be revolved to allow access to both sides of the work piece. Robots work well for repetitive tasks on similar pieces that involve welds in more than one axis or where access to the piece is difficult. Welding robots are used in two ways in manufacturing – as elements in production line and as stand-alone units for batch production. Few companies move from all manual welding to a completely automated production line, so many people introduce robotic welding with a stand-alone cell.

At fabrication or welding trade shows, a variety of welding robots can be seen performing complex maneuvers and elegant pirouettes similar to troupe ballet dancers. These displays are designed to demonstrate the speed and flexibility of today's generation of robots. The fact is, dance moves aside, today's robots can handle a wide range of welding applications. Some of the welding operations that can be performed by robots are as follows:

1. Arc welding
2. Metal inert gas (MIG) welding
3. Tungsten inert gas (TIG) welding
4. Spot welding
5. Stick welding

6.04.2.4 Examples of Welding Robots

This section gives a few examples of current welding robots.

KUKA: Their versatility and flexibility make the KUKA KR 6-2 and KR 16-2 (**Figure 3**) our most popular robots. These masterful movers have a payload of 6 or 16 kg and, thanks to their design, are ideal for all space-saving, cost-effective system concepts. That is why they are used virtually everywhere – both in the automotive components industry and in non-automotive sectors. With minimized disruptive contours and a streamlined robot wrist design, these high-precision multitalents offer outstanding

Figure 3 (a) KUKA KR 6-2 robot and (b) FANUC F-200iB robot. Reproduced from KUKA Industrial Robots. http://www.kuka-robotics.com; FAUNAC Robotics America. www.fanucrobotics.com.

www.iran-mavad.com
مرجع مهندسی مواد و متالورژی

Figure 4 Panasonic Perform Arc robot. Reproduced from PANASONIC Robotics. http://www.panasonicrobotics.eu.

accessibility, even in confined spaces. For cleanroom requirements or environments with a high degree of fouling and high temperatures, the KR 16-2 is also available in the special variants Cleanroom (CR) and Foundry (F) (*29*).

FANUC: The FANUC F-200iB (**Figure 3**) is a 6° of freedom servo-driven parallel link robot designed for use in a variety of manufacturing and automotive assembly processes. The F-200iB is engineered for applications requiring extreme rigidity and exceptional repeatability in a compact, powerful package (*30*).

Panasonic: Panasonic Perform Arc C Series (**Figure 4**) are dedicated customized robot systems, made 100% on customer request. Some of the important features of these robots can be summarized as follows (*31*):

- High-quality welding with high production rate
- Torsion-free design for easy transportation with no programming correction, and for program exchanges between the robots for production expansion
- All from one solutions reduce interfaces from different supplies and increase productivity.

Motoman: Motoman is extending the success of its arc welding robotic arms with the introduction of the first seven-axis arc welding robot. The flexibility of the VA1400 model (**Figure 5**) can be used to reduce floor space and achieve higher robot density for increased production. The unique 'elbow' axis of the arm also allows the robot to reach around tall parts or reach into boxy parts (*32*).

CLOOS: Due to the modular product design, the new generation of CLOOS QIROX welding robots (**Figure 5**) can be optionally equipped with a seventh axis. The offset axis mounted in the robot base permits horizontal movement of the robot up to 550 mm. The welding of complex work pieces is simplified and accelerated thanks to the considerably increased range. The setting and positioning efforts are considerably reduced because, thanks to the eccentric movement, the welding head can be moved around corners or into niches much more easily, for example (*33*).

Daihen: The Daihen FD-V6 (**Figure 5**) is suitable for virtually all MIG, MAG, CO_2, and TIG welding applications, and air plasma cutting applications. The FD-V6 may be used for common materials such as mild steel, stainless steel, aluminum, titanium, as well as other exotic metals (*34*).

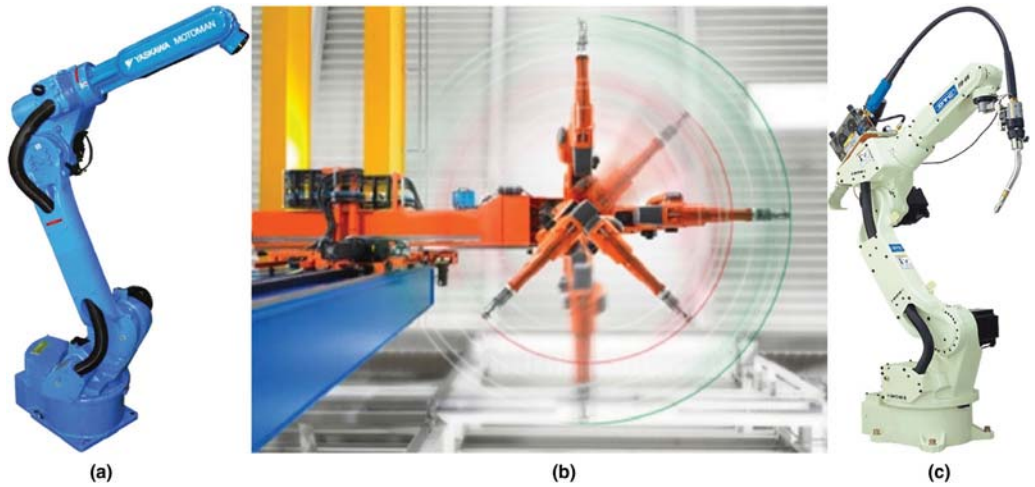

Figure 5 (a) Motoman VA1400 robotic arm (reproduced from YASKAWA MOTOMAN Robotics' Robotics. http://www.motoman.com); (b) CLOOS QIROX welding robots (reproduced from CLOOS Robots. www.cloosrobot.com); and (c) the Daihen FD-V6 robot(reproduced from DAIHEN Robotics. www.daihen-usa.com).

www.iran-mavad.com
مرجع مهندسی مواد و متالورژی

6.04.3 Robotics in Different Welding Techniques

6.04.3.1 Spot Welding

Spot welding is widely used in the automotive industries for the efficient joining of metal sheets (*35*). Classified under resistance welding, spot welding acts by generating heat with use of a high current, approximately about 1000 A–100 000 A. The welding guns are the main part of the welding. There are two different kinds of guns, but the important fact is that they have a similar function, to make a close loop circuit connecting the power supply to the weld spot (**Figure 6**).

The current passes through the sheet metals as the two guns clamps simultaneously. The high current provided will cause the surfaces in contact with the electrodes to melt. After the energy reaches a sufficient level, a weld nugget will start to form. The surfaces (between the sheets, having the highest resistance) heat to a solid–liquid temperature and form a molten weld pool (*36*). The weld spot, which is the so-called HAZ, cools down via the thermal condition, where the heat is transferred to the gun, which is cooled by water that flows through it. The gun is then open to complete the process. The advantages of spot welding are that this method uses an efficient energy that is supplied by electrical power and generates a high current through the generator. This method consumes less time for heating the materials. Plus, with time for changeover of material, this method has less lead time than other methods and enjoys high production rates. In addition, spot welding is easy for automation due to its simple construction and yet it requires no filler materials.

The equipment commonly used in spot welding can be divided into two main types: welding equipment and robotized equipment. The welding robot is available in various sizes, which are classified according to the maximum load the robot can manipulate, how far the robot can reach for welding, and the number of axes that the robot can work on. The welding gun is attached to the end effector of the robot. It is designed to fit the assembly process, which come in two types: C-type, which is to be the cheaper, and X-type. These gun are operated by means of pneumatic actuator, which provides uniform electrode force and hydraulic actuation, which is often used when high pressure is needed in a small or limited space (**Figure 7**). However, a new servo gun was invented, in which a servo motor operates the gun (*37*). This gun has more accurate electrode force control compared to a pneumatic gun (*38*).

Basically, a welding gun applies appropriate pressure and current at the welding spot. This means the gun will be exposed to heat and pressure that will cause deformation of the welding electrodes. An automatic tip dresser is used to sharpen the electrode (**Figure 8**). This is needed because of soft electrode material, high welding current, and high pressure. The dressing is done after each working cycle and takes about 1–2 s. To maintain a good contact surface of the electrode is important; it defines the quality of the welding. In addition, maintaining proper electrode geometry can reduce production downtime and utility cost. One main problem usually encountered during the welding process is position of the cables and hoses, which tend to limit robot movement. A swivel is used to provide compressed air, cooling water, current, and signal within single rotating unit.

A swivel greatly improves the efficiency of robotic welding (**Figure 9**). It maximizes the utilization of access to spot-weld areas. It fits directly onto the robot's end effector without any hoses or cables and ensures the high quality of the spot weld. A spot weld timer is used to control welding time and the current as well as the sequence and time of other parts of the welding cycle.

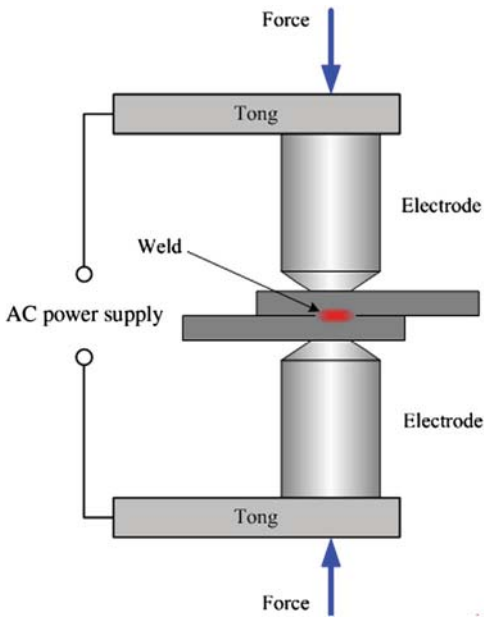

Figure 6 Process of spot welding. Reproduced from Radhakrishnan, V. M. *Welding Technology and Design*; New Age: New Delhi, 2006.

www.iran-mavad.com
مرجع مهندسی مواد و متالورژی

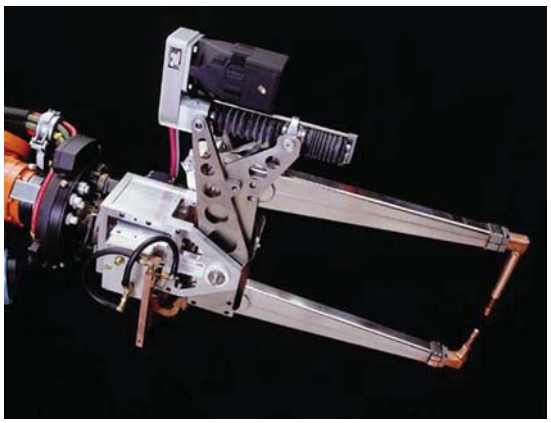

Figure 7 C-type welding gun. Reproduced from Radhakrishnan, V. M. *Welding Technology and Design*; New Age: New Delhi, 2006.

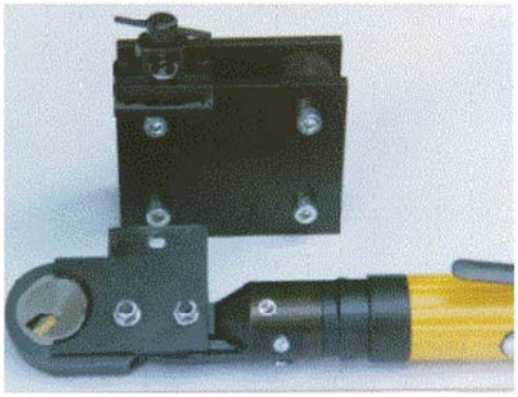

Figure 8 Tip dresser. Reproduced from Timings, R. Fabrication and Welding Engineering; Newnes: Oxford, 2008.

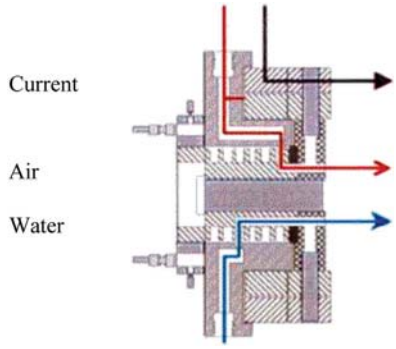

Figure 9 Swivel. Reproduced from Timings, R. Fabrication and Welding Engineering; Newnes: Oxford, 2008.

As with other methods of welding, this method of welding also has a number of parameters that need to be considered during the welding process. It is important to have the optimum control of welding parameters to obtain the satisfactory result of the nugget formation, thus defining the level of quality of the welding itself. Spot welding parameters includes the electro force, the diameter of the electrode contact surface, squeeze time, weld time, hold time, and weld current. A minor adjustment in any of the parameters will influence all other parameters. The diameter of the electrode contact surface has a strong relationship with the electrode force. Lai et al. (*37*) have estimated the electrode face diameter based on a servo gun. A servo gun has more accurate electrode force control. It touches the sheet metal softly, reducing impact and improving the electrode lifetime. In their research, a mathematical model was derived to estimate the face diameter. It shows that an increase in welding current and force will increase the electrode wear rate, and this causes the electrode to be smaller in diameter (*37*). As the electrodes apply force to the metal sheets,

www.iran-mavad.com
مرجع مهندسی مواد و متالورژی

the electrodes are squeezed. The interval between the initial of force applied and the current supplied is necessary to ensure the force has reached the desired level before the weld current reaches overload. This prevents spatter, which would cause the electrode and the sheets to stick together.

The weld time should be as short as possible. This is the time when the nugget is formed and enlarges. This can define the strength of the weld. Aslanlar et al. (39) observed welding time effect on welding joint strength. The welding time of 12 and 15 periods give the optimum tensile shear strength at welding current 10 kA, and a welding time of 10 periods give optimum peel strength at welding current of 11 kA. This is because it is sufficient time for the nugget to grow to its optimal size. It should be at least 20% and not exceeding 80% of the sheet thickness.

The holding time is the time after welding process, when the electrodes are still clamping the sheets. This cools the weld and allows the nugget to solidify and join the sheets. The condition meets the principle of heat transfer. As water cools the electrode, heat from the weld spot is transferred to the cool area to achieve a thermal equivalent. This interval time should not be too long because the weld could become brittle. However, a longer hold time is recommended whenever galvanized carbon steel is used.

Another parameter that significantly influences the welding is the weld current. The weld current is controlled by the setting of the transformer tap switch and the amount of current control. Use of correct current amount also defines the strength of the weld joint. Aslanlar et al. (40) studied the influence of welding current on welding joint strength and found that optimal tensile shear strength and tensile peel strength are attained at 10 and 11 kA of welding current, respectively. The current should be kept as low as possible. Spatter will occur if the current reaches the overload amount.

Technology can be expensive, but it does improve lives. Robotic spot welding not only increases production volume and reduces manufacturing lead time, but also improves the quality of the product. In fact, the best production cost is obtained compared to manual work in small or medium batch manufacturing (41). Common applications of spot welding are manufacturing nickel-cadmium batteries, welding metal sheets in automotive industries, and even in orthodontists' clinics, which is used to resize metal 'molar bands.' As its main purpose is to join metals, the welding process is mostly used in assembly worldwide. It is a complex and difficult to parameterize and to monitor and control effectively. However, the effects on the joint are not fully understood (4).

The main areas of research are in the robotics, sensor technology, control systems, and artificial intelligence. All of these are controlled by the main component called a controller, which acts as a 'brain' for the robot. The controller is used to program the robot, give an order to the robot to activate sensors, move, and activate the welding gun to perform a task. Most of the failures in implementing robots are from the software that controls the robots. Many researchers are studying the problems related to well-defined tasks performed by the controller. Problems not only affect the physical movement of the robot, but also might affect the quality of the welding itself. An algorithm is created to provide a step-by-step process that is used to solve the problems. Lee et al. (42) found that the quality of current resistance spot welding process is poor, with a high expulsion rate. He has come out with neuro-fuzzy algorithm in order to reduce the percentage of specimen error and hence increase welding quality. His research showed that the neuro-fuzzy inference system is an appropriate technique in monitoring the quality of the spot welding process. Too long welding duration and current will decrease the tensile strength because of too much melting. One critical task of the controller is to control the welding parameter and monitor it to maintain the consistency of the parameter's magnitude during the welding process. Jou (43) has investigated the effect of changeable parameters to output signal for a variety of steels in automotive industry. He found that extremely high current yields excessive nugget and led to molten metal expulsion that can cause unpredictable effects. Increased current supply will also increase the rate of joule heating.

Another approach used to solve problems is using artificial neural networks. A mathematical model is used to model complex relationship between inputs and outputs or to find patterns in data. This has been used by Martin et al. (44) to explain a neural network system that is capable of interpreting ultrasonic oscillograms obtained by a pulse echo method. It is able to classify the unused input vectors in training as 10 components vector are used to describe ultrasonic oscillograms. Cho (45) explains a system that is capable of evaluating the quality of resistance spot welding using a dynamic resistance pattern. He found that the Hopfield is established as a welding quality estimation system using the pattern recognition method. This system is suitable for an industrial environment. The neural network produces the best results in strength and nugget diameter estimation. The measurement must be made when current rate of change is equal to zero to avoid inductive noise.

6.04.3.2 Arc Welding

The father of robotics, George Charles Devol, created the first industrial robots in 1954 (46). Industrial robots continued to evolve and are directly influenced by developments in computers and by massive production demand. The development of arc welding robots in terms of design, control system, and sensing ability is seen among engineers as a potential area of growth because it will give highly positive impacts to the whole production. Design is in general defined as the establishment of a new algorithm wherein a mathematical equation describes the physical parameters' setup of the robot (47). The most important part of the arc welding process is the arc itself. The welding process consists of two types of control system, manual control and automatic control (47). Significant differences between automatic control and manual control influence product quality level, numbers of production, error occurrences, hazardous working environments, and total production costs.

Another important consideration in improving the arc welding robot system is its sensing ability. Sensors integrated in the central welding system will convert the information from parameters involved into quantitative data such as digital signal, voltage, and current (47).

www.iran-mavad.com
مرجع مهندسی مواد و متالورژی

An example of an automated welding process is the work done by Lima and Bracarens (48) that used structure for electrode voltage decrement in order to detect temperature change during the process. As a result, the chosen value of arc voltage for the welding process becomes more accurate. Creating control for the right torch angle is also an important factor in ensuring high-quality welding. Silva et al. (49) established a parallel structure robot where the axes are independent of each other. Therefore, if any defect happened at particular axis, it would not influence the other axes, avoiding unnecessary use of a high accuracy actuator. Damage will not spread to other axes, resulting in lower maintenance cost. Previously, some researchers such as Rubinovitz and Wysk (50) used offline programming system in their experiments that improves the productivity and efficiency of the welding process. The total time needed for online programming tasks is reduced because the process of defining specific points is eliminated. The system also lowers the buildup costs of the robot programming system.

By providing new opportunities for welding technologies, the applications of mobile robots have increased rapidly because they can replace human workers in hazardous working environments. Lee et al. (51) designed a mobile welding robot with optimization based on workspace, which is 13% lighter than the original design, as shown in **Figure 10**. Moreover, this robot is beneficial when it comes to building shipyard structures. However, design efficiency is lessened by about 4.9%. Chang et al. (52) developed a method for mobile welding robots to detect seam and plot the 3D configuration of the profile. It is tested by using straight line butt welding. The robot is also robust since it can work accurately with unpredictable profiles and rough bead surfaces. Tung et al. (53) described an image-guided mobile robotic system that is capable of producing higher quality welding compared to manual work by experienced workers. After recognizing the defect part, the robot will move to the intended welding path. The welding path is achieved by using the newly introduced algorithm.

On the other side, Karadeniz et al. (54) observed the influence of welding parameters on welding penetration. Generally, higher welding current and arc voltage lead to higher penetration depth. Welding current has a stronger effect on penetration compared to arc voltage and welding speed. Control of weld shape is also important to ensure that the welding process meets the requirement specifications (55), and a new reinforcement model functions as a feedback element. The system can also be integrated with a teach and playback robot in order to control the welding current and wire feed rate. Apart from weld shape, a uniform cross-section of the bead profile is essential in maintaining product quality. Bead profile forming is also critical for surface quality improvement. Therefore, an optimal model in creating the bead profile is an essential requirement in arc welding. Xiong et al. (56) found that shape of the bead profile is highly affected by the ratio of wire feed rate to welding speed. Using the best model in a single bead section, a perfect smooth surface is achieved by determining the center distance of adjacent beads.

The control system in robotic arc welding is categorized as an open-loop system or a closed-loop system. The open-loop system is the basic concept of any control system in a welding process, while closed-loop system is an improved system. There are optimal control, adaptive control, and intelligent control. For instance, the work done by Daeinabi and Teshnehlab (57) developed an appropriate algorithm for controlling the arc welding process in terms of seam tracking. Using the algorithm, robots are able to perform good quality welding at any point and can work in hazardous environments. Formerly, Murakami et al. (58) found that a fuzzy logic controller reduces the vibration in a tracking locus by using weld-line tracking control. Another important factor that affects product quality is bead width. Xue et al. (59) introduced a fuzzy regression system that is capable of maintaining welding quality by applying a linear regression model together within the fuzzy variable of the triangular membership functions. The system produces accurate measurement of bead width. Sayyaadi and Eftekharian (60) established the application of a SCARA robot in GMAW. Combinations of various methods are used in controlling the system such as feedback linearization, neural network, and fuzzy controller, resulting in improvement in system efficiency. Earlier, an intelligence robotics system named ROBOEDIT (61), an expert

Figure 10 RRX4 mobile welding Robot. Reproduced from Stinchcomb, C. *Welding Technology Today, Principles and Practices*; Prentice-Hall: New Jersey, 1989.

www.iran-mavad.com
مرجع مهندسی مواد و متالورژی

system designed specifically for floor adjustment, was developed. The programming assistant is very efficient and results in an increase in production numbers. The system is also capable of interpreting numerical control robot programming and English-like format.

Dung et al. (62) introduced an adaptive nonlinear controller that improves wheel mobile robot detecting ability, as shown in Figure 11. The system is powerful and hardly affected by disturbances from outside. Multivariable control introduced by Huissoon et al. (63) contains an empirical state space model. It has the ability to identify reference steps and produce fair disturbance rejection.

Incompetent seam tracking has proved to be crucial for quality problems in welding process. Xu et al. (64) established a new technology for seam tracking with a self-designed passive vision sensor that is capable of producing a clear welding image for seam tracking. Then, a segmented self-adaptive proportional-integral-derivative controller will monitor seam tracking in order to surpass seam-forming quality requirements. Without doubt, intelligence control system is currently the best applied method practically. There are a lot of works done by researchers to create the modernized system. For example, Liu et al. (65) created an intelligent motion navigation method that is capable of estimating a zero accident path, thus significantly minimizing energy utilization. The programming also provides a welding process of high quality and efficiency. Chu and Tung (66) produced an automatic control system equipped with a fuzzy gain scheduling controller that is capable of performing human tasks and shielded metal arc welding. Zhu et al. (67) explained in their paper how the starting position of a weld seam is detected using pattern match technology. Faster matching technology avoids a time-consuming process, and the ability of the system gives good technical support to the welding robot.

In a welding process, a sensor is used for estimating the condition of the work piece, then transferring the information to the robotics system for further action. Normally, the sensor is in the form of a portable micro-electronic device and plays an important role in the whole mechanized system. Park et al. (68) explained about mobile welding robots used for application in U-type cells. The system is equipped with a touch sensor to modify any misplaced positioning and dimensioning. Nevertheless, the price of the robot is very high and it is also very heavy. Sweet (69) has developed an application of a vision sensor system using the General Electric P50 as shown in Figure 12. The welding robot produces excellent results for welding joints of 12 mm at 12 cm s^{-1} welding speed. Kim et al. (70) established a system to calculate the position and orientation of end effectors. It adjusts 19 controllers' gains for a six-axis manipulator. The maximum magnitude frequency goes down by 54%. Luo and Chen (71) developed a seam tracking

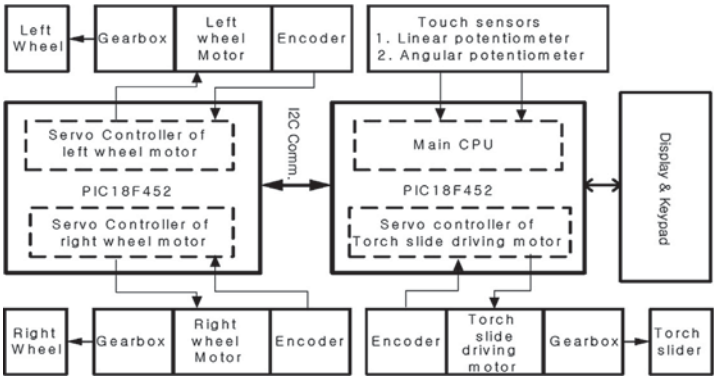

Figure 11 Control system configuration adapted from Dung et al. Reproduced from Dung, N. M.; Duy, V. H.; Phuong, N. T.; Kim, S. B.; Oh, M. S. Two-wheeled Welding Mobile Robot for Tracking a Smooth Curved Welding Path Using Adaptive Sliding-mode Control Technique. *Int. J. Control Autom. Syst.* **2007,** *5* (3), 283–294.

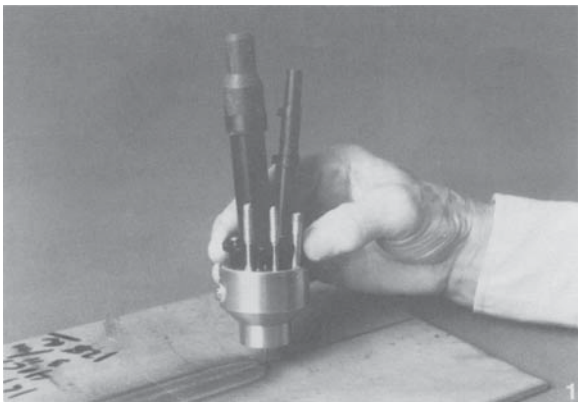

Figure 12 Integrated torch sensor. Reproduced from Kusiak, A. *Modelling and Design of Flexible Manufacturing Systems*; Elsevier: Amsterdam, 1986.

www.iran-mavad.com
مرجع مهندسی مواد و متالورژی

controller that is equipped with a laser-based camera. The system has the capability to calculate the starting welding position and to employ two-point linear interpolation in order to detect missing seam points.

Design and modeling, control system, and sensing ability in robotics arc welding focus on vital factors for innovation. Heat transfer, arc characteristics, and weld bead geometry are the important factors that influence the concept in designing welding robots. These factors will directly affect the total cost and the power supply of the whole production. For the control system, manufacturers concentrate more on weld penetration ability, control of joint profile, and also control of filling rate. Examples presented in this chapter are fuzzy logic control, neural network control, and knowledge-based control. Seam-tracking accuracy is also critical in ensuring a high-quality product. The same goes for sensor ability. It will depend on how fast a sensor can transform the information from the work piece, variety of application of the sensor, and also covered area of the sensor.

6.04.3.3 Friction Stir Welding

In the relatively short time since its invention, a new welding process has found potential applications in a number of industries, including aerospace (military/civilian aircraft, aircraft parts, fuel tanks, rockets), land transportation (tailored blanks, truck bodies, armor plate vehicles, wheel rims, engine and chassis cradles, fuel tankers, motorcycle and bicycle frames), railway (tankers and wagons, container bodies, underground carriages, and trams), shipbuilding and marine (panels for decks, sides, bulkheads and floors, helicopter landing pads, offshore accommodation, hulls and superstructures, aluminum extrusions), construction (aluminum bridges, window frames, aluminum pipelines, heat exchangers, facade panels), electrical (bus bars, electrical connectors, electric motor housings, encapsulation of electronics), and gas (tanks and cylinders) (*72*).

Unlike fusion welding processes, for example, arc welding, electron beam welding, and laser welding, friction stir welding (FSW) takes place in the solid phase below the melting point of the materials being joined (**Figure 13**). Advantages that have been cited for the process include the ability to weld alloys that are difficult to weld by fusion welding processes; excellent mechanical properties; low distortion and shrinkage; no fume, porosity, or spatter (frequently associated with arc welding); energy efficiency; and the ability to be used in all positions (*72*). Additionally, FSW uses a non-consumable tool, requires no filler wire or gas shielding, and is tolerant of thin oxide layers.

FSW applications can be expected to expand substantially when industrial robots are used in place of currently employed heavy-duty machine tool equipment. This will permit welding three-dimensional contours, with the robots offering the advantages of greater flexibility and availability, and relatively low cost (*72*). It was not until the Friction Stir Welding Symposium in Gothenburg, Sweden in 2000 that the first robotic FSW application was demonstrated (*73*). Two research groups presented successful welding in aluminum, where one group used a serial kinematics robot (*74*) and the other used a parallel kinematics robot (*75*). The work by C. Smith was initiated in 1997 with internal feasibility studies at Tower Automotive (*76*) and could be seen as the first investigation of robotic FSW.

The most common design for industrial robots is serial kinematics. It is widely adopted in the automotive industry and has been tested in the area of FSW by several research groups in the past (*77–79*). However, alternative systems have also demonstrated using a parallel kinematic robot (*75*). Such robot systems have a much better stiffness but lack the large workspace that serial kinematics robots offer and are far more expensive. A serial kinematics robot has great advantages but has limited stiffness (*74*). A robot also consists of many components with certain flexibility. Inaccuracies in robotics are mainly caused in the joint by torsional flexibility in the gears, bearing deformation, and shaft windup (*80*).

Since 1996, efforts have been put into creating a robot-based FSW technology (*81*). Early in the development of friction stir welding, it was recognized that it had many advantages over other joining processes for aluminum in numerous applications. However, it was often concluded that FSW was uncompetitive in many of these applications for several reasons. First, the high forces that FSW requires meant there was a need for expensive custom-built machinery (*82*). These custom-built machines also created relatively high productivity losses in many applications, due to the inability to achieve high duty cycles ('on time'). These two factors

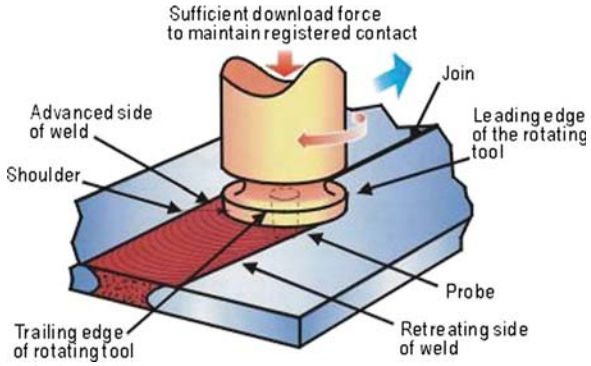

Figure 13 Principle of friction stir welding. Reproduced from Radhakrishnan, V. M. *Welding Technology and Design*; New Age: New Delhi, 2006.

www.iran-mavad.com
مرجع مهندسی مواد و متالورژی

made FSW uncompetitive, especially where robotics is currently employed. To overcome this issue, the robotic FSW solutions were developed (*82*).

Neos Tricept type robots have a parallel kinematic structure, which yields a significantly stiffer structure than the serial structures typically used with other industrial robots (**Figure 14**). This parallel kinematic structure has definite advantages when attempting to develop robotic FSW systems. However, these type of robots have rather limited working envelopes when compared to serial kinematic structures. Additionally, their cost has been significantly higher than standard serial kinematic robots (*82*).

Since the welding procedures do not call for widely varying operating parameters, stable robust force feedback control can be readily implemented with properly sized industrial robots (*72*). For example, Smith (*77*) reported a robotic FSW system based on the use of an ABB IRB 7600 articulated robot arm as shown in **Figure 15**. This robot has a 500 kg payload. The spindle and motor drive for rotating the pin tool are attached to the end plate of the manipulator. The spindle is designed to accept the forces (both axial and radial) required for FSW and it additionally contains force sensing for force feedback control. Smith (*77*) have shown that the system is capable of maintaining constant axial force even under conditions of a programmed 3 mm change in component surface height over the length of the weld. Furthermore, these robots are stiffer than the previous serial kinematic robots. Another important advancement with these new robots is the modern, more powerful control systems that allow for significant improvements in the force control system capability (*82*).

An ABB IRB 940 (**Figure 16**) is a Tricept type robot. Its parallel design provides an extremely stiff structure that is capable of a vertical force of 1300 kg (*83*). The high stiffness of this arm design is derived from the use of three parallel linear actuators connected to a center tube in the middle with three additional axes on the wrist (*72*). The working envelope of this type robot is less than the articulated serial arm and it provides excellent rigidity for stable force feedback control. Strombeck (*84*) reported the use of a parallel robot for robotic FSW with force feedback control and reported an excellent result with the system.

This type of robot is much more competitive with the serial kinematic structures. In applications where a relatively small work envelope is required or where more force capability is required, the use of this type of robot will be competitive with other robotic joining technologies. This type of robot would also be helpful in applications where machining of the part is also required. A further

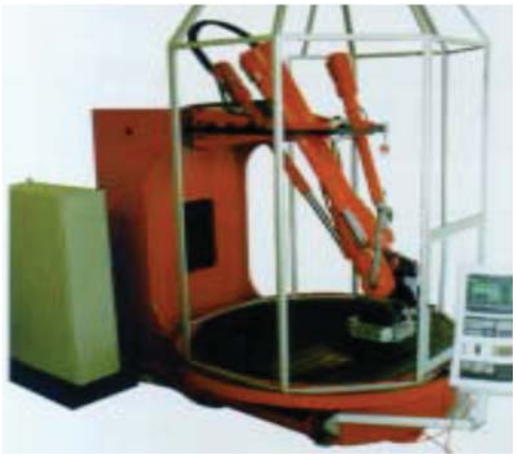

Figure 14 Neos Tricept Robot. Reproduced from Rosheim, M. E. *Robot Evolution: The Development of Anthrobots*; John Willey & Sons: New York, 1994.

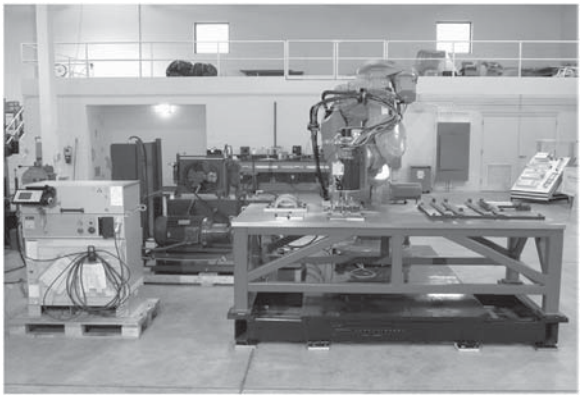

Figure 15 ABB IRB 7600. Reproduced from Agren, B. Sensor Integration for Robotic Arc Welding. Ph.D. Thesis, Lund University, 1995.

www.iran-mavad.com
مرجع مهندسی مواد و متالورژی

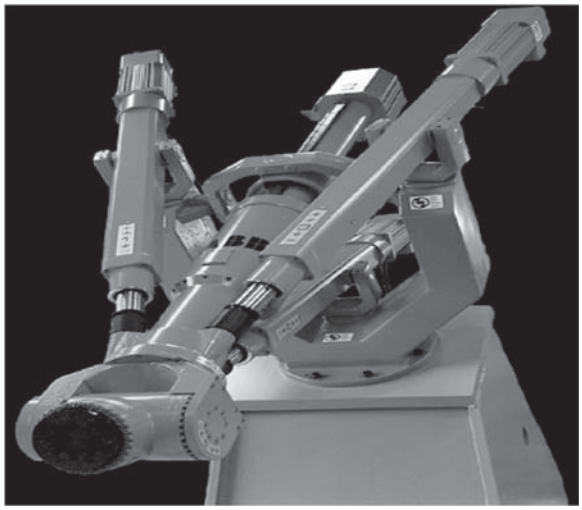

Figure 16 ABB IRB 940. Reproduced from Smith, C. B.; Hinrichs, J. F. *Robotic Friction Stir Welding: State-of-the-Art*, 2005. http://www.frictionstirlink.com/publications/Pub124thFSWSymposiumRoboticFSWpdf.pdf.

benefit of this new solution is that this robot now has a common architecture with the serial kinematic robot, making integration of other FSW hardware and software relatively seamless (*82*).

ABB IRB 6400 robot (**Figure 17**) has the open architecture that is required for any robotic FSW system. This robot system has been used to make thousands of parts, but its applicability in production applications is still questionable for several reasons (*82*). First, the high duty cycles seen in production applications tend to overheat the robot's motors. Second, the response time of the force control is still slower than would be required for production application. Last, the relative lack of stiffness of the robot can make development of weld paths challenging and require a highly skilled robot programmer. Thus, this robot system is relegated to prototype applications (*85*).

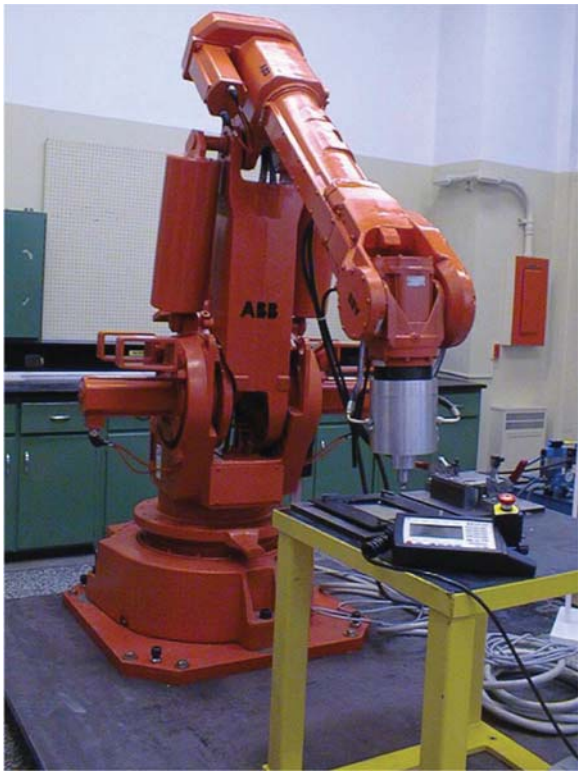

Figure 17 ABB IRB 6400 robot. Reproduced from Hinrichs, J.; Noruk, J.; McDonald, W.; Heideman, R. Challenges of Welding Aluminium Alloys for Automotive Structures. *Svetsaren* 1995, 50 (3), 7–9.

www.iran-mavad.com
مرجع مهندسی مواد و متالورژی

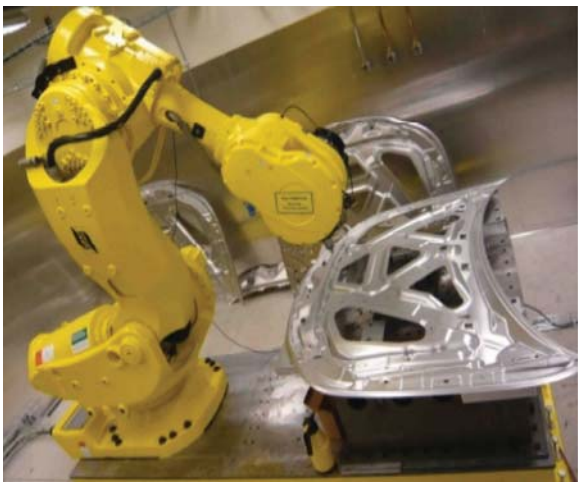

Figure 18 FSW robot welding automotive body parts at the Production Technology Centre. Reproduced from Hinrichs, J.; Noruk, J.; McDonald, W.; Heideman, R. Challenges of Welding Aluminium Alloys for Automotive Structures. *Svetsaren* 1995, 50 (3), 7–9.

An FSW-robot cell was established at the Production Technology Centre in Trollhättan, Sweden. The project aimed to bring robotic FSW closer to industrial applications by eliminating constraints, related to the robotic implementation of the FSW process, and by further control and automation of the process (*83*).

The control system is adapted to a five-axis controller, and a force sensor for direct force control is implemented. The robot comes with several instructions for programming FSW of simple geometries. This robot system also comes with several software features for programming simple geometries such as squares, lines, and circles. These functions require only some teach-points to define that geometry, and the welding path with desired tilt-angle is calculated from those points. However, the robot did not include a function that can use offline-programmed robot paths for FSW.

Industrial robots would be a preferred solution for performing FSW for a number of reasons, including their widespread use in the automotive industry (*86*), their ability to repeatedly follow three-dimensional paths, and their low costs. The use of an industrial robot for FSW could also be a major improvement because many process changes can be intercepted by a software adaption. The first industrial robots had insufficient stiffness and since they could not deliver the required down force, they were not suitable to use for FSW. However, nowadays there are robots with very high payloads of 1000 kg and more that are also very stiff. This makes a breakthrough of robotic FSW possible (**Figure 18**).

As mentioned previously, there are two different robot concepts useful for FSW, which is parallel and serial construction. A parallel construction is much stiffer and provides very good results, but it has a few important drawbacks. The system is more complex, it has a very limited workspace, and the cost, compared to a serial robot with the same payload, is much higher. Nevertheless, the compliance problems are very detrimental in a serial design robot, where the design is more suitable for applications in the industry. The motor that is used in the FSW robots can be either hydraulic or electric. According to Smith, the major advantage of a hydraulic motor is it has a lower volume to power ratio, making it the best motor choice in the industry.

6.04.4 Current Research Topics in Robotic Welding

6.04.4.1 Path/Motion Planning

Once the programmer has defined all of the seams within the vehicle that are to be welded, they then move onto the next programming task, which relates to planning the motions required for the robotic cell to correctly carry out the welds. In welding rapid manufacturing technology, path planning is equally important.

The problem of effective motion planning for industrial welding robots was discussed by Trnka and Bozek (*87*) in two parts. The first part dealt with the current method for off-line motion planning. In the second part, the presented work was done by one of the simulation systems with automatic trajectory generation and off-line programming capability. Some researchers considered a two-robot welding coordination of a complex curve seam, which means one robot grasps the work piece, the other holds the torch, and the two robots work on the same work piece simultaneously (*88*). They built the dual-robot coordinate system at the beginning, and a three-point calibration method of the two robots' relative base coordinate system was presented. After that, the non-master/slave scheme was chosen for the motion planning, the non-master/slave scheme set the poses versus time function of the point u on the work piece, and calculated the two robot end effecter trajectories through the constrained relationship matrix automatically.

Multi-pass weaving welding is usually used in thick plates (*89*). Automatic path layout of multi-pass weaving welding is a key technology to realize robot automatic welding for thick plates. In a study by Zhang et al. (*89*), a user self-defined path layout model was developed to realize teach offline programming for multi-pass weaving welding. Users can set the welding parameters of every pass, the number of layers and passes, and welding sequence according to the real welding technology. The developed system can

www.iran-mavad.com
مرجع مهندسی مواد و متالورژی

produce the position, pose of welding torch, and oscillation displacement of total passes automatically. The multi-pass welding shape is well designed and meets the actual production requirement through robot multi-pass weaving welding experiments for single V-groove thick plates. In order to solve the problem that the welding robot path planning in the production line of body in white (BIW) is inefficient, some researchers analyzed the problem of the welding robot path planning and abstracts it into the traveling salesman problem (TSP) model (*90*). Afterward, the optimal welding path was calculated using ant colony optimization. The result shows that this algorithm is an accurate and effective tool for welding path planning.

A four freedom robot able to carry out automatic welding of offshore platform was introduced (*91*). The kinematic design of the robot has been designed according to the welding seam feature of a T/Y/K-joint. The path planning of T/Y and the obstacle avoidance technique are used to study the robot's collision avoidance welding on a K-joint. In the process of K-joint path planning, the geometrical method was adopted to study the welding torch's posture in branch gap. For ensuring the postural stability of the robot, the robot posture of a series welding points in the single branch pipe condition was adjusted gradually in the K-joint condition. For a mobile welding robot, its kinematic and inverse kinematic model was calculated based on the D-H method (*92*). This method used the approach of interpolation to do path planning of a mobile welding robot with a DOF arm, and adopt the method to make various welding path simulation. When the vehicle is walking across obstacles, it should do the welding at the same time.

Based on the UG/OPEN GRIP platform, a slicing and route planning algorithm was proposed (*93*). The robot NC code can be created automatically after slicing the UG part model and executing the route planning algorithm. By using the RP technology together with welding technology, it directly slices the UG 3D entity model on the UG/OPEN GRIP platform. This method is more effective and can avoid the problem of low precision caused by the conventional slicing method, which uses the triangles to approximate the 3D models. The proposed route planning algorithm generates a continuous route according to the feature of the model, improves the efficiency and quality of the modeling, and largely reduces the stop and start operations of the welding torch.

A path planning optimization method was proposed by Wang and Chi (*94*) to add learning ability to a teaching and playback welding robot. The optimization was divided into the welding points sequence improvement and trajectory improvement, which was done both on-line and off-line. Points sequence optimization was modeled as TSP and was continuously improved by a genetic algorithm (GA)-based strategy, while the trajectory between two welding points was improved on-line by a trial-and-error strategy where the robot tries different trajectories from time to time so as to search for a better plan. Simulation results verified that this control strategy reduced the time and energy cost as compared with the human-made fix-order sequence. In a study by Liu et al. (*95*), the quantic polynomial interpolation was adopted between each two adjacent desired via points, the continuous trajectory is formed in accordance with the time course. The simulation model was developed using Sim Mechnics, the movement parameters and path were obtained by simulating, the simulation results indicated that the motional parameters and path can be accurately and effectively obtained for robot analysis and design. An automated programming system for the combination of a laser beam deflection unit, a laser scanner, and an industrial robot was presented (*96*). According to the optimum path planning of the arc welding robot, a new gene insertion greedy genetic algorithm (GGA) was presented by Sun and Yan (*97*) to optimize the global path planning of the arc welding robot. The algorithm can be used in the multi-joint arc welding robot and also be used in the robot off-line programming. For the optimum welding path planning problem of a six DOF mini welding robot, a path planning method was proposed based on a GA (*98*). The off-line programming system of the MOTOMAN-UP20 arc welding robot based on OpenGL visual technology has a big position error. In order to resolve the problem, a novel method of real-time error correction was proposed (*99*). It reduced position error by optimal path planning, and then the signal of real-time error correction was inputted to a control robot to correct the robot path, which decreased all kinds of errors.

In view of the current lack of a theoretical basis for BIW welding robot path planning , a solution was provided that abstracts the problem of robot path planning into a TSP mathematical model (*100*). After researching the calculation method of the mathematical model, an optimization program based on the ant colony algorithm was given via MATLAB. The results show that this solution is effective and has a faster speed.

A new developed system that can automatically plan the welding path of space weld for an arc welding robot was proposed (*101*). Using VB6.0 as the programming platform, the system can generate the position and posture file of the welding torch directly and automatically from a 3D solid model, and convert the file into the robot program. In the experimental welding of the combined use of UP-6 arc welding robot system and S-350 MAG welding system, the correctness of the system has been validated.

In BIW assembly and joint workstations, several robots are usually used to do spot welding simultaneously. There are many devices and the robot's workspace is cluttered, and the path planning is onerous and hard to optimize by experiential methods. On the basis of analyzing assembly and joint workstations, a workstation with commercial simulation software was modeled and a probabilistic road-map algorithm was applied to implement path planning for the robot automatically (*102*). An automatic path planning method, including the torch pose planning, was proposed to improve the flexibility and automatic planning ability of arc welding robot (*104*). The virtual object, which represents the real object to be welded, was reconstructed first by a non-rational B-spline surface from a geometric polygonal mesh model or a measured point cloud. Based on the reconstructed non-rational surface model, the tangent vector and the tangent plane of each sampling point on the space welding seam were calculated, as well as the normal plane of each sampling point. Thus the position and pose of torch with respect to each sampling point of space seam can be determined by the calculated tangent vector, normal plane, and concrete requirement of the welding process. The final path planning of the arc welding robot in joint space was obtained by its inverse kinematics. Experimental results demonstrated the accuracy and the feasibility of the proposed method.

www.iran-mavad.com
مرجع مهندسی مواد و متالورژی

The omnidirectional path planning in 3D space of the welding robot was presented (*105*). In order to make the obtained trajectory pass through the scheduled position, the spatial pose must be accurately calculated, and the angle of every joint is interpolated using the cubic B-splines. Thus, the accuracy of controlling error is high and the path planning program can be easily compiled.

A planning algorithm for a multi-path/multi-layer circular locus was proposed (*106*). The algorithm was applied to weld the nipples on the header of a boiler. The multi-path/multi-layer circular locus was planned according to three teaching points, which was lapped head on end to satisfy the requirement of technology. For nipples wherever they are arranged, radially or axially, even if there are errors caused by positioning and thermal deformations, providing that nipple's position and orientation relative to the teaching one can be measured, the multi-path/multi-layer circular locus can be planned without any further teaching. This algorithm has been applied in a welding robot for manufacturing power station boilers.

6.04.4.2 Image Processing

With the development of the computer vision technology and image processing methods, numerous welding robots and some automatic welding machines are equipped with corresponding vision sensors to achieve different welding tasks in severe conditions. A weld pool image processing algorithm based on passive light vision has been studied (*107*). First, they designed a kind of method to directly capture the welding pool images of GMAW with a charge-coupled device camera with a narrowband filter. Next, using the median filter and wavelet transform eliminates noise and keeps the details of the image effectively. Then, they proposed to adopt the threshold image segmentation for detecting the welding pool in the image. The segmentation between the connected components and the noises to include the welding pool with the spots and the block has been realized by the method to mark the connected pixels. Finally, through the operations of pixel-by-column scanning and pixel-by-line scanning, the groove centerline and the welding torch centerline can be found correctly, and the deviations of the seam are also obtained. A structured light image processing technology was proposed by Yue et al. (*108*) for a pipeline welding automation project and a vision-based pipeline girth-welding robot. In this process, the welding torch can accurately track the weld and complete the omni-orientation welding automatically.

Some methods have been proposed to improve the robustness and adaptability of arc welding robots (*109*). An image processing algorithm for feature extraction from structured light images of weld seam was discussed in the case of a large amount of strong reflection, arc light, and splash disturbance. The processes consist of defining a target region, selecting an adaptive threshold, and extracting feature points. Then a novel hybrid visual servo control method for arc welding robot was provided, in which the position-based and image-based visual servo method were integrated to increase the robustness of weld seam tracking.

The technology of capturing and processing weld images in real time was analyzed in the study by Xu et al. (*110*), which is very important to the seam tracking and the weld quality control during the robotic GTAW process. An efficient algorithm of weld seam detection for butt joint welding from a single image was proposed (*111*). A robotic vision sensing system for taking and processing the image of a MIG welding pool of aluminum alloy was established (*112*). A series of clear welding pool images were obtained during welding process. The welding pool's image processing and edge detection method was designed, which affects good conditions for MIG welding.

6.04.4.3 Artificial Intelligence

With the rapid development of modern automation and artificial intelligence technologies, their application in welding has become a hot research topic. Recently, there has been a rapid development in computer technology, which has in turn led to develop the fully robotic welding system using artificial intelligence technology. However, the robotic welding system has not been achieved due to difficulties of the mathematical model and sensor technologies. The possibilities of the fuzzy regression method to predict bead geometry such as bead width, bead height, bead penetration, and bead area in the robotic GMA welding process were presented (*113*). A well-known method to deal with the problems with a high degree of fuzziness was used to build the relationship between four process variables and the four quality characteristics, respectively. Using these models, the proper prediction of the process variables for obtaining the optimal bead geometry can be determined.

The possibilities of the fuzzy regression method in modeling the bead width in the robotic arc-welding process were presented by Xue et al. (*114*). Fuzzy regression is a well-known method to deal with the problems with a high degree of fuzziness so that the approach is employed to build the relationship between four process variables and the quality characteristic such as bead width.

It is important to control the penetration depth of the weld pool during welding to obtain a good-quality weld, but it may be difficult to detect the penetration depth directly using a visual sensor. In order to detect the penetration depth, a penetration depth model was proposed by Hirai et al. (*115*) based on a neural network. During welding, a fuzzy controller adjusts the welding current to obtain the desired penetration depth. Since the performance of the fuzzy controller depends on fuzzy variables, its tuning can be performed using the neural network model. The validity of the fuzzy neural network is verified by some welding experiments.

A kinematics model of welding robot was built by Wu et al. (*116*). An improved fuzzy controller (Fuzzy-P) for welding robot mobile platform was designed based on analyzing a seam-tracking control system. A novel robust control of welding robots for weld seam tracking in the task-space was presented in a study by Fateh (*117*). The proposed control law includes a robust Takagi–Sugeno fuzzy controller, and two model-based control transformations named as feedback linearization and inverse kinematics. As the performance of control transformations is degraded due to the uncertainty, the fuzzy controller was used to compensate the effects of imperfect transformations.

www.iran-mavad.com
مرجع مهندسی مواد و متالورژی

Further, a fuzzy coordinator was introduced as a novel application of fuzzy controller by Fateh (*118*). A control transformation from the task space to the joint space is required to control a robot manipulator in the task space. The actuators operate in the joint space and the manipulator is controlled in the task space. A conflict between two spaces is produced due to using an imprecise transformation. The fuzzy coordinator coordinates two spaces by modifying the control transformation affected by uncertainties. The fuzzy coordinator is designed simply and operates as a robust controller. The role of fuzzy coordinator was analyzed and illustrated in the robust control of a welding robot in the task space. A circular trajectory was planned for a welding task performed by a SCARA robot. The fuzzy coordinator was then used to improve the performance of the control system affected by imprecise transformations, including the imprecise path transformation and the approximated feedback linearization.

To solve the seam-tracking problem of the welding mobile robot, an adaptive fuzzy controller and fuzzy-Gaussian neural network (FGNN) controller were designed to complete coordinated controlling of the cross-slider and wheels (*119*). The fuzzy-neural control algorithm was described by applying a Gaussian function as an activation function, taking a lateral slider position and the error between the robot moving direction and the seam direction as the inputs signals, and the adjusted angle for welding torch as the output; a specialized learning architecture was used so that membership function would be tuned in real time by applying the FGNN controller.

In the work of Zhang et al. (*120*), the kinematics modeling of the developed welding mobile robot was presented and a real-time seam-tracking algorithm based on a fuzzy neural network was proposed. At first, the kinematics behavior of the mobile robot body and cross sliders action to the welding torch was investigated by the Denavit-Hartenberg homogeneous transformation method and a full kinematics model was established. Then, a seam-tracking controller based on FGNN was described by applying a Gaussian function as an activation function, taking the lateral slider position and heading angle of the robot as input signals, and the adjusted angle for welding torch as output. For the curved weld seam-tracking problem of a wheeled welding mobile robot used in shipbuilding and large spherical tank welding, a predictive fuzzy control method was proposed (*121*). To overcome the disadvantage of a rotational arc sensor that cannot detect the next seam position, the algorithm employed a weighted least square fitting method to predict the weld seam next position and used a linearization model to predict the robot next orientation and position. In addition, fuzzy control was adopted to deal with the nonlinear characteristic of the system. The main advantages of this predictive fuzzy controller include small tracking error, small robot orientation delay angle, the availability of a linearized predictive model that reduces the computing complexity, and the high tracking quality. A convenient and effective close loop control scheme had been proposed to satisfy the aim of seam tracking based on the analysis of the welding-robot modeling and its control link (*122*). With the introduction of fuzzy controller and PID controller and with the adoption of the simulation on the differentiated modeling, the characteristics of the hybrid manipulator were illuminated.

The transient values of welding voltage and current are measured in real time under the condition of arc welding robot-based seam tracking on a V groove of 10 mm thick mild steel plates. Statistical processing for the transient values was carried out two times, and the characteristic vector was set up for describing the welding electrical parameters under different levels of weaving amplitude and frequency (*123*). Employing the fuzzy pattern recognition technique, the relationship between the characteristic vector and the weaving amplitude frequency was developed to provide the basis for analyzing quantitatively the effects of weaving amplitude frequency on weld penetration of V groove joints. According to the working conditions for the special robot repairing hydraulic turbines and the characteristics of the welding process, such as disturbances, nonlinearity, strong coupling, and so on, a kind of adaptive fuzzy control system for weld was designed on the basis of adaptive theory and fuzzy control theory (*124*).

In the Zhang et al. study (*125*), a GA combined with graph theory was proposed for solving the problem of welding route planning in car BIW manufacture. By regarding the welding point and tool center point frame as a spatial point to establish a relationship graph, transforming constraint factors into directed relationship matrix and using minimum motion distance of welding gun as object function, a TSP model was established. Generation of legal initial population and processing of selection, cross, and mutation genetic operators were based on directed relationship matrix. The trajectory of a revolute welding robot with six joints was planned in order to make the trajectory smooth and working time optimal (*126*). The time intervals between each point to be welded in Cartesian space were coded in binary, and the trajectory was implemented using an adaptive genetic algorithm while considering constraints of displacement, velocity, acceleration, and jerk of each joint. According to the optimal time intervals generated, the results of simulation on robot kinematics show that the method designed for robot trajectory planning can obtain the goal trajectory. This method can solve the premature convergence and slow convergence problems, comparing with the simple genetic algorithm.

The job scheduling method of arc welding robots was proposed by Meng and Chen (*127*). The job scheduling of arc welding robot was considered as a TSP. Welding job scheduling was modeled and relevant job scheduling optimization methods are designed. A genetic algorithm and an ant colony algorithm were applied to robot welding job scheduling first. Then, based on the characteristics of both algorithms, a hybrid genetic ant colony algorithm was designed to improve optimization performance.

For the optimum welding path planning problem of six DOF mini welding robot, a path planning method was proposed based on a GA (*98*). First, the kinematical equation of the wielding robot with a method D-H was found, and then an optimized welding path planning with the fitness function of energy consumption was given. Finally, by means of simulated results on the six DOF welding robot, the correctness and feasibility of this algorithm was testified.

According to analysis of the optimum path planning of the arc welding robot, a new gene insertion GGA was proposed to optimize the global path planning of the arc welding robot (*97*). This algorithm can be used in the multi-joint arc welding robot and also be used in the robot off-line programming.

www.iran-mavad.com
مرجع مهندسی مواد و متالورژی

Based on the GGA, utilizing the operation of gene transplantation improves the performance of the traditional GA. The new algorithm is called the greed genetic algorithm with gene transplantation (GGAGT). This algorithm was applied to find the global sequence plan when the industrial multi-joint manipulator is used in the welding (*128*). It is proven that the convergence of the result is improved and the range of the research is broadened while the scale of the group is not increasing and neither is the computation; at the same time, the algorithm quickens the speed of convergence and makes possible decreased local convergence.

For the error analysis of a welding robot, based on the Vittorio granularity encoding, an enhanced genetic neural network using binary and real-valued blend encoding methods was presented (*129*). The neural network topology adopts binary encoding, which reserves the virtues of Vittorio granularity encoding, and the connection weights adopt real-valued encoding; the Solis and Wets algorithm brings the virtues of evolutionary programming and evolutionary strategy to the new GA.

The problem of coordinating multiple motion devices for welding was considered in the Wu et al. study (*130*). This problem is complex as there are nine axes involved, and a number of permutations are possible, which achieve the same movements of the weld torch. The system is redundant and the robot has singular configurations. As a result, manual programming of the robot system is rather difficult to complete. This proposed approach to the coordination problem is based on a subdivision of tasks. The welding table was coordinated to align the weld point surface to be not parallel to the gravity direction. The six-axis robot was constrained to move the weld torch along the weld trajectory. Robot coordination was achieved by placing the positioning table in a good maneuverability position, i.e., far from its singular configurations and far from the motion limits of the six-axis arm and the motion limits of the track. While considering multiple criteria, including the welding orientation, a GA was employed to globally optimize six relevant redundant degrees of the multiple robotic system for welding. The joint angles of the arm were generated by inverse kinematics.

A model was proposed for using the artificial neural networks when determining the relations of dependency between the observable parameters and the controllable ones in the case of robotic TIG welding. The proposed model was based on the direct observation of welded joints, emphasizing the process variables that have been arranged in the nodes of a neural network. The design of the network is intended to achieve an architecture that contains four nodes in the input layer (all of them being controllable parameters) and two nodes in the output layer (one for each observable parameter).

An attempt has been made to develop a neural network model to predict the weld bead width as a function of key process parameters in robotic GMA welding (*131*). The neural network model was developed using two different training algorithms: the error back-propagation algorithm and the Levenberg–Marquardt approximation algorithm. An intelligent algorithm was proposed to understand relationships between process parameters and bead height, and to predict process parameters on bead height through a neural network and multiple regression methods for robotic multi-pass welding process. Using a series of robotic arc welding, additional multi-pass butt welds were carried out in order to verify the performance of the neural network estimator and multiple regression methods as well as to select the most suitable model.

In order to detect the penetration depth, a penetration depth model was developed based on a neural network. During welding, a fuzzy controller adjusts the welding current so as to obtain the desired penetration depth. Since the performance of the fuzzy controller depends on fuzzy variables, its tuning can be performed by using the neural network model. The validity of the fuzzy neural network was verified by some welding experiments.

6.04.5 Conclusions

In order to fulfill modern-day diversified requirements, significant improvements are needed for each element of welding robots. Robots must be able to integrate with their environment in order to produce optimum performance. The ability to present knowledge by using prior information and newly acquired information is another important element. This would provide people the combination of ideas they have explored. Most of the robots are designed to operate with human capability. Otherwise, it will reduce opportunities to be the main player in the market. People should provide robots with fully autonomous systems rather than using panels to control them. A level of cooperation among robots is also important, especially when solving complicated tasks. Working as a team, each part of the robot should communicate well and perform given tasks using best possible solutions. Power supply is another issue that should be included in the discussion. Since the world is turning toward sustainable ways of living, the developed system must be aligned with them. Instead of using electricity, manufacturers could use renewable energy or a closed-loop system to maintain energy sources. All of the mentioned elements will contribute to a major change in the technology of welding robots.

References

1. Timings, R. *Fabrication and Welding Engineering;* Newnes: Oxford, 2008.
2. Radhakrishnan, V. M. *Welding Technology and Design;* New Age: New Delhi, 2006.
3. Cary, H. B.; Helzer, S. C. *Modern Welding Technology;* Prentice Hall: New Jersey, 2011.
4. Pires, N.; Loureiro, A.; Bölmsjo, G. *Welding Robots, Technology, System Issues and Applications;* Springer-Verlag: London, 2006.
5. Stinchcomb, C. *Welding Technology Today, Principles and Practices;* Prentice-Hall: New Jersey, 1989.
6. Griffin, I. H.; Roden, E. M.; Jeffus, L.; Briggs, C. W. *Welding Processes;* Delmar: New York, 1984.
7. United Nations and International Federation of Robots. *World Industrial Robots 1996: Statistics and Forecasts;* ONU/IFR: New York, 2000.

www.iran-mavad.com
مرجع مهندسی مواد و متالورژی

8. Kusiak, A. *Modelling and Design of Flexible Manufacturing Systems;* Elsevier: Amsterdam, 1986.
9. Kusiak, A. *Computational Intelligence in Design and Manufacturing;* John Wiley & Sons: New York, 2000.
10. Rosheim, M. E. *Robot Evolution: The Development of Anthrobots;* John Willey & Sons: New York, 1994.
11. Rosheim, M. E. In the Footsteps of Leonardo. *Robot. Automat. Mag., IEEE* **1997,** *4* (2), 12–14.
12. Pedretti, C. *Leonardo Architect;* Rizzoli International Publications: New York, 1981.
13. Tesla, N. *My Inventions: Autobiography of Nicola Tesla;* Hart Brothers: Willinston, VT, 1983.
14. Myhr, M. Industrial New Trends: ABB View of the Future. In *International Workshop on Industrial Robotics, New Trends and Perspectives;* Parque das Nações: Lisbon, 1999. http://robotics.dem.uc.pt/ir99/.
15. Bolmsjo, G. *Sensor System in Arc Welding.* Technical Report; Lund Institute of Technology, Production and Materials Engineering Department, 1997.
16. Bolmsjö, G.; Olsson, M.; Nikoleris, G.; Brink, K. Task Programming of Welding Robots. In *Proceedings of the Int. Conf. on the Joining of Materials, JOM* **May–June 1995,** Vol. 7; pp 573–585.
17. Loureiro, A.; Velindro, M.; Neves, F. The Influence of Heat Input and the Torch Weaving Movement on Robotized MIG Weld Shape. *Int. J. Join. Mater.* **1998,** *10* (3), 86–91.
18. Agren, B. Sensor Integration for Robotic Arc Welding. Ph.D. Thesis, Lund University, 1995.
19. Richardson, R. W. Robotic Weld Joint Tracking Systems – Theory and Implementation Methods. *Weld. J.* **1986,** *65* (11), 43–51.
20. Books, B. Welding Robots – The State of the Art. *Weld. Met. Fabr.* **June 1991**.
21. Drews, P.; Starke, G. *Development Approaches for Advanced Adaptive Control in Automated Arc Welding.* Internal Report XII-970; Mechatronics Department: Achen, Germany, 1986.
22. Koyama, T.; Takahashi, Y.; Kobayashi, M.; Morisawa, J. Development of Real Time Welding Control System by Using Image Processing. *Q. J. Jpn. Weld. Soc.* **1989,** *7* (3), 79–83.
23. Dahlén, P.; Bolmsjö, G. Human Factors in the Justification of Advanced Manufacturing Systems. *Int. J. Hum. Factor Manuf.* **1996,** *6* (2), 147–162.
24. Pires, J. N.; Sá da Costa, J. Object-oriented and Distributed Approach for Programming Robotic Manufacturing Cells. *Robot. Comput. Integr. Manuf.* **2000,** *16* (1), 29–42.
25. Pires, J. N.; Monteiro, P.; Schölzke, V. *Using Robot Manipulators on High Efficient Wrapping Machines for Paper Industry;* ISR'2001: Seoul, Korea, April 2001.
26. Pires, J. N. Using MATLAB to Interface Industrial Robotic and Automation Equipment. *IEEE Robot. Autom. Mag.* **2000,** *7* (3).
27. Sá da Costa, J. M. G.; Pires, J. N. Future Welding Robot Developments. *J. Robótica* **January 2001,** *41*.
28. Pires, J. N. Programming Industrial Robotic and Automation Equipment. *Ind. Robot: Int. J.* **July 2000**. MCB University Press.
29. KUKA Industrial Robots. http://www.kuka-robotics.com.
30. FAUNAC Robotics America. www.fanucrobotics.com.
31. PANASONIC Robotics. http://www.panasonicrobotics.eu.
32. YASKAWA MOTOMAN Robotics. http://www.motoman.com.
33. CLOOS Robots. www.cloosrobot.com.
34. DAIHEN Robotics. www.daihen-usa.com.
35. Dennison, A.; Toncich, D.; Masood, S. Control and Process-based Optimisation of Spot-welding in Manufacturing Systems. *Int. J. Adv. Manuf. Technol.* **1997,** *13* (4), 256–263.
36. Tsai, C. L.; Jammal, O. A.; Dickinson, D. W. Modelling of Resistance Spot Weld Nugget Growth. *Weld. J. Res. Suppl.* **1992,** *71,* 47–54.
37. Lai, X.; Zhang, X.; Chen, G.; Zhang, Y. On-line Estimation of Electrode Face Diameter Based on Servo Gun Driven by Robot in Resistance Spot Welding. In *Robotic Welding, Intelligence and Automation;* Tarn, T. J., Chen, S. B., Zhou, C., Eds.; Springer: New York, 2007; pp 195–202.
38. Zhang, X.; Chen, G.; Zhang, Y. Characteristics of Electrode Wear in Resistance Spot Welding Dual-phase Steels. *Mater. Des.* **2008,** *29* (1), 279–283.
39. Aslanlar, S.; Ogur, A.; Ozsarac, U.; Ilhan, E. Welding Time Effect on Mechanical Properties of Automotive Sheets in Electrical Resistance Spot Welding. *Mater. Des.* **2008,** *29* (7), 1427–1431.
40. Aslanlar, S.; Ogur, A.; Ozsarac, U.; Ilhan, E.; Demir, Z. Effect of Welding Current on Mechanical Properties of Galvanized Chromided Steel Sheets in Electrical Resistance Spot Welding. *Mater. Des.* **2007,** *28* (1), 2–7.
41. Kusiak, A. Application of Operational Research Models and Techniques in Flexible Manufacturing Systems. *Eur. J. Oper. Res.* **1986,** *24* (3), 336–345.
42. Lee, S.; Choo, Y.; Lee, T.; Kim, M.; Choi, S. A Quality Assurance Technique for Resistance Spot Welding Using a Neuro-fuzzy Algorithm. *J. Manuf. Syst.* **2001,** *20* (5), 320–328.
43. Jou, M. Real Time Monitoring Weld Quality of Resistance Spot Welding for the Fabrication of Sheet Metal Assemblies. *J. Mater. Process. Technol.* **2003,** *132* (1), 102–113.
44. Martín, Ó.; López, M.; Martín, F. Artificial Neural Networks for Quality Control by Ultrasonic Testing in Resistance Spot Welding. *J. Mater. Process. Technol.* **2007,** *183* (2), 226–233.
45. Cho, Y.; Rhee, S. Quality Estimation of Resistance Spot Welding by Using Pattern Recognition with Neural Networks. *Instrum. Meas. IEEE Trans.* **2004,** *53* (2), 330–334.
46. Ballard, L. A.; Sabanovic, S.; Kaur, J.; Milojevic, S. George Charles Devol, Jr. [History]. *Robot. Automat. Mag., IEEE* **2012,** *19* (3), 114–119.
47. Naidu, D. S.; Moore, K. *Modelling, Sensing and Control of Gas Metal Arc Welding;* Elsevier Science Publishing Company.
48. Lima, E. J.; Bracarens, A. Q. *Robotic Shielded Metal Arc Welding, Mechanical Engineering Department;* Universidade Federal de Minas Gerais: Belo Horizonte, Brazil, 2010.
49. Silva, E. B.; Filho, F. A. R.; Lima, E. J.; Bracarense, A. Q. Development of Parallel Robots for Welding. *ABCM Sym. Ser. Mechatron.* **2010,** *4,* 693–699.
50. Rubinovitz, J.; Wysk, R. A. Task Level Off-line Programming System for Robotic Arc Welding—an Overview. *J. Manuf. Syst.* **1988,** *7* (4), 293–306.
51. Lee, D.; Seo, T.; Kim, J. Optimal Design and Workspace Analysis of a Mobile Welding Robot with a 3P3R Serial Manipulator. *Robot. Auton. Syst.* **2011,** *59* (10), 813–826.
52. Chang, D.; Son, D.; Lee, J.; Lee, D.; Kim, T.-w.; Lee, K.-Y.; Kim, J. A New Seam-tracking Algorithm through Characteristic-point Detection for a Portable Welding Robot. *Robot. Comput. Integr. Manuf.* **2012,** *28* (1), 1–13.
53. Tung, P.-C.; Wu, M.-C.; Hwang, Y.-R. An Image-guided Mobile Robotic Welding System for SMAW Repair Processes. *Int. J. Mach. Tool Manuf.* **2004,** *44* (11), 1223–1233.
54. Karadeniz, E.; Ozsarac, U.; Yildiz, C. The Effect of Process Parameters on Penetration in Gas Metal Arc Welding Processes. *Mater. Des.* **2007,** *28* (2), 649–656.
55. Shen, H.-y.; Wu, J.; Lin, T.; Chen, S.-b. Arc Welding Robot System with Seam Tracking and Weld Pool Control Based on Passive Vision. *Int. J. Adv. Manuf. Technol.* **2008,** *39* (7–8), 669–678.
56. Xiong, J.; Zhang, G.; Gao, H.; Wu, L. Modeling of Bead Section Profile and Overlapping Beads with Experimental Validation for Robotic GMAW-based Rapid Manufacturing. *Robot. Comput. Integr. Manuf.*, in press.
57. Daeinabi, K.; Teshnehlab, M. Seam Tracking of Intelligent Arc Welding Robot. *WSEAS Trans. Syst.* **2006,** *5* (11), 2600–2605.
58. Murakami, S.; Takemoto, F.; Fujimura, H.; Ide, E. Weld-line Tracking Control of Arc Welding Robot Using Fuzzy Logic Controller. *Fuzzy Set Syst.* **1989,** *32* (2), 221–237.
59. Xue, Y.; Kim, I.; Son, J.; Park, C.; Kim, H.; Sung, B.; Kim, I.; Kim, H.; Kang, B. Fuzzy Regression Method for Prediction and Control the Bead Width in the Robotic Arc-welding Process (AMPT/AMME05 Part 2). *J. Mater. Process. Technol.* **2005,** *164,* 1134–1139.
60. Sayyaadi, H.; Eftekharian, A. Modeling and Intelligent Control of a Robotic Gas Metal Arc Welding System. *Sci. Iran.* **2008,** *15* (1), 75–93.
61. Sullivan, E. C.; Rajaram, N. S. A Knowledge-based Approach to Programming Welding Robots. *ISA Trans.* **1992,** *31* (2), 115–133.
62. Dung, N. M.; Duy, V. H.; Phuong, N. T.; Kim, S. B.; Oh, M. S. Two-wheeled Welding Mobile Robot for Tracking a Smooth Curved Welding Path Using Adaptive Sliding-mode Control Technique. *Int. J. Control Automat. Syst.* **2007,** *5* (3), 283–294.
63. Huissoon, J.; Strauss, D.; Rempel, J.; Bedi, S.; Kerr, H. Multi-variable Control of Robotic Gas Metal Arc Welding. *J. Mater. Process. Technol.* **1994,** *43* (1), 1–12.
64. Xu, Y.; Yu, H.; Zhong, J.; Lin, T.; Chen, S. Real-time Seam Tracking Control Technology during Welding Robot GTAW Process Based on Passive Vision Sensor. *J. Mater. Process. Technol.* **2012,** *212* (8), 1654–1662.

www.iran-mavad.com
مرجع مهندسی مواد و متالورژی

65. Liu, Z.; Bu, W.; Tan, J. Motion Navigation for Arc Welding Robots Based on Feature Mapping in a Simulation Environment. *Robot. Comput. Integr. Manuf.* **2010,** *26* (2), 137–144.
66. Chu, W.-H.; Tung, P.-C. Development of an Automatic Arc Welding System Using SMAW Process. *Int. J. Adv. Manuf. Technol.* **2005,** *27* (3–4), 281–287.
67. Zhu, Z. Y.; Lin, T.; Piao, Y.; Chen, S. Recognition of the Initial Position of Weld Based on the Image Pattern Match Technology for Welding Robot. *Int. J. Adv. Manuf. Technol.* **2005,** *26* (7–8), 784–788.
68. Park, J.; Lee, S.-B.; Kim, J.-W.; Kim, J.-Y.; Kim, J.-M.; Park, H.-H.; Seo, J.-W.; Kang, G.-H.; Kim, S.-H. Development of a Portable Welding Robot with EtherCAT Interface. *World Acad. Sci. Eng. Technol.* **2011,** *60,* 733–737.
69. Sweet, L. Sensor-based Control Systems for Arc Welding Robots. *Robot. Comput. Integr. Manuf.* **1985,** *2* (2), 125–133.
70. Kim, K.; Lee, S.; Kim, K.; Lee, K.-Y.; Heo, S.; Park, K.; Jeong, J.-I.; Kim, J. Development of the End-effector Measurement System for a 6-axis Welding Robot. *Int. J. Precis. Eng. Manuf.* **2010,** *11* (4), 519–526.
71. Luo, H.; Chen, X. Laser Visual Sensing for Seam Tracking in Robotic Arc Welding of Titanium Alloys. *Int. J. Adv. Manuf. Technol.* **2005,** *26* (9–10), 1012–1017.
72. Cook, G. E.; Crawford, R.; Clark, D. E.; Strauss, A. M. Robotic Friction Stir Welding. *Ind. Robot: Int. J.* **2004,** *31* (1), 55–63.
73. De Backer, J. *Robotic Friction Stir Welding for Flexible Production;* Lund University, 2012.
74. Smith, C. B. Robotic Friction Stir Welding Using a Standard Industrial Robot. *Kei Kinzoku Yosetsu (J. Light Met. Weld. Construct.)* **2004,** *42* (3), 40–41.
75. Threadgill, P.; Leonard, A.; Shercliff, H.; Withers, P. Friction Stir Welding of Aluminium Alloys. *Int. Mater. Rev.* **2009,** *54* (2), 49–93.
76. Smith, C. B. *Robotic Friction Stir Welding: Phase I Initial Feasibility Study,* May 1997. Report APPT-1493, Tower Automotive Internal Report.
77. Smith, C. B.; Hinrichs, J. F.; Crusan, W. A. *In Robotic Friction Stir Welding: The State-of-the-Art, 4th Friction Stir Welding International Symposium;* Addison-Wesley, 2003.
78. Soron, M. *Robot System for Flexible 3D Friction Stir Welding;* Universitetsbiblioteket: stockholm, 2007.
79. Voellner, G.; Zäh, M.; Kellenberger, O.; Lohwasser, D.; Silvanus, J. 3-Dimensional Friction Stir Welding Using a Modified High Payload Robot. In *Proceedings of the 6th International Symposium on Friction Stir Welding, Saint-Sauveur, Canada;* 2006.
80. Spong, M. W.; Vidyasagar, M. *Robot Dynamics and Control;* John Wiley & Sons: New York, 2008.
81. Soron, M.; Kalaykov, I. A Robot Prototype for Friction Stir Welding, Robotics. In *Automation and Mechatronics, 2006 IEEE Conference on;* IEEE: Bangkok, Thailand, 2006; pp 1–5.
82. Smith, C. B.; Hinrichs, J. F. *Robotic Friction Stir Welding: State-of-the-Art,* 2005. http://www.frictionstirlink.com/publications/Pub124thFSWSymposiumRoboticFSWpdf.pdf.
83. Von Strombeck, A.; Schilling, C.; Dos Santos, J. F. Robotic Friction Stir Welding – Tool, Technology and Applications. *Biuletyn Instytutu Spawalnictwa (Poland)* **2001,** *45* (6), 49–52.
84. ABB Limited, Zurich, Switzerland. 2003, http://new.abb.com/products/robotics.
85. Hinrichs, J.; Noruk, J.; McDonald, W.; Heideman, R. Challenges of Welding Aluminium Alloys for Automotive Structures. *Svetsaren* **1995,** *50* (3), 7–9.
86. Smith, C. B.; Crusan, W.; Hootman, J. R.; Hinrichs, J. F.; Heideman, R. J.; Noruk, J. S. Friction Stir Welding in the Automotive Industry. In *Proceedings of the TMS—Aluminum Automotive and Joining Sessions;* 2001; pp 175–185.
87. Trnka, K.; Božek, P. Optimal Motion Planning of Spot Welding Robot Applications. *Appl. Mech. Mater.* **2013,** *248,* 589–593.
88. Zhang, T.; Ouyang, F. Offline Motion Planning and Simulation of Two-robot Welding Coordination. *Front. Mech. Eng.* **2012,** *7* (1), 81–92.
89. Zhang, H.; Lu, H.; Cai, C.; Chen, S. Robot Path Planning in Multi-pass Weaving Welding for Thick Plates. In *Robotic Welding, Intelligence and Automation;* Tarn, T. J., Chen, S. B., Zhou, C., Eds.; Springer: New York, 2011; pp 351–359.
90. Wang, J. H.; Xiao, R. H.; Ma, Y. L. Research on Welding Robot Path Panning Using Ant Colony Optimization. *Adv. Mater. Res.* **2011,** *201,* 1926–1929.
91. Wang, T. Q.; Li, L. Y.; Gao, T. J.; He, J. J. The Collision Avoidance Path Planning of K-joint Automatic Welding Robot. *Adv. Mater. Res.* **2011,** *317,* 723–726.
92. Zhang, T.; Chen, S. Path Planning and Computer Simulation of a Mobile Welding Robot. In *Robotic Welding, Intelligence and Automation;* Tarn, T., hen, S., Zhou, C., Eds.; Springer: New York, 2011; pp 421–428.
93. Xu, X. M.; Li, C. G.; Zhu, W. Research on UG/OPEN GRIP-based Robot Welding Path Planning. *Manuf. Inform. Eng. China* **2011,** *7,* 008.
94. Wang, Y.; Chi, N. Path Planning Optimization for Teaching and Playback Welding Robot. *TELKOMNIKA Indonesian J. Electr. Eng.* **2013,** *11* (2), 960–968.
95. Liu, S. G.; Du, H. W.; Wang, S. C.; Zhao, Y. N. Path Planning and System Simulation for an Industrial Spot Welding Robot Based on SimMechanics. *Key Eng. Mater.* **2010,** *419,* 665–668.
96. Hatwig, J.; Minnerup, P.; Zaeh, M. F.; Reinhart, G. An Automated Path Planning System for a Robot with a Laser Scanner for Remote Laser Cutting and Welding. In *Mechatronics and Automation (ICMA), 2012 International Conference on;* IEEE, 2012; pp 1323–1328.
97. Sun, L. G.; Yan, B. D. Application of the Improved Genetic Algorithm in the Arc Welding Robot Path Planning. *Tech. Automat. Appl.* **2008,** *4*, 004.
98. Xue-feng, P. Path Planning of a 6 DOF Robot Based on Genetic Algorithm for Line Welding. *Tech. Automat. Appl.* **2010,** *12*, 002.
99. Liu, P.; Chen, H. M.; Xiong, Z. Y. Application of Error Correction for Path Planning of Arc Welding Robot. *Electric Weld. Mach.* **2009,** *4*, 028.
100. Wang, J. H.; Wang, Y. A Study on BIW Welding Robot Path Planning Based on Ant Colony Algorithm. *Manuf. Automat.* **2008,** *5*, 008.
101. Yan, H.; Liu, J. F.; Qiu, S. H.; Wang, Z. L. Research on the Automatic Planning of Arc Welding Robot Welding Path for Space Weld. *Mach. Des. Manuf.* **2005,** *8*, 049.
102. Zhang, Y. Z.; Han, Z. D. Study on Path Planning of Spot Welding Robot in BIW Assembly and Joint Workstation. *Mach. Des. Manuf.* **2006,** *2,* 72–74.
103. Chen, Z.; Yin, S.; Lu, Z. Genetic Simulated Annealing Based Coordinated Path Planning for Arc Welding Robot System. *Jixie Gongcheng Xuebao (Chin. J. Mech. Eng.)* **2005,** *41* (2), 194–198.
104. Chou, W.; You, L.; Wang, T. Automatic Path Planning for Welding Robot Based on Reconstructed Surface Model. *Robot. Weld. Intell. Automat.* **2006,** *362,* 153–161.
105. Gu, Z. R.; Zue, L. W.; Wei, J. H.; You, B. The Working Path Panning of Welding Robot of Hydraulic Turbine Runners. *J. Harbin Univ. Sci Technol.* **2000,** *6*, 016.
106. Lixin, F.; Binwen, F.; Chun, D. Planning of Circle Locus for Multi-path/multi-layer Welding Robot with Automatic Error-correction. *China Weld.* **2000,** *9* (1).
107. Zou, Y.; Li, Y.; Jiang, L.; Xue, L. Weld Pool Image Processing Algorithm for Seam Tracking of Welding Robot. In *Industrial Electronics and Applications (ICIEA), 2011 6th IEEE Conference on;* IEEE, 2011; pp 161–165.
108. Yue, H.; Li, K.; Zhao, H.; Zang, Y. Vision-based Pipeline Girth-welding Robot and Image Processing of Weld Seam. *Ind. Robot: Int. J.* **2009,** *36* (3), 284–289.
109. Xu, D.; Wang, L.; Tan, M. Image Processing and Visual Control Method for Arc Welding Robot. In *Robotics and Biomimetics, 2004. ROBIO 2004. IEEE International Conference on;* IEEE, 2004; pp 727–732.
110. Xu, Y.; Yu, H.; Zhong, J.; Lin, T.; Chen, S. Real-time Image Capturing and Processing of Seam and Pool during Robotic Welding Process. *Ind. Robot: Int. J.* **2012,** *39* (5), 513–523.
111. Shi, F.; Lin, T.; Chen, S. Efficient Weld Seam Detection for Robotic Welding Based on Local Image Processing. *Ind. Robot: Int. J.* **2009,** *36* (3), 277–283.
112. Yu, S.; Zhang, D. F.; Ding, F.; Liang, W. D. Robotic Vision Sensing System for Welding Pool Image Taking and Processing in Aluminum Alloy MIG Welding Process. *Electric Weld. Mach.* **2006,** *3*.
113. Sung, B.; Kim, I.; Xue, Y.; Kim, H.; Cha, Y. Fuzzy Regression Model to Predict the Bead Geometry in the Robotic Welding Process. *Acta Metall. Sin. (English Letters)* **2007,** *20* (6), 391–397.
114. Xue, Y.; Kim, I.; Son, J.; Park, C.; Kim, H.; Sung, B.; Kim, I.; Kim, H.; Kang, B. Fuzzy Regression Method for Prediction and Control the Bead Width in the Robotic Arc-welding Process. *J. Mater. Process. Technol.* **2005,** *164,* 1134–1139.
115. Hirai, A.; Kaneko, Y.; Hosoda, T.; Yamane, S.; Oshima, K. Sensing and Control of Weld Pool by Fuzzy-neural Network in Robotic Welding System, Industrial Electronics Society, 2001. In *IECON'01. The 27th Annual Conference of the IEEE;* IEEE, 2001; pp 238–242.
116. Wu, Y. Q.; Yuan, Z. H.; Wang, J. H. A Fuzzy Controller Design of Seam Tracking for Welding Robot. *Adv. Mater. Res.* **2012,** *442,* 370–374.
117. Fateh, M. M. Fuzzy Task-space Control of a Welding Robot. *Int. J. Robot. Automat.* **2010,** *25* (4).

www.iran-mavad.com
مرجع مهندسی مواد و متالورژی

118. Fateh, M. M.; Farahani, S. S.; Khatamianfar, A. Task Space Control of a Welding Robot Using a Fuzzy Coordinator. *Int. J. Control Automat. Syst.* **2010,** *8* (3), 574–582.
119. Kai, L.; Ting, Z.; Libin, Z.; Shumei, X. Seam Tracking Based on Fuzzy-Gaussian Neural Network for Mobile Welding Robot, Intelligent Networks and Intelligent Systems, 2009. In *ICINIS'09. Second International Conference on;* IEEE, 2009; pp 261–264.
120. Zhang, K.; Wu, Y.; Jin, X. Real-time Seam Tracking Based on Fuzzy-Gaussian Neural Network for Welding Mobile Robot. *Trans. China Weld. Inst.* **2007,** *28* (9).
121. Yanfeng, G.; Hua, Z.; Zhiwei, M.; Junfei, P. Predictive Fuzzy Control for a Mobile Welding Robot Seam Tracking, Intelligent Control and Automation, 2008. In *WCICA 2008. 7th World Congress on;* IEEE, 2008; pp 2271–2276.
122. Ye, J. X.; Zhang, H. Application of Fuzzy-PID Control on Seam Tracking for Welding-robot. *Trans. China Weld. Inst.* **2005,** *26* (11).
123. Xiaoning, D.; Chuansong, W.; Jiakun, H. Fuzzy Pattern Recognition of Weaving Amplitude and Frequency in Seam Tracking of Arc Welding Robot. *Chin. J. Mech. Eng.* **2005,** *41* (9), 228.
124. Li, X.; Zhou, X.; Riu, B. Study of Adaptive Fuzzy Control for Welding Process of the Robot. *J. Harbin Univ. Sci. Technol.* **2004,** *6*.
125. Zhang, C.; Liu, H.; Jiang, D. Robot Welding Route Planning in Car-body Welding Process Based on Genetic Algorithm. *J. Tongji Univ.* **2011,** *4*.
126. Liao, X.; Wang, W.; Lin, Y.; Gong, C. Time-optimal Trajectory Planning for a 6R Jointed Welding Robot Using Adaptive Genetic Algorithms. In *Computer, Mechatronics, Control and Electronic Engineering (CMCE), 2010 International Conference on;* IEEE, 2010; pp 600–603.
127. Meng, Z.; Chen, Q. Hybrid Genetic-ant Colony Algorithm Based Job Scheduling Method Research of Arc Welding Robot. In *Information and Automation (ICIA), 2010 IEEE International Conference on;* IEEE, 2010; pp 718–722.
128. He, G. H.; Yan, B. D.; Sun, L. G.; Tian, F. Application of Genetic Algorithm with Gene Transplantation in Optimal Sequence Plan of Welding Robot. *J. Henan Univ. Sci. Technol.* **2008**.
129. Wang, D.-S.; Xu, X.-H. Genetic Neural Network and Application in Welding Robot Error Compensation. In *Machine Learning and Cybernetics, 2005. Proceedings of 2005 International Conference on;* IEEE, 2005; pp 4070–4075.
130. Wu, L.; Cui, K.; Chen, S. Redundancy Coordination of Multiple Robotic Devices for Welding through Genetic Algorithm. *Robotica* **2000,** *18* (6), 669–676.
131. Kim, I. S.; Son, J. S.; Lee, S. H.; Yarlagadda, P. K. Optimal Design of Neural Networks for Control in Robotic Arc Welding. *Robot. Comput. Integr. Manuf.* **2004,** *20* (1), 57–63.

www.iran-mavad.com
مرجع مهندسی مواد و متالورژی

This page intentionally left blank

www.iran-mavad.com
مرجع مهندسی مواد و متالورژی

6.05 Mathematical Modeling of Weld Phenomena, Part 1: Finite-Element Modeling

AG Olabi, University of the West of Scotland, Paisley, Renfrewshire, UK
G Casalino, DMMM – Politecnico di Bari, Bari, Italy

© 2014 Elsevier Ltd. All rights reserved.

6.05.1	Introduction	101
6.05.2	Application of the FEM to the Welding Processes	101
6.05.3	Thermal Analysis and the Weld Pool	102
6.05.4	Mechanical and Metallurgical Analysis	103
6.05.5	FEM Application to Fusion Welding	104
6.05.6	FEM Application to the Solid-State Welding	106
6.05.7	Concluding Remarks	108
References		108

6.05.1 Introduction

Welding, heat treatment, casting, additive, and subtractive process, such as cutting and machining, are manufacturing processes that play an important role at various stages of the production of mechanical parts. The use of finite-element analysis (FEA) for analyzing manufacturing processes is very important to improve product integrity and quality and to have a better understanding of the influence of different parameters on the manufacturing process output.

Using FEA, the evolution of stresses and deformations can be predicted as well as the susceptibility to failure and fracture; some aspects of the manufacturing process can be optimized by this analysis.

The powerful tool of FEA is the finite-element method (FEM), which is a technique for solving partial differential equations by first discretizing these equations in their space dimensions.

Complicated domains are subdivided into a series of smaller regions in which the equations are approximately solved by the FEM. A set of equations for each region is assembled and the behavior over the entire problem domain is determined. Each region is referred to as an element, and the process of subdividing a domain into a finite number of elements is referred to as discretization. Elements are connected at specific points, called nodes. The equations relate the input at specified nodes of the elements to the output at the same nodes, and the assembly process requires that the solution be continuous along common boundaries of adjacent elements (*1*).

Numerical simulation by the FEM saves time, allows analyzers to see the results in a graphical format, and reduces design and prototyping expenses. It can make complexity possible since it can handle very complicated equations. FEA has become increasingly more precise as computers become more efficient. Since computer efficiency continues to improve, FEA might improve in its accuracy and potential scope indefinitely.

Nowadays, a very large number of general purpose and commercial FEM software is available for scientific and commercial applications.

6.05.2 Application of the FEM to the Welding Processes

The FEM analysis of the welding process involves multiphysics aspects such as thermal, fluid, metallurgical, and mechanical phenomena. To develop a suitable FEM model for welding, the thermal and mechanical boundary conditions, the geometrical discretization, the material nonlinearities, and all physical phenomena involved in welding must be considered.

The discretization of the volume is called meshing. For physically based models, a large number of elements are required to produce the necessary level of detail. In this light, a dual-mesh strategy can be proposed in which a fine submesh resides at the nodal points of a coarse mesh. The fine submesh defines a small domain at which microstructure characteristics and evolution are calculated. These domains should be as small as possible to reduce computational costs; however, they must be large enough to describe the weld and its evolution.

Figures 1 and 2 show the dual-mesh strategy for a butt and a T-joint with filler material.

Very high temperatures are introduced in the region of the welded joint and they cause steep temperature gradients in the structure.

Microstructural transformations occur in the metals during the evolution of the process. Heating and cooling induce localized volumetric changes. The thermal strains that occur in the vicinity of the welding zone are elastoplastic and the resulting stresses react

www.iran-mavad.com
مرجع مهندسی مواد و متالورژی

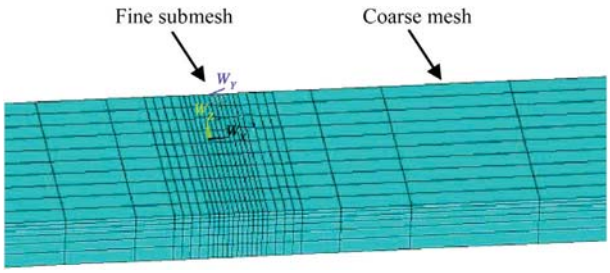

Figure 1 Mesh for a butt joint.

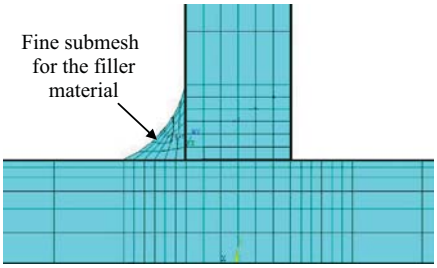

Figure 2 Mesh for a T-joint with filler material.

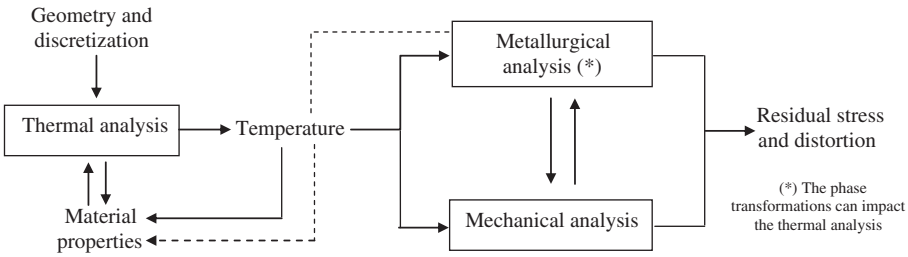

Figure 3 Flowchart of the modeling approach to the FEM of the welding processes.

causing permanent distortions. Distortions introduce residual deformation that complicates the assembly of welded structures and reduces their quality.

The ability to predict the residual stress state allows for the prediction of the final shapes of the parts and a more complete understanding of how residual stresses may affect the load capacity of a structure.

The welding simulation uses a sequentially coupled approach in which a thermal analysis is followed by a mechanical analysis. The temperature results from the thermal analysis are read into the stress analysis as loading to calculate the thermal stress effects.

Figure 3 shows the flowchart of the modeling approach. The geometry and its discretization are the starting point. Then the thermal analysis is performed. Its output is the temperature distribution that feeds the metallurgical and mechanical analysis, which should be fully coupled (double arrow) since the variables of those problems are interdependent. The final output is the residual stress and the thermal distortion.

During the thermal cycle, the material properties must be updated with the updated temperature (double arrow) and the metallurgical transformation (dotted arrow). The temperature field, the metallurgical transformation, the residual stress, and the distortion values are the desired output of the entire analysis that can be used for the evaluation of the impact of the welding process on the joined structure and its suitability for the desired application.

The accuracy of modeling the welding process depends on the capability to simulate first the thermal analysis, which consists of modeling the moving heat source and the weld pool, and then the microstructure and mechanical changes in the weld.

6.05.3 Thermal Analysis and the Weld Pool

The thermal analysis is performed to calculate the heat transfer resulting from the thermal load of a moving heat source.

The governing equation is the energy balance equation that, under fixed assumptions, is based on the linear dependence of the heat flux on the temperature gradient (Fourier's law).

www.iran-mavad.com
مرجع مهندسی مواد و متالورژی

The weak formulation or variational form of the balance equation is derived, supplied by boundary conditions, using the weighted residuals method.

A weak temperature-based form of the governing equation is given as follows:

$$\int_{\Omega} W\rho c\frac{\partial T}{\partial t}\mathrm{d}V + \frac{\partial}{\partial t}\int_{\Omega} W\rho R\Theta \mathrm{d}V + \int_{\Omega} k\nabla T\mathrm{d}V + \int_{\partial\Omega_q} W\overline{q}\mathrm{d}S + \int_{\partial\Omega_c} Wh_{\mathrm{env}}(T - T_{\mathrm{env}})\mathrm{d}S - \int_{\Omega} Wq\mathrm{d}V = 0 \quad [1]$$

where:

Ω is the structure body;
$\partial\Omega_T$, $\partial\Omega_q$, and $\partial\Omega_c$ are nonoverlapping portions of the body boundary $\partial\Omega$;
W is a weighting function;
ρc and $\rho\Theta$ are the unit volume heat capacity and latent heat, respectively;
f_l is a characteristic function of temperature;
q refers to imposed temperature and heat flux yields, T_{env} is the temperature of the environment, whose film coefficient is h_{env}; and
T is the unknown temperature field.

In the finite-element context, the unknown field T is approximated as a linear combination of interpolation functions and the shape functions as follows:

$$T(x, y, z) = \sum_{i}^{N} N_i(x, y, z)T_i \quad [2]$$

T_i is the temperature at each node i ($i = 1,2,\ldots,N$) arising from the discretization of the analyzed domain Ω. The T approximation from eqn [2] can be introduced in eqn [1].

A weighting function W can be adopted for the interpolation function N ($W \equiv N_i$, Galerkin method). A nonlinear system of N ordinary differential equations is set, stated in matrix form as

$$\Psi = \mathbf{C}\frac{\partial \mathbf{T}}{\partial t} + \frac{\partial \mathbf{L}}{\partial t} + \mathbf{KT} - \mathbf{F} \quad [3]$$

where $\mathbf{T}$ is the vector of unknown nodal temperatures, $\mathbf{C}$ is the capacity matrix, $\mathbf{L}$ is the latent heat vector, $\mathbf{K}$ is the conductivity (stiffness) matrix, and $\mathbf{F}$ is the external flux vector.

The transient conduction problem in the absence of phase change has been widely discussed in the classical finite-element literature.

Time integration can be done with the unconditionally stable first-order backward Euler method.

This implicit scheme is applied in eqn [3], which leads to a set of nonlinear equations to be solved for the values of the temperatures at finite-element nodes.

The weld pool is different from one welding technique to another. The forces acting on the weld pool are the gravity or buoyancy, the Lorentz force, and the Marangoni force due to the gradients in surface tension. When an electric arc is used as the welding source, traction due to the arc plasma acts on the surface of the pool (2). When the energy density is very high, as in the case of laser welding, a particular profile of the weld pool is obtained and it is called a key-hole (3). Metal added to the weld pool causes a momentum flux.

6.05.4 Mechanical and Metallurgical Analysis

The structural analysis uses the thermal analysis temperature results as the loading. The objective of the structural analysis is to determine the stresses and strains induced in the weld region during the cooling transient.

Assuming linear kinematics, the strain is induced by microstructure evolution during solid-state phase transformation along with the thermal strain. At the same time, transformation-induced plasticity is also produced. Therefore, the total strain rate ($\dot{\varepsilon}$) can be written as the sum of the individual components of the strain rate as

$$\dot{\varepsilon} = \dot{\varepsilon}^{\mathrm{E}} + \dot{\varepsilon}^{\mathrm{P}} + \dot{\varepsilon}^{\mathrm{T}} + \dot{\varepsilon}^{\Delta\mathrm{V}} + \dot{\varepsilon}^{\mathrm{Trp}} \quad [5]$$

The various components in this equation represent strain rate due to elastic, plastic, and thermal loading, volumetric change, and transformation plasticity, respectively; transformation-induced plasticity is not taken into account. Ignoring this component, the strain increment can be written as follows:

$$\Delta\varepsilon = \Delta\varepsilon^{\mathrm{E}} + \Delta\varepsilon^{\mathrm{P}} + \Delta\varepsilon^{\mathrm{T}} + \Delta\varepsilon^{\Delta\mathrm{V}} \quad [6]$$

www.iran-mavad.com
مرجع مهندسی مواد و متالورژی

The component $\Delta\varepsilon^{\Delta V}$ is caused by a volume change due to phase transformation.

In steel welding, the perlite and ferrite changes to austenite between A_1 temperature and A_3 temperature can be calculated as the strain increment due to the volume change according to the level law. For the sake of simplicity, a linear relation can be assumed. By using the linear approximation, the strain increment can be estimated as follows:

$$\Delta\varepsilon_h^{\Delta V} = \frac{\Delta T_h}{A_3 - A_1} \cdot \varepsilon_h^{\Delta V+} \quad [7]$$

where ΔT_h is the temperature increment during heating.

According to the Koistinen–Marburger relationship, the strain increment due to volume change in the course of the martensitic transformation process can be determined by the following equation:

$$\Delta\varepsilon_c^{\Delta V} = f \cdot \{ -k \cdot \exp[k(T - M_s)]\} \cdot \Delta T_c \cdot \varepsilon_c^{\Delta V+} \quad [8]$$

where ΔT_c is the increment of temperature during the cooling phase (4).

The hypothesis of isotropic hardening is satisfactory for welding applications.

The domain can be discredited using the implicit Euler-backward finite-difference scheme (5).

Given the previous assumptions, the mechanical problem can be solved using the standard quasistatic boundary value problem in solid mechanics (4).

The latter consists in finding the displacement field u that satisfies the following integral equation:

$$\int_{\Omega_s} \sigma : \nabla^s w \cdot dV = \int_{\Omega_s} \rho b \cdot w dV + \int_{\delta\Omega_{s,t}} \bar{t} \cdot w dS \quad [9]$$

Throughout the domain Ω_s for all the admissible displacement is the weighting function w.

Incompressible material behavior may lead to some difficulties in numerical simulation, such as inaccuracy of the solution and divergence. In that case, it is possible to state the standard quasistatic problem in the *mixed u-p* form (6).

Eventually, it is noteworthy to remember that the FEM formulation of the melting/solidification problem must be carefully considered. The material constitutive behavior in the zone of liquid/solid phase transformation strongly influences the dependence of the material parameters on the temperature. Some approaches are available in the literature, such as assigning a very low stiffness to the elements that are in liquid/mushy phases or bringing poor conditioning of the algebraic equation system to be solved. An additive decomposition of strain in actual and current configurations with respect to the reference one enables us to calculate the stress in a simple and accurate way (7).

6.05.5 FEM Application to Fusion Welding

Fusion welding is a joining process that uses fusion of the base metal to make the weld. It is mostly used to join materials of similar compositions and melting points.

In the simulation of the fusion welding, the moving heat source is implemented as a typical transient formulation where the heat source moves along the part. Goldak proposed a Gaussian distribution in a three-dimensional double ellipsoid heat source (**Figure 4**) (8).

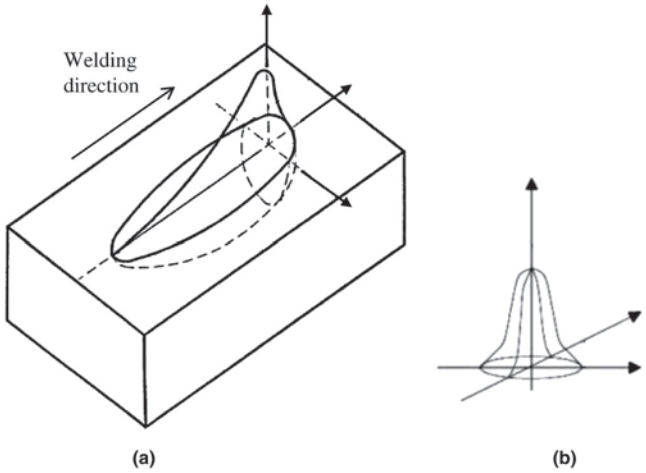

Figure 4 (a) Double-ellipsoidal heat source model; (b) the Gaussian distribution of the heat flux.

www.iran-mavad.com
مرجع مهندسی مواد و متالورژی

It is a flexible model that fits the characteristics of both the shallow of the arc welding and the deeper penetration of the laser and electron beam processes. The sizes of the liquid pool, which is above the melting temperature, the solid heat affected zone, which contains the pool, and the solid region, which is at temperatures below half the melting point, can be calculated. The dimensions of the heat distribution can be adjusted by a trial-and-error approach until the computed weld sizes fit the experimental ones (**Figure 5**).

However, if a complex weld pool shape has to be computed, it can be difficult to find a heat distribution. In this case, a 'prescribed temperature' of the weld pool, such as a quadratic one, can be assumed or estimated (*9*). The arc heating effects can be simulated with an equivalent internal heat input that is assumed constant per unit volume.

Using the FEM formulation, a large number of simulations have been performed for fusion welding of metals and plastics.

The FEM was adopted for predicting the bead geometry in laser welding of 1.6-mm-thick AISI304 stainless steel sheets. A three-dimensional finite-element model was used to analyze the temperature distribution in a T-joint weld produced by the laser welding process (*10*).

Three-dimensional models for thermal and mechanical simulation of both laser and tungsten inert gas welding of INCONEL 625 and AISI 316 were presented using both brick and nonlinear contact elements and elastic and elastic–plastic materials (*11*).

The laser spot welding of AISI 304 stainless steel was performed for predicting the weld bead geometry. The effect of latent heat of fusion and the convective and radiative aspects of boundary conditions are considered while developing the finite-element model. The heat input to the developed model is assumed to be a three-dimensional conical Gaussian heat source (*12*).

An FEM solution of the macroscale heat transfer and fluid flow in industrial castings through the temperature and pressure fields was calculated for the multiscale modeling of solidification microstructures, including microsegregation and microporosity, in an Al–Si–Cu alloy. At the microscale, the FEM model was coupled with a combined stochastic–deterministic approach based on the cellular automata method used to solve multicomponent diffusion in a three-phase system (liquid, solid, and gas), simulating the nucleation and growth of both grains and pores (*13*).

A model based on a double-ellipsoidal volume heat source to simulate the gas metal arc welding (GMAW) heat input and a cylindrical volume heat source to simulate the laser beam heat input was developed to predict the temperature field and thermally induced residual stress in the hybrid laser–gas metal arc welding process. For the simulation of the filling of the groove by a melted wire, a 'death and birth' technique was used (*14*).

A sequentially coupled temperature–displacement analysis was undertaken to simulate the weld pool geometry, transient temperature, and displacement fields in the fabrication of aircraft structures with fuselage panels, made of thin sheets of AA 6056-T4 (an aluminum alloy), in a T-joint configuration (*15*).

The volumetric heat source is suitable for a multipass joint. In a given finite-element model, each weld pass can be divided into a number of small parts (mesh blocks) with the same length (*16*).

Out-of-plane and complex geometry hybrid welding was simulated by a thermal flux through a nail-shaped volume that moved along the seam thanks to a local coordinates system (**Figures 6** and **7**) (*17*).

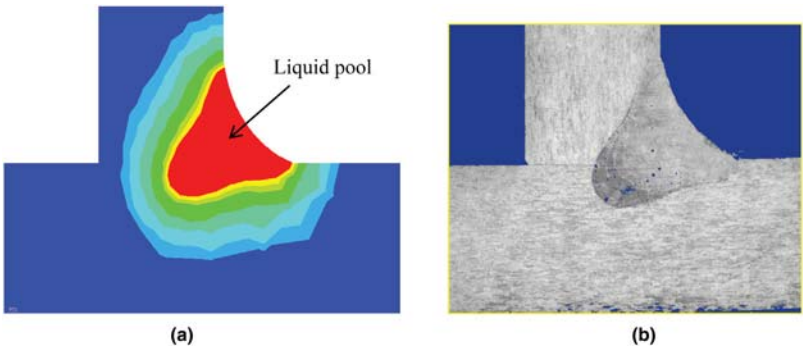

Figure 5 (a) Computed and (b) experimental pictures of the transverse cross-section of an aluminum alloy T-joint.

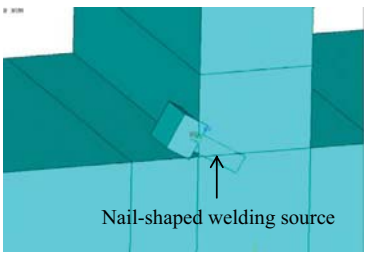

Figure 6 A nail-shaped volume.

www.iran-mavad.com
مرجع مهندسی مواد و متالورژی

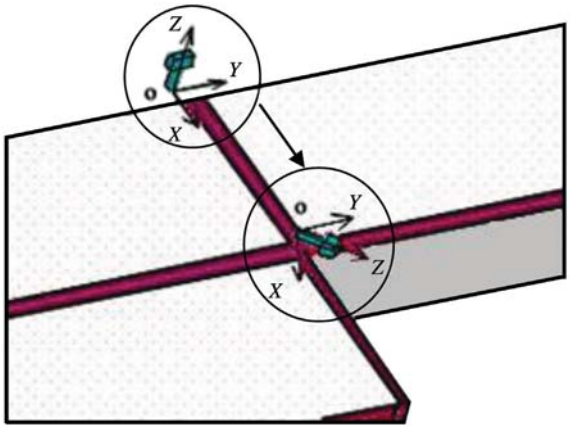

Figure 7 Nail-shaped welding source moving along the seam.

A peak temperature, as high as the molten temperature, was used as the thermal load in the calculation of the deformation in the GMAW of a low carbon steel butt joint. The temperature load was applied progressively in order to simulate the advance of the arc along the seam. In this way, only the cooling phase was simulated. The computational time and the required computer memory were dramatically reduced with respect to the double ellipsoid heat source while the distortions were correctly computed (*18*).

The iterative substructure method is a high-speed large-scale computational method that carries out the FEM based on thermoelastoplastic theory. The technique reduces the computational time by computing the small region near the weld torch as a strong nonlinear region, and the remaining large area as an elastic linear region, so that only the stiffness matrix needs to be remade when the convergence fails. This computational technique allows large-scale computation of welding residual stress (*19*).

A newly developed FEM model for arc welding simulation and analysis was recently developed. It consists of original methods for the modeling of a material deposit allowing a direct simulation of joint formation, instead of usual element birth techniques. Moreover, a dynamic mesh optimization procedure allowing error control was implemented (*20*).

6.05.6 FEM Application to the Solid-State Welding

Solid-state welding is a group of welding processes that produces coalescence at temperatures essentially below the melting point of the base materials being joined, without the addition of brazing filler metal. They are a heterogeneous group of welding techniques that rely on different multiphysics phenomena.

Friction stir welding (FSW) uses primarily viscous dissipation in the workpiece material, driven by high shear stresses at the tool–workpiece interface. The process has been used for the manufacture of butt welds, overlap welds, T sections, fillet, and corner welds. **Figure 8** shows the layout for the butt weld. For each of these joint geometries, specific tool designs are required that are being further developed and optimized (*21*). **Figure 9** shows the tip of a typical FSW tool. Therefore, the heat generation modeling requires some representation of the behavior of the contact interface, together with the viscous dissipation behavior of the material. The modeling process must provide a special focus on the heat generation due to the contact conditions between the FSW tool and the workpiece (*22*).

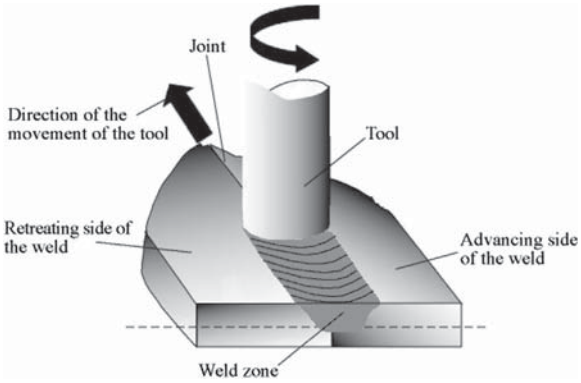

Figure 8 Friction stir welding of a butt joint.

www.iran-mavad.com
مرجع مهندسی مواد و متالورژی

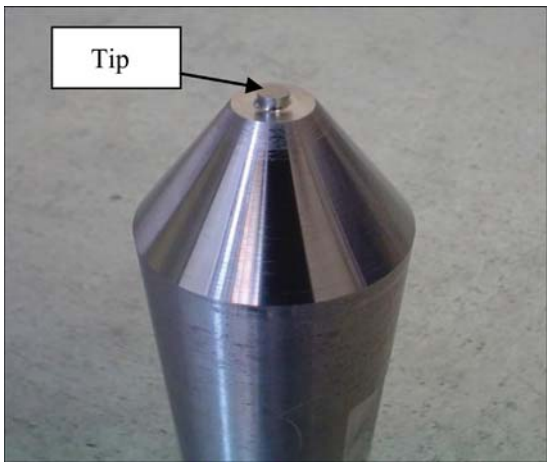

Figure 9 A typical friction stir welding tool.

During the FSW, the heat is generated from both the shoulder and the probe of the FSW tool. The heat input can be divided into surface and volume heat contributions due to frictional or viscous (plastic dissipation) heating, respectively. The heat is dissipated into the workpiece leading to the thermomechanical heat affected and the heat affected zones, depending on the thermal conductivity coefficient of the base material (*23*).

Heat generation and heat dissipation must be adjusted and balanced to obtain an agreement with experimental temperature values.

Flow models should be able to simultaneously capture the thermal and mechanical aspects of a given problem. The material flow around the probe is one of the main parameters that is determinant for the success of FSW (*24*).

As for heat flow analyses, numerical flow models can use either an Eulerian or Lagrangian formulation for the mesh; another solution can be a combination of both (hybrid solution and Lagrangian–Eulerian).

Two analytical approaches can be chosen for modeling the flow field and temperature field in the vicinity of the FSW tool. The first approach was based on a three-dimensional (3D) arbitrary Lagrangian–Eulerian (ALE) hydrodynamics formulation in which the geometry and kinematics of the FSW process are modeled. The advantage of this technique is the ability to model both the workpiece and the tool simultaneously, so that not only the flow and temperature fields in the workpiece but also the stresses and strains and the temperature history of the tool can be calculated. The second approach is based on a computational fluid dynamics approach in which the workpiece is modeled as a fluid with temperature-dependent viscosity. Heat flux and velocities may be provided to the tool–workpiece interface as initial conditions, without actually modeling the tool. The advantage is that it is computationally much faster to achieve the steady-state temperature and velocity fields in the workpiece than in the ALE approach.

The thermal computations should be coupled to the mechanical ones, so the discretized form of the heat equation is solved at each time step. Heat generated by material deformation and by friction with the tool, thermal exchanges by conduction, convection, and radiation should all be taken into account. The unilateral contact conditions between the plate and the tool can be simulated by a splitting or uncoupled approach with the ALE formulation, which handles problems of mesh distortions at the contact or complex free surfaces (*25*).

Resistance spot welding has some exclusive characteristics, such as dynamic changes of the heat and electrical current flow paths, which make its physical process much more difficult to be modeled. Projection welding is a variation of resistance welding in which current flow is concentrated at the point of contact with a local geometric extension of one (or both) of the parts being welded. These projections are used to concentrate heat generation at the point of contact, and, therefore, to generate a weld nugget faster and at a lower current level compared to conventional spot welding (*26*).

The complexity arises from the dynamic changes in heat and electrical current flow paths, and temperature-dependent material properties, information about contact interfaces, and the geometry of the projection areas have to be taken into account. A truly thermal–electrical–mechanical coupled numerical analysis is required for the projection of a welding simulation (*27*).

For the electrical analysis, the governing equation and its boundary condition of electrical potential can be expressed by using the quasi-Laplace equation. The electrical conductivity's dependence on temperature should be considered. Since the electrical contact conductance and the thermal contact conductance play important roles and need to be specified appropriately during the solution of the electrical–thermal problem (*28*), the total welding process can be performed sequentially with three main blocks, as shown in **Figure 10**.

When the projection welding process is realized using a milliseconds electrical discharge, the process is known as capacitive discharge or pulsed welding. For the mechanical calculation, the contact and thermal relaxation must be considered. The numerical model must aim to reproduce the electrical, thermal, and mechanical aspects of the pulse welding process and to evaluate the temperature profile, the piece displacement, and the effects of different welding parameters on the weld seam (*29*).

www.iran-mavad.com
مرجع مهندسی مواد و متالورژی

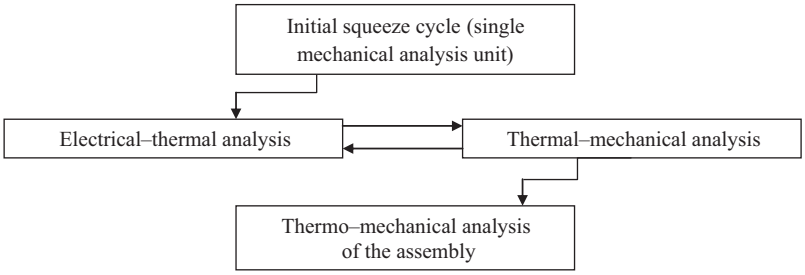

Figure 10 Flowchart of the coupled electrical–thermal–mechanical analysis. Reproduced from Zhu W. F.; Lin Z. Q.; Lai X. M.; Luo A.-H. Numerical Analysis of Projection Welding on Auto-Body Sheet Metal Using a Coupled Finite Element Method. *Int. J. Adv. Manuf. Technol.* **2006,** *28,* 40–52, 2006.

6.05.7 Concluding Remarks

As demonstrated above, the FEM is helpful in the design and the optimization of welding processes. Those calculations can predict the geometry of the welded assembly, including weld bead shape, the thermal and mechanical evolutions in the weld bead, as well as the structural transformations. The final mechanical properties of the assembly, starting from the prediction of residual stresses and structural variables, can be predicted. The risks of defects during the process and in the final assembly can be evaluated.

Nonetheless, despite an abundant literature on welding numerical simulation, there is still a real challenge in the numerical modeling of welding processes, because of the multiphysics nature of the welding phenomena, which are involved at every different time and length of the simulation, and the evolving discontinuities, such as solid-solid phase boundaries (*30*).

In fusion welding, the different phenomena interfering in the melt pool have to be identified and implemented in the computation. The solid–liquid phase change must be handled using more actual assumptions in the continuum formulation.

In friction welding, the simulation of the thermofluid problem must be improved in order to simulate the important material flow around the FSW tool and coupled with a metallurgy model in order to predict the evolution of microstructures.

Moreover, when a much finer mesh is required to describe a complex heat source and large structure, computational work is substantially increased. The calculation speed and the quality of simulation can be affected by the inadequacy of the computational resources. In order to improve the capability, a parallel calculation can be performed by establishing a computer cluster system by ethernet cable connection (*31*).

References

1. Smith, I. M.; Griffiths, D. V. *Programming the Finite Element Method,* 4th ed.; Wiley: Chichester, West Susex, 2004.
2. Edstorp, M. Weld Pool Simulations. Thesis for the degree of licentiate of philosophy; Sweden: Department of Mathematical Sciences, Chalmers University of Technology and University of Gothenburg Goteborg, 2008.
3. Seung, K. B. Simulation of Melt Penetration and Fluid Flow Behavior during Laser Welding. Theses and Dissertations, Lehigh University, Paper 1319, 2013.
4. Deng, D. FEM Prediction of Welding Residual Stress and Distortion in Carbon Steel Considering Phase Transformation Effects. *Mater. Des.* **2009,** *30,* 359–366.
5. Simo, J.; Hughes, T. *Computational Inelasticity;* Springer-Verlag: New York, 1998.
6. Hughes, T. *The Finite Element Method. Linear Static and Dynamic Finite Element Analysis;* Prentice-Hall: Englewood Cliffs, NJ, 1987.
7. Anca, A.; Cardona, A.; Fachinotti, V. Finite Element Modeling of Welded Joints. *Mecánica Computacional* **2008,** *XXVII,* 1445–1470.
8. Goldak, J.; Chakravarti, A.; Bibby, M. A New Finite Element Model for Welding Heat Sources. *Metall. Trans. B* **1984,** *15,* 299–305.
9. Goldak, J.; Bibby, J. A.; Gu, M. Heat and Fluid Flow in Welds. In *Proceedings of the International Institute of Welding. Congress of Joining Research;* North, T. H., Ed.; Chapman: London, 1990; pp 69–82.
10. Shanmugam, N. S.; Buvanashekaran, G.; Sankaranarayanasamy, K.; Ramesh Kumar, S. A Transient Finite Element Simulation of the Temperature and Bead Profiles of T-joint Laser Welds. *Mater. Des.* **2010,** *31,* 4528–4542.
11. Capriccioli, A.; Frosi, P. Multipurpose ANSYS FE Procedure for Welding Processes Simulation. *Fusion Eng. Des.* **2009,** *84,* 546–553.
12. Shanmugam, N. S.; Buvanashekaran, G.; Sankaranarayanasamy, K. Some Studies on Weld Bead Geometries for Laser Spot Welding Process Using Finite Element Analysis. *Mater. Des.* **2012,** *34,* 412–426.
13. Lee, P. D.; Chirazi, A.; Atwood, R. C.; Wang, W. Multiscale Modelling of Solidification Microstructures, Including Microsegregation and Microporosity, in an Al–Si–Cu Alloy. *Mater. Sci. Eng. A* **2004,** *365,* 57–65.
14. Kong, F.; Ma, J.; Kovacevic, R. Numerical and Experimental Study of Thermally Induced Residual Stress in the Hybrid Laser–GMA Welding Process. *J. Mater. Process. Technol.* **2011,** *211,* 1102–1111.
15. Zain-ul-abdein, M.; Nélias, D.; Jullien, J.-F. Dominique Deloison. Experimental Investigation and Finite Element Simulation of Laser Beam Welding Induced Residual Stresses and Distortions in Thin Sheets of AA 6056-T4. *Mater. Sci. Eng. A* **2010,** *527,* 3025–3039.
16. Ogawa, K.; Deng, D.; Kiyoshima, S.; Yanagida, N.; Saito, K. Investigation on Welding Residual Stresses in Penetration Nozzles by Means of Thermal Elastic Plastic FEM and Experiment. *Comput. Mater. Sci.* **2009,** *45,* 1031–1042.
17. Casalino, G.; Curcio, F.; Ludovico, A. D.; Minutolo, F. M. C. FEM Simulation of Metal Sheets Laser Welding with Wire Filler Material. In *Proceedings of SPIE – The International Society for Optical Engineering* **2005,** Vol. 5958; pp 1–11 art. no. 59581V.
18. Casalino, G.; Hu, S. J.; Hou, W. Deformation Prediction and Quality Evaluation of the Gas Metal Arc Welding Butt Weld. *Proc. Inst. Mech. Eng., Part B: J. Eng. Manuf.* **2003,** *217,* 1615–1622.
19. Kawaguchi, A.; Itoh, S.; Mochizuki, M.; Kameyana, M. Large-Scale Computation of Welding Residual Stress. *Prog. Nucl. Sci. Technol.* **2011,** *2,* 613–619.

www.iran-mavad.com
مرجع مهندسی مواد و متالورژی

20. Bellet, M.; Hamide, M.; Pequet, C.; Lasne, P. New Numerical Technologies for the Simulation of Arc Welding Processes. In *Proceedings MCWASP XII, 12th International Conference on Modeling of Casting, Welding and Advanced Solidification Processes, Vancouver & Alaska;* Cockcroft, S., Maijer, D., Eds.; The Minerals, Metals & Materials Society: Warrendale, Pennsylvania, USA, June 7–13, 2009; pp 563–570.
21. Chandra, T.; Wanderka, N.; Reimers, W.; Ionescu, M. Effects of Tool Design and Friction Stir Welding Parameters on Weld Morphology in Aluminum Alloys. *Mater. Sci. Forum* **2010,** *126,* 638–642.
22. Mariano Neto, D.; Neto, P. Numerical Modeling of Friction Stir Welding Process: a Literature Review. *Int. J. Adv. Manuf. Technol.* **2013,** *65,* 115–126.
23. Nandan, R.; Roy, G. G.; Debroy, T. Numerical Simulation of Three-dimensional Heat Transfer and Plastic Flow during Friction Stir Welding. *Metall. Mater. Trans.* **2006,** *37,* 1247–1259.
24. Mishra, R. S.; Ma, Z. Y. Friction Stir Welding and Processing. *Mater. Sci. Eng. R* **2005,** *50,* 1–78.
25. Guerdoux, S.; Fourment, L. A 3D Numerical Simulation of Different Phases of Friction Stir Welding. *Modell. Simul. Mater. Sci. Eng.* **2009,** *17* art. no. 075001.
26. Sun, X. Effect of Projection Height on Projection Collapse and Nugget Formation – A Finite Element Study. *Suppl. Weld. J.* **September, 2001,** *80* (9), 211–216s.
27. Sun, X. Modeling of Projection Welding Processes Using Coupled Finite Element Analyses. *Suppl. Weld. J.* **September, 2000,** *79* (9), 244–251s.
28. Zhu, W. F.; Lin, Z. Q.; Lai, X. M.; Luo, A.-H. Numerical Analysis of Projection Welding on Auto-Body Sheet Metal Using a Coupled Finite Element Method. *Int. J. Adv. Manuf. Technol.* **2006,** *28,* 40–52.
29. Casalino, G.; Ludovico, A. Finite Element Simulation of High Speed Pulse Welding of High Specific Strength Metal Alloys. *J. Mater. Process. Technol.* **2008,** *197,* 301–305.
30. De Borst, R. Challenges in Computational Materials Science: Multiple Scales, Multi-Physics and Evolving Discontinuities. *Comput. Mater. Sci.* **2008,** *43,* 1–15.
31. Tiana, Y.; Wanga, C.; Zhub, D.; Zhouc, Y. Finite Element Modeling of Electron Beam Welding of a Large Complex Al Alloy Structure by Parallel Computations. *J. Mater. Process. Technol.* **2008,** *199,* 41–48.

www.iran-mavad.com
مرجع مهندسی مواد و متالورژی

This page intentionally left blank

www.iran-mavad.com
مرجع مهندسی مواد و متالورژی

6.06 Mathematical Modeling of Weld Phenomena, Part 2: Design of Experiments and Optimization

AG Olabi, University of the West of Scotland, Paisley, Renfrewshire, UK
A Alaswad and KY Benyounis, Dublin City University, Dublin, Ireland

© 2014 Elsevier Ltd. All rights reserved.

6.06.1	**Introduction**	111
6.06.2	**ANN Analysis**	112
6.06.2.1	Weld Bead Geometry	112
6.06.2.2	Mechanical Properties of the Weld Bead	114
6.06.3	**DoE Analysis**	115
6.06.3.1	Factorial Design	115
6.06.3.1.1	Weld Bead Geometry	115
6.06.3.1.2	Mechanical Properties of the Weld Bead	116
6.06.3.2	Response Surface Methodology	117
6.06.3.2.1	Weld Bead Geometry	117
6.06.3.2.2	Weld Bead Mechanical Properties and Operating Cost	119
6.06.3.3	Taguchi Method	121
6.06.3.3.1	Weld Bead Geometry	121
6.06.3.3.2	Mechanical Properties of the Weld Bead	122
6.06.4	**Concluding Remarks**	122
References		122

6.06.1 Introduction

Welding is the most economical and efficient way to permanently join metals. It plays an important role in metals fabrication and repair. It is also used in the fabrication of spacecraft, fighter planes, submarines, and atomic power plants. Welding ranks highly among industrial processes and involves more scientific principles and variables than those involved in any other industrial process. There are many different kinds of welds. Some processes cause sparks and others do not even require extra heat. Welding can be done anywhere, outdoors or indoors, underwater, and in outer space. Numerous welding methods or techniques are in common use for a wide range of applications (*1*,*2*) of which arc welding and laser welding are the most popular.

Arc welding is a type of welding that uses a power supply to create an electric arc between an electrode and the base material to melt the metals at the welding point. Used electrodes can be consumable or nonconsumable. The welding region is usually protected by some type of shielding. Using consumable electrodes, Gas Metal Arc Welding (GMAW) is one of the common welding techniques referred to as MIG welding. MIG welding is a semiautomatic or automatic welding process with a continuously fed consumable wire acting as both electrode and filler metal, along with an inert or semiinert shielding gas flowed around the wire to protect the weld site from contamination. Another popular technique which uses the consumable electrodes is Submerged Arc Welding (SAW) in which the heat is generated by an arc formed when an electric current passes between a welding wire and the workpiece. The tip of the welding wire, the arc, and the weld joint are covered by a layer of granular flux. The generated heat melts the wire, the base metal, and the flux. The flux shields the molten pool from atmospheric contamination, cleans impurities from the weld metal, and shapes the weld bead. On the other hand, nonconsumable electrodes are used in the well-known Gas Tungsten Arc Welding (GTAW) which is frequently referred to as TIG welding. In TIG welding, an arc is formed between a nonconsumable tungsten electrode and the metal being welded. Gas is fed through the torch to shield the electrode and molten weld pool. If filler wire is used, it is separately added to the weld pool.

Laser beam welding (LBW) processes is a unique welding technique used to join multiple pieces of metal through the heating effect of a concentrated beam of coherent monochromatic light known as LASER. LBW is a high-energy-density welding process and well known for its deep penetration, high speed, small heat-affected zone, fine welding seam quality, low heat input per unit volume, and fiber optic beam delivery. The beam provides a concentrated heat source, allowing for narrow, deep welds and high welding rates. The process is frequently used in high volume applications, such as in the automotive industry.

For welding a new component, there are certain weld-joint specifications to be met. The aim of any welding process is to achieve a strong and welding joint which sustains the operating stresses. However, the weld-bead shape is important to control as the mechanical properties of welds are affected by the weld-bead shape (*1*). The fusion layer should not be thicker than necessary in order to avoid wasting of energy, edge burn-off, sagging of the weld pool, and deep weld end craters (*2*). The control of input parameters can be done by (coarse or fine) tuning the welding process's input parameters and inspecting, whether or not, the results comply with the desired specifications. Such a task is usually carried out by skilled personnel or an engineer. However, this

www.iran-mavad.com
مرجع مهندسی مواد و متالورژی

parameter selection process is based on trial and error and is always time and cost consuming. Moreover, this traditional method is nonsystematic and usually does not produce an optimized welding parameters combination, which can be used for different outcomes. This is due to the fact that the welding process is affected by different input and output parameters. Different techniques can be used in welding modeling such as Finite Element Modeling (FEM), Artificial Neural Networks (ANN), and Design of Experiments (DOE).

6.06.2 ANN Analysis

Artificial neural networks are biologically inspired by intelligent techniques. ANNs are generally made up of a number of simple and highly interconnected processing elements organized in layers as shown in **Figure 1**. These processing elements or neurons process information by their dynamic state response to external inputs. ANNs are capable of learning patterns by training with a number of known patterns. The learning process automatically adjusts the weights and thresholds of the processing elements. Once adjusted with minimal difference between ANN output and targeted output, the neural network is said to be trained (*3*,*4*).

6.06.2.1 Weld Bead Geometry

Andersen et al. (*5*) have explained some concepts related to neural networks and how they can be used to model weld-bead geometry, in terms of equipment parameters, in order to evaluate the accuracy of neural networks for weld modeling. They carried out a number of simulations and they used actual GTAW data for this purpose. The data consisted of values for voltage, current, electrode travel speed and wire feed speed, and the corresponding bead width, penetration, reinforcement height, and bead cross-sectional area. The performance of neural networks for weld modeling was presented and evaluated using actual welding data. It was concluded that the accuracy of neural networks modeling is fully comparable with the accuracy achieved by more traditional modeling schemes.

Evaluation of ANN for monitoring and control of the plasma arc welding process was carried out by Cook et al. (*6*). Three areas of welding application were investigated in this work: weld process modeling, weld process control, and weld-bead profile analysis for quality control. A network was constructed to determine the torch standoff, forward current, reverse current, and travel speed for desired crown width and root width. The base material was 2219 aluminium alloy in the form of plates 6.35 mm thick; the joint type was bead-on-plate. It was confirmed that ANNs are powerful tools for analysis, modeling, and control of such applications. Also, the results obtained when analyzing weld profile data suggested that ANNs can yield real-time results of equal or better accuracy and reliability than previously used data analysis algorithms.

Vitek et al. (*7*) have developed a model to predict the weld pool shape parameters (penetration, width, width at half-penetration, and cross-section area) in pulsed Nd-YAG laser welds of Al-alloy 5754 using neural network. They have considered the following

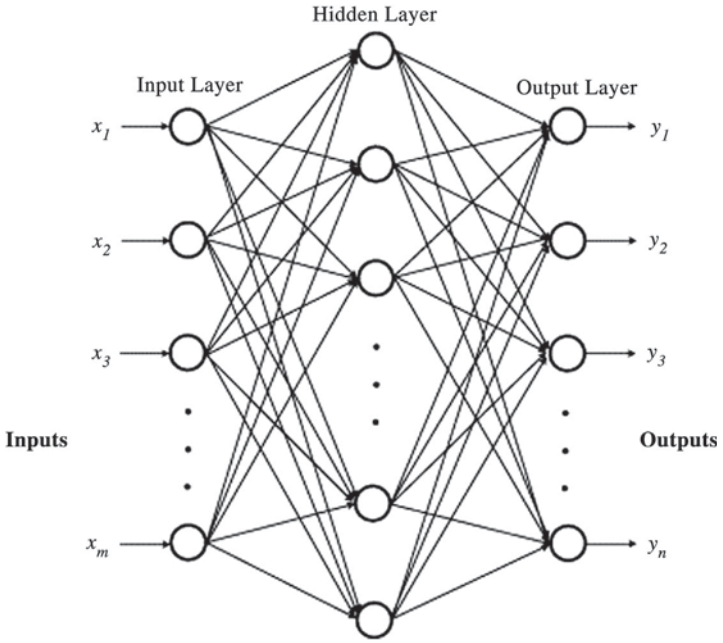

Figure 1 A multilayered preceptor. Reproduced from Ates, H. Prediction of Gas Metal Arc Welding Parameters Based on Artificial Neural Networks. *Mater. Des.* **2007**, *28*, 7, 2015–2023.

www.iran-mavad.com
مرجع مهندسی مواد و متالورژی

process parameters: travel speed, average power, pulse energy, and pulse duration. They developed an excellent routine to convert the shape parameters into a predicted weld profile which was based on the model. They concluded that this approach allows for instantaneous results and therefore, offers advantages in applications where real-time predictions are needed and computationally intensive predictions are too slow.

A comparison between back-propagation and counterpropagation networks in the modeling of the TIG welding process was made by Juang et al. (*8*). The complicated relationships between the welding process parameters and the weld pool features were considered. The input process parameters were welding speed, wire feed speed, cleaning percentage, arc gap, and welding current, while the output features were front height, front width, back height, and back width. The base metal was pure 1100 aluminium with a plate thickness of 1.6 mm. The experimental results, for the TIG welding process, showed that the counterpropagation network has a better learning ability than the Back-Propagation Network (BPN). However, the BPN has better generalization ability than the counterpropagation network.

Chan et al. (*9*) have proposed a model to predict the bead-on-plate weld geometry (bead width, height, penetration, and bag length) in GMAW of low alloy steel with C25 shielding gas. The process parameters were current, voltage, wire travel speed, and workpiece thickness. Back-propagation network was used. Their results revealed that the weld-bead geometry problem can be accurately modeled by using BPN.

Jeng et al. (*10*) have used both BPN and learning vector quantization neural networks to predict the Laser Welding (LW) parameters for butt joints. The input parameters included were workpiece thickness and welding gap, while the output parameters 'responses' were optimal focus position, acceptable welding parameters of laser power, welding speed and weld quality, including weld-width, undercut and distortion. They managed to integrate all the networks together to make an accurate prediction model of the laser welding parameters. Therefore, the limitation in the industrial application of LW for butt joints can be reduced through the use of this well-established model.

Usage of ANN to model the GMAW process was reported by Nagesh and Datta (*11*). BPN was used to associate the welding process parameters (electrode feed-rate, arc power, arc voltage, arc current, and arc length) with output features of bead geometry (bead height and width, penetration depth, and area). The workpiece material was grey cast iron and a mild steel electrode was used. It showed that there was a small error percentage difference between the estimated and experimental values, which indicates that the neural networks can yield fairly accurate results.

Ridings et al. (*12*) have applied a neural networks technique to predict the outer diameter of the weld-bead shape for three wire, single pass per side, submerged-arc, line-pipe seam welds using the following welding process parameters: current, voltage, and angle for the three wires as well as the welding speed, stick out, and spacing of wires. The plates welded were of various thicknesses from 15.9 to 25.4 mm and they were varied in strength from X52 to X65. The welding was carried out using alloyed wires with a 4 mm diameter. It was shown that the applied technique can predict a weld-bead shape with a high degree of confidence. The contribution of each factor to the variation in the final weld-bead shape was determined. Furthermore, it was mentioned that an efficient model can be built using different neural networks to predict the bead shape when using a smaller number of measurements for separate areas. However, the higher the number of measurements the better the accuracy of the technique are.

Christensen et al. (*13*) have developed a multilayer feed forward network for modeling and online adjustment of GMAW process parameters to guarantee a certain degree of quality. In this study, butt joint welding with full penetration of standard steel S135 with 3 mm thickness was carried out. The process parameters were; wire feed speed, voltage, welding speed, and gap width while the network inputs were back-bead width and back-bead height. In open loop control strategy, it has been demonstrated that use of the model to provide high quality welding is feasible and the network training was straightforward and effective. Whereas in the closed loop experiments a single input and single output control scheme was investigated, it was shown that it was applicable for adaptive control of GMAW with some limitations.

Balasubramanian et al. (*14*) investigated the effect of laser power, welding speed, and beam incident angle on the butt weld bead geometry (depth of penetration and bead width). The input and output parameters are analyzed using Neural Networks model (NN) with different network configurations. A suitable neural network model (four neurons with one hidden layer) with best R2 value is arrived at. Expressions for depth of penetration and bead width are extracted from the neural network model.

Dutta et al. (*15*) investigated the effect of input parameters on the weld bead geometry in TIG welding process based on full factorial DOE and two neural network-based approaches (back-propagation algorithm and genetic-neural system). Comparisons were made of the above approaches, after testing their performances on 36 randomly generated test cases. Both the NN-based approaches were seen to be more adaptive compared to the conventional regression analysis, for the test cases. BPNN initially showed a slightly better performance compared to the genetic-neural system, but after about 60 000 iterations, the latter started to perform better than the former. However, the performances of these two approaches were dependent on the nature of the deviation function.

Kim et al. (*16*) presents the development of an intelligent algorithm to understand relationships between process parameters and bead height through a neural network and multiple regression methods for a robotic multipass GMA welding process. Using a series of robotic arc welding, additional multipass butt welds were carried out in order to verify the performance of the neural network estimator and multiple regression methods as well as to select the most suitable model. The results showed that for the studied case, the neural network model produce more accurate results than the empirical models.

Kim et al. (*17*) developed a neural network model to predict the weld bead width as a function of process parameters (number of passes, welding speed, welding current, and arc voltage) in robotic GMA welding. The neural network model is developed using two different training algorithms; the error back-propagation algorithm and the Levenberg–Marquardt approximation algorithm. The accuracy of the neural network models developed in this study has been tested by comparing the simulated data obtained from the

www.iran-mavad.com
مرجع مهندسی مواد و متالورژی

neural network model with that obtained from the actual robotic welding experiments. The result shows that the Levenberg–Marquardt approximation algorithm is the preferred method, as this algorithm significantly reduces the Root Mean Square (RMS) error to a small value, and thus provides better accuracy of prediction. After the 500 cycles of a training process, the result shows that the use of a one hidden-layer of four to one configuration model was more effective and accurate than any other structures. The models developed are able to predict the process parameters required to obtain the desired bead width, to establish guidelines and criteria for the most effective joint design, and further to help the development of an automatic control system of arc welding robots.

Malviya et al. (*18*) used a particle swarm optimization technique for tuning of neural networks utilized for carrying out both forward and reverse mappings of Metal Inert Gas (MIG) welding process. Four approaches have been developed and their performances are compared to solve the said problems. The first and second approaches deal with tuning of multilayer feed-forward neural network and radial basis function neural network, respectively. In the third and fourth approaches, a back-propagation algorithm has been used along with particle swarm optimization to tune radial basis function neural networks. Moreover, in these two approaches, two different clustering algorithms have been utilized to decide the structure of the network. The performances of hybrid approaches (that is, the third and fourth approaches) are found to be better than that of the other two.

6.06.2.2 Mechanical Properties of the Weld Bead

Control of distortion and overall quality of welds were investigated by Casalino et al. (*19*) in order to select the GMAW process parameters that minimize thermal deformation and evaluate weld quality. They integrated the artificial intelligence techniques and FEM with the aid of experimental trials of bead-on-plate welds. The base metal was 1.6 mm thick low-carbon steel, a 0.9 mm diameter copper-coated wire was used as an electrode with a shielding gas consisting of a 75% Ar–25% CO_2 mixture with flow rate of 10–15 $ft^3\ h^{-1}$. ANN was used at first to link the process parameters to the geometry of the molten zone, which allowed the geometries throughout a range of process parameters to be calculated. Then, FEM was applied to predict the residual stress value and distortion in the welded joint. Finally, the fuzzy C-means clustering algorithm was applied to evaluate the quality joints. Mathematical models for GMAW were constructed. Experimentally butt welded joints were validated. It was concluded that the experimental results are in good agreement with the mathematical model.

Li-Ming et al. (*20*) have established a static model for SiCw/6061Al metal matrix composites in diffusion welding using ANN. The relationship between welded joint strength and welding parameters, such as, welding temperature, welding pressure and welding time was presented. The effect of process parameters on the joint strength was demonstrated and optimal technical parameters were obtained. It was proven that the developed static model was in good agreement with the actual data.

Sterjovski et al. (*21*) introduced ANN modeling as an alternative technique to those currently in the literature to predict the hardness of HAZ, and hence, trying to control it to minimize the risk of hydrogen assisted cold cracking in welding in service pipelines by the hot tapping technique. The model developed included materials characteristics; chemical composition and hardness (as inputs), the peak temperature, holding time, and cooling rate of the HAZ thermal cycle simulation were also used as key inputs in the model to predict the HAZ hardness. It was reported that the hardness of HAZ increases with increasing the following: carbon content, original hardness of pipe or fitting material, and more rapid cooling. They compared the predictive capabilities of the models developed with other published works to the neural network model they developed. It was clear that the neural networks model produced a much lower error across a broader range of HAZ hardness values.

Lightfoot et al. (*22*) have used ANN to develop a model to study the Flux Cored Arc Welded (FCAW) process factors affecting the distortion of 6–8-mm thick D and DH grade steel plates. A sensitivity analysis was carried out, which highlighted a number of apparent key factors that influenced distortion. It was proven that the carbon content played a key role in the amount of distortion produced by the welding process. They found that an increase in the carbon content was beneficial in reducing thin plate distortion caused by welding. Also, they identified a number of distortion-related factors, such as carbon content, YS/TS ratio, and rolling treatment. It was concluded that these factors can be controlled to reduce the distortion in 6–8-mm thick plates.

Sterjovski et al. (*23*) have applied the ANN models to predict the mechanical properties of steels in various applications, namely: impact strength of quenched and tempered pressure vessel steel exposed to multiple post weld heat treatment cycles, the hardness of the simulated HAZ in pipeline, and lap fitting steel after in-service welding and the hot ductility and hot strength of various micro alloyed steel over the temperature range for stand or slab straightening in continuous casting process. It was found that the three ANN models successfully predicted the mechanical properties. It was also shown that ANNs could successfully predict multiple mechanical properties and the results of the sensitivity analysis were in agreement with both the findings of the experimental investigation and reported results in the literature. Furthermore, it was mentioned that the use of ANNs resulted in large economic benefits for organizations through minimizing the need for expensive experimental investigation and/or inspection of steels used in various applications.

Okuyucu et al. (*24*) developed a model using ANN for the analysis and simulation of the correlation between friction stir welding parameters of aluminium plates and mechanical properties of the welded joint. The process parameters consist of weld speed and tool rotation speed verses the output mechanical properties of weld joint, namely tensile strength, yield strength, elongation, hardness of WZ, and hardness of HAZ. Good performance of the ANN model was achieved and the model can be used to calculate mechanical properties of the welded plates and a function of process parameters. Also, it was found that the correlation between the measured and predicted values of tensile strength, hardness of HAZ, and hardness of weld metal were better than those of elongation and yield strength.

www.iran-mavad.com
مرجع مهندسی مواد و متالورژی

Ates et al. (25) employed ANN for the prediction of gas metal arc welding parameters. Input parameters of the model consist of gas mixtures, whereas outputs of the ANN model include mechanical properties such as tensile strength, impact strength, elongation, and weld metal hardness, respectively. ANN controller was trained with the extended delta–bardelta learning algorithm. The results showed that the outcomes of the calculation were in good agreement with the measured data, indicating that the novel technique presented in this work shows the good performance of the ANN model.

Acherjee et al. (26) establishes a correlation between the laser transmission welding parameters and output variables through a nonlinear model, developed by applying ANN. The process parameters of the model include laser power, welding speed, standoff distance, and clamping pressure; whereas the output parameters of the model include lap-shear strength and weld-seam width. Experimental data is used to train and test the network. Furthermore, a comparison is made between multiple regression models and ANN models for prediction of laser transmission welding outputs.

Pal et al. (27) developed a multilayer neural network model to predict the Ultimate Tensile Stress (UTS) of welded plates. Six process parameters, namely pulse voltage, back-ground voltage, pulse duration, pulse frequency, wire feed rate, and the welding speed, and the two measurements, namely root mean square values of welding current and voltage, are used as input variables of the model and the UTS of the welded plate is considered as the output variable. A series of experiments were carried out by applying the response surface method, which evenly distributes the process parameters over the operating range. Then the obtained experimental data was used to train and test ANN model of various architectures.

6.06.3 DoE Analysis

Design of Experiments (DOE) is a powerful technique used for exploring new processes, gaining increased knowledge of the existing processes, and optimizing these processes for achieving world class performance. In performing the design of experiments for a process, structural and systematic changes are made to the input parameters in order to observe changes in the output process (28,29). The information gained from properly planned, executed, and analyzed experiments can be used in the modeling of the process output as a function of input parameters. Most popular design strategies are:

1. 'Factorial' or 'Classical DOE' was the first technique used with designed experiments. It allows you to see which factors are most important and helps you to identify important interactions among the factors. It does not predict the best factor levels to meet your goals.
2. Response Surface Methodology (RSM) uses your model to make contour plots of predicted behavior. Using these plots you can actually predict the best combination of factors to meet your goals. Among the RSM designs, two popular types of experimental designs exist for developing second-order models: central composite design and Box–Behnken Design (BBD).
3. Taguchi is interested in finding a 'robust' answer to the experimental question. It seeks an answer that is insensitive to factor variations and noise. It does not predict the best combination of factors to achieve your goals.

6.06.3.1 Factorial Design

6.06.3.1.1 Weld Bead Geometry

Kim et al. (30) developed mathematical models for the selection of process parameters and the prediction of bead geometry (bead width, bead height, and penetration) in robotic GMA welding using factorial design of design of experiments technique. Three factors were incorporated into the factorial model: arc current, welding voltage, and welding speed. Sensitivity analysis was investigated to represent the effectiveness of the processing parameters on the empirical equations and showed that the change of process parameters affects the bead width and bead height more strongly than penetration relatively.

Karaoğlu et al. (31) employed the sensitivity analysis of parameters and fine tuning requirements of the parameters for optimum weld bead geometry. Changeable process parameters such as welding current, welding voltage, and welding speed were used as design variables while the objective function was calculated using width, height, and penetration of the weld bead. Mathematical models were constructed by using multiple curvilinear regression analysis. After carrying out a sensitivity analysis using developed empirical equations, relative effects of input parameters on output parameters were obtained. Effects of all the three design parameters on the bead width and bead height show that even small changes in these parameters play an important role in the quality of the welding operation. The results also revealed that the penetration is almost nonsensitive to the variations in voltage and speed. Current was found as the most important parameter in determining the penetration.

Raveendra and Parmar (32) have built mathematical models using the fractional factorial technique to predict the weld-bead geometry and shape relations (penetration, width, and reinforcement height, width to penetration ratio and percentage dilution). The base metal was a 13-mm thick low-carbon structural steel plate. The parameters of the FCAW process considered in this work were: arc voltage, welding current, welding speed, gun angle, and nozzle-to-plate distance. They have developed models which can be used either to predict the bead geometry or to determine a combination or a range of parameters to obtain the desired bead geometry dimensions within the factors domain. Furthermore, these models can also be used in a production system for automatic control of welding conditions.

Gupta and Parmar (33) have used the fractional factorial technique 2^{5-1} to develop mathematical models to predict the weld-bead geometry and shape relationships for the SAW of micro alloyed steel; the thickness ranged between 10 and 16 mm.

www.iran-mavad.com
مرجع مهندسی مواد و متالورژی

They investigated bead penetration, weld-width, reinforcement; dilution, width/penetration, and width/reinforcement as affected by wire feed-rate, open-circuit voltage, nozzle-to-plate distance, welding speed, and workpiece thickness. It was found that the fractional factorial technique was convenient for the prediction of the main effects and the interaction effects of different combinations of welding parameters. Mathematical models were developed which can effectively be used to predict the weld zone dimensions. Moreover, they mentioned that, if a specific set of requirements for weld-bead dimensions is given, these models can be used in a computer program to determine a combination of parameters which will meet the requirements.

The development of the mathematical models using the five level factorial technique to predict the weld-bead geometry for depositing 316L stainless steel onto structural steel IS2062 in single wire surfacing using the SAW process was studied by Murugan et al. (*34*). They investigated the following weld-bead parameters (penetration, reinforcement, width, and dilution) as affected by the following SAW process variables (open-circuit voltage, wire feed-rate, welding speed, and nozzle-to-plate distance). It was shown that the developed models can be easily employed in automated or robotic welding, in the form of a program, for obtaining the desired high quality welds. The results demonstrated that the bead penetration is not significantly affected by the voltage and nozzle-to-plate distance and the width is not affected by the latter. Furthermore, it was proven that the dilution increased when voltage and welding speed are increased from its lowest level to its center level, but dilution is not affected by changes in voltage when the welding speed is at its center level. They found that the dilution decreased with increasing voltage when the welding speed is increased from its center level to its highest level.

Murugan and Parmar (*35*) used a four-factors, five-levels factorial technique to predict the weld-bead geometry (penetration, reinforcement, width, and dilution%) in the deposition of 316L stainless steel onto structural steel IS2062 using the MIG welding process. The following process parameters were controlled: open-circuit voltage, feed-rate, welding speed, and nozzle-to-plate distance. It was demonstrated that this factorial technique can be easily employed for developing mathematical models to predict the weld-bead geometry within the factors ranges and these models can be fed into automatic robotic surfacing in a form of program to obtain the desired high quality. In addition to this, the effects of each factors on the weld features were determined and graphically presented.

6.06.3.1.2 Mechanical Properties of the Weld Bead

Application of the factorial technique for weld quality prediction for the Plasma Transferred Arc (PTA) weld cladding process on mild steel was investigated by Harris and Smith (*36*). The process variables considered were current, powder feed-rate, torch travel speed, oscillation width, and torch stand-off distance. Four deposit quality features were measured, namely: deposit height, width, hardness, and dilution. It was confirmed that all the process variables were acting as main process parameters in controlling the deposit quality. Also, it was reported that the PTA process is an excellent choice for depositing high quality hard-facing deposits at low controlled dilution.

Optimization of friction welding of dissimilar materials using factorial design was studied by Murti and Sundaresan (*37*). They studied the friction welding of three industrially useful dissimilar materials: low alloy steel to austenitic stainless steel, medium carbon steel to high speed steel, and aluminium to stainless steel. The main aim was to determine the metallurgical and mechanical behavior of the friction welded joints produced using optimum welding conditions. Three mathematical models were developed to relate the Notched Tensile Strength (NTS) and shear energy to the process parameters, namely: friction pressure, friction time, and forging pressure with different levels according to the two materials which formed the joint. It was reported that the statistical experimental design was useful for reducing the number of trials necessary to optimize the welding conditions for friction welding. Also, the strength of the joint which was produced by using the optimized condition was in fair agreement with the predicted results. Moreover, in all cases, the joint strength was at least as high as those of the softer of the two materials that formed the joint.

Control of distortion in robotic CO_2-shielded FCAW was investigated by Arya and Parmar (*38*). A three level fractional factorial technique was used to develop mathematical models to predict the angular distortion in 10-mm thick low-carbon steel. The effect of arc voltage, wire feed-rate, welding speed, and groove angle on the angular distortion in single 'V' butt welds was investigated with and without sealing run. It was concluded that the developed models were fairly accurate and can be usefully employed for controlling the angular distortion in automated welding lines using the FCAW process.

Zhou et al. (*39*) have utilized factorial experimentation to investigate the influence of joining parameters (rotational speed, frictional time, and pressure) on the NTS of dissimilar aluminium-based metal matrix composite MMC/AISI304 stainless steel friction joints. It was observed that frictional pressure and rotational speed have a statistically significant effect on the NTS values. Moreover, they reported that the highest NTS occurs in joints produced at a high frictional pressure of 120 MPa.

Fatigue endurance of FCAW cruciform joints containing lack of penetration using design of experiment was studied by Balasubramanian and Guha (*40*). The aim was to optimize some dimensional factors that affected the fatigue life of cruciform joints made of quenched and tempered steel (ASTM 517 F grade). It was mentioned that the techniques described in this work were fairly simple and economical to optimize the time-consuming fatigue tests. It was also reported that some factors affecting the fatigue endurance were optimized to attain a maximum fatigue life, but the validity of the procedure is limited to the factors domain considered for the investigation. It was noted that the Analysis-of-Variance (ANOVA) technique is the most convenient to identify the significance of the main effects and interaction effects of joint dimensions. The same authors (*41*) continued their investigation by developing mathematical models using design of experiment to predict the fatigue life of Shielded Metal Arc Welding (SMAW) and FCAW cruciform joints failing from root and toe regions. Using the developed models, the fatigue life of SMAW and FCAW cruciform joint can be predicted at a 95% confidence level, however, the validity of the models is limited to the factors domain. It was found that the factorial experimentation technique design of experiment is more economical for predicting the effect of various factors on fatigue life through conducting a minimum number of experiments.

www.iran-mavad.com
مرجع مهندسی مواد و متالورژی

Koganti et al. (42) have employed a full factorial design to define the optimum weld MIG process parameters for nontreatable 5754 aluminium alloys. The effects of weld process parameters on the lap joint failure load (tensile-shear strength) and weld penetration were investigated. The process parameters were: power input, torch speed, voltage, current, wire feed-rate, pulse frequency, and gas flow rate. The joint strengths and weld penetration were measured for various operating ranges of weld factors. It was indicated that the power input and the gas flow rate were the two significant factors based on lap shear load to failure and weld penetration data. It was reported also, that the lower the power input, the lower the shear load to failure and depth of penetration and vice versa. The optimum factor settings for higher joint strength were high power input and high gas flow rate.

Sampath (43) has presented an innovative constrains-based approach that proved quite efficient in developing a specification for consumable solid-wire electrodes for GMAW of HSLA-80 and HSLA-100 steels that meet or exceed the US Navy requirements. Initially, he converted the US Navy requirements into a set of constraints which related the chemical composition of steels to certain metallurgical characteristics. Subsequently, a 2^3 factorial design was used to develop a batch of welding electrodes in order to evaluate their performance. Among the eight electrodes used, it was shown that two electrodes met or exceeded ER-100s requirements, while one electrode met or exceeded ER-120s requirements. It was concluded that the use of this approach greatly reduced the risk inherent in developing electrode specifications.

Pine et al. (44) have presented an experimental and numerical study to determine the torsional stiffness, elastic limit, and ultimate strength of spot welded, adhesively bonded, and weld-bonded box sections. They investigated a variety of factors, namely: joining technique, sheet thickness, steel strength, section area, section design, and end weld using factorial design techniques to determine their effects on the torsional properties of box sections. The authors have concluded that the joining technique, section area, and section thickness were the main factors which have the greatest effect on the torsional stiffness of the box sections. It was found that the torsional stiffness can be improved without substantial weight gain by changing the joining technique from 50 mm pitch spot welds to adhesive bonding, increasing the section area and to a lesser extent, changing the section design. Furthermore, the steel strength was the most important factor in determining the elastic limit and ultimate strength.

Khan et al. (45) employed full factorial design to optimize the laser welding process in order to obtain the most desirable weld quality in terms of weld bead geometry and mechanical strength, and determine the corresponding optimal settings of welding parameters. Laser power and welding speed were indicated as the most important factors affecting the weld bead geometry as well as the shearing force of the weld. Maximum achievable weld resistance length and hence, the weld shearing force, were energy-limited for the welding conditions, joint configuration, and materials used. Optimum results were presented numerically and graphically which allows quicker search for the optimal settings for laser welding.

6.06.3.2 Response Surface Methodology

6.06.3.2.1 Weld Bead Geometry

Yang et al. (46) have used linear-regression equations for computing the weld features (melting rates, total fusion area, penetration, deposit area, bead height and bead width) from SAW process variables (electrode extensions range, welding voltage, welding current, welding speed and electrode diameter) using both positive and negative electrode polarity. The base material was a 19 mm thick ASTM A36 steel plate. They managed to develop regression equations for each weld feature in both polarity conditions. Their results indicated that the linear-regression equations were equally useful for computing the various features of the SAW process.

The effect of process parameters (welding current, travel speed, gap width, bead height and arc deflection current) on the bead shape in a narrow gap-GTAW process with magnetic arc oscillation was studied by Starling et al. (47). Two AISI 304L stainless steel plates (9.5 and 6 mm thick) were employed to prepare the narrow gap joints and an AWS ER308L wire of 0.96 mm diameter was used as a filler metal. Statistical experimental design and linear-regression modeling were used in this investigation to develop the model. It was shown that the arc oscillation has little effect on the lateral fusion of the joint. However, this oscillation does improve bead shape by increasing its concavity. It was reported that when the gap width was reduced, the undercutting level tended to remarkably increase. Also, the effects of other welding parameters were in good agreement with the results of previous works.

Kim et al. (48) have studied the interrelationship between robotic CO_2 arc welding parameters and bead penetration by developing mathematical models using factorial techniques to predict the desired bead penetration. Partial-penetration and single-pass welds were fabricated in 12 mm SS400 plates based on controlling four different process parameters (arc voltage, welding current, welding speed, and welding angle). They found that all the investigated parameters affect the bead penetration. They suggested extending the empirical formula to plates of varying thickness and many other parameters which were not included in their research.

Kim et al. (49) have employed factorial design to correlate the robotic GMAW process parameters (welding voltage, welding speed, and arc current) to three responses (bead width, bead height, and penetration) for optimization purposes. The material used included plates of AS 1204 mild steel adopting the bead-on-plate technique. Electrode wire with a diameter of 1.2 mm with the same mechanical and physical properties of the base metal was used. Their results showed that all process parameters influenced the responses and the models developed are able to predict the responses with 0–25% accuracy.

Murugan and Parmar (50) developed mathematical models using RSM to study the direct and interaction effects of SAW parameters (open-circuit voltage, wire feed-rate, welding speed, and nozzle-to-workpiece distance) on the cladding geometry (depth of penetration, height of reinforcement, weld-width, and dilution%). The process parameters obtained from the developed models were employed to clad IS2062 structural steel plate of 20-mm thickness using 316L stainless steel wire of 3.15 mm diameter. They concluded that a low dilution of 22.57% can be produced by both high voltage and high welding speed or by low voltage and low

www.iran-mavad.com
مرجع مهندسی مواد و متالورژی

welding speed. It was reported that the hardness of the existing martensitic structures at the intermediate mixed zones in overlays was below 400 VHN, due to low carbon content in the cladding.

Gunaraj and Murugan (51) have highlighted the use of RSM to develop mathematical models and plot contour graphs relating important input parameters namely the open-circuit voltage, wire feed-rate, welding speed, and nozzle-to-plate distance to some responses namely, the penetration, reinforcement, width, and percentage dilution of the weld bead in SAW of pipes. They demonstrated that all responses decrease with increasing welding speed. Also, when the nozzle-to-plate distance increases all responses decrease, but reinforcement increases. Moreover, an increase in the wire feed-rate results in an increase in all responses, but the width remains unchanged.

In 1999, Gunaraj and Murugan (52) also studied the effect of SAW parameters on the heat input and the area of HAZ for low-carbon steel with two joint types, bead-on-plate, and bead-on-joint, using mathematical models developed by RSM. They found that for the same heat input, the area of the HAZ is greater for the bead-on-plate than that for bead-on-joint. They found that the effect of SAW parameters on the area of HAZ in both cases follows the same trend.

Koleva (53) has developed models to investigate the influence of Electron Beam Welding (EBW) parameters namely electro beam power, welding velocity, distance from the main surface of the magnetic lens to the focus point, and the distance between the magnetic lens and the sample surface on the welding depth and width. The experiment was performed with samples of austenitic steel, type 1H18NT. Also, the desirability approach was used to find the optimal welding conditions which would lead to the desired depth and width. The author has suggested the use of the developed models for online control of the process. This allows the selection of the optimal levels, eliminates the time required for testing, and prevents losses of components.

Gunaraj and Murugan have divided their study into two parts; in the first part (54), they developed a model to relate the weld-bead volume to SAW parameters with slightly changed open-circuit voltage limits from those used in their previous work (52). This change is reflected in the development of new models to correlate the rest of the responses mentioned earlier to the process. Their results revealed that the penetration reduces, and the bead width and dilution considerably increase as welding voltage increases. Also, they proved that the reinforcement is least when all SAW parameters are at their upper limits and the wire feed-rate is at its lower limit. In the second part (55), the total volume of the weld bead was optimized (minimized) by keeping the other bead parameters as constraints to obtain sound welded pipes. Also, sensitivity analysis was carried out to predict the effect of the other bead parameters on the total volume.

Gunaraj and Murugan (56) continued their previous study and successfully investigated the effect of SAW parameters on HAZ characteristics. They pointed out that the heat input and wire feed-rate has a positive effect, but welding speed has a negative effect on all HAZ characteristics. They also concluded that the width of HAZ is at a maximum (about 2.2 mm) when the wire feed-rate and the welding speed are at their minimum limits.

The effect of the laser welding parameters on the bead geometry of 2.5-mm thick AISI304 stainless steel has been investigated by Manonmani et al. (57). In this study, the relationship between the process parameters (beam power, welding speed, and beam incidence angle) and the weld-bead parameters (penetration, bead width, and area of penetration) has been developed using RSM. To verify the developed models, a conformity test run was carried out using intermediate values of the process parameters. It was confirmed that the model developed was accurate since the error percentages were between −4.317% and 3.914%. It demonstrated that the depth of penetration and penetration area increase as the beam power and the beam angle increase. Also, as the welding speed increases, the width decreases, whereas the penetration depth and area increase to an optimum value and then decrease with further increases in welding speed. This is due to the fact that the effect of key holing is predominant at a lower speed and as the welding speed is increased, the mode of heat transfer changes from key holing to conduction type of welding. It was reported that the variation in the bead width is slightly affected by the process parameters.

In 2005, Gunaraj and Murugan (58) extended their study and managed to establish mathematical expressions to predict the penetration size ratio 'PSR' (the ratio of bead width to the height of penetration) and the reinforcement form factor (RFF, the ratio of bead width to the height of reinforcement). These expressions and the others developed earlier can be fed into a computer, relating the weld-bead dimensions to the important SAW parameters, in order to optimize the process to obtain the required bead shape and weld quality.

Koleva (59) has carried out another work by applying RSM to establish the relationship between performance characteristics (weld-depth, weld-width, and thermal efficiency) and its influencing factors (beam power, welding velocity, focus position, focusing current of the beam and the distance to the sample surface) for EBW of austenitic stainless steel. Optimal welding regimes were found through the thermal efficiency optimization. New statistical approaches were proposed to choose the focus position at a condition of maximum thermal efficiency and welding depth.

Benyounis et al. (60) have applied RSM to investigate the effect of laser welding parameters (laser power, welding speed, and focal point position) based on four responses (heat input, penetration, bead width, and width of HAZ) in CO_2 laser butt welding of medium carbon steel plates of 5-mm thick. They found that the heat input plays an important role in the weld-bead parameters; welding speed has a negative effect while laser power has a positive effect on all the responses. Again, Benyounis et al. (61) have used the previous models (60) to optimize the process. Two optimization criteria were considered; the desirability approach was used to find the optimal conditions in the numerical optimization. They reported that full penetration has a strong effect on the other bead parameters. Also, strong, efficient, and low cost weld joint could be achieved using the optimal conditions.

Koleva and Vuchkov (62) have established the relationship between EBW parameters (beam power, welding velocity, and focus position) and weld-depth and weld-width using RSM in order to improve the quality of the process in mass production.

www.iran-mavad.com
مرجع مهندسی مواد و متالورژی

They reported that the optimal process parameters values when welding stainless steel are: power 6.5–8 kW, welding velocity 11.667–1.333 mm s^{-1}, and focus position 78 mm below the sample surface.

Kannan and Murugan (63) have studied the effect of flux cored arc welding process parameters (welding current, welding speed, nozzle-to-plate distance, and welding torch angle with reference to vertical) on the duplex stainless steel clad quality in terms of penetration, width, reinforcement, and percentage dilution. It was demonstrated that the process parameters have a significant effect on the bead geometry of the clad. The effect of the input process parameters on the clad quality parameters have been presented in graphical form, which assist in finding the welding parameters combination that would quickly lead to the desired clad quality.

Acherjee et al. (64) investigated the laser transmission contour welding process using Finite Element Analysis (FEA) and DoE techniques. Four key process parameters, namely power, welding speed, beam diameter, and carbon black content in absorbing polymer, are considered as input parameters, while maximum temperature at weld interface, weld width, and weld depths in transparent and absorbing polymers are considered as output parameters. First of all, a three-dimensional thermal model is developed to simulate the laser transmission contour welding process with a moving heat source. The commercial finite element code ANSYSs multiphysics is used to obtain the numerical results by implementing a volumetric Gaussian heat source, and combined convection–radiation boundary conditions. DoE together with regression analysis is then employed to plan the experiments and to develop mathematical models based on the simulation results. The developed empirical models are used in sensitivity analysis to determine the relative influence of different parameters on the process outputs. In the results, laser power was found to have a positive effect on all the responses investigated, whereas welding speed was recognized to have a negative effect. In another work, the same authors employed the FEA and DoE to study the effects of process parameters on the temperature field and weld bead dimensions (65). The thermal field is simulated by solving a three-dimensional transient heat diffusion equation with temperature dependent material properties using the ANSYS's multiphysics. Response surface methodology is then applied for developing mathematical models based on simulation results. The effect of parameters and their interactions on the responses are studied using the developed response surface models. Laser power was found to have the most dominant effect on the maximum temperature in the weld zone (Tmax), the maximum temperature at weld interface (Tweld), and the weld width (WW), and it is followed by welding time and beam width. While, welding time was seen as the most important factor affecting the DT and DA, and it is followed by power and beam width. The mathematical models were further used in search of the optimal process window for obtaining an acceptable weld using the graphical optimization results.

Ruggiero et al. (66) investigated the effect of laser power, welding speed, and focal point position on the weld-bead geometry (i.e., weld-bead area, upper width, lower width, and middle width) and on the operating cost using RSM. The experimental plan was based on BBD. Linear and quadratic polynomial equations for predicting the weld-bead geometry were developed. Based on the resultant response surface models, multiobjective optimization was performed that would minimize both the middle width and the weld-bead area, keeping the cost relatively low.

Zhao et al. (67) studied the effect of the laser welding parameters (i.e., laser power, welding speed, gap, and focal position) on the weld bead geometry (i.e., weld depth, weld width, and surface concave) of 0.4-mm thick galvanized SAE1004 steel. The process windows of the concerned process parameters were therefore determined. Then, RSM was used to develop models to predict the relationship between the processing parameters and the laser weld bead profile and identify the correct and optimal combination of the laser welding input variables to obtain superior weld joint. Under the optimal welding parameters, defect-free weld were produced, and the average aspect ratio increased about 30%. Aspect ratio, obtained by dividing weld depth by weld width was defined as the optimization goal.

Correia et al. (68) selected the best values of three control variables (reference voltage, wire feed rate, and welding speed) based on four quality responses (deposition efficiency, bead width, depth of penetration, and reinforcement), inside a previous delimited experimental region using two different techniques, RSM and genetic algorithms (GA). For the RSM, an experimental design was chosen and tests were performed in order to generate the proper models. In the GA case, the search for the optimal was carried out step by step, with the GA predicting the next experiment based on the previous, and without the knowledge of the modeling equations between the inputs and outputs of the GMAW process.

It was found that the GA can be a powerful tool in experimental welding optimization, even when the experimenter does not have a model for the process. The most important response (depth of penetration) had a difference from its target lower than 4%. However, the optimization by the GA technique requires a good setting of its own parameters, such as population size, number of generations, etc. Otherwise, there is a risk of an insufficient sweeping of the search space.

The RSM technique found a better compromise between the evaluated responses than the GA. Besides, the RSM generated models can be useful in further investigations of the search space, avoiding the experiments with undesired predicted responses. An inconvenience of the RSM (and similar techniques) is that it provides good results over regular experimental regions, i.e., with no irregular points. However, it is often very difficult to establish an arc, and melt-through may occur under certain experimental points needed to satisfy the specific experimental design. The data obtained may be impossible to analyze or may provide poor results, both of which often forces the experimenter to modify the design space (69).

6.06.3.2.2 Weld Bead Mechanical Properties and Operating Cost

Wang and Rasmussen (70) have investigated the inertia welding process of low-carbon steels using RSM, with the purpose of establishing an empirical functional relationship between the process parameters (the axial pressure, the initial rubbing velocity, and the total moment of inertia) and the breaking strength of the joint. It was concluded that a relatively wide range of operating conditions would produce successful welds. Also, they observed that the average microhardness at the weld was about 27% higher

www.iran-mavad.com
مرجع مهندسی مواد و متالورژی

than the base material and the ideal weld should be made with the least possible amount of kinetic energy as long as full penetration at the interface is achieved.

Yamaguchi et al. (71) have investigated the friction welding process of 5056 aluminium alloy using RSM. Their aim was to find the optimal welding conditions that would yield maximum tensile strength at the weld. The process input parameters were friction pressure, up-set pressure, friction time, rotating speed, and braking time. It was reported that the successful welds showed 89.2% joint efficiency in tensile strength. It was also observed that the friction layer formed at the friction interface disappeared in these successful weld runs.

Koichi et al. (72) have studied the combination of welding conditions that produce maximum notched tensile strength of friction welded joints of S4 5C carbon steel using RSM. They managed to correlate the process parameters (friction pressure, up-set pressure, friction time, rotation speed, and braking time) to the tensile strength of the weld joint. Successful weld strength was obtained using the optimal welding condition predicted by the empirical equation.

Benyounis et al. (73) have proposed models using RSM to investigate the effect of welding parameters in SAW (welding current, arc voltage, and welding speed) on the impact strength at two testing temperatures of 50 °C and 27 °C. The aim was to predict and optimize the impact strength of the spiral-welded joints with respect to the process parameters. It was observed that the welding current was the most significant factor associated with the impact strength, then the welding speed, whereas the welding voltage has no significant effect within the factors domain investigated. They listed the optimal welding conditions that would lead to acceptable impact strength with improving the process productivity.

The production of strong and stiff, aluminium–titanium, multilayered composites (laminates) by explosive welding was undertaken by Ege et al. (74). The study was performed using RSM to investigate the mechanical behavior of the laminates with changes in two characteristic variables: abundance of interfaces and volume percentage of the more ductile component. Eighteen laminates were produced and then one-step welding of these laminates was carried out by explosive-introduced pressuring. Yield strength, ultimate tensile strength, and elongation were the responses under consideration. A second-order model was fitted to define the relationship between the yield strength and the two variables. It was reported that the mechanical properties of the laminates strongly depend on the relative amounts of the components, but only weakly depend on the abundance of the interface within the selected operability region. It was also mentioned, that with the aid of the developed model, it is possible to fabricate laminates that are tailored to strength, density, and load specifications.

Allen et al. (75) have proposed a model based on central composite design with the alpha parameter set equal to two, for robotic gas metal arc welding of sheet metal of 409-gage, stainless steel. The six factors controlled in this study were: wire feed speed, weld travel speed, arc voltage, contact-tube-to-work distance, root opening, and offset. The objective was to minimize the weld cycle time by maximizing welding speed, while maintaining predictable weld quality over a range of worst-case processing conditions. The optimal welding conditions for this type of material with a lap joint were reported and confirmed by experimental tests. The effect of the process parameters was graphically presented.

Raghukandan (76) has conducted experiments to clad low-carbon steel and copper plates using nitro-glycerine explosive (2500 m s^{-1} detonation velocity). The aim was to adopt RSM to relate the bond and shear strength of the clad to four process factors (flyer thickness, loading ratio, angle of inclination, and stand-off distance). Mathematical models were developed and the effect of process parameters on the responses was discussed. It was found that the flyer thickness, the loading ratio, and the angle of inclination have significant contribution to the interfacial morphology of explosive clad.

Murugan and Gunaraj (77) have implemented RSM to correlate the angular distortion in GMAW of a structural steel plate (IS: 2062) to the process parameters, namely: time gap between successive passes, number of passes, and wire feed-rate. The main and interaction effects of the process parameters were analyzed and presented. It was found that the number of passes had a strong effect on the response; therefore, to control the angular distortion in practice, the number of passes has to be carefully monitored. Moreover, it was demonstrated that all the process parameters have a negative effect on the angular distortion.

Benyounis et al. (78) have studied the effect of CO_2 laser welding parameters (laser power, welding speed, and focus position) on the impact strength and NTS of butt joints made of medium carbon steel plates. Two mathematical models were developed using RSM to describe the influence of the process parameters on the two responses. The main, quadratic, and interaction effects of the process parameters on the two responses were quantitatively determined and graphically presented. It was reported that the welding speed is the main factor affecting the two responses; it was found that decreasing the welding speed from its highest level to lowest level would result in increasing both responses by 89.3% and 76.45%, respectively. Laser power and focal point position have also strong effect on both investigated responses.

Benyounis et al. (79) have done another work to predict the residual stress for CO_2 laser butt-welding joints of AISI304 stainless steel plates. The investigation is carried out using RSM to develop models in terms of the process input parameters mentioned earlier in Ref. (76) to predict the principal residual stress and its direction. It was observed that the travel speed and laser power were the main factors affecting the behavior of the maximum residual stress. It was recommended to use the developed models to find the optimal welding conditions to obtain the welded joint with a minimum distortion.

Olabi et al. (80) have established the relationship between the CO_2 laser welding parameters (laser power, welding speed, and focus position) and the residual stress magnitude and distribution using RSM for butt joint welded components. The base material was AISI304 stainless steel plates with 3-mm thickness. The incremental hole drilling procedure with the standard seven increments was followed to measure the residual stress magnitude and distribution at three locations, on HAZ, 10 mm and 20 mm from weld centerline repetitively. Twenty-one models were developed to describe the residual stress behavior. A procedure of four steps was presented to use the developed models in order to predict the residual stress magnitude at the proposed welding conditions and at

www.iran-mavad.com
مرجع مهندسی مواد و متالورژی

a given position. Also, the effect of the process parameters on residual stress behavior has been quantitatively determined and graphically presented.

Benyounis et al. (81) have developed a mathematical model using RSM to relate the failure load to the laser welding parameters namely: laser power, welding speed, and focal position. The effect of the process parameters on the failure load and the tensile-shear strength of the lap joint made of AISI304 with 1-mm thickness have been investigated. It was found that the main factor affecting the joint strength is the welding speed and the other two factors are slightly affecting the joint strength.

Olabi et al. (82) explored the effect of laser power, welding speed, and focal point position on mechanical properties (ultimate tensile strength and impact strength) and on the operating cost C using RSM. The experimental plan was based on BBD; linear and quadratic polynomial equations for predicting the mechanical properties were developed.

Acherjee et al. (83) investigated the effect of the laser welding parameters such as laser power, welding speed, stand-off distance, and clamp pressure on weld strength and weld width using RSM. Planned experiments and subsequent analyses were carried out to develop the mathematical models to establish the correlation between the process parameters and the responses. The adequacy of the developed models was tested using the sequential F-test, lack-of-fit test, and the ANOVA technique. Furthermore, numerical and graphical, multiobjective optimization techniques, in which the RSM is incorporated, was used to find the optimum solutions, according to the desired optimization criteria. In a further investigation, Acherjee et al. examined the effects of process parameters, namely, laser power, welding speed, size of the laser beam, and clamp pressure, on the lap-shear strength and weld-seam width for laser transmission welding of acrylic (polymethyl methacrylate) (84). Response surface methodology was employed to develop mathematical relationships between the welding process parameters and the output variables of the weld joint to determine the welding input parameters that lead to the desired weld quality. In the results, it has been found that for each power level, there is a threshold line energy value, at which the lap-shear strength reaches maximum. The optimum weld strength can be achieved at a favorable value of line energy with an appropriate combination of laser power and welding speed. In addition, using response surface plots, the interaction effects of process parameters on the responses were analyzed and discussed; in the case of stand-off-distance, the lap-shear strength increases with the stand-off-distance until it reaches its center value, the strength then starts to drop as stand-off-distance is increased above the center limit. However, it was observed that the welding speed has a stronger effect on lap-shear strength. In contrast, welding speed and stand-off-distance both have stronger effects on weld-seam width. These parameters should be carefully selected, because the responses are very sensitive to these process parameters.

Reisgen et al. (85) carried out a numerical and graphical optimization of the CO_2 laser beam welding of dual phase (DP600)/transformation induced plasticity (TRIP700) steel sheets using RSM based on BBD. The aim of the optimization study was to improve the weld quality, increase the productivity, and minimize the total operation cost by adjusting the welding parameters of laser power, welding speed, and focus position. As an outcome of this study, the welding cost was reduced to around 11.7 cents comparing to 14.7 before the optimization study. However, the welding speed was located in the maximum or nearly maximum of the design range in all optimization criteria which leads to increasing production rate.

Gunaraj et al. (86) investigated the SAW process and selected the optimum combination of input variables for achieving the required qualities of weld by the development of mathematical models through effective and strategic planning and the execution of experiments by RSM. A four-factor, five-level central composite rotatable design matrix with full replication was used for planning, conduction, execution, and development of mathematical models.

6.06.3.3 Taguchi Method

6.06.3.3.1 Weld Bead Geometry

Dongxia et al. (87) used the Taguchi approach as a statistical design of experimental technique for optimizing the selected welding parameters. From the experimental results, it is found that the effect of welding parameters on the welding quality decreased in the order of welding speed, wire feed rate, and laser power.

Xiansheng et al. (88) used the Taguchi method to optimize the selection of laser seal welding thin titanium shell, including the main parameters such as laser power, welding speed, defocusing amount, and shield gas. The results were experimentally confirmed and the device is properly equipped in medical treatments. According to the Taguchi experiment results, it was reported that the laser power and weld speed have the greatest influence on the S/N ratio, and the laser power, defocusing amount and weld speed have influence on average of penetration depth to width. The Taguchi method has been proved that it is very efficient method to find the dominant factor given the complex interactions within laser welding parameters, such as laser power, welding speed, defocusing amount, and pulse frequency.

Anawa et al. (89) selected the laser power, welding speed, and defocusing distance combinations with the objective of producing welded joint with complete penetration, minimum fusion zone size, and acceptable welding profile. Fusion zone area and shape of dissimilar austenitic stainless-steel with ferritic low carbon steel were evaluated as a function of the selected laser welding parameters. The Taguchi approach was used as the statistical DOE technique for optimizing the selected welding parameters in terms of minimizing the fusion zone.

Juang and Tarng (90) have adopted a modified Taguchi method to analyze the effect of each welding process parameter (arc gap, flow rate, welding current, and speed) on the weld pool geometry (front and back height, front and back width) and then to determine the TIG welding process parameters combination associated with the optimal weld pool geometry. It was experimentally reported that, the four smaller-the-better quality characteristics, 'four responses' of the weld pool in the TIG welding of S304 stainless steel of 1.5-mm in thickness are greatly improved by using this approach.

www.iran-mavad.com
مرجع مهندسی مواد و متالورژی

Lee et al. (91) have used the Taguchi method and regression analysis in order to optimize Nd-YAG laser welding parameters (nozzle type, rotating speed, title angle, focal position, pumping voltage, pulse frequency, and pulse width) to seal an iodine-125 radioisotope seed into a titanium capsule. The accurate control of the melted length of the tube end was the most important to obtain a sound sealed state. It was demonstrated that the laser pulse width and focal position were the laser welding parameters that had the greatest effects on the S/N ratios of the melted length. The optimal welding conditions were obtained at a pulse width of 0.86 ms and a focal position of 3.18–3.35 mm. Furthermore, confirmation experiments were conducted at the optimal welding conditions, it can be said that the titanium tube ends were perfectly sealed.

6.06.3.3.2 Mechanical Properties of the Weld Bead

Laser butt-welding of a thin plate of magnesium alloy using the Taguchi method has been optimized by Pan et al. (92). They studied the effect of Nd-YAG laser welding parameters (shielding gas type, laser energy, conveying speed, laser focus, pulse frequency, and pulse shape) on the ultimate tensile stress. Their result indicated that the pulse shape and energy of the laser contributed most to thin plate butt-welding. It was found that the optimal combination of welding parameters for laser welding were argon as a shielding gas, a 360 W laser energy, a workpiece speed of 25 mm s^{-1}, a focus distance of 0 mm, a pulse frequency of 160 Hz, and type III pulse shape. It was also found that the superior ultimate tension stress was 169 MPa at an overlap of the welding zone of approximately 75%.

Anawa et al. (93) have applied the Taguchi approach to optimize the laser welding process of dissimilar materials, namely: plain carbon steel and AISI316 with the same thickness of 1.5-mm. The process parameters were laser power, welding speed, and focus position against one response NTS. The experimental results indicated that the process could be optimized using the Taguchi method in order to obtain superior welded joints. Anawa and Olabi (94) have continued their investigation and studied the effect of the laser mentioned above welding parameters on the impact strength of the same joint at room temperature using the same optimizing technique. The results indicated that the laser power has the most significant effect on the impact strength. Also, it was mentioned that the optimal settings to obtain excellent impact strength were the highest laser power, a welding speed of 750 mm min^{-1}, and a focus position of −0.5 mm.

Tarng et al. (95) used the grey-based Taguchi methods for the optimization of the SAW process parameters in hard facing with considerations of multiple weld qualities. A grey relational grade obtained from the grey relational analysis was used as the performance characteristic in the Taguchi method. Then, optimal process parameters were determined by using the parameter design proposed by the Taguchi method. The proposed analysis can convert the optimization of the multiple performance characteristics into the optimization of a single performance characteristic called the grey relational grade. As a result, the optimization of the complicated multiple performance characteristics can be greatly simplified and the SAW process such as deposition rate, dilution, and hardness were improved together by using the method proposed by this study.

6.06.4 Concluding Remarks

Different analysis and optimization techniques were covered in this review in order to understand the influence of the welding factors and parameters on the weld bead shape and mechanical properties, and to explore the operating cost and its relation with the input parameters. This paper reveals the importance of application of design of experiments techniques and artificial neural network to predict the process output and to optimize the welding process. Moreover, different comparative studies of the used techniques were conducted, but still there is a lack of such studies. Integration of finite element modeling and optimization techniques was covered in few studies. However, this new technique is promising and it will be proposed in the future work.

References

1. Althouse, A. D.; Turnquist, C. H.; Bowditch, W. A.; Bowditch, K. E. *Modern Welding;* The Goodheart-Willcox Co., Inc: USA, 1984.
2. Cary, H. B. *Modern Welding Technology;* Prentice-Hall, Inc: New Jersey, 1979.
3. Ates, H. Prediction of Gas Metal Arc Welding Parameters Based on Artificial Neural Networks. *Mater. Des.* **2007,** *28* (7), 2015–2023.
4. Bhadeshia, H. K. D. H. Neural Networks in Materials Science. In *Encyclopedia of Materials: Science and Technology,* 2nd ed., 2008; pp 1–5.
5. Andersen, K.; Cook, G.; Karsai, G.; Ramaswamy, K. Artificial Neural Network Applied to Arc Welding Process Modelling and Control. *IEEE Trans. Ind. Appl.* **1990,** *26* (5), 824–830.
6. Cook, G.; Barnett, R. J.; Andersen, K.; Strauss, A. M. Weld Modelling and Control Using Artificial Neural Networks. *IEEE Trans. Ind. Appl.* **1995,** *31* (6), 1484–1491.
7. Vitek, J. M.; Iskander, Y. S.; Oblow, E. M. Neural Network Modelling of Pulsed-laser Weld Pool Shapes in Aluminum Alloy Welds. In *Proceedings of 5th International Conference on Trends in Welding Research, Pine Mountain, GA, June 1–5;* ASM International, 1998; pp 442–448.
8. Juang, S. C.; Tarng, Y. S.; Lii, H. R. A Comparison between the Backpropagation and Counter-propagation Networks in the Modelling of the TIG Welding Process. *J. Mater. Process. Technol.* **1998,** *75,* 54–62.
9. Chan, B.; Pacey, J.; Bibby, M. Modelling Gas Metal Arc Weld Geometry Using Artificial Neural Network Technology. *J. Can. Metall. Quarter* **1999,** *38* (1), 43–51.
10. Jeng, J. Y.; Mau, T.; Leu, S. Prediction of Laser Butt Joint Welding Parameters Using Back Propagation and Learning Vector Quantization Networks. *J. Mater. Process. Technol.* **2000,** *99,* 207–218.
11. Nagesh, D. S.; Datta, G. L. Prediction of Weld Bead Geometry and Penetration in Shielded Metal-arc Welding Using Artificial Neural Networks. *J. Mater. Process. Technol.* **2002,** *123,* 303–312.
12. Ridings, G. E.; Thomson, R. C.; Thewlis, G. Prediction of Multiwire Submerged Arc Weld Bead Shape Using Neural Network Modelling. *J. Sci. Technol. Weld. Joining* **2002,** *7* (5), 265–279.

www.iran-mavad.com
مرجع مهندسی مواد و متالورژی

13. Christensen, K. H.; SØrensen, T.; Kristensen, J. K. Gas Metal Arc Welding of Butt Joint with Varying Gap Width on Neural Networks. *J. Sci. Technol. Weld. Joining* **2005,** *10* (1), 32–43.
14. Balasubramanian, K. R.; Buvanashekaran, G.; Sankaranarayanasamy, K. Modeling of Laser Beam Welding of Stainless Steel Sheet Butt Joint Using Neural Networks. *CIRP J. Manuf. Sci. Technol.* **2010,** *3* (1), 80–84.
15. Parikshit, D.; Pratihar, D. K. Modeling of TIG Welding Process Using Conventional Regression Analysis and Neural Network-based Approaches. *J. Mater. Process. Technol.* **2007,** *184* (1), 56–68.
16. Kim, I. S.; Son, J. S.; Park, C. E.; Lee, S. H.; Yarlagadda, P. K. D. V. A Study on Prediction of Bead Height in Robotic Arc Welding Using a Neural Network. *J. Mater. Process. Technol.* **2002,** *130,* 229–234.
17. Kim, I. S.; Son, J. S.; Lee, S. H.; Yarlagadda, P. K. D. V. Optimal Design of Neural Networks for Control in Robotic Arc Welding. *Robot. Comput. Integrated Manuf.* **2004,** *20* (1), 57–63.
18. Malviya, Rakesh; Pratihar, D. K. Tuning of Neural Networks Using Particle Swarm Optimization to Model MIG Welding Process. *Swarm Evolutionary Computation* **2011,** *1* (4), 223–235.
19. Casalino, G.; Hu, S. J.; Hou, W. Deformation Prediction and Quality Evaluation of the Gas Metal Arc Welding Butt Weld. *J. Eng. Manuf.* **2003,** *217B,* 1615–1622.
20. Li-Ming, L.; Mei-Li, Z.; Ji-Tai, N.; Zhong-Dian, Z. Predicting Effects of Diffusion Welding Parameters on Welded Joint Properties by Artificial Neural Network. *J. Trans. Nonferrous Metal Soc. China* **2001,** *11* (4), 475–478.
21. Sterjovski, Z.; Nolan, D.; Dunne, D.; Norrish, J. Predicting the HAZ Hardness of Pipeline and Tap fitting Steels with Artificial Neural Networks. In *Proceedings of the 4th International Conference on Pipeline Technology;* Scientific Surveys: New South Wales, Australia, 2004; pp 1233–1245.
22. Lightfoot, M. P.; Bruce, G. J.; McPherson, N. A.; Woods, K. The Application of Artificial Neural Networks to Weld-induced Deformation in Ship Plate. *Weld. J., AWS and WRC* **February 2005,** *84,* 23-s–26-s.
23. Sterjovski, Z.; Nolan, D.; Carpenter, K. R.; Dune, D. P.; Norrish, J. Artificial Neural Network for Modelling the Mechanical Properties of Steels in Various Applications. *J. Mater. Process. Technol.* **2005,** *170* (3), 336–344.
24. Okuyucu, H.; Kurt, A.; Arcaklioglu, E. Artificial Neural Network Application to the Friction Stir Welding of Aluminium Plates. *J. Mater. Des.* **2007,** *29,* 78–84.
25. Benyounis, K. Y.; Olabi, A. G. Optimization of Different Welding Processes Using Statistical and Numerical Approaches – A Reference Guide. *Adv. Eng. Software* **June 2008,** *39* (6), 483–496.
26. Acherjee, B.; Mondal, S.; Tudu, B.; Misra, D. Application of Artificial Neural Network for Predicting Weld Quality in Laser Transmission Welding of Thermoplastics. *Appl. Soft Comput.* **2011,** *11* (2), 2548–2555.
27. Sukhomay, P.; Surjya, K. P.; Samantaray, A. K. Artificial Neural Network Modeling of Weld Joint Strength Prediction of a Pulsed Metal Inert Gas Welding Process Using Arc Signals. *J. Mater. Process. Technol.* **2008,** *202* (1), 464–474.
28. Antony, J. *Design of Experiments for Engineers and Scientists*; Butterworth-Heinemann: Oxford, 2003; Vol. 26.
29. Montgomery, D. C. *Design and Analysis of Experiments,* 2nd ed., Wiley: New York, 1984.
30. Kim, I. S.; Son, K. J.; Yang, Y. S.; Yaragada, P. K. D. V. Sensitivity Analysis for Process Parameters in GMA Welding Processes Using a Factorial Design Method. *Int. J. Mach. Tools Manuf.* **2003,** *43* (8), 763–769.
31. Serdar, K.; Seckin, A. Sensitivity Analysis of Submerged Arc Welding Process Parameters. *J. Mater. Process. Technol.* **2008,** *202* (1), 500–507.
32. Raveendra, J.; Parmar, R. S. Mathematical Models to Predict Weld Bead Geometry for Flux Cored Arc Welding. *J. Metal Construct.* **1987,** *19* (2), 31R–35R.
33. Gupta, V. K.; Parmar, R. S. Fractional Factorial Technique to Predict Dimensions of the Weld Bead in Automatic Submerged Arc Welding. *IE(I) J-MC* **November 1989,** *70,* 67–75.
34. Murugan, N.; Parmar, R. S.; Sud, S. K. Effect of Submerged Arc Welding Process Variables on Dilution and Bead Geometry in Single Wire Surfacing. *J. Mater. Process. Technol.* **1993,** *37,* 767–780.
35. Murugan, N.; Parmar, R. S. Effects of MIG Process Parameters on the Geometry of the Bead in the Automatic Surfacing of Stainless Steel. *J. Mater. Process. Technol.* **1994,** *41,* 381–398.
36. Harris, P.; Smith, B. L. Factorial Techniques for Weld Quality Prediction. *J. Metal Construct.* **November 1983,** *15,* 661–666.
37. Murti, K. G. K.; Sundaresan, S. Parameter Optimization in Friction Welded Dissimilar Materials. *J. Metal Construct.* **1983,** *15* (6), 331–335.
38. Arya, S. K.; Parmar, R. S. Mathematical Models for Predicting Angular Distortion in CO_2-shielded Flux Cored Arc Welding. In *The Proceedings of International Conference on Joining of Metals (JOM-3);* Helsingor: Denmark, 1986; pp 240–245.
39. Zhou, Y.; Li, Z.; Hu, L.; Fuji, A.; North, T. H. Mechanical Properties of Particulate MMC/AISI 304 Friction Joints. *J. ISIJ Int.* **1995,** *35* (10), 1315–1321.
40. Balasubramanian, V.; Guha, B. Assessment of Some Factors Affecting Fatigue Endurance of Welded Cruciform Joints Using Statistical Techniques. *Int. J. Fatigue* **1999,** *21,* 873–877.
41. Balasubramanian, V.; Guha, B. Fatigue Life Prediction of Load Carrying Cruciform Joints of Pressure Vessel Steel by Statistical Tools. *J. Mater. Des.* **2004,** *25,* 615–623.
42. Koganti, R.; Karas, C.; Joaquin, A.; Henderson, D.; Zaluzec, M.; Caliskan, A. Metal Inert Gas (MIG) Welding Process Optimization for Joining Aluminium Sheet Material Using OTC/DAIHEN Equipment. In *Proceedings of IMECE'03, November 15–21, 2003;* ASME International Mechanical Engineering Congress: Washington, DC, 2003; pp 409–425.
43. Sampath, K. Constrains-based Modelling Enables Successful Development of Welding Electrode Specification for Critical Navy Application. *Weld. J., AWS* **August 2005,** *84,* 131-s–138-s.
44. Pine, T.; Lee, M. M.; Jones, T. B. Factors Affecting Torsional Properties of Box Sections. *J. Ironmarking Steelmarking* **1998,** *25* (3), 205–209.
45. Khan, M. M. A.; Romoli, L.; Fiaschi, M.; Dini, G.; Sarri, F. Experimental Design Approach to the Process Parameter Optimization for Laser Welding of Martensitic Stainless Steels in a Constrained Overlap Configuration. *Opt. Laser Technol.* **2011,** *43* (1), 158–172.
46. Yang, L. J.; Bibby, M. J.; Chandel, R. S. Linear Regression Equations for Modelling the Submerged-arc Welding Process. *J. Mater. Process. Technol.* **1993,** *39,* 33–42.
47. Starling, C. M. D.; Marques, P. V.; Modenesi, P. J. Statistical Modelling of Narrow-gap GTA Welding with Magnetic Arc Oscillation. *J. Mater. Process. Technol.* **1995,** *51,* 37–49.
48. Kim, I. S.; Son, J. S.; Kim, I. G.; Kim, O. S. A Study on Relationship between Process Variable and Bead Penetration for Robotic CO_2 Arc Welding. *J. Mater. Process. Technol.* **2003,** *136,* 139–145.
49. Kim, I. S.; Son, K. J.; Yang, Y. S.; Yaragada, P. K. D. V. Sensitivity Analysis for Process Parameters in GMA Welding Processes Using a Factorial Design Method. *Int. J. Mach. Tools Manuf.* **2003,** *43,* 763–769.
50. Murugan, N.; Parmar, R. S. Effect of Welding Conditions on Microstructure and Properties of Tupe 316L Stainless Steel Submerged Arc Welding Cladding. *Weld. J., AWS* **1997,** *76* (5), 210s–220s.
51. Gunaraj, V.; Murugan, N. Application of Response Surface Methodology for Predicting Weld Bead Quality in Submerged Arc Welding of Pipes. *J. Mater. Process. Technol.* **1999,** *88,* 266–275.
52. Gunaraj, V.; Murugan, N. Prediction and Comparison of the Area of the Heat-affected Zone for the Bead-on-plates and Bead-on-joint in Submerged Arc Welding of Pipes. *J. Mater. Process. Technol.* **1999,** *95,* 246–261.
53. Koleva, E. Statistical Modelling and Computer Programs for Optimisation of the Electron Beam Welding of Stainless Steel. *J. Vacuum* **2001,** *62,* 151–157.
54. Gunarai, V.; Murugan, N. Prediction and Optimization of Weld Bead Volume for the Submerged Arc Process – Part 1. *Weld. J., AWS* **October 2000,** *79,* 286s–294s.
55. Gunarai, V.; Murugan, N. Prediction and Optimization of Weld Bead Volume for the Submerged Arc Process – Part 2. *Weld. J., AWS* **November 2000,** *79,* 331s–338s.
56. Gunaraj, Murugan Prediction of Heat-affected Zone Characteristics in Submerged Arc Welding of Structural Steel Pipes. *Weld. J., AWS* **January 2002,** 94s–98s.
57. Manonmani, K.; Murugan, N.; Buvanasekaran, G. Effect of Process Parameters on the Weld Bead Geometry of Laser Beam Welded Stainless Steel Sheets. *Int. J. Joining Mater.* **2005,** *17* (4), 103–109.

www.iran-mavad.com
مرجع مهندسی مواد و متالورژی

58. Gunaraj, Murugan Prediction and Control of Weld Bead Geometry and Shape Relationships in Submerged Arc Welding of Pipes. *J. Mater. Process. Technol.* **2005,** *168,* 478–487.
59. Koleva, E. Electro Beam Weld Parameters and Thermal Effciency Improvement. *Vacuum J.* **2005,** *77,* 413–421.
60. Benyounis, K. Y.; Olabi, A. G.; Hashmi, M. S. J. Effect of Laser Welding Parameters on the Heat Input and Weld-bead Profile. *J. Mater. Process. Technol.* **2005,** *164–165,* 978–985.
61. Benyounis, K. Y.; Olabi, A. G.; Hashmi, M. S. J. Optimizing the Laser-welded Butt Joint of Medium Carbon Steel Using RSM. *J. Mater. Process. Technol.* **2005,** *164–165,* 986–989.
62. Koleva, E.; Vuchkov, I. Model-based Approach for Quality Improvement of Electro Beam Welding Applications in Mass Production. *J. Vacuum* **2005,** *77,* 423–428.
63. Kannan, T.; Murugan, N. Effect of Flux Cored Arc Welding Process Parameters on Duplex Stainless Steel Clad Quality. *J. Mater. Process. Technol.* **2006,** *176,* 230–239.
64. Acherjee, B.; Kuar, A. S.; Mitra, S.; Misra, D. Modeling of Laser Transmission Contour Welding Process Using FEA and DoE. *Opt. Laser Technol.* **2012,** *44* (5), 1281–1289.
65. Acherjee, B.; Kuar, A. S.; Mitra, S.; Misra, D. Modeling and Analysis of Simultaneous Laser Transmission Welding of Polycarbonates Using an FEM and RSM Combined Approach. *Opt. Laser Technol.* **2012,** *44* (4), 995–1006.
66. Ruggiero, A.; Tricarico, L.; Olabi, A. G.; Benyounis, K. Y. Weld-bead Profile and Costs Optimisation of the CO_2 Dissimilar Laser Welding Process of Low Carbon Steel and Austenitic Steel AISI316. *Opt. Laser Technol.* **2011,** *43* (1), 82–90.
67. Zhao, Y.; Zhang, Y.; Hu, W.; Lai, X. Optimization of Laser Welding Thin-gage Galvanized Steel via Response Surface Methodology. *Opt. Lasers Eng.* **2012,** *50* (9), 1267–1273.
68. Correia, D. S.; Gonçalves, C. V. Comparison between Genetic Algorithms and Response Surface Methodology in GMAW Welding Optimization. *J. Mater. Process. Technol.* **2005,** *160* (1), 70–76.
69. Kim, D.; Rhee, S. Optimization of Arc Welding Process Parameters Using a Genetic Algorithm. *Weld. J.* **2001,** *80,* 184–189.
70. Wang, K. K.; Rasmussen, G. Optimization of Inertia Welding Process by Response Surface Methodology. *J. Eng. Ind.* **1972,** *94* (4), 999–1006.
71. Yamaguchi, H.; Ogawa, K.; Sakaguchi, K. Optimization of Friction Welding Condition of 5056 Aluminium Alloy. *J. Jpn. Inst. Light Metal.* **1991,** *41* (10), 716–720.
72. Koichi, O.; Hiroshi, Y.; Seiichi, K.; Kazuhiko, S. Optimization of Friction Welding Condition for S4 5C Carbon Steel Using a Statistical Technique. *J. Jpn. Weld. Soc.* **1993,** *24* (2), 47–53.
73. Benyounis, K. Y.; Bettamer, A. H.; Olabi, A. G.; Hashmi, M. S. J. Prediction the Impact Strength of Spiral-welded Pipe Joints in Submerged Arc Welding of Low Carbon Steel. In *Proceedings of IMC21;* Limerick, 1–3 September 2004; pp 200–210.
74. Ege, E. S.; Inal, O. T.; Zimmerly, C. A. Response Surface Study on Production of Explosive-welded Aluminium–titanium Laminates. *J. Mater. Sci.* **1998,** *33,* 5327–5338.
75. Allen, T. T.; Richardson, R. W.; Tagliabue, D. P.; Maul, G. P. Statistical Process Design for Robotic GMA Welding of Sheet Metal. *Weld. J., AWS* **May 2002,** *81,* 69s–77s.
76. Raghukandan, K. Analysis of the Explosive Cladding of Cu-low Carbon Steel Plates. *J. Mater. Process. Technol.* **2003,** *139,* 573–577.
77. Murugan, V. V.; Gunaraj, V. Effects of Process Parameters on Angular Distortion of Gas Metal Arc Welded Structural Steel Plates. *Weld. J., AWS* **November 2005,** 165s–171s.
78. Benyounis, K. Y.; Olabi, A. G.; Hashmi, M. S. J. Estimation of Mechanical Properties of Laser Welded Joints Using RSM. In *Proceedings of IMC22, 31 August–2 September 2005;* Institute of Technology Tallaght: Dublin, Ireland, 2005; pp 565–571.
79. Benyounis, K. Y.; Olabi, A. G.; Hashmi, M. S. J. Residual Stresses Prediction for CO_2 Laser Butt-welding of 304-stainless Steel. *Appl. Mech. Mater.* **2005,** *3* (4), 125–130. Trans Tech Publications.
80. Olabi, A. G.; Benyounis, K. Y.; Hashmi, M. S. J. Application of RSM in Describing the Residual Stress Distribution in CO_2 Laser Welding of AISI304. *Strain J.* **2007,** *43* (1), 37–46.
81. Benyounis, K. Y.; Olabi, A. G.; Hashmi, M. S. J. Effect of Laser Welding Parameters on the Tensile-shear Strength of AISI304 Sheet. In *Published in AMPT2006 Proceedings, July 30–August 3, 2006;* Ohio University: Athens, OH, USA, 2006.
82. Olabi, A. G.; Alsinani, F. O.; Alabdulkarim, A. A.; Ruggiero, A.; Tricarico, L.; Benyounis, K. Y. Optimizing the CO_2 Laser Welding Process for Dissimilar Materials. *Opt. Laser Technol.* **2013,** *51* (7), 832–839.
83. Acherjee, B.; Kuar, A. S.; Mitra, S.; Misra, S.; Acharyya, S. Experimental Investigation on Laser Transmission Welding of PMMA to ABS via Response Surface Modelling. *Opt. Laser Technol.* **2012,** *44* (5), 1372–1383.
84. Acherjee, B.; Misra, D.; Bose, D.; Venkadeshwaran, K. Prediction of Weld Strength and Seam Width for Laser Transmission Welding of Thermoplastic Using Response Surface Methodology. *Opt. Laser Technol.* **2009,** *41* (8), 956–967.
85. Reisgen, U.; Schleser, M.; Mokrov, O.; Ahmed, E. Optimization of Laser Welding of DP/TRIP Steel Sheets Using Statistical Approach. *Opt. Laser Technol.* **2012,** *44* (1), 255–262.
86. Gunaraj, V.; Murugan, N. Application of Response Surface Methodology for Predicting Weld Bead Quality in Submerged Arc Welding of Pipes. *J. Mater. Process. Technol.* **1999,** *88* (1), 266–275.
87. Dongxia, Y.; Xiaoyan, L.; Dingyong, H.; Zuoren, N.; Hui, H. Optimization of Weld Bead Geometry in Laser Welding with Filler Wire Process Using Taguchi's Approach. *Opt. Laser Technol.* **2012,** *44* (7), 2020–2025.
88. Xiansheng, N.; Zhenggan, Z.; Xiongwei, W.; Luming, L. The Use of Taguchi Method to Optimize the Laser Welding of Sealing Neuro-stimulator. *Opt. Lasers Eng.* **2011,** *49* (3), 297–304.
89. Anawa, E. M.; Olabi, A. G. Using Taguchi Method to Optimize Welding Pool of Dissimilar Laser-welded Components. *Opt. Laser Technol.* **2008,** *40* (2), 379–388.
90. Juang, S. C.; Tarng, Y. S. Process Parameters Selection for Optimizing the Weld Pool Geometry in the Tungsten Inert Gas Welding of Stainless Steel. *J. Mater. Process. Technol.* **2002,** *122,* 33–37.
91. Lee, H. K.; Han, H. S.; Son, K. J.; Hong, S. B. Optimization of Nd-YAG Laser Welding Parameters for Sealing Small Titanium Tube Ends. *J. Mater. Sci. Eng.* **2006,** *A415,* 149–155.
92. Pan, L. K.; Wang, C. C.; Hsiso, Y. C.; Ho, K. C. Optimization of Nd-YAG Laser Welding onto Magnesium Alloy via Taguchi Analysis. *J. Opt. Laser Technol.* **2004,** *37,* 33–42.
93. Anawa, E. M.; Olabi, A. G.; Hashmi, M. S. J. Optimization of Ferritic/Austenitic Laser Welded Components. In *Presented at AMPT2006 International Conference July 30–August 3, 2006, Las Vegas, NV, USA;* 2006.
94. Anawa, E. M.; Olabi, A. G. Effect of Laser Welding Conditions on Toughness of Dissimilar Welded Components. *J. Appl. Mech. Mater.* **2006,** *5* (6), 375–380.
95. Tarng, Y. S.; Juang, S. C.; Chang, C. H. The Use of Grey-based Taguchi Methods to Determine Submerged Arc Welding Process Parameters in Hardfacing.". *J. Mater. Process. Technol.* **2002,** *128* (1), 1–6.

www.iran-mavad.com
مرجع مهندسی مواد و متالورژی

6.07 Welding Defects and Implications on Welded Assemblies

F Yusof and MF Jamaluddin, University of Malaya, Kuala Lumpur, Malaysia

© 2014 Elsevier Ltd. All rights reserved.

6.07.1	**Introduction**	125
6.07.2	**Types of Welding Defects**	125
6.07.2.1	Undercuts	126
6.07.2.2	Lack of Fusion	127
6.07.2.3	Porosity	127
6.07.2.4	Cracks in Weld Metal	128
6.07.2.4.1	Cold Cracking	128
6.07.2.4.2	Hot Cracking	128
6.07.2.4.3	Lamellar Cracking	129
6.07.2.5	Inclusions	129
6.07.2.5.1	Oxide Inclusions	130
6.07.2.5.2	Slag Inclusions	130
6.07.2.5.3	Tungsten Inclusions	130
6.07.2.6	Others	130
6.07.2.6.1	Spatter	130
6.07.3	**Welding Defects in Several Industries and Applications**	130
6.07.3.1	Automotive	130
6.07.3.2	Aeronautics and Aerospace	131
6.07.3.3	Underwater Welding	131
6.07.3.4	Engineering Structures	132
6.07.3.5	Electronics, Medical Devices, and Precision Instruments	132
6.07.3.6	Railways	132
6.07.4	**Concluding Remarks**	133
References		133

6.07.1 Introduction

Welding defects can be defined as weld surface irregularities, discontinuities, imperfections, or inconsistencies that occur in welded parts. Defects in weld joints could result in the rejection of parts and assemblies, costly repairs, significant reduction of performance under working conditions and, in extreme cases, catastrophic failures with loss of property and life.

These defects originate from various sources. In most cases, the defects occur as a result of improper weld design and unsuitable welding processes and choice of incompatible materials. In addition, a lack of knowledge of the process, poor workmanship, and inadequate training of the welder can also contribute to these defects. Furthermore, there are always certain flaws in the welding due to the inherent weakness in welding technology and the characteristics of metals (*1*).

Critical welding quality assessment can control the welding defects to within acceptable levels. Nondestructive evaluation or nondestructive testing (NDT) methods can be used to indirectly quantify the weld quality without destroying the material or component. It is important to evaluate the weld quality, as welded joints are often the locations of crack initiation due to inherent metallurgical geometrical defects, as well as heterogeneity in mechanical properties and the presence of residual stresses. Various NDT methods have been developed, each having advantages and limitations in terms of applications, detectable defects, required skills, and costs. A combination of different NDT tests can be used to provide assurance that the component is fit for use.

In practice, it is practically impossible to obtain a perfect weld and, in most circumstances, it is not necessary to provide the adequate service functions required. Thus, for many industries, the specifications and tolerances for welds have been established to determine what is acceptable and fit for service. These are specified as codes or standards, and permit a variety of flaw types, sizes, and frequencies. Since some codes are more strict than others, the same weld might be acceptable under one code but not under another code.

This chapter will describe the welding defects, their causes, and detection methods. Examples of common types of defects in various industries will also be presented.

6.07.2 Types of Welding Defects

Welding defects can be classified into two main categories, namely, process related, and materials/metallurgical related. These defects mainly occur at weld metal (WM), heat affected zone (HAZ), and base metal (BM). **Figure 1** shows the common location of the defects.

www.iran-mavad.com
مرجع مهندسی مواد و متالورژی

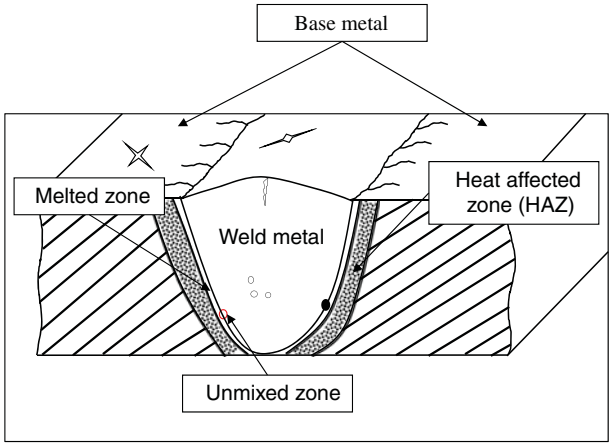

Figure 1 Common location of the welding defects.

6.07.2.1 Undercuts

Undercuts in welded parts usually occur adjacent to the weld toe of the BM. Figure 2 illustrates a schematic of undercut defects on a T-joint and a butt joint. An incomplete welded groove is formed since the melt flow does not completely fill the welded area. The melt flow characteristics during welding will depend on material interactions, temperature-dependent viscosity, and surface tension of the melt (2).

In fusion welding processes such as shielded metal arc welding (SMAW), undercuts are formed due to high welding current, excessive arc length welding, unsuitable stick electrodes, and overheated BM. Other than welding parameters, the surface condition of the BM could also influence the formation of undercuts. In laser hybrid arc welding of 10-mm-high strength steel, two kinds of undercuts were observed due to differences in surface conditions. The BM with removed surface oxides, exhibited a slight undercut curve close to the top surface whereas the metal base with surface oxides, the undercut formed at a lower level with sharp angle (2).

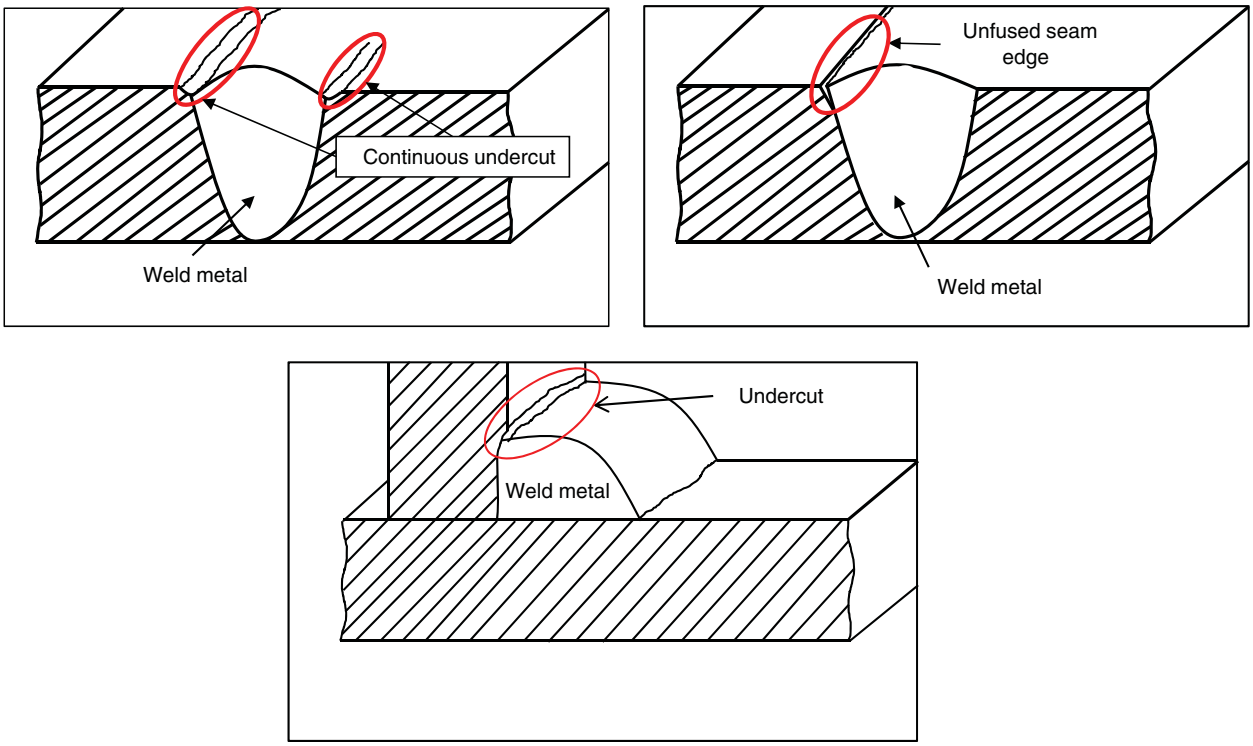

Figure 2 Typical undercuts occur in weld metals.

www.iran-mavad.com
مرجع مهندسی مواد و متالورژی

Undercuts can be classified as geometrical welding defects, and radiography is usually employed to observe the severity of the welding defects.

6.07.2.2 Lack of Fusion

Lack of fusion (LOF) is described as incomplete attachment or penetration between the WM and the BM. This defect occurs when the WM does not fully melt to form a cohesive bond with the BM. There are three types of LOFs found in metallurgical examinations:

1. Pure LOFs are formed when the weld metal does not fully melt during welding and adheres to the BM.
2. Open LOF occurs when internal stresses due to weld solidifications induce the separation of faces in the internal weldment. A narrow gap will form between weldment faces and is difficult to distinguish from a crack.
3. LOF comprised of inclusions occurs when the inclusions are uniformly distributed across the entire surface of the LOF defect. Spherical shapes of defects are formed in the weldments.

In arc welding (SMAW, metal active gas (MAG), and flux core arc welding (FCAW)), LOF can occur under low welding current conditions, rapid or slow welding speed, arc blow effects, uncontrollable weld pool movement, and improper fixture (*3–5*). **Figure 3** shows the influence of welding parameters on the effect of LOF. LOF is considered to be a very dangerous weld defect in a welded structure because of the notch effect, a crack may further propagate under the smallest load applied.

Lack of penetration (LOP) occurs when the WM has not completely penetrated to the bottom of the weld joint. Failure of the joint can initiate either at the weld toe or at the LOP region depending on the severity of the LOP. The LOP may be caused by low welding current, excessive travel speed, improper electrode application, or the presence of surface contaminants that prevent full melting of the BM (*6–8*).

Possible techniques used to observe these kinds of defects are radiography, ultrasonic particle inspection, and magnetic particle inspection. However, radiography is unable to detect small discontinuity areas. While for magnetic particle inspection, radiography is only applicable for thin sheet samples.

6.07.2.3 Porosity

Porosity or voids in weld metal is a cavity-type discontinuity that can form when gas is entrapped inside the molten metal. In general, the pores are formed from the evaporation of low boiling point elements, hydrogen rejection from solid phase during solidification, shielding gas entrapment in high density welding, decrease in solubility of dissolved elements in the molten pool during cooling and solidification, imperfect keyhole phenomenon, and turbulent weld pool flow (*9–12*). **Table 1** gives a summary of the causes of porosity formation in welding processes. The appearance, distribution, and quantity of pores will depend on factors such as weld parameters, weld solidification, cooling rate, convective weld molten flow, and shielding gas mixture. **Figure 4** illustrates the pores in the weld metal.

Visual inspection can be effective if the pores lie in the weldment surface. For porosity that forms in subsurface weldment, ultrasonic and eddy current methods are able to detect the porosity. However, ultrasonic inspection is not regularly used for porosity detection except for thick sections or inaccessible areas where radiography is unable to observe defects.

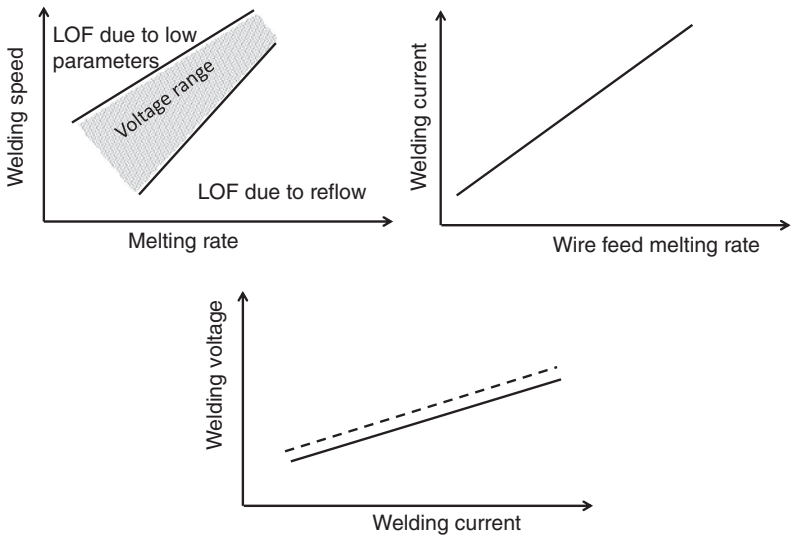

Figure 3 Influence of welding parameters on the effect of lack of fusion (LOF).

www.iran-mavad.com
مرجع مهندسی مواد و متالورژی

Table 1 Summary of the causes of porosity formation in welding processes

No.	*Welding type*	*Common causes*	*References*
1.	Gas metal arc welding (GMAW)	• Low travel speed • Low wire speed • Shielding gas mixture • Too little shielding gas • Improper welding parameter (high welding ampere, arc length too long, or excessive welding voltage) • Contamination on BM surface	(*13–16*)
2.	Laser beam welding (LBW)	• Collapse of the keyhole • High heat input • Low travel speed	(*17–20*)
3.	Flux core arc welding (FCAW)	• Shielding gas combination (oxygen and nitrogen)	(*21*)
4.	Plasma arc weld (PAW)	• Low welding current and speed • Low plasma flow rate gas	(*22*)
5.	Gas tungsten arc welding (GTAW)	• Too high heat input • Diffusion of hydrogen in the weld metal during welding	(*15,23,24*)
6.	Electron beam welding (EBW)	• Improper weld geometry • Diffusion of hydrogen in the weld metal during welding • Surface contaminations • Keyhole stabilization	(*25,26*)

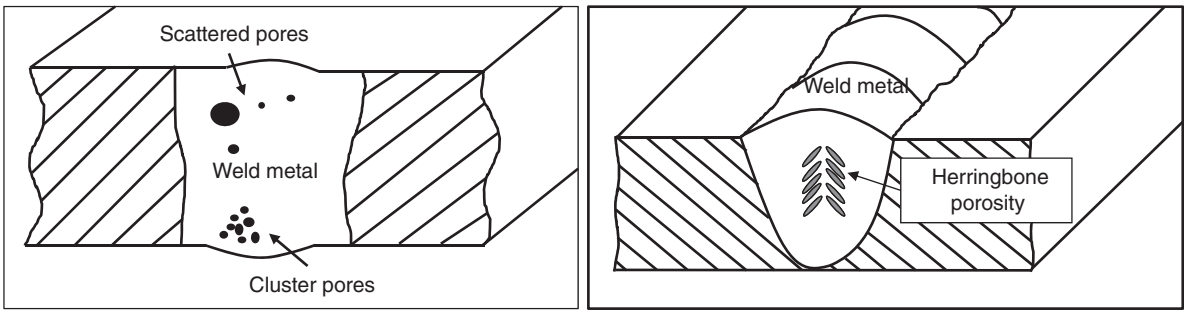

Figure 4 Several types of porosity formed in the weld metals.

6.07.2.4 Cracks in Weld Metal

A crack in welding is a severe welding defect, especially when subjected to fatigue loading conditions. Some of the common types of cracks that can occur are cold cracking, hot cracking, centerline cracking, transverse cracking, and longitudinal cracking. These types of cracks are further elaborated upon in the following section.

6.07.2.4.1 Cold Cracking

Cold cracking is formed after solidification in the WM at a temperature of approximately below 200 °C and is usually induced by hydrogen dissolution. **Figure 5** illustrates the location of cold cracking in welding. The phenomenon of cold cracking in welding usually occurs when the thermal cycle causes nonuniform heating and cooling in the material, thus inducing a harder HAZ, residual stress, and cold cracking susceptibility in the WM and BM especially for ferrous materials (*27–30*).

To alleviate these problems, heat treatment before welding (preheating) and after welding postweld heat treatment (PWHT) can be utilized. The suitable preheating temperature can be determined using the equation (*31*):

$$T_{\mathrm{wm}}(^{\circ}\mathrm{C}) = A\,R_{\mathrm{m}} + B\log(HD) + C\,h_w + D \qquad [1]$$

where R_{m} is the tensile strength of WM in MPa, HD is the hydrogen diffusion in milliliter per hundred grams, h_w is WM height in mm, and A, B, C, and D are constants.

Parameters for PWHT will be based on the specific alloys and filler metals used in the welding.

6.07.2.4.2 Hot Cracking

Hot cracking is a defect which forms during solidification and liquation of the WMs. The solidification cracks appear mostly in the WM, while liquation cracks occur in the HAZ. Many researchers have studied the solidification crack formation and the details of the

www.iran-mavad.com
مرجع مهندسی مواد و متالورژی

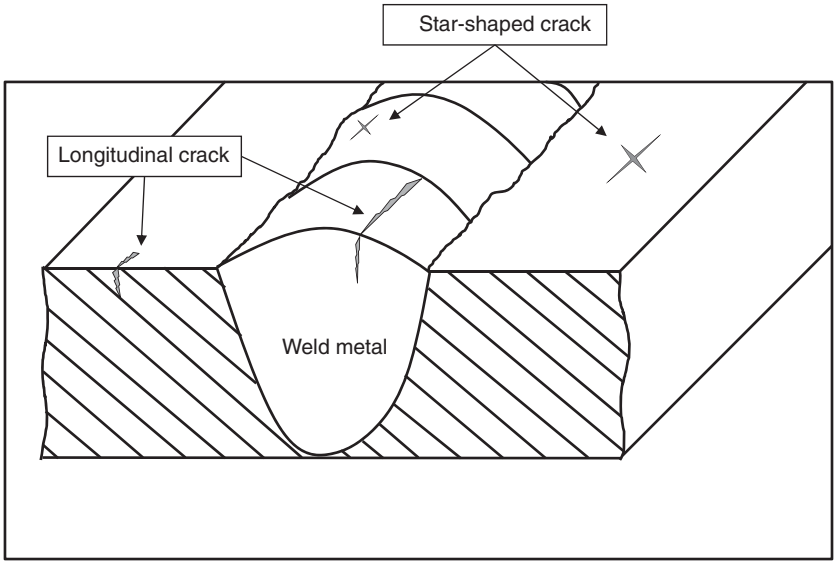

Figure 5 Typical cold cracking that occur in the weldments.

mechanisms can be found elsewhere (*32–35*). The formation of solidification cracks originates when microfissures form in the welding due to shrinkage, and propagate as microcracks as the weld cools down.

Liquation, or grain boundary melting, when accompanied by sufficient thermal stress, can initiate crack formation along the HAZ grain boundaries and propagates into the fusion zone. In some specific special alloys such as aluminum–magnesium–silicon, the occurrence of hot cracking is more severe due to high dissolution of hydrogen.

6.07.2.4.3 Lamellar Cracking

Lamellar cracking is a cleavage in the form of steplike or subsurface terraces in the BM with a basic orientation parallel to the BM surface. The main causes of these defects are inadequate BM ductility in terms of thicknesses, high sulfur content in the BM, the presence of high hydrogen content during welding, inclusion existence in the BM, and high-tension stress with regard to the thickness of BMs. An example of lamellar cracking is shown in **Figure 6**.

The most effective way to inspect the crack in weldment is using ultrasonic inspection. The ultrasonic technique is able to detect most of the cracks in the WMs such as transverse cracks, longitudinal cracks, craters, and hot cracks. Other techniques such as radiography can also be used to inspect the cracks in weldment. But the composition differences in WMs and BMs can create shadows which hide the true cracks in the weldment. Liquid penetration is usually for cracks that are interconnected up to the weld surface.

6.07.2.5 Inclusions

The entrapment of solid particles, created from extraneous materials during the welding process, can also give rise to welding defects. The source of solid particles may be from surface oxides, sulfide, tungsten electrodes, and slag. Oxides and slag inclusions

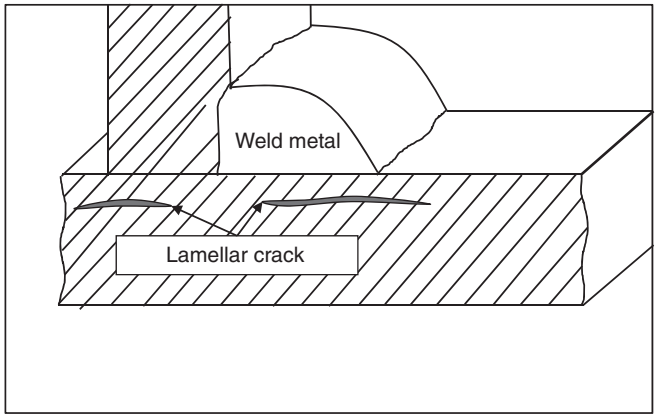

Figure 6 Lamellar cracking.

www.iran-mavad.com
مرجع مهندسی مواد و متالورژی

can be found at the surface near the weld root, inside the WM, between weld bead for multiple passes welding, and side of the weld root.

6.07.2.5.1 Oxide Inclusions

Oxide inclusion during the welding process is mainly attributed to the strong affinity of the WMs toward oxygen. Surface oxides are formed in three stages: (1) oxygen chemisorption, (2) formation of the oxide layer, and (3) thickening of the oxide (9). For example, in laser beam welding (LBW) process, the keyhole formation is unstable and the position may change over time. This phenomenon will lead to the entrapment of air or shielding gas and vaporization of metals in the weld pool. The interaction between the metal at the interface and the molten metal at the weld pool, as well as the vaporized metal/shielding gas will form oxidized layers due to entrapment of air and gas shielding. The brittle oxides layer can be of two types: (1) particles and (2) films. The welded joint quality is not as compromised if the oxides are in particle forms. However, in the case of welding magnesium alloy using LBW, the folded film-type oxides will greatly affect the performance of the welded joint (9). These folded film oxides, in the form of cracklike discontinuities, would promote crack formations since they will act as incipient cracks and as the nucleation starts points for new cracks (9).

6.07.2.5.2 Slag Inclusions

Welding processes with the presence of slag would be susceptible to slag inclusion defects. During welding, the slag may spill ahead of the arc and, as a result, gets covered by incoming weld pool due to unfit joint configuration, poor joint design, incorrect electrode manipulation, or the movement of arc blow. In multiple pass welding, the complete removal of slag from the previous pass is very important, and incomplete slag removal will generate slag entrapments anywhere along the welding direction.

6.07.2.5.3 Tungsten Inclusions

The nonconsumable tungsten electrode in gas tungsten arc welding (GTAW) is the main factor for tungsten particle entrapments. Excessive current, electrodes which are too long, physical contact between the tips of electrodes and hot tips of the electrodes, lack of shielding gas, and the improper shielding gas combinations are the factors that intensify tungsten inclusion.

Magnetic particle inspection, ultrasonic inspection, and radiography inspection are suitable methods for detecting the inclusions. The most reliable method is ultrasonic inspection, and it can be used for any kind of material. Radiography inspection also can be used for any type of material but cost is more expensive as compared to other methods. However, the types of inspection methods will be based on the size, shape, orientation, and location of slag inclusions.

6.07.2.6 Others

6.07.2.6.1 Spatter

Spatter can be found easily in metal inert gas (MIG), MAG, and manual metal arc welding (MMAW) as compared to other welding processes. Spatter is not considered a serious defect if it does not exceed the quality standard. There are three quantity levels (B, C, and D) to evaluate spatter acceptance, as determined by ISO 5817. Spatter is a typical surface imperfection, and it has minimal detrimental effect on mechanical strength. The general causes of spatter in MIG/MAG and MMAW processes are as follows:

1. too long of an arc,
2. unsuitable filler materials,
3. improper shielding gas combination with regard to BMs and filler metals, and
4. contaminations of filler metals.

6.07.3 Welding Defects in Several Industries and Applications

Almost every manufacturing industry uses some type of welding process during manufacturing or in the repair and maintenance of process equipment. The following section describes some welding defects commonly found in several industries and applications.

6.07.3.1 Automotive

A lap joint is the most common type of joint in automotive assembly applications (36). Resistance spot welding is extensively used for lap joining of car body assemblies (36,37), which may contain around 4500 spot welds (38). Common weld defects in spot welding are stick weld, missing or open weld points, burned through weld points, and too small of a weld spot (39).

Observable defects in this process include metal expulsions during the welding cycle (40). Expulsion is the eruption of molten metal particles, visible as hot sparks thrown into the air, which are ejected from the welding area during the welding process. The metal expulsion decreases the cross section of the joint, weakens the weld (41), and may contain discontinuities which can spread with vibration and lead to weld failure (40). However, spot welding without expulsion seldom occurs in production, and some studies have indicated that although increased indentation may occur during expulsion, the welds are not necessarily of reduced strength (42). In addition, the expulsed molten particles may adhere and solidify on the BM as

www.iran-mavad.com
مرجع مهندسی مواد و متالورژی

weld spatter. It is only considered a significant defect if it interferes with the part serviceability or subsequent operations, such as painting. Weld spatter can be carefully removed by blasting or mechanical grinding. Nevertheless, spatter is an important factor in most welding processes because of the cost of subsequent removal and the potential to cause in-service defects such as pit corrosion and microcracks (43).

Galvanized or zinc-coated steel sheets are used abundantly in the fabrication of automobile frames. Predominantly dip-coated steels are used, which may sometimes have an uneven coating thickness. This affects the resistance factor from weld to weld; thus, it is quite difficult to maintain the integrity of the galvanized coating when performing resistance spot welding (41). Welding a lap joint configuration would involve two layers of zinc coatings in between two steel sheets. Zinc vaporizes at 907 °C, whereas the melting point of steel is in the range of 1425–1540 °C. The different boiling points and melting points causes zinc vaporization, resulting in porosity in the weld and a general weakening of the expected shear strength. In a study by Marya and Gayden (44) on dual phase steel, it was found that the effect of zinc was most prominent in welds that were made abnormally quickly and resulted in solidification cracking. Furthermore, voids could be controlled by process parameters such as high welding forces and reduced sheet thickness.

Laser welding is used increasingly in the fabrication of various automotive body parts. The technique offers high scanning speed, high strength, and low distortion of joints, and flexible implementation of the system in the production line (36). The common defects of laser welding at high power include heavy spatter ejection (45), intrinsic pore formation (38), holes, drop outs, and LOP (46).

Laser welding is also used in the fabrication of tailor welded blanks (TWBs) (47), made up of two more sheets of metals welded together in a single plane prior to forming. The sheets can be identical, or have different thicknesses, mechanical properties, or surface coatings (48). TWBs are used in automobile manufacturing to produce body, frame, and closure panels (49). There are several challenges in the laser welding of zinc-coated steel sheets. Due to the high energy density of the laser, both zinc and steel in the weld pool would begin to vaporize and get trapped in between the sheets. A degassing process would occur if the vapor pressure exceeds the pressure of the weld pool (50). This would result in cavities in the weld seam when the liquid steel is spattered out of the welding zone. Improper degassing of the vapor would also cause porosities in the weld. Schmidt et al. (50) suggest that the zinc vapor is also generated beside the weld pool and, because it does not have a direct dissipation path, creates degassing channels as it expands toward the liquid weld pool.

6.07.3.2 Aeronautics and Aerospace

Welding in the aeronautical industry is characterized by low unit production, high unit cost, extreme reliability, and severe operating conditions (51). Welding for aerospace materials used in flight hardware includes, but is not limited to arc welding, solid state welding, resistance welding, and high energy density welding (52). Most aerospace-welded assemblies are made of aluminum, and a few are made of titanium alloy and stainless steel.

GTAW is used in aerospace since it is suitable for welding aluminum alloys. Among the major challenges is the high hydrogen solubility in liquid aluminum leading to gas entrapment and porosity in the solidified weld (53,54). Furthermore, the high coefficient of thermal expansion and volume shrinkage during solidification results in severely distorted weld joint or cracks during solidification (55).

Laser welding is another process being considered for welding airframe structures, although the process is generally perceived to be difficult because of the initial high surface reflectivity and high thermal conductivity of aluminum (56) Porosities can be formed due to high solubility of hydrogen in aluminum, collapse of unstable keyholes, and entrapment of gases by surface turbulence (57). Titanium alloys, such as Ti–6Al–4V, have been successfully joined using laser welding (58). Defects detected include porosities caused by accumulated gases in the weld material and the formation of craters at the surface of the material when the peak power of the laser is increased too much (58). Welding has also been used in the repair of titanium gas turbine engine fan blades. Although internal porosity distribution is present, it is well within the inspection limits developed for the repair procedure (59).

EBW of Inconel 718 is performed in a vacuum in most aerospace applications, requiring a near-zero joint gap to ensure fusion of the parts. The most prominent potential defects are improper seam tracking and microfissuring. Full penetration welds may result in excessive spatter (54).

Friction stir welding (FSW) is a solid-state welding technique first incorporated to join structural components of the Eclipse 500, a six-person, twin-engine jet (51). Although FSW has a low incidence of defects as compared to conventional arc welding, the process does have its own characteristic flaws. Voids may be formed when insufficient weld pressure and high travel speed, coupled with slow tool rotation speed, are used. Joint line remnants in the form of root flaw may be caused by inadequate tool plunge depth or poor tool-to-joint alignment (55).

6.07.3.3 Underwater Welding

Underwater welding is used in the repair of offshore structures and pipelines, ships, submarines, and nuclear reactors. Current techniques that are generally used are wet underwater welding and hyperbaric welding.

The most commonly used wet welding technique is SMAW and FCAW including self-shielded FCAW (60). Welds produced underwater are subjected to increased cooling rates, and a higher current may be needed to compensate for the

www.iran-mavad.com
مرجع مهندسی مواد و متالورژی

quenching effect (61), which may cause undercutting. The process itself breaks down water into its component elements, thus producing high levels of hydrogen and oxygen – both of which are detrimental to the mechanical properties of the weld. Underwater wet welds are known to contain high amounts of porosity, formed by molecular hydrogen, carbon monoxide, or water vapor (60). The resultant welds may exhibit unacceptable weld defects, lack ductility, and will likely suffer from hydrogen embrittlement, where the hydrogen penetrates into the weld pool. These cracks could, potentially, propagate into the parent metal thus causing more severe damage than the repair was intended to resolve. In multipass welds, there may be LOF between passes because of the problem of trying to maintain interpass temperature (61). Furthermore, visibility conditions for achieving wet welds is generally poor, thus relying much on the coordination skills of the welder.

In hyperbaric welding, it has been found that with increasing depth and pressure, the cooling rate becomes high and WM cracking tendency increases substantially. Increased pressure makes welding arc unstable, and the presence of diffusible hydrogen and brittle microstructure in the welds can be the reasons for crack formation (60).

6.07.3.4 Engineering Structures

Modern structures are typically built from steel or concrete or a combination of both. Engineering and structural welding are usually subjected to high stress levels thus requiring proper size, length, and penetration of weld, which should completely meet design requirements. For many types of structures, the appearance of a weld is not critical except for exposed aesthetic requirements. The material weldability, nature of failure that prompted the repair, and involvement of any code requirements should be considered before attempting a welding repair (62).

The majority of construction materials used today are mild, or low-carbon steel, which are readily weldable. Defects can arise from use of electrodes, which were not suitably protected and kept dry in an electrode storage oven. Moisture absorbed by the electrodes would be released as hydrogen gas during the welding process and get entrapped in the solidifying WM. This may result in immediate or delayed cracking. Medium and high carbon steel (over 0.25% C) requires proper preheat, interpass temperature, and PWHT to ensure fusion of the WM and the BM, to prevent distortion and to ensure dimensional stability. Uncontrolled cooling would also result in fusion line cracking.

6.07.3.5 Electronics, Medical Devices, and Precision Instruments

There is a lack of weldability information for some metal alloys often used for medical devices including titanium, Nitinol, MP35N, MP35N, platinum, 316 stainless steel, Kovar, and nickel. Furthermore, very limited studies have been conducted on the weldability of these material combinations, where the presence of intermetallics can result in brittle joints.

Small-scale resistance spot welding (SSRSW) is commonly used for medical devices and electronic components, because the welded parts are thinner and smaller compared to common resistance spot welding applications (63). Fukumoto and co-authors reported that SSRSW exhibits a fast cooling rate, as well as fast heating rate, and may cause porosity in the joint (64).

Nitinol alloys, used in the fabrication of vascular stents, guidewires, and orthodontic arc wires can be joined using microresistance spot welding in cross-wired configuration (65). Undesired weld defects in the form of large amounts of expulsion and excessive flashes were detected for increased welding currents, which cause subsequent separation of the joined wires (66).

Laser microwelding has been successfully used as a noncontact microjoining tool in the electric and electronics industry where miniaturization, high strength, and high heat resistance are constantly required (67). In the laser microwelding of thin copper circuits and thick brass electrodes, alloyed zinc in the brass would easily evaporate, forming porosity in the weld, which can be controlled by using a pulse waveform of heat input (67).

Laser microwelding has also been used to weld aluminum-based metal matrix composites (MMCs) in the fabrication of passive heat sinks. An Al–Gr composite heat sink was welded using Nd:YAG, with the laser power kept between 30 W and 40 W to avoid severe ejection of material, blowholes, and porosities. The required laser power to generate the molten zone is relatively smaller than the welding of pure aluminium (68).

Ultrathin geometries of precision parts were successfully welded using laser microwelding, resulting in clean weld with no spatter or plasma plume. Diode lasers are more suitably used for welding ultrathin sheets than Nd:YAG lasers. However, intermittent weld beads can form by condensation of the molten metal due to surface tension. Gaps in laser welding of a microbutt joint will lead to welding defects such as shallow penetrations with underfilling or nonbonded joints (69,70).

6.07.3.6 Railways

The welding of railway tracks involves a number of technological differences as compared to conventional welding processes (71). Flash butt welding (FBW) and aluminothermic welding (ATW) are commonly used in the welding of rail tracks. Rail steels contain relatively large amounts of alloying elements, particularly carbon (72). Due to the higher level of carbon, there is a tendency to form weld cracking and brittle zones in the weld area. Fractures originate more frequently from ATW than from FBW, and they generally arise from porosity, LOF, or hot tears within the WM.

www.iran-mavad.com
مرجع مهندسی مواد و متالورژی

6.07.4 Concluding Remarks

Obtaining the 'perfect' weld is extremely rare and, in most cases, unnecessary for all but the most critical applications. To make an informed decision on the proper selection of the welding process requires a full understanding of the welding requirements whether the needs fall within critical, semicritical, or noncritical applications, and the process limitations and resources required. It can be seen that porosities are present in almost all welding processes. Although the effect may be minor, uncontrolled porosity formations may lead to other serious defects during operation. Other general types of defects were also presented to show their nature and implications on the weld operations and output. Common welding problems in some industry and applications are highlighted for the benefit of practitioners in various industries.

References

1. Sargunar, P. N. J.; Sukanesh, R. Automatic Detection of Weld Defects in Pressure Vessels Using Fuzzy Neural Network. *Int. J. Comp. Appl.* **2010,** *1* (12), 111–116.
2. Karlsson, J.; Norman, P.; Kaplan, A.. F. H.; Rubin, P.; Lamas, J.; Yañez, A. Observation of the Mechanisms Causing Two Kinds of Undercut during Laser Hybrid Arc Welding. *Appl. Surf. Sci.* **2011,** *257,* 7501–7506.
3. Tušek, J.; Bajcer, B.; Taljat, B.; Hrzenjak, M. Analysis of Lack of Fusion in Welds at Water Heater. *Metalurgija* **2007,** *46* (2), 111–116.
4. Padmanaban, G.; Balasubramanian, V. Optimization of Pulsed Current Gas Tungsten Arc Welding Process Parameters to Attain Maximum Tensile Strength in AZ31B Magnesium Alloy. *Trans. Nonferrous Met. Soc. China* **2011,** *21* (3), 467–476.
5. Mourad, A.-H. I.; Khourshid, A.; Sharef, T. Gas Tungsten Arc and Laser Beam Welding Processes Effects on Duplex Stainless Steel 2205 Properties. *Mater. Sci. Eng. A* **2012,** *549,* 105–113.
6. Karadeniz, E.; Ozsarac, U.; Yildiz, C. The Effect of Process Parameters on Penetration in Gas Metal Arc Welding Processes. *Mater. Des.* **2007,** *28* (2), 649–656.
7. Nowacki, J.; Rybicki, P. The Influence of Welding Heat Input on Submerged Arc Welded Duplex Steel Joints Imperfections. *J. Mater. Process. Technol.* **2005,** *164–165,* 1082–1088.
8. Li, R.; Li, Z.; Zhu, Y.; Rong, L. A Comparative Study of Laser Beam Welding and Laser–MIG Hybrid Welding of Ti–Al–Zr–Fe Titanium Alloy. *Mater. Sci. Eng. A* **2011,** *528* (3), 1138–1142.
9. Cao, X.; Jahazi, M.; Immarigeon, J. P.; Wallace, W. A Review of Laser Welding Techniques for Magnesium Alloys. *J. Mater. Process. Technol.* **2006,** *171* (2), 188–204.
10. Zhao, H.; DebRoy, T. Pore Formation during Laser Welding of Die-Cast Magnesium Alloy AM60B – Mechanism and Remedy. *Weld. J.* **2001,** *80* (8), 204S–210S.
11. Fujii, H.; Nogi, K.; Aoki, Y.; Umatoshi, H. Bubble Formation in Aluminum Alloy during Electron Beam Welding. *J. Mater. Process. Technol.* **2004,** *155–156,* 1252–1255.
12. Ribic, B.; Palmer, T. A.; DebRoy, T. Problems and Issues in Laser-Arc Hybrid Welding. *Int. Mater. Rev.* **2009,** *54* (4), 223–244.
13. Wei, E.; Farson, D.; Richardson, R.; Ludewig, H. Detection of Weld Surface Porosity by Statistical Analysis of Arc Current in Gas Metal Arc Welding. *J. Manuf. Process.* **2001,** *3* (1), 50–59.
14. Mendes da Silva, C.; Scotti, A. The Influence of Double Pulse on Porosity Formation in Aluminum GMAW. *J. Mater. Process. Technol.* **2006,** *171* (3), 366–372.
15. Liu, Y.; Wang, W.; Xie, J.; Sun, S.; Wang, L.; Qian, Y.; Meng, Y.; Wei, Y. Microstructure and Mechanical Properties of Aluminum 5083 Weldments by Gas Tungsten Arc and Gas Metal Arc Welding. *Mater. Sci. Eng. A* **2012,** *549,* 7–13.
16. Dong, H.; Liao, C.; Yang, L. Microstructure and Mechanical Properties of AZ31B Magnesium Alloy Gas Metal Arc Weld. *Trans. Nonferrous Met. Soc. China* **2012,** *22* (6), 1336–1341.
17. Chakraborty, N. The Effects of Turbulence on Molten Pool Transport during Melting and Solidification Processes in Continuous Conduction Mode Laser Welding of Copper–Nickel Dissimilar Couple. *Appl. Therm. Eng.* **2009,** *29* (17–18), 3618–3631.
18. Paleocrassas, A. G.; Tu, J. F. Inherent Instability Investigation for Low Speed Laser Welding of Aluminum Using a Single-mode Fiber Laser. *J. Mater. Process. Technol.* **2010,** *210* (10), 1411–1418.
19. Katayama, S.; Kawahito, Y.; Mizutani, M. Elucidation of Laser Welding Phenomena and Factors Affecting Weld Penetration and Welding Defects. *Phys. Procedia* **2010,** *5* (B), 9–17.
20. Yusof, F.; Yukio, M.; Yoshiharu, M.; Shukor, M. H. A. Effect of Anodizing on Pulsed Nd:YAG Laser Joining of Polyethylene Terephthalate (PET) and Aluminium Alloy (A5052). *Mater. Des.* **2012,** *37,* 410–415.
21. Kannan, T.; Murugan, N. Effect of Flux Cored Arc Welding Process Parameters on Duplex Stainless Steel Clad Quality. *J. Mater. Process. Technol.* **2006,** *176* (1–3), 230–239.
22. Liu, L.; Jiang, J. Formation and Disappearance of Pores in Plasma Arc Weld Bonding Process of Magnesium Alloy. *Mater. Trans.* **2009,** *50* (7), 1649–1654.
23. Zhao, L.; Tian, Z. L.; Peng, Y. Control of Nitrogen Content and Porosity in Gas Tungsten Arc Welding of High Nitrogen Steel. *Sci. Technol. Weld. Joining* **2009,** *14* (1), 87–92.
24. Kumar, S.; Shahi, A. S. Effect of Heat Input on the Microstructure and Mechanical Properties of Gas Tungsten Arc Welded AISI 304 Stainless Steel Joints. *Mater. Des.* **2011,** *32* (6), 3617–3623.
25. Huang, J. L.; Warnken, N.; Gebelin, J.; Strangwood, M.; Reed, R. C. On the Mechanism of Porosity Formation during Welding of Titanium Alloys. *Acta Mater.* **2012,** *60* (6–7), 3215–3225.
26. Luo, Y.; Wu, W.; Wu, G.; Ye, H. Influence of Gravity State upon Bubble Flow in the Deep Penetration Molten Pool of Vacuum Electron Beam Welding. *Vacuum* **2013,** *89,* 26–34.
27. Srivastsva, B. K.; Tewari, S. P.; Prakash, J. A Review on Effect of Preheating and/or Post Weld Heat Treatment (PWHT) on Mechanical Behavior of Ferrous Metals. *Int. J. Eng. Sci. Technol.* **2010,** *2* (4), 625–631.
28. Shvachko, V. I. Cold Cracking of Structural Steel Weldments as Reversible Hydrogen Embrittlement Effect. *Int. J. Hydrogen Energy* **2000,** *25* (5), 473–480.
29. Stevenson, M. E.; Lowrie, S. L.; Bowman, R. D.; Bennett, B. A. Metallurgical Failure Analysis of Cold Cracking in a Structural Steel Weldment: Revisiting a Classic Failure Mechanism. *Prac. Fail. Anal.* **2002,** *2* (4), 55–60.
30. Pokhodnya, I. K.; Shvachko, V. I. Cold Cracks in Welded Joints of Structural Steels. *Mater. Sci.* **1996,** *32* (1), 45–55.
31. Seo, J. S.; Kim, H. J.; Ryoo, H. S. Microstructural Parameter Controlling Weld Metal Cold Cracking. *J. Achieve. Mater. Manuf. Eng.* **2008,** *27* (2), 199–202.
32. Yinan, L.; Xuesong, L.; Jiuchun, Y.; Lin, M.; Chunfeng, L. Effect of Ti on Hot Cracking and Mechanical Performance in the Gas Tungsten Arc Welds of Copper Thick Plates. *Mater. Des.* **2012,** *35,* 303–309.
33. Huang, C. J.; Cheng, C. M.; Chou, C. P.; Chen, F. H. Hot Cracking in AZ31 and AZ61 Magnesium Alloy. *J. Mater. Sci. Technol.* **2011,** *27* (7), 633–640.
34. Ankara, A.; Ari, H. B. Determination of Hot Crack Susceptibility in Various Kinds of Steels. *Mater. Des.* **1996,** *17* (5–6), 261–265.
35. Cicală, E.; Duffet, G.; Andrzejewski, H.; Grevey, D.; Ignat, S. Hot Cracking in Al–Mg–Si Alloy Laser Welding – Operating Parameters and Their Effects. *Mater. Sci. Eng. A* **2005,** *395* (1–2), 1–9.
36. Ma, J.; Kong, F.; Carlson, B.; Kovacevic, R. Mitigating Zinc Vapor Induced Weld Defects in Laser Welding of Galvanized High-strength Steel by Using Different Supplementary Means. In *Welding Processes;* Kovacevic, Radovan, Ed.; InTech, ISBN 978-953-51-0854-2; 2012. http://dx.doi.org/10.5772/53562.
37. Ouisse, M.; Cogan, S. Robust Design of Spot Welds in Automotive Structures: A Decision-Making Methodology. *Mech. Syst. Signal Process.* **2010,** *24* (4), 1172–1190.

www.iran-mavad.com
مرجع مهندسی مواد و متالورژی

38. Ribolla, A.; Damoulis, G. L.; Batalha, G. F. The Use of Nd:YAG Laser Weld for Large Scale Volume Assembly of Automotive Body in White. *J. Mater. Process. Technol.* **2005,** *164–165,* 1120–1127.
39. Zhao, X.; Zhang, Y. S.; Chen, G. L. Ultrasonic Fast Identification of Automotive Body Spot Weld Defect Based on Echo Characteristics Qualitative Analysis. *Sci. Technol. Weld. Joining* **2006,** *11* (6), 731–736.
40. Arthi, N.; Wylie, S. R.; Cullen, J. D.; Al-Shamma'a, A. I. Ultrasonic Non-Destructive Evaluation for Spot Welding in the Automotive Industry. In *Proceedings of the IEEE Sensors 2009 Conference;* Christchurch, New Zealand, 2009, October 25–28, 2009; pp 1518–1523.
41. *Handbook for Resistance Spot Welding;* Miller Electric Mfg. Co, 2012 (cited Feb 20, 2013).
42. Kimchi, M. *Spot Weld Properties When Welding with Expulsion – A Comparative Study;* Welding Research Supplement, 1984; pp 58s–63s.
43. Schwab, G.; Steele, J. P. H.; Vincent, T. L. Vision-Based Spatter Classification for Contaminant Detection. *Suppl. Weld. J.* **2009,** *88,* 121s–129s.
44. Marya, M.; Gayden, X. Q. Development of Requirements for Resistance Spot Welding Dual-phase (DP600) Steels Part 1 – the Causes of Interfacial Fracture. *Weld. J.* **2005,** *84* (11), 172s–182s.
45. Karlsson, J.; Kaplan, A. F. H. Analysis of a Fibre Laser Welding Case Study, Utilising a Matrix Flow Chart. *Appl. Surf. Sci.* **2011,** *257* (9), 4113–4122.
46. Saludes Rodil, S.; Arnanz Gómez, R.; Bernárdez, J. M.; Rodríguez, F.; Miguel, L. J.; Perán, J. R. Laser Welding Defects Detection in Automotive Industry Based on Radiation and Spectroscopical Measurements. *Int. J. Adv. Manuf. Technol.* **2009,** *49* (1), 4133–4122.
47. Ono, M.; Yoshitake, A.; Ohmura, M. Laser Weldability of High Strength Steel Sheets in Fabrication of Tailor Welded Blanks. *NKK Tech. Rev.* **2002,** *86,* 13–18.
48. Saunders, F. I.; Wagoner, R. H. The Use of Tailor-Welded Blanks in Automotive Applications. In *Simulation of Materials Processing: Theory, Methods and Applications, Numiform'95, Proceedings of the Fifth International Conference in Numerical Methods in Industrial Forming Processes, 18–21 June 1995;* Shen, Dawson, Eds.; Ithaca: New York, USA, 1995; pp 157–164.
49. Stephen, W. K.; Roger, A. K.; Marvin, B. K.; Bacher, G. D.; Bruno, P. In-Process Detection of Weld Defects Using Laser-based Ultrasound. In *Proceedings SPIE,* Wang, Anbo, Ed; **1999,** Vol. 3852.
50. Schmidt, M.; Otto, A.; Kägeler, C. Analysis of YAG Laser Lap-Welding of Zinc Coated Steel Sheets. *CIRP Ann. Manuf. Technol.* **2008,** *57* (1), 213–216.
51. Mendez, P. F.; Eager, T. W. New Trends in Welding in the Aeronautic Industry. In *New Manufacturing Trends,* Bilboa, Spain*;* 2002; pp 1–10.
52. Mulville, D. R. *General Fusion Welding Requirements for Aerospace Materials Used in Flight Hardware*; NASA Technical Standard No. NASA-STD-5006, 1999.
53. Verhaeghe, G. Low-Porosity Laser Welding of 12.7mm Thickness Aerospace Aluminium. In *Proceedings of the 10th International Conference on Joints in Aluminium (INALCO 2007);* Oct 24–26, 2007. Tokyo.
54. *Welding Practices for 2219 Aluminum and Inconel 718*; NASA Welding Practice No. PD-ED-1205, 1998. Available from: http://engineer.jpl.nasa.gov/practices/1205.pdf (cited Feb 20, 2013).
55. Leonard, A. J.; Lockyer, S. A. Flaws in Friction Stir Welds. In *Proceedings of the 4th International Symposium on Friction Stir Welding;* May 14–16, 2003. Park City, Utah, USA.
56. Verhaeghe, G.; Hllton, P. Laser Welding of Low-Porosity Aerospace Aluminium Alloy. In *Proceedings of the 34th International MATADOR Conference;* July 2004. Manchester, UK.
57. Kumar, D. H.; Somireddy, A. Laser Welding of Certain Materials: A Perspective, International Journal of Advanced Science. *Eng. Technol.* **2013,** *2* (1), 109–119.
58. Akman, E.; Demir, A.; Canel, T.; Sönmazçelik, T. Laser Welding of Ti6Al4V Titanium Alloys. *J. Mater. Process. Technol.* **2009,** *209* (8), 3705–3713.
59. Azar, P.; Ping, Li.; Patnaik, P. C.; Thamburaj, R.; Immarigeon, J.-P. Electron Beam Weld Repair and Qualification of Titanium Fan Blades for Military Gas Turbine Engines. In *RTO AVT Specialists' Meeting on Cost Effective Application of Titanium Alloys in Military Platforms, Loen, Norway;* May 7–11, 2001.
60. Łabanowski, J.; Fydrych, D.; Rogalski, G. Underwater Welding – A Review. *Adv. Mater. Sci.* **December 2008,** *8* (3), 11–22.
61. Bayliss, M.; Short, D.; Bax, M. Underwater Inspection by Plymouth Oceans Projects Ltd, 1988.
62. Sutter, V. Repair Welding. In *Weld Integrity and Performance;* Lampman, S. R., Ed.; ASM International, 1997.
63. Salem, M. Control and Power Supply for Resistance Spot Welding. Ph.D. Thesis, The University of Western Ontario, London, Ontario, Canada, 2011.
64. Fukumoto, S.; Matsuo, T.; Kuroda, D.; Yamamoto, A. Weldability of Nickel-Free Austenitic Stainless Steel Thin Sheet by Small-Scale Resistance Spot Welding. *Mater. Trans.* **2008,** *49* (12), 2844–2849.
65. Tam, B.; Khan, M. I.; Zhou, Y. Micro-Resistance Spot Welding of 55.8wt% Ni-Ti Cross Wires. In *Proceedings from the Materials and Processes for Medical Devices Conference 2009, August 10–12;* Gilbert, J., Ed.; Minnesota, USA, 2009; pp 207–209.
66. Tam, B.; Pequegnat, A.; Khan, M. I.; Zhou, Y. Resistance Microwelding of Ti-55.8 wt pct Ni Nitinol Wires and the Effects of Pseudoelasticity. *Metall. Mater. Trans. A* **2012,** *43* (8), 2969–2978.
67. Ismail, M. I. S.; Okamoto, Y.; Okada, A.; Uno, Y.; Ueoka, K. Direct Micro-Joining of Flexible Printed Circuit and Metal Electrode by Pulsed Nd:YAG Laser. *Int. J. Precis. Eng. Manuf.* **2012,** *13* (3), 321–329.
68. Ismail, M. I. S.; Okamoto, Y.; Okada, A. Micro-Welding of Super Thermal Conductive Composite by Pulsed Nd:YAG Laser. In *Nd YAG Laser;* Dumitras, Dan. C., Ed.; InTech, ISBN 978-953-51-0105-5; 2012.
69. Hiroshi, K.; Yousuke, K.; Katayama, S. In-process Monitoring and Adaptive Control for Micro Welding of Titanium. *Trans. JWRI* **2010,** *39* (2), 201–203.
70. Yousuke, K.; Masayuki, K.; Katayama, S. Adaptive Gap Control in Butt Welding with a Pulsed YAG Laser. *Trans. JWRI* **2007,** *36* (2), 5–10.
71. Jessop, T. *Institute-of-Rail-Welding-IoRW-ten-years-on,* 2012 (cited Feb 20, 2013). Available from: http://www.iorw.org/Institute-of-Rail-Welding-IoRW-ten-years-on.pdf.
72. Popovic, O.; Prokic-Cvetkovic, R. Surface Welding as a Way of Railway Maintenance. In *Mechanical Engineering;* Gokcek, Murat, Ed.; InTech, ISBN 978-953-51-0505-3; 2012.

www.iran-mavad.com
مرجع مهندسی مواد و متالورژی

6.08 9% Nickel Steels and Their Welding Behavior

Q Ahsan, Universiti Teknikal Malaysia Melaka (UTeM), Melaka, Malaysia
ASMA Haseeb, University of Malaya, Kuala Lumpur, Malaysia
NI Syahriah Binti Hussein and SY Chang, Universiti Teknikal Malaysia Melaka (UTeM), Melaka, Malaysia

© 2014 Elsevier Ltd. All rights reserved.

6.08.1	**Introduction**	135
6.08.2	**9% Nickel Steel for Cryogenic Applications**	135
6.08.2.1	Features of Ni-Alloyed Ferritic Steels	135
6.08.2.2	Metallurgy of 9%Ni Steel	136
6.08.2.3	Heat Treatment and Microstructures	136
6.08.2.3.1	Double Normalizing and Tempering – ASTM A 353	136
6.08.2.3.2	Quench and Temper – ASTM A 553	136
6.08.2.4	Mechanical Properties of 9%Ni Steel	139
6.08.2.4.1	Tensile Properties	139
6.08.2.4.2	Impact Properties	139
6.08.3	**Welding of 9% Nickel Steel**	141
6.08.3.1	Filler Metal Selection	141
6.08.3.2	Filler Metal Grades	141
6.08.3.2.1	Covered Electrodes for Shielded Metal Arc Welding	141
6.08.3.2.2	Flux-Cored Wires for Flux Core Arc Welding	141
6.08.3.2.3	Welding Wires for Gas Tungsten Arc Welding, Gas Metal Arc Welding and Submerged Arc Welding	141
6.08.3.3	Welding Procedure and Process	143
6.08.4	**Weldability of 9% Nickel Steel**	144
6.08.4.1	Factors Influencing Weldability of 9% Nickel Steel	144
6.08.4.2	Structural Decomposition at Heat Affected Zone	145
6.08.5	**Quality Control of Weldment**	146
6.08.5.1	Cracking Problems in 9% Nickel Steel Welding	146
6.08.5.2	Weldability Testing	147
6.08.5.3	Inspection of Welding	147
6.08.6	**Concluding Remarks and Future Directions**	148
References		148

6.08.1 Introduction

The 9% nickel steels were first developed by the International Nickel Company, USA, in 1942. In 1962, this steel was demonstrated to have improved notch toughness at liquid nitrogen temperature and to provide a tough welded pressure vessel at −196 °C without the need for postweld heat treatment (*1*). The addition of 9% nickel as alloying element to the steel and its further heat treatment are the primary source for the high strength and excellent fracture toughness of this steel (*2*). Later, Japanese steel companies started producing large tonnages of 9% nickel steel. Since then, developments in Ni steels allow them to very effectively sustain cryogenic temperatures. As a result, steels are mainly used in connection with storage and transporting of liquefied natural gas (LNG).

The greater issue is raised when the steel is welded, which is inevitable for storage tank construction. The weld heat-affected zone properties of a wide variety of steels have been evaluated utilizing weld simulation devices, Charpy V-notch impact testing and metallographic investigation. The fundamental mechanical properties of 9% nickel steel must conform to the requirements of ASTM 353 or ASTM 553 ASTM 353 and 533 Type I specify double-normalize-and-temper (NNT) and quench-and-temper (QT) heat treatments, respectively. These specifications require measurement of impact absorption energy at liquid nitrogen temperatures, –196 °C. However, at the LNG storage temperature of −162 °C, these steels, in the wrought condition, safely exceed the ASTM specifications.

With the world wide increase in the demand of LNG as a clean source of energy, the 9% nickel steels are going to be even more important in the construction of welded tanks and vessels. Demands for improved mechanical properties, better reliability, optimum usage of steel and lower cost are the main driving forces for the new developments. This chapter is intended to review the main aspects of the 9%Ni steels and their welding behavior in the current as well as future context.

6.08.2 9% Nickel Steel for Cryogenic Applications

6.08.2.1 Features of Ni-Alloyed Ferritic Steels

In the case of carbon and most low alloy ferritic steels, as the temperature drops below 24 °C, generally the tensile strength and hardness increase while the tensile ductility and notch toughness drastically decrease (*3*). In the case of applications at temperatures

www.iran-mavad.com
مرجع مهندسی مواد و متالورژی

below −50 °C, Ni-alloyed steels containing nickel in the range from 1.0 to 9.0% are favored. Nickel is not a carbide or nitride forming element and it remains in substitutional solid solution in the α lattice. This improves the hardenability and the notch toughness at low temperatures (4). Among the Ni-alloyed steels, 9%Ni steel has been recognized by the American Society of Mechanical Engineers (ASME) Boiler and Pressure Vessel Code for cryogenic applications since 1952 and the specification is covered by ASTM A 353 and ASTM A 553.

A large number of researches have been carried out to improve the strength and specially notch and fracture toughness in Ni-steel through improving the manufacturing process (5,6). Thanks to clean steel technology in which S and P inclusions are kept to a minimum, Al is added to refine grain size, and Mo and Mn are added to improve the strength and toughness of the Ni-steel at low temperatures (6). The chemical compositions of 9%Ni steel for cryogenic applications are listed in **Table 1**.

6.08.2.2 Metallurgy of 9%Ni Steel

The transformation of low carbon 9%Ni steel is similar to that of a Fe–Ni alloy (4). As illustrated in **Figure 1**, with the addition of nickel as an austenite stabilizing element, the ferrite–austenite transformation occurs at appreciably low temperatures. Thus, the role of nickel is to retard the high temperature transformation ferrite/pearlite products. The resultant microstructure possesses higher strength and superior notch/fracture toughness at cryogenic temperatures due to the presence of stable retained austenite (2,7–10).

The addition of nickel lowers the martensite finish temperature. Consequently, upon cooling from the austenitization temperature to room temperature, heat-treated structures usually contain a substantial amount of retained austenite or tempered austenite, which remains stable even at the liquid nitrogen temperature. Previous investigations (8,10,11) have shown that if tempering is performed in the two-phase $\gamma + \alpha$ region above the lower critical temperature, i.e., above approximately 580 °C, the high nickel content stabilizes the austenite and the final product contains 5–10 vol.% 'retained' austenite. The presence of the stable austenite indirectly improves the impact strength after conventional heat treatment by taking the carbides into solution, which prevents the formation of embrittling carbides and nitrides. Thus, the fine grained structure of nickel–ferrite in 9%Ni steel, which is devoid of embrittling carbide networks, results in excellent low-temperature notch impact properties.

6.08.2.3 Heat Treatment and Microstructures

For cryogenic applications, the 9%Ni steel is usually heat-treated either by NNT or QT to meet the requirements of the ASME Boiler and Pressure Vessel Code (12). Typical heat treatment procedures are described below.

6.08.2.3.1 Double Normalizing and Tempering – ASTM A 353

The 9% nickel steel plate is heated to a uniform temperature of 900 ± 15 °C, held at this temperature for a minimum of 2.4 min mm^{-1} of thickness; but in no case less than 15 min; cooled in air. Reheat until the plate is reheated to attain a uniform temperature of 790 ± 15 °C; held at this temperature for a minimum of 2.4 min mm^{-1} of thickness, but in no case less than 15 min; cooled in air. For tempering treatment, reheating is done to a uniform temperature within the range of 565–605 °C; held at this temperature for a minimum of 2.4 min mm^{-1} of thickness, but in no case less than 15 min; cooled in air or quenched in water at a rate not less than 165 °C h^{-1}. If hot forming is performed within the range 900–955 °C, the first normalizing treatment may be omitted (8).

The first normalizing treatment usually produces a fully homogeneous structure followed by a second normalizing treatment that gives a structure of low carbon martensite and bainite with a hardness value of 400 HV. The first normalized treatment at 900 °C produces martensite and bainite. In the second cycle of the normalizing treatment at 750 °C, fine grained austenite forms and subsequent air cooling transforms the austenite to martensite and bainite. Tempering at 565–610 °C causes reversion of metastable products to 10–15% austenite, which remains stable upon air or water cooling (1). This retained austenite contributes to high notch toughness down to liquid nitrogen temperature (9).

6.08.2.3.2 Quench and Temper – ASTM A 553

Here, the plate is heated to a uniform temperature of 800–925 °C; held at this temperature until uniform temperature is obtained throughout the plate thickness; and quenched in water. It is then reheated until the plate attains a uniform temperature of 565–605 °C; held at this temperature for a minimum of 1.2 min mm^{-1} of thickness, but in no case less than 15 min; cooled in air or quenched in water at a rate not less than 165 °C h^{-1} (13). Similar microstructure is also produced after quenching in QT process.

The phase transformation of 9%Ni steel is illustrated in **Figure 2**. Subsequent tempering in both the heat treatment processes results in strong tough Ni-rich ferrite and carbide, and reforms some retained austenite enriched with dissolved carbide. This austenite remains stable below −196 °C. Finally, the microstructure of heat-treated 9%Ni steel consists of bainite, Ni-rich ferrite, and stable carbide-rich, retained austenite. The metallurgically stable retained austenite is very important in developing the superior cryogenic toughness of the steels (5). A typical microstructure of 9%Ni steel after QT process is illustrated in **Figure 3**. The microstructure of this material largely consists of tempered martensite (TM). The TM is a mixture of ferrite and carbide which has precipitated during the tempering heat treatment of as-quenched martensite (2).

It was also reported (14) that temper embrittlement may occur if these steels are subjected to tempering at 370–540 °C for prolonged periods. An extended holding period was suggested to make austenite unstable leading to the formation of martensite during cooling with lower notch toughness (1).

www.iran-mavad.com
مرجع مهندسی مواد و متالورژی

Table 1 Compositions and properties of 9%Ni steels specified by various national codes and specifications

		Composition								*Mechanical properties*			
												KCV, J	
Country	*Code/specification*	*C*	*Si*	*Mn*	*S*	*P*	*Ni*	*Mo*	*Others*	*Yield stress, MPa*	*UTS, MPa*	*+20 °C*	*−196 °C*
USA	ASTM A553-70 Grade A	0.13 max	0.15–0.30	0.90 max	0.040 max	0.035 max	8.50–9.50	–	–	517–586	689–821	–	34
USA	ASTM A353-70	0.13 max	0.15–0.30	0.90 max	0.040 max	0.035 max	8.50–9.50	–	–	–	–	–	–
UK	BS 1501-509	0.10 max	0.10–0.30	0.30–0.80	0.030 max	0.025 max	8.75–9.75	–	–	–	–	–	–
Belgium	NBN 630-70 10Ni 36	0.10 max	0.15–0.35	1.00 max	0.030 max	0.030 max	8.50–9.50	–	–	–	–	–	–
Czechoslovakia	17 501	0.10 max	0.15–0.35	0.30–0.80	0.030 max	0.025 max	8.50–10.5	–	–	490	637–833	–	29
Czechoslovakia	Vitkovice	0.06–0.12	0.10–0.35	0.30–0.80	0.025 max	0.025 max	8.50–10.5	0.4–0.6	0.02–0.04Al	650	833	184	90
BRD	DIN 17280 17173, 17174	0.10 max	0.10–0.35	0.30–0.80	0.035 max	0.035 max	8.50–9.50	–	–	490	637–834	–	R3 41
France	NFA 36-208	0.10 max	0.15–0.30	0.80 max	0.030 max	0.030 max	8.50–9.50	–	–	–	–	–	–
Italy	UNI 5920-66 X10 Ni9	0.10 max	0.15–0.30	0.90 max	0.035 max	0.035 max	8.50–9.50	–	–	–	–	–	–
Norway	DnV (1971) NV 20-2	0.08 max	0.15–0.35	0.40–0.70	0.025 max	0.020 max	9.00 max	–	–	–	–	–	–

Reproduced from Guide to the Welding and Weldability of Cryogenic Steels, Document IIS/IIW-844-87, Sub-commission IXG of Commission IX of the International Institute of Welding, the Welding Institute, UK, 1987.

www.iran-mavad.com
مرجع مهندسی مواد و متالورژی

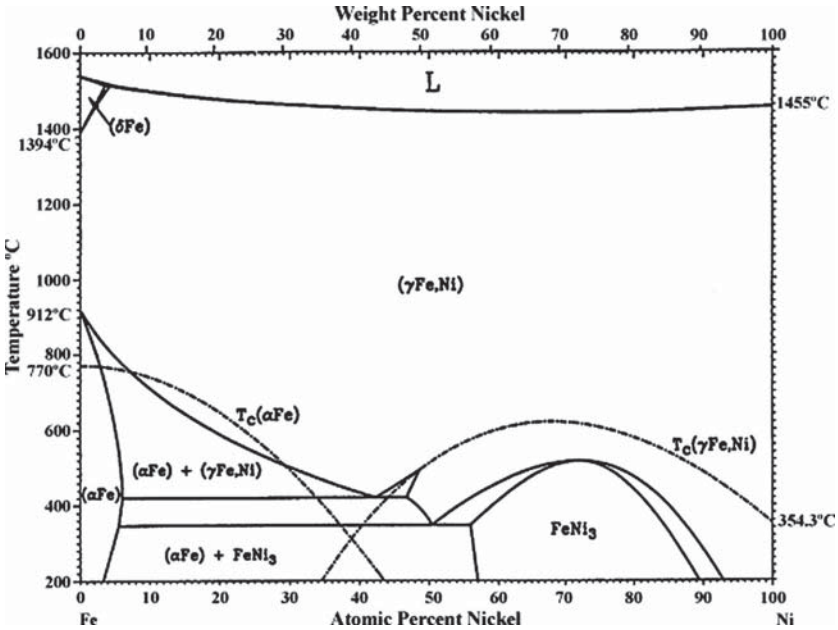

Figure 1 Fe–Ni phase diagram. Reproduced from Swartzendruber, L.J. The Fe-Ni (Iron-Nickel) System, *J. Phase Equilibria* **1991,** *12*, 288–312.

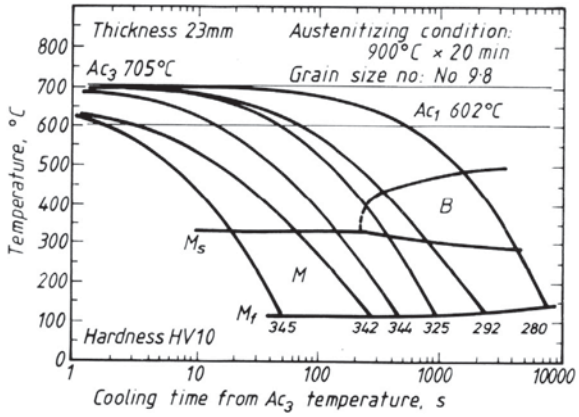

Figure 2 Austenite decomposition diagram for 9%Ni steel (0.09C–0.22Si–0.68Mn–9.02Ni–0.008P–0.009S–0.031Al). Reproduced from Guide to the Welding and Weldability of Cryogenic Steels, Document IIS/IIW-844-87, Sub-commission IXG of Commission IX of the International Institute of Welding, the Welding Institute, UK, 1987.

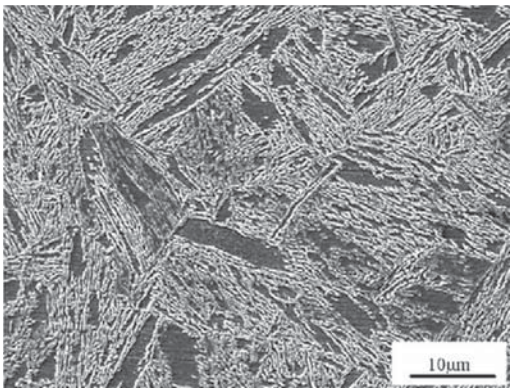

Figure 3 9%Ni steel with heat treated microstructure. Reproduced from Du, W. S.; Cao, R.; Yan, Y. J.; Tian, Z. L.; Peng, Y.; Chen, J. H. Fracture Behavior of 9% Nickel High-strength Steel at Various Temperatures Part I. Tensile Tests. *Mater. Sci. Eng. A* **2008**, *486*, 611–625.

www.iran-mavad.com
مرجع مهندسی مواد و متالورژی

6.08.2.4 Mechanical Properties of 9%Ni Steel

6.08.2.4.1 Tensile Properties

Mechanical testing of 9%Ni steel, in terms of tensile and yield stress, is usually carried out from room temperature to cryogenic service temperatures. These values along with hardness and elongations at different temperatures for different heat treated steels are shown in Table 2.

With decreasing test temperature, the yield strength, tensile strength and Brinell hardness show an increasing trend while the elongation holds the same value. It is also observed from Table 2 that the yield strength of ASTM A 553 is higher than that of ASTM A 353 at any temperature, while the tensile strength values are almost the same for both steels at any tested temperature. Du et al. observed similar tensile behavior in the 9%Ni 1000 MPa grade steel regardless of the test specimen orientation (15). The fracture morphologies at different test temperatures are distinctive and can be categorized into four types of fracture features. These fracture features result from the change of tensile fracture orientation with temperature. At cryogenic temperature, the initial tensile fracture surface, which propagated along the tensile direction at the end of necked region, bifurcates of its orientation at two ends by developing two opposite transverse cracks perpendicular to the tensile direction. These multiple orientations of the crack may cause the sharp rise in fracture stress at −196 °C. As the temperature increases, the size of the longitudinal crack length reduces. On the other hand, at room temperature, the fracture surfaces were composed of microvoid coalescence regions at the center with typical shear lips at the end so it does reduce the fractures stress.

Du et al. (15) suggested that a considerable amount of retained austenite is responsible for the ductile behavior of the steel even at low temperature. As a result, the elongation or the reduction in area does not vary considerably when the test is conducted from room temperature to −196 °C. The longitudinal crack initiated at the center of the necking region propagated along the austenite grain boundaries with a cleavage-type morphology. The crack further extended into a transverse direction through halves of the cross-section in opposite directions. Quasi-cleavage morphology was observed at the transverse crack. The crack propagation is prohibited or resisted by the austenite and bainite, which resulted in the formation of dimple strips and shear ridges with the suppression of cleavage cracks.

In order to study the resistance to sudden blow, Shin et al. (16) evaluated the impact tensile behavior of 9%Ni steel at low temperature under the dynamic tensile load with a varying strain rate range of 10^{-3} to 5×10^{2} s^{-1}. Their results showed that at a low temperature of −196 °C and a high strain rate of 250 s^{-1}, the elongation of 9%Ni steel held the same value as that of the static loading case at 20 °C. This indicates that the resistance to brittle fracture of nickel steel remains the same in the range of 20 to −196 °C. It may be noted that microvoid coalescence occurred at the center of tested samples for all temperatures.

6.08.2.4.2 Impact Properties

Toughness of 9%Ni steel is largely assessed by Charpy V-notch test. As previously mentioned, the improved toughness properties can be achieved with clean steel production technologies (5), as shown in Figure 4. The benefit of lower carbon, sulfur and phosphorous, and higher nickel levels is seen in terms of improvement in toughness.

It is not only the chemical composition that controls the toughness of the steel, heat treatment conditions also greatly determine the improved toughness of the 9%Ni steel. Generally, QT steel shows better Charpy V notch impact values as compared to NNT steel over the temperature range (3). Charpy V-notch test results of QT and NNT plates for different rolling directions at temperatures starting from room temperature to −196 °C are shown in Figure 5.

Figure 5 reveals that all steels have the lower shelf impact energy values at around −185 °C, whereas the upper shelf energy values start from −45 °C and held constant up to the ambient temperature. It is difficult to determine the ductile-to-brittle transition temperature of this material from these data because the lower energy shelf is not clearly defined and it is assumed that the lower energy shelf begins at −196 °C (2). It was also observed that at any direction, impact values of QT products were higher than that of NNT products at temperatures below −130 °C. This was attributed to the fact that (5) the yield strength to tensile strength ratio and lateral expansion increased with increasing cooling rate in the heat treatment cycle. The fracture surface of all Charpy test samples

Table 2 Mechanical properties of 9% nickel steel plates at various temperatures

		Test temperature, °C							
Properties	*Heat treatment*	*−196*	*−155*	*−130*	*−100*	*−70*	*−45*	*−20*	*20*
Yield strength[a] (offset 0.2%), MPa	NNT (ASTM A 353)	860	723	655	618	606	586	586	580
	QT (ASTM A 553)	997	881	827	796	753	732	721	711
Tensile strength[a], MPa	NNT (ASTM A 353)	1188	1071	1008	933	891	827	781	724
	QT (ASTM A 553)	1172	1080	1012	943	896	839	805	736
Elongation[a], %	NNT (ASTM A 353)	33.1	30.8	30.0	30.0	30.0	30.0	30.8	33.1
(50 mm)	QT (ASTM A 553)	33.1	31.5	30.4	29.2	27.7	27.7	27.7	27.7
Brinell hardness, HV	NNT (ASTM A 353)	358	325	300	280	263	242	233	220
	QT (ASTM A 553)	351	327	308	289	273	258	239	231

[a]Plate thickness (9.5 mm).

Reproduced from Low Temperature Properties of Nickel Alloy Steels: The International Nickel Company, Inc (INCO), Copyright@1975.

www.iran-mavad.com
مرجع مهندسی مواد و متالورژی

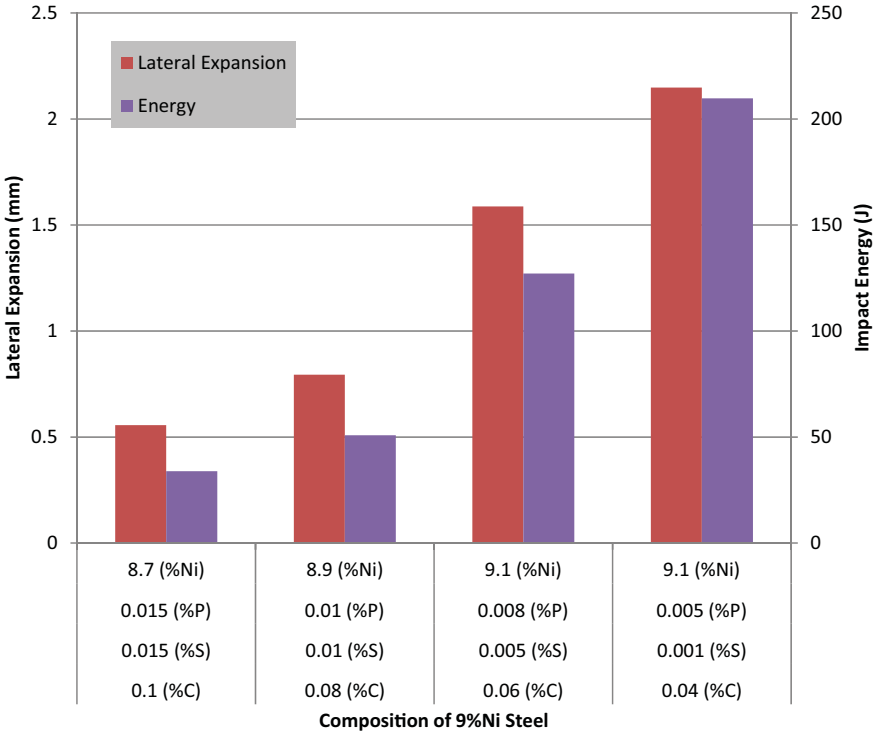

Figure 4 9%Ni steel process improvements. Data Reproduced from 9% Nickel steel: for use at cryogenic temperatures, Technical Report, ArcelorMittal USA, Dec 2010.

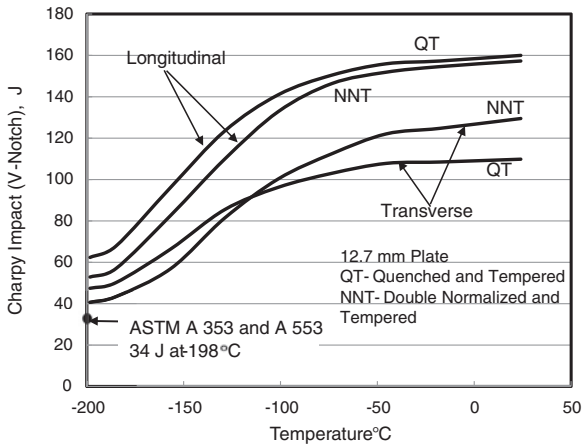

Figure 5 Effect of heat treatment and rolling direction on Charpy V-notch impact of low carbon 9%Ni steel plate. Data reproduced from Low Temperature Properties of Nickel Alloy Steels: The International Nickel Company, Inc (INCO), Copyright@1975.

were found to be 100% shear fracture even at −196 °C (*17*). Nevertheless, all impact values of both NNT and QT materials substantially exceed the supplementary requirements of ASTM A 353 and A 553 standards for Ref. (*18*).

Although the Charpy V notch test at cryogenic temperature is considered as the important quality control tool for assessing the energy absorption, the crack initiation or catastrophic crack propagation in brittle materials in terms of stress intensity factors may not properly be evaluated by the test. In order to evaluate the safety performance of the steel plate against the initiation of brittle crack and resistance to brittle crack propagation, fracture toughness testing under low strain rates of full plate thickness in the presence of a very sharp crack or notch has been developed. Based on classical linear elastic fracture mechanics, under plane strain condition stress intensity factor K_I in brittle materials is usually determined subjected to slow stressing in tension and bending of a test sample containing a sharp crack with no plastic deformation at the crack tip. In the case of more ductile materials, yielding occurs at the crack tip with stable crack propagation, which can be monitored by measuring crack tip opening displacement (CTOD) value under elastic–plastic fracture mechanic system. However, crack propagation in 9%Ni steel even at the lowest cryogenic system is such that the crack becomes blunt and is arrested. Hence, it is difficult to achieve a completely brittle failure.

www.iran-mavad.com
مرجع مهندسی مواد و متالورژی

Table 3 Fracture toughness test results of QT 9%Ni steel in 75 mm plate thickness at different temperatures

Temperature, °C	*0.2% Yield strength, MPa*	K_Q, *MPam*$^{1/2}$
24	636	105
		111
		111
−75	666	110
		108
		105
−196	858	125
		110
		117

Data reproduced from Low Temperature Properties of Nickel Alloy Steels: The International Nickel Company, Inc (INCO), Copyright@1975.

In numerous fracture toughness tests of 5–9%Ni steel plate of 20–50 mm thickness at around −196 °C, valid K_{IC} values associated with more brittle behavior were not obtained because insufficient specimen size led to conditional plane strain fracture toughness, K_Q. TRW Inc. (3) conducted fracture toughness tests of 9%Ni steel plate of 75 mm thickness at 24, −75 and −196 °C and K_Q values are shown in Table 3. In order to obtain valid K_{IC} values, the specimen thickness is required to be 110–125 mm to fulfill the plane strain condition as the toughness of the material appeared to be high based on high plastic zone size factor $(K_Q/\sigma_{ys})^2$.

Usually, 9% nickel steel exhibits the ductile type CTOD curve in which the steel has the ability to absorb high local stress around a sharp notch. Crack tip opening displacement fracture toughness tests on a plate up to 75 mm thick at −196 °C gave $CTOD_{max}$ values of 0.25–0.4 mm at the first onset of maximum load and K_{max} values of 110 MPam$^{1/2}$. Only minor differences in fracture toughness properties of QT and NNT plate up to 30 mm thickness were found.

6.08.3 Welding of 9% Nickel Steel

6.08.3.1 Filler Metal Selection

Wrought or cast structural members of cryogenic alloys of 9%Ni steel are usually joined using filler materials with compositions that are similar, but not identical, to the base material. The welding consumables that are generally used for welding 9%Ni steel are high Ni alloy such as the Inconel type (Ni–Cr alloy) and the Hastelloy type (Ni–Mo alloy). Although the strength of these high Ni alloys is lower than that of 9%Ni steel, it does not cause brittle fractures, even at cryogenic temperatures, because of its full austenitic microstructure (19).

The weld composition is optimized to compensate for the inherent differences in the properties of weld and parent material that are due to grain structure, inclusion content, and cooling rate differences. The goal is to match, as closely as possible, the mechanical and physical properties of the weld and parent material. When nonmatching weld compositions are most appropriate, differences between the welds and parent material in terms of thermal contraction, corrosion and other factors must be considered.

6.08.3.2 Filler Metal Grades

Recommended filler metal grades or welding consumables for 9%Ni steel include covered electrodes for shielded metal arc welding (SMAW), flux-cored wires for flux core arc welding (FCAW), and welding wire for gas metal arc welding (GMAW), gas tungsten arc welding (GTAW) and submerged arc welding (SAW).

6.08.3.2.1 Covered Electrodes for Shielded Metal Arc Welding

AWS specifications for covered electrodes used in SMAW for welding 9%Ni steel are shown in Table 4.

Kobelco Welding (19) has developed a new covered electrode for SMAW namely PREMIARC™ NI-C70H. Specifications of this electrode are listed in Table 5. The electrode has much higher 0.2% proof strength and tensile strength than other conventional covered electrodes for the 9%Ni steel.

6.08.3.2.2 Flux-Cored Wires for Flux Core Arc Welding

The application of flux-cored wires (FCWs) for LNG tanks made of 9%Ni steel had been limited because tight control of welding conditions in a narrow range was required to prevent hot cracks, and the all-position welding was difficult. However, as shown in Table 6, Kobe Steel has developed two types of the FCWs for welding 9%Ni steel that solve these problems, and recently, they have been put into operation. PREMIARC™ DW-N70S is designed for down-hand welding and a new FCW, PREMIARC™ DWN709SP, for all position welding as shown in Table 6.

6.08.3.2.3 Welding Wires for Gas Tungsten Arc Welding, Gas Metal Arc Welding and Submerged Arc Welding

AWS specifications for welding wires used in GTAW and GMAW for welding of 9%Ni steel are shown in Table 7. In the SAW process, the wire used by the industry is according to AWS specifications of A5.14 ERNiMo-8.

www.iran-mavad.com
مرجع مهندسی مواد و متالورژی

Table 4 AWS specification for welding 9%Ni steel using SMAW compositions

Element (%)	*ENiCrFe-9 [A5.11]*	*ENiCrMo-6 [A5.11] [OK 92.55]*	*ENiCrMo-8 [A5.11]*	*ENiCrMo-3 [OK 92.45]*
C	≤0.15	≤0.10	≤0.10	<0.03
Si	≤0.75	≤1.0	≤0.75	–
Mn	1.0–4.5	2.0–4.0	≤1.5	0.4
Ni	≥55.0	≥55.0	≥60.0	60.0
Cr	12.0–17.0	12.0–17.0	0.5–3.5	21.0
Mo	2.5–5.5	5.0–9.0	17.0–20.0	9.5
W	≤1.5	1.0–2.0	2.0–4.0	–
Nb + Ta	0.5–3.0	0.5–2.0	–	3.3
Fe	≤12.0	≤10.0	≤10.0	–
0.2% PS (MPa)	–	–	–	–
TS (MPa)	≥650	≥620	≥650	–
Charpy V (J) at −196 °C	–	85	–	50

Reproduced from Kobelco's Welding Consumables for LNG Storage Tanks Made of 9% Ni Steel. *Kobelco Weld. Today* **2011**, 3–8; *Welding Liquid Natural Gas Tanks and Vessels in 5% and 9% Nickel Steels, ESAB AB*, 2001. Online available at: www.esab.com (accessed 18 March 2013).

Table 5 PREMIARC™ covered electrodes for 9%Ni steel

	Ni–C70S ENiCrFe-9	*Ni–C70H ENiCrMo-6*	*Ni–C1S ENiCrMo-8*
Feature	Inconel type	Inconel type	Hastelloy type
Polarity	AC	AC	AC
C	0.09	0.08	0.03
Si	0.26	0.42	0.49
Mn	2.26	2.85	0.28
Ni	67.6	68.1	68.6
Cr	13.9	12.9	1.9
Mo	3.7	7.1	18.6
W	0.6	1.2	2.9
Nb + Ta	1.7	0.9	–
Fe	9.8	5.5	6.8
0.2% YS (MPa)	430	460	440
TS (MPa)	705	725	730
El (%)	41	42	48
Charpy V (J) at −196 °C	62	77	83

Reproduced from *Welding Liquid Natural Gas Tanks and Vessels in 5% and 9% Nickel Steels, ESAB AB*, 2001. Online available at: www.esab.com (accessed 18 March 2013).

Table 6 PREMIARC™ flux-cored wires for 9%Ni steel used in FCAW

AWS A5.34	*DW-N70S* –	*DW-N709SP ENiMo13-T*
Feature	Applicable for downhand welding	● Hastelloy type for all position welding ● Excellent hot-crack
Shielding gas	80% Ar – 20% CO_2	80% Ar – 20% CO_2
C	0.05	0.02
Si	0.20	0.21
Mn	5.91	2.75
Ni	62.6	62.1
Cr	16.8	6.9
Mo	10.2	17.6
W	–	2.4
Nb + Ta	2.0	–
Fe	1.8	7.7
0.2% PS (MPa)	425	450
TS (MPa)	715	710
El (%)	46	46
Charpy V (J) at −196 °C	106	90
LE (mm) at −196 °C	–	1.40

Reproduced from Kobelco's Welding Consumables for LNG Storage Tanks Made of 9% Ni Steel. *Kobelco Weld. Today* **2011**, 3–8.

www.iran-mavad.com
مرجع مهندسی مواد و متالورژی

Table 7 AWS specifications for GTAW and GMAW wires for 9%Ni steel

	AWS A5.14 ERNiMo-8	*TG-S709S*
Features	–	● Hastelloy type wire and rod ● Suitable for automatic GTAW
C	≤0.10	0.02
Si	≤0.75	0.03
Mn	≤1.5	0.03
Ni	≥60.0	70.4
Cr	0.5–3.5	2.0
Mo	17.0–20.0	19.0
W	2.0–4.0	3.0
Fe	≤10.0	5.5
0.2% PS (MPa)	≥360	460
TS (MPa)	≥660	730
El (%)	≥25	47
Charpy V (J) at −196 °C	Av ≥ 34	160

Reproduced from Kobelco's Welding Consumables for LNG Storage Tanks Made of 9% Ni Steel. *Kobelco Weld. Today* **2011**, 3–8.

As discussed above, for the construction of the tanks for cryogenic service, 9% nickel steels are usually welded with Ni-based filler materials. Although sufficient toughness is attained in weld deposit, the strength of the weld deposit is lower than that of a 9% nickel steel plate. In addition, the total cost of 9% nickel steel welded structures is rather high because of the high prices of the Ni-based filler materials. Attempts have been made to overcome the situation by using matching fillers that have similar composition to 9%Ni steel (*20*). It is suggested by Nako et al. (*21*) that such filler materials can be applied to some extent to the construction of LNG storage tanks with the attainment of a good balance of toughness and strength in the weldment. They investigated the microstructures of the weldment of 9%Ni steel with similar weld metals composition. The high toughness level of the welds was mainly attributed to the fine martensite–bainite mixed microstructure of the reheated zone. The fine microstructure at the reheated zone was attained because of the refinement of the prior austenite structure by reverse transformation (*21*). However, the difficulties in using similar composition fillers are in the control of the heat input, especially in the GTAW process. The high heat input causes a reduction in the toughness of the weld metal. It was reported that the lowering of the toughness level by high heat input is related to the retained austenite (*22*).

Koshiga et al. (*23*) studied the cryogenic fracture toughness of weldments of 9% nickel steel using a filler with 11%Ni. They found that brittle fracture initiation characteristics and fatigue properties of the welded joint with matching ferritic filler metal were as good as those with high-nickel alloy filler metals. This was recognized as suitable for the welding of 9% nickel steel by the Japan Welding Engineering Society and the Japan High Pressure Institute.

6.08.3.3 Welding Procedure and Process

The 9%Ni steels have very good weldability and are proven to be welded with SMAW with covered electrodes and with SAW (*19,24*). For SAW, an endless wire on spool and a suitable flux is used. The wire is alloyed with all of the required chemical elements in the ASME code. Starting with the SMAW process, welding of 9%Ni steel now has widespread use of automatic welding processes such as SAW, GTAW and GMAW in the fabrication of storage or transport tanks. GMAW and GTAW have been used occasionally.

In LNG tank fabrication, the welding positions 1G, 2G (flat and horizontal seams) and 3G (vertical seams) are the most used with SMAW according to ASME code section IX part QW. But, other positions are also possible for welding on the stiffeners, bottom and roof of the tank. It is necessary, therefore, that the electrodes are able to weld in all positions except upside down. It is especially important to show that all required mechanical properties are achievable after welding with the stick electrode in all welding positions (*25*).

As the second welding process, the SAW is usually used on LNG tanks. It is a mechanized and continuous process and, therefore, has higher efficiency than the SMAW. The SAW is used especially in the 2G position and in nearly all 1G positions of the tank. This means that all horizontal seams are welded with SAW. Therefore, special equipment to hold the flux is necessary. For LNG tanks, a Ni-base alloy wire according to ASME SFA 5.14, material ER NiCrMo-3/UTP UP 6222Mo or ER NiCrMo-4 UTP UP 776, with the suitable flux for low temperature applications are mostly used.

The electrode is welded with a slight tilt and a short arc for the SMAW. Stringer beads (no weaving) are to be welded and the right parameters like voltage and amperage have to be used. The heat input for the SMAW and the SAW should be approx. 12 kJ cm^{-1}, and the interpass temperature approx. 150 °C. Unless the constructions are heavily restrained, there is no need for preheating or postheat treatment when welding 9%Ni steel (*25*). The interpass temperature should be kept below 150 °C. The magnetic properties of 9%Ni steel mean that arc blow will be encountered during welding. AC welding is therefore often preferred. In order to obtain

www.iran-mavad.com
مرجع مهندسی مواد و متالورژی

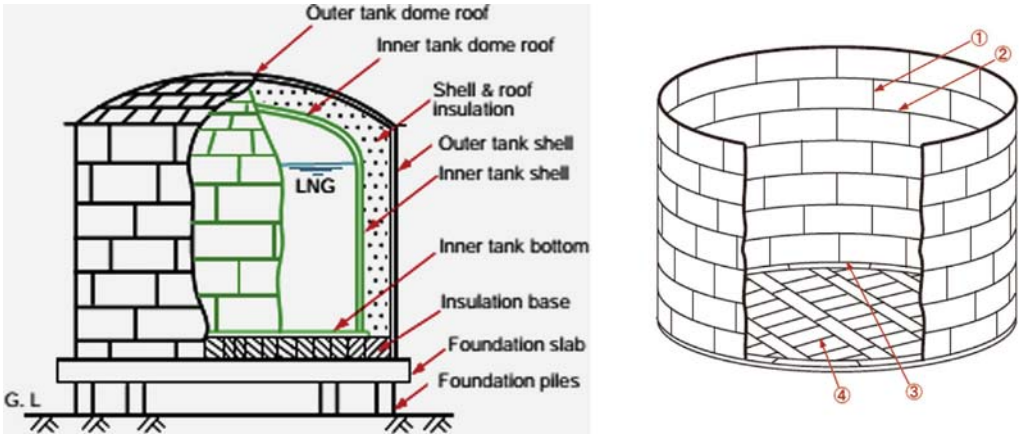

Figure 6 General elevation and cross-sectional view of typical welding joints in the shell and bottom of a 9%Ni steel tank in on-site fabrication. The components are 1 and 2 – side shell, 3 – bottom to side shell, and 4 – bottom. Reproduced from Kobelco's Welding Consumables for LNG Storage Tanks Made of 9% Ni Steel. *Kobelco Weld. Today* **2011**, *14* (2), 3–8.

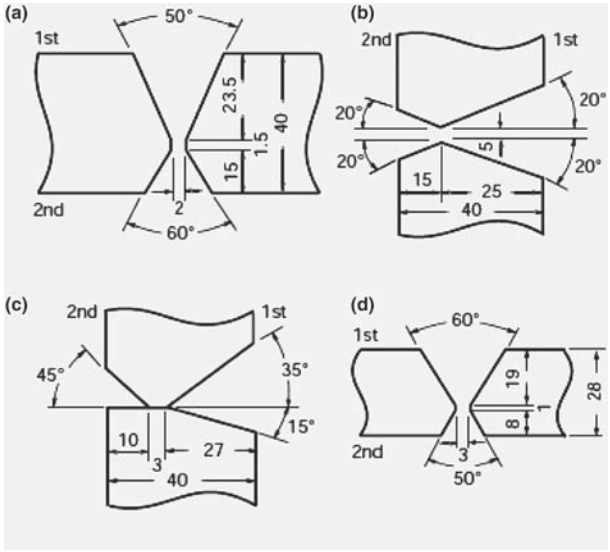

Figure 7 Typical groove configurations for double V joint for (a) 1 G by SMAW, (b) 2 G by GTAW, (c) 2 G by SAW, and (d) 3 G by FCAW. Reproduced from Kobelco's Welding Consumables for LNG Storage Tanks Made of 9% Ni Steel. *Kobelco Weld. Today* **2011,** *14* (2), 3–8.

high impact resistance in the weld metal and to facilitate these welds, the use of a small diameter of 1.6 mm wire is recommended. The welding joints that are typically carried out on 9%Ni steel components are shown in Figure 6. The common type of joint employed is double V with multiple pass of weld deposition.

Typical groove configurations for the double V joint for SMAW, GTAW, SAW and FCAW are shown in Figure 7.

6.08.4 Weldability of 9% Nickel Steel

6.08.4.1 Factors Influencing Weldability of 9% Nickel Steel

In LNG tank construction, welding or joining of structural components is usually carried out by SMAW, SAW, and GTAW processes. As these welding processes are associated with fusion of weld metal onto base metal; weld integrity, weld dilution and structure–property relationship are vital issues that need to be considered in the construction of weldment. Therefore, the following sections will describe the 'process-induced' and 'metallurgical-induced' factors in the welding of 9% nickel steel.

Typically, a 9% nickel steel vessel, e.g., an LNG tank, is covered by a composite layer with an outermost covering of mild steel. There exists a thermal gradient between the inner and outer layers and the vessel is subjected to expansion and contraction while in service. For dissimilar compositions of weld fillers and base metal, a significant difference in coefficient of thermal expansion (CTE) 's values exist. When the CTE between weld and the 9% nickel steel is large, a thermal stress, in addition to a residual stress,

www.iran-mavad.com
مرجع مهندسی مواد و متالورژی

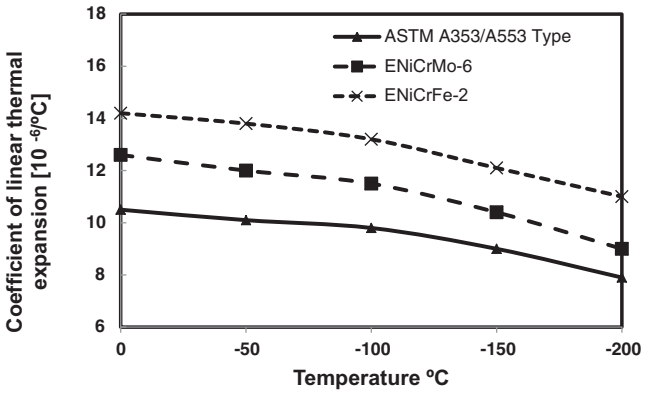

Figure 8 Comparison of the coefficient of linear thermal expansion of 9%Ni Steel with that of conventional welding consumables. Reproduced from Hilkes, J.; Fred, N.; Welding 9% Nickel steel for LNG application, Singapore Welding Society Newsletter, March 2007, 5–9.

develops during welding, which obviously lowers the fatigue life. In order to avoid this problem, a filler metal is chosen (e.g., ENiCrMo-6 type of consumable) so as to make the CTE value of weld deposit as close as possible to that of 9%Ni steel. Figure 8 shows the CTE of different electrodes as compared to 9% nickel steel plate in the temperature range of 0 to −200 °C. The recently developed ultrasonic peening method may alleviate the residual stress, which may improve the fatigue life of weldment (*26*). Recent attempts have been made to use martensitic Ni-alloyed or ferritic (Fe–Ni base) filler materials for 9% nickel steel welding. It was found that the CTE for these fillers are very much closer to 9%Ni steel (*23,27*).

A large difference in Ni content between filler and base metal makes dilution of base metal, which affects the mechanical properties by decreasing the tensile strength of the weld metal. It is customary to conduct the all weld test and transverse weld test to check the welding conditions and to ensure that the tensile strength, yield strength and notch toughness conform to code and standard values.

In general, this steel can become easily and very strongly magnetized during handling and transportation and can develop residual magnetism. The magnetic properties of the steel cause arc blow in welding that can be minimized if an alternating current is used. In the case of DC welding, an ac current coil is wound around the test piece to minimize the arc blow effect. Precautions include the avoidance of magnetic handling, demagnetization and to ensure that magnetic fields are below 50 Oersted (*28*). When arc blow is encountered, the area can be demagnetized by using a coil of welding cable attached to an AC transformer.

6.08.4.2 Structural Decomposition at Heat Affected Zone

The mechanical properties of the weld metal or of the heat-affected zone (HAZ) may not match those of the base metal, as the welding can alter the metallurgical properties and the stress state of the material immediately adjacent to the weld joint. Figure 9 shows a typical weld configuration and the microstructures of different regions of a 9% nickel steel plate welded with nickel-based filler metal (*29*).

Weld deposit shows the dendritic as-cast structure with coarse grains at HAZ and tempered martensitic structure at the base metal area (Figure 9). The thickness requirement of a steel plate essentially demands multipass welding. The intense heat from an arc in each pass of welding will generate thermal cycles. The thermal cycles to some extent alter the metallurgical structure of the base

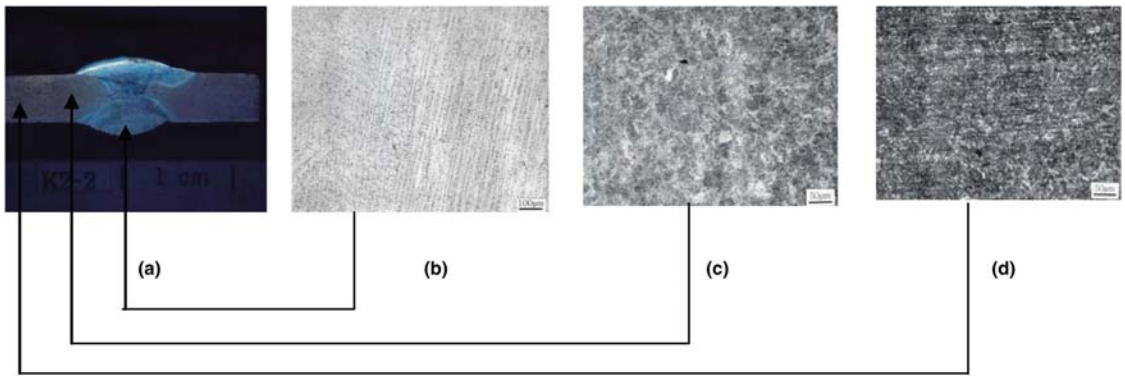

Figure 9 (a) Typical 9% nickel steel plate welded with nickel-based alloy filler with microstructure at (b) weld deposit (c) HAZ and (d) base metal. Reproduced from Uznanski, D.; Château, E.; Legrandais, J. P.; Yang, Y. M.; Yamashita, M.; Cherasse, J. M.; Jana, S.; Goeminne, D.; Capelle, J. Y. Investigations into the Aging Extent of the 9% Nickel 500 m^3 LNG Storage Tank of the Nantes Cryogenic Testing Station.

www.iran-mavad.com
مرجع مهندسی مواد و متالورژی

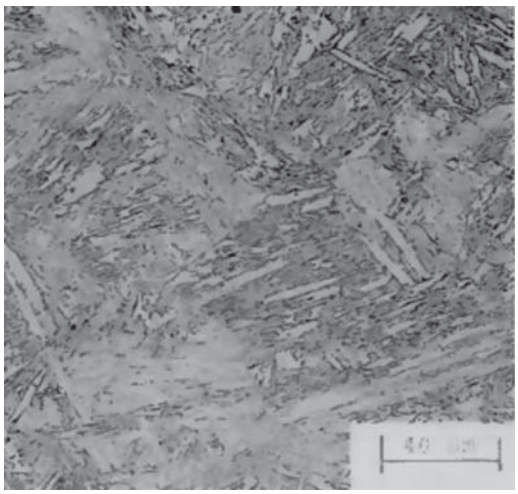

Figure 10 Microstructure of coarse grained HAZ area of 9% nickel steel. Reproduced from Nippes, E. F.; Balaguer, J. P. A Study of the Weld Heat-affected Zone Toughness of 9% Nickel Steel. *Weld. Res. Suppl.* **September 1986**, pp 237–243.

material near the weld vicinity (HAZ). The base metal region close to the fusion line is heated to peak temperature causing grain growth. A typical microstructure of the coarse-grained region of the true HAZ in a 9% nickel steel weld (*2*) is shown in **Figure 10**.

Depending on the heat input and section thickness of this region for subsequent welding, fast or slow cooling may induce transformation products that may differ from the original condition. The coarse grain of austenite usually retards the nucleation site for fine ferrite–carbide products. It is reported that (*1*,*2*,*7*,*8*) with a presence of nickel at moderate heat inputs, the dwell time at peak temperature is short. So, grain growth is restricted both in degree and in the volume of metal affected. As a result, subsequent rapid cooling is enough to produce fine ferrite-carbide structures or martensite depending on the cooling structure. The reheating cycles associated with multipass welding partially refines the coarsened weld deposit structure and tempers hardened regions. Consequently, the notch toughness of the HAZ may not be significantly altered by welding at low heat input. However, the upper-shelf impact energy decreases at −196 °C when high heat input causes grain coarsening of the primary austenite (*30*).

The change of microstructure in HAZ, resulting from thermal cycling of welding, has been extensively studied by Nippes et al. (*2*) and others (*31*). The methodology of simulating the weld HAZ used in this study, i.e., reproduction of measured weld thermal cycles in a small specimen using the Gleeble machine, is an intrinsic part of the welding literature. A detailed discussion of these techniques can be found elsewhere (*32*–*34*). Toughness of this steel, subjected to three different artificial thermal cycles, was measured using the Charpy V-notch impact test. It was found that the material subjected to high peak-temperature thermal cycles still met the ASTM toughness requirements at liquid nitrogen temperatures. The upper shelf energy for this steel was lowest for an intermediate thermal cycle of 1000 °C (1832 °F) peak temperature. Simulated thermal cycling of this material to peak temperatures of 500 °C and 1300 °C significantly decreases the retained austenite content. Synthetic thermal cycling to a peak temperature of 1000 °C reduces the retained austenite content to an undetectable level. The decreased impact toughness of this material, after synthetic thermal cycling, is apparently partly caused by local reductions in the retained austenite content. The reduction in retained austenite content results in a decrease in the upper shelf of the impact energy versus temperature curve for all three thermal cycles.

The impact of weld deposit and the associated heat from fused weld deposit in fusion welding will inevitably induce the change in HAZ microstructure, which primarily consists of tempered martensite along with 5% retained austenite resulting from the full heat-treatment of 9%Ni steel (*1*). The microstructure of fused weld and the transformed microstructure in HAZ areas are determined by the temperature gradient formed during welding. It has already been mentioned that the HAZ part of the heat treated base material undergoes structural decomposition at a peak temperature in the range of 600–800 °C. The presence of nickel usually suppresses the eutectoid reaction temperature so that the structural changes are much pronounced at 700 °C, where the residual austenite is more likely changed to secondary tempered products (*4*) and the total austenite content drops. Research results (*1*,*4*) also indicate that beyond 700–900 °C, due to the presence of grain refinement agents (such as Al) present in the HAZ, fine grains are developed as compared to the low temperature region. In addition, austenite content is also low in this region. The occurrence of fine grain size contributes to hardening in an HAZ band with decrease in notch toughness at −196 °C (*29*,*35*). A typical hardness profile across the HAZ zone (*29*) is shown in **Figure 11**.

6.08.5 Quality Control of Weldment

6.08.5.1 Cracking Problems in 9% Nickel Steel Welding

The major concerns in welding of 9% nickel steel are the avoidance of hot cracking in the welded joint and to yield acceptable properties in the weld metal and HAZ. Literature shows that the restriction of impurities, especially S and P to low levels, is essential

www.iran-mavad.com
مرجع مهندسی مواد و متالورژی

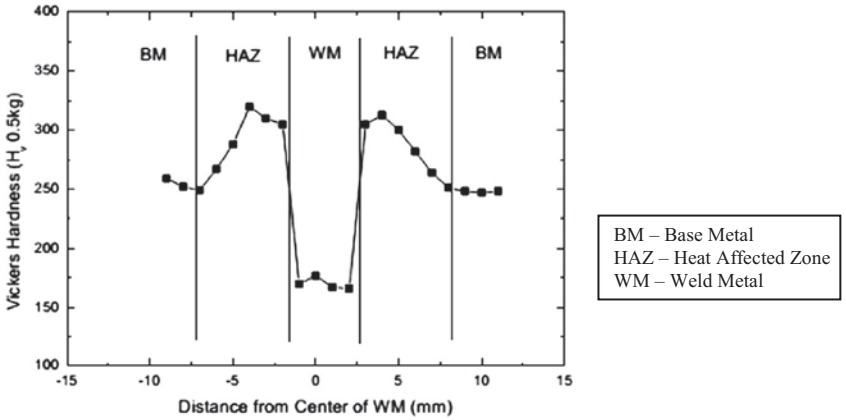

Figure 11 Hardness distribution across welded joint in a 9%Ni steel. Reproduced from Uznanski, D.; Château, E.; Legrandais, J. P.; Yang, Y. M.; Yamashita, M.; Cherasse, J. M.; Jana, S.; Goeminne, D.; Capelle, J. Y. Investigations into the Aging Extent of the 9% Nickel 500 m^3 LNG Storage Tank of the Nantes Cryogenic Testing Station.

to produce sound welds (*1,2*). The soundness in structure associated with improved fracture strength usually resist hot cracking for welding in excessive constraint conditions of the joint.

The outstanding features of welding of 9% nickel steel is that it is not susceptible to cold cracking as usually found in normal welding of carbon manganese steel. Cold cracking or hydrogen cracking occurs due to hydrogen pick up during welding and the hydrogen causes brittle fracture in the stressed region. Field work as well as laboratory research demonstrated that the hydrogen embrittlement or cold (delayed) cracking are generally not observed in the hardened zone because austenite in the steel absorbs hydrogen (*36*). Hence, preheating or postweld heat treatment operations may not be required when welded with low hydrogen consumables. But in some instances, preheating at 100–150 °C is also helpful in avoiding hydrogen or restraint cracking.

Usually, LNG tanks are welded with much dissimilar high Ni alloy welding consumables that are hot crack sensitive in general. Liquification cracking or hot cracking can be a notable feature if nickel-sulfide or the aluminium-oxide is present in the weld. Weld simulator tests are usually carried out to evaluate the sensitivity of the steel to liquation cracking. In addition, crater cracks can also form. It is recommended that a crater be ground off after the termination of each welding.

6.08.5.2 Weldability Testing

Although a large number of test techniques have been introduced to assess or quantify high temperature cracking susceptibility in weld, only a few of them are standardized. In general, test techniques can be grouped into two categories: representative (self-restraint) and simulative (externally loaded) (*37,38*). The former observes 'cracking' or 'no-cracking' conditions for actual welding condition without quantifying the cracking susceptibility of the material under different welding conditions. On the other hand, for the quantification of cracking susceptibility, simulative tests introduce thermal cycling combined with applied mechanical strain in order to produce cracks. This procedure is executed on a thermo mechanical simulator where the hot tensile test or strain induced crack opening test in combination with thermal cycle are carried out on weld samples. The simulative testing allows the determination of temperatures at which the cracks occur, measurement of critical strains and strain rates to fracture that are associated with the hot cracking (*2,37*).

6.08.5.3 Inspection of Welding

A wide range of regulations and standards defines the design, construction, inspection and maintenance of LNG tanks made of 9% Ni steel. Some of the relevant ASME, API, BS EN, and JIS standards are listed below:

1. ASME Sec. VIII, Div. 1: Design and fabrication of pressure vessels; Div. 2: Alternative rules.
2. API Standard 620: Design and construction of large, welded, low-pressure storage tanks; Appendix Q: Low pressure storage tanks for liquefied hydrocarbon gases at temperature not lower than −270 °F (−168 °C).
3. BS EN 14620-1(2006): Design and manufacture of site built, vertical, cylindrical, flat-bottomed steel tanks for the storage of refrigerated, liquefied gases with operating temperatures between 0 °C and −165 °C, Part 1: General.
4. JIS B8265(2010): Construction of pressure vessel — General principles; JIS B8267(2008): Construction of pressure vessel.

The most commonly applied regulations and standards worldwide are ASME Sec. VIII and API 620.

www.iran-mavad.com
مرجع مهندسی مواد و متالورژی

6.08.6 Concluding Remarks and Future Directions

The 9%Ni steel will continue to remain the mainstay material for the storage and transportation of liquefied natural gas in the foreseeable future. A number of factors are driving new developments in this area. The need for bigger tanks for efficient storage and transportation demands steel with even higher strength. Increasingly stringent safety requirements mean that the fracture properties of the steel need further improvement. These requirements are being addressed by improving the steel making process, steel chemistry and adopting innovative heat treatments procedures. Use of cleaner steels with lower S, P etc. is being pursued. Some small beneficial alloy additions, such as Cu, are being investigated. Researchers are investigating higher nickel content steels for improved toughness. On the other hand, in an effort to lower cost for some applications, lower nickel content steels with other minor alloy additions are also being investigated. As for improved heat treatment procedure, direct-quenching and tempering processes have been reported (*39*) that can provide better ability to arrest brittle crack propagation.

Traditionally, filler metals with high nickel contents have been used. Recently, the ever increasing pressure to reduce costs has prompted researchers to develop low nickel filler metal. However, the effects of low Ni filler metal on the weld impact strength and toughness remains a concern. Work is underway on the achievement of acceptable weld quality using low Ni filler metals by adopting appropriate welding techniques and parameters. Specially, the aim is to achieve a narrow band of reheat zone or HAZ area in GTAW. Researchers are investigating the development of an appropriate new postweld heat treatment to homogenize the whole weldment structure for improved impact and fracture toughness. Researchers are also working on improvements in the welding process for higher productivity, lower cost and better reliability. Vertical submerged arc welding (*40*) for tank construction, electron beam welding (*41*) procedures with lower heat input, etc. are being pursued.

Future developments in this area can also result from a deeper understanding of fracture behavior weldments in this steel (*42*). Fracture toughness testing are being conducted not only under Mode I but also under Mode II and Mode III tests in order to study crack bifurcation from high toughness to low toughness area in weldment. The influence of a local brittle zone embedded in HAZ area on crack arrest behavior is of future interest.

Industry is interested in understanding the ageing behavior of LNG vessels in an effort to extend their service life and inspection frequency. The behavior of a 9%Ni steel welded structure under sudden impact caused by accidents is another area of future research.

References

1. Pense, A. W.; Stout, R. D. Fracture Toughness and Related Characteristics of the Cryogenic Nickel Steels. *WRC Bulletin* **1975,** *205*.
2. Nippes, E. F.; Balaguer, J. P. A Study of the Weld Heat-affected Zone Toughness of 9% Nickel Steel. *Weld. Res. Suppl.* **September 1986,** 237–243.
3. Low Temperature Properties of Nickel Alloy Steels: The International Nickel Company, Inc (INCO), Copyright@1975.
4. Guide to the Welding and Weldability of Cryogenic Steels, Document IIS/IIW-844-87, Sub-commission IXG of Commission IX of the International Institute of Welding, the Welding Institute, UK, 1987.
5. Technical Report *9% Nickel Steel: For Use at Cryogenic Temperatures;* ArcelorMittal: USA, Dec 2010.
6. Hoshino, M.; Saitoh, N.; Muraoka, H.; Saeki, O. Development of Super-9%Ni Steel Plates with Superior Low-temperature Toughness for LNG Storage Tanks, Nippon Steel Technical Report 90, 2004, 20–24.
7. Wilson, A. D. Variables Influencing the Toughness of 9% Nickel Steel. In *American Gas Association Transmission Conference, Atlanta, Georgia;* May 1981.
8. Strife, J. R.; Passoja, D. E. The Effect of Heat Treatment on Microstructure and Cryogenic Fracture Properties of 5 Ni and 9 Ni Steel. *Met. Trans.* **1980,** *11A* (8), 1341–1350.
9. Marschall, C. W.; Hehemann, R. F.; Troiano, A. R. The Characteristics of 9% Nickel Low Carbon Steel. *Trans. ASM* **1962,** *55* (1), 135–148.
10. Syn, C. K.; Jin, S.; Morris, J. W., Jr. Cryogenic Fracture Toughness of 9 Ni Steel Enhanced through Grain Refinement. *Met. Trans.* **1976,** *7A* (12), 1827–1832.
11. Kim, K. J.; Schwartz, L. H. On the Effects of Intercritical Tempering on the Impact Energy of Fe-9Ni-0.1C. *Mater. Sci. Eng.* **1978,** *33,* 5–20.
12. *ASME Boiler and Pressure Vessel Code, Section VIII, Division 1: Design and Fabrication of Pressure Vessels;* American Society For Mechanical Engineers (ASME), 2007.
13. Standard Specification for Pressure Vessel Plates, Alloy Steel, Quenched and Tempered 8 and 9 percent Nickel, Designation: A 553/A 553M – 95; ASTM International, Reapproved 2000, 282–284.
14. Pense, A. W.; Kottcamp, E. H.; Stout, R. D. A Study of Subcritical Embrittlement in Pressure Vessel Steels. *Weld. J.* **1963,** *42* (12), 541s–546s.
15. Du, W. S.; Cao, R.; Yan, Y. J.; Tian, Z. L.; Peng, Y.; Chen, J. H. Fracture Behavior of 9% Nickel High-strength Steel at Various Temperatures Part I. Tensile Tests. *Mater. Sci. Eng. A* **2008,** *486,* 611–625.
16. Shin, H. S.; Lee, H. M.; Kim. Impact Tensile Behavior of 9% Nickel Steel at Low Temperature. *Int. J. Impact Eng.* **2000,** *24,* 571–581.
17. Swartzendruber, L. J. The Fe-Ni (Iron-nickel) System. *J. Phase Equil.* **1991,** *12,* 288–312.
18. Standard Specification for Pressure Vessel Plates, Alloy Steel, 9 percent Nickel, Double-Normalized and Tempered, Designation: A 353/A 353M – 93, ASTM International, Reapproved 1999, 169–171.
19. Kobelco's Welding Consumables for LNG Storage Tanks Made of 9% Ni Steel. *Kobelco Weld. Today* **2011,** *14* (2), 3–8.
20. Ichihara, I.; Sugiyama, T.; Aida, I.; Nishikawa, Y. Kobe Steel Engineering Reports; Vol. 28, 1978, 4–46.
21. Nako, H.; Okazaki, Y.; Takeda, H.; Suenaga, K.; Nakanishi, K. Comparison of Microstructures at as Welded Zone and Reheated Zone in 9%Ni Steel Similar Composition Weld Metal. Trans Tech Publications. *Mater. Sci. Forum* **2010,** *638–642,* 3693–3698.
22. Tamura, H.; Onzawa, T.; Uematsu, S.; Maekawa, K. *Trans. Japan Weld. Soc.* **1981,** *12,* 25.
23. Koshiga, F.; Tanaka, J.; Watanabe, I.; Takamura, T. Matching Ferritic Consumable Welding of 9% Nickel Steel to Enhance Safety and Economy. Sponsored by the American Welding Society and the Welding Research Council. *Weld. Res. Suppl., Supplement to the Welding Journal* **1984,** 105–115.
24. *Welding Liquid Natural Gas Tanks and Vessels in 5% and 9% Nickel Steels, ESAB AB,* 2001. Online available at: www.esab.com (accessed 18 March 2013).
25. *Welding of 9% Ni-steel Tanks;* Newsletter, UTP, Josef Heinemann and Stefan Eich, UTP Schweissmaterial GmbH: Germany, 2009.
26. Kudryavtsev, Y.; Kleiman, J. *Residual Stresses in Welded Elements: Measurements, Fatigue Analysis and Beneficial Redistribution*; Structural Integrity Technologies, Inc. (SINTEC), www.sintec.ca.
27. Tamura, H. Notch Toughness and Retained Austenite in 9% Ni Steel Welds Using Ferritic Filler Metals. *Trans. JWS* **1981,** *12* (1), 25–30.
28. Avery, R. E.; Parsons, D. *Welding Stainless and 9% Nickel Steel Cryogenic Vessels;* Nickel Development Institute, November 1995. NiDi Reprint Series No. 14037, Printed with permission from Welding Journal.

www.iran-mavad.com
مرجع مهندسی مواد و متالورژی

29. Uznanski, D.; Château, E.; Legrandais, J. P.; Yang, Y. M.; Yamashita, M.; Cherasse, J. M.; Jana, S.; Goeminne, D.; Capelle, J. Y. Investigations into the Aging Extent of the 9% Nickel 500 m^3 LNG Storage Tank of the Nantes Cryogenic Testing Station.
30. *Fracture Characteristics of Nine Percent Nickel Steel Plate and Its Welded Joint;* Nippon Steel Corporation, June 1980.
31. Dhooge, A.; Provost, W.; Vinckier, A. *Weldability and Fracture Toughness of Quench and Tempered 9% Nickel Steel, Part I–Weld Simulation Testing, Part II—Wide Plate Testing.* WRC Bulletin No. 279, July 1982.
32. Nippes, E. F. The Weld Heat-affected Zone. *Weld. J.* **1959,** *38* (1), 1-s–18-s.
33. Nippes, E. F.; Savage, W. F. Development of Specimen Simulating Weld Heat-affected Zones. *Weld. J.* **1949,** *8* (11), 534s–546s.
34. Nippes, E. F.; Sibley, C. R. Impact Performance of Synthetically Reproduced Heat-affected Zone Microstructures in, T-1 Steel. *Weld. J.* **1956,** *35* (10), 473s–480s.
35. Yan, C. Y.; Yang, S. Z.; Zhao, J. H.; Li, W. S. Prediction of Hardness in Heat Affected Zone of 9%Ni Steel. *Adv. Mater. Res.* **2012,** *455–456,* 406–412.
36. Tsuboi, J.; Hirai, Y. Welding Materials for Low Temperature Service. *Kawasaki Steel Report* **1971,** *3* (2), 108–123.
37. Lippold, J. C. *Recent Developments in Weldability Testing for Advanced Materials, Joining of Advanced and Specialty Materials VII (#05116G);* ASM International, 2005.
38. Collins, M. G.; Ramirez, A.; Lippold, J. C. An Investigation of Ductility-dip Cracking in Ni-base Filler Metals – Part 3. *Weld. J.* **2004,** *83* (2), 39s–49s.
39. 9% Ni Steel With High Brittle Crack Arrestability, JFE Technical Report, No. 11, June 2008; Originally published in JFE GIHO No. 18, Nov. 2007, 75–76.
40. Sakamoto, R.; Kobayashi, K.; Iijima, T.; Nishimura, Y.; Mizo, Y. Development of Vertical Submerged Arc Welding Method for Aboveground LNG Storage Tank Construction. *IHI Eng. Rev.* **2010,** *43* (2), 55–62.
41. Kim, S. H.; Kang, C. Y.; Bang, K. S. Weld Metal Impact Toughness of Electron Beam Welded 9% Ni Steel. *J. Mater. Sci.* **2010,** *36,* 1197–1200.
42. Cao, R.; Zhu, S. S.; Feng, W.; Peng, Y.; Jiang, F.; Du, W. S.; Tian, Z. L.; Chen, J. H. Effects of Weld Metal Property and Fraction on the Toughness of Welding Joints of a 8%Ni 980 MPa High Strength Steel. *J. Mater. Process. Technol.* **2011,** *211,* 759–772.

www.iran-mavad.com
مرجع مهندسی مواد و متالورژی

This page intentionally left blank

www.iran-mavad.com
مرجع مهندسی مواد و متالورژی

6.09 Weldability of Nickel-Base Alloys

JL Caron, Haynes International, Inc., Kokomo, IN, USA
JW Sowards, National Institute of Standards and Technology, Boulder, CO, USA

© 2014 Elsevier Ltd. All rights reserved.

6.09.1	**Introduction**	152
6.09.2	**Welding Considerations**	153
6.09.2.1	General Welding Considerations	153
6.09.2.2	Specific Welding Process Considerations	155
6.09.2.2.1	Gas Tungsten Arc Welding	155
6.09.2.2.2	Gas Metal Arc Welding	156
6.09.2.2.3	Shielded Metal Arc Welding	156
6.09.2.2.4	Submerged Arc Welding	156
6.09.2.2.5	Flux-Cored Arc Welding	157
6.09.2.2.6	Electron Beam and Laser Beam Welding	157
6.09.2.3	Examples of Relevant Welding Codes and Standards	157
6.09.3	**Discontinuities in Ni-Base Weldments**	158
6.09.3.1	Weld Process- or Procedure-Related Defects	158
6.09.3.2	Metallurgical-Related Defects	158
6.09.3.2.1	Weld Solidification Cracking	160
6.09.3.2.2	Liquation Cracking	162
6.09.3.2.3	Ductility-Dip Cracking	164
6.09.3.2.4	Strain-Age Cracking	165
6.09.4	**Dissimilar Welding**	167
6.09.4.1	General Considerations	167
6.09.4.2	Applications and Techniques	168
6.09.4.2.1	Over-Alloyed Filler Metal	168
6.09.4.2.2	Buttering	168
6.09.4.2.3	Universal Filler Metal	168
6.09.4.2.4	Weld Overlay	169
6.09.4.2.5	Joining Non-Ni-Base Alloys	169
6.09.5	**Special Material Considerations**	169
6.09.5.1	Welding of Castings	170
6.09.5.2	Welding of Specialty Alloys	170
6.09.5.2.1	Nickel Aluminides	170
6.09.5.2.2	Oxide Dispersion Strengthened Alloys	170
6.09.5.3	Repair Welding	171
6.09.5.3.1	Solid-Solution Strengthened Alloys	171
6.09.5.3.2	Precipitation-Strengthened Alloys	171
6.09.5.3.3	Single Crystal Superalloys	171
6.09.6	**Influence of Welding on Service Performance**	171
6.09.6.1	Mechanical Performance	171
6.09.6.1.1	As-Welded Mechanical Properties	171
6.09.6.1.2	Thermal Stability	171
6.09.6.2	Corrosion Resistance	172
6.09.6.2.1	WM Dendrite Coring	172
6.09.6.2.2	HAZ Sensitization	172
6.09.6.2.3	Other Forms of Corrosion	172
6.09.7	**Weldability Testing Techniques**	173
6.09.7.1	The Hot-Ductility Test	174
6.09.7.2	The Varestraint Test	175
6.09.7.3	The Sigmajig Test	176
6.09.7.4	The Strain-to-Fracture Test	176
6.09.7.5	Other Techniques	177
6.09.8	**Concluding Remarks**	178
References		178

www.iran-mavad.com
مرجع مهندسی مواد و متالورژی

6.09.1 Introduction

The Ni-base alloys are used in a wide range of applications in the engineering of systems that are exposed to extreme conditions, including highly corrosive and high-temperature environments. Most of these applications require the use of welding (i.e., materials joining) processes during manufacture of system components. In these demanding environments, the weld must perform to a level similar to the base metal. The topic of weldability (or joinability) addresses the issues that arise during welding and fabrication, and is specifically defined as the ability of a material to be welded and to perform satisfactorily in the imposed service environment. Weldability of Ni-base alloys is well developed as a field of scientific study, and the results of weldability studies have direct impact on industrial fabrication. In fact, there have been several comprehensive review papers (see, e.g., (*1–3*)) and a recent text book (*4*) dedicated to the topic of Ni-base alloy weldability that cover both the breadth and depth of this important field. However, due to the extent of this topic, it is simply the objective of this chapter to address the major issues relating to the weldability of Ni-base alloys, and provide an understanding of how to approach these issues from a practical engineering standpoint.

To better understand the main weldability concerns, we briefly review the effects of alloying elements in Ni-base alloys and the major Ni-base alloy classifications. While one is referred to other reference books (*5*) for more detailed descriptions of Ni-base alloy metallurgy, here, a brief review is important in order to understand weldability issues that will be discussed in this chapter. Nickel has a face-centered cubic (FCC) 'austenite' structure at all temperatures and can be alloyed with several different elements to produce alloys with uniquely superior properties to many other materials. Nickel exhibits extensive solid solubility with many different metal elements, including copper, iron, chromium, molybdenum, and cobalt, which act as solid-solution strengtheners and form the basis for many of the binary (e.g., Ni–Cu and Ni–Mo alloys) and ternary (e.g., Ni–Fe–Cr and Ni–Cr–Mo alloys) types of Ni-base alloys. Chromium is an essential element in most Ni-base alloys in order to form a passive Cr_2O_3 surface oxide film that is needed for corrosion resistance. Since nickel has a high solid solubility for chromium, and a narrow solidification temperature range when alloyed with chromium, it is an ideal element to form the basis of most of the Ni-base alloys. Significant strengthening can be achieved through the formation of long-range ordered domains/precipitates of the $Ni_2(Mo,Cr)$ phase. Elements such as aluminum, titanium, and niobium are added to form strengthening precipitates in high-temperature alloys. Aluminum and titanium promote the formation of the γ' $Ni_3(Ti,Al)$ precipitate, which is an ordered FCC phase that provides for excellent high-temperature strength. However, these alloys suffer from strain-age cracking during postweld heat treatment (PWHT) to the point where several alloys are considered unweldable. When sufficient amounts of niobium are added, formation of the γ'' Ni_3Nb precipitate is promoted, which several commercial alloys rely on for strengthening. While γ'' strengthened alloys are relatively immune from strain-age cracking, the formation of Nb-rich eutectic phases during weld solidification renders them susceptible to solidification cracking. Boron and zirconium are added to improve elevated-temperature creep strength and ductility by enhancing grain boundary strength. However, these two elements have an extremely damaging effect on weld hot cracking resistance. Most Ni-base alloys also contain appreciable levels of carbon, which forms various types of carbides with elements such as chromium, molybdenum, tungsten, titanium, niobium, and tantalum. The carbon content is usually held to an 'as low as possible' level in corrosion-resistant alloys, typically below 0.01 wt%. Lower carbon levels hinder the formation of carbides in the heat-affected zone (HAZ), which act to impair the overall corrosion resistance of these alloys by depleting the austenite matrix of critical alloying elements, namely chromium and molybdenum. Carbon levels are intentionally higher in high-temperature alloys, typically in the range of 0.05–0.1 wt%, to form strengthening carbides. Aluminum is also added to high-temperature alloys to provide corrosion protection by the formation of a tenacious Al_2O_3 oxide film on the surface of the alloy. Even though impurity elements such as sulfur, phosphorus, and lead are held to very low levels in Ni-base alloys, they can have a significantly adverse effect on weldability since they are essentially insoluble in nickel and promote hot cracking by forming low-melting-point eutectic phases. Magnesium and manganese are added to control the effects of sulfur. An extensive review of the effect of alloying elements in Ni-base alloys is provided elsewhere (*6*).

The composition of Ni-base alloys has been constantly evolving since their first usage began in the early 1900s (*7*). In the century following, the compositions of the various Ni-base alloys have become quite extensive as the applications have increased with particular emphasis on aqueous corrosion resistance and high-temperature service. Two companies have been at the forefront in the development of advanced Ni-base alloys. Special Metals Corporation, originating as the International Nickel Company (INCO) in 1902, is well known for the development of alloys with trade names such as INCONEL® and INCOLOY®, including the production of the first industrial alloy known as MONEL® metal. Haynes International, Inc., founded as the Haynes Stellite Company in 1912, has developed numerous successful alloys for both corrosion-resistant and high-temperature applications, better known by their HASTELLOY® and HAYNES® trade names. **Table 1** provides an overview of the main Ni-base alloy systems with common commercial examples, as well as the main weldability concerns associated with each system.

A Ni-base alloy will be defined in this text as one in which nickel is the plurality element, but not necessarily more than 50% of the total atomic or weight percent. Since there is not a systematic classification system similar to that for other alloy systems, Ni-base alloys are better known by their trade names or by the alloy name/number that was originally assigned by the alloy producer. The unified numbering system (UNS) number designated to each alloy allows cross-reference by chemical composition. The definition of a Ni-base alloy sometimes includes alloys that have significant additions of nickel, such as the low-expansion INVAR alloys, which are technically Fe–Ni alloys, or Alloy 800 and its derivatives, which are technically Fe–Ni–Cr alloys but have UNS numbers beginning with the letter N to indicate they are a part of the Ni-base alloy family. Since some of the Ni-base alloys that are used at high temperatures have such a good combination of elevated-temperature strength and corrosion resistance, they have become known as 'superalloys' (*8*).

www.iran-mavad.com
مرجع مهندسی مواد و متالورژی

Table 1 Overview of commercial Ni-base alloys and the main weldability concerns associated with each alloy system

Alloy family	*Alloy system*		*Commercial alloy examples*	*Main weldability concerns*
Corrosion-resistant	Solid-solution strengthened	Ni	Nickel 200	WM porosity
		Ni–Cu	400, K-500	WM porosity, solidification cracking
		Ni–Mo	B-2, B-3®	WM and HAZ corrosion
		Ni–Cr–Mo	G-35®, 59	WM and HAZ corrosion
		Ni–Cr–Mo–W	C-276, C-22®, 686	WM and HAZ corrosion
		Ni–Cr–Mo–Cu	C-2000®	WM and HAZ corrosion
		Ni–Mo–Cr	HYBRID-BC1®	WM and HAZ corrosion
High-temperature	Solid-solution strengthened	Ni–Fe–Cr	800H, RA330®, HR-120®	Liquation cracking
		Ni–Cr–Fe	600, 690	Ductility-dip cracking
		Ni–Cr–Fe–Mo	HASTELLOY X	Liquation cracking
		Ni–Cr–Mo–Nb	625, 625SQ®	Solidification cracking
		Ni–Cr–Co–Mo	617	Liquation cracking
		Ni–Cr–W–Mo	230®	Solidification and liquation cracking
		Ni–Co–Cr–Si	HR-160®	Solidification cracking
	Precipitation-strengthened	$Ni_2(Mo,Cr)$	242®, 244®	Solidification cracking
		γ'	Waspaloy, René 41, 282®	Strain-age cracking
		γ''	718, 718 Plus®	Solidification and liquation cracking
	Nickel aluminides	Ni_3Al	IC-25, IC-218	Solidification and liquation cracking
	Oxide-dispersion strengthened	Y_2O_3	MA754, MA6000	Oxide agglomeration/flotation
	Single-crystal superalloys	N/A	CMSX-4, TMS 162	Stray grain formation, solidification cracking

6.09.2 Welding Considerations

6.09.2.1 General Welding Considerations

If proper techniques and procedures are followed, welding of Ni-base alloys is usually successfully achieved without any undue difficulties. The development and qualification of welding procedures is suggested to achieve quality production welds. These procedures are usually required for fabrication to code requirements (e.g., American Society of Mechanical Engineers (ASME) Pressure Vessel and Piping Code) and should take into account parameters such as welding process, base and filler metals, joint design, preheat/interpass temperatures, and PWHT requirements. Any modern welding power supply with adequate output and controls may be used with the common arc welding processes. Generally, it is preferred that welding heat input be controlled in the low to moderate range. Stringer bead welding techniques, with some electrode/torch manipulation, are preferred; wide weave beads are not recommended.

Compared to other alloys, Ni-base alloys exhibit both gish welding and shallow penetration characteristics, which is mainly due to the low viscosity of molten nickel. Therefore, joint design and weld bead placement need to be carefully considered to ensure that proper weld bead fusion is achieved. Ni-base alloys also have a tendency to crater crack, so grinding of starts and stops is recommended. Another important aspect to achieve sound welds is cleanliness of the weld joint region. Contamination by grease, oil, corrosion product, lead, sulfur, and other low-melting-point elements can lead to severe cracking problems. It is suggested that the base metals are in the solution annealed condition prior to welding. Welding of materials that have a large amount of residual cold work can result in cracking in the weld metal (WM) and/or HAZ. Generally, annealing is not required if cold work is below 7% outer-fiber elongation.

The three most common welding processes that are used to join Ni-base alloys are gas tungsten arc welding (GTAW), gas metal arc welding (GMAW), and shielded metal arc welding (SMAW). In addition to these common welding processes, other welding processes such as flux-cored arc welding (FCAW), submerged arc welding (SAW), plasma arc welding, resistance spot welding, laser beam welding (LBW), and electron beam welding (EBW) are used. The plasma arc cutting process is commonly used to cut alloy plate into desired shapes and prepare the weld geometry. The use of oxyacetylene welding and cutting is not recommended because of carbon pickup from the flame. For all welding processes, weld parameter selection, as it relates to heat input, is extremely important due to the greater possibility of hot cracking as heat input increases.

Correct weld joint design is critical to the successful fabrication of Ni-base alloys. Poor joint design can negate even the most optimum selection of other welding parameters. Weld joint designs for Ni-base alloys are shown in **Figure 1**. A square-groove (not shown) does not require any joint preparation, but is generally limited to material thickness less than 3.2 mm. For joints where access to only one side of the joint is possible, such as the square-groove and single-v groove joints, GTAW is the suggested method for depositing the root pass even when GMAW or SMAW is being employed elsewhere. A J-groove design is acceptable for groove welds on heavy section plates (greater than 19 mm thickness) to reduce the amount of filler metal and time required to complete the

www.iran-mavad.com
مرجع مهندسی مواد و متالورژی

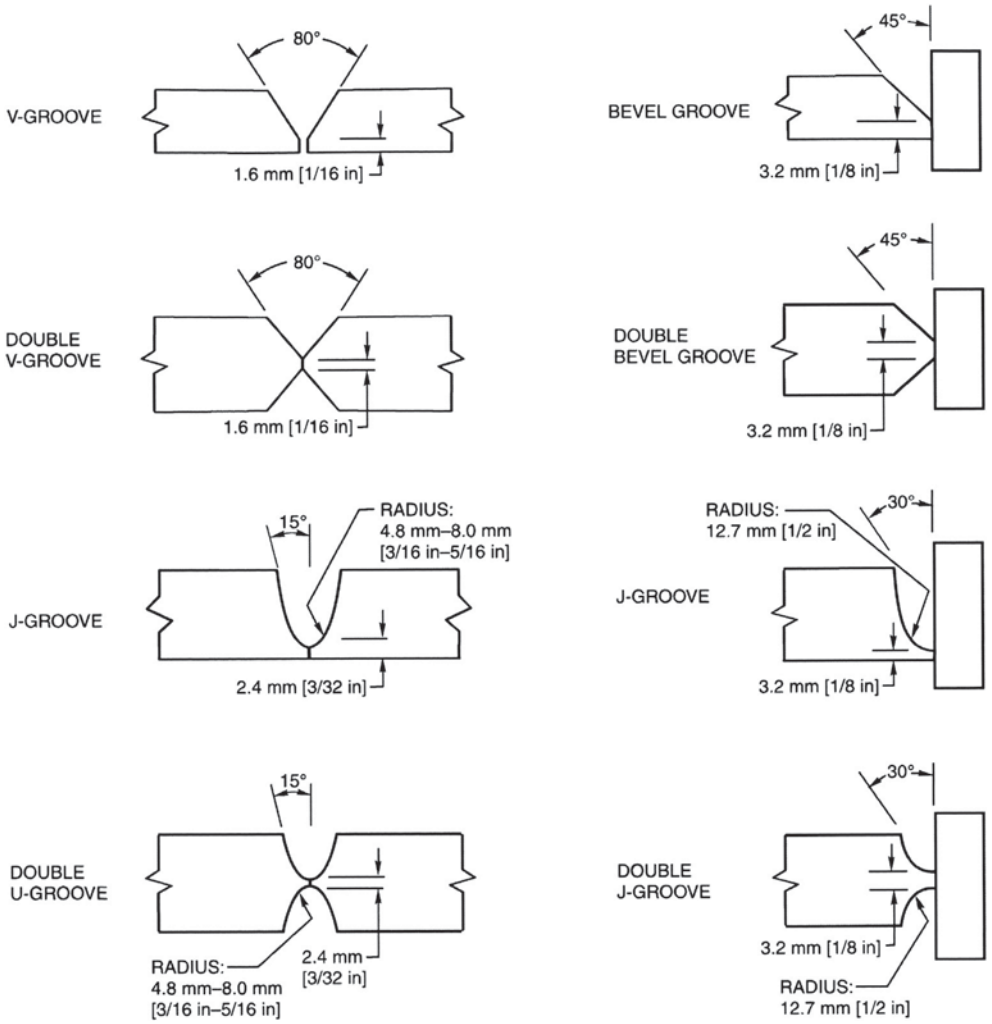

Figure 1 Weld joint designs for Ni-base alloys. From AWS G2.1M/G2.1:2012, Guide for the Joining of Wrought Nickel-Based Alloys.

weld. The actual number of passes required to fill the joint depends upon a number of factors that include filler metal size (electrode or wire diameter), power supply amperage, and travel speed.

While the welding characteristics of Ni-base alloys are similar in many ways to those of the austenitic stainless steels, there are some important differences that should be noted. For example, a Ni–Cr–Mo alloy such as C-276 (UNS N10276) alloy has lower thermal expansion, lower thermal conductivity, and higher electrical resistivity compared to an Fe–Cr–Ni alloy such as 304 (UNS S30400). Since Ni-base WM is comparatively 'sluggish,' meaning it is not as fluid compared to carbon or stainless steel, and does not flow out as readily and 'wet' the sidewalls, the welding arc and filler metal must be manipulated to properly place the molten metal. In addition to the sluggish nature of the weld pool, the shallow penetration characteristics of Ni-base alloys compared to that of stainless steel increase the possibility of incomplete fusion. The sluggish behavior of Ni-base WM must also be understood when considering weld joint design. Care must be taken to ensure that the groove opening is wide enough to allow proper electrode manipulation and placement of the weld bead to achieve proper fusion.

Proper preparation of the weld joint region is considered a very important part of welding Ni-base alloys. A variety of mechanical and thermal cutting methods are available for the preparation of weld angles. Potential processes include plasma cutting, machining, grinding, and air carbon arc gouging. It is necessary to condition all thermal cut edges to bright, shiny metal prior to welding, which is particularly important if air arc gouging is being used due to the possibility of carbon pickup from the carbon electrode, which is detrimental to weld soundness. In addition to the weld angle, a 25 mm wide band on the top and bottom (face and root) surface of the weld zone should be conditioned to bright metal prior to welding. This can be accomplished with an 80-grit flapper wheel or disk. Furthermore, the welding surface and adjacent regions should be thoroughly cleaned with an appropriate solvent, such as acetone, prior to any welding operation. All greases, cutting oils, crayon marks, machining solutions, corrosion products, paints, scale, dye penetrant solutions, and other foreign matter should be completely removed.

www.iran-mavad.com
مرجع مهندسی مواد و متالورژی

Cleaning of the WM between weld passes can be accomplished with stainless steel wire brushing. The grinding of starts and stops is recommended for all arc-welding processes. Any localized cracking should be removed by grinding prior to further welding. Attempting to remelt or 'wash-out' welding cracks is not recommended. If oxygen- or carbon dioxide-bearing shielding gas is used during GMAW, light grinding is necessary between weld passes prior to wire brushing. Slag removal during SMAW requires chipping and grinding followed by wire brushing. Surface iron contamination in the form of rust staining typically results from the contact of steel in the weld region. While this is not expected to be a serious problem for the performance of the weld joint, and it is usually not necessary to remove such rust stains prior to service, reasonable care should be exercised so as not to introduce iron contamination. If the iron or rust may act as a contaminant in the process that it serves, it should be removed from the surface.

Distortion characteristics of Ni-base alloys are similar to those of austenitic stainless steels. However, the lower coefficient of thermal expansion (CTE) of Ni-base alloys, compared to austenitic stainless steels, makes them less susceptible to distortion and residual stresses for a given weld geometry. To control distortion, jigs, fixturing, cross supports, bracing, bead placement, and weld sequence can be used. Balanced welding about the neutral axis should be employed where possible to assist in keeping distortion to a minimum. Proper fixturing and clamping of the assembly makes the welding operation easier and minimizes buckling and warping of thin sections. It is suggested that extra material be added to the overall width and length where possible. The excess material can then be removed after welding to obtain final dimensions.

Heating of Ni-base alloys prior to welding ('preheat') is generally not required. Preheat is usually specified only as room temperature. The base material may require warming to raise its temperature above freezing or to prevent condensation of moisture, which may occur, for instance, if the alloy is brought into a warm shop from cold outdoor storage. Warming should be accomplished by indirect heating if possible, such as infrared heaters or natural warming to room temperature. If oxyacetylene warming is used, the heat should be evenly applied over the base metal rather than being concentrated in the weld zone. The torch should be adjusted so that the flame is not carburizing. It is recommended that a 'rosebud' tip be used to evenly distribute the flame. Care should be taken to avoid local or incipient melting as a result of the warming process. The temperature between weld passes ('interpass temperature') should be maintained at relatively low levels, such as being maintained below 100–150 °C. To achieve this condition, auxiliary cooling methods can be used. Water quenching or rapid air cooling are preferred to cool the assembly; natural cooling is also permissible, although in some cases the weld zone will be in a deleterious intermediate temperature range for prolonged periods of time, which should be avoided if possible. In the vast majority of service environments, Ni-base alloys can be used in the as-welded condition and PWHT is not required. If deemed necessary, solution anneal or stress relief heat treatments can be employed. These temperatures are alloy dependent, with typical temperatures for solution annealing being in the 1050–1200 °C range. The intermediate temperature range (approximately 600–650 °C) where stress relief is effective may also promote secondary phase precipitation in the microstructure, which is detrimental to corrosion resistance and/or mechanical properties. For example, Ni–Mo alloys should never be heat treated in the 538–816 °C temperature range, which can cause intermediate temperature cracking.

6.09.2.2 Specific Welding Process Considerations

Process considerations specific to the more commonly used welding processes are discussed in this section. Suggested welding parameters for many processes are provided by material suppliers and are available in other references (9). The suggested parameters usually provide a suitable starting point in developing a qualified weld procedure, with the particular parameters for each situation being dependent on alloy, weld geometry, and welding equipment.

6.09.2.2.1 Gas Tungsten Arc Welding

Since the GTAW process is a very versatile, all-position welding process, it is often used to join Ni-base alloys. It offers high quality, low distortion welds that are free of spatter. It can be used with or without filler metal and can be completed manually or adapted to automatic equipment. It is a process that offers great control and is therefore routinely used during tack welding and root pass welding. The major drawback of GTAW is productivity, since manual GTAW WM deposition rates are low. It also requires more welder dexterity and hand–eye coordination than manual GMAW or SMAW.

Electrical polarity should be direct current electrode negative (DCEN). Two-percent thoriated tungsten electrodes (AWS A5.12 EWTh-2) are suggested. It is recommended that the electrode be ground to a cone shape (included angle of 30–60°) with a 1.6 mm flat ground at the point.

Welding-grade argon of 99.996% minimum purity is recommended as a shielding gas for all normal fabrication situations. Flow rates are normally in the 12–15 l min^{-1} range. To provide optimum shielding gas coverage of the weld puddle, the welding torch should be equipped with a gas diffuser screen ('gas lens'). Also, the gas cup should be as large as practical. When proper shielding is achieved, the as-deposited WM should have a bright-shiny appearance and require only minor wire brushing between passes. On special occasions, argon–helium or argon–hydrogen shielding gases are used in high travel speed, highly specialized mechanized welding systems. In addition to welding torch shielding gas, a 'back-purge' at the root side of the weld joint is employed with welding-grade argon with flow rates of 2.5–5 l min^{-1}. Copper backing bars are often used to assist in developing the desired bead shape on the root side of GTAW welds. Backing gas is often introduced through small holes along the length of the backing bar. In situations where backing bars cannot be used, such as pipe or tube circumferential butt welding, open-butt welding is often performed. When access to the root side of the joint is not possible, modified gas flow conditions can be used. The torch flow rates are reduced to approximately 5 l min^{-1} and the back-purge flow rates are increased to approximately 20 l min^{-1}.

www.iran-mavad.com
مرجع مهندسی مواد و متالورژی

It is recommended that the torch essentially be held perpendicular to the workpiece when welding. Stringer bead techniques are recommended, which use only enough current to melt the base material and allow proper fusion of the filler metal. During welding, the tip of the welding filler material should always be held under the shielding gas to prevent oxidation of the hot welding filler wire. Standing still or 'puddling' the weld adds to the welding heat input and is not recommended.

6.09.2.2.2 Gas Metal Arc Welding

The GMAW process offers a significant increase in productivity when compared to GTAW and is well suited to both manual and automatic welding situations. Although the level of control is reduced compared to GTAW, WM deposition rates and ease of operation are considerably higher. The modes of metal transfer that are possible with GMAW are (1) short-circuiting, (2) globular, (3) spray, and (4) pulsed spray. The selection of WM transfer mode requires information on joint design/thickness, welding position, desired deposition rates, and welder skill levels.

The short-circuiting transfer mode is used in all welding positions, provides good weld puddle control, and is considered to be a low heat-input welding process. However, since this transfer mode operates at the lowest range of amperage, it is more prone to incomplete fusion defects. The globular mode is mainly used only for weld overlay applications such as cladding. Spray transfer occurs at the highest current and voltage levels and is thus characterized as a moderate to high heat input welding process with relatively high deposition rates. Spray transfer is well suited to welding thick sections in the flat position due to its good fusion, high productivity, and low spatter characteristics. While spray transfer is less susceptible to incomplete fusion defects when compared to short-circuiting, its relatively high heat input can induce secondary phase precipitation in the HAZ of corrosion-resistant Ni-base alloys and reduce their as-welded corrosion resistance. Pulsed-spray mode is a variation of spray transfer in which the welding power is cycled from low to high levels. While spray transfer is still achieved at the highest current levels, the lower average power allows pulsed-spray welding to be used on thinner base metals and in all welding positions. Its main advantage relates to a lower average current that decreases overall weld heat input and its concomitant benefits. In order to produce the pulsed output, a specially designed power source is required. Electrical polarity in GMAW is direct current electrode positive (DCEP). Generally, shielding gas flow rates are in the 15–20 l min^{-1} range. To obtain optimum shielding, it is suggested that the welding torch gas cup be as large as possible. Shielding gases that can be used include pure Ar and mixes of Ar + He, Ar + He + CO_2, and He + Ar + CO_2. The gases containing CO_2 produce a very stable arc, excellent out-of-position welding characteristics, and excellent Ni-base to carbon steel welding characteristics. However, because carbon dioxide is present, the WM surface will be highly oxidized. This oxidized condition can increase the possibility of incomplete fusion defects. It is therefore strongly recommended that multi-pass welds made with CO_2-containing gases be lightly ground between passes to remove the oxidized surface. When using Ar + He mixes, the weld surface is expected to be bright and shiny with minimal oxidation. During multi-pass welding, it is not mandatory to grind between passes. If 100% Ar is used, some oxidation may be noted on the weld surface. Heavy wire brushing and/or light grinding (80 grit) between passes is recommended. As with GTAW, back-purging is required to ensure the root side of the weld joint is not heavily oxidized. As an alternative, fabricators may weld without back-purging if they grind the root side of the weld to remove oxidation.

6.09.2.2.3 Shielded Metal Arc Welding

The SMAW process is a manual welding process whereby an arc is generated between a flux-covered consumable electrode and the workpiece. This process is well known for its versatility because it can be used in all welding positions, and in both production and repair situations. Generally, it is not useful on thin sheet material. It requires no special equipment and can be easily operated in remote locations. The flux covering decomposes to generate a shielding gas and to provide fluxing elements to protect the molten WM. The electrode coating formulations vary depending on the particular alloy and are generally classified as slightly basic to slightly acidic. All electrodes are suitable for use in the AC or DC mode (AC–DC), but are recommended to be used with DCEP electrical characteristics. So that the electrode coating does not absorb moisture, it is important that all electrodes be stored in a dry rod oven, maintained at approx. 120–200 °C, after the canister has been opened. This is especially important in humid conditions and for low-moisture coating formulations.

For maximum arc stability and control of the molten puddle, it is important to maintain a short arc length. The electrode is generally directed back toward the molten puddle (backhand welding) with a 20–40° drag angle. Stringer bead welding techniques are typical with some electrode manipulation to place the molten WM where needed. During vertical welding, the weave bead technique and larger diameter electrodes are used to maintain a relatively flat bead profile. It is particularly important that when welding Ni-base alloys, all starts and stops be ground to sound WM. Starting porosity, which may occur because the electrode requires a short time to begin generating a protective atmosphere, can be minimized by using a starting tab of the same alloy as the workpiece or by grinding each start to sound WM. Small crater cracks may also occur at the stops, which can be minimized by using a slight back-stepping motion to fill the crater just prior to breaking the arc.

6.09.2.2.4 Submerged Arc Welding

The advantages of the SAW process are attractive to many fabricators, which compared to GMAW include higher deposition rates, thicker weld beads, better arc stability, and smoother weld surfaces. Furthermore, it is attractive from a safety point of view because the welder is not exposed to the arc since it is concealed by the flux and virtually no welding fume is generated. Unfortunately, the SAW process is generally not recommended by Ni-base alloy producers since the high heat input to the base metal and slow cooling of the weld act to increase weld restraint and promote cracking. It has been successfully used to join solid-solution alloys such as

www.iran-mavad.com
مرجع مهندسی مواد و متالورژی

Alloys 400 and 600. Even so, it is mainly limited to thick-section welds (greater than 12.7 mm thickness). It should not be considered for joining precipitation-strengthened alloys.

GMAW spool wire is used to complete the weld, with larger diameters being employed at higher weld heat inputs. The SAW process can be used with either DCEP or DCEN. For butt welding, DCEP is preferred because it produces a flatter weld bead with deeper penetration. For weld overlay applications, DCEN is preferred because it gives a higher deposition rate with lower penetration.

The type of flux plays a crucial role in the success of welding and should be carefully selected for each alloy/wire. Crucial alloying elements such as Cr can be lost during welding. The chemistry of the weld deposit can suffer due to the pickup of silicon from the flux, which further exacerbates weld solidification cracking susceptibility.

6.09.2.2.5 Flux-Cored Arc Welding

Some Ni-base alloys are joined by the FCAW process, which provides for higher deposition rates in all-position welding than SMAW or GMAW, with less operator skill required. Disadvantages include slag detachment and higher welding fume generation rates. The equipment and setup is either identical or very similar to that used for GMAW. While the use of FCAW is generally limited in Ni-base alloys, more applications are being identified to utilize its advantages. These include welding and cladding of power generation vessels, dissimilar welding of offshore platform components, and joining of corrosion-resistant alloys in the petrochemical industry. At the current time, alloys 600 and 625 are among the Ni-base alloys that are joined with FCAW. Commercial electrodes for both gas-shielded and self-shielded processes are available for these alloys.

6.09.2.2.6 Electron Beam and Laser Beam Welding

High energy density beam welding processes offer the advantages of low heat input, high weld depth-to-width ratio, narrow HAZ, and reduced distortion. Most Ni-base alloys that can be joined with conventional arc welding processes can be joined with EBW and LBW. These processes typically provide better overall weld properties compared to arc welding. It is even considered more suitable for some alloys that are difficult to arc weld. This may be attributed to the shorter time spent in the solidification temperature range. However, joint preparation and fit-up are especially important with these processes. As well, EBW generally needs to be performed in a vacuum environment, which limits its applicability. Porosity can be a weldability issue due to the rapid solidification rates and deep weld pools that do not readily allow for dissolved gases to escape; this effect is promoted by high weld travel speeds. Agitation of the weld pool by the weaving of the beam may help the gases to escape and reduce porosity. Susceptibility to liquation cracking in the 'nail-head' region of the HAZ is a particular weldability problem due to the stress/strain state in this region. Slower weld travel speeds are beneficial toward reducing liquation cracking susceptibility, as it produces a shallower temperature gradient whereby the stress/strain experienced in a given location of the partially melted zone (PMZ) is reduced.

6.09.2.3 Examples of Relevant Welding Codes and Standards

There are many national and international codes and standards that are relevant to the welding and joining of Ni-base alloys. The ASME code is typically followed for welding of pressure vessels, whereas the American Petroleum Institute (API) code is followed by the oil and gas industry. The American Welding Society (AWS) publishes approximately 300 standards and technical documents with several exclusively written for Ni-base alloys. The International Organization for Standards (ISO) publishes many standards that are internationally recognized and accepted. A condensed list is provided below that shows some of the commonly used codes for joining nickel and its alloys. This list is not meant to be all-inclusive, but merely to provide a source for the reader of this chapter to pursue.

American Society of Mechanical Engineers

ASME Boiler and Pressure Vessel Code, Section II-B: Provides material specification for nonferrous materials used in pressure vessel construction.

ASME Boiler and Pressure Vessel Code, Section IX: Provides welder and procedure qualification guidelines.

American Petroleum Institute

API RP 582 Recommended Practice and Supplementary Welding Guidelines for the Chemical, Oil, and Gas Industries.

American Welding Society

AWS A5.11/A5.11M Specification for Nickel and Nickel-Alloy Welding Electrodes for SMAW.
AWS A5.14/A5.14M Specification for Nickel and Nickel-Alloy Bare Welding Electrodes and Rods.
AWS A5.34/A5.34M Specification for Nickel-Alloy Electrodes for FCAW.
AWS B2.1/B2.1M Specification for Welding Procedure and Performance Qualification.
AWS B4.0M Standard Methods for Mechanical Testing of Welds.
AWS D17.1/D17.1M Specification for Fusion Welding for Aerospace Applications.
AWS G2.1M/G2.1 Guide for the Joining of Wrought Nickel-Based Alloys.

International Standards Organization

ISO 5817 Welding – Fusion-welded joints in steel, nickel, titanium and their alloys (beam welding excluded) – Quality levels for imperfections.

www.iran-mavad.com
مرجع مهندسی مواد و متالورژی

ISO 9606-4 Approval testing of welders – Fusion welding – Part 4: Nickel and nickel alloys.

ISO 14172 Welding consumables – Covered electrodes for manual metal arc welding of nickel and nickel alloys – Classification.

ISO 15792-1 Welding consumables – Test methods – Part 1: Test methods for all-WM test specimens in steel, nickel and nickel alloys.

ISO 18274 Welding consumables – Solid wire electrodes, solid strip electrodes, solid wires and solid rods for fusion welding of nickel and nickel alloys – Classification.

6.09.3 Discontinuities in Ni-Base Weldments

Weld quality is highly dependent on the considerations that are made prior to fabrication. The welding procedures and practices should be carefully developed and meticulously followed not only to meet design specifications, but to ensure welds are free of unacceptable discontinuities. The presence of weld discontinuities can influence the fitness-for-service of the fabricated component, particularly with respect to fatigue life and corrosion resistance. Inspection and maintenance should also be considered when allowable discontinuities are present during the service life of the component. This section examines some of the more prevalent weld discontinuities that are formed during fabrication of Ni-base alloys with fusion welding processes.

6.09.3.1 Weld Process- or Procedure-Related Defects

Defects can occur in Ni-base weldments due to the welding process or procedure. One possible defect is porosity, which can develop in Ni-base WM due to contamination by hydrogen, oxygen, nitrogen, or carbon monoxide. Commercially pure (CP) Ni and Ni–Cu alloys are particularly susceptible to porosity, especially when welded autogenously (without filler metal). To achieve porosity-free autogenous welds in these alloys, it is important that the weld puddle is properly shielded by use of dry torch gases and sufficient shielding gas flow rates. To alleviate the issue of porosity, weld filler metals for welding CP Ni and Ni–Cu alloys are alloyed with gas-absorbing elements aluminum and titanium. For example, the AWS A5.14 ERNi-1 electrode that is used to weld Nickel 200 contains a maximum of 1.5 wt% Al and 2.0–3.5 wt% Ti. Both aluminum and titanium combine with oxygen and nitrogen to form oxides and nitrides, thereby controlling porosity in the WM. Since most of the other Ni-base alloys contain Cr, which has a natural affinity for the gases that are formed during welding, they are not as susceptible to porosity. Formation of gas holes can occur due to hydrogen pickup from moisture or dissociation of hydrocarbons. This form of porosity can be minimized by keeping the weld joint area and filler metal dry and free of hydrocarbon contaminants. Nitrogen-induced porosity occurring from nitrogen pickup from air is mainly related to improper or insufficient shielding of the weld pool. The susceptibility to this form of porosity is mainly related to the extent of nitrogen solubility in the particular alloy. In order for carbon monoxide to form in the weld pool, all of the deoxidizing elements such as aluminum and silicon would have to be depleted, making this an unlikely cause of WM porosity in Ni-base WM.

Inclusions in Ni-base WM can form as a result of oxides that become trapped in the weld pool. This can occur from the tenacious oxide film that forms on the surface of most Ni-base alloys. Since the melting temperatures of surface oxides are usually much higher than the base metal, they are more likely to stay solid during welding and become mixed in the weld pool. For example, pure nickel melts at 1455 °C, while NiO and Cr_2O_3 melt at much higher temperatures of 1982 and 2260 °C, respectively. Thus, it is especially important that surface oxides be removed prior to welding and between passes in multi-pass welds. Tungsten inclusions can be produced in the WM during GTAW if the tungsten electrode accidently contacts the molten weld pool or if there is excessive weld current. Elements with a strong affinity for oxygen such as aluminum or magnesium can combine with oxygen to form oxide inclusions in the WM. Slag inclusions are associated with flux processes such as SMAW, SAW, and FCAW. These inclusions form in the WM when residual slag becomes entrapped in cavities or pockets that form due to inadequate weld bead overlap, excessive undercut at the weld toe, or an uneven surface profile of the preceding weld bead. The entrapped slag is not melted out during subsequent weld passes. Thus, an important consideration in flux processes is the ease with which the slag can be removed between weld passes. Inclusions must be ground out from the weld or they will act to initiate fracture prematurely, which can have a detrimental effect on mechanical properties.

Other common process-related defects that are encountered in Ni-base welds are undercut, incomplete fusion/penetration, and distortion. These defects are generally attributed to improper welding technique and/or welding parameters. Undercut is a groove that is melted into the base metal, usually at the root or toes of the weld, and can occur due to excessive welding current. This discontinuity creates a notch at the periphery of the weld and can significantly weaken the strength of the weldment. As previously discussed, incomplete fusion/penetration is a common defect in Ni-base welds due to the sluggish nature of the WM and the poor penetration characteristics. Although distortion can occur in a weldment, Ni-base alloys are less susceptible than comparable austenitic stainless steel weldments because of their lower CTE.

6.09.3.2 Metallurgical-Related Defects

Metallurgical phenomena that occur during fabrication of Ni-base alloys can lead to formation of various types of defects in the fusion zone (FZ), PMZ, and HAZ. The sluggish behavior of weld deposits may result in formation of an unmixed zone (UMZ). **Figure 2** illustrates a schematic representation of the various regions in a fusion weld (*10*). It is recognized that the magnitude of metallurgical

www.iran-mavad.com
مرجع مهندسی مواد و متالورژی

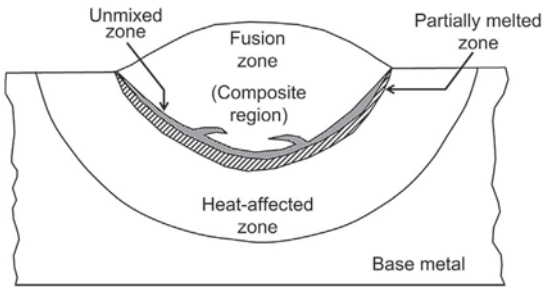

Figure 2 Schematic representation of the regions in a fusion weld. Adapted from Baeslack, W. A.; Lippold, J. C.; Savage, W. F. *Weld. J.* **1979,** *58*, S168.

phenomena occurring in the various weld regions is sometimes controlled by the welding process conditions, and adjustments to the welding parameters can often alleviate or exacerbate the formation tendency of these defects. However, the defects to be discussed in this section mainly form as a result of metallurgical phenomena that are often associated with the temperature range in which they occur. Weld cracking in Ni-base alloys is typically grouped into two categories, namely 'hot cracking,' which is associated with some form of liquid film embrittlement, and 'warm cracking,' which is associated with elevated temperatures where no liquid is present in the system.

Hot cracking phenomena are associated with a metallurgical structure consisting of both solid and liquid phases. Hot cracking refers to two distinct forms of cracking discussed below that include weld solidification cracking and liquation cracking in the HAZ and WM. WM typically refers to the FZ, except when it is reheated in multi-pass welds. Since liquid must be present for hot cracks to form, these defects are associated with the FZ and PMZ, i.e., regions of the weldment where the microstructure is subjected to temperatures at or above the effective solidus temperature. The solidus occurs at a discrete temperature in pure metals, and more aptly in the Ni-base alloys, the solidus occurs over a range of temperatures. The solidus temperatures in Ni-base alloys are defined on the equilibrium phase diagram appropriate for the particular alloy system. Many of the Ni-base alloys contain eutectic compounds. The eutectic composition has the lowest solidus temperature in the system. This is important, because the presence of a eutectic can effectively suppress the temperature at which an alloy solidifies, which often promotes hot cracking. As previously noted, even minute additions of impurities such as sulfur and phosphorus form eutectic compounds with melting points far below that of the nickel alloy itself. These impurities are typically most detrimental to the formation of hot cracks.

Cracks that form at elevated temperatures below the solidus temperature, i.e., in the solid-state, are found in the FZ and HAZ. Consequently, such defects are not associated with the liquid phase and are typically related to microstructural phase transformations or other physical phenomena that cause embrittlement of the microstructure. Ni-base alloys are primarily susceptible to two forms of solid-state cracking discussed in this section: ductility-dip cracking and strain-age cracking.

The mechanical metallurgy of welds is also related to each form of weld cracking in the Ni-base alloys. Metallurgical-related defects in welds are associated with a loss of ductility in the microstructure, due either to the presence of liquid or other embrittling phenomena. **Figure 3** shows a schematic representation of weld ductility in a fusion weld as a function of temperature. Solidification and liquation cracking are associated with the brittle temperature range (BTR) and ductility-dip cracking is associated with the ductility-dip temperature range (DTR). These regions are approximated with the liquidus temperature (T_L) and solidus temperature (T_S). Given that temperature is distributed spatially in a weld, the cracks associated with each embrittlement region occur in different physical locations of the weld, as shown.

Aside from the physical region where cracking is observed (e.g., FZ, HAZ, etc.), metallographic evaluation of cracking is key to understanding the mechanism of crack formation. FZs in austenitic alloys such as Ni-base alloys contain three distinct boundary types. These boundary types are illustrated in **Figure 4** (*11*). Solidification subgrain boundaries (SSGBs) are low misorientation angle boundaries resulting from perturbations of the solid–liquid interface at the trailing edge of the weld pool and define the intersection of cells or cellular-dendrites. They typically have compositional gradients as a result of the microsegregation process during solidification, and the tendency of particular alloying elements to segregate to cell/dendrite cores or boundaries depends on the solute redistribution coefficient, k, which is defined as the ratio of the composition of the solid (C_S) to the composition of the liquid (C_L), i.e., $k = C_S/C_L$. Enrichment or depletion of a particular solute occurs if the value of k is less than or greater than unity and is typically described with the Scheil–Gulliver solidification model (*12*). The second boundary type is the solidification grain boundaries (SGBs), which are typically high-misorientation angle boundaries that define the intersection of packets of cells/dendrites at the trailing edge of the weld pool. These boundaries have a significant composition component from macrosegregation. Solidification cracking typically occurs along the SGBs and less frequently on the SSGBs. The third type of boundary is the migrated grain boundary (MGB). These boundaries result when a grain growth-like phenomenon occurs to reduce the energy associated with the tortuous SGB surface area. The effective grain boundary area is reduced as the SGB's crystallographic component 'migrates' away from the compositional component as the weld cools through lower temperatures, is reheated by subsequent passes, or undergoes a PWHT. There is little impediment to this migration behavior in single-phase WMs. When secondary phases are present in Ni-base alloys, they can inhibit migration by pinning the boundary. The ductility-dip cracking phenomenon occurs along the MGB.

www.iran-mavad.com
مرجع مهندسی مواد و متالورژی

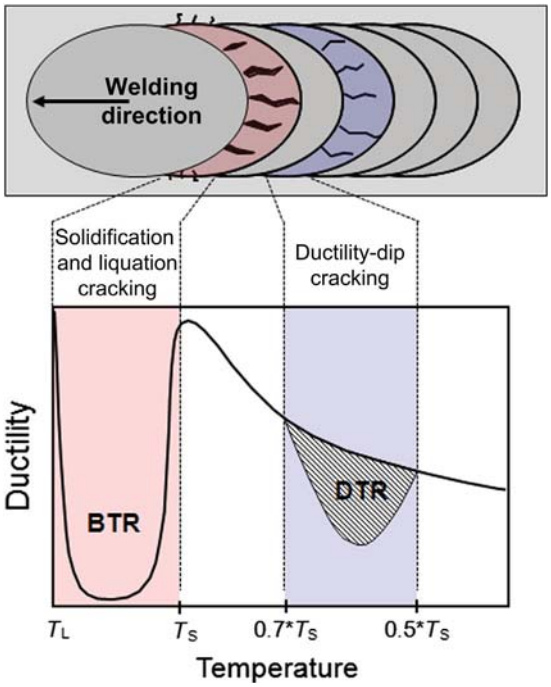

Figure 3 Schematic representation of weld ductility as a function of temperature and two temperature regions where weld cracking occurs in Ni-base alloys.

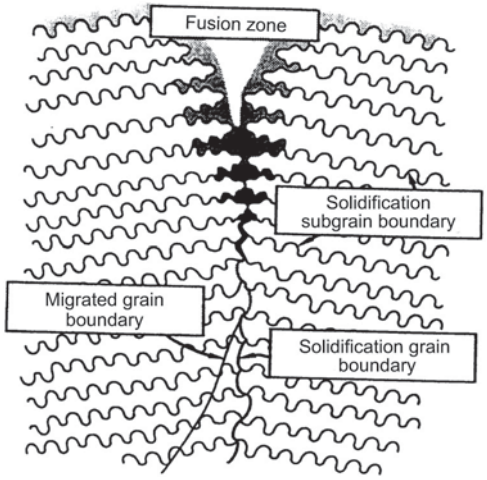

Figure 4 Types of weld metal boundaries observed in austenitic weld metals. Adapted from Lippold, J. C.; Clark, W. A. T.; Tumuluru, M. In *The Metal Science of Joining*, Proceedings of a Symposium Sponsored by the TMS Solidification Committee/MDMD and the Physical Metallurgy Committee/SMD; Cieslak, M. J., Perepezko, J. H., Kang, S., Glicksman, M. E., Eds.; TMS: Cincinnati, OH, 1991.

6.09.3.2.1 Weld Solidification Cracking

Ni-base alloys solidify as austenite from the liquid phase. The FCC crystal structure of the austenite phase is tight-packed and has lower solubility and diffusivity for solute elements than many ferritic alloys, which have the body-centered cubic structure. This gives the Ni-base alloys the tendency to segregate alloying elements during solidification, and strongly promotes solidification cracking in the WM. Segregation results in the distribution of low-melting-temperature liquid films along the SGBs during the terminal phase of solidification. Solidification-induced shrinkage of the FZ causes accumulation of tensile strains across the weld, which can separate the grains at boundaries containing continuous coatings of liquid. The temperature range over which an alloy is susceptible to solidification cracking (and liquation cracking) is defined as the BTR, which is schematically shown in **Figure 3** in Section 6.09.3.2 above. Cracking typically occurs in the low-temperature region of the BTR where the microstructure mostly contains the solid austenite phase, but also sufficient liquid distributed at the SGW.

www.iran-mavad.com
مرجع مهندسی مواد و متالورژی

Metallographic evaluation of the cracks reveals that they have an intergranular morphology and typically occur along SGBs and SSGBs. An example of a solidification crack in a Varestraint sample of 242 alloy is shown in Figure 5. Investigation of the fracture surface features reveals a dendritic structure that is associated with the liquid film present along the grain boundary at the instant of strain-induced grain separation. Weld solidification cracks are typically identified by these features. Many of the Ni-base alloys form low volume fractions of eutectic, resulting in liquid films distributed along the SGW at the end of solidification. This is a metallurgical structure that is highly susceptible. Alloys that form a significant volume fraction of eutectic at the end of solidification can exhibit crack healing, where additional liquid is pulled into the solidification crack front by, e.g., capillary forces. The crack can be completely healed with the eutectic liquid in this manner. Some alloys exhibit crack healing behavior whereby the eutectic constituent penetrates down the tip of the crack.

Weldability is typically governed by the combination of thermally induced weld deformation and microstructure in the two-phase liquid + solid region at the trailing edge of the weld pool. Successful control of cracking requires managing of these factors as discussed below.

6.09.3.2.1.1 Solid-Solution Strengthened Alloys

Solid-solution strengthened alloys typically possess good weldability. Alloys that do not form eutectic compounds, such as those based on the Ni–Cu and Ni–Fe–Cr systems, typically exhibit a narrow BTR. The solidification cracking tendency is mostly governed by the impurity content (sulfur, boron, and phosphorus). The binary equilibrium phase diagrams of Ni–S, Ni–B, and Ni–P metallurgical systems exhibit low-melting-point eutectics, which can effectively widen the BTR. The phase diagrams also exhibit the presence of many intermetallic phases indicating the low solubility of these elements in nickel. Low solubility promotes interdendritic segregation and liquid film formation at the grain boundaries. Higher alloyed materials containing elements such as Mo and Nb tend to form interdendritic eutectics (such as Laves phase, Sigma phase, and NbC) at the end of solidification. The eutectic liquids can suppress the effective solidus temperature of the material, which tends to widen the physical dimensions of the mushy zone during welding. Lippold et al. have studied the weldability of five solid-solution Ni-base alloys with the Transvarestraint weldability test (*13*). They found a good correlation between the solidification temperature range calculated with Scheil–Gulliver simulations, and the solidification cracking temperature range (SCTR) parameter determined during Transvarestraint testing. The SCTR estimates the BTR for a given set of welding conditions. In general, the alloys that solidify over a wider temperature range are more susceptible to cracking. Techniques such as the Varestraint test allow a qualitative classification of solidification cracking susceptibility such as that proposed by DuPont et al. (*4*), and shown here in Table 2. The table shows a simplistic view on the solidification cracking tendency based on solid-solution alloying additions.

6.09.3.2.1.2 Precipitation-Strengthened Alloys

The cracking tendency of the Ni-base superalloys is typically controlled by minor alloying additions and impurities. To enhance the grain boundary creep properties, minor additions of B, Hf, Zr, and C are made to the superalloys. Impurities such as P and S are minimized, as they have to metallurgical benefit and only promote weldability concerns. Alloys strengthened with γ'' contain Nb. Cracking susceptibility typically increases as the alloying levels of each of these elements increases since they strongly segregate to the interdendritic regions and grain boundaries during solidification. Since all of these alloying elements are intentionally included for promoting high-temperature properties (except S and P), little can be done to control the solidification cracking except for process and design considerations.

6.09.3.2.1.3 Metallurgical Considerations

The presence of liquid films along the grain boundaries is largely responsible for solidification cracking. Liquid volume fraction, grain boundary area (grain size), and film wetting characteristics are important components that control the nature of the film behavior. Volume fraction, and distribution of liquid, can be predicted with solidification simulations such as with the Scheil–Gulliver equation. The solidification models are typically dependent on solute redistribution coefficients, although the weld thermal gradient can also play a role in how liquid phase is distributed in the weld. A steeper thermal gradient minimizes the

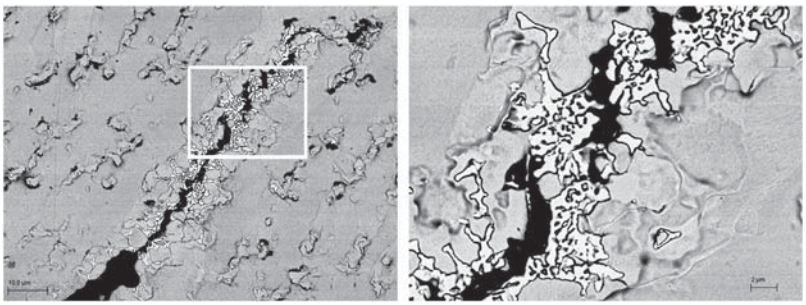

Figure 5 Weld solidification crack in a Varestraint sample of 242 alloy. Cracking is associated with the Mo-rich carbide eutectic phase that forms at the end of solidification.

www.iran-mavad.com
مرجع مهندسی مواد و متالورژی

Table 2 Classification of solidification cracking susceptibility in several Ni-base alloys

	Cracking susceptibility		
Alloy type	*Low*	*Moderate*	*High*
Ni alloys	200, 270, 271, 280		
Ni–Cu	400		
Ni–Mo	B2, B3		
Ni–Cr		600, 601, 230	
Ni–Cr–Mo	C-4, C-22, C-276, C-2000	Hast W,242, Hast X,617	
Ni–Cr–Mo–Nb		625	
Ni–Co–Cr–Si			HR-160

From DuPont, J. N., Lippold, J. C., Kiser, S. D. *Welding Metallurgy and Weldability of Nickel-Base Alloys*, John Wiley & Sons: Hoboken, NJ, 2009.

physical size of the two-phase liquid + solid region (i.e., the mushy zone). Liquid-film wetting behavior is controlled by the surface tension at the liquid–solid interface. Grain size is important, since long straight grain boundaries can be more easily wet by the liquid films, whereas a smaller grain size can prevent liquid film penetration along a grain boundary. Controlling sulfur typically reduces wetting of the liquid films as sulfur is a surface-active component in the Ni-base alloy metallurgical systems. Other minor impurities such as phosphorus and boron can contribute to solidification cracking as they form low-melting eutectics with nickel.

6.09.3.2.1.4 Process and Design Considerations

Solidification cracks can occur in single-pass and multi-pass welds. Increasing weld travel speed tends to increase cracking susceptibility since the weld pools shape is altered from an elliptical shape to a 'teardrop' shape at the trailing edge of the weld pool of austenitic materials. This behavior is illustrated in **Figure 6(a)** (*14*). The teardrop weld pool results in a distinct centerline along the weld where segregation is enhanced and transverse stresses can be high. Reduction of weld travel speed, use of pulsed current power supplies, or weaving the weld bead can be effective at eliminating the teardrop shape. Weld geometry plays a key role as large concave weld beads are more susceptible than small convex weld beads. This is illustrated in **Figure 6(b)**. Note the tensile stress across the large concave bead and resulting solidification crack. Small convex beads tend to have lower tensile stresses along the outer fibers and tend to exhibit no cracks. Application of smaller convex weld beads can reduce productivity, but will also help reduce stresses across the weld that result in solidification cracking. Reduction of weld heat input will have some effect as the thermal gradients will become steeper than those in high heat input welds. This restricts the size of the 'mushy' zone at the trailing edge of the weld pool. Weld bead depth-to-width ratio can play a significant role too, in that narrow, deeper penetration welds experience significantly higher transverse stresses during cooling than those with a proper depth-to-width ratio where stresses are radially distributed from the weld. This is illustrated in **Figure 6(c)**.

6.09.3.2.2 Liquation Cracking

The metallurgical basis for liquation cracking involves the presence of continuous liquid films at grain boundaries. Liquation cracking may occur either in the HAZ or reheated WM. The simultaneous presence of continuous liquid films and a critical level of restraint are necessary to induce cracking. If these liquid films are unable to accommodate the strains that accompany thermal and mechanical restraints during cooling, a crack forms along a grain boundary. The likelihood of grain boundary liquation is increased by welding process parameters that result in relatively high heat inputs, such as GMAW spray transfer mode. However, reducing

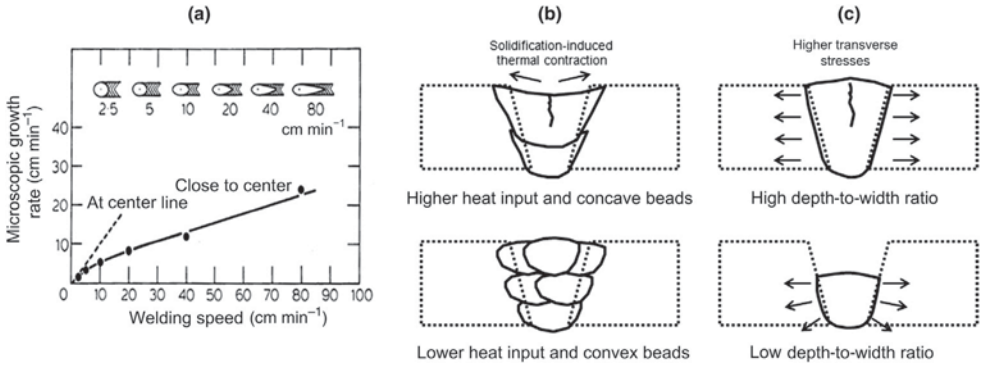

Figure 6 The effects of welding process and design variables including: (a) Travel speed on weld pool shape (Reproduced from David, S. A.; Vitek, J. M. *Int. Mater. Rev.* **1989,** *34,* 213); (b) Heat input and bead shape on solidification cracking; (c) Bead depth-to-width ratio on solidification cracking.

www.iran-mavad.com
مرجع مهندسی مواد و متالورژی

HAZ liquation cracking susceptibility is best achieved by adjusting material composition and microstructure. This form of cracking is sometimes referred to as 'microfissuring' due to the relatively small crack sizes that are observed.

All engineering alloys melt and solidify over a range of temperatures and, in general, this range is wider with increased alloy content. Since Ni-base alloys are highly alloyed, they exhibit relatively wide melting and solidification temperature ranges. During the weld thermal cycle, the base metal adjacent to the WM experiences a range of peak temperatures that are between the liquidus and solidus temperatures of the alloy. Since nonequilibrium conditions occur during the weld thermal cycle, the microstructure in this region is susceptible to partial melting and is termed the PMZ.

The two major mechanisms responsible for HAZ liquation cracking in Ni-base alloys are the segregation and penetration mechanisms (*12*). In both of these mechanisms, grain boundary melting occurs due to the suppression of its local melting temperature. In the segregation mechanism, alloy and/or impurity elements segregate to the HAZ grain boundaries through diffusion. In the penetration mechanism, localized melting that occurs in the microstructure is intersected by a mobile grain boundary, which leads to liquid penetration and wetting of the grain boundary. The penetration mechanism occurs in Ni-base alloys containing secondary phases, such as carbides, intermetallics, and other solute-rich precipitates. The two forms of the penetration mechanism are constitutional liquation and eutectic melting. While constitutional liquation and eutectic melting are more commonly associated with precipitation-strengthened alloys, these mechanisms can occur in solid-solution strengthened alloys since they sometimes contain remnant constituents from the original melting or casting process that do not dissolve during subsequent thermal-mechanical processing.

For solid-solution strengthened alloys that are primarily single-phase austenite, segregation of solute elements is the dominant mechanism leading to HAZ liquation cracking. While the grain boundaries of solid-solution strengthened alloys typically experience some liquation in the PMZ due to solute element segregation, it is the formation of continuous liquid films that ultimately results in HAZ liquation cracking. The segregation of impurity elements such as sulfur, phosphorus, and boron to grain boundaries is expected to occur to a certain extent in the HAZ of all Ni-base alloys. To avoid cracking, impurities should be held to levels as low as possible, which can be promoted by utilizing double-melting techniques. While some elements, such as sulfur and phosphorus, are always considered impurities, boron is intentionally added to some Ni-base alloys to improve creep strength (*6*). The significant effect of boron on liquation cracking was well exhibited by the hot-ductility results from two heats of HAYNES® 214® alloy, which is a solid-solution strengthened Ni–Cr–Al–Fe alloy that exhibits excellent oxidation resistance. The two heats of 214 alloy were identical except for an increase in boron from 0.0002 to 0.003 wt% (*15*). The temperature range that exhibited zero ductility expanded by a factor of five for the higher-boron heat. The liquation cracking susceptibility may also be dependent on the grain boundary character, where segregation is higher for high-angle boundaries compared to low-angle boundaries, such as twin boundaries (*16*). Grain growth within the HAZ also contributes to increased grain boundary segregation as solute elements are 'swept' into the boundary as it migrates. The amount of grain growth is a function of the initial base metal grain size, the amount of cold work, and the HAZ thermal cycle, which is determined by weld heat input. During optical metallographic examination of a polished and etched sample, the solidified solute-rich grain boundaries in the PMZ often appear as thick boundaries.

Constitutional liquation was first proposed by Pepe and Savage (*17*), and involves the reaction between a 'constituent' particle and the surrounding matrix to create a composition gradient around the particle. The composition of the reaction zone then undergoes melting below the melting temperature of the surrounding matrix. The rapid heating of the weld thermal cycle does not allow sufficient time for complete dissolution of the secondary phase within the austenite matrix. Furthermore, the constituent particle does not melt; rather it is an intermediate composition in the reaction zone that melts. When the interfacial liquid film reaches the eutectic composition, this represents the onset of constitutional liquation. The detailed mechanism of constitutional liquation is explained in more detail elsewhere (*4*). The earliest studies by Owczarski et al. (*18,19*), in order to better understand HAZ cracking, found that as MC and M_6C carbides (where M represents a metal such as molybdenum, niobium, or titanium) decomposed during the rapid heating of the weld thermal cycle, constitutional liquation occurred in the vicinity of the carbides. The constitutional liquation mechanism has been observed in several different Ni-base alloys, including precipitation-strengthened alloys such as Waspaloy and 718 alloys, and solid-solution strengthened alloys such as alloy X and alloy 625.

Another form of the penetration mechanism involves localized melting of residual eutectic constituents. The rapid heating associated with the weld thermal cycle does not allow for dissolution of the eutectic constituent and it melts when the temperature exceeds the eutectic temperature. When the maximum solid solubility of the alloy is exceeded by the eutectic composition, the eutectic constituent cannot dissolve without localized melting occurring, regardless of the heating rate.

Localized melting in the microstructure is not sufficient to promote cracking. The penetration mechanism requires the intersection of the liquid with moving grain boundaries. It is also essential that the liquid species penetrate and wet the boundary to create a continuous liquid film that limits solid–solid contact along the grain boundaries.

The susceptibility of an alloy to liquation cracking is a function of the amount of liquid that forms, the liquation temperature range, and the penetration/wetting characteristics of the liquid. Of the two forms of liquation, the penetration mechanism usually results in greater cracking susceptibility since it generally produces more liquid that ultimately melts and solidifies at lower temperatures. The distance to which liquid films are present in the PMZ is also dependent on the temperature gradient in the HAZ, which is influenced by weld heat input.

Liquation cracking susceptibility has been shown to be linearly dependent on grain size (*20*). The benefits of a finer grain size toward improved HAZ liquation cracking resistance is based on strain accommodation and liquid distribution arguments. Since the total grain boundary area increases with a decreased grain size, a smaller fraction of the total strain is required to be accommodated by a given grain boundary and grain boundary triple points. This reduces the potential for grain boundary sliding and crack

www.iran-mavad.com
مرجع مهندسی مواد و متالورژی

initiation. Below a critical level of strain, the grain boundary is not expected to crack. Furthermore, for a fixed volume percent of liquid, the liquid boundary film is expected to be thinner or discontinuous with a finer grain size. Liquid discontinuity increases the extent of solid–solid contact at the grain boundaries. Larger grain sizes promote thicker liquid layers, which require longer time periods to resolidify on cooling and increase the region over which the alloy exhibits essentially zero ductility in the HAZ. Thus, control of grain size should be considered for improved HAZ liquation cracking resistance in any Ni-base alloy. This can be particularly effective in concert with low heat input welds, where HAZ grain growth is inhibited by relatively rapid heating and cooling rates. In high heat input welds, grain growth will be more pronounced and the alloy more prone to metallurgical phenomena, leading to HAZ liquation. While a finer grain size will generally have a favorable effect on material properties, it may adversely affect creep resistance, and thus may not be a suitable strategy for limiting HAZ liquation cracking in alloys operating at elevated temperatures.

Minimization of welding restraint can be the most effective method for controlling liquation cracking in highly susceptible alloys. This can be achieved through optimized weld joint design. Also, low heat-input welding parameters reduce the amount of thermal expansion and contraction experienced by the WM and HAZ regions, thereby lowering the amount of thermal strain.

Liquation cracking in the WM occurs in the same manner as described for HAZ liquation cracking, except that the previously deposited WM represents the HAZ in a multi-pass weld. Localized melting in the underlying WM can easily occur during reheating since there is built-in segregation along the WM grain boundaries. For similar reasons, liquation cracking susceptibility of cast alloys is greater than their wrought versions, which can also be attributed to their typically larger grain size. In practice, it may be difficult to differentiate liquation cracks from ductility-dip cracks because they can occur in the same temperature range.

6.09.3.2.3 Ductility-Dip Cracking

The solid-state phenomenon known as ductility-dip cracking has become more prevalent in recent years as the Ni-base filler metals containing higher Cr have seen more use in the power generation industry. However, ductility-dip cracking is not limited to high-Cr Ni-base alloys, and has been observed in other nickel-base grades, and materials including copper alloys, titanium alloys, and austenitic stainless steels. This form of cracking occurs as a susceptible material experiences an abrupt drop in ductility at temperatures above approximately half the solidus temperature to just below the solidus temperature. The DTR associated with ductility-dip cracking has already been shown schematically in **Figure 3**. There are several proposed metallurgical mechanisms that attempt to explain ductility-dip cracking (*21–23*), although there is not a great consensus of the mechanism at this time. The proposed mechanisms generally describe cracking as a result from grain boundary sliding (a creep-like phenomenon) at elevated temperatures and include the effect of secondary phases such as carbides on pinning the grain boundaries to prevent sliding. However, the segregation of sulfur to grain boundaries likely plays some role in promoting cracking as well.

Ductility-dip cracking typically occurs in thick-section multi-pass weldments of Ni-base weld deposits. The cracks have an intergranular morphology and are observed on the MGB as shown in **Figure 7(a)** presented earlier. The MGBs follow a characteristically straight path and provide little impediment to the creep-like grain boundary sliding. In Ni-base alloy WM deposits, the columnar austenitic grains can be quite large compared to the base metal. This tends to also exacerbate the ductility-dip cracking phenomenon. The WM grain boundaries typically contain chromium-rich carbides (such as $M_{23}C_6$) or Nb-rich carbides (NbC) that form near the end of weld solidification. The $M_{23}C_6$ is relatively ineffective at pinning the grain growth that occurs as the MGBs straighten upon cooling during typical welding process conditions. The NbC are much more effective at inhibiting the boundary migration, and WM grain boundaries typically exhibit a tortuous structure in its presence. **Figures 7(b) and 7(c)** show the straight boundaries seen in alloys containing $M_{23}C_6$ and the tortuous boundaries observed in alloys containing NbC precipitates.

Various test methods have shown that grain boundary pinning will significantly reduce the ductility-dip cracking susceptibility. The strain-to-fracture test method was developed to specifically evaluate this form of cracking. Details of the test method are discussed in greater detail below. **Figure 8** shows cracking envelopes obtained with the strain-to-fracture test (*24,26*). The cracking envelopes allow direction comparison of alloy susceptibility. The lines plotted in the figure represent the threshold strain level for ductility-dip cracking. If welding strains are maintained at levels below the threshold strain, then cracking will not occur. Note that alloy 690 and Filler Metal 52 is a typical Ni-base combination of base metal and filler metal, respectively. Both have a low threshold strain for cracking across a wide range of temperatures and are considered quite susceptible to ductility-dip cracking when weld restraint is high. The Filler Metal 82 weld deposits contain NbC and have significantly higher threshold strains. Thus, Filler Metal 82 is more resilient to ductility-dip cracking than Filler Metal 82 and alloy 690. Note that an austenitic stainless steel (310) is shown for comparison. Stainless steels typically exhibit higher threshold strains than Ni-base alloys, especially when they contain a small volume fraction of ferrite from weld solidification.

Material selection is one method of controlling ductility-dip cracking. Ni-base filler metals containing high Cr contents, such as Filler Metal 52, are most susceptible to this form of cracking. The filler metals with higher chromium content may not be necessary unless superior corrosion resistance is required for the final application. Selection of filler metals containing lower alloying additions of Cr or selection of alloys that produce sufficient morphology and volume fraction of secondary phases at the end of solidification will help to reduce ductility-dip cracking. These filler metals should be implemented if they provide a weld deposit composition that will maintain the necessary corrosion resistance in-service. Some filler metals have been designed to have sufficient Cr content for the most aggressive environments, yet also have additions of Nb to form a favorable distribution of NbC that act as grain boundary pinning sites. This can effectively prevent the creep-like grain boundary sliding that results in cracking. Filler Metal 52MSS is an example of a new alloy that may accomplish this. However, the formation of NbC at the end of solidification can

www.iran-mavad.com
مرجع مهندسی مواد و متالورژی

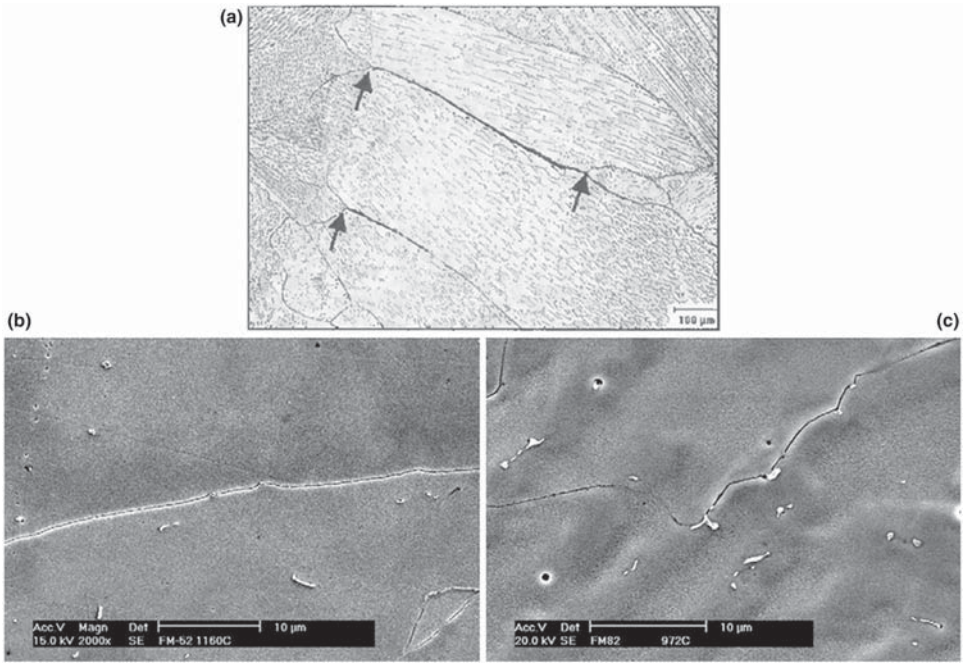

Figure 7 Optical micrographs of nickel-base weld deposits showing: (a) Ductility-dip cracking along migrated grain boundaries in Filler Metal 52 weld deposit (Reproduced from Collins, M. G.; Lippold, J. C. *Weld. J.* **2003,** *82,* 288S); (b) The straight boundaries most susceptible to cracking (Filler Metal 52) (Reproduced from Ramirez, A. J.; Lippold, J. C. *Mater. Sci. Eng. A – Struct. Mater. Prop. Microstruct. Process.* **2004,** *380,* 245); (c) Tortuous grain boundaries that are pinned by NbC precipitates (Filler Metal 82) (Reproduced from Ramirez, A. J.; Lippold, J. C. *Mater. Sci. Eng. A – Struct. Mater. Prop. Microstruct. Process.* **2004,** *380,* 245).

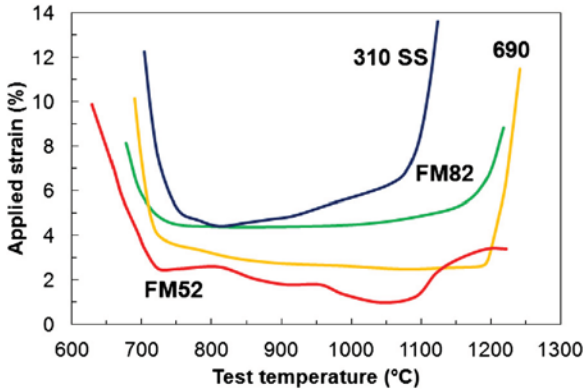

Figure 8 Strain-to-fracture test results are plotted to compare ductility-dip cracking susceptibility of several nickel-base and stainless steel alloys. Adapted from Nissley, N. E.; Lippold, J. C. *Weld. J.* **2003,** *82,* 355S and Collins, M. G.; Lippold, J. C. *Weld. J.* **2003,** *82,* 288S.

aggravate the tendency for solidification cracking. Elevated levels of NbC can also increase WM liquation cracking susceptibility in multi-pass welds.

Thick-section, high-restraint welds are generally the most susceptible during welding due to accumulation of thermally induced contraction strains. Therefore, from a process control standpoint, it is desirable to minimize weld heat input and deposit smaller weld beads to reduce accumulation of residual stresses in the joint. This could decrease productivity, as additional weld passes may be required to weld the components. The costs of reduced productivity should be weighed against the potential for cracking in the weldments, which could cause the component to fail inspection. Also, joint configurations can be managed to reduce the restraint of the nickel-base weld deposit.

6.09.3.2.4 Strain-Age Cracking

Strain-age cracking occurs during PWHT in the Ni-base alloys strengthened by precipitation hardening with the γ' intermetallic phase $Ni_3(Ti,Al)$. This form of cracking has also been known more generically as 'PWHT cracking.' During welding of the precipitation

www.iran-mavad.com
مرجع مهندسی مواد و متالورژی

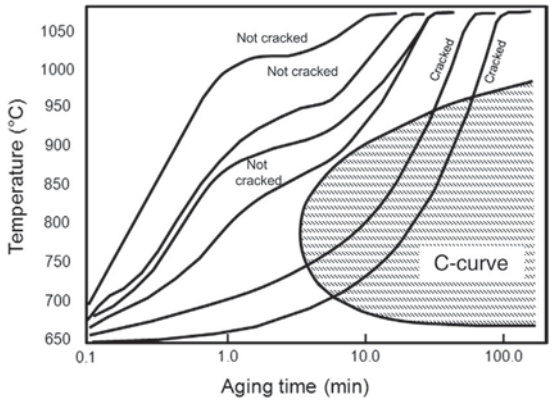

Figure 9 Strain-age cracking susceptibility curve of René 41. Adapted from Berry, T. F.; Hughes, W. P. *Weld. J.* **1969,** *48,* S505.

hardened alloys, the γ' precipitates in the material are solutionized in the HAZ where simultaneous grain growth occurs. PWHT is necessary after welding to relieve residual stresses and completely solutionize the material before an aging treatment is performed. The final aging treatment is necessary to form a favorable distribution of γ' to maximize the elevated-temperature strength and creep resistance. The precipitation of γ' is governed by the 'C-Curve' kinetics described in **Figure 9** (*27*). If the PWHT heating rate is sufficiently fast to the stress relief temperature (above 1050 °C in the example shown), the nose of the precipitation curve can be avoided. If the heating rate is slow and passes through the nose of the precipitation curve, γ' will form before reaching the stress relief temperature. The precipitates typically nucleate and grow within the austenite grain interiors, which localizes stresses at the grain boundaries. Simultaneous precipitation of intergranular carbides typically accompanies the γ' precipitation, and tends to further the embrittlement of the grain boundaries. Residual stresses from the welding process relax at elevated temperature, resulting in thermally induced strains. Intergranular fracture results from the simultaneous action of the aging and strain.

Cracking susceptibility is generally attributed to the rate of age-hardening, i.e., the rate at which the γ' precipitates, which is described by the C-Curve kinetics shown in **Figure 9**. C-Curves that are further to the right exhibit more sluggish precipitation, and generally have a lower strain-age cracking susceptibility. As the C-Curve shifts toward the left, the strain-age cracking susceptibility increases since precipitation of γ' takes less time. Generally, higher (Ti + Al) content in the alloy will promote strain-age cracking since rapid precipitation of the Ni_3(Ti,Al) intermetallic leads to embrittlement before stress relief. The diagram shown in **Figure 10** describes composition ranges of immune and susceptible nickel-base superalloys. The gray band running through the plot represents the critical value of (Ti + Al) where strain-age cracking susceptibility is a concern. Alloys that are situated above the gray band are generally susceptible to cracking and increase in susceptibility with additional (Ti + Al) content. Alloys with compositions below the band are generally immune to strain-age cracking. Some of the more susceptible alloys are essentially unweldable due to their rapid aging response in the HAZ, where cracking will occur due merely to the welding thermal cycle. The alloy René 41 (R-41) is situated just on the susceptible side, making it possible to avoid cracking during PWHT by carefully controlling the aging response as shown in **Figure 9**. Recent alloy developments resulted in HAYNES 282 alloy, which has excellent creep strength in the 650–900 °C temperature range, comparable to René 41 with significantly better fabricability and resistance to strain-age cracking (*28*). The unique properties of this alloy were achieved through optimizing chemical composition to produce sluggish γ' precipitation kinetics.

Alloy 718 was developed to be a weldable superalloy with regards to strain-age cracking. This was accomplished by alloying with Nb instead of Ti and Al. The γ'' (Ni_3Nb) precipitation kinetics are significantly slower than the γ' kinetics. This allows 718 to be heated to the solutionizing temperature range without experiencing precipitation. However, the γ'' precipitation strengthening mechanism in the 718 alloy is limited to applications below 650 °C, above which the γ' strengthened alloys are employed for their much higher strength. Alloy 718 and many of the other Ni-base superalloys are susceptible to liquation cracking, which has been discussed in a previous section.

Strain-age cracking is identified by metallographic techniques and fractography. If cracking is found in a weldment, the metallographic evaluation typically shows that cracking occurs near to the fusion boundary and has the intergranular morphology. Evaluation of the fracture surface reveals intergranular fracture mode that can either have a smooth faceted appearance, or some ductile features. Liquation cracking will sometimes accompany the strain-age cracking, particularly in alloys that have a significant volume fraction of carbides. As a result, the presence of liquid films can also be observed along the fractured grain boundaries.

Strain-age cracking can be controlled in many alloys, yet some are unweldable if the Ti + Al content is sufficiently high. Thermal stress management is a key to controlling cracking during the welding process. This is done by using low weld heat input and selection of a joint design that will minimize stresses. Low weld heat input also minimizes grain growth in the HAZ, and decreases the potential for liquation cracking to occur. Both of these can both contribute to strain-age cracking. PWHT heating rates can be selected so that the nose of the C-Curve is avoided. If the nose is unavoidable, rapid heating through the nose can sometimes alleviate cracking. An alternative is to heat to a temperature just below the C-Curve and hold for a period of time to partially relieve the residual stresses, and then heat through the C-Curve to the solutionizing temperature. If possible, the selection of a weldable alloy such as Alloy 718 will also minimize cracking.

www.iran-mavad.com
مرجع مهندسی مواد و متالورژی

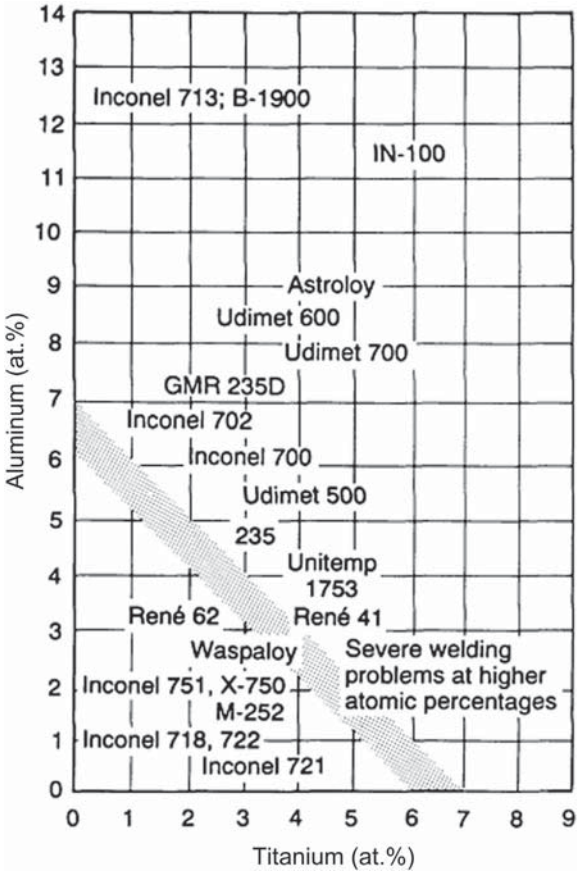

Figure 10 Plot showing the strain-age cracking susceptibility of many commercial nickel-base superalloys. Adapted from Thompson, R. G.; Olson, D. L., Siewert, T. A., Liu, S., Edwards, G. R., Eds.; ASM International: 1993; Vol. 6, p 566.

6.09.4 Dissimilar Welding

Dissimilar welding refers to the joining of two alloys that have nominally different chemical compositions. Ni-base alloys are commonly joined to other Ni-base alloys having dissimilar compositions, as well as carbon and stainless steels. This section discusses some of the key considerations of dissimilar welding, and provides examples of applications and techniques involving Ni-base alloys.

6.09.4.1 General Considerations

The successful completion of dissimilar welds involves consideration of several important factors. These include metallurgical compatibility of the base and filler metals, dilution control, proper filler metal selection, CTE differences, and PWHT requirements.

In almost all dissimilar welds, a filler metal will be used to join the alloys together. It is important that the filler metal exhibits good metallurgical compatibility with the base metals. The base and filler metals should be metallurgically compatible such that the as-deposited WM does not form a deleterious microstructure or contain deleterious phases that might promote hot cracking, embrittlement, or other metallurgical issues. The formation of an UMZ (see **Figure 2**) in the WM can occur during dissimilar welding, such as when making welds between a Ni-base filler metal and a ferritic steel base metal. The UMZ is found between the composite region of the filler metal that has been completely mixed with the base metal, and the PMZ in the HAZ. This UMZ has the composition of the base metal, but has melted and solidified without mixing with the filler metal. They are typically observed as islands that exhibit a distinct metallurgical structure from the FZ when etched with metallographic techniques. These zones, particularly in dissimilar welds of carbon steels, can form hard martensitic structures. In welds where the base metal is an austenitic stainless steel, a solidification structure can form that contains a different phase balance than the base metal. Often, the use of Ni-base filler metals prevents the formation of the UMZ on other materials, but the weld process may need to be tightly controlled. Care should be taken to avoid the formation of an UMZ as it can degrade corrosion performance.

The composition of the WM is a function of the filler metal and the amount of dilution from the two base metals, which varies with the welding process/parameters, joint design, and welding technique. Dilution is defined as a (percent) change in the filler metal composition by mixing with the base metal. Dilution is primarily controlled by weld geometry and welding parameters.

www.iran-mavad.com
مرجع مهندسی مواد و متالورژی

For a given metal feed rate, dilution increases with higher heat input. To reduce dilution of the filler metal, the welding arc can be manipulated so that it primarily impinges on the base metal nearest in composition to the filler metal. When joining Ni-base alloys to carbon or low-alloy steels, the arc may have a tendency to drift toward the steel side of the weld joint. Proper grounding techniques, such as a short arc length and torch/electrode manipulation, are necessary to compensate for this problem. Unless dilution levels are very high (>75%), dissimilar welds between Ni-base alloys and steels will provide a fully austenitic matrix microstructure. Constitution diagrams developed for stainless steels, such as the Schaeffler Diagram, can be used to predict the phases that will form in the WM. However, these diagrams predict only austenite, ferrite, and martensite phases. Secondary phases that readily develop in dissimilar Ni-base welds are not predicted by the diagrams. Solidification cracking susceptibility in dissimilar welds between Ni-base alloys and steels is highly dependent on the amount of dilution. This is attributed to widening of the solidification temperature range due to increased Fe content of the weld deposit.

Proper selection of a filler metal is often the most crucial design consideration in dissimilar welding applications. In many cases, there may be several different filler metals that exhibit metallurgical compatibility such that the base alloys can be successfully joined together. However, it is important that the weld region adequately performs in the intended service environment. Ideally, it should exhibit properties that are at least equivalent to one of the base metals. The selection of filler metals for dissimilar welds is often based upon experience as much as engineering judgment. When a new dissimilar combination is being joined, it is strongly recommended that welding procedure qualification be performed to assure that the joint can be readily fabricated and is appropriate for the intended service conditions. Many alloy producers and material suppliers provide filler metal suggestions for dissimilar welds involving their alloys and should be contacted during the procedure qualification process to ensure that a proper filler metal is selected.

The CTE differences between the base metals should be carefully considered when designing a dissimilar weld joint. If the CTE of one alloy is much lower than the other, it will try to constrain it from expanding. As a result, locally higher stresses will be generated at their interface. Cracking can even occur in the WM if the CTE difference is large enough. Large CTE differences can also result in high local stresses when a dissimilar weld joint is heated to elevated temperatures. If welded joints are going to be thermally cycled repeatedly in service and there is a significant mismatch in CTE, premature thermal fatigue failure can result.

PWHT is not usually suggested or required when joining Ni-base alloys. However, when joining Ni-base alloys to steels, PWHT is often performed since it is a code requirement for the steel. In most cases due to the relatively short time periods involved, PWHT will have negligible effects on the properties of the Ni-base alloy. If there are concerns over possible adverse microstructural effects in the Ni-base alloy, the PWHT schedule may be modified to be performed at more advantageous conditions, such as employing longer time periods at lower temperatures that are outside of precipitation regimes.

6.09.4.2 Applications and Techniques

6.09.4.2.1 Over-Alloyed Filler Metal

In aqueous corrosion-resistant applications, several different alloys are often used at various locations in the same structure. For these applications, either (1) a matching-composition filler metal or (2) an 'over-alloyed' filler metal can be selected. When the matching-composition filler metal technique is used, the filler metal is generally chosen to match the more highly alloyed and/or more corrosion-resistant base metal. For the over-alloyed filler metal technique, a more highly alloyed and/or more corrosion-resistant filler metal than either of the base metals is selected. Using an over-alloyed filler metal reduces the likelihood for preferential corrosive attack of the WM since it will contain a higher concentration of critical alloying elements compared to a matching filler metal. A common example of this is when higher alloyed Ni–Cr–Mo weld filler metals such as ERNiCrMo-10 and ERNiCrMo-14 are used to weld less corrosion-resistant Ni–Cr–Mo alloys such as Alloy 625.

6.09.4.2.2 Buttering

A useful technique in dissimilar welds is a butter layer, which is an intermediate layer of WM that is applied to the surface of the joint. The butter layer provides better metallurgical compatibility for the filler metal that is subsequently used to complete the weld. A classic example of this technique involves the joining or cladding of carbon steel to Alloy 400. A butter or barrier layer of ERNi-1 (Nickel 61, UNS N02061) provides a compositional and microstructural barrier between the high-Fe and -C steel and ERNiCu-7 (Filler Metal 60, UNS N04060), which is normally used to join Alloy 400 (UNS N04400). The benefit of the ERNi-1 is that it has a much higher tolerance to dilution by carbon steel than ERNiCu-7 before becoming susceptible to weld solidification cracking. The higher sulfur and phosphorus contents typically present in steel, and their dilution into the Ni-base WM, also act to increase cracking susceptibility. Thus, dilution needs to be carefully controlled in order to use the ERNiCu-7 weld filler metal directly on the carbon steel without experiencing weld cracking.

6.09.4.2.3 Universal Filler Metal

In situations where many different alloys will be welded together, it may be advantageous to select a 'universal' filler metal that can be used for all or most dissimilar welds. The advantages include the ability to join many different alloys without additional qualification in an alloy that exhibits good weldability and obtains adequate mechanical properties and corrosion resistance in the welded condition. The HAYNES 556® alloy (AWS A5.9 ER3556) has excelled at being a versatile filler metal for a variety of dissimilar high-temperature welding applications involving Ni-, Fe-, and Co-base alloys due to its excellent welding characteristics and outstanding all-weld-metal strength and corrosion resistance (*30*). While it is technically an Fe-base alloy, when one considers

www.iran-mavad.com
مرجع مهندسی مواد و متالورژی

the combined content of Ni and Co (which have essentially complete solid solubility with one another), it can easily be viewed as a Ni-base alloy. It has been shown to possess better high-temperature strength and corrosion resistance than the base metals being welded in many dissimilar combinations. The use of a universal filler metal can also apply to aqueous corrosion environments involving several different alloys, whereby the most corrosion-resistant alloy is selected for all joints. This is especially true where 'upset' conditions are likely to occur or in multi-purpose facilities where a wide variety of acids will be encountered.

6.09.4.2.4 Weld Overlay

A unique type of dissimilar weld involves the weld overlay technique. Weld overlay is a cladding technique that involves the application of a relatively thin layer of WM onto the surface of another alloy. It often involves the application of a highly corrosion-resistant Ni-base alloy on the surface of a less corrosion-resistant alloy, such as a low-alloy or carbon steel. In many applications, it is an accepted alternative to solid construction. Weld overlay of tube sheets and of large diameter shafts are common applications. Another area where weld overlay is used is in the local repair and refurbishment of chemical process components.

It is important to understand that the corrosion resistance of a weld overlay deposit is not equivalent to the wrought base metal of similar composition. The corrosion resistance of a weld overlay deposit is affected by several factors. One factor that is common to all Ni-base welds is segregation of alloying elements during weld solidification, as previously outlined. However, the most important factor to control in weld overlay is dilution of the WM by the base metal substrate. Dilution lowers the chemical contents of critical alloying elements (such as Ni, Cr, Mo, W) in the WM layer, which lowers the corrosion resistance of the weld overlay. The most effective method to overcome dilution in Ni-base weld overlays is by using multiple weld layers. As a general rule, the outer layer of a three-layer deposit, even with relatively high base metal dilution, will approach the weld filler metal composition. With careful control of welding parameters, a two-layer deposit may also achieve this goal.

Dilution can also be minimized through welding techniques and welding parameter selections that impart lower heat input to the base metal. Dilution can be controlled by using welding processes that have low penetration patterns. For example, globular and short-circuiting GMAW transfer modes have lower penetration patterns when compared to the spray transfer mode. In addition, oscillation of the welding torch will lower penetration and thus, dilution. Finally, bead placement affects total substrate dilution. In some cases, during GMAW short-circuiting mode, beads can be overlapped in such a way that part of the weld penetration is in the previous weld bead, rather than in the substrate base metal. When a low penetration welding process is coupled with welding torch oscillation, dilution can be limited to less than 10% in a two-layer deposit.

6.09.4.2.5 Joining Non-Ni-Base Alloys

Ni-base weld filler metals are often employed in situations where neither of the alloys being joined is in the Ni-base alloy family. Strictly speaking, these are not considered dissimilar Ni-base alloy welds; however, they are included here as examples of the wide-ranging applications involving Ni-base alloys due to their attractive properties. Dissimilar weld applications involving the use of Ni-base filler metals include the following:

- Ni-base filler metals are used to join austenitic stainless steels to carbon steels in power plant applications that require creep and thermal fatigue resistance. The large difference in CTE between the two alloys can lead to failures in the HAZ of the carbon steel during long-term exposure at elevated temperatures. Since the CTE of a Ni-base filler metal such as ERNiCr-3 is in between that of the carbon and austenitic stainless steels, it provides a gradation in CTE across the weld joint that results in a better stress distribution between the carbon steel and stainless steel at elevated temperatures.
- Filler metals such as ERNiCrMo-3 and ERNiCrMo-4 are commonly used to weld 5 and 9% Ni cryogenic steels. Their CTE closely matches that of the steels and they exhibit superior low-temperature impact strength in the as-welded condition. However, weld solidification cracking can be an issue when Ni-base filler metals are used to join these steels due to completely austenitic solidification at relatively high-Fe contents.
- Overalloyed filler metals such as ERNiCrMo-10 (UNS N06022) are used to weld 'superaustenitic' stainless steels such as AL-6XN®. The increased Mo additions of approximately 6–7.5 wt% to the superaustenitic alloys are crucial to their corrosion resistance. However, when autogenously welding superaustenitic alloys or with matching filler metals, the dendrite cores of the WM become depleted in critical alloying elements, particularly molybdenum, to the extent that their corrosion superiority to the standard 300-series austenitic stainless steels is negated. As such, overalloyed Ni-base alloys containing higher levels of molybdenum, chromium, and tungsten are used to provide for higher concentration of critical alloying elements in the dendrite core and minimize preferential corrosive attack (*31*).
- When a PWHT is not possible during the fabrication of super duplex stainless steels such as Alloy 2507, Ni-base filler metals such as ERNiCrMo-14 (UNS N06686) are used to provide better corrosion resistance of the WM in the as-welded condition.
- Ni and Ni–Fe alloys are commonly used for joining and repair of cast irons since these filler metals can accept dilution by iron and carbon while maintaining ductility and good machining characteristics.

6.09.5 Special Material Considerations

The discussion of weldability of Ni-base alloys has thus far focused on wrought alloys. There are situations where castings and specialty alloys require welding. Repair welding of wrought and single crystal superalloys is also discussed.

www.iran-mavad.com
مرجع مهندسی مواد و متالورژی

6.09.5.1 Welding of Castings

Cast Ni-base alloys can be readily joined by the common arc welding processes assuming that the casting itself is of proper integrity. The general guidelines outlined in previous sections for welding of wrought Ni-base alloys can be applied to the welding of cast alloys. Surface oxides and 'casting skin' should be removed from the weld region either by abrasive grinding or machining. The ASTM A494/A494M, Standard Specification for Castings, Nickel and Nickel Alloy (*32*) covers Ni, Ni–Cu, Ni–Cu–Si, Ni–Mo, Ni–Cr, and Ni–Cr–Mo alloy castings for corrosion-resistant service. Several of the alloys in the specification are cast equivalents of wrought solid-solution strengthened alloys. For example, the cast alloy CX2MW (UNS N26022) is the cast equivalent to the wrought alloy C-22 (UNS N06022). The nominal compositions are similar except for slight modifications to enhance castability and properties. Higher concentrations of carbon and manganese are employed for improved deoxidation and cracking resistance. The largest increase typically relates to silicon, which is increased from a maximum of 0.08–0.80 wt% to enhance fluidity during casting. Unfortunately, this dramatic increase in silicon has an adverse effect on weldability. In Ni-base alloys, silicon promotes weld solidification cracking through the formation of low-melting-point Ni–Si 'silicide' phases. Therefore, for similar levels of restraint and welding parameters, cast alloys are more susceptible to hot cracking than wrought alloys. To improve their weldability, castings should be a solution annealed prior to welding to relieve residual casting stresses and homogenize the microstructure. Some cast alloys, such as the precipitation-strengthened Alloy 713C, are considered virtually unweldable; some success can be achieved by using dissimilar filler metals.

Surface defects of castings are commonly repaired by welding. The defect is typically removed by grinding to form a cavity. The cavity should then be dye-penetrant inspected to ensure that all defects have been removed and thoroughly cleaned. Due to the low penetration characteristics of Ni-base alloy WM, the cavity must be sufficiently broad and provide enough sidewall clearance to allow for proper manipulation of the weld bead with the welding electrode. It is not recommended that defects or cracks be remelted or washed-out by autogenous welding or by depositing additional filler metal on the surface. The particular welding process employed during repair of weld castings is dependent on the sizes of the casting and defect. The GTAW process is preferred for repairing smaller castings and small, shallow defects. Larger defects can be more efficiently repaired with GMAW and SMAW.

6.09.5.2 Welding of Specialty Alloys

6.09.5.2.1 Nickel Aluminides

The nickel aluminides are candidate materials for high-temperature structural applications particularly in the aerospace and automotive fields (*33*). These materials are based on intermetallic systems including the binary Ni–Al and ternary Ni–Fe–Al systems. Such as the Ni-base superalloys, the nickel aluminides exhibit increasing strength with temperature up to approximately 900 K. Weldability studies have been performed on various nickel aluminide materials and they have exhibited solidification cracking and liquation cracking issues in the FZ and HAZ, respectively.

Iron-nickel aluminide (including the alloys: IC-2, IC-6, IC-14, IC-15, IC-18, IC-19, and IC-25) weldability has been studied during GTAW and EBW (*34*). Gas tungsten arc welds exhibited severe cracking the FZ and HAZ due to the complex solidification paths during the transition from liquid to solid. HAZ cracking was intergranular, and FZ cracking exhibited interdendritic morphology, which was associated with the presence of NiAl phase. Electron beam welds, made under a narrow range of processing conditions, exhibited no cracking. The NiAl phase was reportedly eliminated during a PWHT. Several filler wires (IC-221LA and IC-221W) are successfully used for welding similar and dissimilar joints, and for repair welding of castings with the GTAW process (*35*). The IC-221LA filler metal is used for a wide range of applications. It can be used for closely matching WM and base metal strength, and for applications that require the component to operate at temperatures higher than 900 °C. The yield strength, tensile strength, and creep resistance of welds made with these filler metals are lower than the IC-221M base metal. This shows that welding of nickel aluminides can be successfully implemented from a weldability standpoint, but that design for service life should be carefully considered. It has been suggested that for consistently making high-quality gas tungsten arc welds, carbon, sulfur, silicon, boron, and zirconium levels need to be closely controlled (*36*). Boron additions of approximately 250 ppm have greatly reduced cracking severity in welds, although even slight decreases or increases from the level will exacerbate cracking (*34*).

6.09.5.2.2 Oxide Dispersion Strengthened Alloys

Oxide dispersion strengthened alloys are produced by mechanical alloying nanoparticles of ytterbium-oxide (Y_2O_3) with powders containing nickel and chromium. Depending on the alloy, other elements are added including aluminum, titanium, tungsten, molybdenum, tantalum, carbon, boron, and zirconium. The powders are then processed into the final shape with various powder metallurgy methods including hot isostatic pressure followed by final heat treatment to achieve desired grain structure and mechanical properties. Components made with this technique have excellent high-temperature creep and corrosion resistance. Creep resistance is improved over the superalloys strengthened only with γ', because the nanoscale oxides are insoluble and will not undergo coarsening and dissolution. Fusion welding processes will destroy the distribution of the oxides in the FZ and cause a drastic decrease in creep strength compared to base metal. Laser beam and EBW produce much steeper thermal gradients during welding which shortens the time period necessary for solidification to occur, resulting in less alteration to the oxide distribution and more favorable creep resistance than gas tungsten arc welds (*37*). Brazing, diffusion welding, or pulsed electric current sintering appear to be more viable processes than fusion welding during the joining of these materials, as they have better potential to avoid high-temperature property degradation.

www.iran-mavad.com
مرجع مهندسی مواد و متالورژی

6.09.5.3 Repair Welding

Since Ni-base alloys are relatively expensive and single crystal superalloys especially so, they require repair rather than replacement to make their use economically viable. Repair is often performed via welding on both as-cast defects and damage experienced during elevated temperature exposure (wear, erosion, fatigue, etc.). Due to microstructural differences, the procedures for repair welding may significantly differ from those used during original fabrication.

6.09.5.3.1 Solid-Solution Strengthened Alloys

There are several issues that can occur during service exposure of the corrosion-resistant alloys. Carburizing environments and extremely oxidizing environments can render the alloys unweldable during repair. If the areas damaged by such conditions are localized, sections of the component can be removed by grinding or cutting, and new material welded in place. Test welds are typically necessary to determine the feasibility of making a repair weld. This is typically performed by grinding and cleaning the component, then making a weld representative of the intended repair procedure. This test weld should be thoroughly examined for cracking issues. This can be accomplished with nondestructive testing or with destructive evaluation if the material removal will not ultimately compromise the component. The test repair weld shall be free of cracks before repair procedures are implemented.

6.09.5.3.2 Precipitation-Strengthened Alloys

The superalloys are susceptible to oxidation, carburization, void formation (creep-related), and fatigue at elevated temperatures. It is not uncommon to find such damage that has completely penetrated the thickness of the component. This essentially renders the component unusable as attempts to repair weld will likely be unsuccessful. If the damage is localized then repair welding may be successful. Any corrosion must be removed from the component before the repair weld is made. The alloy is typically annealed to restore weldability. Turbine blades can be repair welded without a thermal treatment by using a filler metal with higher ductility (and lower strength) than the component. Repair weld procedures should be carefully evaluated to avoid cracking issues.

6.09.5.3.3 Single Crystal Superalloys

Single crystal superalloys are produced through directional solidification techniques whereby the final component comprises only a single grain. The absence of grain boundaries in single crystal superalloys provides for superior creep and thermal fatigue resistance compared to polycrystalline alloys. Another advantage of these alloys is an increased incipient melting temperature due to the absence of secondary elements such as B and Zr, which are employed for grain boundary strengthening in wrought Ni-base alloys. For these reasons, they are used in gas turbine engines as blades and vanes. The chemical compositions of several single crystal superalloys are provided in Ref. (*6*).

One of the major difficulties in achieving successful weld repair of single crystal superalloys is the formation of equiaxed 'stray' grains in the weld, which is attributed to constitutional supercooling (*38*,*39*). High energy density processes (e.g., EBW, LBW) that offer steeper temperature gradients to minimize undercooling of the liquid are favorable for avoiding the formation of stray grains (*40*–*42*). However, due to the high degree of undercooling at the weld centerline, equiaxed growth and loss of the single crystal structure is difficult to avoid. Studies on CMSX-4 alloy using both GTAW and LBW demonstrated that both reduced power and increased travel speed were beneficial toward preserving the single crystal structure (*43*). The LBW process allowed for a larger processing window, presumably due to the steeper temperature gradient in the weld pool.

Solidification cracking is another issue that is encountered during weld repair of single crystal superalloys (*38*). Cracking typically occurs along the stray grain boundaries, particularly along high-angle boundaries that provide easy paths for crack propagation. Elemental partitioning and the presence of low-melting-point eutectic phases during nonequilibrium solidification are contributing factors to cracking susceptibility. Preheating has been shown to mitigate cracking through a reduction in thermal stresses. Parameter optimization studies have shown that cracking resistance is enhanced by high power density and low heat input (*44*).

6.09.6 Influence of Welding on Service Performance

6.09.6.1 Mechanical Performance

6.09.6.1.1 As-Welded Mechanical Properties

The welds of solid-solution strengthened alloys primarily used for their aqueous corrosion resistance generally exhibit similar mechanical properties to the base metal. They can be put into service in the as-welded condition without PWHT being required. WM strength is typically comparable to that of the base metal with good ductility. The HAZ may undergo a slight amount of grain growth that can lead to local softening. Since the precipitation-strengthened alloys require PWHT to develop properties similar to the base metal in the aged condition, the as welded properties typically are not of concern.

6.09.6.1.2 Thermal Stability

Significant microstructural changes can occur during elevated temperature exposure. One possibility occurs during PWHT to relieve residual stresses. Certain alloys can undergo microstructural embrittlement at intermediate temperatures. Alloy 625 WM exhibits embrittlement mainly in the 750–950 °C range due to the formation of Nb-rich δ (delta) phase (*45*). The needle-type morphology

www.iran-mavad.com
مرجع مهندسی مواد و متالورژی

of this phase has a catastrophic effect on mechanical properties. At lower temperatures in the 600–750 °C range, the γ″ phase can form and have a slightly adverse effect on ductility. As such, the 625 alloy is usually carefully postweld annealed in the 955–980 °C range to avoid embrittlement and limit grain growth. Stress relief treatments at lower temperatures (<600 °C) do not cause severe embrittlement. In C-22 alloy, the effect of aging at temperatures from 425 to 760 °C for up to 40 000 h was investigated (46). Long-range ordering in the form of $Ni_2(Cr,Mo)$ was observed in welds aged below 600 °C. Significant strengthening at 593 °C was attributed to ordering. At higher temperatures, topologically closed packed (TCP) phases (σ, P, and μ) were found to nucleate and grow near the original TCP phases in the weld interdendritic regions. The presence and growth of the TCP phases drastically decreased Charpy impact toughness. Proper solution anneal treatments are effective at restoring the mechanical properties of C-22 welds (47). Severe embrittlement of solid-solution strengthened high-temperature alloy welds during aging in the 538–871 °C range was attributed to carbide precipitation (48).

6.09.6.2 Corrosion Resistance

6.09.6.2.1 WM Dendrite Coring

Microsegregation and macrosegregation during weld solidification results in localized variations in composition in the WM. Chromium and molybdenum, two alloying elements that typically promote corrosion passivity to the Ni-base alloys, have a tendency to segregate to interdendritic regions during solidification of the WM. The dendrite cores can see a significant reduction in chromium and molybdenum concentration, thereby decreasing their corrosion resistance. PWHT is performed on the weldments to reduce the concentration gradients and restore corrosion resistance. An *index of residual concentration* (δ) is useful for predicting the PWHT temperatures and times necessary to restore uniformity of the WM composition (4). This index is defined below where D is alloying element diffusivity in the matrix (and is a function of temperature), t is time, and λ is the dendrite spacing:

$$\delta = \exp\left(-\frac{4\pi^2 Dt}{\lambda^2}\right)$$

The index δ begins at unity and decreases toward zero with homogenization time. Increasing the temperature, and time at temperature, tend to accelerate homogenization, and smaller dendrite spacing tends to also reduce time for homogenization. However, these may not be practical from a welding process standpoint. This equation merely illustrates a simple method for considering a PWHT to enhance the corrosion resistance.

6.09.6.2.2 HAZ Sensitization

Alloys primarily used for their aqueous corrosion resistance can become susceptible to corrosive attack in the HAZ. In Ni–Cr–Mo 'C-type' alloys, this form of intergranular attack occurs when Cr- or Mo-rich precipitates, such as $M_{23}C_6$ and TCP phases, form along grain boundaries in the HAZ, which creates a Cr-depleted zone along the grain boundary that is 'sensitive' to corrosive attack (49). As such, this metallurgical phenomenon is known as 'sensitization.' In Ni–Mo 'B-type' alloys, Mo-rich $M_{12}C$ carbides and the NiMo (δ) intermetallic compound have been identified to form along the HAZ grain boundaries (50). Again, the formation of these precipitates depletes the adjacent matrix of molybdenum and renders the grain boundary region susceptible to corrosion. Sensitization manifests itself as rapid attack of the grain boundary regions, which can lead to 'ditching' of the grain boundaries and individual grains even dropping out of the microstructure. The characteristic 'wagon tracks' appearance of sensitized welds after corrosive attack occurs along symmetric sensitized bands in the HAZ that run parallel to the weld seam. Sensitization occurs at some distance from the weld interface since these precipitates form in an intermediate temperature range; the higher peak temperatures closer to the weld interface are typically above their solvus temperatures. Sensitization is best controlled in Ni-base alloys by utilizing low heat-input welding parameters and maintaining low preheat/interpass temperatures. These strategies act to increase the cooling rate in the HAZ so that there is insufficient time for the precipitates to form upon cooling. Certain alloys are more susceptible to HAZ sensitization due to their more rapid precipitation kinetics.

6.09.6.2.3 Other Forms of Corrosion

The solid-solution strengthened alloys see heavy use in applications that require extremely high corrosion resistance such as, e.g., aqueous and petrochemical service, whereas the precipitation-strengthened and oxide dispersion strengthened alloys typically require good high-temperature oxidation resistance as they are used at elevated temperatures. Many applications for Ni-base alloys require both chemical resistance and high-temperature oxidation resistance. Welding can have the undesired effect of altering the base metal microstructure and increasing residual stresses in these alloy systems, both of which typically result in reduced corrosion resistance. PWHT is typically employed on weldments to relieve the residual stresses, dissolve undesired secondary phases, and homogenize the microstructure to combat corrosion issues. This generally increases the resistance to stress corrosion cracking.

Galvanic corrosion, particularly in dissimilar metal welds, is a corrosion issue that should be considered. If a particular base metal is more 'noble' than the weld deposit on the galvanic series, then preferential corrosion of the weld deposit will occur if both materials are simultaneously exposed to the same environment. Ni-base alloys are typically more noble than other alloys such as carbon steels and stainless steels so galvanic corrosion is generally not a problem. However, this should carefully be considered before exposing dissimilar metal welds to a corrosive environment.

www.iran-mavad.com
مرجع مهندسی مواد و متالورژی

6.09.7 Weldability Testing Techniques

A variety of test methods are employed to evaluate the weldability of Ni-base alloy base metals, and filler metals, with the purpose of determining the susceptibility to various forms of cracking. Over the years, many novel test procedures have been developed and employed to evaluate material susceptibility to, e.g., solidification cracking and liquation cracking (*51*), strain-age cracking (*52*), and ductility-dip cracking (*26*). This is done so that the formation of defects can be studied from a metallurgical and process standpoint, and perhaps more importantly to reduce or eliminate the formation of defects during fabrication. There are four broad classifications of weldability tests including: mechanical, nondestructive, service performance, and specialty (*4*). All but the nondestructive techniques involve sectioning of the welds for metallographic evaluation, and thus are unsuited to the production and fabrication environments where nondestructive methods are preferred. The specialty tests are typically designed such that a specific metallurgical defect can be studied, e.g., solidification cracking or ductility-dip cracking. These tests are most suited to alloy development or selection and are discussed next since they are most applicable to testing susceptibility to the elevated temperature cracking issues common to Ni-base alloys.

Weldability tests suitable for evaluating elevated temperature cracking are classified into three categories including: representative tests, simulative tests, and high-temperature mechanical tests. Representative (or 'self-restraint') tests are used to reproduce actual welding conditions, and results are particular to a unique welding scenario involving a specific combination of material, weld parameters, and restraint. Variation in welding parameters and restraint may significantly affect the results of the test. Also, these tests are not well suited for comparing weldability of different materials as the metallurgical variables are not well isolated from process variables when interpreting results. Therefore, results are typically qualitative such as 'go' or 'no go' for a given weld scenario. Simulative tests are externally restrained with the controlled application of stress or strain. Therefore, these test approaches allow the separation of process variables from the metallurgical variables and allow quantification of metallurgical susceptibility to cracking. Simulative tests are suitable for comparing cracking susceptibility across different alloys or heats of a single alloy type. However, they have the inherent drawback that restraint conditions are not necessarily representative of actual welding conditions. Lastly, the high-temperature mechanical tests provide a measure of elevated temperature strength and ductility. Weld cracking issues are connected to embrittlement phenomena that are indicated by an increase in strength or decrease in ductility.

Several of the commonly used weldability test techniques are shown by classification in **Figure 11** (*53*), and are discussed in greater detail below. Solidification and liquation cracking are some of the more prevalent weld defects in the Ni-base alloys. Ductility-dip cracking is also becoming more prevalent as filler metals with higher alloy content are being developed. Most of the following discussions place emphasis on evaluating the formation of those defects. However, other forms of weld embrittlement occur and the last section briefly discusses tests for evaluating those issues.

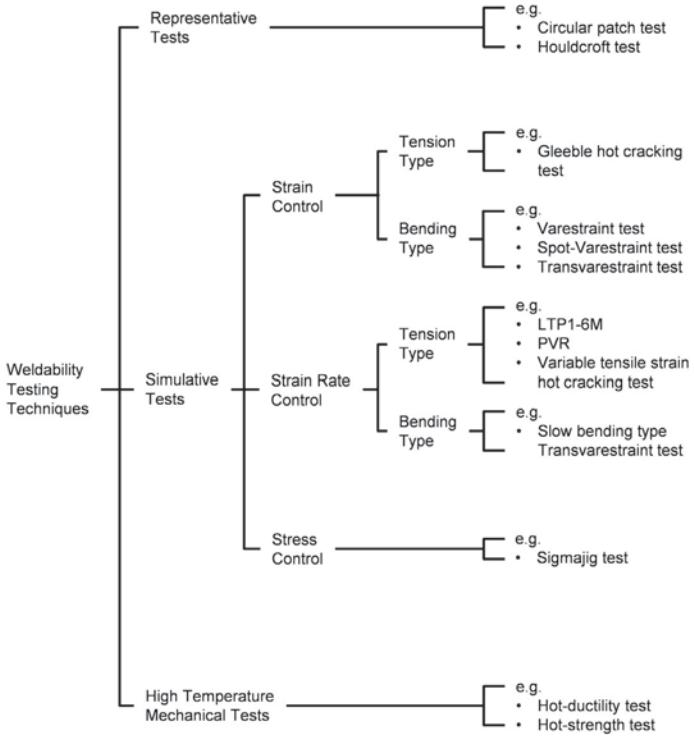

Figure 11 General classification and common weldability test techniques. Reproduced from Lin, W. -E. The Ohio State University: 1991.

www.iran-mavad.com
مرجع مهندسی مواد و متالورژی

6.09.7.1 The Hot-Ductility Test

The hot-ductility test is used to evaluate the susceptibility of an alloy to cracking at elevated temperatures, such as HAZ liquation cracking (*54*). Since there is no definitive mechanism to describe HAZ liquation cracking in Ni-base alloys, the hot-ductility test is useful for determining the relative cracking susceptibilities of different alloys. The hot-ductility test simulates the metallurgical degradation that occurs during a weld thermal cycle and provides a measure of the ductility of the alloy at high temperatures. Ductility is a key component of overall weldability since weld cracking is often associated with an exhaustion of available ductility. It was first applied to Ni-base superalloys in order to better understand their poor weldability and the basic mechanisms responsible for HAZ cracking (*18,19*). The hot-ductility test has been used to evaluate the liquation cracking susceptibility of various Ni-base alloys (*15,55–58*). The hot-ductility test has also been used to evaluate ductility-dip cracking in Ni-base alloys (*23*).

Both on-heating and on-cooling ductility tests are performed to obtain a complete ductility 'signature' of the alloy, as schematically shown in **Figure 12**. The nil-ductility temperature (NDT) is defined as the on-heating temperature where ductility is reduced to zero (*4*). Essentially, this can be viewed as the temperature of liquation onset, where grain boundary surfaces are coated by a thin continuous liquid film (*59*). As the amount of liquid increases, the nil-strength temperature (NST) is reached, representing the point where the strength of the alloy drops to essentially zero. This is observed when boundaries are coated by a substantial thickness of liquid, such that the boundaries are unable to accommodate any stress. At the NST, the continuous liquid layer present at the NDT has thickened to the point where minimal capillary exists. To determine the on-cooling curve, samples are typically heated to a temperature somewhere between the NDT and NST, and brought to the test temperature at a prescribed cooling rate. The temperature at which measurable ductility is regained is called the ductility recovery temperature (DRT). At the DRT, the liquid that has formed during the heating cycle has solidified extensively enough during cooling that measurable ductility is achieved in the sample. While the NDT is viewed as being a constant for a given heating rate, the DRT is known to be a function of the on-cooling peak temperature (*60*). The peak temperature is representative of different locations in the HAZ, with the peak temperature at the weld fusion line approximated to the liquidus temperature. As such, employing an on-cooling peak temperature that is closer to the NST than the NDT provides a more discriminating test of cracking susceptibility.

A number of criteria can be used to interpret hot-ductility curves. Among the various criteria, the temperature range between the NST and DRT, referred to as the liquation cracking temperature range (LCTR), is the most widely utilized in assessing HAZ liquation cracking susceptibility (*61*). An alloy with a narrower LCTR is deemed to have better resistance to HAZ liquation cracking. The thermal crack susceptible region (CSR), identified by Lin (*60*), describes and quantifies the region in the HAZ where liquation cracking may occur for a specific alloy. The temperature range between the liquidus temperature and NDT represents the extent of the thermal CSR in the on-heating portion of the HAZ thermal cycle. The on-cooling CSR corresponds to the temperature range between the on-cooling peak temperature and the corresponding DRT (**Figure 13**).

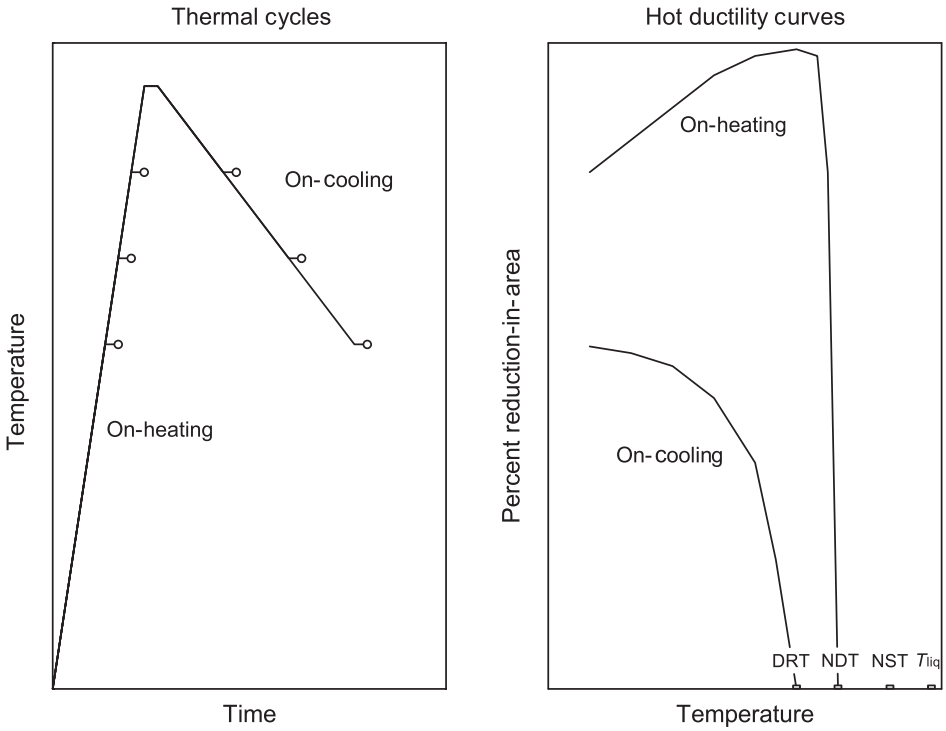

Figure 12 Schematic illustration of hot-ductility testing illustrating thermal cycles and ductility curves with critical temperatures identified.

www.iran-mavad.com
مرجع مهندسی مواد و متالورژی

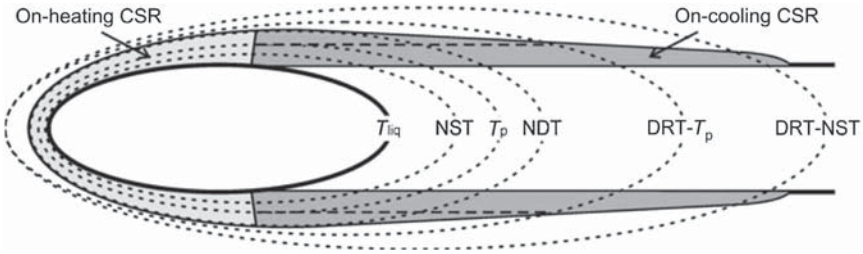

Figure 13 Schematic illustration of the theoretical thermal CSR.

6.09.7.2 The Varestraint Test

The longitudinal Varestraint (Variable Restraint) test was developed to isolate the metallurgical variables from welding process variables by applying a strain while making a weld on the alloy of interest (62). Since the development of the original test, there have been significant modifications, which allow the evaluation of both solidification and liquation cracking susceptibility. Testing typically consists of making an autogenous gas tungsten arc weld (although welding processes using filler metals can also be employed) and simultaneously applying a strain to the weldment to produce cracking in regions that contain a microstructure susceptible to 'hot' cracking, i.e., solidification and liquation cracking. Test specimens of known thickness (t) are bent over a die block with a known radius (R) so that the applied strain (ε) is quantifiable by:

$$\varepsilon = \frac{t}{2R + t}$$

There are three varieties of the test that include the longitudinal, transverse, and spot Varestraint test methods. The longitudinal and transverse (also known as Transvarestraint) methods are schematically shown in **Figures 14(a) and 14(b)**, respectively. During longitudinal Varestraint testing, strain is applied in the direction that the weld is oriented, producing solidification cracking in the FZ and liquation cracking in the HAZ. During transverse testing, strain is applied across the FZ where cracking is essentially restricted, thus inducing predominantly solidification cracking. The spot test (which is not shown) consists of making a spot weld and bending the weldment during cooling from the molten state. This test tends to isolate cracking in the HAZ for the evaluation of liquation cracking susceptibility. Bending is typically performed with the transverse configuration during the spot Varestraint test.

The solidification and liquation cracking susceptibilities can be quantified by several methods. Welds are typically evaluated under low powered microscopy. The numbers of cracks are counted to determine a total number of cracks. Each crack length is also measured. The longest crack is defined as the maximum crack length, and total crack length is the algebraic sum of the individual crack lengths. The maximum crack length is typically plotted as a function of the applied strain resulting in a cracking envelope.

The concept of maximum crack distance (MCD) is slightly different from the maximum crack length defined above. The differences are illustrated in **Figure 15(a)**. The MCD is always measured in a direction perpendicular to the weld pool solidification boundary, and follows the thermal gradient of the weld pool. Often is the case where the longest crack is observed along the centerline of the weld. This usually means the maximum crack length and MCD are equal. The MCD reaches saturation where its length does not increase beyond a certain level of applied strain. The level of strain where cracks reach their maximum length is the saturated strain. The minimum level of strain to initiate solidification cracks is the threshold strain. A lower threshold strain and

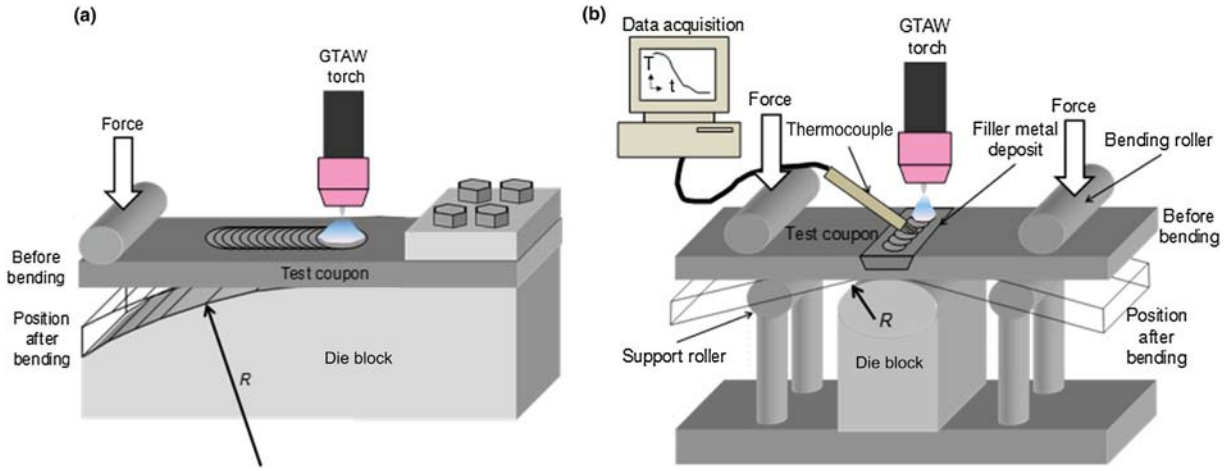

Figure 14 Schematic diagrams of: (a) The longitudinal Varestraint test; (b) The transverse Varestraint test.

www.iran-mavad.com
مرجع مهندسی مواد و متالورژی

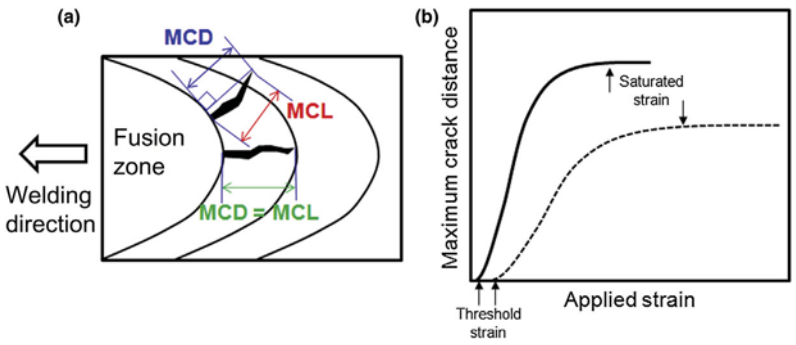

Figure 15 Schematic illustration showing: (a) The concept of maximum crack distance (MCD) which lies in a perpendicular direction to the weld isotherms; (b) The solidification cracking envelope.

lower saturated strain typically indicates a greater propensity for solidification cracking during fabrication. The MCD is plotted versus the applied strain resulting in a cracking envelope that is shown schematically in **Figure 15(b)** for two hypothetical alloys. The alloy which exhibits the behavior of the dashed line would have a lower solidification cracking susceptibility than the alloy that exhibits the behavior indicated by the solid line.

The concept SCTR was developed by Lippold and Lin (*63*) to quantify the solidification cracking tendency of a material, and allows direct comparison of weldability between different materials. Cooling rate (CR = dT/dt where T is temperature and t is time) of the solidifying weld pool is determined during transverse Varestraint testing by plunging a thermocouple into the trailing edge of the molten FZ at the weld centerline (shown in **Figure 14(b)**). The MCD is determined at the level of saturated strain. Once the cooling rate and MCD are determined, and given that the welding torch travel speed (TS = dx/dt where x is distance and t is time and is equal to the solidification rate at the trailing edge of the weld pool) is fixed during the Transvarestraint test, SCTR is calculated with

$$\mathrm{SCTR} = \frac{\mathrm{MCD} * \mathrm{CR}}{\mathrm{TS}} = \frac{dT}{dt}\frac{dt}{dx}\mathrm{MCD}$$

Note that the division of the cooling rate (dT/dt) by the travel speed (dx/dt) gives the thermal gradient (dT/dx) along the direction of crack growth. This implies that welds that exhibit longer cracks and higher thermal gradients will have higher values of SCTR, and thus have a higher susceptibility to solidification cracking.

6.09.7.3 The Sigmajig Test

The Sigmajig test was developed at Oak Ridge National Laboratory in the late 1980s to evaluate solidification cracking susceptibility of thin sheets of material since Varestraint testing is limited to testing materials with thicknesses greater than approximately 3 mm (*64*). Other tests (e.g., the Houldcroft (*65*) test) are suitable for evaluating solidification cracking in thin sheet, but they rely on self-imposed restraint, whereas the Sigmajig test has variable loading capability. The ability to vary the restraint allows the quantification of cracking as a function of the applied stress. Thin sheets of material (50 × 50 mm) are clamped in the test fixtures and a transverse tensile stress is applied by applied force to the sheet with instrumented bolts as shown in **Figure 16(a)**. The bolts are instrumented with strain gages so that transverse stress imposed on the sheet is readily determined. The original, and most typical, form of the Sigmajig test procedure utilizes an autogenous GTAW process to make a weld along the centerline of the sheet specimen. A typical welding current of 20 A is used and the torch is moved along the centerline at a travel speed of approximately 15 mm s^{-1}. Other autogenous welding processes have been implemented for Sigmajig testing including LBW and EBW. Selection of the process is made based on the fabrication method implemented for welding the actual sheet component. The test results are highly dependent on welding conditions, and may require high welding torch travel speeds to induce cracking.

Multiple coupons are evaluated during a round of testing. A low stress level is applied on the first test sample and then linearly increased in each subsequent sample until centerline weld solidification cracking is initiated. This stress level required to initiate a crack is assigned as the threshold stress. This value is a good indicator of solidification cracking susceptibility when comparing different alloys or heats of a given alloy. Stress is typically increased beyond the threshold level until complete specimen separation occurs along the sample length. The stress range over which solidification cracking occurs is also useful in comparing cracking susceptibility. Test results are typically plotted in the fashion shown in **Figure 16(b)**. Note that the figure illustrates a material with a low and high susceptibility to solidification cracking.

6.09.7.4 The Strain-to-Fracture Test

The strain-to-fracture test was developed at The Ohio State University to quantify susceptibility to ductility-dip cracking (*26*), which is a solid-state, elevated temperature cracking phenomenon that occurs in high-restraint austenitic weldments. Strain-to-fracture test

www.iran-mavad.com
مرجع مهندسی مواد و متالورژی

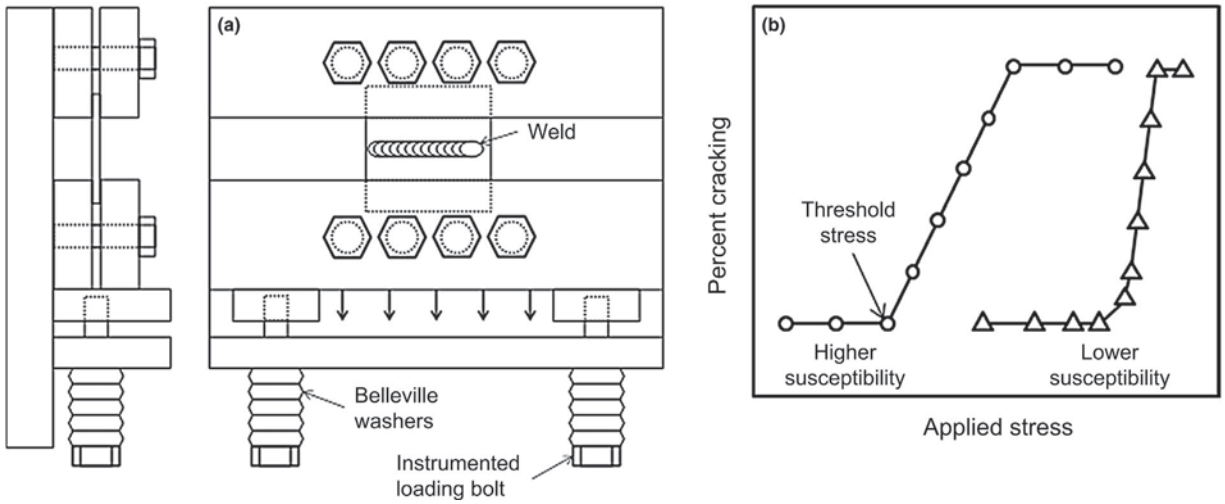

Figure 16 Schematic illustrations of: (a) The Sigmajig test; (b) Typical test results adapted from Goodwin. Reproduced from Goodwin, G. M. *Weld. J.* **1987,** *66,* S33.

specimens are fabricated by machining a tensile sample from a base material, and then making an autogenous gas tungsten arc weld in the center necked region as shown in **Figure 17(a)**. This spot weld provides a weld microstructure similar to that, which would be found during the fabrication of the component. The specimen is tested in a Gleeble™ thermo-mechanical simulator by heating to an elevated temperature, where ductility-dip cracking occurs, and then straining the necked region under tension at a constant displacement rate until the desired applied strain level is achieved. **Figure 17(b)** shows the typical test configuration where the specimen is clamped between chilled copper grips. Current is passed through the grips and the specimen, which resistively heats the sample to the desired test temperature. This is typically performed in a vacuum or inert gas such as argon. A fairly flat and symmetric temperature gradient is maintained in between the grips, as shown in the figure. Temperature is controlled by a thermocouple directly attached to the specimen. Tensile deformation is applied to the specimen at the desired test temperature and then it is cooled to room temperature. Multiple samples are tested in this manner at various temperatures, and applied strain levels to quantify the DTR. The specimens are inspected under a low-powered microscope to evaluate cracking.

The extent of ductility-dip cracking is typically determined by counting the total number of cracks present in the spot weld region. Higher strains typically increase the number of cracks that are observed. The minimum level of applied strain that induces cracking in the spot weld is the threshold strain level. The threshold strain is determined as a function of the test temperature and plotted as shown in **Figure 8**. This cracking envelope represents the ductility-dip cracking susceptibility of an alloy. If a given material exhibits a lower threshold strain and wider cracking envelope, it generally has a greater susceptibility to ductility-dip cracking than an alloy with a higher threshold strain and narrower envelope.

6.09.7.5 Other Techniques

Tests for evaluating solidification and liquation cracking are numerous and have seen application in many of the solid-solution strengthened and precipitation-strengthened nickel-based alloys. These tests have been reviewed elsewhere in-depth (*51*) and general focus on evaluating an alloy's BTR, which corresponds to the welding temperatures where weld restrain overcomes material

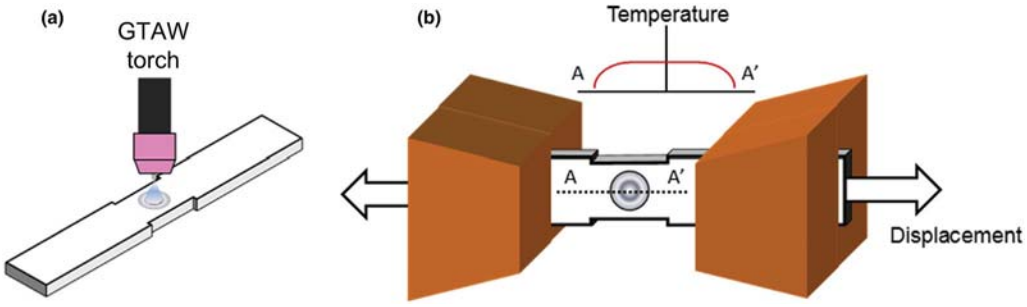

Figure 17 Schematic illustrations showing strain-to-fracture testing procedures: (a) The sample is prepared with a gas tungsten arc spot weld; (b) The Gleeble™ thermo-mechanical system performs the heating and deformation.

www.iran-mavad.com
مرجع مهندسی مواد و متالورژی

ductility to induce solidification and liquation cracks. Critical strain rate tests in bending configuration include: the *Murex test*, *VDR test* (Japan), *Bargyanski test* (Russia), *KSLA test* and *Smit test* (Netherlands), and the *HDR test* and *MVT test* (Germany). Critical strain rate tests in tearing mode include *VUZ-LTP-1-6 test* (Czech Republic), *IMET-TsNII ChM test* (Russia), *PVR test* (Austria), *VTS test* (Japan), and the *Hot tear test* (Germany). Tests that determine a critical strain include *Varestraint* and *Transvarestraint test* (USA and other countries) and the *MVT test* (Germany). Another method known as the *Cast Pin Tear test*, which was originally developed in the 1950s, has been revived and modified by researchers at The Ohio State University (66). This test has the advantage over many other weldability tests in that much smaller quantities of material are needed to obtain cracking envelopes, making this suitable for alloy development purposes.

Tests for determining strain-age cracking susceptibility have been reviewed by Thamburaj et al. (52) and include six categories: restraint tests, hot tensile tests, constant-load rupture tests, stress-relaxation tests, notched stress-rupture tests, and fracture-mechanics tests. 'Screening tests' are also used to select heats of material that are not susceptible to strain-age cracking, since even small composition changes can have significant influence on cracking susceptibility. Several more recent test methods have been developed which utilize the Gleeble® thermo-mechanical simulator (67–69). These tests typically control the stress, strain, and temperature during simulated weld and PWHT thermal cycling to evaluate embrittlement by γ' precipitation.

6.09.8 Concluding Remarks

Ni-base alloys are implemented in a wide array of applications that require extreme service performance. Fabrication of these highly engineered materials often requires special consideration beyond that of more conventional materials. This chapter has covered the major challenges encountered when joining the numerous classes of Ni-base alloys. The authors encourage interested readers to seek the many documents referenced here for more specific information on: implementation of the various welding processes, usage of proper welding techniques, materials and consumable selection, and methods to overcome the various difficulties in joining the various alloys.

References

1. Lehockey, E.; Palumbo, G.; Lin, P. *Metall. Mater. Trans. A* **1998,** *29,* 3069.
2. Babu, S. S.; David, S. A.; Park, J. W.; Vitek, J. M. *Sci. Technol. Weld. Join.* **2004,** *9,* 1.
3. Henderson, M. B.; Arrell, D.; Larsson, R.; Heobel, M.; Marchant, G. *Sci. Technol. Weld. Join.* **2004,** *9,* 13.
4. DuPont, J. N.; Lippold, J. C.; Kiser, S. D. *Welding Metallurgy and Weldability of Nickel-Base Alloys;* John Wiley & Sons: Hoboken, NJ, 2009.
5. Davis, J. R. *Nickel, Cobalt, and Their Alloys;* ASM International: OH, 2000; Vol. 8.
6. Geddes, B.; Leon, H.; Huang, X. *Superalloys: Alloying and Performance;* ASM International, 2010.
7. Hodge, F. *J. Miner., Met. Mater. Soc.* **2006,** *58,* 28.
8. Decker, R. F. *J. Miner., Met. Mater. Soc.* **2006,** *58,* 32.
9. *AWS G2.1M/G2.1:2012*; American Welding Society: Doral, FL, 2012.
10. Baeslack, W. A.; Lippold, J. C.; Savage, W. F. *Weld. J.* **1979,** *58,* S168.
11. Lippold, J. C.; Clark, W. A. T.; Tumuluru, M. The Metal Science of Joining. In *Proceedings of a Symposium Sponsored by the TMS Solidification Committee/MDMD and the Physical Metallurgy Committee/SMD;* Cieslak, M. J., Perepezko, J. H., Kang, S., Glicksman, M. E., Eds.; TMS: Cincinnati, OH, 1991.
12. Kou, S. *Welding Metallurgy;* John Wiley & Sons, Inc.: New Jersey, 2003.
13. Lippold, J. C.; Sowards, J. W.; Murray, G. M.; Alexandrov, B. T.; Ramirez, A. J. *Hot Cracking Phenomena in Welds II,* 2008; p 147.
14. David, S. A.; Vitek, J. M. *Int. Mater. Rev.* **1989,** *34,* 213.
15. Cieslak, M. J.; Stephens, J. J.; Carr, M. J. *Metall. Trans. A – Phys. Metall. Mater. Sci.* **1988,** *19,* 657.
16. Guo, H.; Chaturvedi, M. C.; Richards, N. L. *Sci. Technol. Weld. Join.* **1998,** *3,* 257.
17. Pepe, J. J.; Savage, W. F. *Weld. J.* **1967,** *46,* S411.
18. Owczarski, W. A.; Duvall, D. S.; Sullivan, C. P. *Weld. J.* **1966,** *45,* S145.
19. Duvall, D. S.; Owczarski, W. A. *Weld. J.* **1967,** *46,* S423.
20. Thompson, R. G.; Cassimus, J. J.; Mayo, D. E.; Dobbs, J. R. *Weld. J.* **1985,** *64,* S91.
21. Zhang, Y. C.; Nakagawa, H.; Matsuda, F. *Trans. JWRI* **1985,** *14,* 125.
22. Ramirez, A. J.; Lippold, J. C. *Mater. Sci. Eng. A – Struct. Mater. Prop. Microstruct. Process.* **2004,** *380,* 259.
23. Noecker, F. F.; DuPont, J. N. *Weld. J.* **2009,** *88,* 62S.
24. Collins, M. G.; Lippold, J. C. *Weld. J.* **2003,** *82,* 288S.
25. Ramirez, A. J.; Lippold, J. C. *Mater. Sci. Eng. A – Struct. Mater. Prop. Microstruct. Process.* **2004,** *380,* 245.
26. Nissley, N. E.; Lippold, J. C. *Weld. J.* **2003,** *82,* 355S.
27. Berry, T. F.; Hughes, W. P. *Weld. J.* **1969,** *48,* S505.
28. Pike, L. M. *TMS* **2008,** 191.
29. Thompson, R. G., Olson, D. L., Siewert, T. A., Liu, S., Edwards, G. R., Eds.; ASM International, 1993; Vol. 6, p 566.
30. Ernst, S. C.; Lai, G. Y. *Life Assessment & Repair: Technology for Combustion Turbine Hot Section Components;* ASM International, 1990; p 303.
31. Banovic, S. W.; DuPont, J. N.; Marder, A. R. *Sci. Technol. Weld. Join.* **2002,** *7,* 374.
32. *ASTM A494/494M - 13*; ASTM International: 2013. (DOI: 10.1520/A0494_A0494M-13).
33. Yamaguchi, M.; Inui, H.; Ito, K. *Acta Mater.* **2000,** *48,* 307.
34. David, S. A.; Jemian, W. A.; Liu, C. T.; Horton, J. A. *Weld. J.* **1985,** *64,* S22.
35. Sikka, V. K.; Deevi, S. C.; Viswanathan, S.; Swindeman, R. W.; Santella, M. L. *Intermetallics* **2000,** *8,* 1329.
36. Deevi, S. C.; Sikka, V. K.; Liu, C. T. *Prog. Mater. Sci.* **1997,** *42,* 177.
37. Molian, P. A.; Yang, Y. M.; Patnaik, P. C. *J. Mater. Sci.* **1992,** *27,* 2687.
38. David, S. A.; Vitek, J. M.; Babu, S. S.; Boatner, L. A.; Reed, R. W. *Sci. Technol. Weld. Join.* **1997,** *2,* 79.

www.iran-mavad.com
مرجع مهندسی مواد و متالورژی

39. Vitek, J. M.; David, S. A.; Boatner, L. A. *Sci. Technol. Weld. Join.* **1997,** *2,* 109.
40. Rappaz, M.; David, S. A.; Vitek, J. M.; Boatner, L. A. *Metall. Trans. A – Phys. Metall. Mater. Sci.* **1989,** *20,* 1125.
41. Gaumann, M.; Bezencon, C.; Canalis, P.; Kurz, W. *Acta Mater.* **2001,** *49,* 1051.
42. Yang, S.; Huang, W. D.; Liu, W. J.; Zhong, M. L.; Zhou, Y. H. *Acta Mater.* **2002,** *50,* 315.
43. Fujita, Y.; Saida, K.; Nishimoto, K. In *Advanced Structural and Functional Materials Design, Proceedings*; Umakoshi, Y., Fujimoto, S., Eds.; Trans Tech Publications Ltd: Zurich-Uetikon, 2006; Vol. 512, p 313.
44. Anderson, T. D.; Dupont, J. N. *Weld. J.* **2011,** *90,* 27S.
45. Cortial, F.; Corrieu, J. M.; Vernotloier, C. *Metall. Mater. Trans. A – Phys. Metall. Mater. Sci.* **1995,** *26,* 1273.
46. Edgecumbe-Summers, T. S.; Rebak, R. B.; Seeley, R. R. *Influence of Thermal Aging on the Mechanical and Corrosion Properties of C-22 Alloy Welds;* Lawrence Livermore National Laboratory, 2000.
47. El-Dasher, B. S.; Edgecumbe, T. S.; Torres, S. G. *Metall. Mater. Trans. A – Phys. Metall. Mater. Sci.* **2006,** *37A,* 1027.
48. Ireland, D. R. *Weld. J.* **1967,** *46,* S270.
49. Gorhe, D. D.; Raja, K. S.; Namjoshi, S. A.; Radmilovic, V.; Tolly, A.; Jones, D. A. *Metall. Mater. Trans. A – Phys. Metall. Mater. Sci.* **2005,** *36A,* 1153.
50. Cao, S.; Brooks, C. R.; Whittaker, G. *Mater. Charact.* **1994,** *33,* 21.
51. Wilken, K.; Kleistner, H. *Weld. World* **1990,** *28,* 37.
52. Thamburaj, R.; Wallace, W.; Goldak, J. A. *Int. Met. Rev.* **1983,** *28,* 1.
53. Lin, W. -E. The Ohio State University, 1991.
54. Campbell, R.; Walsh, D.; Olson, D. L.; Siewert, T. A.; Liu, S.; Edwards, G. R., Eds. ASM International: 1993; Vol. 6, p 603.
55. Lin, W.; Nelson, T. W.; Lippold, J. C.; Baeslack, W. A. *International Trends in Welding Science and Technology.* Gatlinburg, TN, 1993; p 695.
56. Qian, M.; Lippold, J. C. *Weld. J.* **2002,** *81,* 233S.
57. Qian, M.; Lippold, J. C. *Weld. J.* **2003,** *82,* 145s.
58. Ramirez, J. E. *Weld. J.* **2012,** *91,* 122S.
59. Weiss, B.; Grotke, G. E.; Stickler, R. *Weld. J.* **1970,** *49,* S471.
60. Lin, W. *Weld. World* **1992,** *30,* 236.
61. Lin, W.; Lippold, J. C.; Baeslack, W. A. *Weld. J.* **1993,** *72,* S135.
62. Savage, W. F.; Lundin, C. D. *Weld. J.* **1965,** *44,* S433.
63. Lippold, J. C.; Lin, W. In *Aluminium Alloys: Their Physical and Mechanical Properties, Pts 1–3*; Driver, J. H., Dubost, B., Durand, F., Fougeres, R., Guyot, P., Sainfort, P., Suery, M., Eds.; Transtec Publications Ltd: Zurich-Uetikon, 1996; Vol. 217, p 1685.
64. Goodwin, G. M. *Weld. J.* **1987,** *66,* S33.
65. Houldcroft, P. *British Weld. J.* **1955,** *2,* 471.
66. Alexandrov, B. T.; Lippold, J. C.; Nissley, N. E. *Evaluation of Weld Solidification Cracking in Ni-base Superalloys Using the Cast Pin Tear Test;* Springer-Verlag Berlin: Berlin, 2008.
67. Norton, S. J. Ohio State University, 2003.
68. Metzler, D. A. *Weld. J.* **2008,** *87,* 249S.
69. Metzler, D. A. *Weld. J.* **2012,** *91,* 163S.

www.iran-mavad.com
مرجع مهندسی مواد و متالورژی

This page intentionally left blank

www.iran-mavad.com
مرجع مهندسی مواد و متالورژی

6.10 Review of Microstructures, Mechanical Properties, and Residual Stresses of Ferritic and Martensitic Stainless-Steel Welded Joints

AG Olabi, University of the West of Scotland, Paisley, Renfrewshire, UK
R Lostado, University of La Rioja, Spain
KY Benyounis, Dublin City University, Dublin, Ireland

© 2014 Elsevier Ltd. All rights reserved.

6.10.1	**Introduction**	181
6.10.2	**Microstructure and Hardness Testing**	182
6.10.2.1	Tungsten Inert Gas Welding	182
6.10.2.2	Laser Beam Welding	183
6.10.2.3	Friction Welding	183
6.10.2.4	Submerged Arc Welding	184
6.10.2.5	Shielded Metal Arc Welding	184
6.10.2.6	Flux Cored Arc Welding	184
6.10.2.7	Plasma Arc Welding	184
6.10.3	**Mechanical Properties**	185
6.10.3.1	Laser Beam Welding	185
6.10.3.2	Tungsten Inert Gas Welding	185
6.10.3.3	Friction Welding	186
6.10.3.4	Submerged Arc Welding	186
6.10.3.5	Plasma Arc Welding	186
6.10.4	**Residual Stresses**	186
6.10.4.1	Laser Beam Welding	186
6.10.4.2	Metal Inert Gas Welding	186
6.10.4.3	Flux Cored Arc Welding	186
6.10.4.4	Tungsten Inert Gas Welding	187
6.10.5	**Impact Strength Testing**	188
6.10.5.1	Tungsten Inert Gas Welding	188
6.10.5.2	Metal Inert Gas Welding	188
6.10.5.3	Friction Welding	188
6.10.5.4	Plasma Arc Welding	188
6.10.6	**Discussions**	189
6.10.7	**Concluding Remarks**	191
References		192

6.10.1 Introduction

Welding is a metal joining process, which is commonly used in many industries. A wide range of materials can be joined by means of the welding process, but it is most widely used in joining stainless steel and low carbon steel. Due to the intense concentration of heat in a small area, the regions near the weld line undergo severe thermal cycles. These thermal cycles mainly generate changes in the microstructure, inhomogeneity in the distribution of the phases, variations in the mechanical properties, and the appearance of residual stresses. These various changes depend mainly on the type of welding process, the materials joined, and cooling and heating rates of the welded joints.

To study the changes in the microstructures and the inhomogeneities in the distribution of the phases, some researchers have used optical microscopy to obtain micrographs. These micrographs reveal important details of the microstructures, such as the distribution of chemical compositions, grain sizes, and phase changes over the different parts of welded joints (parent material, weld beam, and heat-affected zone (HAZ)) (*1*). Hardness testing is commonly employed as a simple method to investigate microstructures by surface hardness mapping. This test reveals the hardness level of each of the microstructural phases and, for this reason, is performed to identify all the different phases in the parts of welded joints (*2*). High hardness in the welded zone may be attributed to fine grain size, needle-shaped ferrite, or the existence of widmanstätten inside ferrite grains (*3,4*). Lower hardness in the HAZ may be related to grain growth and the existence of a ferrite phase in this region (*5,6*). Nowadays, this method is used to measure the strength of each microconstituent in the microstructure by determining the average hardness of each phase (*7*). Some researchers (*8,9*) have developed equations that relate hardness and tensile strength and yield strength, and these can be used to assess the strength of the welded joint.

www.iran-mavad.com
مرجع مهندسی مواد و متالورژی

Impact strength or toughness is defined as the ability of a material to absorb mechanical energy in the process of deformation and fracture, without plastic deformation under impact loading. Toughness can be affected by an excessive grain size, and increased crack initiation and growth. Thus, toughness represents the chemical composition, microstructure, and grain size of welded joints (*3–10*).

Longitudinal and transversal tensile properties such as yield strength, tensile strength, and percentage of elongation are important values in the characterization of welded joints. This test reveals hardening and softening of different areas (parent material, weld bead, and HAZ) from the computation of the accumulated plastic strain until ultimate failure of the welded components (*11*). Most of the time yielding occurred in the softened zone, and then the majority of the plastic deformation was accumulated in that zone until final failure.

Residual stresses in welded union are produced mainly by nonuniform heat distributions, plastic deformations, and phase transformations. These changes generate different residual stress patterns for welded regions and can provide information on changes in microstructural phases (*12*). For instance, residual stresses in tensile strength are induced by shrinkage of the molten region, and residual stresses in compression are induced by the effects of phase transformations (*13*).

In this chapter, a comparative study of hardness and microstructures, mechanical properties, and the residual stresses for the parent material, weld beam, and HAZ for different welding processes is carried out. The work focuses on ferritic and martensitic stainless-steel steel materials, for similar and dissimilar materials. The chapter is organized as follows. In Section 6.10.2, the microstructures and hardness values for different welding processes and different materials are shown. Section 6.10.3 presents the mechanical properties of yield and tensile strengths. Section 6.10.4 and Section 6.10.5 show the values of residual stresses and toughness for different materials and welding processes, respectively. The discussion then takes place in Section 6.10.6. Finally, the conclusions are presented in Section 6.10.7.

6.10.2 Microstructure and Hardness Testing

The microstructure of a material can strongly influence physical properties such as strength, toughness, and hardness, and is usually obtained with optical microscopy or a scanning electron microscope (SEM). **Figure 1** shows details of a micrograph in which weld metal, base material, and different HAZs are shown.

The microhardness test is carried out by using a microVickers hardness testing machine. This test is mainly employed to map surface hardness values for different points across a weld cross-section, as well as across the surface of the specimen at various thicknesses (**Figure 2**). The procedure for preparing the optical microscopy and microhardness test for a welded joint starts with grinding, polishing, and etching of the test specimens in nital or picric solution in order to obtain clear images of the microstructure, independent of the welding process used.

Many researchers have studied the microstructure and the microhardness of a test weld of the parent metal, the weld material, and the HAZ, focusing on specific welding processes. The most common welding processes are as follows.

6.10.2.1 Tungsten Inert Gas Welding

Gas tungsten arc (tungsten inert gas (TIG)) welding is most commonly used to weld stainless steel, carbon steels, and nonferrous materials. Preheating and postweld heat treatment (PWHT) is generally required in TIG welding for low alloy steels and martensitic and ferritic chromium stainless steels to prevent the formation of martensite in the HAZ, thus avoiding the fragilization of the weld joint.

One of the first studies to obtain surface hardness mapping in TIG welding, in the case of a number of different PWHTs, was proposed by Olabi (*14*) in 1998. This work was carried out on pieces made from AISI 410 high-chromium steel welded for aircraft engines. Vickers hardness variations were obtained at a depth of 1 mm across the specimen thickness and then also at different depths from the surface after the application of PWHT with different heating rates. With these data, a map of hardness as a function

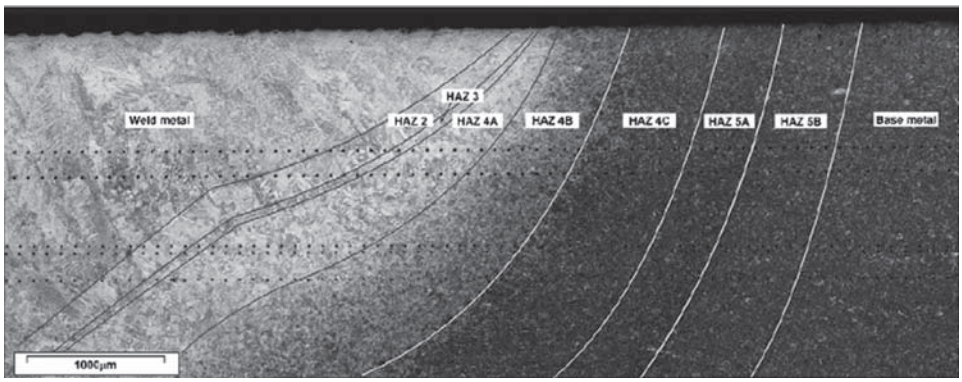

Figure 1 Micrograph of weld metal, base material, and different HAZs. Reproduced from Thibault, D.; Bocher, P.; Thomas. M. Residual Stress and Microstructure in Welds of 13%Cr–4%Ni Martensitic Stainless Steel. *J. Mater. Process. Technol.* **2009**, *20* (9), 2195–2202.

www.iran-mavad.com
مرجع مهندسی مواد و متالورژی

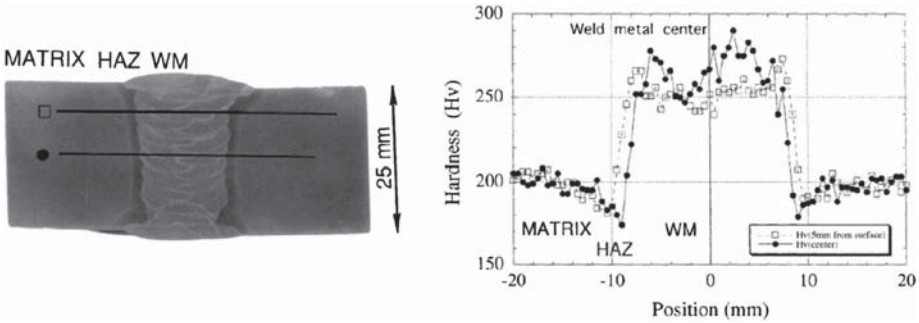

Figure 2 Cross-sectional macrostructure and hardness distribution across the weld joint. Reproduced from Inoue, N.; Muroga, T.; Nishimura, A.; Motojima, O. Correlation between Microstructure and Hardness of a Low Activation Ferritic Steel (JLF-1) Weld Joint. *J. Nucl. Mater.* **1998**, *258–263*, 1248–1252.

of different cooling rates for the welded parts was generated. Other authors, such as Inoue et al. (*2*), obtained microhardness distributions in a cross-section of a weld joint at two depths in weld metal. In this case, the weld cord was applied over parts based on low activation ferritic steel in a nuclear fusion reactor. Furthermore, the study of the microstructure showed that a fine lath structure was observed for the moderately tempered martensitic phase, as well as the well-tempered martensitic phase in the weld metal and the base metal. On the other hand, for a deeply tempered martensitic phase, the HAZ presented a coarsened lath structure.

Ghazanfari et al. (*7*) carried out a comparative study of the microstructure and microhardness of AISI 4130 welds in order to obtain hardness maps of the weld cord, base metal, and the HAZ for the TIG welding process. The structure of the base plate in this case was ferrite and pearlite, but these were not heated sufficiently to change its microstructure, with the plates showing Vickers hardness values of 210–250 HV. Adjacent to the weld metal zone, the HAZ contained a variety of microstructures and a wide range of hardness (250–400 HV). The results of the experiments showed good correlations between the various microstructures and the strength and hardness values of the weld union.

Lakshminarayanan et al. (*15*) studied the microstructure and fracture surface morphology of AISI 409M ferritic stainless-steel steel grade, welded by single-pass butt welded joints with continuous current gas tungsten arc welding (CC TIG), and pulsed current gas tungsten arc welding (PC TIG). In this case, the hardness of the weld region is greater than that of the HAZ region and the base metal region, irrespective of the welding processes. The optical micrographs of the welded joints showed that the fusion zone (FZ) region and the HAZ region primarily consisted of ferrite grains. The measured average grain diameter of CC TIG joints was 40 μm, while the average grain diameter of PC TIG joints was 25 μm.

6.10.2.2 Laser Beam Welding

Laser beam welding (LBW) is a welding technique that provides a concentrated heat source for melt and weld of the materials. This type of welding usually provides a high power density of energy for melt and concentrates the heat in a small area. For this reason, a reduced HAZ combined with high heating and cooling rates can crack the welded union, especially where high-carbon steels are used as the parent material.

A study undertaken by Zambon et al. (*16*) of this technique of welding, using AISI 904L superaustenitic stainless-steel sheets, showed an increase of the microhardness in the weld bead compared to the parent metal, as well as the microstructural refinement induced by a rapid cooling of the FZ. These data can be used to establish a methodology for optimizing the process parameters. The micrographic examination showed that the extension of the HAZ was negligible, and a fully dendritic microstructure in this area was detected in the weld bead.

Furthermore, an evaluation of the microstructural change after laser welding and its effect on the tensile and fatigue properties in DP600 steel was made by Farabi et al. (*17*). In this case, the study was based on the increment of hardness in the FZ and the formation of a soft zone in the outer HAZ. The values observed in the FZ were approximately 1.5 times higher than those of the base metal. An SEM examination of this region indicated that the phases apparent in the FZ appeared predominantly martensite in conjunction with ferrite and bainite. The formation of this martensite in the FZ resulted from the rapid cooling of the weld pool during the laser welding process.

Sathiya et al. (*18*) studied the increase in hardness in a weld bead with respect to the base metal (AISI 904L super-austenitic stainless steel) and its relationship with the microstructural refinement induced by rapid cooling of the weld zone. The cross-sectioned area of the bead profiles confirmed that the weld structure was fully austenitic and dendritic. Hardness values increased in the weld bead with respect to the base metal, mainly due to microstructural refinement induced by rapid cooling of the weld zone.

6.10.2.3 Friction Welding

Friction welding (FW) is a particular welding process that generates heat through mechanical friction between a moving workpiece and a stationary component. The combination of force and heat, direct at the weld interface, yields relatively small HAZs. There are

www.iran-mavad.com
مرجع مهندسی مواد و متالورژی

mainly two types of FW, *rotary FW* and *friction stir welding*. In rotary FW, one component is rotated against the other, while in friction stir welding, a nonconsumable rotating tool is pushed into the materials welding them together. These welding techniques generally avoid grain growth in high-strength steels and heat-treated steels.

In 2009, Lakshminarayanan and Balasubramanian (*11*) studied the microstructure and mechanical characterization of friction in a stir welded 409M ferritic stainless-steel steel joint, using a welding speed of 50 mm min^{-1} and a rotation speed of 1000 rpm. In this case, the optical micrographs of the base metal at different regions showed that the coarse ferrite grains in the base material were changed to very fine grains consisting of a duplex structure of ferrite and martensite. These changes were caused primarily due to the rapid cooling rate and high strain induced by severe plastic deformation caused by frictional stirring. The microhardness was measured in the weld joint across the thickness, and the value of the base metal was about 170 HV. Also, the hardness in the stir zone varied from 320 to 382 HV depending on the grain size of each zone. Tiejun Ma et al. (*19*) studied the variation of the microstructure and microhardness for carbon steel (grade 45) using rotary FW and after quenching. In this case, a progressive reduction in hardness was observed from the parent metal to the weld center despite the position. The microhardness of the quenched 45 steel was measured with a variation of 23 HV from one area to another area. This relatively large variation in hardness (23 HV) could be associated with the amount of the soft residual austenite after quenching. The parent 45 steel showed the typical martensite structure and a small quantity of austenite.

6.10.2.4 Submerged Arc Welding

Submerged arc welding (SAW) is a welding process in which the molten weld and the arc zone are protected from atmospheric contamination under a fusible flux. The process is normally limited to a horizontal-fillet welding position, but with a high deposition rate. This welding process is usually applied to carbon steels, low alloy steels, stainless steels, and nickel-based alloys. Deep weld penetration and thick materials may be welded with this process. For this welding process, Hashemi et al. (*20*) studied the hardness and the microstructure of the fusion zone, the base metal, and the HAZ of double submerged arc welded (SAW welding) in a line pipe steel of grade API X65 manufactured and welded by spiral forming. The hardness of the FZ was slightly higher than the hardness of the base metal and this can be attributed to the presence of lower temperature transformation products (i.e., bainite and Widmanstatten ferrite) in the FZ. The microstructure showed that the HAZ did not experience melting, but its microstructure changed due to phase transformation. In this case, the base metal region remained unaffected.

6.10.2.5 Shielded Metal Arc Welding

Shielded metal arc welding (SMAW), also known as manual metal arc welding, is a manual arc welding process that uses a consumable and protected electrode. As the electrode melts, a cover that protects the electrode melts and protects the weld area from oxygen and other atmospheric gases. With this method, the porosity is often not visible without the use of advanced nondestructive testing methods, and this defect usually strongly affects the strength and the quality of the weld. This welding process is used for carbon steel, low alloy steel, high alloy steel, stainless steel, cast iron, and ductile iron. In this process, the electrodes coated with rutile, provide deep weld penetration, but most of the time it is necessary to carry out PWHT in order to prevent excessive risk of cracking.

In this way, some researchers like *Oñoro* (*21*) studied 9–12Cr steels in welded materials that required good mechanical properties and corrosion resistance at high temperature. This steel normally has a fully martensite microstructure, and is also susceptible to the formation of delta ferrite, mainly during the welding process. In this study, the specimens were welded with SMAW, and a PWHT was carried out at 760 ° C for 2 h. Analyses were made of the weld metal microstructures produced by SMAW using electrodes with different compositions of Cr and other alloy elements such as Mo, W, Cu, and Co, in order to obtain a martensitic microstructure free of delta ferrite in the FZ.

6.10.2.6 Flux Cored Arc Welding

Flux-cored arc welding (FCAW) is an arc welding process which requires a continuously fed consumable tubular electrode, with an externally supplied shielding gas sometimes being used to generate the necessary protection from the atmosphere. This welding process is interesting because it generally provides good penetration into the base metal, and is normally used in mild alloy steels and low alloy steels, stainless steels, and in high nickel alloys.

Using this welding process, Thibault et al. (*1*) studied the microstructural changes in the HAZ induced by welding over 13% Cr–4% Ni stainless-steel steel plates, welded with 410NiMo material deposited in six passes with the FCAW process used in hydraulic turbine fabrication. The microstructure analysis showed that mainly martensite was formed, with a small amount of ferrite formed at high temperature. This ferrite did not transform to austenite during the cooling process. In the same way, the microhardness testing was applied across the whole weld in the six beads, but had a high dispersion, probably due to the presence of ferrite stringers.

6.10.2.7 Plasma Arc Welding

Plasma arc welding (PAW) is an arc welding process quite similar to gas TIG. In this case, the electric arc is formed between an electrode and the pieces to be welded. This process uses a nonconsumable tungsten electrode, and can be used to join metals like low alloy steels, martensitic and ferritic chromium stainless steels, and austenitic stainless steels.

www.iran-mavad.com
مرجع مهندسی مواد و متالورژی

Using this welding process, Lakshminarayanan et al. (*15*) studied the microstructure and fracture surface morphology of AISI 409M ferritic stainless-steel steel grade welded by single pass butt welded joints, with (CC TIG) PAW welding, with CC TIG and PC TIG. From the micrographs of the welded joints it was observed that as the average grain diameter of PAW joints was 10 μm. This indicates a reduction in grain diameter of 30 μm for CC TIG, and 15 μm for PC TIG.

6.10.3 Mechanical Properties

Transverse tensile properties such as yield strength, tensile strength, and percentage of elongation are important values used in the characterization of the welded joints. In most cases, the preparation of specimens is the most expensive test phase for obtaining mechanical properties and must always be prepared according to (*22*) ASTM E190-92 (Standard Test Method for Guided Bend Test for Ductility of Welds) and (*23*) ASTM E8M-04 (Standard Test Methods for Tension Testing) guidelines. In contrast to obtaining microhardness and microstructure, obtaining the mechanical properties of the welded materials differs greatly depending on the type of welding process used.

Specimens are usually taken perpendicular to the weld, which is centered in the specimen, but sometimes specimens can be taken along the weld and consist entirely of weld metal. For example, in TIG (*2*), laser (*1*), and friction stir (*11*) welding, the specimens are machined in a cylindrical shape or rectangular cross sections in a perpendicular or parallel direction to the cord direction, and at other times, specimens are machined the same way but welded using friction (*19*) (**Figure 3**).

6.10.3.1 Laser Beam Welding

In a study presented by Zambon et al. (*16*) on parts welded by laser, the dimensions of the specimens did not follow the standard indications. These tests showed tensile stresses very close to the yield strength (YS) and in the longitudinal direction in the weld bead. The stresses were compressive in the transverse direction and in the base material. In this case, the tensile strength of the weld bead exceeded the value of the base metal.

6.10.3.2 Tungsten Inert Gas Welding

Divya et al. (*24*) studied the mechanical properties of welded parts with TIG welding techniques in order to obtain the YS and ultimate tensile strength (UTS) in the cross weld tensile. In this case, the tested material was AISI 410 steel for the plates and

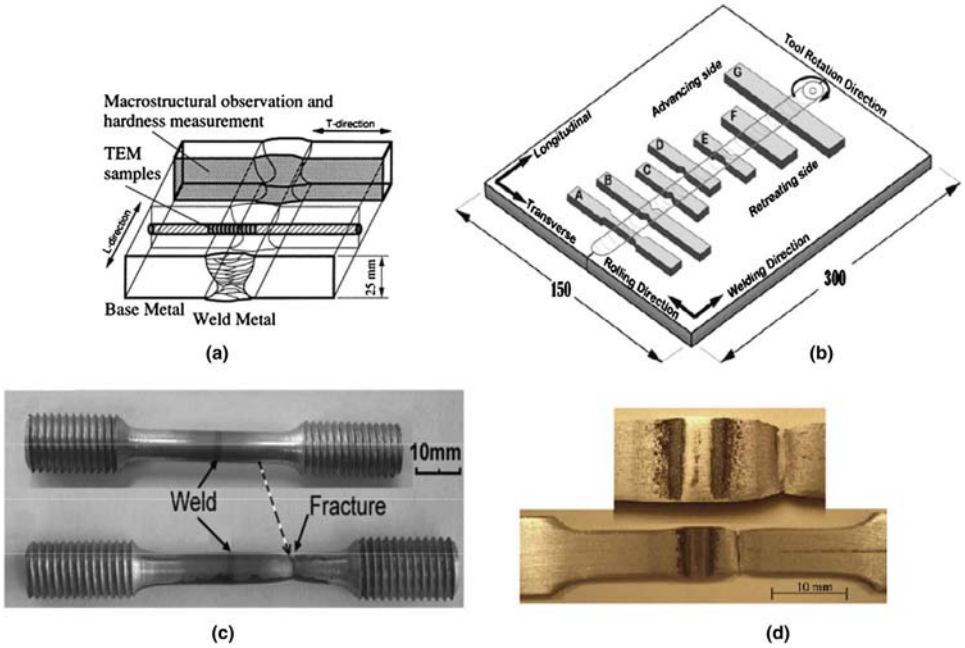

Figure 3 Diagrams of extraction of specimens for mechanical testing: (a) TIG (Reproduced from Inoue, N.; Muroga, T.; Nishimura, A.; Motojima, O. Correlation between Microstructure and Hardness of a Low Activation Ferritic Steel (JLF-1) Weld Joint. *J. Nucl. Mater.* **1998**, *258–263*, 1248–1252); (b) Friction stir (Reproduced from Lakshminarayanan, A. K.; Balasubramanian, V. An Assessment of Microstructure, Hardness, Tensile and Impact Strength of Friction Stir Welded Ferritic Stainless Steel Joints. *Mater. Des.* **2010**, *31*, 4592–4600); (c) Friction (Reproduced from Ma, T.; Li, W. Y.; Xu, Q.; Zhang, Y.; Li, J.; Yang, S.; Liao, H. Microstructure Evolution and Mechanical Properties of Linear Friction Welded 45 Steel Joint. *Adv. Eng. Mater.* **2007**, *9* (8)); (d) Laser (Reproduced from Thibault, D.; Bocher, P.; Thomas, M. Residual Stress and Microstructure in Welds of 13%Cr–4%Ni Martensitic Stainless Steel. *J. Mater. Process. Technol.* **2009**, *20* (9), 2195–2202).

www.iran-mavad.com
مرجع مهندسی مواد و متالورژی

410NiMo for the cord. Similarly, Lakshminarayanan et al. (15) studied the effects of different arc welding processes on yield strength (YS) and UTS of AISI 409M ferritic stainless-steel steel grade. In this case, the plates were welded by a single pass butt-welded joints with CC TIG and PC TIG. An increase of 30% in strength values in CC TIG welding, and 35% in strength values in PC TIG, was detected compared to the unwelded base metal.

6.10.3.3 Friction Welding

The tensile properties of the 45 steel after Rotary FW were studied by Tiejun Ma et al. (19). In this case, tensile properties of the welded joint were improved both in strength and ductility, and the fractures of all specimens seemingly occurred in the HAZ far from the weld and close to the parent metal.

6.10.3.4 Submerged Arc Welding

Hashemi et al. (20) measured the tensile properties of X65 base steel welded by double submerged arc welded (SAW Welding) in a line pipe steel of grade API X65 manufactured and welded by spiral forming. In this case, three flat tensile bars were taken from the original pipe in its hoop direction, and the values for the material tensile properties for this parent metal was yield strength (YS) $>$ 448 MPa and tensile strength (TS) $>$ 531 MPa.

6.10.3.5 Plasma Arc Welding

Lakshminarayanan et al. (15) studied the YS and UTS of AISI 409M ferritic stainless steel welded by single pass butt welded joints with CC TIG (PAW Welding). This work indicated that there is an increase of 30% in strength values from the base metal with CC TIG and 35% with PC TIG welding, and showed that the joints fabricated by the PAW process exhibit higher strength values than CC TIG and PC TIG.

6.10.4 Residual Stresses

Material and structural properties such as fatigue, strength, and corrosion resistance in welded components are commonly influenced by residual stresses, and is one of the most important factors taken into account during the design and manufacturing of different products. Obtaining residual stresses by researchers over recent years has forced the development of new methods specific for the welded material and the welding process used. According to Rossini et al. (12), these methods can be classified as destructive, semidestructive, and nondestructive techniques. In **Figure 4**, some of the most used methods to obtain the values of residual stresses are shown. **Figure 4(a)** shows the procedure for obtaining the residual stress through drilling a hole. **Figures 4(a) and 4(b)** show the residual stress contour obtained with the method and the neutron diffraction respectively.

6.10.4.1 Laser Beam Welding

In this welding process, Olabi et al. (25) studied the minimization of the residual stress in the HAZs of welded AISI 304 plates. This optimization was performed by means of several design of the experiments (DOE) techniques, and the residual stresses were obtained with the hole drilling method. Others authors, such as Zambon et al. (16), used techniques based on X-ray diffraction (XRD) and the residual stresses in AISI 904L superaustenitic stainless-steel steel sheets. In this case, the maximum tensile stresses were close to the YS value, and were located in the longitudinal direction in the weld bead. Likewise, in the transverse direction and in the base material, the values were compressive. **Figure 5** presents the laser welding machine.

6.10.4.2 Metal Inert Gas Welding

The effect of PWHTs on the residual stress of low carbon steel AISI 1020 components welded with metal inert gas (MIG) welding was studied by Olabi et al. (26). In this study, different PWHT parameters were applied in different soaking temperatures at 450, 550, and 650 °C. The hole drilling method was applied to determine the magnitude and distribution of residual stresses before and after the application of the PWHTs. Likewise, Thibault et al. (27) studied residual stress characterization by neutron diffraction and the contour method on 13% Cr–4% Ni welds that were made using 410NiMo weld filler metal. The transverse, longitudinal, and normal components of stress were measured by neutron diffraction, and the longitudinal stress distribution was also measured by the contour method.

6.10.4.3 Flux Cored Arc Welding

Paradowska et al. (28) studied residual stress due to various restraints for a single bead, and in fully restrained samples with different numbers of beads with the FCAW process with low-carbon steel plates. In this case, a neutron diffraction technique was used in order to investigate the residual stress distribution during the welding process. Similarly, the distribution of residual stresses induced

www.iran-mavad.com
مرجع مهندسی مواد و متالورژی

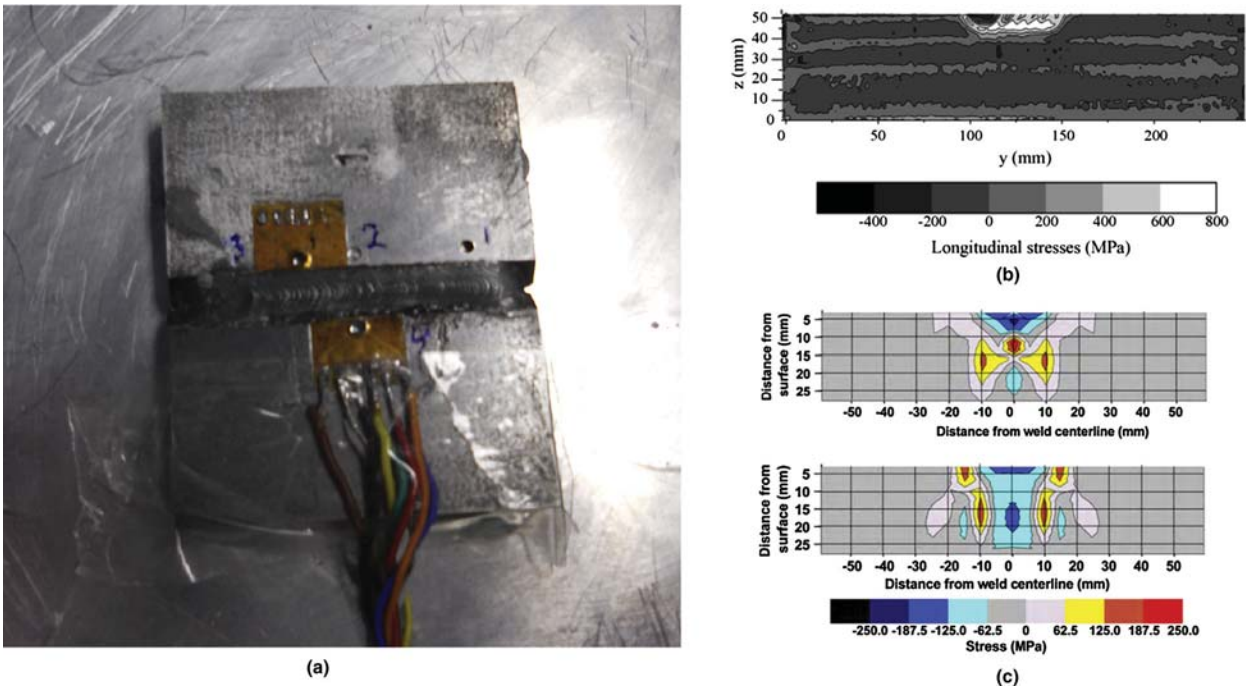

Figure 4 (a) Obtaining residual stresses by hole drilling; (b) longitudinal stresses measured by the contour method (Reproduced from Thibault, D.; Bocher, P.; Thomas, M. Residual Stress and Microstructure in Welds of 13%Cr–4%Ni Martensitic Stainless Steel. *J. Mater. Process. Technol.* **2009**, *20* (9), 2195–2202); (c) Normal residual stress distributions measured by neutron diffraction (Reproduced from Thibault, D.; Bocher, P.; Thomas, M.; Gharghouri, M.; Côté, M. Residual Stress Characterization in Low Transformation Temperature 13%Cr–4%Ni Stainless Steel Weld by Neutron Diffraction and the Contour Method. *Mater. Sci. Eng. A* **2010**, *527*, 6205–6210).

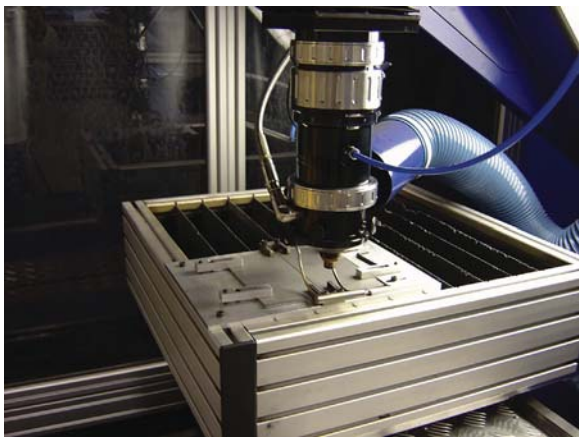

Figure 5 The laser welding machine.

by welding in the HAZ over 13% Cr–4% Ni stainless-steel steel plates welded with 410NiMo material deposited was studied by Thibault et al. (*1*). In this case, hole-drilling, XRD, and the contour methods were used after welding. The contour method allowed quantification of the residual stresses at the core of the plate, and produced a complete pattern of perpendicular residual stresses on an entire plane.

6.10.4.4 Tungsten Inert Gas Welding

The residual stress in high-chromium steel AISI 410 used in aircraft engines and heating and cooling at different rates were investigated by Olabi (*14*). The hole-drilling method was used in order to determine the magnitude and distribution of the residual stresses in the welded component before and after the application of PWHT.

www.iran-mavad.com
مرجع مهندسی مواد و متالورژی

6.10.5 Impact Strength Testing

Impact Strength Testing or Charpy Impact Testing is an ASTM standard method for determining impact energy. Impact tests are used for studying the toughness of material, which represents the absorbed energy during plastic deformation of the materials. For determining the impact energy in welded components, standard shaped impact specimens were machined by following the guideline according to the German Standard (DIN-50121) with a V-notch. The value of this energy is normally obtained in the HAZ zone and the base metal of the welded union, and for this reason, the V-notch is located in this area (**Figure 6**).

6.10.5.1 Tungsten Inert Gas Welding

Olabi and Hashmi (*14*) studied the absorption of impact energy of high-chromium steel AISI 410 used in aircraft engines welded by laser after heating and cooling at different rates. This study detected a substantial improvement in the impact energy after applying a very slow cooling rate and by applying PWHT for long time durations, but with only slight improvement in the impact energy by decreasing the heating rate. In **Figure 7**, the schematic diagram of the double shielded TIG welding process is shown (*29*).

6.10.5.2 Metal Inert Gas Welding

Divya et al. (*24*) studied the impact toughness in welded parts made by the TIG welding techniques. In this case, the tested material was AISI 410 steel for the plates and 410NiMo for the cord. The results of this impact test showed that the weld metal, after a two stage heat treatment, possessed excellent toughness, and the fracture mode showed a quasi cleavage in the stretch zone and ductile in the center region. The effect of PWHTs on the toughness of low carbon steel AISI 1020 welded components with MIG was studied by Olabi et al. (*26*). The soaking temperatures were 450, 550, and 650 °C for the application of PWHT, and it was found that the maximum improvement in the toughness was obtained at 650 °C. **Figure 8** presents a schematic diagram of MIG welding set-up (*30*).

6.10.5.3 Friction Welding

The toughness of friction in a stir welded 409M ferritic stainless-steel steel joint was studied by Lakshminarayanan and Balasubramanian (*11*) for friction stir welding. The maximum value of toughness was on the unwelded base metal, and this value reduced toward the weld centerline and HAZ region. **Figure 9** presents a schematic drawing of the four linear FW stages: (a) initial, (b) transition, (c) equilibrium, and (d) deceleration stage (*31*).

6.10.5.4 Plasma Arc Welding

The work presented by Lakshminarayanan et al. (*15*) showed that for AISI 409M ferritic stainless-steel steel grade, the values obtained with the PAW process exhibit 25% higher impact toughness values compared to PC TIG joints, and 50% higher compared to

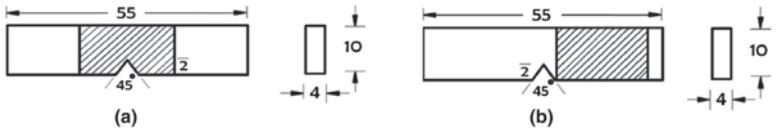

Figure 6 (a) Impact specimen (notch at weld center); (b) Impact specimen (notch at HAZ). Reproduced from Lakshminarayanan, A. K.; Balasubramanian, V. An Assessment of Microstructure, Hardness, Tensile and Impact Strength of Friction Stir Welded Ferritic Stainless Steel Joints. *Mater. Des.* **2010**, *31*, 4592–4600.

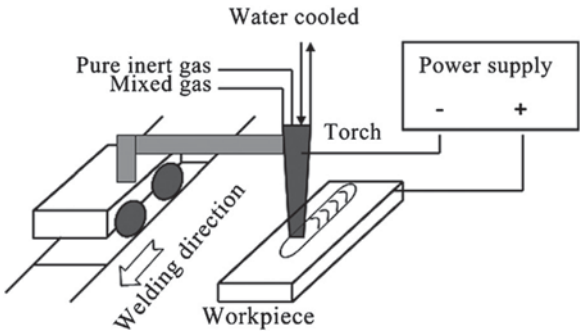

Figure 7 Schematic diagram of the double shielded TIG welding process. Reproduced from Li, D.; Lu, S.; Dong, W.; Li, D.; Li, Y. Study of the Law between the Weld Pool Shape Variations with the Welding Parameters under Two TIG Processes. *J. Mater. Process. Technol.* **2012**, *212* (1), 128–136.

www.iran-mavad.com
مرجع مهندسی مواد و متالورژی

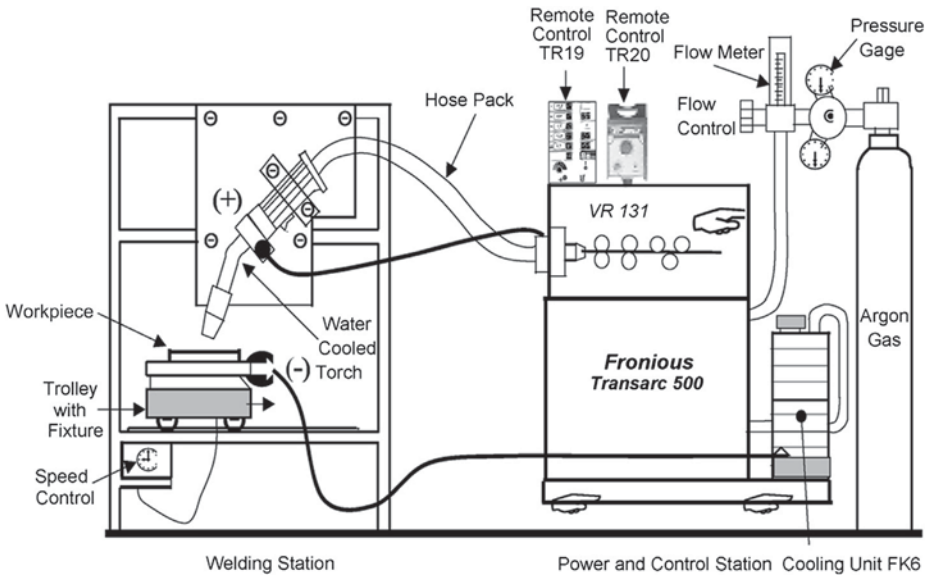

Figure 8 A schematic diagram of MIG welding setup. Reproduced from Ganjigatti, J. P.; Pratihar, D. K.; Roy Choudhury, A. Global versus Cluster-wise Regression Analyses for Prediction of Bead Geometry in MIG Welding Process. *J. Mater. Process. Technol.* **2007**, *189* (1–3, 6), 352–366.

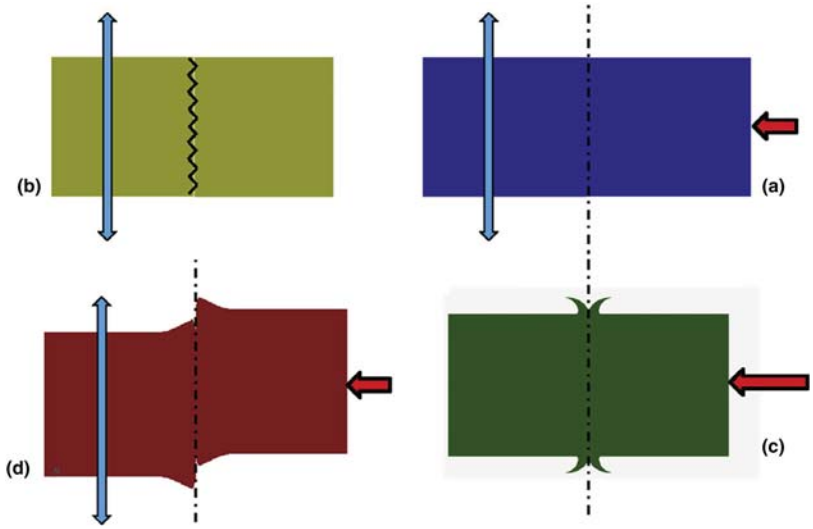

Figure 9 A schematic drawing of the four linear FW stages: (a) Initial; (b) Transition; (c) Equilibrium; (d) Deceleration stage. Reproduced from Fratini, L.; Buffa, G.; Campanella, D.; La Spisa, D. Investigations on the Linear Friction Welding Process through Numerical Simulations and Experiments. *Mater. Des.* **2012**, *40*, 285–291.

CC TIG joints. Likewise, there is a 55% reduction in the toughness value due to CC TIG welding, and 31.82% reduction for PC TIG joints when compared to that in the base metal. Figure 10 presents a schematic of keyhole PAW process (*32*).

6.10.6 Discussions

A comparative study of hardness and microstructure, mechanical properties, and the residual stresses for the parent material, weld bead, and HAZ for different welding processes is discussed in this chapter. The study solely covers ferritic and martensitic stainless-steel materials, as well as on dissimilar materials.

First, different microstructures formed in different welding processes were compared. As a general rule, the MIG process produces coarser grains compared to the SMAW and TIG processes. The heat input supplied by the MIG process is relatively high compared to that of the SMAW and TIG processes and, for this reason, the variations in heat input of the welding processes influence the weld

www.iran-mavad.com
مرجع مهندسی مواد و متالورژی

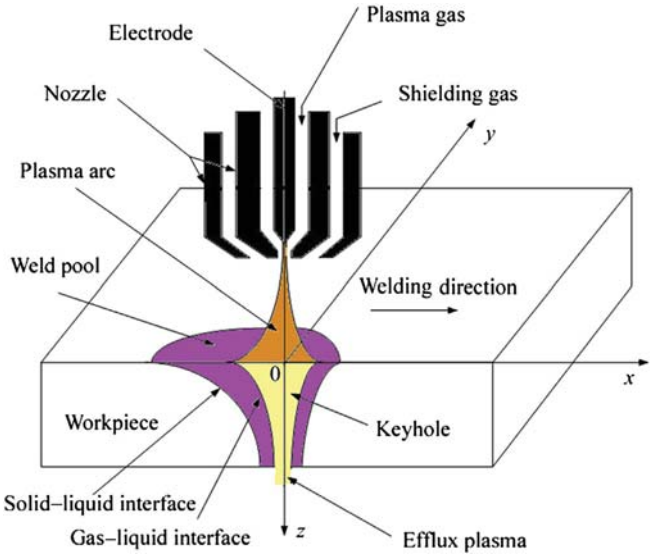

Figure 10 Schematic of keyhole PAW process. Reproduced from Sun, J.; Wu, C. S.; Feng, Y. Modeling the Transient Heat Transfer for the Controlled Pulse Key-holing Process in Plasma Arc Welding. *Int. J. Therm. Sci.* **2011**, *50* (9), 1664–1671.

thermal cycle and subsequently causes important variations in microstructures. Ferritic stainless steels lose their toughness, ductility, and corrosion resistance to be soldiers mainly because of grain growth and the formation of martensite. This excessive grain growth can be avoided by using lower welding heat inputs. For instance, AISI 430 ferritic stainless steel has greater ductility and strength if it is welding with TIG compared to the SMAW process.

Austenitic stainless steels can be easily welded using high power density sources, such as laser, and the major advantages of these welding processes are a small HAZ, which cools very rapidly with very little distortion (*16*). Superaustenitic stainless steels obtained by means of PAW shows fully dendritic and austenitic microstructures. Generally, in austenitic and superaustenitic steels, the welds produced with TIG flux, exhibited equivalent or improved microstructure and properties when compared to the autogenous nonflux welds.

Likewise, the values of Vickers hardness, toughness (Charpy), YS, and tensile strength are shown in **Table 1** for different materials and for different manufacturing processes. The first column of the table shows the manufacturing process, and the next three

Table 1 Summary of Vickers hardness, tensile, and Charpy testing for materials and welding processes

Vickers hardness, Charpy, and tensile for materials and process											
Process	*Material*	*HV base*	*HV weld*	*HV HAZ*	*Charpy base*	*Charpy weld*	*Charpy HAZ*	*B. tens. st. (MPa)*	*B. yie. st. (MPa)*	*W. tens. st. (MPa)*	*W. yie. st. (MPa)*
TIG (*7*)	AISI 4130	275	440	325	–	–	–	–	–	1575	1260
TIG (*2*)	Low activation ferritic steel	200	280	180	–	–	–	–	–	–	–
SAW (*20*)	API X65	211	218	208	271	163	199	490	552	600	758
TIG (*14*) minimum PWT	AISI 410	–	–	–	–	–	–	–	–	–	10
TIG (*14*) maximum PWT	AISI 410	–	–	–	–	–	–	–	–	–	25
Laser (*18*)	AISI 904S	175	210	–	–	–	–	–	–	–	–
TIG (CC) (*15*)	AISI 409M	–	–	–	22	10	–	359	524	510	600
TIG (PC) (*15*)	AISI 409M	–	–	–	22	15	–	359	524	550	650
Laser (*16*)	AISI 904L	180	195	–	–	–	–	–	–	–	–
Laser (*17*)	DP600	325	200	195	–	–	–	380	610	410	600
FCAW (*1*)	Martens-s-s 13%Cr–4%Ni	300	375	375	–	–	–	–	–	–	–
Friction stir (*11*)	AISI 409M	170	375	–	34	28	–	364	536	610	906
SMAW (*29*)	AISI 409M	325	290	–	20	18	–	359	480	230	285
MIG (*29*)	AISI 409M	325	275	–	20	16	–	359	480	215	270
MIG (*29*) maximum PWT	AISI 1020	220	–	275	–	80	–	–	–	–	458
PAW (*15*)	AISI 409M	–	–	–	22	20	–	359	524	840	990

www.iran-mavad.com
مرجع مهندسی مواد و متالورژی

Table 2 Summary of residual stresses of base metal and welded joints

Residual stresses of base metal and welded joints								
Process	*Material*	*Long. res. mat. (MPa)*	*Trans. res. mat. (MPa)*	*Long. res. HAZ (MPa)*	*Trans. res. HAZ (MPa)*	*Long. res. weld (MPa)*	*Trans. res. weld (MPa)*	*Measuring residual stresses*
FCAW (*28*) single bead	Low-carbon steel	−300	0	360	0	–	–	Neutron diffraction
FCAW (*28*) multi beads	Low-carbon steel	−40	200	480	60	–	–	Neutron diffraction
TIG (*14*) (no PWT)	AISI 410	−30		225				Hole drilling
Laser (*16*)	AISI 904L	–	–	128	−113	239	−345	X-ray
Laser (*25*)	AISI 304	–	–	104	–	–	–	Hole drilling
FCAW (*1*)	13%Cr–4%Ni martensitic stainless steel	0	−10	340	460	–	–	Hole-drilling, x-ray, contour method
MIG (*27*) (no PWT)	13%Cr–4%Ni martensitic stainless steel (410NiMo weld filler)	−50	−30	−350	−180	−360	−100	Neutron diffraction, contour method

columns are the Vickers hardness for base material, weld, and HAZ, respectively. The next three columns show the values of toughness measured in the base material, weld bead, and HAZ, respectively. The last four columns show the values of YS and tensile strength for the base material and for the weld bead. From this table, it is observed that the material AISI 4130 welded with TIG (*7*) presents the highest values of YS and tensile strength (1575 MPa and 1260 MPa). In addition, this material exhibits the highest value for the Vickers Hardness Weld Cord (440) and for the beam (325). Similarly, the AISI 409M material welded with friction stir (*11*) has the next highest values, having 906 MPa and 610 MPa for the values of tensile strength and YS, respectively. However, this material has a value of 375 Vickers hardness for the HAZ, and not a very high value for the base material (170), but a value of 28 J for the weld cord and 34 J for the base material. Also, this same material AISI 409M, welded with SMAW (*11*), exhibited values of 285 MPa and 230 MPa for YS and tensile strength, a value of 18 J for the weld beam and 20 J for the base material, and values of 290 and 325 for Vickers hardness of the weld beam and for the HAZ, respectively. This same material welded with MIG (*11*) presents a slightly lower value of YS, tensile strength, toughness, and Vickers hardness than if it had been welded with SMAW (*11*). However, this material welded with PAW (*15*) exhibited 990 MPa YS, and 20 J toughness of the weld beam. But if this material is welded with CC TIG (*15*) and PC TIG (*15*), it exhibited values of 650 MPa for the YS and values of 10 J and 15 J for the weld beam, respectively. Furthermore, the material AISI 1020 welded with MIG exhibited values of 458 MPa for YS, 80 J for the beam weld, and 275 for Vickers hardness, once the material has been subjected to several PWT (*33*). From **Table 1**, it is deduced that welds that present high values of TS and YS, usually also show high Vickers hardness values on the weld beam. Likewise, TIG joints exhibiting superior tensile properties and impact toughness compared to SMAW and MIG joints. During tensile tests, all the specimens invariably failed at the HAZ irrespective of tensile test, and similarly all the specimens invariably failed at the HAZ irrespective of welding processes. This implies that the FZ region is much stronger than the HAZ.

Likewise, in **Table 2**, values of the residual stresses measured in the longitudinal and transverse directions for the base metal, the HAZ, and the weld beam are shown. The first column of the table shows the manufacturing process and the materials welded, and the next six columns are the residual stresses measured in the longitudinal and transverse directions for the base metal, the HAZ, and the weld beam, respectively. The last column shows the procedure used for obtaining the values of the residual stresses. From **Table 2** it is clear that low carbon steel welded with FCAW (*28*) exhibits maximum values of 480 MPa and 360 MPa in the HAZ with multibeads and single beads, respectively. Likewise, in welded material for multibeads and single beads the values are −300 MPa and −40 MPa. MIG (*27*) welding process for 13% Cr–4% Ni martensitic stainless steel showed maximum values on the surface for the weld cord in longitudinal and transversal directions of −360 MPa and −100 MPa, respectively. The values in the HAZ was −350 MPa in longitudinal and −180 MPa in transversal direction, and −50 MPa for longitudinal direction in base material. From **Table 2** it is concluded that FCAW shows high longitudinal residual stress values on the weld beam for multibeads and single beads in the HAZ for low carbon steel. The values obtained in FACW for martensitic stainless steel in HAZ (*1*) was 340 for longitudinal and 460 for transversal stresses, demonstrating that the value for transversal stress is higher for this material than low carbon steel.

6.10.7 Concluding Remarks

This study reveals the great interest in examining the microstructure, microhardness, residual stresses, and the mechanical properties for ferritic and martensitic stainless-steel welded joints. In addition, this study clearly shows that the microstructural and the internal stresses play a major role in describing how well the welded joint will serve in a real application. Furthermore, the amount of distortion varies significantly from one welding process to another. This variation is a function of the heat input that is introduced to the welded joint and to the cooling rate. Some welding processes may result in a high heat input such as SAW, while other processes may result

www.iran-mavad.com
مرجع مهندسی مواد و متالورژی

in very little amounts of heat input such as in laser welding processes. In terms of microstructure and hardness of the HAZ and the fusion zone, greater heat input leads to an increase in grain size, which in return causes coarse microstructure and lower hardness.

Also, high heat input may improve the welded structure in the actual application where high toughness is required, because it improves the impact strength of the welded joint. Similarly, the size of the FZ has an impact on the properties of the welded joint. Very high cooling rates can be achieved in some welding processes like laser welding. The amount of heat introduced to the small melted area is conducted to the bulk materials resulting in higher cooling rates. The residual stress distribution, magnitude, and sign affect the mechanical properties of the welded joint. Generally, compressive residual stresses improve the performance of welded components because they reduce service tensile stresses and curb crack nucleation. On the other hand, tensile residual stresses will speed up crack nucleation, which may result in early failure of the welded component.

On balance, to achieve a welded joint with desirable properties is a matter of compromise. Engineers often search for conditions that will optimize the welding process, and they therefore attempt to determine the values of the welding process input parameters that will result in properties of the welded joint to reach their optimum. The optimum could be either a minimum or a maximum of a particular function in terms of the process input parameters. Residual stress microstructure (RSM) based on design of experiment is one of the optimization techniques currently used to describe the performance of the welding process and to find the optimal properties of the welded joint.

References

1. Thibault, D.; Bocher, P.; Thomas, M. Residual Stress and Microstructure in Welds of 13%Cr–4%Ni Martensitic Stainless Steel. *J. Mater. Process. Technol.* **2009,** *20* (9), 2195–2202.
2. Inoue, N.; Muroga, T.; Nishimura, A.; Motojima, O. Correlation between Microstructure and Hardness of a Low Activation Ferritic Steel (JLF-1) Weld Joint. *J. Nucl. Mater.* **1998,** *258–263,* 1248–1252.
3. Gharibshahiyan, E.; Raouf, A. H.; Parvin, N.; Rahimian, M. The Effect of Microstructure on Hardness and Toughness of Low Carbon Welded Steel Using Inert Gas Welding. *Mater. Des.* **2011,** *32,* 2042–2048.
4. Reed-hill, R. E.; Abbaschian, R. *Physical Metallurgy Principles,* 3rd ed.; PWS Publishing Company, 1994.
5. Ramazan, K.; Koray, K. Effect of Controlled Atmosphere on the MIG–MAG Arc Weldment Properties. *Mater. Des.* **2005,** *26,* 508–516.
6. Loureiro Altino, J. R. Effect of Heat Input on Plastic Deformation of Undermatched Weld. *J. Mater. Process. Technol.* **2002,** *128,* 240–249.
7. Ghazanfari, H.; Naderi, M.; Iranmanesh, M.; Seydi, M.; Poshteban, A. A Comparative Study of the Microstructure and Mechanical Properties of HTLA Steel Welds Obtained by the Tungsten Arc Welding and Resistance Spot Welding. *Mater. Sci. Eng. A* **2012,** *534,* 90–100.
8. Cahoon, J. R.; Broughton, W. H.; Kutzak, A. R. *Metall. Trans.* **1971,** *2,* 1979–1983.
9. Challenger, K. D.; Moteff, J. *Scr. Metall.* **1972,** *6,* 155–160.
10. Karl, M.; Ratan, D.; Horst, Z. Effects of Heat Input on the Microstructure and Toughness of the 8MnMONi 5 5 Shape-welded Nuclear Steel. *J. Nucl. Mater.* **2005,** *340,* 25–32.
11. Lakshminarayanan, A. K.; Balasubramanian, V. An Assessment of Microstructure, Hardness, Tensile and Impact Strength of Friction Stir Welded Ferritic Stainless Steel Joints. *Mater. Des.* **2010,** *31,* 4592–4600.
12. Rossini, N. S.; Dassisti, M.; Benyounis, K. Y.; Olabi, A. G. Methods of Measuring Residual Stresses in Components. *Mater. Des.* **2012,** *35,* 572–588.
13. Macherauch, E.; Origin, K. H. Measurements and Evaluation of Residual Stresses. *Residual Stress Sci. Technol.* **1987,** 3–26.
14. Olabi, A. G.; Hashmi, M. S. J. Effects of the Stress-relief Conditions on a Martensite Stainless-steel Welded Component. *J. Mater. Process. Technol.* **1998,** *77,* 216–225.
15. Lakshminarayanan, A. K.; Shanmugam, K.; Balasubramanian, V. Effect of Autogenous Arc Welding Processes on Tensile and Impact Properties of Ferritic Stainless Steel Joints. *J. Iron Steel Res., Int.* **2009,** *16* (1), 62–68.
16. Zambon, A.; Ferro, P.; Bonollo, F. Microstructural, Compositional and Residual Stress Evaluation of CO_2 Laser Welded Superaustenitic AISI 904L Stainless Steel. *Mater. Sci. Eng. A* **2006,** *424,* 117–127.
17. Farabi, N.; Chen, D. L.; Li, J.; Zhou, Y.; Dong, S. J. Microstructure and Mechanical Properties of Laser Welded DP600 Steel Joints. *Mater. Sci. Eng. A* **2010,** *527,* 1215–1222.
18. Sathiya, P.; Abdul Jaleel, M. Y. Measurement of the Bead Profile and Microstructural Characterization of a CO_2 Laser Welded AISI 904 L Super Austenitic Stainless Steel. *Opt. Laser Technol.* **2010,** *42,* 960–968.
19. Ma, T.; Li, W. Y.; Xu, Q.; Zhang, Y.; Li, J.; Yang, S.; Liao, H. Microstructure Evolution and Mechanical Properties of Linear Friction Welded 45 Steel Joint. *Adv. Eng. Mater.* **2007,** *9* (8).
20. Hashemi, S. H.; Mohammadyani, D. Characterisation of Weldment Hardness, Impact Energy and Microstructure in API X65 Steel. *Int. J. Pressure Vessels Piping* **2012,** *98,* 8–15.
21. Oñoro, J. Martensite Microstructure of 9–12%Cr Steels Weld Metals. *J. Mater. Process. Technol.* **2006,** *180,* 137–142.
22. ASTM E190-92, Standard Test Method for Guided Bend Test for Ductility of Welds.
23. ASTM E8-04, Standard Test Methods for Tension Testing of Metallic Materials.
24. Divya, M.; Das, C. R.; Ramasubbu, V.; Albert, S. K.; Bhaduri, A. K. Improving 410NiMo Weld Metal Toughness by PWHT. *J. Mater. Process. Technol.* **2011,** *211,* 2032–2038.
25. Olabi, A. G.; Casalino, G.; Benyounis, K. Y.; Rotondo, A. Minimisation of the Residual Stress in the Heat Affected Zone by Means of Numerical Methods. *Mater. Des.* **2007,** *28,* 2295–2302.
26. Olabi, A. G.; Hashmi, M. S. J. Stress Relief Procedures for Low Carbon Steel (1020) Welded Components. *J. Mater. Process. Technol.* **1996,** *56,* 552–562.
27. Thibault, D.; Bocher, P.; Thomas, M.; Gharghouri, M.; Côté, M. Residual Stress Characterization in Low Transformation Temperature 13%Cr–4%Ni Stainless Steel Weld by Neutron Diffraction and the Contour Method. *Mater. Sci. Eng. A* **2010,** *527,* 6205–6210.
28. Paradowska, A.; Price, J. W. H.; Ibrahim, R.; Finlayson, T. A Neutron Diffraction Study of Residual Stress due to Welding. *J. Mater. Process. Technol.* **2005,** *164–165,* 1099–1105.
29. Li, D.; Lu, S.; Dong, W.; Li, D.; Li, Y. Study of the Law between the Weld Pool Shape Variations with the Welding Parameters under Two TIG Processes. *J. Mater. Process. Technol.* **2012,** *212* (1), 128–136.
30. Ganjigatti, J. P.; Pratihar, Dilip Kumar; Roy Choudhury, A. Global versus Cluster-wise Regression Analyses for Prediction of Bead Geometry in MIG Welding Process. *J. Mater. Process. Technol.* **2007,** *189* (1–3, 6), 352–366.
31. Fratini, L.; Buffa, G.; Campanella, D.; La Spisa, D. Investigations on the Linear Friction Welding Process through Numerical Simulations and Experiments. *Mater. Des.* **2012,** *40,* 285–291.
32. Sun, J.; Wu, C. S.; Feng, Y. Modeling the Transient Heat Transfer for the Controlled Pulse Key-holing Process in Plasma Arc Welding. *Int. J. Therm. Sci.* **2011,** *50* (9), 1664–1671.
33. Olabi, A. G.; Hashmi, M. S. J. The Microstructure and Mechanical Properties of Low Carbon Steel Welded Components after the Application of PWHTs. *J. Mater. Process. Technol.* **1996,** *56,* 88–97.

www.iran-mavad.com
مرجع مهندسی مواد و متالورژی

6.11 Quality Control in Welding Process

AG Olabi, University of the West of Scotland, Paisley, Renfrewshire, UK
RL Lorza, University of La Rioja, Spain
KY Benyounis, Dublin City University, Dublin, Ireland

© 2014 Elsevier Ltd. All rights reserved.

6.11.1	**Introduction**	193
6.11.2	**Testing the Quality of the Weld**	193
6.11.3	**Distortion in Weldment**	194
6.11.4	**Measuring Methods of Residual Stress**	194
6.11.4.1	Mechanical Methods	196
6.11.4.1.1	Hole-Drilling Technique	196
6.11.4.1.2	Deep Hole Method	198
6.11.4.1.3	Sectioning Technique	198
6.11.4.1.4	Contour Method	200
6.11.4.1.5	Other Destructive Methods	200
6.11.4.2	Diffraction Techniques	202
6.11.4.2.1	X-ray Diffraction Method	202
6.11.4.2.2	Neutron Diffraction Method	203
6.11.4.3	Other Nondestructive Techniques	205
6.11.4.3.1	Barkhausen Noise Method	205
6.11.4.3.2	Ultrasonic Method	206
6.11.5	**Concluding Remarks**	208
References		210

6.11.1 Introduction

Welded components are designed to serve in a certain structure, which contains other welded and/or mechanical components. To ensure that these welded components will achieve their planned function, they need to be tested to examine their quality. The tests can be done by observing the welded structure in actual service, which is costly and time consuming. Alternatively, a standardized test procedure could be followed in order to predict the performance of the welded joint. Some of these tests are distractive and some are nondistractive. These tests measure a variety of properties and distortion which occur in the welded joint as a result of thermal loading. The most important cause of this distortion is the residual stresses.

Residual stresses are internal stresses that remain in the component without any external loading. Residual stress exists in practically all mechanical components, whether they are metal or not (ceramic, glass, polymer, wood, etc.). They are self-balanced internal stresses; therefore, the resultant force and moment produced by them must be equal to zero. Residual stresses can be classified as macro stresses and micro stresses. Macro stresses occur over a long range and they are self-equilibrated in the cross-section of the manufactured part. In all welded structures, residual stresses are produced in regions around the welded joint. Whereas, micro stresses are of a short range. They are homogenous or inhomogeneous on a micro scale (*1*).

This chapter discusses the effect of residual stresses on the welded components. Comprehensive details will be addressed to present the quality control in welding process; good quality of welded components would be achieved by reducing or eliminating the residual stresses. Residual stresses should be measured to insure the high quality of the welding process; this chapter also will discuss in detail the different methods of measuring the residual stresses which would help researchers and investigators to choose the correct measurement method which could be implemented. Then, further discussions are introduced to present the effect of Post Weld Heat Treatment (PWHT) on the residual stresses and its role in producing high quality of welded components.

6.11.2 Testing the Quality of the Weld

All manufacturing and fabricating processes introduce residual stresses into the manufactured part. Extreme service loading may also change the state of residual stress in the part. The effect of residual stress may be either beneficial or detrimental, depending upon the sign, magnitude, and distribution of the stress. In fact, compressive residual surface stresses are important because notches, scratches, sharp changes in cross-section, etc., concentrate additional applied tensile stresses near the surface and can initiate a crack. These additional applied tensile stresses must overcome the residual compressive stresses to initiate the crack. Thus, the presence of surface compressive residual stresses is a highly favorable condition. On the other hand, tensile residual stresses will speed up crack nucleation, which may result in early failure of the welded component (*2*,*3*).

www.iran-mavad.com
مرجع مهندسی مواد و متالورژی

There are three phenomena in welded components by which the transverse residual stress would be generated; these phenomena are as follows:

1. Variation in shrinkage of the areas which are heated in a different ways,
2. Surface quenching,
3. Nonequilibrium transformation of austenite.

In reality, the various stress origins are not independent. At least two or even three different kinds of stress on cooling welded joint are superimposed, leading to a complicated total state of stress (4,5).

6.11.3 Distortion in Weldment

As previously discussed, welding involves highly localized heating. Also, the temperature is nonuniformly distributed. Upon cooling, the weld pool solidifies and shrinks resulting in stresses in WZ and HAZ. If the stresses produced from thermal expansion and contraction exceed the yield strength of the material being welded, localized plastic deformation in the component occurs. Therefore, the component dimensions change and destroy the structure. Three different types of residual stress induced distortion can be found in welded structures. Longitudinal and transverse shrinkage can cause in-plane distortion of the component. Plane or axis-symmetrical angular shrinkage can cause distortion perpendicular to the plane of the welded component. Another distortion is bending due to grids with longitudinal and transverse welds (6). Examples of distortion that can occur during welding are illustrated in **Figure 1** (6).

The maximum value of the harmful residual stress is about 360 N mm^{-2} (tensile stress) near the welding line and it decreases to be about 165 N mm^{-2} at the distance of 80 mm from the welding axis. The minimum residual stress is about 90 N mm^{-2} near the welding line and it becomes about 60 N mm^{-2} in compression at the distance of about 60 mm, then it reduces to about 10 N mm^{-2} in tension at 80 mm distance from the axis. Such high tensile residual stresses are the result of thermoplastic deformations during the welding process and are one of the main factors leading to the origination and propagation of fatigue cracks in welded elements.

Welding is a vital production process for industry, and generates residual stresses at a remarkable level. They are formed in the structure as the result of differential contractions which occur as the weld metal solidifies and cools to ambient temperature. In fact, welding introduces high heat input to the material being welded. As a result, nonuniform heat distributions, plastic deformations, and phase transformations occur on the material. These changes generate different residual stresses patterns for weld region and in the Heat Affected Zone (HAZ). Each stress generating mechanism has its own effects on the residual stress distribution as shown in **Figure 2**. Residual stresses induced by shrinkage of the molten region are usually tensile. Transformation induced residual stresses occur at the parts of the HAZ where the temperature exceeds the critical values for phase transformations. When the effect of phase transformations is dominant, compressive residual stresses are formed in the transformed areas (7).

6.11.4 Measuring Methods of Residual Stress

During the past years, many different methods for measuring the residual stresses in different types of components have been developed. Techniques to measure Type I (except for techniques such as diffraction, which selectively sample 'special' grains,

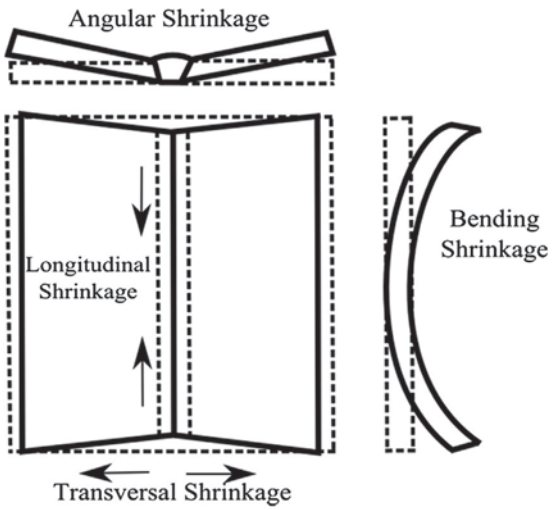

Figure 1 Distortion in weldment. Reproduced from American Welding Society. *Welding Handbook, Welding Technology*, 7th ed.; American Welding Society: Miami, 1981, ISBN: 0-87171-126-5.

www.iran-mavad.com
مرجع مهندسی مواد و متالورژی

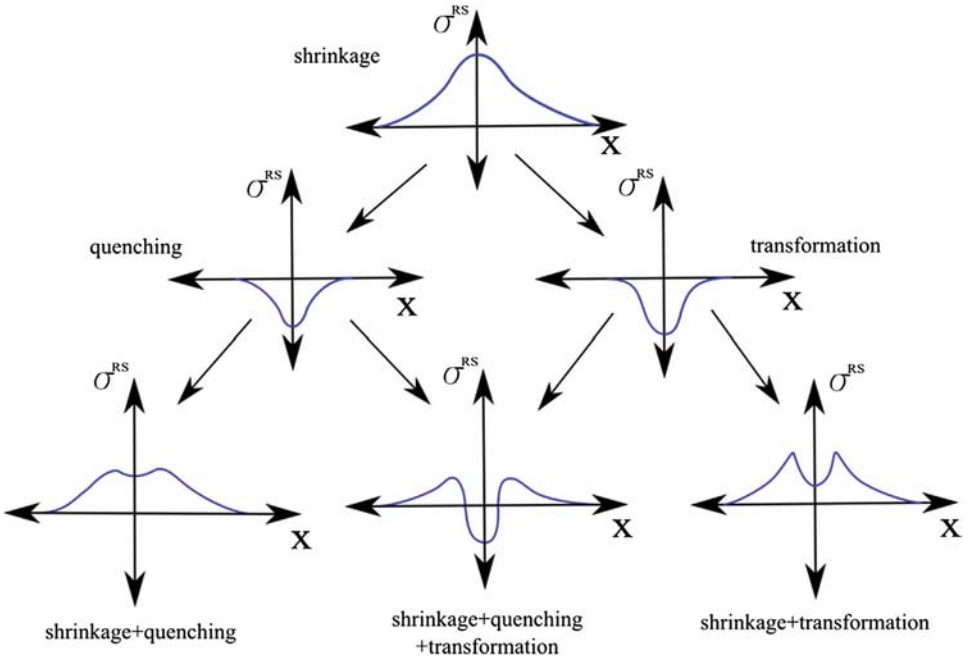

Figure 2 Change of residual stress due to metallurgical processes during welding. Reproduced from Macherauch, E.; Kloos, K. H. Origin, Measurements and Evaluation of Residual Stresses. *Residual Stress Sci. Technol.* **1987,** 3–26.

i.e., those correctly oriented for diffraction) residual stresses may be classified as either destructive or semi-destructive or nondestructive as shown in Figure 3. The destructive and semi-destructive techniques, called also mechanical method, are dependent on inferring the original stress from the displacement incurred by completely or partially relieving the stress by removing the material. These methods rely on the measurement of deformations due to the release of residual stresses upon removal of material from the specimen. Sectioning, contour, hole-drilling, ring-core, and deep-hole are the principal destructive and semi-destructive techniques used to measure residual stresses in structural members. Nondestructive methods include X-ray or neutron diffraction, ultrasonic methods, and magnetic methods. These techniques usually measure some parameter that is related to the stress. For the assessment of fatigue-related damage, they become increasingly important since many structural components, e.g., bridges, aircraft structures, or offshore platforms, need to be periodically inspected to prevent major damage or even failure. For inspection in the field or on large constructions, small, mobile, and easy to handle devices are essential. Additionally, cost minimizing requires short measuring times without time-consuming preparation of the part prior to the test (*8*).

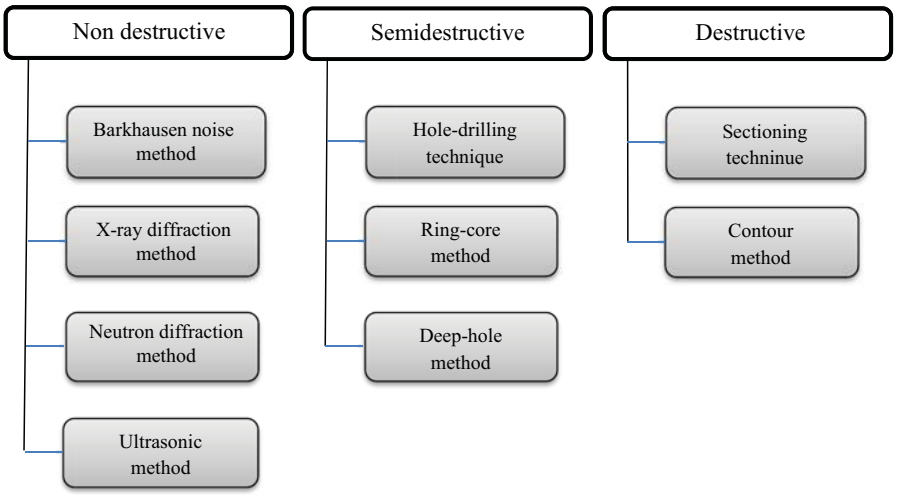

Figure 3 Residual stresses measuring techniques.

www.iran-mavad.com
مرجع مهندسی مواد و متالورژی

6.11.4.1 Mechanical Methods

These techniques are called stress-relaxing methods, which analyze the stress-relaxation produced in a metal part when the material is removed. By measuring the deformation caused by relaxation, the values of the residual stresses present in the part before the metal was removed can be determined by analyzing the successive state of equilibrium (*9*). The most common mechanical methods are as follows.

6.11.4.1.1 Hole-Drilling Technique

The hole-drilling method is relatively simple and quick; it is one of the most popularly used semi-destructive methods of residual stress evaluation which can provide the measurement of residual stress distribution across the thickness in magnitude, direction, and sense. It has the advantages of good accuracy and reliability, standardized test procedures, and convenient practical implementation. The damage caused to the specimen is localized to the small drilled hole, and is often tolerable or repairable. The principle involves introduction of a small hole (of about 1.8 mm diameter and up to about 2.0 mm deep) at the location where residual stresses are to be measured. Due to the drilling of the hole, the locked up residual stresses are relieved and the corresponding strains on the surface are measured using suitable strain gages (see **Figure 4**) bonded around the hole on the surface (*10*). From the strains measured around the hole, the residual stresses are calculated using appropriate calibration constants derived for the particular type of strain gage rosette used, as well as the most suitable analysis procedure for the type of expected stresses (*11*).

The ring-core method (*12,13*) is an 'inside-out' variant of the hole-drilling method. Whereas the hole-drilling method involves drilling a central hole and measuring the resulting deformation of the surrounding surface, the ring core method involves measuring the deformation in a central area caused by the cutting of an annular slot in the surrounding material. As with the hole-drilling method, the ring-core method has a basic implementation to evaluate in-plane stresses (*13*), and an incremental implementation to determine the stress profile (*14*). The ring-core method has the advantage over the hole-drilling method because it provides much larger surface strains. However, it is less frequently used because it creates much greater specimen damage and is much less convenient to implement in practice.

In comparison to other residual stress measuring techniques, the hole-drilling method is applicable in general to all groups of materials. First, the materials should be isotropic and the elastic parameters should be known. Second, the analyzed materials should be machinable, i.e., the boring of the hole should not prejudice the measured strain. The method determines macro residual stresses. Most in-depth evaluation algorithms provide a solution to determine an elastic plane stress state. However, to avoid local yielding because of the stress concentration due to the hole, the maximal magnitude of measured residual stress should not exceed 60–70% of local yield stress. The local resolution of the method is dependent on the equipment used. Laterally, the resolution ranges in the area of produced hole diameter. The minimal analyzable depth of the hole does not exceed $0.5 \times d_0$ (hole diameter) (*15*). Vishay measurements group have explained the practical steps of the implementation of the hole-drilling method (*16*).

Many investigators have applied this method to study the residual stresses in components produced by welding. Liu et al. (*17*) have measured the residual stresses present around thick aluminium friction stir welded butt joints using the hole-drilling method. The relieved strain caused by the drilling operation was detected by the electric resistance rosette strain gage

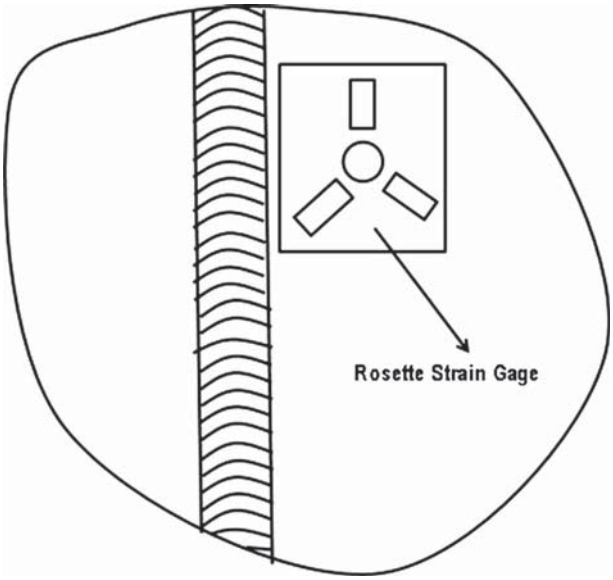

Figure 4 Schematic illustrations of the application of hole-drilling methods for residual stress measurement. Reproduced from Olabi, A. G.; Hashmi, M. S. J. Stress Relief Procedures for Low Carbon Steel (1020) Welded Components. *J. Mater. Process. Technol.* **1996**, *56*, 552–562.

www.iran-mavad.com
مرجع مهندسی مواد و متالورژی

(BE120-2CA-K) and was displayed on an ASM7.0 strain indicator. In their investigations, Olabi and Hashmi (*10*,*18*,*19*) have applied the hole drilling method to evaluate the magnitude and the distribution of residual stresses, before and after the application of PWHTs, of I-beam welded box-sections in structural steel materials and high-chromium steel AISI 410 used in aircraft engines. The RS-200 hole-drilling technique was employed and the strain-gage rosettes were installed along the same line across the welding at different distances from the welding axis. A number of preparations were made in assessing the residual stress according to the following steps: (1) surface and strain gage preparation and installation; (2) after bonding the strain gages to the test part at points where the residual stresses were to be determined, each rosette grid element was connected to a strain indicator P-3500 and 'zero' readings were recorded; (3) the RS-200 milling guide was positioned over the center of the gage and securely attached to the test part by using a special kind of cement; (4) finally, the principal residual stresses and their directions were computed by using appropriate equations. The results of this test show that there is a tensile stress near the welding zone and that it decreases as the distance from the welding zone increases. Moreover, suitable PWHTs have a significant effect on reducing the residual stresses for different levels. Olabi et al. (*20*) have used the hole-drilling method to measure residual stresses in the heat affected zones of AISI 304 steel welded plates and to establish the relationship between laser welding input parameters and principal residual stresses magnitude and direction. Benyounis et al. (*21*) have applied the hole-drilling method to measure the maximum residual stress in the heat-affected zone of dissimilar butt jointed welds of AISI 304 and AISI 1016. The holes were drilled at two locations one on the center of each side and as close as possible to the weld seam to ensure the holes are located in the HAZ. In all previous studies, a strain gage rosette used was of type CEA-06-062UM-120, which allows the measurement of the residual stresses close to the weld-bead.

The drilling of the hole for residual stress measurements needs to be done with significant care to avoid introduction of errors. There are three main error sources: introduction of machining stresses (adding to the residual stresses to be measured), non-cylindrical hole shape, and eccentricity, but so far it is the only method for measurement of residual stresses that is accepted as an ASTM standard (*22*). In general, the magnitude of this additional induced stress depends on the drilling method employed and working parameters as well. The additional stress induced by High-Speed (HS) hole-drilling technique is relatively lower than that generated by other hole-drilling techniques (*23*). Furthermore, the HS hole-drilling technique has the advantages of a simple experimental setup, a straightforward operation, and improved accuracy. Although the HS hole-drilling strain gage method has the advantage when used to measure the residual stress in specimens with high hardness and high toughness, a severe wear on the drill will occur. However, the tool wear will further cause the induced stress to increase and therefore cause significant measurement errors (*24*). In extreme cases, the tool wear may be so severe that the tool fails catastrophically. The Electrical Discharge Machining (EDM) process has the advantage of no constraint on mechanical properties of ferrous materials, and has proven its capability to drill highly precise holes on various metals. Hence, EDM hole-drilling provides as an alternative method for the measurement of residual stresses where HS hole-drilling is failed to employ in the stain gage method. In the investigation performed by Ghanem et al. (*25*), it has been shown that a tensile residual stress is formed within the EDM transformation layer. Ekmekci et al. (*26*) have developed a modified empirical equation to scale the residual stress in a machined surface, and reported that the stress increases from the surface and reaches a maximum value, this maximum stress value is around ultimate tensile strength of the material, and then it gradually falls to zero or even to a small compressive residual stress at greater depths. When using the EDM hole-drilling strain gage method to measure the residual stress within a component, part of the released strain detected by the strain gage originates not from the original component, but from the residual stress induced in the transformation layer during the hole-drilling process. This additional strain inevitably introduces a measurement error unless it is taken into account in some manner. In 2003, Lee and Hsu (*27*) have employed a series of stress-free and prestressed specimens to perform the stress measurement with both high-speed hole-drilling and EDM hole-drilling methods. Experimental results reveal that the application of the EDM method provides the same degree of measurement reliability and stability as the high-speed method. Furthermore, they also found that the measurement error induced by EDM is dependent on the working parameters employed, and independent on the magnitude of residual stress within original component. Consequently, it was suggested by Lee et al. (*28*) that the accuracy of the residual stresses measurements obtained using the hole-drilling technique could be improved by calibrating the measurement results using the hole-drilling induced stress (σ_{IS}). However, the application of this calibration scheme requires the use of a separate machining operation in order to determine the value of σ_{IS} for the particular material of interest. Keeping this in mind, the objective of the following study (Mayer and Hsu (*29*)) was to enhance this correction scheme such that the calibration factor, σ_{IS}, can be directly predicted from the material properties of the specimen without the need for any auxiliary machining trial. Furthermore, Lee and Liu (*30*) found that provided the dielectric fluid retains a high level of purity, the value of σ_{IS} is primarily determined by the thermal conductivity and carbon equivalent of the specimen.

In most practical cases, the residual stresses are not uniform with depth. The incremental hole drilling method is an improvement on the basic hole drilling method, which involves carrying out the drilling in a series of small steps, which improves the versatility of the method and enables stress profiles and gradients to be measured. A high-speed pneumatic drill which runs above 200 000 rpm is used to drill the hole without introducing any further machining stresses and thereby modifying the existing stress system. The strain data at predetermined depths are precisely acquired. Nevertheless, the precision of the method depends on the number of increments and their respective depths. The greater the number of drilling increments for the same laminate thickness, the more representative the residual stress profile. With regard to the influence of the depth increment, it would seem that choosing an increment that is too significant (one increment per ply) can lead to the slight overestimation of the stress. The slight relative overestimation of the stresses in the case of the drilling of an increment per ply seems to be caused by too significant stresses relaxation during and after the drilling. Indeed, the more the increment depth is large, the more the drilling time is significant and

www.iran-mavad.com
مرجع مهندسی مواد و متالورژی

the more the contact between the tool and material can be prejudicial. At the same time, it would seem that by reducing the respective depth of each increment, the sensitivity of the method for determining the residual stress profile in the through-depth of the material can be increased, particularly within each ply of the laminate (31). The incremental hole-drilling method has been employed by Olabi et al. (32) to measure the magnitude and the distribution of the maximum residual stress in AISI 304 steel welded plates. The aim of this study was to create mathematical models to determine the relationship between laser welding parameters and the magnitude of the residual stress at different locations by using Response Surface Methodology (RSM). Two types of strain gage rosettes were used: the first type was CEA-06-062UM-120 which allows measurement of the residual stresses close to the weld-bead; the second type was CEA-06-062UL-120 which has been used for measuring the residual stress at the other two locations of 10 and 20 mm from the weld center line.

Recent work (33,34) has concentrated on the use of full-field optical techniques to measure the deformations around a drilled hole. These developments have greatly expanded the scope of hole-drilling residual stress measurements, notably by providing a very rich source of available data. These additional data can provide detailed information about residual stress distributions, and can enable issues such as nonlinear material behavior and nonuniform stresses to be taken into account.

6.11.4.1.2 Deep Hole Method

The deep hole method (35,36) is a further variant procedure that combines elements of both the hole-drilling and ring-core methods. In the deep-hole method, a hole is first drilled through the thickness of the component. The diameter of the hole is accurately measured and then a core of material around the hole is trepanned out, relaxing the residual stresses in the core. The diameter of the hole is remeasured finally allowing the residual stresses to be calculated from the change in diameter of the hole. The deep hole method is classified as a semi-destructive method of residual stresses measurement since although a hole is left in the component, the diameter of the hole can be quite small and could coincide with a hole that needs to be subsequently machined. The main feature of the method is that it enables the measurement of deep interior stresses. The specimens can be quite large, for example, steel and aluminium castings weighing several tons. Initial development of the deep-hole method was carried out by Zhandanov and Gonchar (37), Beaney (38), and Jesensky and Vargova (39). Zhadanov and Gonchar (37) used the deep-hole method to measure residual stresses in steel welds. They drilled 8 mm diameter holes and trepanned out a 40 mm diameter core. In their method, the trepanning was incrementally carried out. Beaney (38) used a 3-mm gun-drill and an electro-chemical machining process to trepan the core. He measured the diameter of the hole using two strain gaged beams that were drawn along the sides of the hole. His methodology was later improved by Procter and Beaney (40) with the introduction of noncontacting capacitance gages to measure the hole diameter. Jesensky and Vargova (39) again measured residual stresses in steel welds, but used strain gages attached to the sides of the hole to measure the strain relaxation following trepanning. More recent improvements to the deep-hole method have been made by Smith and his coworkers (35,41–43). They have followed an approach of gun-drilling a hole of 3 mm nominal diameter and measuring the change in diameter of the hole using an air probe. The air probe works by calculating the clearance between the gage and the hole from the pressure required to blow air from the gage into the gap. Trepanning the core is carried out using an EDM operation (44–47).

The deep-hole method has become a standard technique for the measurement of residual stresses in isotropic materials. The method is particularly suited to thick components. Some investigators (48) have developed an extension to the method to allow the measurement of residual stress in orthotropic materials such as thick laminated composite components.

6.11.4.1.3 Sectioning Technique

The sectioning technique (49) and (50) is a destructive method that relies on the measurement of deformation due to the release of residual stress upon the removal of material from the specimen. It has been extensively used to analyze residual stresses in structural carbon steel, aluminium, and stainless steel sections (51–53). The sectioning method consists in making a cut on an instrumented plate in order to release the residual stresses that were present on the cutting line. For this, the cutting process used should not introduce plasticity or heat, so that the original residual stress can be measured without the influence of plasticity effects on the cutting planes' surface. **Figure 5** shows an example of the sectioning method, where a sequence of cuts was made to evaluate the residual stresses in an I-beam section (50).

The strains released during the cutting process are generally measured using electrical or mechanical strain gages. In general, the strips of material released by the sectioning process may exhibit both axial deformation and curvature, corresponding to membrane and bending (through thickness) residual stresses, respectively. Membrane residual stresses σ_m generally dominate in hot rolled and fabricated sections, whereas bending residual stresses σ_b are generally dominant in cold formed sections. These two residual stress components are illustrated in **Figure 6**, where the bending stresses are assumed to be linearly varying through the thickness. From this assumption, it follows that the combined membrane and bending residual stress pattern σ_{rc} is always a linear relationship (54).

Excellent residual stresses measurement results obtained with this method are presented in the literature, e.g., Ref. (55), for welded stiffened aluminium structures and center cracked tension specimens accordingly. Cruise and Gardner (56) have carried out an experimental program to quantify the residual stresses in stainless steel sections from three different production routes. Comprehensive residual stress distributions have been obtained for three hot rolled angles, eight press braked angles, and seven cold rolled box sections. In the hot rolled and press braked sections, residual stresses were typically found to be below 20% of the material 0.2% proof stress, though for the cold rolled box sections, whilst membrane residual stresses were relatively low, bending residual stresses were found to be between 40 and 70% of the material 0.2% proof stress.

www.iran-mavad.com
مرجع مهندسی مواد و متالورژی

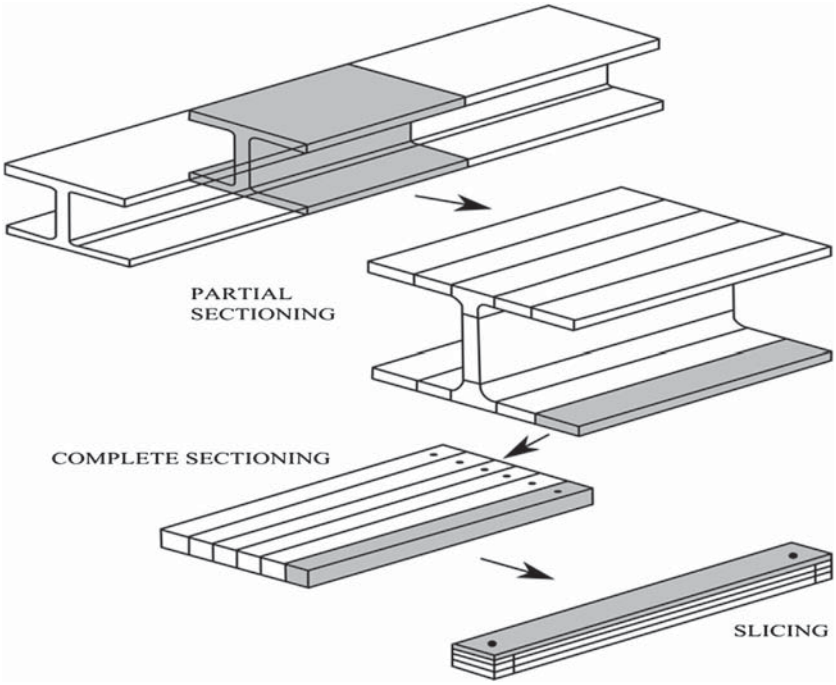

Figure 5 Sectioning method. Reproduced from Tebedge, N.; Alpsten, G.; Tall, L. Residual-Stress Measurement by the Sectioning Method. *Exp. Mech.* **1973**, *13* (2), 88–96.

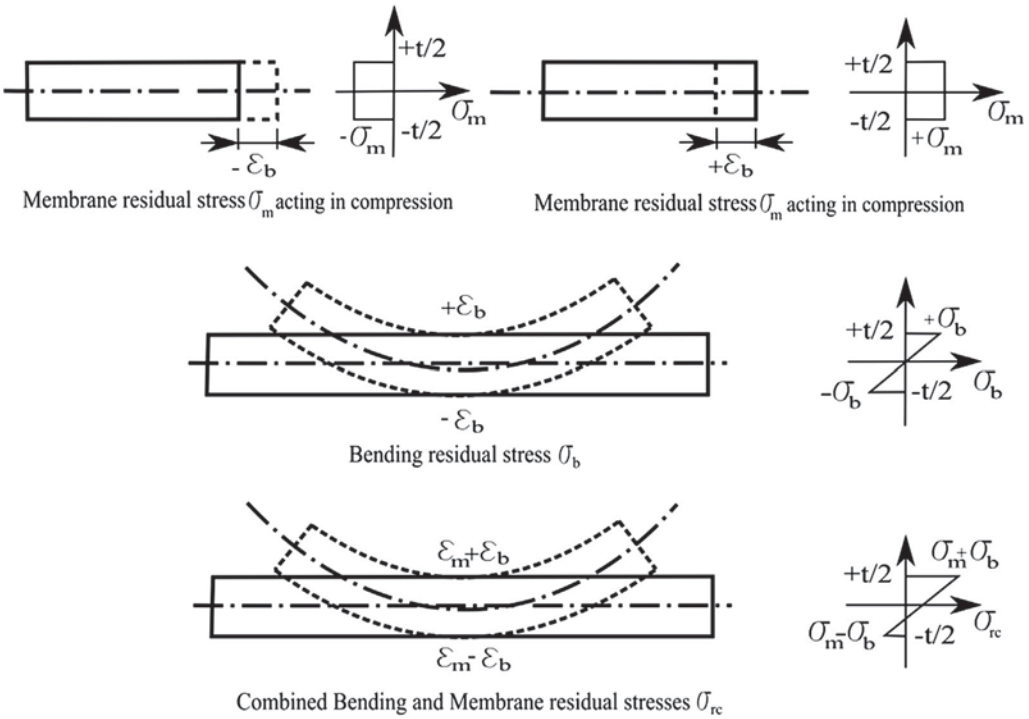

Figure 6 Modeling of residual stresses with membrane and bending stress components. Reproduced from Cruise, R. B.; Gardner, L. Strength Enhancements Induced during Cold Forming of Stainless Steel Sections. *J. Construct. Steel Res.* **2008**, *64* (11), 1316–1320.

www.iran-mavad.com
مرجع مهندسی مواد و متالورژی

6.11.4.1.4 Contour Method

The contour method, first proposed in 2000 (57), is a newly invented relaxation method that enables a 2D residual stress map to be evaluated on a plane of interest. The contour method provides higher spatial resolution, while the sectioning technique is easier to apply since almost no calculations are needed. The method has found a number of applications: for example, carbon steel tee-join welded (58) and (59), quenched and impacted thick plates (60), cold-expanded hole (45), and aluminium alloy forging (11). It offers improvements over conventional relaxation methods of measuring residual stresses (61,62). The theory of the contour method is based on a variation of Bueckners elastic superposition principle (63). The method was first published in detail in 2001, where the contour method was numerically verified by 2D Finite Element (FE) simulation and experimentally validated on a bent steel beam having a known residual stress distribution (62). The potential of the contour method was later demonstrated on a 12-pass TIG BS4360 steel weld to measure a complex 2D stress variation across the weld section (58). The result obtained from the contour method was in excellent quantitative agreement with the outcome measured by a completely different technique nondestructive neutron diffraction. A high stress component, over the initial yield stress of the material, was measured in that case. The contour method was also successfully used for measuring the residual stresses induced by impact in a high-strength low-alloy steel (HSLA-100) with thickness up to 51 mm (60). The comparison with explicit FE simulation of the impact process indicated a good match, and the as-received HSLA-100 quenched plate showed a typical quenching residual stress distribution. Another application was an EN8 steel plate with a cold-expanded hole where a characteristic profile of 2D longitudinal residual stresses was measured by the contour method (64). The measured cold expansion stress profile was compared with the result predicted by 3D FE modeling, and the comparison was encouraging although there were certain errors at edges, including hole edges. The latest application of the contour method was a 7075 aluminium alloy hand forging, in which three cuts were performed in orthogonal directions to obtain three directions of the stress tensor (61). The measured stresses were in good agreement with the FE-predicted outcomes.

Application of the contour method primarily involves four steps: specimen cutting, contour measurement, data reduction, and stress analysis, which will be detailed as follows.

Weld cutting: specimen cutting is the first and the most critical step in implementing the contour method, as the subsequent procedures of contour measurement, data reduction, and stress analysis are all reliant on the quality of the cutting. Wire EDM has been identified as a suitable method of cutting for the contour method (63), as it uses electrical discharges (sparks) instead of hard cutting tools to remove the material. A single flat cut is important to achieve high accuracy in using the contour method. Proper constraint of a specimen to avoid its movement during cutting is essential. A constant width of cut is also crucial to guarantee flat cutting. This is found to be strongly related to the type of cutting wire chosen, the material to be cut, the geometry of the specimen, and the EDM operating parameters. The cutting wire should be as thin as possible so that minimum material is removed, which is particularly important for cases where there is a high stress gradient.

Contour measurement: following the weld cut, a contoured surface is formed owing to the release of residual stresses, which needs to be measured on both the cut surfaces. A Coordinate Measuring Machine (CMM) has been proved to be sufficiently accurate for surface profile measurement (60–62). A CMM is designed to measure complex shapes with high precision, and is typically used to measure manufactured parts to determine if tolerance specifications are met. It uses a ruby-tipped stylus as a sensor for detecting a specimen surface. A mechanical assembly moves the sensor or stylus to contact the surface to be measured. The deflection of the stylus triggers a computer to record the position of each contact point.

Data reduction: the very first step of data reduction is to average each pair of measured points, which should be at the mirror positions from the two cut planes. It is unavoidable that the measured data contain errors from cutting and measurement. In particular, stress evaluation magnifies any error in the measured data. Smoothing of the measurements to minimize the errors in the data is, therefore, crucial to achieve accurate stress evaluation with the contour method.

Stress analysis and result: finite element modeling and analysis were performed to calculate the original stress. The smoothed data were input to an FE model, with opposite sign, as displacement boundary conditions.

In the conventional contour method, the measured displacements are used to predict the original residual stress. In contrast, the principle of the multiaxial contour method is based on computing the eigenstrain from the measured displacement, and then the residual stresses are derived from the eigenstrain. The source of all residual stresses is incompatible strain in a body which is the so-called eigenstrain. Many researchers (65–69) have studied residual stresses in engineering components using eigenstrain. The motivation for using eigenstrain to determine residual stresses in the contour method is that the eigenstrain remains constant upon residual stress redistribution. In other words, a change in the geometry of a body alters the residual stress distribution, but not the eigenstrain. Hence, multiple cuts can be made without changing the eigenstrain distribution. Moreover, as long as the eigenstrain variation in the body is known, its residual stress can be calculated for any configuration sectioned from this body. The multiaxial contour stress measurement technique was successfully applied to the measurement of the residual stresses in a VPPA-welded plate (70). The measurements were compared with previously obtained results using neutron diffraction, and good agreement was obtained. The method has therefore been successfully validated.

6.11.4.1.5 Other Destructive Methods

Other less used methods such as excision, splitting, curvature, layer removal, and slitting, are described as follows. Excision is a simple quantitative method for measuring residual stresses. It entails attaching one or more strain gages on the surface of the specimen, and then excising the fragment of material attached to the strain gage(s). This process releases the residual stresses in the material, and leaves the material fragment stress-free. The strain gage(s) measure the corresponding strains. Excision is typically applied with thin plate specimens, where the cutting of a small material fragment around the strain gage(s) is straightforward.

www.iran-mavad.com
مرجع مهندسی مواد و متالورژی

Application on thicker specimens is also possible. Full excision is possible, but is not usually done because the inconvenience of the undercutting process required to excavate the material fragment. Indeed, partial excision by cutting deep slots at each end of the strain gage (71–73) is a more practical procedure. **Figure 7(a)** illustrates the splitting method (74). A deep cut is sawn into the specimen and the opening (or possibly the closing) of the adjacent material indicates the sign and the approximate size of the residual stresses present. This method is widely used as a quick comparative test for quality control during material production. The 'prong' test shown in **Figure 7(b)** is a variant method used for assessing stresses in dried lumber (75). The splitting method is usually used to assess the residual stresses in thin-walled tubes. **Figure 7** shows two different cutting arrangements (76), (c) for evaluating longitudinal stresses and (d) for circumferential stresses. The latter arrangement is commonly used for heat exchanger tubes, and is specified by ASTM standard E1928 (77). The thin-wall tube splitting method illustrated in **Figure 7(c) and 7(d)** is also an example of Stoney's Method (78), sometimes called the curvature method. This method consists in measuring the deflection or curvature of a thin plate caused by the addition or removal of material containing residual stresses. The method was first developed for evaluating the stresses in electroplated materials, and is also useful for assessing the stresses induced by shot-peening (79).

The layer removal method is a generalization of Stoney's Method. It involves observing the deformation caused by the removal of a sequence of layers of material. The method is suited to flat plate and cylindrical specimens where the residual stresses are known to vary with the depth from the surface, but to be uniform parallel to the surface. **Figure 8** illustrates examples of the layer removal method, the method involves measuring deformations on one surface, for example using strain gages, as parallel layers of material

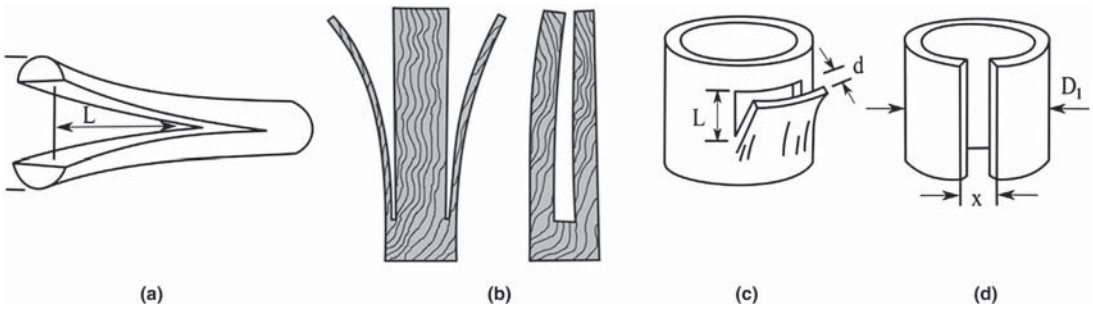

Figure 7 The splitting method: (a) for rods (reproduced from Kartal, M. E.; Liljedahl, C. D. M.; Gungor, S.; Edwards, L.; Fitzpatrick, M. E. Determination of the Profile of the Complete Residual Stress Tensor in a VPPA Weld Using the Multi-axial Contour Method. *Acta Mater.* **2008**, *56*, 4417–4428); (b) for wood (reproduced from Gunnert, R. *Method for Measuring Residual Stresses and Its Application to a Study of Residual Welding Stresses*; Almqvist & Wiksell: Stockholm, 1955); (c) for axial stresses in tubes (reproduced from Schwaighofer, J. Determination of Residual Stresses on the Surface of Structural Parts. *Exp. Mech.* **1964**, *4* (2), 54–56); and (d) for circumferential stresses in tubes (reproduced from Baldwin, W. M. Residual Stresses in Metals. In *Philadelphia: Proc. American Society for Testing and Materials*, 1949, 49).

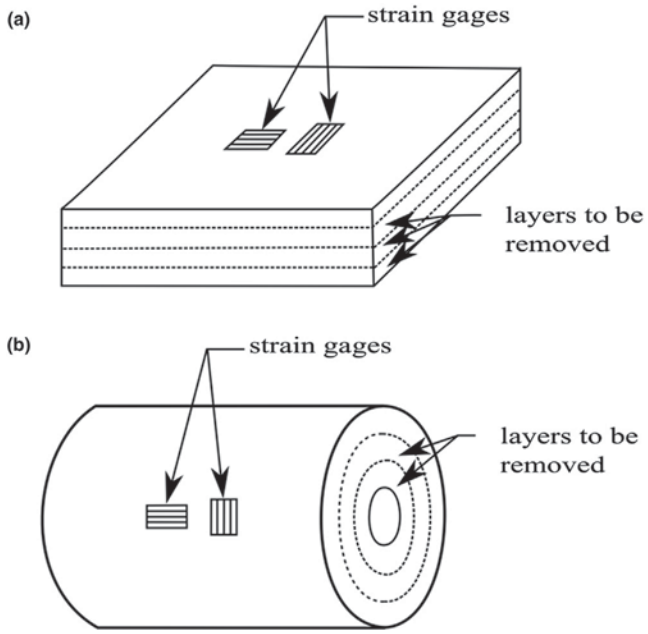

Figure 8 Layer removal method: (a) flat plate and (b) cylinder. Reproduced from Treuting, R. G.; Read, W. T. A Mechanical Determination of Biaxial Residual Stress in Sheet Materials. *J. Appl. Phys.* **1951**, *22* (2), 130–134.

www.iran-mavad.com
مرجع مهندسی مواد و متالورژی

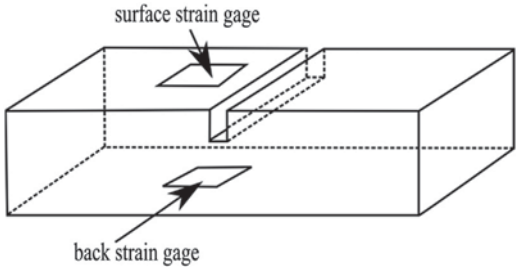

Figure 9 Slitting method. Reproduced from Fetullazad, E.; Akyildiz, H. K.; Saritas, S. Effects of the Machining Conditions on the Strain Hardening and the Residual Stresses at the Roots of Screw Threads. *Mater. Des.* **2010**, *31* (4), 2025–2031.

are removed from the opposite surface (*80*). In the case of a hollow cylindrical specimen, deformation measurements can be made on either the outside or the inside surface, while annular layers are removed from the opposite surface. Applied to cylindrical specimens, the layer removal method is commonly called 'Sachs' Method' (*81*). The method is a general one; it is typically applied to metal specimens, e.g., but can be applied to other materials, e.g., paperboard (*82*).

Investigators (*83,84*) have applied this method using ECM for the measurement of the residual stresses in a metallurgy steel. Since it is a nonmechanical metal removal process, ECM is capable of machining any electrically conductive material with attendant high removal rates, regardless of mechanical properties. In particular, the removal rate in ECM is independent of the hardness and toughness of the material being machined.

The slitting method (*85–87*) is also very similar to the hole-drilling method, but uses a long slit rather than a hole. **Figure 9** illustrates the geometry. Strain gages are attached either on the front or back surfaces, or both, and the relieved strains are measured as the slit is incrementally increased in depth. The slit can be introduced by a thin saw, milling cutter or wire EDM. Due to this, the residual stresses perpendicular to the cut can then be determined from the measured strains using finite element calculated calibration constants, in the same way as for hole-drilling calculations. Overall, the slitting method has the advantage over the hole-drilling method in that it can evaluate the stress profile over the entire specimen depth, the surface strain gage providing data for the near-surface stresses, and the back strain gage providing data for the deeper stresses. However, the slitting method provides only the residual stresses normal to the cut surface, whereas the hole-drilling method provides all three in-plane stresses. Additional cuts can be made to find other stress components, in which case, the overall procedure resembles the sectioning method (*88–90*). The slitting method can also be applied to estimate the stress intensity factor caused by residual stresses, which is very useful for fatigue and fracture studies (*91*).

6.11.4.2 Diffraction Techniques

Diffraction methods are based on determining the elastic deformation which will cause changes in the interplanar spacing, d, from their stress free value, d_0. Then, the strain could be calculated by using Bragg's law and of course it is necessary to have an accurate measure of stress-free interplanar spacing. The most common diffraction methods are as follows.

6.11.4.2.1 X-ray Diffraction Method

The X-ray method is a nondestructive technique for the measurement of residual stresses on the surface of materials. X-ray diffraction techniques exploit the fact that when a metal is under stress, applied or residual stress, the resulting elastic strains cause the atomic planes in the metallic crystal structure to change their spacings. X-ray diffraction can directly measure this interplanar atomic spacing; from this quantity, the total stress on the metal can then be obtained (*92,93*).

Since metals are composed of atoms arranged in a regular three-dimensional array to form a crystal, most metal components of practical concern consist of many tiny crystallites (grains), randomly oriented with respect to their crystalline arrangement and fused together to make a bulk solid. When such a polycrystalline metal is placed under stress, elastic strains are produced in the crystal lattice of the individual crystallites. In other words, an externally applied stress or one residual within the material, when bellow the yield strength of the material, is taken up by interatomic strains in the crystals by knowing the elastic constants of the material and assuming that stress is proportional to strain, a reasonable assumption for most metals and alloys of practical concern (*94*). Therefore, X-ray diffraction residual stresses measurement is applicable to materials that are crystalline, relatively fine grained, and produce diffraction for any orientation of the sample surface. The sample may be metallic or ceramic, provided a diffraction peak of suitable intensity and free of interference from neighboring peaks can be produced in the high back-reflection region with the radiations available (*95*).

Some investigators have used the X-ray method to evaluate the residual stress distribution in dissimilar metal welds of maraging steel to quenched and tempered medium alloy medium carbon steel across the weldment (i.e., perpendicular to welding direction) (*96*) and to measure the residual stresses on the top side of a double-electrode butt welded steel plates in longitudinal and transversal directions (*97*). Indeed, some problems arise when using diffraction to determine the residual stresses in large welds because the limited space available on most beam lines or X-ray diffractometers means that samples often need to be cut-down in

www.iran-mavad.com
مرجع مهندسی مواد و متالورژی

order to be measured. The geometry has to be such that an X-ray can both hit the measurement area and still be diffracted to the detector without hitting any obstructions. Portable diffractometers that can be taken out into the field for the measurements of structures such as pipelines, welds, and bridges are now available (*98*). It could be also combined with some form of layer-removal technique so that a stress profile can be generated, but then the method becomes destructive and the current results clearly indicate that such cutting must be done with care to ensure the stress state is not unduly altered (*99*). Moreover, in the case of a nanostructured material, it is not easy to use diffraction techniques because of the difficulty involved in analyzing the shape of the nanomaterial diffraction peak. It is difficult to pinpoint the peak location or to determine the peak shift in order to study the macroscopic stress due to severe plastic deformation for many materials. For this reason, mechanical methods are the only techniques known for the study of residual stresses in all kinds of surface nanostructured materials without the effect of nanostructure (*100*). The speed of measurement depends on a number of factors, including the type of material being examined, the X-ray source, and the degree of accuracy required. The gage volume is a trade-off between the need for spatial resolution within the expected strain field and the time available for data collection. With careful selection of the X-ray source and test set-up, speed of measurement can be minimized. New detector technology has also greatly reduced the measurement time.

Third generation synchrotron sources provide access to high X-ray energies. At these high (hard) energies, the attenuation length, defined as the path length over which the intensity falls to $e - 1$, markedly increases. This combined with the very high X-ray intensities they produce leads to path lengths of centimeters even in steel (*101*). The main advantages are the high intensity and the high collimation of the beam, which allow data acquisition rates of the order of seconds if not milliseconds, and the definition of millimeter to micron size sampled gage dimensions (*102*). The intense beams of high energy synchrotron X-rays available at synchrotron sources offer unparalleled spatial resolution lateral to the beam (1–100 μm) and fast data acquisition times (say 1 ms). These make the method well suited to the collection of detailed maps of the strain field in two or three dimensions, or to monitor phase transformations where neutron diffraction would be unfeasibly slow. In counterpoint, there are serious drawbacks in the application of the synchrotron method. First, the low scattering angles mean that the sampling gage is usually very elongated. This means that the spatial variation is very different in different directions, being excellently lateral to the beam, but much poorer along the beam. Secondly, the low scattering angles mean that the method is well-suited to plate geometries where the significant stresses are in-plane, but for large or geometrically complex samples, it can be difficult to achieve short path lengths for all measurement directions. Consequently, it is often not possible to derive the stresses (which require at least three perpendicular strain values) without invoking simplifying assumptions, e.g., plane stress. As a solution, researchers have developed hybrid methods whereby synchrotron diffraction is used to provide two components of strain and another method, e.g., neutron diffraction used to determine the third (*103*). It should also be noted that neutron diffraction is often more appropriate for multiphase or composite materials containing both high and low atomic number elements. Finally, in many cases, the high spatial resolutions achievable in theory cannot be realized in practice because the powder method breaks down due to insufficient grain sampling. Even at similar gage dimensions to the neutron method, the very low divergence of the incident X-ray beam means that in many cases too few grains satisfy the diffraction condition to provide results representative of the bulk (*104*).

A novel, multiscale methodology for determining the residual stress field within a polycrystalline work piece from diffraction data has been presented by McNelis et al. (*105*). The method employs a finite element discretization of the work piece for introducing the lattice strain data, which are taken over a broad expanse of the work piece, and for imposing constraints of mechanical equilibrium and the effects of traction free boundaries. The diffraction data consist of thousands of elastic lattice strain measurements from several families of lattice planes. The methodology produces the distribution of residual macroscopic stress over the work piece along with the orientation-dependent distribution of crystal-scale elastic strains at each diffraction volume. The solution is the one that best satisfies the macroscopic constraints of equilibrium and traction boundary conditions while simultaneously matching the lattice strain data, which are directly linked to straining at the crystal scale. The finite element framework enables interpolation of the continuum stress components over the full domain of the work piece enabling the designer to understand the residual stress field at any location.

6.11.4.2.2 Neutron Diffraction Method

Neutron diffractions method is very similar to the X-ray method as it relies on elastic deformations within a polycrystalline material that cause changes in the spacing of the lattice planes from their stress-free condition. The application of neutron diffraction in solving engineering relevant problems has become widespread over the past two decades. The advantage of the neutron diffraction methods in comparison with the X-ray technique is its larger penetration depth. In fact, the X-ray diffraction technique has limits in measuring residual stresses through the thickness of a welded structure. On the other hand, a neutron is able to penetrate a few centimeters into the inside of a material, thus it can be widely applied to evaluate an internal residual stress of materials. It enables the measurement of residual stresses at near-surface depths around 0.2 mm down to bulk measurement of up to 100 mm in aluminium or 25 mm in steel (*106*). This is especially useful for alloys of high average atomic numbers because the penetration of the X-rays falls off rapidly in this regime. With high spatial resolution, the neutron diffraction method can provide complete three-dimensional maps of the residual stresses in material. At each measurement point, strain was measured in three orthogonal directions: along the sample axis (axial strain ε_A), transverse to it (transverse strain ε_T), and through the wall (normal strain ε_N). This was achieved by mounting each sample in three different orientations as shown in **Figure 10** (the strain measurement direction bisects the incident and diffracted beam directions) (*107*). However, compared to other diffraction techniques such as X-ray diffraction, the relative cost of application of the neutron diffraction method, is much higher, mainly because of the equipment cost. It is too expensive to be used for routine process quality control in engineering applications.

www.iran-mavad.com
مرجع مهندسی مواد و متالورژی

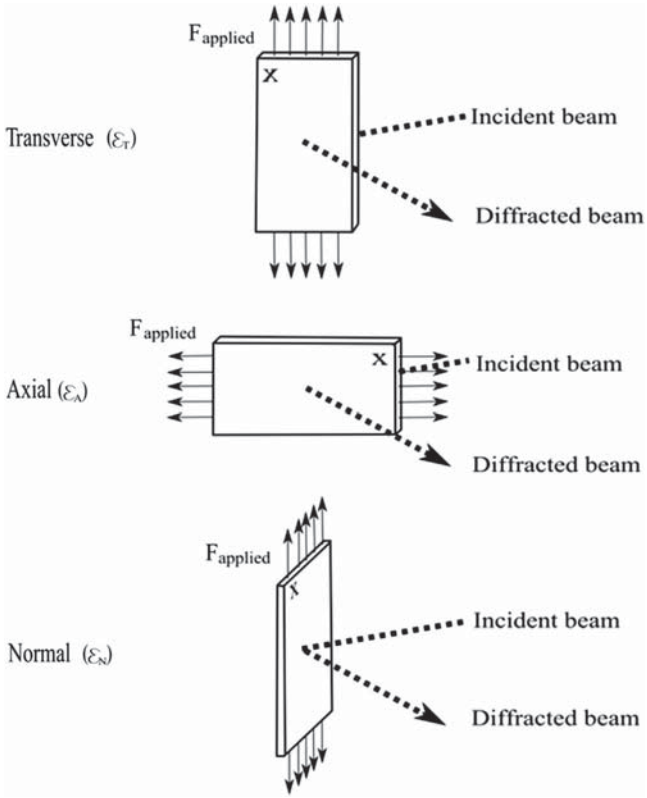

Figure 10 The three different orientations used to determine transverse strain (ε_T), axial strain (ε_A), and normal strain (ε_N). Also shown are the applied load direction ($F_{applied}$) and also the direction of the incident and diffracted neutron beam. The strain measurement direction bisects the incident and diffracted beam directions. Reproduced from Claphama, L.; Abdullah, K.; Jeswiet, J. J.; Wild, P. M.; Roggec, R. Neutron Diffraction Residual Stress Mapping in Same Gauge and Differential Gauge Tailor-welded Blanks. *J. Mater. Process. Technol.* **2004**, *148* (2), 177–185.

In 2001, after a series of round robin studies an International Organization for Standardization Technology Trends Assessment document was produced recommending procedures for the measurement of residual stress by neutron diffraction in polycrystalline materials (*108*). It outlines the method to be followed, calibration procedures, recommends diffraction peaks to be used for different materials, how to deal with elastic and plastic anisotropy, methods for inferring the strain free lattice parameter, and reporting guidelines. In the past, neutron diffractometers have generally been built as 'all-purpose' instruments, with designs that are compromises, balancing competing requirements to simultaneously measure the intensities, positions, and widths of diffraction peaks. In contrast, the newly constructed diffractometer ENGIN-X (*109*) was designed with the single aim of making engineering strain measurements; essentially the accurate measurement of polycrystalline lattice parameters, at a precisely determined position. Under this design philosophy, considerable performance improvements have been obtained compared to the existing instrument. The improvement in count times obtained allows for more complete studies, either through more detailed scanning experiments of components, or for parametric studies. The improvement in intensity and low background also means that larger path lengths than previously possible can now be achieved, allowing for the study of large parts. Finally, the improved count times allow the study of shorter timescale phenomena. Dann et al. (*110*) detailed the design philosophy of this instrument, including tuneable incident resolution, together with the approaches used to realize the performance required. The improved instrument performance was demonstrated, with the results obtained during the commissioning of ENGIN-X. These results include strain mapping experiments, and demonstrate the influence of resolution on required count times, and provide a direct comparison with measurements from the existing ENGIN instrument at ISIS.

There are several experimental reports about neutron diffraction measurements of weld stresses; Martinson et al. (*111*) have applied the neutron diffraction technique to characterize laser and resistance spot welds to gain an understanding of residual stresses of different joint geometries used in the automotive industry. Paradowska et al. (*112*) had used the neutron diffraction technique to investigate and compare the residual stresses characteristics in fully restrained samples with different numbers of beads. The aim of the research was to characterize the residual stress distribution which arises in a welded component with increasing the number of passes or beads. The resolution of the measurements carried out in this work achieves a new level of detail and reveals significant features of the residual stress pattern in multibead welding. The findings have important consequences for the design of welding procedures, demonstrating the effects of placing new beads on prior welding.

Taken together with the complementary synchrotron method, it can provide nondestructive evaluation for the introduction of new process technologies or for structural integrity assessment at the component or plant scale. Recently, neutrons have even been

www.iran-mavad.com
مرجع مهندسی مواد و متالورژی

used to study welding process induced stresses. At the device level, neutron diffraction can provide information into the activation of smart transformations, while at the material level, it delivers phase or grain family information for optimizing the performance of alloys and composites. With the increasing number and performance of dedicated neutron strain measurement instruments around the world, there is no doubt that neutron diffraction will continue to make a significant contribution to basic science and applied engineering over the coming years (*113*).

6.11.4.3 Other Nondestructive Techniques

These methods are based on measurements of electromagnetic, optical, and other physical phenomena in the residual stress zone. The common methods among this category are as follows.

6.11.4.3.1 Barkhausen Noise Method

The Magnetic Barkhausen Noise (MBN) method is of particular interest because of its potential as a nondestructive industrial tool to measure surface residual stress and other microstructural parameters. The MBN technique is applicable to ferromagnetic materials, which are composed of small order magnetic regions called magnetic domains. Each domain is spontaneously magnetized along the easy axes of the crystallographic magnetization direction. However, magnetization vectors inside the domains are oriented in such a way that the total magnetization of the material is zero except for the natural magnets. Domains are separated from each other by domain walls also called bloch walls. There are two types of bloch walls in a ferromagnetic material. Bloch walls of 180° have greater mobility than 90° walls so their contribution to MBN is bigger (*114*). If an external D.C. magnetic field is applied to a ferromagnetic substance, the magnetization of the sample changes due to the domain wall movements. Domains with alignments parallel or nearly parallel to the applied field vector expand and others annihilate during magnetization. When all of the magnetization vectors inside the domains align themselves in the direction of the applied field by domain wall movements, the saturation occurs (*9*).

Grain boundaries, lattice dislocations, second phase materials (e.g., carbides in iron), and impurities in the ferromagnetic material act as an obstacle for the movement of domain walls. By the application of higher magnetization force values, force on the domain wall exceed the restraining force due to pinning sites, so there is an increase in the magnetization in small jumps, which also give rise to hysteresis. This increase can be determined by placing an inductive coil near to the specimen being magnetized. Because of this magnetization change, an electrical pulse is induced on the coil. When all electrical pulses produced by all domain movements added together, a noise-like signal called Barkhausen noise is generated (*9*). **Figure 11** schematically shows the design of a micromagnetic sensor. A U-shaped yoke is excited by a coil connected to a bipolar power-supply unit. By the orientation of the poles, the direction of the resulting alternating magnetic field is defined and thus, the corresponding stress component can be measured. The Barkhausen noise is detected by a small air coil whereas the tangential field strength is measured by a hall probe. Both signals are amplified, filtered, and evaluated in the micromagnetic testing system (*115*).

Stewart et al. (*116*) have made measurements on a welded steel plate. Away from the weld, the results are consistent with the expected compressive stress parallel to the weld direction. At a point near one edge of the weld, the amount and character of the MBN sharply changed, suggesting a concentration of stress. MBN is sensitive to changes in the applied stress. This phenomenon of elastic properties interacting with domain structure and magnetic properties of the material is called a 'magneto–elastic interaction.' As a result of magneto–elastic interaction in materials with positive magnetic anisotropy (iron, most steels and cobalt), compressive stresses will decrease the intensity of Barkhausen noise while tensile stresses increase it. This fact can be exploited so that by measuring the intensity of Barkhausen noise, the amount of residual stresses can be determined. As well as being sensitive to the stress state of ferromagnetic materials, Barkhausen noise is also affected by the microstructural state of the material. This implies that the stress dependent Barkhausen signal will change from one material to the next. Therefore, for MBN to be effective in determining residual or applied stresses, different materials must be individually calibrated. In their study, Yelbay et al. (*117*) have concluded

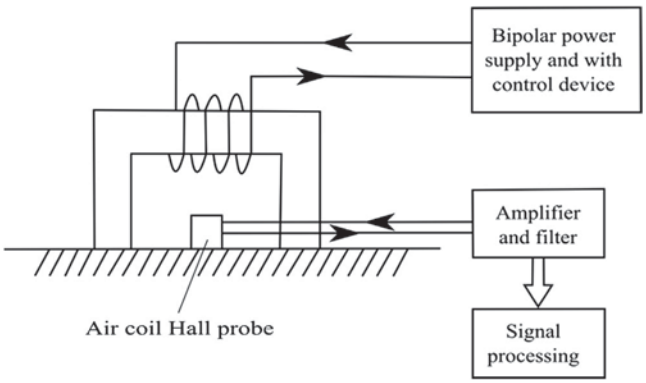

Figure 11 Micromagnetic sensor setup. Reproduced from Theiner, W.; Höller, P. Magnetische Verfahren zu Spannungsermittlung. In *HTMBeiheft: Eigenspannungen und Lastspannungen*; Hauk, V.; Macherauch, E., hrsg.; Hanser, 1982, pp 156–163.

www.iran-mavad.com
مرجع مهندسی مواد و متالورژی

that the calibration procedure is very important for accurate and reliable results. Each zone having remarkably different microstructure should be separately considered for calibration.

Previous studies (*118,119*) on steels have shown that the maximum amplitude of the MBN signal decreases with the reduction in grain size, however, it increases with increasing misorientation angles at the grain boundary. From a similar viewpoint, it is almost impossible to use the MBN to assess residual stresses in weldments containing HAZ, since HAZ have very rapid microstructural gradients. Ju et al. (*120*) have developed a modified magnetic Barkhausen noise method to obtain the residual stress distribution in an API X65 pipeline weldment. In order to reflect the microstructural variations in the heat-affected zone, calibration samples were extracted from four different regions: weld metal, coarse-grained HAZ (CGHAZ), fine-grained HAZ, and base metal. This approach yielded that compressive residual stresses existed in the CGHAZ contrary to the tensile results using the base-metal-based calibration method. Compared with the results from the mechanical cutting method, it can be concluded that the data obtained with the HAZ-based calibration method were more reliable.

The MBN method is also limited by the saturation of the MBN energy signal in either tension or compression. When either minimum or maximum energy values arise, the stress can no longer alter the MBN energy level. This limits the correlation between stress and MBN energy to maximum tensile and maximum compressive stress values. However, this magnetic BN method has the advantages of being rapid, suitable for the circular geometry such as rings, and requiring no direct contact. Some investigators (*121*) have developed BN methods to evaluate surface residual stress in aeronautic bearings, in particular in contact zones between ball or roller bearings and their raceways, with the aim to move this method out of the laboratory and into the industrial environment.

The measurement depth mainly depends on the permeability of the material and it is typically up to 0.2 mm for surface hardened components. Since this depth is 100 times more than that of X-ray diffraction, the Barkhausen noise method is also capable of quantifying subsurface stress without the need of removing the surface layer.

6.11.4.3.2 Ultrasonic Method

One of the promising directions in the development of nondestructive techniques for residual stresses measurement is the application of ultrasound. Ultrasonic method, called also refracted longitudinal (LCR) wave techniques, is not limited by the types of material under study, and can be utilized for residual stresses measurements on thick samples. Ultrasonic stress measurement techniques are based on the acoustic-elasticity effect, according to which the velocity of elastic wave propagation in solids is dependent on the mechanical stress (*122,123*). The most important advantages of the development technique and equipment are the possibility to determinate the residual and applied stresses in samples and real structure elements. The relationships between the changes of the velocities of longitudinal ultrasonic waves and shear waves with orthogonal polarization under the action of tensile and compressive loads in steel and aluminium alloys are presented in **Figure 12** (*124*). As can be seen, the intensity and character of these changes can be different, depending on the material properties. Different configurations of ultrasonic equipment can be used for residual stresses measurements. Overall, waves are launched by a transmitting transducer, propagate through a region of the material, and are detected by a receiving transducer, as show in **Figure 13** (*125*).

The technique in which the same transducer is used for excitation and receiving of ultrasonic waves is often called the pulse-echo method. This method is effective for the analysis of residual stresses in the interior of the material. In this case, the trough-thickness average of the residual stresses is measured. In the configuration shown in **Figure 13**, the residual stress in a (sub)surface layer is

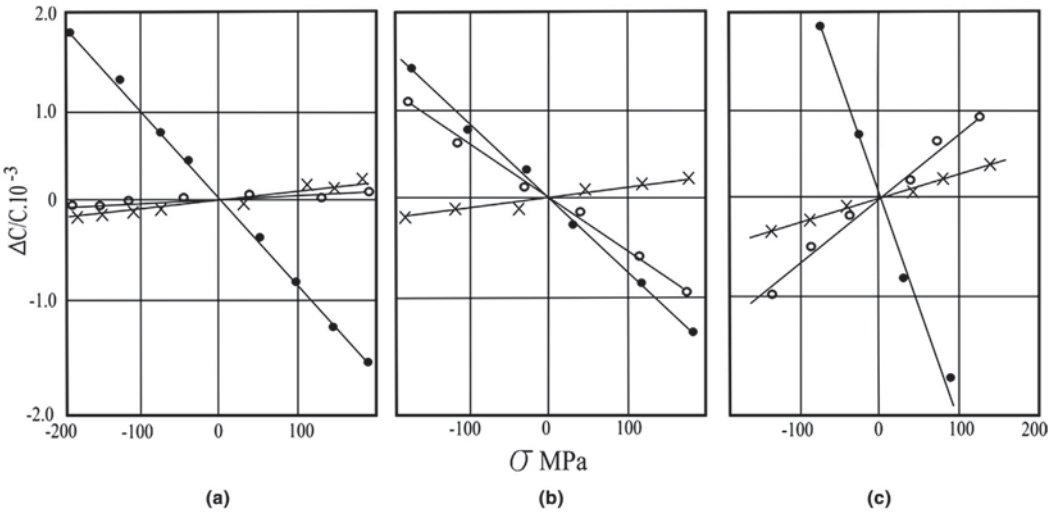

Figure 12 (a–c) Change of ultrasonic longitudinal wave velocity (CL) and shear waves velocities of orthogonal polarization (CSX3; CSX2) depending on the mechanical stress σ in steel A (a), steel B (b), and aluminium alloy (c): ● – CSX3; ○ – CSX2; x – CL. Reproduced from Kudryavtev, Y.; Kleiman, J.; Gushcha, O.; Smilenko, V.; Brodovy, V. Ultrasonic Technique and Device for Residual Stress Measurement. In *X Int. Congress and Exposition on Experimental and Applied Mechanics*, 2004, pp 1–7.

www.iran-mavad.com
مرجع مهندسی مواد و متالورژی

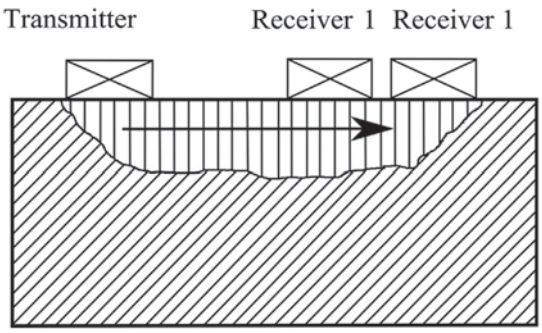

Figure 13 Schematic view of ultrasonic measurement configuration: surface pitch–catch. Reproduced from Park, M. J.; Yang, H. N.; Jang, D. Y.; Kim, J. S.; Jin, T. E. Residual Stress Measurement on Welded Specimen by Neutron Diffraction. *J. Mater. Process. Technol.* **2004**, *155–156*, 1171–1177.

determined. The depth of this layer is related to the ultrasonic wave-length, often exceeding a few millimeters, and hence is much greater than that obtained by the X-ray method. Other advantages of the ultrasonic technique are the facts that instrumentation is convenient to use, quick to step up, portable, inexpensive, and free of radiation hazards. This method is suitable for routine inspection procedures for large components such as steam turbine disks (*126,127*).

In the technique proposed by Kudryavtsev et al. (*124*), the velocities of longitudinal ultrasonic waves and shear waves with orthogonal polarization are measured at a considered point to determinate the uni- and biaxial residual stresses. The bulk waves in this approach are used to determine the stresses averaged over the thickness of the investigated elements. Surface waves are used to determine the uni- and biaxial stresses at the surface of the material. The mechanical properties of the material are represented by the proportionality coefficients, which can be calculated or experimentally determinate under external loading of a sample of the considered material. They developed the Ultrasonic Computerized Complex (UCC) that includes measurement unit supporting software and a laptop with an advanced database and expert system for the analysis of the influence of residual stresses on the fatigue life of welded components. The UCC allows the determination of uni- and biaxial applied and residual stresses for a wide range of materials. In general, the change in the ultrasonic wave velocity in structural materials under mechanical stress amounts to only tenths of a percentage point. Therefore, the equipment for practical application of ultrasonic technique for residual stress measurement should be of high resolution, reliable, and fully computerized. Ya et al. (*128*) have used an ultrasonic method to measure the nonuniform residual stresses in the transverse direction of the aluminium alloys. Aluminium alloys are widely used in the automotive, aerospace, and other industries because of their high strength/weight ratio. They show that the LCR technique offers advantages not possible with other acoustic techniques, such as acoustic birefringence. Specifically, the LCR technique is less sensitive to texture, most sensitive to stress, and is capable of indicating stress gradients. Furthermore, the LCR technique does not require opposite parallel surfaces and, therefore, does not impose any strict geometric limitations on the test specimens.

Currently, the main difficulty with such methods is that the relative deviations of ultrasonic velocities produced by the presence of stress are extremely small. Time-of-flight measurements are usually carried out to determine the velocity difference. The accuracy of such measurements obviously depends on the time duration of a probe pulse. On the other hand, the duration of a probe pulse cannot be reduced indefinitely, because the attenuation of ultrasound in metals is usually proportional to the second or even fourth degree of frequency. Nonetheless, a compromise can be achieved with the application of wide-band ultrasonic pulses. However, traditional piezoelectric techniques are inefficient for excitation over a very wide frequency range. Karabutov et al. (*129*) have developed a new laser ultrasonic method for residual stress measurements. The optoacoustic phenomenon can be employed for producing a large frequency band.

The ultrasonic transients excited by the absorption of laser radiation in a metal follow the time envelope of the laser pulse intensity. In this way, it is possible to obtain nanosecond ultrasonic pulses with an aperiodic temporal profile, a wide frequency spectrum, and pressure amplitudes up to a few hundreds of MPa. Javadi et al. (*130*) have applied L_{CR} method (known as FEL_{CR}) a 3D thermo-mechanical finite element analysis to evaluate welding residual stresses in austenitic stainless steel plates of AISI 304L. The finite element model has been verified by the hole drilling method. The validated FE model is then compared with the ultrasonic stress measurement based on acoustoelasticity. It was found that this method is able to evaluate the pipe residual stresses through the thickness. In another research, Javadi et al. (*131*) have investigated the ultrasonic method in axial and hoop stress measurement through the thickness of an austenitic stainless steel pipe. The residual stresses calculated by FE simulation are then compared with those obtained from the ultrasonic measurement while a good agreement is observed. It is demonstrated that the residual stresses through thickness of the stainless steel pipe can be evaluated by combining FE and L_{CR} method. Also, Javadi et al. (*132*) have presented a comparison of contact and immersion waves used to measure residual stresses in a dissimilar welding of AISI 304 to carbon steel (A106). Longitudinal critically refracted (L_{CR}) wave propagated by 2 MHz contact and immersion ultrasonic transducers is employed to measure the residual stresses. The same validated FE model of the welding process proposed in Ref. (*131*) is used to verify the ultrasonic results. The best agreement is observed in the parent material while the maximum difference is measured in the HAZ. The results show no considerable difference between using contact and immersion transducers in ultrasonic stress measurement of dissimilar joints.

www.iran-mavad.com
مرجع مهندسی مواد و متالورژی

6.11.5 Concluding Remarks

The main advantage of the nondestructive methods of measuring residual stresses is the preservation of the welded specimen, and they are particularly useful for production quality control and for measurement of valuable specimens. However, these methods commonly require detailed calibrations on representative specimen material to give required computational data. The diffraction methods such as X-ray and neutron diffraction can be applied for the polycrystalline and fine grained materials as well as metallic or ceramic. However, they cannot be used for large welds because the limited space available on most beam lines or X-ray diffractometers or for nanostructured materials because of the difficulty involved in analyzing the shape of the nanomaterial diffraction peak. The advantage of the neutron diffraction method in comparison with the X-ray technique is its larger penetration depth as X-ray method is limited for the measurement of residual stresses on the surface of materials. However, the relative cost of application of the neutron diffraction method, is much higher, mainly because of the equipment cost and it is not recommended to be used for routine process quality control in engineering applications.

The MBN method is applicable to ferromagnetic materials. It is affected by the 'magneto–elastic interaction,' by the saturation of the MBN energy signal in either tension or compression and by the microstructural state of the material, therefore, different materials must be individually calibrated. However, this magnetic BN method has the advantages of being rapid, suitable for the circular geometry such as rings, requiring no direct contact and the penetration is 100 times more than that of X-ray diffraction. The ultrasonic method, is not limited by the types of material understudy and can be utilized for residual stresses measurements on thick samples. Although this method is completely portable and cheap to perform, the wave's velocities depend on microstructural in-homogeneities and there are difficulties in separating the effects of multiaxial stresses. This method is especially recommended for routine inspection procedures for large components such as steam turbine disks.

In comparison to the nondestructive method, the destructive and semi-destructive residual stresses measurement methods generally require much less specific calibrations because they measure fundamental quantities such as displacements or strains, thus

Table 1 Comparison of the residual stresses measurement techniques

Technique	*Advantage*	*Disadvantage*
X-ray diffraction	Ductile Generally available Wide range of materials Hand-held systems Macro and micro RS	Lab-based systems Small components Only basic measurements
Hole drilling	Fast Easy use Generally available Hand-held Wide range of materials	Interpretation of data Semi-destructive Limited strain sensitivity and resolution
Neutron diffraction	Macro and micro RS Optimal penetration & resolution 3D maps	Only specialist facility Lab-based system
Barkhausen noise	Very quick Wide sensitive to Microstructure effects especially in welds Hand-held	Only ferromagnetic materials Need to divide the microstructure signal from that due to stress
Ultrasonic	Generally available Very quick Low cost Hand-held	Limited resolution Bulk measurements over whole volume
Sectioning	Wide range of material Economy and speed Hand-held	Destructive Interpretation of data Limited strain resolution
Contour	High-resolution maps of the stress normal to the cut surface Hand-held Wide range of material Larger components	Destructive Interpretation of data Impossible to make successive slices close together
Deep hole drilling	Deep interior stresses measurement Thick section components Wide range of material	Interpretation of data Semi-destructive Limited strain sensitivity and resolution
Synchrotron	Improved penetration & resolution of X-rays Depth profiling Fast Macro and micro RS	Only specialist facility Lab-based systems

Reproduced from Rossini, N. S.; Dassisti, D.; Benyounis, K. Y.; Olabi, A. G. Methods of Measuring Residual Stresses in Components. *Mater. Des.* **March 2012**, *35*, 572–588.

www.iran-mavad.com
مرجع مهندسی مواد و متالورژی

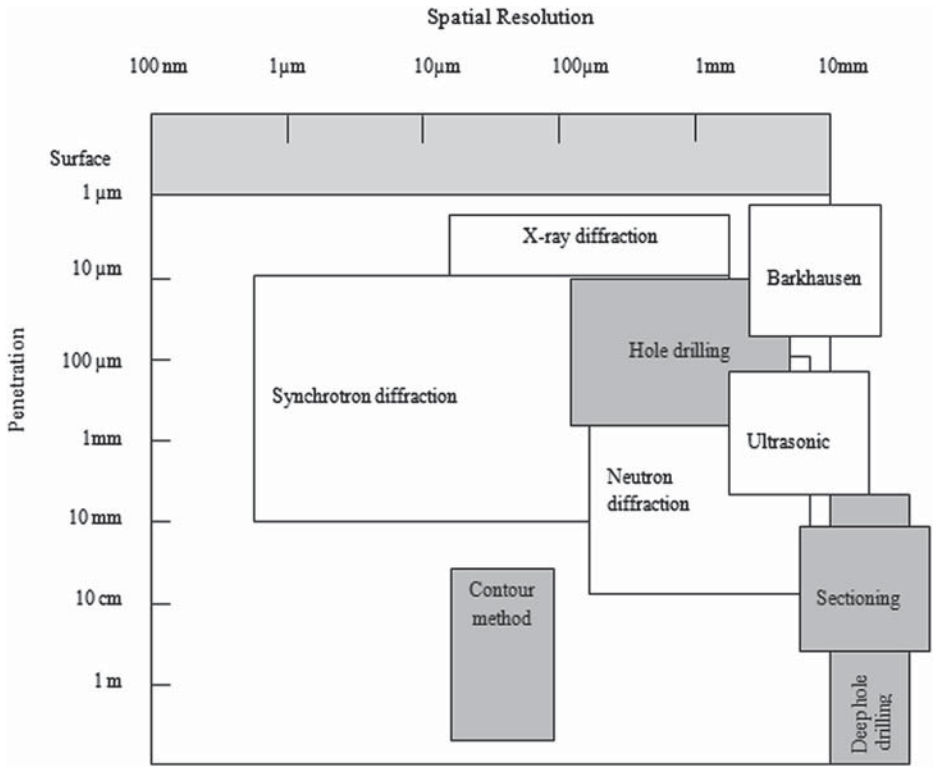

Figure 14 Penetration and the spatial resolution of the various techniques. The destructive and semi-destructive methods are colored grey. Reproduced from Rossini, N. S.; Dassisti, D.; Benyounis, K. Y.; Olabi, A. G. Methods of Measuring Residual Stresses in Components. *Mater. Des.* **March 2012**, *35*, 572–588.

giving them a wide range of application. The hole-drilling method is a cheap, fast, and popular semi-destructive method. It could be applied to isotropic and machinable materials whose elastic parameters are known. The main problem of this method is the introduction of machining stresses. The HS hole-drilling technique allows to resolve this problem inducing a lower additional stress and it has got the advantages of a simple experimental setup, a straightforward operation, and an improved accuracy. HS hole-drilling is suggested to measure the residual stresses in specimens with high hardness and high toughness. However, the tool wear will further cause the induced stress to increase and therefore, cause significant measurement errors. EDM hole-drilling provides as an alternative method for the measurement of residual stresses where HS hole-drilling is failed to employ in the stain gage method. It has got the advantage of no constraint on mechanical properties of ferrous materials, and has proven its capability to drill highly precise holes on various metals. When the residual stresses are not uniform with depth, the incremental hole-drilling method is recommended. It needs the appropriate trade-off with regard to both the number of the drilling increments and the depth of each increment.

The ring-core method is a variant of the hole drilling method suitable for much larger surface strains, but it creates much greater specimen damage and is much less convenient to implement in practice. The semi-destructive deep hole method combines elements of both the hole-drilling and ring-core methods. It enables the measurement of deep interior stresses for quite large specimens as steel and aluminium castings weighing several tons and it has become a standard technique for the measurement of residual stress in isotropic materials. The sectioning technique is a destructive method that gives only the average residual stresses for the area from which the piece was removed, but it is still counted as a simple and accurate method for measurement in structural carbon steel, aluminium, and stainless steel sections.

Many of these methods are the subject of continual advancement, but two in particular are of particular interest for the future because they have only recently become routinely available. As regards destructive methods, the contour method promises to be a useful complement to existing methods, being the first destructive method to provide high-resolution maps of the stress normal to the cut surface. However, it is not possible to make successive slices close together or at right angles to one another in order to comprehensively map the stress tensor due to stress relaxation caused by each successive cut. The method finds a number of application, for example, steel welds, quenched and impacted thick plates, cold-expanded hole, and aluminium alloy forging. By the nature of the cutting process, provided one can find an electro-discharge machine big enough, the contour method can reveal the stress fields over large areas. This makes it ideal for identifying hot-spot locations in residual stress. As regards the nondestructive method, the use of synchrotron radiation to perform strain scanning is a relatively recent development in residual stresses measurement, and its advantages lie in favorable combination of high X-ray intensity and penetration, combined with count times that range from several minutes per point to well under a minute, depending on the synchrotron source and the details of the experimental set-up. It is particularly useful for relatively thin plates of light element materials, such as aluminium alloys. Finally, in **Table 1** summarized the advantages and the disadvantages of each methods, while **Figure 14** shows the penetration and the spatial resolution (*133*).

www.iran-mavad.com
مرجع مهندسی مواد و متالورژی

References

1. Macherauch, E.; Kloos, K. H. Origin, Measurement and Evaluation of Residual Stress. In *Residual Stress in Science and Technology;* Macherauch, E., Hank, V., Eds.; DGM Verlag: Oberursel, 1987; pp 3–26.
2. Noyan, I. C.; Cohen, J. B. *Residual Stress Measurement by Diffraction and Interpretation;* Springer-Verlag: New York, 1987; pp 1–12.
3. Macherauch, E.; Wohlfahrt, H. Different Sources of Residual Stress as a Result of Welding. In *Conf. on Residual Stresses in Welded Construction and Their Effect, London, UK;* 15–17 Nov. 1977; pp 267–282.
4. Totten, G. *Handbook on Residual Stress;* SEM: Bethel, 2005. ISBN: 978-0871707291; Vol. 1, p 417.
5. Trufyakov, V.; Mikheev, P.; Kudryavtsev, Y. *Fatigue Strength of Welded Structures;* Harwood Academic: London, 1999; p 100.
6. American Welding Society. *Welding Handbook, Welding Technology,* 7th ed.; American Welding Society: Miami, 1981. ISBN 0-87171-126-5.
7. Macherauch, E.; Kloos, K. H. Origin, Measurements and Evaluation of Residual Stresses. *Residual Stress Sci. Technol.* **1987,** 3–26.
8. Lachmann, C.; Nitschke-Pagel, Th; Wohlfahrt, H. Non-destructive Characterization of Fatigue Processes in Cyclically Loaded Welded Joints by the Barkhausen Noise Method. In *Stanford University: 2nd International Workshop on Structural Health Monitoring;* 1999.
9. Lu, J. *Handbook of Measurement of Residual Stresses;* SEM: Bethel, 1996. Vol. 1, ISBN 978-0132557382; pp 319–322.
10. Olabi, A. G.; Hashmi, M. S. J. Stress Relief Procedures for Low Carbon Steel (1020) Welded Components. *J. Mater. Process. Technol.* **1996,** *56,* 552–562.
11. Kandil, F. A.; Lord, J. D. *A Review of Residual Stress Measurement Methods. A Guide to Technique Selection.* NPL Report MAT(A)04, 2001.
12. Milbradt, K. P. Ring-method Determination of Residual Stresses. *Proc. SESA* **1951,** *9* (1), 63–74.
13. Kiel, S. Experimental Determination of Residual Stresses with the Ring-core Method and an On-line Measuring System. *Exp. Tech.* **1992,** *16* (5), 17–24.
14. Ajovalasit, A.; Petrucci, G.; Zuccarello, B. Determination of Non-uniform Residual Stresses Using the Ring-core Method. *J. Mater. Process. Technol.* **1996,** *118* (2), 224–228.
15. Scholtes, B. *Residual Stress Analysis of Components with Real Geometries Using the Incremental Hole-drilling Technique and a Differential Evaluation Method;* Kassel University Press GmbH, 2007.
16. Vishay Measurements Group. (accessed 1 March 2011), http://www.vishaypg.com/, 2007.
17. Liu, J.; Zhu, H.; Xu, W. Analysis of Residual Stresses in Thick Aluminum Friction Stir Welded Butt Joints. *Mater. Des.* **2011,** *32* (4), 2000–2005.
18. Olabi, A. G.; Hashmi, M. S. J. The Effect of Post-weld Heat-treatment on Mechanical-properties and Residual-stresses Mapping in Welded Structural Steel. *J. Mater. Process. Technol.* **1995,** *55,* 117–122.
19. Olabi, A. G.; Hashmi, M. S. J. Effects of the Stress-relief Conditions on a Martensite Stainless-steel Welded Component. *J. Mater. Process. Technol.* **1998,** *77,* 216–225.
20. Olabi, A. G.; Casalino, G.; Benyounis, K. Y.; Rotondo, A. Minimisation of the Residual Stress in the Heat Affected Zone by Means of Numerical Methods. *Mater. Des.* **2007,** *28,* 2295–2302.
21. Benyounis, K. Y.; Olabi, A. G.; Abboud, J. H. Assessment and Minimization of the Residual Stress in Dissimilar Laser Welding. *Appl. Mech. Mater.* **2007,** *7–8,* 139–144.
22. Schajer, G. S. Hole-drilling Residual Stress Measurements at 75: Origins, Advances, Opportunities. *Exp. Mech.* **2009,** *50,* 245–253.
23. Flaman, M. T.; Herring, G. A. Comparison of Four Hole-producing Techniques for the Center-hole Residual-stress Measurement Method. *Exp. Tech.* **1985,** *9,* 30–32.
24. Flaman, M. T.; Herring, G. A. Ultra-high-speed Center-hole Technique for Difficult Machining Materials. *Exp. Tech.* **1986,** *10,* 34–35.
25. Ghanem, F.; Braham, C.; Sidhom, H. Influence of Steel Type on Electrical Discharge Machined Surface Integrity. *J. Mater. Process. Technol.* **2003,** *142,* 163–173.
26. Ekmekci, B.; Tekkaya, A. E.; Erden, A. A Semi-empirical Approach for Residual Stresses in Electric Discharge Machining (EDM). *Int. J. Mach. Tools Manuf.* **2006,** *46,* 858–868.
27. Lee, H. T.; Hsu, F. C. Feasibility Evaluation of EDM Hole Drilling Method for Residual Stress Measurement. *Mater. Sci. Technol.* **2003,** *19,* 1261–1265.
28. Lee, H. T.; Rehbach, W. P.; Hsu, F. C.; Ta, T. Y.; Hsu, E. The Study of EDM Hole-drilling Method for Measuring Residual Stress in SKD 11 Tool Steel. *J. Mater. Process. Technol.* **2004,** *149,* 88–93.
29. Mayer, J.; Hsu, F. C. Application of EDM Hole-drilling Method to the Measurement of Residual Stress in Tool and Carbon Steels. *J. Mater. Process. Technol.* **2006,** *128,* 468–475.
30. Lee, H. T.; Liu, C. Calibration of Residual Stress Measurements Obtained from EDM Hole Drilling Method Using Physical Material Properties. *Mater. Sci. Technol.* **2008,** *24,* 1462–1469.
31. Sicot, O.; Gong, X. L.; Cherouat, A.; Lu, J. Determination of Residual Stress in Composite Laminates Using the Incremental Hole-drilling Method. *J. Compos. Mater.* **2003,** *37,* 831–844.
32. Olabi, A. G.; Benyounis, K. Y.; Hashmi, M. S. J. Application of Response Surface Methodology in Describing the Residual Stress Distribution in CO_2 Laser Welding of AISI304. *Strain* **2007,** *43* (1), 37–46.
33. Baldi, A. A. New Analytical Approach for Hole Drilling Residual Stress Analysis by Full Field Method. *J. Mater. Process. Technol.* **2005,** *127* (2), 165.
34. Schajer, G. S.; Steinzing, M. Full-field Calculation of Hole-drilling Residual Stresses from ESPI Data. *Exp. Mech.* **2005,** *45* (6), 526–532.
35. Leggatt, R. H.; Smith, D. J.; Smith, S. D.; Faure, F. Development and Experimental Validation of the Deep Hole Method for Residual Stress Measurement. *J. Strain Anal.* **1996,** *31* (3), 177–186.
36. DeWald, A. T.; Hill, M. R. Improved Data Reduction for the Deep Hole Method of Residual Stress Measurement. *J. Strain Anal.* **2003,** *38* (1), 65–78.
37. Zhandano, I. M.; Gonchar, A. K. Determining the Residual Welding Stresses at Depth in Metals. *Automat. Weld.* **1978,** *31,* 22–24.
38. Beaney, E. M. *Measurement of Sub-surface Stress.* Report Rd/B/N4325; Central Electricity Generating Board, 1978.
39. Jesensky, M.; Vargova, J. Calculation and Measurement of Stresses in Thickwalled Pressure Vessels. *Svaracske Spravy* **1981,** *4,* 79–87.
40. Procter, E.; Beaney, E. M. Advances in Surface Treatments: Technology Application Effects. In *New York: Int. Guide Book Residual Stresses* **1987,** Vol. 14, pp 165–198.
41. Bonner, N. W.; Smith, D. J. Measurement of Residual Stresses Using the Deep-hole Method. *Pressure Vessels Piping* **1996,** *327,* 53–65.
42. George, D.; Bouchard, P. J.; Smith, D. J. Evaluation of Through Wall Residual Stresses in Stainless Steel Weld Repairs. *Mater. Sci. Forum* **2000,** *347–349,* 646–651.
43. George, D.; Smith, D. J. The Application of the Deep-hole Technique for Measuring Residual Stresses in Auto Frettaged Tubes. *ASME PVP High Pressure Technol.* **2000,** *406,* 25–31.
44. George, D.; Smith, D. J. Residual Stress Measurement in Thick Section Components. In *Seattle: Proc. ASME Pressure Vessels Pip. Conf.* **2000,** Vol. 410, pp 275–282.
45. Smith, D. J.; Bouchard, P. J.; George, D. Measurement and Prediction of Through Thickness Residual Stresses in Thick Section Welds. *J. Strain Anal.* **2000,** *35,* 287–305.
46. George, D.; Kingston, E.; Smith, D. J. Measurement of Through-thickness Stresses Using Small Holes. *J. Strain Anal.* **2002,** *37,* 125–139.
47. Wimpory, R. C.; May, P. S.; O'Dowd, N. P.; Webster, G. A.; Smith, D. J.; Kingston, E. Measurement of Residual Stresses in T-plate Weldments. *J. Strain Anal.* **2003,** *38,* 349–365.
48. Bateman, M. G.; Miller, O. H.; Palmer, T. J.; Breen, C. E. P.; Kingstonb, E. J.; Smith, D. J., et al. Measurement of Residual Stress in Thick Section Composite Laminates Using the Deep-hole Method. *Int. J. Mech. Sci.* **2005,** *47,* 1718–1739.
49. Shadley, J. R.; Rybicki, E. F.; Shealy, W. S. Application Guidelines for the Parting Out in a Through Thickness Residual Stress Measurement Procedure. *Strain* **1987,** *23,* 157–166.
50. Tebedge, N.; Alpsten, G.; Tall, L. Residual-stress Measurement by the Sectioning Method. *Exp. Mech.* **1973,** *13* (2), 88–96.
51. Mazzolani, F. M. *Aluminium Alloy Structures,* 2nd ed.; E&FN Spon, an imprint of Chapman and Hall: London, 1995. ISBN 978-0419177708.
52. Lagerqvist, O.; Olsson, A. Residual Stresses in Welded I-girders Made of Stainless Steel and Structural Steel. In *Helsinki: Proceedings of the Ninth Nordic Steel Construction Conference;* 2001; pp 737–744.

www.iran-mavad.com
مرجع مهندسی مواد و متالورژی

53. Young, B.; Lui, W. M. Behavior of Cold-formed High Strength Stainless Steel Sections. *J. Struct. Eng., ASCE* **2005,** *131* (11), 1738–1745.
54. Schafer, B. W.; Peköz, T. Computational Modelling of Cold-formed Steel: Characterizing Geometric Imperfections and Residual Stresses. *J. Construct. Steel Res.* **1998,** *47* (3), 192–210.
55. Lanciotti, A.; Lazzeri, L.; Polese, C. Presentation at the Porto Meeting of the European Union DaToN Project, 2007.
56. Cruise, R. B.; Gardner, L. Strength Enhancements Induced during Cold Forming of Stainless Steel Sections. *J. Construct. Steel Res.* **2008,** *64* (11), 1316–1320.
57. Prime, M. B.; Gonzales, A. R. In *Proceedings of the Sixth International Conference on Residual Stresses;* IOM Communications Ltd.: Oxford, UK, 2000; pp 617–624.
58. Prime, M. B.; Hughes, D. J.; Webster, P. J.. Portland, OR In *Proceedings of 2001 SEM Annual Conference on Experimental and Applied Mechanics Bethel,* 2001; pp 608–611.
59. Murugan, N.; Narayanan, R. Finite Element Simulation of Residual Stresses and Their Measurement by Contour Method. *Mater. Des.* **2009,** *30* (6), 2067–2071.
60. Prime, M. B.; Martineau, R. L. Mapping Residual Stresses after Foreign Object Damage Using the Contour Method. *Mater. Sci. Forum* **2002,** *404–407,* 521–526.
61. Zhang, Y.; Fitzpatrick, M. E.; Edwards, L. Measurement of the Residual Stresses around a Cold Expanded Hole in an EN8 Steel Plate Using the Contour Method. *Mater. Sci. Forum* **2002,** *404–407,* 527–534.
62. Prime, M. B. Cross-sectional Mapping of Residual Stresses by Measuring the Surface Contour after a Cut. *J. Eng. Mater. Technol.* **2001,** *123* (2), 162–168.
63. Bueckner, H. F. The Propagation of Cracks and the Energy of Elastic Deformation. *Trans. ASME* **1958,** *80,* 1225–1230.
64. Prime, M. B.; Newborn, M. A.; Balog, J. A. Quenching and Cold-work Residual Stresses in Aluminum Hand Forgings: Contour Method. *Mater. Sci. Forum* **2003,** *426–432,* 435–440.
65. DeWald, A. T.; Hill, M. R. Multi-axial Contour Method for Mapping Residual Stresses in Continuously Processed Bodies. *Exp. Mech.* **2006,** *46,* 473–490.
66. Ueda, Y. M.; Fukuda, K.; Kim, Y. C. New Measuring Method of Axisymmetric Three-Dimensional Residual Stresses Using Inherent Strains as Parameters. *J. Eng. Mater. Technol.* **1986,** *108* (4), 328–335.
67. Ueda, Y. M.; Fukuda, K. New Measuring Method of Three-dimensional Residual Stresses in Long Welded Joints Using Inherent Strains as Parameters-Lz Method. *J. Eng. Mater. Technol.* **1989,** *111* (1), 1–8.
68. Hill, M. R. Determination of Residual Stress Based on the Estimation of Eigenstrain. Ph.D. Thesis, Stanford University, USA, 1996.
69. DeWald, A. T. Measurement and Modelling of Laser Peening Residual Stresses in Geometrically Complex Specimens. Ph.D. Thesis, University of California, Davis, USA, 2005.
70. Kartal, M. E.; Liljedahl, C. D. M.; Gungor, S.; Edwards, L.; Fitzpatrick, M. E. Determination of the Profile of the Complete Residual Stress Tensor in a VPPA Weld Using the Multi-axial Contour Method. *Acta Mater.* **2008,** *56,* 4417–4428.
71. Gunnert, R. *Method for Measuring Residual Stresses and Its Application to a Study of Residual Welding Stresses;* Almqvist & Wiksell: Stockholm, 1955.
72. Schwaighofer, J. Determination of Residual Stresses on the Surface of Structural Parts. *Exp. Mech.* **1964,** *4* (2), 54–56.
73. Jullien, D.; Gril, J. Growth Strain Assessment at the Periphery of Small-diameter Trees Using the Two-grooves Method: Influence of Operating Parameters Estimated by Numerical Simulations. *Wood Sci. Technol.* **2008,** *42* (7), 551–565.
74. Walton, H. W. *Deflection Methods to Estimate Residual Stress. Handbook of Residual Stress and Deformation of Steel;* ASM International: Materials Park, 2002. ISBN 0-87170-729-2; pp 89–98.
75. Fuller, J.. Research Paper *Conditioning Stress Development and Factors that Influence the Prong Test,* Vol. 537; USDA Forest Products Laboratory: Madison, WI, 1995; p 6.
76. Baldwin, W. M. Residual Stresses in Metals. In *Philadelphia: Proc. American Society for Testing and Materials;* 1949; p 49.
77. *ASTM: Standard Practice for Estimating the Approximate Residual Circumferential Stress in Straight Thin-walled Tubing. Standard Test Method E1928–07;* American Society for Testing and Materials: West Conshohocken PA, 2007.
78. Stoney, G. G. The Tension of Thin Metallic Films Deposited by Electrolysis. *Proc. R. Soc. London* **1909,** *82,* 172–175.
79. Cao, W.; Fathallah, R.; Castex, L. Correlation of Almen Arc Height with Residual Stresses in Shot Peening Process. *Mater. Sci. Technol.* **1995,** *11* (9), 967–973.
80. Treuting, R. G.; Read, W. T. A Mechanical Determination of Biaxial Residual Stress in Sheet Materials. *J. Appl. Phys.* **1951,** *22* (2), 130–134.
81. Sachs, G.; Espey, G. The Measurement of Residual Stresses in Metal. *Iron Age* **1941,** *148,* 63–71.
82. Ostlund, M.; Ostlund, S.; Carlsson, L. A.; Fellers, C. Experimental Determination of Residual Stresses in Paperboard. *Exp. Mech.* **1985,** *45* (6), 493–497.
83. Kafkas, F.; Karatas, C.; Sozen, A.; Arcaklioglu, E.; Saritas, S. Determination of Residual Stresses Based on Heat Treatment Conditions and Densities on a Hybrid (FLN2–4405) Powder Metallurgy Steel Using Artificial Neural Network. *Mater. Des.* **2007,** *28* (9), 2431–2442.
84. Fetullazad, E.; Akyildiz, H. K.; Saritas, S. Effects of the Machining Conditions on the Strain Hardening and the Residual Stresses at the Roots of Screw Threads. *Mater. Des.* **2010,** *31* (4), 2025–2031.
85. Prime, M. B. Residual Stress Measurement by Successive Extension of a Slot: The Crack Compliance Method. *Appl. Mech. Rev.* **1999,** *52* (2), 75–96.
86. Germaud, M.; Cheng, W.; Finnie, I.; Prime, M. B. The Compliance Method for Measurement of Near Surface Residual Stresses Analytical Background. *J. Eng. Mater. Technol.* **1994,** *119* (4), 550–555.
87. Cheng, W.; Finnie, I. *Residual Stress Measurement and the Slitting Method;* Springer: New York, 2007. ISBN 978-144194241.
88. Prime, M. B.; Hill, M. R. Residual Stress, Stress Relief, and in Homogeneity in Aluminum Plate. *Scr. Mater.* **2002,** *46* (1), 77–82.
89. Nervi, S.; Szabó, B. A. On the Estimation of Residual Stresses by the Crack Compliance Method. *Comput. Methods Appl. Mech. Eng.* **2007,** *196* (37–40), 3577–3584.
90. An, Y.; Schajer, G. S. Residual Stress Determination Using Cross-slitting and Dual-axis ESPI. *Exp. Mech.* **2010,** *50* (2), 169–177.
91. Schindler, H. J.; Cheng, W.; Finnie, I. Experimental Determination of Stress Intensity Factors due to Residual Stresses. *Exp. Mech.* **1997,** *37* (3), 272–277.
92. Norton, J. H.; Rosenthal, D. Stress Measurement by X-ray Diffraction. *Proc. Soc. Exp. Stress Anal.* **1944,** *1* (2), 73–76.
93. Norton, J. H.; Rosenthal, D. Application of the X-ray Method of Stress Measurement to Problems Involving Residual Stress in Metals. *Proc. Soc. Exp. Stress Anal.* **1944,** *1* (2), 81–90.
94. Ruud, C. O. A Review of Selected Non-destructive Methods for Residual Stress Measurement. *NDT Int.* **1982,** *15* (1), 15–23.
95. Prevéy, P. S. X-ray Diffraction Residual Stress Techniques. *Lambda Technol.* **2006,** *10,* 380–392.
96. Venkata Ramana, P.; Madhusudhan Reddy, G.; Mohandas, T.; Gupta, A. V. S. S. K. S. Microstructure and Residual Stress Distribution of Similar and Dissimilar Electron Beam Welds – Maraging Steel to Medium Alloy Medium Carbon Steel. *Mater. Des.* **2010,** *31* (2), 749–760.
97. Estefen, S. F.; Gurova, T.; Castello, X.; Leontiev, A. Surface Residual Stress Evaluation in Double-electrode Butt Welded Steel Plates. *Mater. Des.* **2010,** *31* (3), 1622–1627.
98. Lu, J.; Retraint, D. A Review of Recent Developments and Applications in the Field of X-ray Diffraction for Residual Stress Studies. *J. Strain Anal.* **1998,** *33* (2), 127–136.
99. Cheng, X.; Fisher, J.; Prask, H.; Gnauper, T.; Yen, B.; Roy, S. Residual Stress Modification by Post-weld Treatment and Its Beneficial Effect on Fatigue Strength of Welded Structures. *Int. J. Fatigue* **2003,** *25,* 1259–1269.
100. Ya, M.; Xing, Y.; Dai, F.; Lu, K.; Lu, J. Study of Residual Stress in Surface Nanostructured AISI 316L Stainless Steel Using Two Mechanical Methods. *Surf. Coat. Technol.* **2003,** *168* (2–3), 148–155.
101. Withers, P. J. Depth Capabilities of Neutron and Synchrotron Diffraction Strain Measurement Instruments. I. The Maximum Feasible Path Length. *J. Appl. Crystallogr.* **2004,** *37* (4), 596–606.
102. Reimers, W.; Broda, M.; Brusch, B.; Dantz, D.; Liss, K.-D.; Pyzalla, A., et al. Evaluation of Residual Stresses in the Bulk of Materials by High Energy Synchrotron Diffraction. *J. Nondestruct. Eval.* **1998,** *17* (3), 129–140.
103. Ganguly, S.; Fitzpatrick, M. E.; Edwards, L. Use of Neutron and Synchrotron X-ray Diffraction for Evaluation of Residual Stresses in a 2024–T351 Aluminum Alloy Variable-polarity Plasma-arc Weld. *Metall. Mater. Trans.* **2006,** *37* (2), 411–420.
104. Withers, P. J. Mapping Residual and Internal Stress in Materials by Neutron Diffraction. *Comp. Rendus Phys.* **2007,** *8* (7–8), 806–820.

www.iran-mavad.com
مرجع مهندسی مواد و متالورژی

105. McNelis, Kevin P.; Dawson, Paul R.; Miller, Matthew P. A Two-scale Methodology for Determining the Residual Stresses in Polycrystalline Solids Using High Energy X-ray Diffraction Data. *J. Mech. Phys. Solids* **February 2013,** *61* (2), 428–449.
106. Kim, Seok-Hoon; Kim, Jong-Bum; Lee, Won-Jae Numerical Prediction and Neutron Diffraction Measurement of the Residual Stresses for a Modified 9Cr–1Mo Steel Weld. *J. Mater. Process. Technol.* **2009,** *209* (8), 3905–3913.
107. Claphama, L.; Abdullah, K.; Jeswiet, J. J.; Wild, P. M.; Roggec, R. Neutron Diffraction Residual Stress Mapping in Same Gauge and Differential Gauge Tailor-welded Blanks. *J. Mater. Process. Technol.* **2004,** *148* (2), 177–185.
108. Polycrystalline Materials – Determinations of Residual Stresses by Neutron Diffraction. In *ISO/TTA3 Technology Trends Assessment, Geneva, Switzerland;* Webster, G. A., Ed.; 2001.
109. Dann, J. A.; Daymond, M. R.; James, J. A. J.; Santisteban, J. R.; Edwards, L. A New Diffractometer Optimized for Stress Measurements. In *ENGIN-X Proc. ICANS XVI* **2003,** Vol. 1, pp 231–238.
110. Dann, J. A.; Daymond, M. R.; Edwards, J. A.; James, J. A.; Santisteban, J. R. A Comparison between Engin and Engin-X, a New Diffractometer Optimized for Stress Measurement. *Phys. B* **2004,** *350* (1–3), E511–E514.
111. Martinson, P.; Daneshpour, S.; Koçak, M.; Riekehr, S.; Staron, P. Residual Stress Analysis of Laser Spot Welding of Steel Sheets. *Mater. Des.* **2009,** *30* (9), 3351–3359.
112. Paradowska, A.; Price, J. W. H.; Ibrahim, R.; Finlayson, T. R.; Blevins, R.; Ripley, M. Residual Stress Measurements by Neutron Diffraction in Multi-bead Welding. *Phys. B* **2006,** *385–386* (2), 890–893.
113. Woo, W.; Feng, Z.; Wang, X.-L.; An, K.; Bailey, W. B.; David, S. A., et al. *Mater. Sci. Forum* **2006,** *524–525,* 387–392.
114. Altpeter, I.; Dobmann, G.; Kröning, M.; Rabung, M.; Szielasko, S. Micro-magnetic Evaluation of Micro Residual Stresses of the IInd and IIIrd Order. *NDT&E Int.* **2009,** *42,* 283–290.
115. Theiner, W.; Höller, P. Magnetische Verfahren zu Spannungsermittlung. In *HTMBeiheft: Eigenspannungen und Lastspannungen;* Hauk, V., Macherauch, E., Eds.; Hanser, 1982; pp 156–163.
116. Stewart, D. M.; Stevens, K. J.; Kaiser, A. B. Magnetic Barkhausen Noise Analysis of Stress in Steel. Original Res. Article. *Curr. Appl. Phys.* **2004,** *4* (2–4), 308–311.
117. Ilker Yelbay, H.; Cam, Ibrahim; Hakan Gur, C. Non-destructive Determination of Residual Stress State in Steel Weldments by Magnetic Barkhausen Noise Technique. *NDT&E Int.* **2010,** *43,* 29–33.
118. Anglada-Rivera, J.; Padovese, L. R.; Capo-Sanchez, J. Magnetic Barkhausen Noise and Hysteresis Loop in Commercial Carbon Steel: Influence of Applied Tensile Stress and Grain Size. *J. Magn. Magn. Mater.* **2001,** *231,* 299–306.
119. Yamaura, S.; Furuya, Y.; Watanabe, T. The Effect of Grain Boundary Microstructure on Barkhausen Noise in Ferromagnetic Materials. *Acta Mater.* **2001,** *49,* 3019–3027.
120. Ju, Jang-Bog; Lee, Jung-Suk; Jang, Jae-il; Kim, Woo-sik; Kwon, Dongil *Int. J. Pressure Vessels Piping* **2003,** *80* (9), 641–646.
121. Desvaux, S.; Duquennoy, M.; Gualandri, J.; Ourak, M. The Evaluation of Surface Residual Stress in Aeronautic Bearings Using the Barkhausen Noise Effect. Original Res. Article. *NDT&E Int.* **2004,** *37* (1), 9–17.
122. Balahcene, F.; Lu, J. Study of Residual Stress Induced in Welded Steel by Surface Longitudinal Ultrasonic Method. In *Proceedings of SEM Annual Conference on Theoretical, Experimental and Computational Mechanics;* Bethel, 1999; pp 331–334.
123. Leon-Salamanca, T.; Bray, D. E. Residual Stress Measurement in Steel Plates and Welds Using Critically Refracted Waves. *Res. Nondestruct. Eval.* **1996,** *7* (4), 169–184.
124. Kudryavtsev, Y.; Kleiman, J.; Gushcha, O.; Smilenko, V.; Brodovy, V. Ultrasonic Technique and Device for Residual Stress Measurement. In *X Int. Congress and Exposition on Experimental and Applied Mechanics;* 2004; pp 1–7.
125. Park, M. J.; Yang, H. N.; Jang, D. Y.; Kim, J. S.; Jin, T. E. Residual Stress Measurement on Welded Specimen by Neutron Diffraction. *J. Mater. Process. Technol.* **2004,** *155–156,* 1171–1177.
126. Lee, H. Y.; Nikbin, K. M.; Dowd, P. O. A Generic Approach for a Linear Fracture Mechanics Analysis of Components Containing Residual Stress. *Int. J. Pressure Vessels Piping* **2005,** *82,* 797–806.
127. Paradowska, A.; Price, J. W. H.; Ibrahim, R.; Finlayson, T. A Neutron Diffraction of Residual Stress due to Welding. *J. Mater. Process. Technol.* **2005,** *164–165,* 1099–1105.
128. Ya, M.; Marquette, P.; Belahcene, F.; Lu, J. Residual Stresses in Laser Welded Aluminium Plate by Use of Ultrasonic and Optical Methods. *Mater. Sci. Eng.* **2004,** *382* (1–2), 257–264.
129. Karabutov, A.; Devichensky, A.; Ivochkin, A.; Lyamshev, M.; Pelivanov, I.; Rohadgi, U., et al. Laser Ultrasonic Diagnostics of Residual Stress. *Ultrasonics* **2008,** *48* (6–7), 631–635.
130. Javadi, Y.; Akhlaghi, M.; Najafabadi, A. M. Using Finite Element and Ultrasonic Method to Evaluate Welding Longitudinal Residual Stress through the Thickness in Austenitic Stainless Steel Plates. *J. Mater. Des.* **2013,** *45,* 628–642.
131. Javadi, Y.; Pirzaman, H. S.; Raeisi, M. H.; Najafabadi, A. M. Ultrasonic Inspection of a Welded Stainless Steel Pipe to Evaluate Residual Stresses through Thickness. *Mater. Des.* **August 2013,** *49,* 591–601.
132. Javadi, Y.; Najafabadi, M. H. Comparison between Contact and Immersion Ultrasonic Method to Evaluate Welding Residual Stresses of Dissimilar Joints. *Mater. Des.* **May 2013,** *47,* 473–482.
133. Rossini, N. S.; Dassisti, D.; Benyounis, K. Y.; Olabi, A. G. Methods of Measuring Residual Stresses in Components. *Mater. Des.* **March 2012,** *35,* 572–588.

www.iran-mavad.com
مرجع مهندسی مواد و متالورژی

6.12 Safety and Security Conditions in Welding Processes

TS Hong and M Ghobakhloo, Universiti Putra Malaysia, Selangor, Malaysia

© 2014 Elsevier Ltd. All rights reserved.

6.12.1	**Introduction**	213
6.12.2	**Welding Fumes and Gases**	213
6.12.2.1	Welding Fumes and Gases-Related Diseases	214
6.12.2.1.1	Pulmonary Effects	214
6.12.2.1.2	Lung Cancer	215
6.12.2.2	Minimizing Welding Fume and Gas Hazards	215
6.12.3	**Electric Shock Hazards in Welding**	216
6.12.3.1	Criticality of Electric Shock Injury	217
6.12.3.2	Potential Risk of Electric Shock from Welding Activities	218
6.12.3.3	Electric Shock in Underwater Welding	219
6.12.4	**Burning Hazards**	220
6.12.4.1	Burn Injuries in Welding Activities and Relative Effects	220
6.12.4.2	Safety Measures to Prevent Burns	221
6.12.5	**Welding Noise Effects**	222
6.12.6	**Ultraviolet Radiation/Infrared Radiation Hazards**	223
6.12.6.1	Reducing the Effect of UVR/IR Beam during the Welding Process	223
6.12.7	**Hazards of Welding Equipment**	223
6.12.7.1	Minimizing the Hazards of Engine Powered Equipment	223
6.12.7.2	Hazards of Compressed Gas Cylinder	224
6.12.7.2.1	Minimizing the Hazard of Compressed Gas Cylinder	224
References		224
Relevant Website		225

6.12.1 Introduction

Welding can be classified as one of the most risky professions in the world, as the processes in welding are associated with unique exposure, extreme heat, high radiant energy, high electromagnetic fields, molten metal splatter, and smoke (*1*). Welding is considered to be a dangerous profession for the following reasons (*2*,*3*):

- There are various factors that jeopardize the welder's health, such as temperature, burns, radiation, noise, gas, and electric shock;
- Large variety in the chemical composition of the metal vapors results during the welding processes, which differ according to the material, the method, and the shielded gas used. The particles and gas generated during the welding operation are considered the most harmful in comparison with other reactions that result following the welding operation.

The major dangers linked with the welding operation that affect the health of the human personnel are smoke and gas. Moreover, dangers can exist as follows: electrical shock, fire and explosions, burns due to the splashes of molten metal, eye and skin diseases due to ultraviolet emissions, effects due to heat radiation, and effects associated with the powerful noise during plasma arc welding (*4*–*6*).

6.12.2 Welding Fumes and Gases

Welding may produce fumes and gases hazardous to health, particularly if inhaled or ingested by the welder (*7*). ('Welder' or 'welding operator' as used herein are intended to designate any operator of electric or oxyfuel gas welding or cutting equipment, or allied processes.) Fumes are solid particles that originate from welding consumables, the base metal, and any coatings present on the base metal (Safety and Health Fact Sheet No. 1). The consumable, however, produces 80–95% of the fumes (*8*). The welding fumes generated during the welding process include at least 14 metals, comprising manganese (Mn), beryllium (Be), cadmium (Cd), chromium (Cr), cobalt (Co), copper (Cu), iron (Fe), lead (Pb), mercury (Hg), molybdenum (Mo), nickel (Ni), zinc (Zn), antimony (Sb), and vanadium (V) (*9*). Besides fumes, significant levels of different toxic gases such as CO, CO_2, F, and HF might be released during common welding processes (*8*). Although essential for health in small doses, pure manganese is a neurotoxin that can cause manganese poisoning in large doses. Similarly, chromium and nickel can be carcinogenic. Chromium, nickel, and manganese do not exist as pure elements in welding fumes; rather, they are present as impure compounds. The heated and vaporized metals react with air, producing metal oxides. Although these compounds do not present the same toxic risk as pure elements, their toxicity is of serious concern (*9*). Welding fume particles range in size from 0.005 to 20 μm, although less than

www.iran-mavad.com
مرجع مهندسی مواد و متالورژی

10–30% (depending on the welding process) of the fume mass is larger than 1 μm. These particles are small enough to become and remain airborne and are easily inhaled. Accordingly, overexposure to welding fumes and gases may indeed cause possible effects. Depending on the material involved, these effects range from irritation of eyes, skin, and respiratory system to more severe complications. Effects may also occur immediately or at some later time (*10*).

6.12.2.1 Welding Fumes and Gases-Related Diseases

Many investigators have examined the effects of welding fumes and gases on welders and exposed operators' health. The composition and the rate of generation of welding fumes and gases are characteristic of the individual welding processes and may be affected by the welding current, shielding gases, and even the technique and skill of the welder (*11*). Accordingly, the severity of exposure to welding fumes and gases varies within different welding contexts. Prior studies, however, have reported that a certain level of exposure to welding fumes and gases may indeed cause symptoms such as nausea, headaches, dizziness, and metal fume fever. The possibility of more serious health effects exists when highly toxic materials are involved. For example, manganese overexposure can affect the central nervous system resulting in impaired speech and movement. **Table 1** which is adapted from Antonini et al. (*11*) lists the common fume components and their uses and potential hazards.

6.12.2.1.1 Pulmonary Effects

Pulmonary effects are the most expected effects of welding fume and gas inhalation among welders. Mur et al. (*12*) conducted an epidemiological, cross-sectional study in order to assess nonneoplastic effects on the lung due to chronic exposure to arc welding fumes and gases. Their study demonstrated that arc welders have had a slightly higher bronchial hyper-reactivity to acetyl-choline and a lower lung diffusing capacity for CO. Moreover, nonspecific radiologic abnormalities such as reticulation and micro-nodulation as well as obstructive signs were found to be more frequent in the more exposed welders than in those working in well ventilated workplaces. The study of Mur et al. (*12*), however, revealed that the nature of the metal welded (mild steel, stainless steel, or aluminum) did not seem to have an influence on respiratory impairments.

Many investigators have reported that transient effects on pulmonary function can occur at the time of exposure in the workplace and then return to normal during unexposed nonworking periods (*11*). Akbar-Khanzadeh (*13*), for example, measured the forced vital capacity (FVC); the forced expiratory volume in 1 s (FEV_1) and the transfer factor for the lung (TL) were measured before and after an 8-h work shift in groups of welders and nonwelder controls in a shipyard. Akbar-Khanzadeh (*13*) reported that although the lung function indices in both the welder and control groups decreased from morning through afternoon, the welders demonstrated significantly higher reduction in the indices than the control group. Similarly, Donoghue et al. (*14*) compared the peak expiratory flow (PEF) of welders and nonwelders over a 12-h period. These researchers measured the PEF before the start of work and 15 min, 30 min, and 1, 2, 4, 7, and 12 h after the start of welding and found an immediate type reaction in welders, similar to that seen in some cases of occupational asthma yet not as severe. Consistently, Beckett et al. (*15*) conducted a 3-year survey to measure the respiratory symptoms, spirometry, and methacholine reactivity annually in welders and nonwelder control subjects to determine whether welding-related symptoms are associated with accelerated decline in lung function or changes in airway reactivity. There scholars reported that the welders have had significantly more reversible work-related symptoms of cough, phlegm, wheeze, and chest tightness than the nonwelder shipyard control subjects. They also found that pulmonary symptoms were significantly more

Table 1 Elemental constituents commonly found in welding fumes

Fume	*Uses*	*Potential hazard concern*
Aluminum	Alloy and filler metal	Conducive to ozone production
Barium	Fluxing agent	Eye, nose, and throat irritant
Cadmium	Plating and brazing alloy	Respiratory irritant, metal fume fever
Chromium	Stainless steel alloy	Lung carcinogen
Copper	Alloy and coating material	Respiratory irritant, metal fume fever
Fluorine	Fluxing agent	Respiratory irritant
Iron	Most common fume component when welding steel	Siderosis
Lead	Brass, bronze, and steel alloy	Nervous system and kidney effects
Magnesium	Light metal alloy	Respiratory irritant, metal fume fever
Manganese	Steel alloy	Nervous system effects, respiratory irritant
Molybdenum	Steel alloy	
Nickel	Stainless steel alloy	Lung carcinogen
Silicon	Fluxing agent	
Tin	Bronze and solder alloy	Metal fume fever
Titanium	Fluxing agent	
Zinc	Galvanized steel, paint coatings	Metal fume fever

Adapted from Antonini, J. M.; Lewis, A. B.; Roberts, J. R.; Whaley, D. A. Pulmonary Effects of Welding Fumes: Review of Worker and Experimental Animal Studies. *Am. J. Ind. Med.* **2003**, *43* (4), 350–360 and Antonini, J. M.; Taylor, M. D.; Zimmer, A. T.; Roberts, J. R. Pulmonary Responses to Welding Fumes: Role of Metal Constituents. *J. Toxicol. Environ. Health, Part A* **2004**, *67* (3), 233–249.

www.iran-mavad.com
مرجع مهندسی مواد و متالورژی

frequent among welders as compared with controls throughout the study, but the complaints subsided as welding exposure diminished during the course of the 3-year period.

The dose effect of years of welding on lung function has been documented by prior studies. Meo et al. (16) investigated the nonsmoking manual metal arc welders who work without the benefit of welding fume control ventilation or respiratory protective devices and demonstrated that welding workers, with exposures longer than 9 years, have a significant reduction in spirometry (FEV_1, FEV_1/FVC%, and PEF). In a comprehensive longitudinal study in the period of 1987 and 2004 by Christensen et al. (17), lung function was measured by spirometry among steel welders and nonwelding production workers to investigate if long-term exposure to welding fume particulates accelerates the age-related decline in lung function. Christensen et al. (17) analyzed the decline in FEV_1 in relation to cumulated exposure to fume particulates among welders during the follow-up period and concluded that long-term exposure to welding emissions may accelerate the age-related decline of lung function.

6.12.2.1.2 Lung Cancer

Prior studies have extensively investigated the potential association between welding and the development of lung cancer. In 1990, the International Agency for Research on Cancer (IARC) categorized welding fumes as possibly carcinogenic to humans on the basis of 23 epidemiologic studies (18). Alternatively, the National Institute of Occupational Safety and Health (NIOSH) announced that there is an elevated risk of lung cancer among welders that cannot be completely accounted for by smoking or asbestos exposure. More recent literature, however, has provided more evidence to support the view that welding fumes can increase the risk of lung cancer (19,20). The welding community generally believes that mild steel welding, which roughly accounts for 90% of all welding, poses a slight risk for the development of lung cancer (19,21). In most cancer studies in relation to welding fumes the focus falls upon nickel, chromium or chromium(VI), and other possible carcinogens (20). Thus, investigators generally believe the risk is confined to stainless steel welding, in which chromium and nickel (known human carcinogens) have been measured in significant quantities in welding fumes (11).

Sørensen et al. (22) studied welders working in Danish stainless or mild steel industrial companies and found that among the stainless steel welders, the risk of cancer increases significantly with increasing accumulative welding particulate exposure. Sørensen et al. (22), however, did not find any exposure–response relation for mild steel welders, even after adjustment for tobacco smoking and asbestos exposure. Seel et al. (19) similarly conducted a retrospective exposure assessment of asbestos, welding fumes, chromium, and nickel (in stainless steel welding fumes) at the Portsmouth Naval Shipyard for a nested case-control study of lung cancer. Seel et al. (19) found that asbestos and welding fume exposure estimates were positively associated with lung cancer in their nested case-control study. Ambroise et al. (23) conducted a meta-analysis of 60 published research papers on the relation between welding and lung cancer to assess whether lung cancer risk is significantly higher among welders. According to this meta-analysis, the estimate of lung cancer risk among welders, as compared with nonwelders, has been 1.26. This means that the meta-analysis by Ambroise et al. (23) showed a 26% excess of lung cancer for welders. Inconsistent with some studies suggesting that stainless steel welders are more susceptible to lung cancer compared to mild steel welders, Ambroise et al.'s (23) meta-analysis did not support the hypothesis that stainless steel welders are at higher lung cancer risk than mild steel welders (there is 26% excess of lung cancer risk for both stainless and mild steel compared to nonwelders), despite their probable exposure to chromium and nickel compounds in welding fumes. Further, Siew et al. (20) analyzed the associations between exposure to iron and welding fumes and the incidence of lung cancer among Finnish men and found that the relative risks for lung cancer increase as the cumulative exposures to iron and welding fumes increase. Interestingly, Siew et al. (20) found a higher standardized lung cancer ratio for mild steel welders in comparison with stainless steel welders, which challenges the contention that stainless steel welders are at higher lung cancer risk than mild steel welders.

Prior studies suggest that pulmonary effects of welding fumes and gases are not limited to lung functions and lung cancer. In fact, it is possible that welding fumes may increase susceptibility to metal fume fever (24), pneumoconiosis/fibrosis (25,26), and infection/immunity (27,28) in welders. The effects of welding fume inhalation on metal fume fever, pneumoconiosis/fibrosis, and infection/immunity are summarized in **Table 2**.

6.12.2.2 Minimizing Welding Fume and Gas Hazards

Welding fumes are a complex mixture of potentially toxic fumes and noxious gases. Some of the frequently observed diseases resulting from exposure to welding fumes and gases were discussed in Section 6.12.2.1. It is, however, imperative to notice that welding fumes are a complex mixture of metals and metal oxides, and exposure to welding fumes is unique. Many questions remain unanswered concerning the effects of welding fume and gas exposure on human health (2). In particular, it has been suggested that new welding fume hazards will likely be introduced into the workplace due to the development of increasingly sophisticated welding technologies that may alter the properties of the freshly formed fumes (11,29). Accordingly, avoiding these fumes and gases would be the main practical strategy for minimizing the hazards of welding fumes and gases. Based on the recommendations provided by the American Conference of Governmental Industrial Hygienists (ACGIH), the American Welding Society (AWS), the American National Standards Institute (ANSI), and the Occupational Safety and Health Administration (OSHA), the following strategies are recommended to minimize the hazards of exposure to welding fumes and gases.

- When welding, welders should keep their heads out of the fumes, and they must not breathe the fumes.
- Enough ventilation or exhaust (or both) should be used at the arc to keep fumes and gases from the welders' breathing zone and general area.

www.iran-mavad.com
مرجع مهندسی مواد و متالورژی

Table 2 Summary of welding fume effects on metal fume fever, pneumoconiosis/fibrosis, and infection/immunity.

Effects	*Worker studies*	*Animal studies*
Metal fume fever	● Most frequent acute respiratory complaint ● Self-limiting, short duration ● Caused by oxides of zinc, copper, magnesium, or cadmium ● Proinflammatory cytokines may be involved	● No *in vivo* animal studies specifically evaluating the effect of welding fumes on metal fume fever available ● Lung responses to zinc oxide in animals similar to humans
Pneumoconiosis/fibrosis	● Siderosis: significant lung accumulation of iron; benign pneumoconiosis without evidence of progressive fibrosis	● Fumes generated from MMAW processes using SS electrodes are more pneumotoxic; likely due to presence of soluble metals and production of macrophage-derived inflammatory cytokines
Infection/immunity	● Reports of interstitial fibrosis; possibly due to improper ventilation or exceedingly high fume exposures ● Increase in frequency, duration, and severity of upper and lower respiratory tract infections ● Increased mortality due to pneumonia ● Evidence of immunosuppression in welders	● Exposure to exceedingly high levels of either MS or SS welding fumes can cause interstitial pulmonary fibrosis ● *In vivo* animal studies limited ● Soluble metals and fluxing agents present in shielded MMAW fumes suppress macrophage function and other lung defense mechanisms

Adapted from Antonini, J. M.; Lewis, A. B.; Roberts, J. R.; Whaley, D. A. Pulmonary Effects of Welding Fumes: Review of Worker and Experimental Animal Studies. *Am. J. Ind. Med.* **2003**, *43* (4), 350–360.

- The use of mechanical ventilation will improve air quality. In some cases, however, natural air movement provides enough ventilation and fresh air.
- Where ventilation is questionable, air sampling should be done to determine the need for corrective measures.
- Welding with some electrodes such as stainless or hard facing or on lead or cadmium plated steel and other metals or coatings produce highly toxic fumes and thus require special ventilation. In such circumstances, exposure should be kept as low as possible and below threshold limit values. Local exhaust or mechanical ventilation can be used for this purpose.
- Welding operations in a confined space should be done only if it is well ventilated or while wearing an air-supplied respirator. Welding fumes and welding-created oxygen depletion can alter air quality, causing injury or death. Similarly, shielding gases used for arc welding can displace air and cause injury or death. It should be made sure that breathing the air is safe.
- Welding operations should not be done in locations near chlorinated hydrocarbon vapors coming from degreasing, cleaning, or spraying operations. The heat and rays of the arc can react with solvent vapors to form phosgene, a highly toxic gas, and other irritating products.
- It is crucial to have a qualified specialist in 'industrial hygiene' or 'environmental services' check the operation and air quality and make recommendations for the specific welding operation.
- Welding operators should read and understand the material safety data sheet (MSDS) for welding equipment and consumables. MSDS forms are available from your welding distributor or from the manufacturer. Welding operators also need to strictly follow their employer's safety practices.

6.12.3 Electric Shock Hazards in Welding

Injuries related to electrical shocks are common accidents occurring every year and everywhere, especially when it comes to occupational incidents. Most workplaces nowadays are equipped with electrical source and open electrical equipment that may expose workers to the hazard of being electrocuted. In Japan, 13% of fatal occupational accidents are contributed by electric shock cases (*30*). In United States, the U.S. Department of Health and Human Services, together with NIOSH, reported that under the surveillance system of National Traumatic Occupational Fatalities (NTOF), electrocutions were the fifth leading cause of death, accounting for 7% of all workplace fatalities from 1980 through 1992. Welding works are not exempted from contributing into the statistics. From the Fatality Assessment and Control Evaluation (FACE) Program established by NIOSH, below are several electric shock cases summarized which are related to welding works (*31*):

- A maintenance worker electrocuted as he attempted to turn off a welder. Due to exposed cable, broken insulation and water on floor;
- Production welder plugged cord of a portable welder into a defective extension cord and was electrocuted;
- Two pipefitters electrocuted when the boom of the crane moving a metal welding shed contacted a 12 400 V overhead power line. Victims were standing on the ground grasping the shed to guide it into place;
- Welder/pipefitter killed when he contacted an energized 110 V conductor while removing a fluorescent light fixture and fell 29 feet to the floor. He cut into the energized wire with uninsulated metal wire cutters;

www.iran-mavad.com
مرجع مهندسی مواد و متالورژی

- Welder electrocuted when he contacted a conductor on an overhead crane. He was engaged in adding reinforcing steel to the bridge of an overhead crane at a steel fabrication firm. Victim believed crane to be de-energized.

From the cases mentioned above, an exposed electrical conductor, wet environment and clothing, defective tools and appliances, and ignorance may be the leading causes of electric shock accidents. When a person accidentally becomes the path of current with energized conductors such as open electrical wires (*32*), noninsulated cables or circuit, he/she would experience a shocking reaction, the criticality of which may vary depending on many factors.

Rather than voltage (measured in volts, V), magnitude of current (measured in amperes, A) plays a more significant role that can impose physiological effects on the victims during electrical shock. The level of current passing through the human body is directly related to the resistance of its path through the body (*31*). The resistance of the path through the body can be related directly to the amount of current engaged in an electric flow. Human skin in dry conditions gives higher resistance while wet skin provides the opposite. As far as Ohm's law is concerned, current (I) equals voltage (V) divided by resistance (R, measured in Ohms): $I = VR^{-1}$. As wet skin means lower path resistance, the amount of current is more significant compared to the skin when it is dry. Dry skin's resistance normally falls between the range of 40 000–100 000 Ω cm^{-2}. When skin is wet, resistance is reduced to as low as 1000 Ω (cm^2)$^{-1}$ (*33*). Thus current is far greater on wet versus dry skin during electrical shock. Apart from moisture level, open skin wounds also can lower the resistance of the current pathway through the body (*31*). In accidental electric shock, the ability to release oneself would depend somewhat on the type of contact as well as the magnitude of the current (*34*).

The flow of electricity during an electrical shock is from the source through the body and to the ground (*32*). In the model of electrocution injury, energy is transferred from its source to the human body, causing injury such as cardiac arrest, skin burn, tissue damage, internal bleeding, respiratory arrest, etc. As high voltage may break the skin and reduce its pathway resistance, an amount of current may enter the body and the body will act as part of electrical circuit. However, electrocution will not happen if there is a layer of safeguard that limits the energy to be transferred to the human's body. The amount of current imposed will cause different reactions of the body. **Table 3** shows the general relationship between the amount of current received and the reaction when current flows from the hand to the foot for just 1 s (*32*,*35*).

6.12.3.1 Criticality of Electric Shock Injury

The criticality or severity of the electric shock depends on several factors, namely amount of current flowing through the body, the current's path through the body, the length of time the body remains in the circuit, and the current's frequency (*32*).

Current is the main criteria of shock intensity. From factors listed above, various amounts and conditions of current and other variables may influence the outcome of an electric shock on humans. One of the effects from electrical shock is cardiac arrest. A study was conducted to investigate the current threshold that can cause heart fibrillation (*34*). A current threshold is the maximum amount of current allowed for ventricular fibrillation to happen which a man may be safely subjected to. The study used a few groups of animals as the specimens. Different factors mentioned above were tested on these animals, and the results and analysis are summarized as follows.

Species and size of animal

A test was conducted using alternating currents of 208 V, 60 cycle frequency to a few groups of animals that were kept under surgical anesthesia. These groups of animals represent different ranges of body and heart weight. From the studies, threshold current increases roughly with both heart weight and body weight of different species of animals. Thus, it can be concluded that the heavier the body and heart weight, the higher the threshold of current it takes to produce heart fibrillation. If using these data to forecast the

Table 3 Amount of current through the body and its reaction

Current	*Reaction*
Below 1 mA	Generally not perceptible
1 mA	Faint tingle
5 mA	Slight shock felt; not painful but disturbing. Average individual can let go. Strong involuntary reactions can lead to other injuries.
6–25 mA (women)	Painful shock, loss of muscular control[a]
9–30 mA (men)	The freezing current or 'let-go' range.[a] Individual cannot let go, but can be thrown away from the circuit if extensor muscles are stimulated.
50–150 mA	Extreme pain, respiratory arrest, severe muscular contractions. Death is possible.
1000–4300 mA	Rhythmic pumping action of the heart ceases. Muscular contraction and nerve damage occur; death likely
10 000 mA	Cardiac arrest, severe burns; death probable

[a]If the extensor muscles are excited by the shock, the person may be thrown away from the power source.

Reproduced from Ferris, L.; King, B.; Spence, P.; Williams, H. Effect of Electric Shock on the Heart. *Trans. Am. Inst. Electr. Eng.* **1936**, *55* (5), 498–515; Lee, R. C.; Dougherty, W. Electrical Injury: Mechanisms, Manifestations, and Therapy. *IEEE Trans. Dielectr. Electr. Insul.* **2003**, *10* (5), 810–819.

www.iran-mavad.com
مرجع مهندسی مواد و متالورژی

current threshold for a man of 70 kg (roughly 330 g heart weight) to get heart fibrillation, the average current threshold would be around 0.26 A. However, the threshold of current may differ compared to other individuals.

Path of current through the body

The position or location of the electric shock applied to certain parts of the body plays an important role in getting heart fibrillation as well. Rightfully, if the shock is applied directly to the heart, the threshold of current is lower. The same settings of frequency, types of current, and conditions applied to a group of sheep, except for the position of the shock applied on the body. From the results, shock to some part of the body affects a proportion of current reaching the heart. It can be seen from the data that higher threshold achieved up to 12 A for the position of hind leg to hind leg, and relatively lower current threshold achieved 0.36 A for the position of right to left side of chest. This may apply to humans as well, as a welder engaged in a shock at his feet may not experience cease of rhythmic heart rate as critically as if he gets the electric shock at the chest area.

The length of time the body remains in the circuit

In another test to see the effect of current threshold with respect to the duration of shock applied to a body, a 60 cycle alternating current was applied at the right forelegs and left hind legs of a group of sheep. From the outcome, independent variables of shock duration of 0.03, 0.1, and 0.12 s show a similar trend in current threshold (2.8 A) while increased duration of 0.47 and 3 s presented lower current threshold, respectively, at 2 and 9 times lower than that for 0.03, 0.1, and 0.12 s. From these studies, it can be concluded that a welder is most likely to be badly injured if he was electrocuted for a longer duration of time, rather than shorter exposure to current.

Current's frequency

Frequency of current also can determine the maximum current allowed for heart fibrillation to happen. In the same study, 25 and 60 cycle alternative currents were tested for 3 s on a sheep's right foreleg and left hind legs. Additional variables of using direct current were introduced as well. The results showed that 25 cycle threshold current is about 25% higher than the 60 cycle and direct current having 4 and 6 times, respectively, higher compared to 25 and 60 cycle. Thus, it is more likely for a welder to get cardiac arrest at the above threshold current if he was exposed to the lower frequency of current rather than the higher ones, and alternating current will have bigger effect on an electrocuted welder rather than direct current.

Therefore, from the outcomes of the studies discussed above, it can be concluded that a welder is subjected to electrocution risk depending on how much current he/she is exposed to, which is closely related to the size of the body, location of the electric shock in contact to the body parts, and duration as well as frequency of the current.

6.12.3.2 Potential Risk of Electric Shock from Welding Activities

There are many types of welding available nowadays, but shielded metal arc welding (SMAW), commonly known as stick welding, and gas tungsten arc welding (GTAW) are two of the most general welding methods widely used in the world. For example, over 40% of welding works performed in the United States are stick welding (*36*). Stick and GTAW welding are relatively identical methods, except for the fact that instead of using consumable electrode, GTAW welding uses tungsten nonconsumable electrode and GTAW welding machines can produce a constant stream of electricity for welding without changing the voltage much at all. These manual types of welding offer huge advantages for both professional and amateur welders because they are lightweight, portable, cheap, and widely available in the market. Stick welding, in particular, is very flexible, whereby it can be performed in a confined space. Although the huge advantages attract a higher number of users, especially amateurs, a higher risk of accidents, particularly electric shocks, while working on these methods are expected. As mentioned previously, electric shock can be caused by exposed electrical conductor, wet environment and clothing, defective tools and appliances, as well as welder ignorance. In stick and GTAW welding operations, risk of electrocution may come from the sources discussed below.

Equipment setup and installation

Stick and GTAW welding machines are the most imperative components in both welding methods. Using bad and legally unapproved Stick and GTAW welding machines can bring electrical hazards to the users. As quoted by AWS (*37*):

> Equipment should meet applicable National Electrical Manufacturers Association (NEMA) or American National Standards Institute (ANSI) standards, such as ANSI/UL 551, Safety Standard for Transformer Type Arc Welding Machines, latest edition. When special welding and cutting processes require open circuit voltages higher than those specified in ANSI/NEMA Publication EW-1, Electrical Arc Welding Apparatus, insulation and operating procedures must be provided that are adequate to protect the welder from these higher voltages.

AWS also emphasizes the correct machine installation to take place prior to welding activities. Installation of machines and other components is also being highlighted to ensure that the requirement of ANS1/NFPA 70, National Electric Code, and local codes are met. Disconnecting, fusing, and incoming power lines are also included.

Grounding is also important in the welding component setup. Lack of grounding measures exposes welders to a high risk of electrocution hazard. Also quoted by AWS (website 1):

www.iran-mavad.com
مرجع مهندسی مواد و متالورژی

The workpiece being welded and the frame or chassis of all electrically powered machines must be connected to a good electrical ground. Grounding can be done by locating the workpiece or machine on a grounded metal floor or platen, or by connecting it to a properly grounded building frame or other satisfactory ground. Chains, wire ropes, cranes, hoists, and elevators must not be used as grounding connectors or to carry welding current.

Power source

Stick welding is very flexible in terms of the power used. Both direct current generators and transformers are feasible. Generators produce electricity from fuels such as gasoline, diesel, or natural gas, while transformers and inverters can be plugged into a wall outlet and the welder is able to adjust the amperes to be used. Electrocution may occur if the transformer or inverter is plugged into defective or overutilized wall outlets.

Heat sparks and spatters

Stick welding produces more heat sparks and spatter than any other welding process (*36*). These spark and spatter temperature and intensity can pose a risk of melting off any electrical insulators situated nearby without the welder realizing it. Contact with defective, energized, noninsulated wires lying nearby the welding area can cause serious electrocution injury to the welder.

Exposed electrode holder, ground clamp, and torches

Electrode holders and ground clamps that are not properly insulated will pose a risk of electrocution during welding. Good ground clamps facilitate to ground the welding table and ensure that the workpiece conducts electricity well. Torches used in GTAW serve many purposes. One of them is insulating welders from dangerous electrical connections. Usage of torches in bad conditions puts welders at risk of coming in contact with a high intensity of electric shock.

Wet environment

Welding areas that contain stagnant water pose a critical risk to welders, as a wet environment facilitates the occurrence of electrical shock. Leaking roofs, contained water at uneven flooring activities involving water existing nearby the welding area will pose a great electrical hazard during welding. Apart from that, wet clothing or personal protective equipment exerts a similar risk.

Using wrong amperage settings or specifications on welding machine

Welding machines and electrodes used in welding are normally provided with a guideline of amperage setting for welders to follow. Careful studies and research has been carried out by the manufacturers to determine the right amperage setting range for every type of electrode and machine. The correct range of current use during stick welding determines the quality of the stick weld. Not only that, as mentioned earlier, the higher amount of current that goes through a person's body will increase the risk and severity of the electrical shock injury. Therefore, working with the incorrect amperage setting range may cause catastrophic injuries.

6.12.3.3 Electric Shock in Underwater Welding

Underwater welding work is needed when there are any structures or ships that require salvage. It is also needed whenever there are urgent repairs required. Apart from that, it comes in handy when there is a need of installation of new offshore drilling structures, subsea pipelines and hot taps, docks and harbor facilities, as well as modifications and additions to underwater structures. The depth in underwater welding work can go as low as from 30 to 400 feet of salinity water (FSW). Underwater welding works often are carried out for the repair of underwater pipelines below drilling platforms, on some portion of the rigs, or the platform structure itself. The damages that need repairing normally are due to marine accidents as well as corrosion and fatigue. Oil and gas drilling are not the only industry that is adopting underwater welding works. Navy forces are often engaged in this activity as well. They normally use these techniques to perform salvation of ships or harbor clearance operations (*38*). It is advised that only trained and qualified persons should be allowed to perform underwater welding. Basically, there are two types of underwater welding: wet and dry. Dry welding means the welding works are carried out in atmospheric pressure in a chamber from which water has been displaced. The welder may completely or partially be in the chamber depending on the size and configuration of the chamber. During this activity, the welder is wearing the usual welders' attire, dive gear, or both. The chamber acts as a habitat, also known as a hyperbaric chamber, and provides the welder-diver with all the necessary welding equipment in a dry environment. Upon using hyperbaric chambers during welding activity, several precautions need to be taken into account as well. Hyperbaric chambers or diving bells' condition is extremely damp. Even though the welder would not be welding surrounded by water, electrocution hazard will exist as per normal conditions. In this welding condition, alternating or direct current may be used. However, different settings are needed depending on the types of current used. If direct current is used, the ripple factor needs to be considered and ensured to be in its acceptable limit (*39*). Guidelines provided by International Marine Contractors Association (IMCA) state that the conditions in the chamber are as follows: The pressure inside of the bell shall depend on the depth of immersion; however, the range of pressure shall be between 0 and 25 bar and the temperature is normally set at 25–35 °C. Welders are advised to wear full diver suits when working in the diving bell, while the attire used when working in the hyperbaric chamber is much lighter. There are many electrical hazards identified while welding in this enclosed space. Considerations such as type of current installation ripple factors (if direct current is used), electrical power supply and control, responsiveness of trip device, maximum voltage, and

www.iran-mavad.com
مرجع مهندسی مواد و متالورژی

modifications should be made to the original equipment setting. A safe and correct voltage level needs to be ensured during the works so there is no hazard of high voltage exposure to the welder. The trip device needs to be verified and confirmed that it works effectively by responding to emergency switch off during a faulty incident. Failure to respond in a timely manner shall increase the severity of injury related to electrical shocks as more current may flow through the body in a longer period of time. Welders also need to check if the equipment had gone through any modifications that change any of its original settings. This is important as insulation or electrical protection for the equipment may be tampered with and may cause an unexpected incident during the works. IMPA Code of Practice also suggests that there are two ways to ensure the safety of welders against electrical shock (*39*):

- If the operating voltage of the equipment is under the maximum safe voltage level of 30 V dc (7.5 V ac).
- If the operating voltage is under the maximum safe voltage level of 250 V ac (285 V dc) and a trip device is fitted with a reaction time of less than 20 ms.

Wet welding, on the other hand is performed, totally immersed underwater. Wet welding exposes welders to much more electrical hazard. Lethal electrical current, if engaged at a closer than safety distance, shall involve severe electrocution injury such as cardiac arrest or even death. The presence of a spark and electrode tip temperatures in excess of 10 000 °F also can trigger catastrophic explosion due to combination of oxygen and hydrogen rich gases underwater (*38*). In contrast with dry welding, wet welding is strictly off limits for alternating currents. This is because exposure of alternating current underwater will prevent voluntary relaxation of the muscles controlling the hand, which hinders the welder to let go of his body or equipment out of the electric circuit. First of all, the diver/welder must be qualified personnel trained in emergency response such as CPR and first aid. These types of welding cannot be done by only one person. A surface helper shall be on standby to monitor and control the knife switch whenever the diver signals for it. In wet welding, the current will only be on once the electrode is positioned against the work. Whenever the electrode is consumed and finished, the welder shall send a signal to the surface helper to open the knife switch. There are many factors that contribute to electrical accidents underwater such as adverse currents, unstable footing, poor visibility and low alertness of welders/surface helpers or both. Being underwater, the diver must not connect any body part or equipment with the grounded work when the safety switch is closed, as this will make the body or equipment part of the electric circuit. This shall apply to any loose metal tools brought together underwater during the welding works.

In sum, and regardless of dry or wet welding, safe usage of power supply must be ensured at all times. The source of power supply must be verified by trained personnel according to a specific plan. Welding machines must be tested to ensure the validity and safety of operations before commencing work. Components of welding equipment should also become obsolete due to any modifications or age factors of the equipment.

6.12.4 Burning Hazards

Welding activity is widely implemented in many industries such as marine, construction, fabrications, and manufacturing engineering. In Non-Fatal Occupational Injuries and Illnesses 2008, Bureau of Labor Statistics, in US Department of Labor reported that welders, solderers, brazers, and cutters in various industry sectors, namely construction, manufacturing, trade, transportation and utilities, national resource, and mining, made up total of 21 720 cases of nonfatal occupational injuries and illnesses in that year. An incident rate of 12.5 per 10 000 full-time welders, solderers, brazers, and cutters was reported to involve in heat burn injuries within the same year, which placed welders as the third highest in burn-related injuries occurring in workers by occupation (*40*). Welding activities involve an intense source of radiation and heat. The nature of welding works that normally emit high intensity and temperature of sparks and spatters exposes welders to burn hazards. A welder commonly works with temperatures as high as 10 000 F (*41*). Burn injuries resulting from welding activities are mainly contributed by the exposure of high temperature heat, radiant energy, or other causes such as improper work setup or defectiveness of equipment.

For high temperature sources, it is common for welding methods to produce sparks and spatters, regardless of its magnitude of intensity. It is well known that the SMAW or stick welding method produces more sparks and spatters compared to others (*36*). Even though the range of spark intensity is varied, safety measures such as wearing protective clothing should always be in place and welders are required to adhere to this for the sake of their safety and health. Radiant energy emitted by the welding ray may also contribute to burn injuries. The light radiation given off during welding works emits electromagnetic energy, which can damage the welder's skin tissues and cause severe effects. Bright, visible, infrared, and ultraviolet light released by welding flames can lead to serious illnesses and immediate injury. Ultraviolet is known as the light rays that are outside of the visual spectrum at the violet end. These rays are comparatively intense in arc welding. Thus, personal protective equipment in terms of gowning procedures and eye protection is needed to shield the welder from direct exposure that may cause immediate injuries or long-term illnesses. Apart from sparks and spatters and radiant energy, other burn hazards can be closely related to the work setup. An improper environment provided for welding, such as keeping flammable materials too close to the working area, high human traffic in the work area, or cluttered work stations, may increase the danger of burn accidents for workers or people around them.

6.12.4.1 Burn Injuries in Welding Activities and Relative Effects

High temperature heat sources can easily cause an accident during welding works. The probability of being involved with a burn-related injury is higher whenever manual welding methods are used, such as SMAW, GTAW, GMAW, and dry welding in submerged

www.iran-mavad.com
مرجع مهندسی مواد و متالورژی

conditions, as mentioned previously. However, underwater welding for wet environments (wet welding) is not included, as the activity takes place underwater and the heat exposure is much less than that of dry welding (welding done underwater but in a welding bell or hyperbaric chamber). Dry welding done underwater shall be treated similarly as welding works conducted on land due to the comparable atmospheric conditions.

The manual method will impose a higher chance of welders getting a burn injury because of the close proximity to the source of heat. For example, SMAW operates by melting the end of the electrode and the base metal that welders are trying to weld. The electrode is protected by a flux to ensure the integrity of metal inside from any contaminants, and to protect from porosity, which is melted to form a shielding gas. As the metal inside the electrode melts, it goes across the arc and deposits itself in the molten pool of metal to form the weld bead. Special attention should be paid for stick welding because it is the welding method with most sparks and spatter produced compared to the others (*36*). Hot slags, mostly known as molten metal, are also a dangerous piece of spatter from the outcome of welding activities. Plus, arc flashes are also formed from arcing, where the electric arcs and resulting radiation and shrapnel cause severe skin burns, hearing damage, and eye injuries. These sparks and spatters hold sufficiently high energy to cause a burn to the skin if it is not protected. More serious burn injuries also can occur when these sparks are in touch with fuels located around them, causing ignition that further leads to an explosion. As mentioned earlier, power generators used to fire up a welding machine normally use diesel or gasoline as fuel. Sparks and spatters can be a very dangerous source of ignition for these flammable fuels as they can fly as far as to 35 feet (*38*). Sparks, with their small size, can also fly and end up getting into compartments of the welder's clothing or any opening that allows contact with the welder's skin. The severity of injury due to this incident varies and depends on the heat intensity, thickness, or material of the welder's clothing. It is also advised and implemented by US Navy that the use of any gas cylinder as a roller or support is forbidden, even if it is empty. It is believed that there might be some residual gases still trapped in the compressed cylinder. In underwater welding, other hydrocarbon fuels might not be the primary source of explosion, but oxygen is. Oxygen is commonly used in underwater welding, and it is stored in high pressure cylinders that can lower the ignition temperature. That is why it is advised that the cylinder valve must be open or closed in the right manner and the cylinders must not be dropped. Opening a gas cylinder must not be done using a forced action such as knocking it with a hammer. Firing arc onto the body of cylinders is prohibited, as it might cause brittleness at some area which may lead to rupture under rough handling.

Burn accidents do not only affect the welder's skin but also may cause injury to the welder's eyes as well. The ray is capable of emitting high intensity ultraviolet radiation (UVR) that can cause burning of the retinas and cataracts (*42*). For more advanced welding methods such as laser arc welding, additional hazards are identified which may affect human eyes as the near infrared laser beam is used in the operation. Therefore, extra care needs to be taken during the operation of this welding method by ensuring the activity takes place within an interlocked, light-tight enclosure (*43*).

6.12.4.2 Safety Measures to Prevent Burns

The ultimate safety measure to be taken to prevent burn injuries during welding is wearing proper protective clothing and working in a safe environment. A proper set of protective clothing should be able to protect welders from direct heat that is severe enough to cause an injury when in contact to the body.

First of all, welders need to ensure that their clothes and protective equipment are worn comfortably. Uncomfortable conditions may cause welders to be unfocused, and this can cause accidents. The best fire-resistant clothing is made of 100% wool, with full sleeves and sufficient thickness to prevent any spatters burning through it. The other reason to wear thicker clothes with full sleeves is because it can prevent welders from exposure to electrical arc, as the effect is the same as getting sunburned (*36*). It is advised as well for the clothes not to have pockets sewn to them, as spatters or hot slags may fly and end up inside the welder's pocket. For underwater welding, a complete neoprene wet suit may be used if it is in good condition and has no tears and holes (*38*).

It is important for welders to ensure that ample eye protection is worn. To keep the welder's eyes from spatters, hot slags, or intense arc rays, an eye safety shield must be worn. An eye safety shield in the form of transparent goggles should be worn for persons with prescription glasses or safety glass for welders without (*41*). This transparent eye safety shield can be worn together with a flame proof skull cap. The cap can protect the welder's hair from catching fire. As welding arcs emit ultraviolet radiation, it is highly important for welders to protect their eyesight during welding with the helmet's filter lens. According to OSHA, there are different types of shades classified for the lens, and this depends on types of welding method, electrode sizes, and arc currents. **Table 4** lists the shade numbers according to its welding method (*44*).

As electric arc emits dangerous ultraviolet rays, not only welders are required to protect themselves, but other passersby must take action to protect themselves as they come near anyone who performs welding. Welders have to be aware of anyone around the welding area.

Hands are the body parts which are easily injured in welding works. High temperature work conditions require welders to protect their hands with appropriate gloves. Working with hot equipment means that welders should be wearing leather gloves. Plastic gloves must not be worn during welding because they can melt and burn through the skin and make the injury more severe (*45*).

Safety shoes are generally equipped with protective barriers such as steel toes, steel intersoles, and nonslip oil-resistant soles to shield the welder's feet from any falling objects, sharp object penetration, and slippage. Wearing safety shoes can also protect a welder's feet from getting injured from flying hot debris from welding works.

Safe protection is compulsory during welding, and welders must ensure that safe working conditions are always implemented. With the nature of welding works, fire hazard is high if the work area is situated near flammable and easily ignited materials.

www.iran-mavad.com
مرجع مهندسی مواد و متالورژی

Table 4 Filter lenses for protection during welding and cutting operations

Operation	*Arc current (amperes)*	*OSHA minimum protective shade number*	*ANSI & AWS shade number recommendation*
Gas metal arc welding (GMAW) and flux cored arc welding (FCAW)	Fewer than 60	7	–
	60–160	10	11
	More than 160–250	10	12
	More than 250–500	10	14
Gas tungsten arc welding (GTAW)	Fewer than 50	8	10
	50–150	8	12
	More than 150–500	10	14
Air carbon arc cutting (CAC-A) (light)	Fewer than 500	10	12
Air carbon arc cutting (CAC-A) (heavy)	500–1000	11	14
Plasma arc welding (PAW)	Fewer than 20	6	6–8
	20–100	8	10
	More than 100–400	10	12
	More than 400–800	11	14
Plasma arc cutting (PAC) (light)	Fewer than 300	8	9
Plasma arc cutting (PAC) (medium)	300–400	9	12
Plasma arc cutting (PAC) (heavy)	More than 400–800	10	14
Torch brazing (TB)	Nil	3	3 or 4
Torch soldering (TS)	Nil	2	2
Carbon arc welding (CAW)	Nil	14	14

Reproduced from OSHA. *Eye Protection against Radiant Energy during Welding and Cutting in Shipyard Employment*, 2012, http://www.osha.gov/Publications/OSHAfactsheet-eyeprotection-during-welding.pdf.

Before commenting on the welding operations, welders need to ensure that the work setup is proper and no wooden structures or combustible materials are located in the vicinity of welding operations (*45*). As mentioned in electric shock section, a working table shall be used whenever possible. Work areas also need to be free of clutter. During fire or burn emergencies, a neat work area with sufficient space to move can help welders to escape or to seek emergency treatment in a timely manner. Fire exits also must be known and briefed to all the welders so that during emergencies, all the people would know where to go to for assembly. Fire-fighting equipment is also needed to be readily available at convenient places. There are different classes of fire extinguishers which are used in different situations (*36*):

- Class A: Takes care of any fires that produce ash. These fires usually involve wood, cloth, or paper.
- Class B: Fights fires caused by flammable liquids such as gasoline, oils, and paints.
- Class C: Electrical fires call for class C fire extinguishers. It is imperative to note that water- or foam-based extinguishers must not be used instead of class C on an electric fire, as serious shock can occur.
- Class D: Takes care of metal fires. Combustible metals like magnesium, potassium, and sodium are extremely flammable, and fires based on these materials are very dangerous. Class D extinguishers are best for these fires because the other classes often disperse a metal fire instead of putting it out, making the situation worse.

Hot work permits are also important in performing any works which areas are not normally assigned for. This can alert the key personnel of that area about the unexpected danger that may be exposed during the activity. The permit consists of a checklist of precautions that includes the thorough checking and verification of the fire extinguishers' availability and functionality, establishment of fire watches if necessary, inspection for nearby combustible materials, as well as safety instruction (*37*).

In sum, welding works involve high temperature and high risk of fire hazard. Welders and area users are advised to observe and take precautionary actions before entering or starting work on welding. Safe work setup is extremely important to eliminate any fire hazard. Burn from arc ray can be prevented if the welders or people around it protect themselves with sufficient personal protective equipment mentioned above. Apart from that, these injuries also can be avoided by adhering to professional working behavior, as playing around with high temperature equipment will always end up with bad accidents.

6.12.5 Welding Noise Effects

Welders, and in general anyone close to welding sites, are frequently exposed to the excessive noise that can cause short-term and long-term negative effects (*46*). Sometimes people are exposed to noises that can cause potential damage to hearing. Sound travels through the air in the form of a series of moving pressure disturbances or waves. Moreover, pressure waves are formed by the vibration or motion of the sound source, which are caused by minute back and forth movements of the air molecules. The welding process itself generates harmful levels of noise. Besides the welding process itself, which is noisy, the other tasks that a welder will typically do are also noisy, and welding is generally carried out in a noisy environment. The dangers caused by welding noise can be

www.iran-mavad.com
مرجع مهندسی مواد و متالورژی

reduced by applying the control measures (46). The most effective option for reducing environmental welding noise pollution is to eliminate the noisy process (47). For example, noise from arc welding directly increases with wire/rod diameter and operating current, and thus, using appropriate wire/rod size and current should help minimize the noise levels. Moreover, welding in areas where sound may be reflected (e.g., confined spaces or corner of a workshop) would cause higher noise levels compared to welding which is carried out in an open space. In such circumstances, performing welding in open spaces if possible or using sound absorbing materials around the welding area can decrease the impact of the welding noise on others working nearby. Nevertheless, eliminating noisy processes in welding is not always feasible, thus hearing protection such as ear plugs or ear muffs should be used as the main solution to reducing welding noise exposure.

6.12.6 Ultraviolet Radiation/Infrared Radiation Hazards

Laser welding, demonstrated for thermoplastics in the 1970s, is suitable for a wide range of applications like electronic packages, joining sheets, film, molded thermoplastics, textiles, and automotive components. It uses a laser beam to melt the material in the joint region. Lasers are well suited to deliver controlled amounts of energy to a precise location due to the ease of controlling the beam size available (10 μm–100 mm width) and the range of methods available for precise positioning and movement of the beam (48). Harmful UVR and IR exposure may occur during welding operations. Their respective frequencies and wavelengths, in part, determine their biomedical effects on human beings that can cause damage to the skin and eyes causing burning and photo-keratoconjunctivitis. Likewise, infrared can burn the skin but it has a propensity to affect the lens causing cataract formation (49). The infrared radiation (IR) during the welding process depends on the melt pool temperature and the amount of melted volume. The UVR signal is an indication of the coupling between the laser beam and the workpiece, as this signal is emitted by the plasma plume. Consequently, IR and UVR signals are simultaneously stored with the electronic temperature values (50).

6.12.6.1 Reducing the Effect of UVR/IR Beam during the Welding Process

The arcs associated with arc welding emit high levels of UVR, and this often causes acute injuries in the workplace, particularly photo keratoconjunctivitis and damage to the skin. It is important to know the level of UVR emitted by arc welding under various conditions. Actinic UVR can be reflected significantly from some common surfaces, and these reflections might also create potentially harmful exposure to unprotected personnel. Unpainted metals, particularly aluminum and concrete floors, readily reflect actinic UVR. On the other hand, lightly colored paints often use pigments of zinc oxide or titanium oxide and have a low reflectance of actinic UVR. Therefore, even lightly pigmented paints are good absorbers of actinic UVR (51). In either case, the same protection can be used to minimize UVR hazards to persons working nearby. For electric arc welding, the use of proper eye wear with a proper glass that filters UVR and IR should afford full protection for those engaged in welding (49). Persons in the vicinity of welding operations can be protected from exposure to actinic UVR by the use of screens, curtains, or adequate distance from aisles, walkways, etc. Welders' helpers, overhead crane operators, and forklift operators who have a line of sight to any open arcs should consider wearing appropriate safety equipment such as safety glasses with side shields or even a clear, full-face shield and long-sleeved shirts. Skin protection has not been uniformly prescribed for other personnel who work in the vicinity of open arcs. Fabric measurements have shown that natural materials (leather, cotton, wool) are better for absorbing actinic UVR than synthetic materials (polyester, nylon) (52). Incidental personnel should also consider wearing a long-sleeved shirt.

6.12.7 Hazards of Welding Equipment

When welding with welding equipment, the welding operators are exposed to hazards such as heat burns, toxic fumes, and fire. The equipment will produce heat during its operation, and the fuel poses a fire risk. In addition, equipment like engine-driven generators sometimes emits high noise that could affect the human hearing (www.aws.org). Most of the references on engine-powered welding focused on the safety aspects on ventilation, fire prevention, and personal protection.

6.12.7.1 Minimizing the Hazards of Engine Powered Equipment

It is important to follow the safety instruction of the operation of equipment as provided by the machine manufacturer. Only qualified welding operators should handle the operation. The welding operators should be aware of the danger zone when they are working with moving parts of engine powered equipment. If possible, an enclosure must be created with an entrance that can be monitored with safety switches or a pressure sensitive mat that could detect the presence of a person (53). The working area should be well-ventilated either in an outdoor open space or with an exhaust vent to direct the engine exhaust directly outdoors. For fire prevention measures, the engine must be turned off before conducting any troubleshooting or maintenance work. For refueling purposes, the engine must be cooled down to prevent the formation of fuel vapor that can ignite fire (54). Any spilled fuel should be wiped up immediately. For prompt first aid response, the welding area should be equipped with a fire blanket and a first aid kit. All equipment safety guards, covers, and devices must be in good condition and installed correctly at the equipment (55). In the case of performing maintenance work, the guards should be carefully removed and promptly replaced upon completion. To prevent

www.iran-mavad.com
مرجع مهندسی مواد و متالورژی

physical injury, welding operators need to keep their hands, hair, and clothing away from moving parts, e.g., engine fans. To prevent a scalding injury, the radiator pressure cap can only be removed when the engine has cooled off (56). Personal protective equipment like helmets, gloves, and eyewear are necessary to protect against the hazards. Clothing should be suitable to minimize skin burns caused by potential sparks; for the case of high noise level, appropriate ear protection should be worn. The general classification for high noise level is when the decibel level exceeds 85 dB. According to OSHA standards (OSHA act 1994), exposure while working in a high noise level area should not be more than 8 h.

6.12.7.2 Hazards of Compressed Gas Cylinder

Compressed gas cylinders used in the welding work can cause different hazards due to their high pressures and contents. An example of acetylene gas, which is used in oxyacetylene welding, is a combustible gas and could cause explosion and fire (37). Propane is also commonly used in welding and is a flammable material. The pressurized oxygen gas is also dangerous and must be treated with care as the other flammable gases. Besides combustion and fire, there are dangers of oxygen displacement and toxic gas exposure as well as physical injury to the human body. It is vital for a welding operator to be properly trained on the right procedure and safety precaution to minimize the hazards associated with the compressed gas cylinder.

6.12.7.2.1 Minimizing the Hazard of Compressed Gas Cylinder

Basic components of the compressed gas cylinder are the regulator, the cylinder, the valve cap, and the hose (ESAB, 2000). As a part of standard operating procedure, all the equipment used must be suitable for the application and fit for use. When the cylinder is not in use and when moved from one place to another, the valve protection cap must be hand tightly fitted. Safe handling should be exercised during lifting and moving of the cylinder. The valve must be opened by hand and not with hard tools like a hammer or wrench (55,56). For handling and storage, the cylinder must be positioned upright and located away from where it can be damaged physically or where leakage could occur. During usage, the cylinder must be kept at a safe distance from any source of heat and spark that can cause fire. If the work area is limited in space, the fire resistant cover should be used (57). The welding operator needs to protect the head and face from possible outburst of the compressed gas when opening the cylinder valve outlet. Protective eyewear can be worn to minimize possible injury. Welding experts have emphasized the significance of wearing safety glasses for protecting the eyes (58). As a fire prevention measure, hot parts like the electrode and its holder should be kept at a distance from touching the cylinder. The welding work cannot be done on area where flammable paint has been applied. Heavy dust concentration also poses as a fire risk to be avoided (37). It is compulsory for the welding work area to have a fire extinguisher ready with the welding operator trained on how to use it. A respiratory mask should be worn if the welding work is done in a confined space. It is also necessary to have a supply of clean air. This is to prevent the worker from inhaling the welding fumes that will spread. General ventilation requirement should be thorough to reduce the risk of exposure.

References

1. Meo, S. A.; Al-Khlaiwi, T. Health Hazards of Welding Fumes. *Saudi Med. J.* **2003,** *24* (11), 1176–1182.
2. Antonini, J. M.; Taylor, M. D.; Zimmer, A. T.; Roberts, J. R. Pulmonary Responses to Welding Fumes: Role of Metal Constituents. *J. Toxicol. Environ. Health, Part A* **2004,** *67* (3), 233–249.
3. Palmer, W. G. *Effects of Welding on Health IV;* American Welding Society, 1983. https://pubs.aws.org/Download_PDFS/EWH-IV-PV.pdf.
4. Hewitt, P. J.; Hirst, A. A. A Systems Approach to the Control of Welding Fumes at Source. *Ann. Occup. Hyg.* **1993,** *37* (3), 297–306.
5. Hewitt, P. Reducing Fume Emissions through Process Parameter Selections. *Occup. Hyg.* **1994,** *1* (1), 35–45.
6. Pedersen, B.; Thomsen, E.; Stern, R. Some Problems in Sampling, Analysis and Evaluation of Welding Fumes Containing Cr (VI). *Ann. Occup. Hyg.* **1987,** *31* (3), 325–338.
7. Blunt, J.; Balchin, N. C. *Health and Safety in Welding and Allied Processes,* 5th ed. Woodhead Publishing: Boca Raton, Florida, 2002.
8. Racette, B. A.; McGee-Minnich, L.; Moerlein, S.; Mink, J.; Videen, T.; Perlmutter, J. Welding-related Parkinsonism Clinical Features, Treatment, and Pathophysiology. *Neurology* **2001,** *56* (1), 8–13.
9. Li, G. J.; Zhang, L. L.; Lu, L.; Wu, P.; Zheng, W. Occupational Exposure to Welding Fume among Welders: Alterations of Manganese, Iron, Zinc, Copper, and Lead in Body Fluids and the Oxidative Stress Status. *J. Occup. Environ. Med.* **2004,** *46* (3), 241–248.
10. Jenkins, N.; Eagar, T. Chemical Analysis of Welding Fume Particles. *Weld. J.* **2005,** *84* (6), 87–93.
11. Antonini, J. M.; Lewis, A. B.; Roberts, J. R.; Whaley, D. A. Pulmonary Effects of Welding Fumes: Review of Worker and Experimental Animal Studies. *Am. J. Ind. Med.* **2003,** *43* (4), 350–360.
12. Mur, J.; Teculescu, D.; Pham, Q.; Gaertner, M.; Massin, N.; Meyer-Bisch, C.; Moulin, J.; Diebold, F.; Pierre, F.; Meurou-Poncelet, B. Lung Function and Clinical Findings in a Cross-sectional Study of Arc Welders. *Int. Archiv. Occup. Environ. Health* **1985,** *57* (1), 1–17.
13. Akbar-Khanzadeh, F. Short-term Respiratory Function Changes in Relation to Workshift Welding Fume Exposures. *Int. Archiv. Occup. Environ. Health* **1993,** *64* (6), 393–397.
14. Donoghue, A. M.; Glass, W.; Herbison, G. Transient Changes in the Pulmonary Function of Welders: A Cross Sectional Study of Monday Peak Expiratory Flow. *Occup. Environ. Med.* **1994,** *51* (8), 553–556.
15. Beckett, W. S.; Pace, P. E.; Sferlazza, S. J.; Perlman, G. D.; Chen, A. H.; Xu, X. P. Airway Reactivity in Welders: A Controlled Prospective Cohort Study. *J. Occup. Environ. Med.* **1996,** *38* (12), 1229–1238.
16. Meo, S. A.; Azeem, M. A.; Subhan, M. Lung Function in Pakistani Welding Workers. *J. Occup. Environ. Med.* **2003,** *45* (10), 1068–1073.
17. Christensen, S. W.; Bonde, J. P.; Omland, O. A Prospective Study of Decline in Lung Function in Relation to Welding Emissions. *J. Occup. Med. Toxicol.* **2008,** *3* (6), 1–8.
18. IARC. Chromium, Nickel and Welding. In *IARC Monographs on the Evaluation of Carcinogenic Risks to Humans* **1990,** *Vol. 49.* *http://monographs.iarc.fr/ENG/Monographs/vol49/mono49.pdf.*
19. Seel, E.; Zaebst, D.; Hein, M.; Liu, J.; Nowlin, S.; Chen, P. Inter-rater Agreement for a Retrospective Exposure Assessment of Asbestos, Chromium, Nickel and Welding Fumes in a Study of Lung Cancer and Ionizing Radiation. *Ann. Occup. Hyg.* **2007,** *51* (7), 601–610.
20. Siew, S. S.; Kauppinen, T.; Kyyrönen, P.; Heikkilä, P.; Pukkala, E. Exposure to Iron and Welding Fumes and the Risk of Lung Cancer. *Scand. J. Work Environ. Health* **2008,** *34* (6), 444–450.

www.iran-mavad.com
مرجع مهندسی مواد و متالورژی

21. Stern, R. M. Assessment of Risk of Lung Cancer for Welders. *Archiv. Environ. Health* **1983,** *38* (3), 148–155.
22. Sørensen, A. R.; Thulstrup, A. M.; Hansen, J.; Ramlau-Hansen, C. H.; Meersohn, A.; Skytthe, A.; Bonde, J. P. Risk of Lung Cancer According to Mild Steel and Stainless Steel Welding. *Scand. J. Work Environ. Health* **2007,** *33* (5), 379–386.
23. Ambroise, D.; Wild, P.; Moulin, J. J. Update of a Meta-analysis on Lung Cancer and Welding. *Scand. J. Work Environ. Health* **2006,** *32* (1), 22–31.
24. Mueller, E. J.; Seger, D. L. Metal Fume Fever—A Review. *J. Emerg. Med.* **1985,** *2* (4), 271–274.
25. Buerke, U.; Schneider, J.; Rösler, J.; Woitowitz, H. J. Interstitial Pulmonary Fibrosis after Severe Exposure to Welding Fumes. *Am. J. Ind. Med.* **2002,** *41* (4), 259–268.
26. Roesler, J.; Woitowiltz, H. Welder's Siderosis Progressing to Interstitial Pulmonary Fibrosis after Ongoing Exposure to Welding Fumes. *Eur. Resp. J. Suppl.* **1996,** *9* (1), 220S.
27. Coggon, D.; Inskip, H.; Winter, P.; Pannett, B. Lobar Pneumonia: An Occupational Disease in Welders. *The Lancet* **1994,** *344* (8914), 41–43.
28. Tuschl, H.; Weber, E.; Kovac, R. Investigations on Immune Parameters in Welders. *J. Appl. Toxicol.* **1997,** *17* (6), 377.
29. Hewitt, P. J. Strategies for Risk Assessment and Control in Welding: Challenges for Developing Countries. *Ann. Occup. Hyg.* **2001,** *45* (4), 295–298.
30. Ichikawa, N. Japanese Trends in Fatal Accidents Caused by Electric Shocks and the Prevention of the Accidents. In *Electrical Safety Workshop (ESW), 2012 IEEE IAS;* IEEE: Piscataway, NJ, 2012; pp 1–2.
31. NIOSH. *Worker Deaths by Electrocution;* NIOSH Pub: Cincinnati, OH, 1998; pp 98–131, http://www.cdc.gov/niosh/docs/98-131/pdfs/98-131.pdf.
32. Chao, E. L.; Henshaw, J. L. *Controlling Electrical Hazards,* 2002. http://www.osha.gov/Publications/3075.html.
33. Kouwenhoven, W.; Langworthy, O. R. Effect of Electric Shock. *Trans. Am. Inst. Electr. Eng.* **1930,** *49* (1), 381–394.
34. Ferris, L.; King, B.; Spence, P.; Williams, H. Effect of Electric Shock on the Heart. *Trans. Am. Inst. Electr. Eng.* **1936,** *55* (5), 498–515.
35. Lee, R. C.; Dougherty, W. Electrical Injury: Mechanisms, Manifestations, and Therapy. *IEEE Trans. Dielectr. Electr. Insul.* **2003,** *10* (5), 810–819.
36. Farnsworth, S. R. *Welding for Dummies;* Wiley Publishing, Inc: New York, 2010.
37. O'brien, R. L. *Jefferson's Welding Encyclopedia;* American Welding Society: Opa-locka, Florida, 1997.
38. US Navy. *Underwater Cutting & Welding Manual,* 1989. http://www.hnsa.org/doc/pdf/cut_weld.pdf.
39. IMCA. *Code of Practice for the Safe Use of Electricity under Water,* 2010. http://www.imca-int.com/documents/divisions/rov/docs/IMCAR015.pdf.
40. BLS. *Nonfatal Occupational Injuries and Illnesses Requiring Days Away from Work,* 2011. http://www.bls.gov/news.release/osh2.nr0.htm.
41. Fluegel, L.; Rein, B. *Arc Welding Safety,* 1989. http://nasdonline.org/static_content/documents/1087/d000873.pdf.
42. Clark, P. K. *Male Infertility and Welding Engineers,* 1992. https://www.osha.gov/pls/oshaweb/owadisp.show_document?p_table=INTERPRETATIONS&p_id=20909.
43. Olsen, F. O. *Hybrid Laser-arc Welding;* CRC Press: Boca Raton, Florida, 2009.
44. OSHA. *Eye Protection against Radiant Energy during Welding and Cutting in Shipyard Employment,* 2012. http://www.osha.gov/Publications/OSHAfactsheet-eyeprotection-during-welding.pdf.
45. Timings, R. *Fabrication and Welding Engineering;* Routledge: Oxford, 2012.
46. Futamata, M. Welding Noise as a Health Hazard—Methods of Protection. *Weld. Int.* **1988,** *2* (7), 596–601.
47. Firenze, R. J. *The Process of Hazard Control;* Kendall/Hunt Publishing Company: Dubuque, Iowa, 1978.
48. Troughton, M. *Handbook of Plastics Joining: A Practical Guide;* William Andrew, Inc: Norwich, New York, 2008.
49. Rayman, R. The Electromagnetic Spectrum and Chemical Hazards. In *Occupational Health in Aviation: Maintenance and Support Personnel;* Ribak, J., Rayman, R. B., Froom, P., Eds.; Academic Press: San Diego, 1995; pp 117–165.
50. Sforza, P.; de Blasiis, D. On-line Optical Monitoring System for Arc Welding. *NDT & E Int.* **2002,** *35* (1), 37–43.
51. Sliney, D. H.; Wolbarsht, M. *Safety with Lasers and other Optical Sources: A Comprehensive Handbook;* Plenum Press: New York, 1980.
52. Sliney, D. H.; Benton, R. E.; Cole, H. M.; Epstein, S. G.; Morin, C. J. Transmission of Potentially Hazardous Actinic Ultraviolet Radiation through Fabrics. *Appl. Ind. Hyg.* **1987,** *2* (1), 36–44.
53. ESAB. *Welding and Cutting-measures and Risks,* 2013. http://www.esab.com/global/en/about/upload/weldinga.pdf.
54. Henderson, J. Oxyfuel Safety: It's Everyone's Responsibility. *Weld. J.* **2012,** *91* (8), 48–53.
55. ESAB. *Precautions and Safe Practices for Arc Welding, Cutting and Gouging,* 2009. http://www.esabna.com/us/en/support/upload/Precautions-and-Safe-Practices-for-Arc-Welding-Cutting-and-Gouging.pdf.
56. ESAB. *Precautions and Safe Practices for Gas Welding, Cutting and Heating,* 2009. http://www.esabna.com/us/en/support/upload/Precautions-and-Safe-Practices-for-Gas-Welding-Cutting-and-Heating.pdf.
57. ESAB. *Inspection Guide for Gas Apparatus,* 2000. http://www.esabna.com/us/en/support/upload/F_7218_A_GasApp_InsGuide_Now_Gas_1039.pdf.
58. Bulan, J.; Cull, E.; Stupczy, F. Safeguarding Your Vision. *Weld. J.* **2012,** *91* (8), 58–60.

Relevant Website

http://www.scribd.com/doc/86890919/AWS-Module-2.

www.iran-mavad.com
مرجع مهندسی مواد و متالورژی

This page intentionally left blank

www.iran-mavad.com
مرجع مهندسی مواد و متالورژی

6.13 Optimum Speed of Friction Stir Welding on 304L Stainless Steel by Finite Element Method

S Sulaiman and S Emamian, Universiti Putra Malaysia, Selangor, Malaysia

© 2014 Elsevier Ltd. All rights reserved.

6.13.1	**Introduction**	227
6.13.2	**Model Description**	229
6.13.2.1	Heat Generation and Transfer	229
6.13.2.2	Mechanical Properties	230
6.13.2.3	Velocity of Welding	231
6.13.2.4	Mesh and Boundary Condition	231
6.13.3	**Computational Process**	232
6.13.4	**Result and Discussions**	232
6.13.5	**Conclusion**	235
6.13.6	**Future Study**	235
References		235

6.13.1 Introduction

The process of two pieces of metals joining together occurs at the original boundary surfaces of the pieces. This phenomenon takes place at a level in which the bounding is accompanied by a significant interatomic penetration. At the welding points, the boundaries fade away and the development of the integrating crystals occur across them. By the use of pressure or heat, or sometimes both, the welding process is carried out and there is no added metal.

The general processes of welding are divided into two main categories: fusion welding and solid-state welding. In fusion welding, the joint point is locally melted, and similar to casting, the joining process will occur without hammering or pressure. The energy for melting will be supplied through many ways. In solid-state welding, the temperature of the two pieces for welding should be more than the recrystallization temperature $\left(T > \frac{tm}{2}\right)$ (tm is melting point of metal and usually the recrystallization temperature is $\frac{tm}{2}$), and then the two pieces will be welded by pressure.

One of the nonfusion welding methods that was invented by The Welding Institute (TWI) in UK in 1991 is friction stir welding (FSW) (*1*). The application of this method is in marine, aerospace, automotive, rail, and construction industries. This process was developed for Al, Mg, Cu, and Zn and demonstrated in steels, Ti, and Ni (*2*). This invention works well with aluminium alloy joints and low melting temperature materials. By applying this process, there is no need for filler metals, better joint strengths are achieved, and distortion and residual stresses are decreased.

It is notable that friction stir welding has many applications for aluminium, and extensive research has been carried out in this field. Applying this method to other metals, particularly stainless steels, will help in production efficiency. This chapter describes implementing friction stir welding on 304L stainless steel. 304L Stainless steel is used in heavy production such as pressure vessels and heat exchangers. To substitute fusion welding with FSW in these productions in order to reduce the cost of production, it is impossible to study all aspects of the FSW. Therefore, this study can be considered as a small part of the whole process. Hence, discussion in this chapter is about 304L stainless steel, to find an optimum traveling speed of welding. **Figure 1** shows the illustration of friction stir welding.

The aim of optimum speed in welding is that welding can be performed with low changes in microstructures due to different thermal and stress conditions, and a high-quality weld is left behind. It is clear that high and low speed would cause problems in joining the materials. For instance, high speed would cause lack of penetration and lack of material aggregation. On the other hand, too hot processing conditions can cause flash formation or nugget collapse. Under too cold conditions, insufficient flowing or lack of fill would occur on the advancing side (*3*).

Since the friction between the tool and the base metal causes the generated heat, it is essential to consider the speed of the tool and welding speed. Many scholars have focused their studies on thermal issues and heat generation on the stainless steels, and their results can be useful here.

Reynolds et al. (*4*) used 3.2 mm thick sheets to be joined by FSW. Two different rates were applied for the tool rotation speed at one traveling speed. Relative to the base metal, the resulting welds were overmatched. Residual stresses of 304L stainless steel in FSW are the same in character and magnitude as in fusion welding. Furthermore, lower energy input due to lower tool rotation can result in lower weld temperature and a fine weld nugget grain size. Cho et al. (*5*) conducted FSW on stainless steel type 409. The tool that they used in their study was Polycrystalline Cubic Boron Nitride (PCBN). By using friction stir welding, defect free welds with high quality were successfully created on 409 ferritic stainless steel. Fine grained can be achieved in the stir zone and fraction of low angle grain boundary will be increased compared to base metal. Increasing the plunging depth can cause more fraction of low angle grain

www.iran-mavad.com
مرجع مهندسی مواد و متالورژی

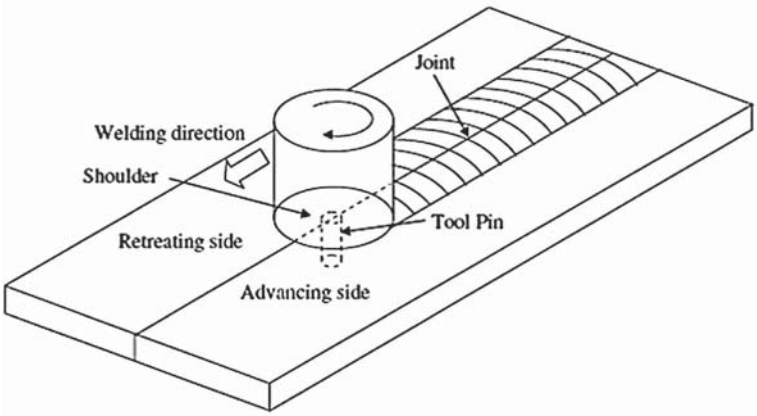

Figure 1 Schematic illustration of friction stir welding. Reproduced from Nandan, R.; DebRoy, T.; Bhadeshia, H. K. D. H. Recent Advances in Friction-stir Welding – Process, Weldment Structure and Properties. *Prog. Mater. Sci.* **2008**, *53* (6), 980–1023

boundary, reduce the grain size, and increase the hardness in the stir zone. They found that fine-grained microstructure was settled by dynamic recrystallization because of high heat generation and shear deformation.

Lakshminarayanan and Balasubramanian (*6*) studied the crack, fatigue, tensile properties, and residual stresses in friction stir welding of 409M, which is a type of ferritic stainless steel. The following conclusions were reached:

1. The fatigue strength improved by friction stir welding on 409M ferritic stainless steel.
2. The strength of fatigue growth is around 24% compared to the base metal.
3. The notch sensitivity factor and fatigue notch of the 409M were decreased by friction stir welding.
4. The main reasons for improving the fatigue performance in the friction stir welding joint in comparison with base metal are larger tensile properties, dual ferritic–martensitic microstructure, and squeezed residual stress vertical to the direction of crack growth.

Esmailzadeh et al. (*7*) in their study indicate that joining of lean duplex stainless steels without transformation can be obtained when friction stir welding is carried out under suitable conditions. To achieve the sound joints, suitable parameters should be selected carefully. By increasing the tool speed, strain rate enhances and peak temperature will be reduced. They suggested that the joint with fine grain and good mechanical properties could be achieved with low heat input friction stir welding.

Ahn et al. (*8*) performed FSW on 409L stainless steel using an Si_3N_4 tool with a rotation speed of 700 rpm and a traveling speed of 60 mm min^{-1}. Microstructural characteristics, mechanical properties, and corrosion were studied. Their results are as follows:

1. A good FSW joint was achieved.
2. With regard to intergranular corrosion resistance, the weld had the same corrosion properties as the base metal.
3. Regarding corrosion resistance, friction stir welding using an Si_3N_4 tool is a fine welding method. They found that the Vickers hardness of the stir zone was same as that of the base metal.

Park et al. (*9*) evaluated the corrosion properties of a friction stir welded 304 stainless steel. In the heat affected zone, the degree of sensitization was relatively low after FSW. This phenomenon can be explained by the short duration of sensitization temperatures. Yet in the advancing side of the stir zone, many grain boundaries were deeply corroded. The severely deteriorated corrosion resistance was attributed to the formation of the sigma phase during FSW.

Jata and Semiatin (*10*) have proposed that stainless steels type 304 and 304L have lower stacking fault energy. They developed a basic understanding of the improvement of microstructure in the dynamically recrystallized area and related it to the deformation process variables of strain, strain rate, and temperature. The main results contained optical, transmission electron microscope (TEM), and orientation imaging microscopy (OIM) characterization of parent material and the weld piece. Optical and TEM microstructure of FSW of an Al–Li alloy were studied to obtain the mechanism of the evolution in the dynamically recrystallized region. They found recrystallized grains in the dynamically recrystallized region form using a continuous mechanism.

Sato et al. (*11*) have examined recrystallization in type 304L and found dynamic recrystallization during intense deformation. In their study, OIM was used to examine the recrystallization event of 304L stainless steel during friction stirring. A component with a fiber texture, which contained a dominant orientation, was observed in the stir zone from the center to the advancing side. In the as-processed condition, the grains included a high density of dislocations, which contained this dominant fiber texture component. Twinning, grain growth, and a change in texture resulted from the post-process heat treatment in most of the grains, which had this fiber component. Without rotation of orientation, during the heat treatment, twinning and grain growth was experienced by the grains, which had an orientation other than the fiber component. These

www.iran-mavad.com
مرجع مهندسی مواد و متالورژی

results showed that during the friction stir, 304L stainless steel partly endures static recrystallization, which is followed by dynamic recrystallization.

Park et al. (12) found that stir zone and thermomechanically affected zone (TMAZ) were dynamically recrystallized. During the friction stir welding, sigma phase formation rapidly occurred in 304 stainless steel. It was concluded that one of the possibilities that was a cause of this phenomenon was that at the high temperature, delta-ferrite emergence can accelerate the sigma formation, and the friction stirring, under recrystallization and high strain, induces the subsequent decomposition of the ferrite.

In 304 stainless steel, during FSW, the microstructural evolution was examined. The Stir Zone (SZ) and TMAZ showed typical dynamically recrystallized and recovered microstructures, respectively. At the advancing side of the stir zone, the sigma phase, which included several stacking faults, was formed, and it was revealed by microstructural observation.

Saeid et al. (13), found that increase in welding speed decreases the recrystallized grain size. The focus of their study was on SAF2205 duplex stainless steel and how, in FSW, the mechanical properties and microstructure of the stir zone in this type of steel are affected by the welding speed. A WC-based material tool was used to weld plates with a specific thickness at a specific constant rotational speed. Then X-ray radiography revealed that in a particular range for the welding speed, sound welds were successfully achieved, while at a higher speed, a groove-like defect was formed. In addition, in the stir zone, the size of grains was decreased by the increase of the welding speed. So the tensile strength and the average hardness value of the stir zone were improved by this increase. These achieved results are interpreted with respect to the interaction between the peak temperature and the welding speed in FSW.

Fine equiaxed grains were included in the microstructure of the stir zones and by an increase in the welding speed, their grain sizes decreased. This type of behavior is credited to the lower input of heat at the higher welding speed. Due to refinement of grain of the microstructure, with the increased welding speed, the hardness and tensile strength of the SAF2205 duplex stainless steel increased. The other factor that can help in understanding FSW, and especially have a role in determining the speed of welding is strain rate, is the material flow in the stir zone. Thus, many researchers have tried to find the strain rate during FSW (3).

This study attempts estimate optimum speed of welding during FSW on 304L stainless steel by choosing the cases of study to analyze with ABAQUS software. It is noteworthy that experimental studies were considered during the study.

6.13.2 Model Description

Chiumenti et al. (15) presented a strategy that is adopted for the FSW process numerical simulation. A coupled thermomechanical solution of both the momentum and energy balance equations is presented. In order to deal with the specific motion description in the friction stir welding problem, a general kinematic framework has been used. To explain the relationship involving the mesh movement and the material in the ST, the arbitrary Lagrangian–Eulerian (ALE) formulation of the balance equations has been introduced. Coupling the thermal and mechanical models, the two diverse heat generation mechanisms that come from friction and stirring have been described. The numerical benchmarks have shown the accuracy of both the thermal and the mechanical responses when an FSW process is simulated.

To review and analyze friction stir welding on stainless steel 304L, a finite element method (FEM) is provided that is performed through ABAQUS software, and ALE framework is employed with suitable meshing to consider elastic–plastic deformations (14). For process modeling and analytical calculations that are described in the next section, a mathematical analysis of related parts is proposed in this section.

In numerical simulation, three parts of the process are investigated which have their own solving method. The work piece is solved in an Eulerian framework, pin is solved in Lagrangian framework, but in the stir zone that is based on this chapter ALE method would be solved (15).

6.13.2.1 Heat Generation and Transfer

FSW is a thermomechanical phenomenon. There is much material motion and shear force and the temperature will increase to below the melting point (16,17). Friction stir welding is a process that is strongly influenced by heat generation and heat flow (18). Contact between the tool and the work piece, while the tool is rotating, and also traveling along the weld, causes the friction, which is the source of heat generation in FSW. The welding tool, as mentioned before, consists of the pin and shoulder, and the surface of the shoulder can generate the majority of the heat (16). According to Ref. (16), there are three contact conditions, which are sticking, sliding, and partial sticking/sliding. If friction shear stress (τ_{friction}) is bigger than yield shear stress (τ_{yield}) then contact surface would be sticking. Inversely, sliding would be defined for contact surface. Total heat generation is sum of Q_1 under the tool shoulder and Q_2 at the side of the pin and Q_3 at the head of pin. The heat generated at the tilted segment is modified as

$$dQ = \omega r dF = \omega r^2 \tau_{\text{contact}} d\theta dr(1 + \tan \alpha) \quad [1]$$

where rotation speed of the pin is ω and r shows distance, and α is cone angle for the shoulders that is conical. By integration of eqn [1], Q_1 may be calculated.

www.iran-mavad.com
مرجع مهندسی مواد و متالورژی

$$Q_1 = \int_0^{2\pi} \int_{R_{pin}}^{R_{shoulder}} \omega \tau_{contact} r^2 (1 + \tan\alpha) dr d\theta = \frac{2}{3}\pi\tau_{contact}\omega\left(R^3_{shoulder} - R^3_{pin}\right)(1 + \tan\alpha) \quad [2]$$

Heat generation at the side of the pin is calculated by

$$Q_2 = \int_0^{2\pi} \int_0^{H_{pin}} \omega \tau_{contact} R^2_{pin} dz d\theta = 2\pi\tau_{contact}\omega R^2_{pin} H_{pin} \quad [3]$$

where R_{pin} is radius of the pin and H_{pin} is height of the pin.

Heat generation at the head of the pin is

$$Q_3 = \int_0^{2\pi} \int_0^{R_{pin}} \omega \tau_{contact} r^2 dr d\theta = \frac{2}{3}\pi_{contact}\omega R^3_{pin} \quad [4]$$

Total heat generation is calculated by combination of (Q_1), (Q_2), and (Q_3):

$$Q_{total} = Q_1 + Q_2 + Q_3$$

$$Q_{total} = 2/3\pi\tau_{contact}\omega\left(R^3_{shoulder} + 3R^2_{pin}H_{pin}\right) \quad [5]$$

According to von Mises criteria, $\tau_{yield} = \frac{\sigma_{yield}}{\sqrt{3}}$; therefore, in the sticking contact condition,

$$Q_{total,sticking} = \frac{2}{3}\pi\frac{\sigma_{yield}}{\sqrt{3}}\omega\left(\left(R^3_{shoulder} - R^3_{pin}\right)(1 + \tan\alpha) + R^3_{pin} + 3R^2_{pin}H_{pin}\right) \quad [5a]$$

For the sliding condition, Coulomb's friction law is chosen to describe shear stress. Thus, $\tau_{contact} = \tau_{friction} = \mu p = \mu\sigma$ where ρ and σ are contact pressures and μ is the friction coefficient. Thus, total heat generation for the sliding condition is

$$Q_{total,sliding} = \frac{2}{3}\pi\mu\rho\omega\left(\left(R^3_{shoulder} - R^3_{pin}\right)(1 + \tan(\alpha)) + R^3_{pin} + 3R^2_{pin}H_{pin}\right) \quad [6]$$

The heat transfer equation in the ALE is

$$\rho o c(\partial T/\partial t|x + c\cdot\nabla T) = \dot{D}_{mesh} + \rho o\dot{r} - \nabla\cdot q \quad [7]$$

where c is specific heat capacity, $\dot{D}_{mesh}$ is mechanical dissipation, $\dot{r}$ is the rate of heat source per unit of mass, $q = -k\nabla T$ that is the heat flux, per unit of surface, where ∇T is temperature gradient, and k is thermal conductivity. It is obvious that in this equation the enthalpy rate is replaced by temperature rate, as $\rho o\dot{h} = \rho o c\dot{T}$ (15).

6.13.2.2 Mechanical Properties

Austenitic stainless steels have good ductility, high strength, corrosion resistance, and good weldability. Hence, it is popular and has been the focus of researchers (19). During the welding, friction between the tool and the work piece will cause the plastic deformation, which in turn is the cause of the heat generation (20). Recrystallization and recovery occur simultaneously (21). Dislocation may increase during deformation (22). Dislocation is a crystallographic defect in material science and is irregularity within a crystal structure. The mechanical properties of an FSW joint, strength and toughness (15,23), are related to the properties of the different zones in the weld (2). Different regions of the weld are shown in **Figure 2**.

The material flow during friction stir welding is quite dependent on the tool geometry, process parameters, and material to be welded. It is of practical importance to understand the material flow characteristics for optimal tool design and to obtain high structural efficiency welds.

In summary, the material flow during FSW is complicated and the understanding of deformation process is limited. It is important to point out that there are many factors that can influence the material flow during FSW. These factors include tool

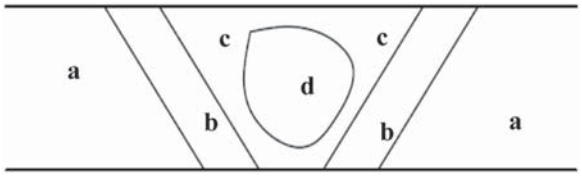

Figure 2 (a) Base metal; (b) Heat affected zone (HAZ); (c) Thermomechanically affected zone (TMAZ); (d) Stir zone.

www.iran-mavad.com
مرجع مهندسی مواد و متالورژی

geometry (pin and shoulder design, relative dimensions of pin and shoulder), welding parameters (tool rotation rate and direction, clockwise or counter clockwise, traverse speed, plunge depth, spindle angle), material type, and work-piece temperature. It is very likely that the material flow within the nugget during FSW consists of several independent deformation processes (*23*).

The material properties of 304L stainless steel are obtained from the Zhu and Chao (*24*) and *Metals Handbook* of Brown et al. (*24,25*). The thermal and mechanical properties that were used in simulation are shown in **Figure 3** and **Table 1**.

6.13.2.3 Velocity of Welding

In FSW, there are two important factors, tool rotating (ω, rpm) and travel speed (v, mm/min). A high-speed rotating tool causes more heat due to friction. One issue that should be considered is that for high melting materials, such as stainless steels, preheating is one of the factors to make a suitable plastic area in this process (*23*). Arbegast (*26*) presented an equation for maximum FSW process temperature that indicates the effects of rotational and welding speeds on the welding temperature.

$$\frac{T}{T_m} = k\left(\frac{\omega^2}{v \times 10^4}\right)^a \quad [8]$$

where T is the FSW temperature (°C), T_m is the melting temperature of the sheet material (°C), a and k are two defined constants, and ω and v are the tool rotational and welding speeds, respectively. According to eqn [8], the FSW process temperature is related to the ω^2/v ratio. It means that increasing the rotational speed at a constant welding speed or decreasing the welding speed at a constant rotational speed leads to a higher welding temperature. It also indicates that the variations of tool rotational speed have higher effects on the process temperature than the welding speed variations (*26,27*).

On the other hand, too hot processing conditions can cause flash formation or nugget collapse. And under too cold conditions, insufficient flow or lack of fill would occur on the advancing side (*3*).

Frictional heat is calculated by $q_f = F_f V$, where F_f is local friction force that according to Coulomb's friction law can be calculated as $F_f = \mu F_n$.

In these equations, V is rotational velocity of the pin, where $V_f = 2\pi RN$ and μ is the friction coefficient between the tool and work piece, and F_n is the normal force applied to the work piece. In the velocity equation, R is the distance of calculated point from the tool axis and N is the rotational speed of the tool (*28*).

6.13.2.4 Mesh and Boundary Condition

In this section, mesh and boundary conditions are explained. In nonlinear simulations there are large deformations, and because of these deformations, finite elements would distort. Therefore, it is necessary to use adaptive meshing tools to reduce the distortion in

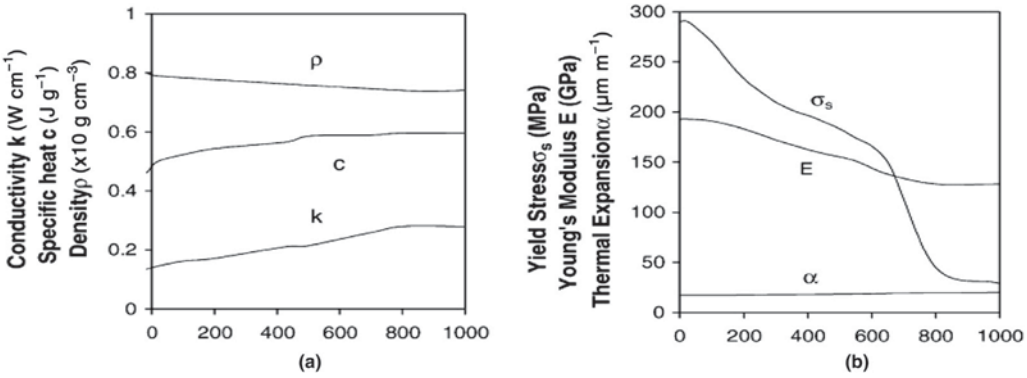

Figure 3 Variation of material properties with temperature of 304L stainless steel. (a) Thermal properties; (b) Mechanical properties. Reproduced from Zhu, X. K.; Chao, Y. J. Numerical Simulation of Transient Temperature and Residual Stresses in Friction Stir Welding of 304L Stainless Steel. *J. Mater. Process. Technol.* **2004**, *146* (2), 263–272.

Table 1 Thermal and mechanical properties of 304L stainless steel

Temperature (° C)	*100*	*200*	*300*	*400*	*500*	*600*	*700*	*800*	*900*	*1000*
Yield strength (MPa)	270	240	210	197	180	167	117	45	30	30
Young's modulus (GPa)	193	180	170	160	153	140	130	125	125	125
Thermal exp. (μm m^{-1} K^{-1})	17	17	18	18	18	19	19	19	20	20
Density (kg m^{-3})	7800	7700	7600	7500	7500	7400	7400	7300	7200	7200
Thermal cond. (W m^{-1} K^{-1})	15	16.5	18.5	20	20	22	23	27	27	27
Heat capacity (J kg^{-1} K^{-1})	510	520	530	540	550	550	550	560	560	560

www.iran-mavad.com
مرجع مهندسی مواد و متالورژی

the mesh. The ALE method is used in this study, because it combines Lagrangian and Eulerian analysis. Thus, mesh motion at free boundaries is constrained to the material motion and material, and mesh motions are independent.

Because 700 mesh and 576 elements of C3D8R were used for the analysis, eight nodes are used with radius integration. However, for better results, deployment of mesh needs to be calculated and is analyzed after the diagram.

In the boundary condition, the reference point of the welding tool should be fixed in all directions except in the x and y rotation axes. In the next step, degree of freedoms should be constrained.

6.13.3 Computational Process

The dimensions of the deformable solid plates, which are made of 304L stainless steel, are 200 mm length, 100 mm width, and 6.4 mm thickness.

In the first stage of analysis, the workpiece is constrained at the bottom surface at surface normal direction (z) to prevent bending of the surface. The tool is modeled as an analytical rigid surface with no thermal degrees of freedom. For the contact interaction between the tool and the work piece, the tool is modeled as a master surface and the work piece as a slave one. Since friction coefficient is variable with an uncertain manner in an FSW process, a constant friction coefficient of 0.6 for contact property is applied. The convection coefficients on various surfaces of the work piece play an important role in the determination of the transient temperature fields.

In order to model the process, the ALE mesh technique was employed to prevent the distortion of the mesh throughout the analysis by regenerating the mesh automatically and allowing the mesh to move independent of the material. The ALE technique improves the results and increases the computation time. For faster and more accurate simulation, two methods are applied: the first one is the adaptive mesh scheme to improve the solutions and the second one is the mass-scaling technique.

In the mass-scaling technique, the explicit procedure is integrated over small time increments. The mass-scaling technique increases the time increment by artificially increasing the material density in the model and improves the computational efficiency, while the results remain accurate. In the second step of analysis, the temperature history generated by the previous model is utilized as thermal input to a static general step. In this step, the tool was removed and fixtures were modeled. In comparison with the experimental method that done for FSW on stainless steels, Sato et al. (*11*) have used PCBN for pin material, but the shape of the pin was three flats.

6.13.4 Result and Discussions

For conducting this study, after investigations of affective conditions in the solution processes and choosing the proper data by regarding the type of workpiece that mentioned before, the following issues were considered that are discussed in the results and conclusions.

To achieve the results, and according to experimental papers such as Sato et al. (*11*), the cases in **Table 2** are considered.

As explained in Ref. (*11*), there was only one traveling speed (120 mm min^{-1}); however, in this study two other velocities were chosen in order to compare thermal and stress conditions. To obtain optimal conditions in FSW, investigating the optimum speeds are essential. It is obvious that rotational and traveling speeds are main factors in heat generation and heat input issues. The relation between speed and heat input is complex during FSW. Too much or too low heat input will affect the weld quality. If the heat input is too low, suitable plastic conditions prevented that causing voids during welding and in extreme cases, the tool may break. On the other hand, with high heat input weld properties are excessively deteriorated. Generally, lower heat input in friction stir welding causes improved mechanical properties as well as decreased distortion and residual stress (*29*).

In comparison with Saeid et al. (*13*), traveling speed changes with temperature would be determined as follows. According to Refs. (*13,30*), the following equation describes the heat input during FSW:

$$Q = \frac{4}{3}\pi^2 \frac{\eta \mu \rho \omega R^3}{v} \quad [9]$$

where Q is the heat input per unit per length, η is the heat input efficiency, R is the radius of the shoulder, and μ is the friction coefficient. According to the equation, by increasing the traveling speed (v) and decreasing the rotation speed, heat input (Q) will decrease. Also, peak temperature decreases by increasing welding speed at a constant tool rotation speed.

Table 2 Cases of study

Case 1	Rotation speed	300 rpm		
	Traveling speed	120 mm min^{-1}	300 mm min^{-1}	600 mm min^{-1}
Case 2	Rotation speed	450 rpm		
	Traveling speed	120 mm min^{-1}	300 mm min^{-1}	600 mm min^{-1}

www.iran-mavad.com
مرجع مهندسی مواد و متالورژی

Before considering the findings of this study, it is better to discuss about the effect of speed on the recrystallization phenomenon. Sato et al. (*11*) proposed that 304L stainless steel undergoes dynamic recrystallization during the heating of friction stir. The result of dynamic recrystallization is fine grains in the stir zone (*12*,*13*). Saeid et al. (*13*) found that an increase in welding speed decreases the recrystallized grain size. In addition, approximate grain sizes at the stir zone under the highest and lowest heat input were much smaller than the base metal. They also found that microstructure of the stir zones includes fine grains of α and γ phases, and their sizes decrease with increasing welding speed. Other studies found that recrystallized grain size could be reduced by decreasing the tool rotational speed or increasing the welding speed (*13*).

Figures 4 and 5 show the relation between traveling speed in constant rotation with temperature and stress according to the two case studies. According to these figures and in comparison with affirmation experimental studies, it is obvious that by increasing traveling speed with constant rotational speed, temperature will be reduced and stress will be increased.

By matching the temperature and stress graphs from each case, which are indicated in **Figure 4**, and understanding the best conditions in FSW from experimental data that was described earlier, the range of optimum speed could be estimated, and it is illustrated in **Figure 5**.

The obtained results from case 1 and case 2 show that if the rotational speed increases, then the optimum traveling speed, decreases.

Figure 6 illustrates the von Mises simulation. It shows the differences between cases 1 and 2.

Figure 7 illustrates the comparison between the two cases from temperature, heat input, and stress points of view.

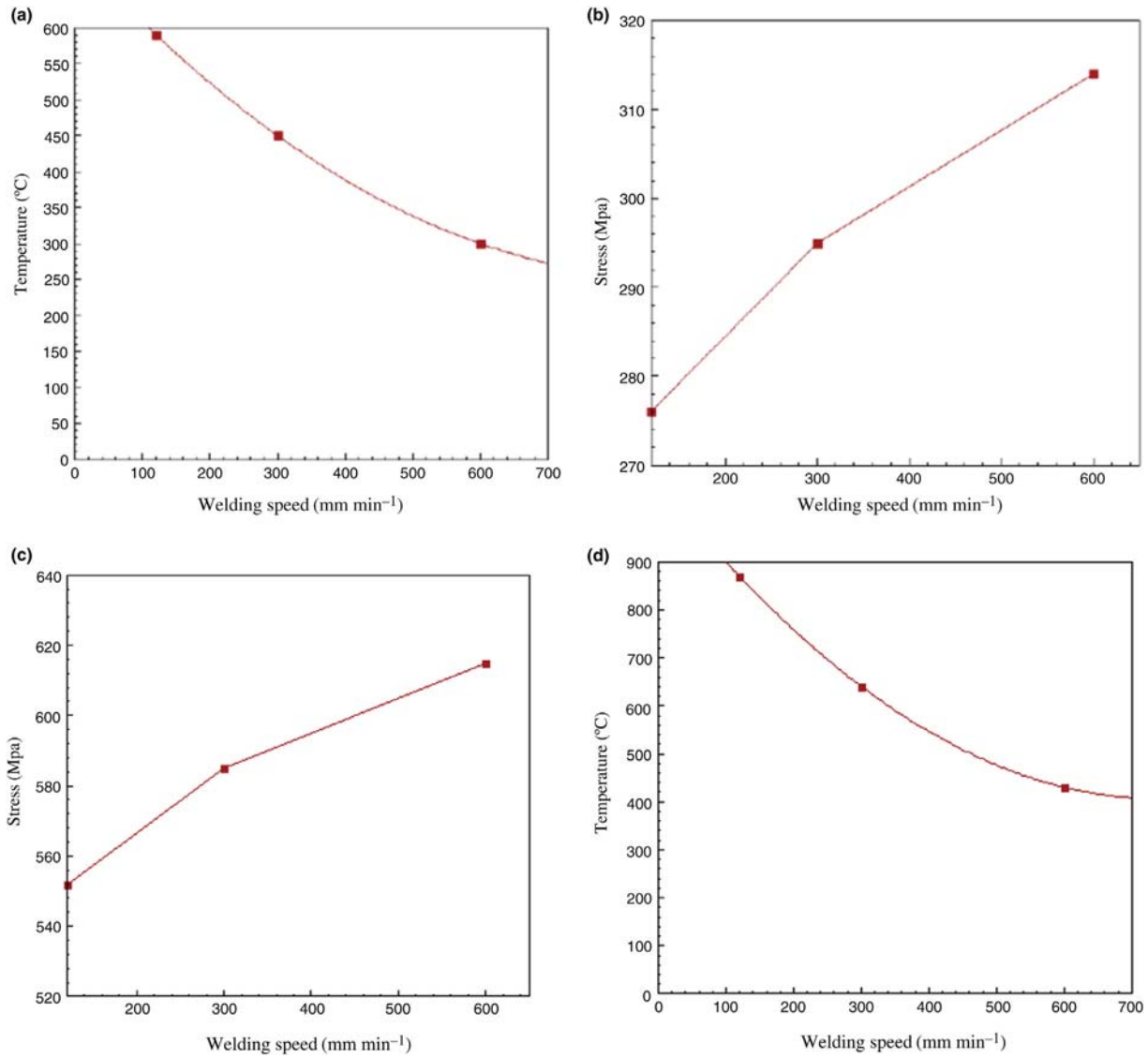

Figure 4 Relation between traveling speed with (a) temperature from case 1, and (b) stress from case 1, and (c) stress from case 2, and (d) temperature from case 2.

www.iran-mavad.com
مرجع مهندسی مواد و متالورژی

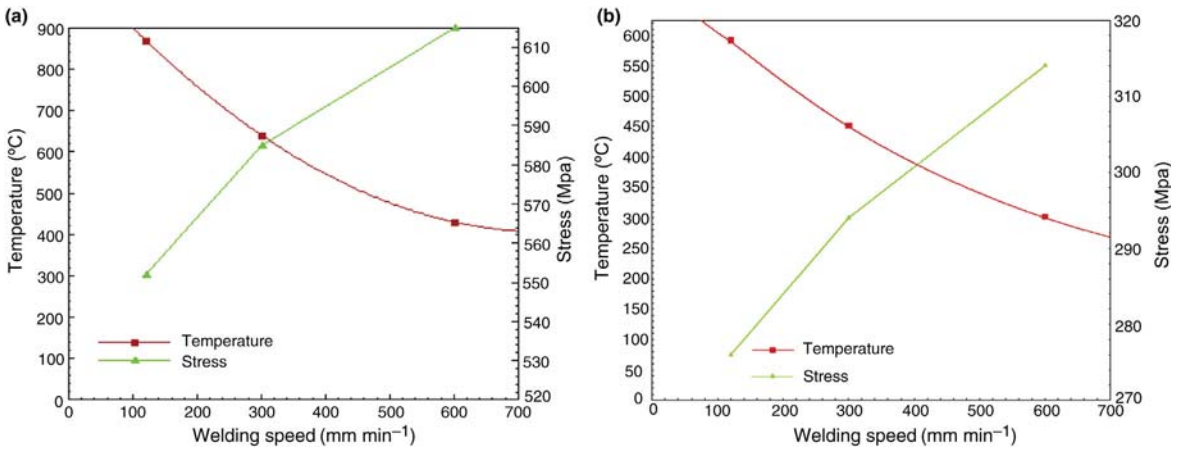

Figure 5 (a) Matching the stress and temperature graphs for case 1. (b) Matching the stress and temperature graphs for case 2.

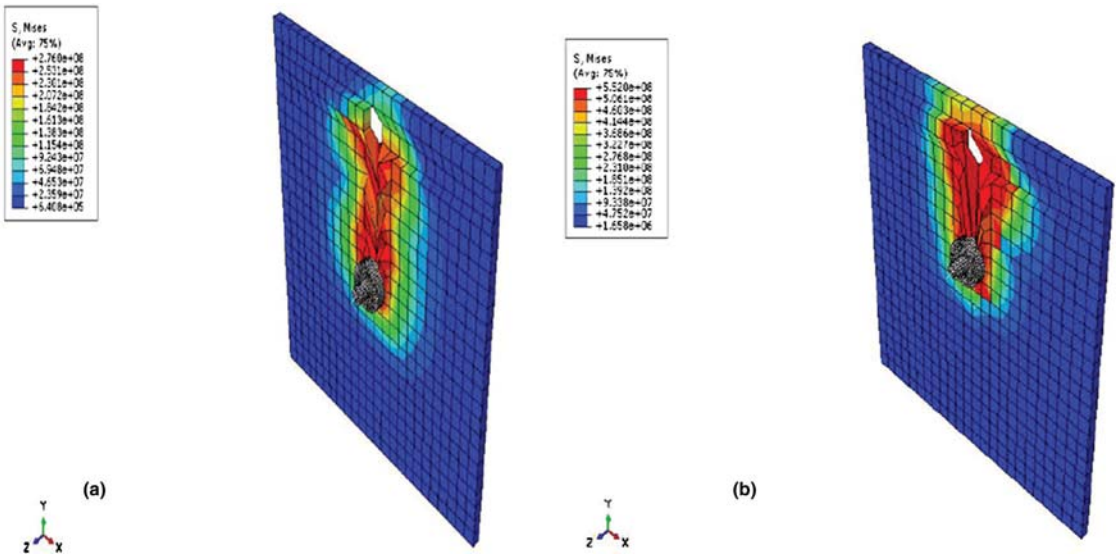

Figure 6 Stress von Mises (a) Case 1; (b) Case 2.

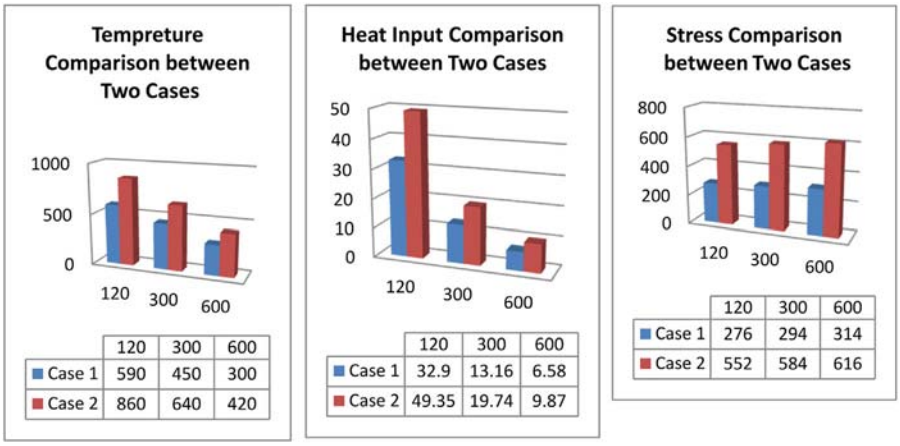

	120	300	600
Case 1	590	450	300
Case 2	860	640	420

	120	300	600
Case 1	32.9	13.16	6.58
Case 2	49.35	19.74	9.87

	120	300	600
Case 1	276	294	314
Case 2	552	584	616

Figure 7 Comparisons between two cases.

www.iran-mavad.com
مرجع مهندسی مواد و متالورژی

From the temperature diagram, it is clear that increasing the rotational speed will lead to temperature enhancement. In addition, increasing the traveling speed will reduce the temperature. The heat input diagram shows that higher rotational speed will provide more heat input, and increasing the traveling speed will significantly reduce heat input.

The stress diagram illustrates that by increasing the rotational speed, stress will go up significantly, while the traveling speed will increase gradually.

6.13.5 Conclusion

Since it is impossible to study all aspects of FSW, this chapter can be considered an aid in understanding this marvel method. According to a survey that was performed in the previous steps, characteristics of 304L stainless steel have been considered. FSW with its tool geometry and design were investigated and the strengths and weaknesses of the process were considered. Experimental studies were compared with simulations and optimum speed of welding during FSW on 304L stainless steel can be obtained as follows. By increasing traveling speed in a constant rotational speed, heat temperature and the amount of heat input would be reduced and stress would be increased. The obtained results from case 1 and case 2 show that if the rotational speed increases, then the optimum traveling speed decreases. The results of this study are summarized as follows:

1. By increasing traveling speed in a constant rotational speed, heat temperature and the amount of heat input would be reduced and stress would be increased.
2. Comparing the two cases shows that higher rotational speed cause generates more heat than the traveling speed.
3. By increasing rotational speed 1.5 times, from 300 to 450 rpm, the amount of temperature and stress would be increased, respectively, to 70% and 50%.
4. By matching two graphs of stress and temperature, the optimum speed of welding can be achieved. At a constant rotational speed of 300 rpm, the optimum speed will be around 400 mm min^{-1} and at a constant rotational speed of 450 rpm, the optimum speed will be around 300 mm min^{-1}.

6.13.6 Future Study

To obtain accurate data and documented results, experimental analysis for process of friction stir welding on 304L stainless steel and radiography of samples to find suitable results of microstructures and grin size of stir zone are recommended. Meanwhile, considering the rate of cooling is another important factor that can be helpful in simulation and experimental analysis.

References

1. Thomas, W. M. Friction Stir Butt Welding. International Patent Appl. No. PCT/GB92/02203 and GB Patent Appl. No. 9125978.8, Dec. 1991, U.S. Patent No. 5460,317, 1991.
2. Russell, M. *Friction Stir Welding at TWI;* TWI: Cambridge, 2010.
3. Qian, J.; Li, J.; Sun, F.; Xiong, J.; Zhang, F.; Lin, X. An Analytical Model to Optimize Rotation Speed and Travel Speed of Friction Stir Welding for Defect-free Joints. *Scr. Mater.* **2013,** *68* (3–4), 175–178.
4. Reynolds, A. P.; Tang, W.; Gnaupel-Herold, T.; Prask, H. Structure, Properties, and Residual Stress of 304L Stainless Steel Friction Stir Welds. *Scr. Mater.* **2003,** *48* (9), 1289–1294.
5. Cho, H.; Han, H. N.; Hong, S.; Park, J.; Kwon, Y.; Kim, S.; Steel, R. J. Microstructural Analysis of Friction Stir Welded Ferritic Stainless Steel. *Mater. Sci. Eng., A* **2011,** *528* (6), 2889–2894.
6. Lakshminarayanan, A. K.; Balasubramanian, V. Assessment of Fatigue Life and Crack Growth Resistance of Friction Stir Welded AISI 409M Ferritic Stainless Steel Joints. *Mater. Sci. Eng., A* **2012,** *539,* 143–153.
7. Esmailzadeh, M.; Shamanian, M.; Kermanpur, A.; Saeid, T. Microstructure and Mechanical Properties of Friction Stir Welded Lean Duplex Stainless Steel. *Mater. Sci. Eng., A* **2013,** *561,* 486–491.
8. Ahn, B. W.; Choi, D. H.; Kim, D. J.; Jung, S. B. Microstructures and Properties of Friction Stir Welded 409L Stainless Steel Using a Si_3N_4 Tool. *Mater. Sci. Eng., A* **2012,** *532,* 476–479.
9. Park, S. H. C.; Sato, Y. S.; Kokawa, H.; Okamoto, K.; Hirano, S.; Inagaki, M. Corrosion Resistance of Friction Stir Welded 304 Stainless Steel. *Scr. Mater.* **2004,** *51* (2), 101–105.
10. Jata, K. V.; Semiatin, S. L. Continuous Dynamic Recrystallization during Friction Stir Welding of High Strength Aluminum Alloys. *Scr. Mater.* **2000,** *43* (8), 743–749.
11. Sato, Y. S.; Nelson, T. W.; Sterling, C. J. Recrystallization in Type 304L Stainless Steel during Friction Stirring. *Acta Mater.* **2005,** *53* (3), 637–645.
12. Park, S. H. C.; Sato, Y. S.; Kokawa, H.; Okamoto, K.; Hirano, S.; Inagaki, M. Rapid Formation of the Sigma Phase in 304 Stainless Steel during Friction Stir Welding. *Scr. Mater.* **2003,** *49* (12), 1175–1180.
13. Saeid, T.; Abdollah-zadeh, A.; Assadi, H.; MalekGhaini, F. Effect of Friction Stir Welding Speed on the Microstructure and Mechanical Properties of a Duplex Stainless Steel. *Mater. Sci. Eng., A* **2008,** *496* (1–2), 262–268.
14. Buffa, G.; Hua, J.; Shivpuri, R.; Fratini, L. A Continuum Based FEM Model for Friction Stir Welding—Model Development. *Mater. Sci. Eng., A* **2006,** *419* (1), 389–396.
15. Chiumenti, M.; Cervera, M.; Agelet de Saracibar, C.; Dialami, N. Numerical Modeling of Friction Stir Welding Processes. *Comput. Meth. Appl. Mech. Eng.* **2013,** *254,* 353–369.
16. Schmidt, H.; Hattel, J.; Wert, J. An Analytical Model for the Heat Generation in Friction Stir Welding. *Modell. Simul. Mater. Sci. Eng.* **2004,** *12* (1), 143–157.
17. Assidi, M.; Fourment, L.; Guerdoux, S.; Nelson, T. Friction Model for Friction Stir Welding Process Simulation: Calibrations from Welding Experiments. *Int. J. Mach. Tool. Manuf.* **2010,** *50* (2), 143–155.
18. Schmidt, H. B.; Hattel, J. H. Thermal Modelling of Friction Stir Welding. *Scr. Mater.* **2008,** *58* (5), 332–337.

www.iran-mavad.com
مرجع مهندسی مواد و متالورژی

19. Lee, W. S.; Cheng, J. I.; Lin, C. F. Deformation and Failure Response of 304L Stainless Steel SMAW Joint under Dynamic Shear Loading. *Mater. Sci. Eng., A* **2004,** *381* (1), 206–215.
20. Nandan, R.; DebRoy, T.; Bhadeshia, H. K. D. H. Recent Advances in Friction-stir Welding – Process, Weldment Structure and Properties. *Prog. Mater. Sci.* **2008,** *53* (6), 980–1023.
21. Bever, M. B.; Holt, D. L.; Titchener, A. L. The Stored Energy of Cold Work. *Prog. Mater. Sci.* **1973,** *17,* 190.
22. Zhu, Q.; Sellars, C. M.; Bhadeshia, H. K. D. H. Quantitative Metallography of Deformed Grains. *Mater. Sci. Technol.* **2007,** *23* (7), 757–766.
23. Mishra, R. S.; Ma, Z. Y. Friction Stir Welding and Processing. *Mater. Sci. Eng., R* **2005,** *50* (1), 1–78.
24. Zhu, X. K.; Chao, Y. J. Numerical Simulation of Transient Temperature and Residual Stresses in Friction Stir Welding of 304L Stainless Steel. *J. Mater. Process. Technol.* **2004,** *146* (2), 263–272.
25. Brown, W. F.; Mindlin, H.; Ho, C. Y. *Aerospace Structural Metals Handbook;* CINDAS/Purdue University, 2001.
26. Bisadi, H.; Tavakoli, A.; Tour Sangsaraki, M.; Tour Sangsaraki, K. The Influences of Rotational and Welding Speeds on Microstructures and Mechanical Properties of Friction Stir Welded Al5083 and Commercially Pure Copper Sheets Lap Joints. *Mater. Des.* **2013,** *43,* 80–88.
27. Ghosh, M.; Kumar, K.; Mishra, R. S. Friction Stir Lap Welded Advanced High Strength Steels: Microstructure and Mechanical Properties. *Mater. Sci. Eng., A* **2011,** *528* (28), 8111–8119.
28. Awang, M.; Mucino, V. H.; Feng, Z.; David, S. A. Thermo-mechanical Modeling of Friction Stir Spot Welding (FSSW) Process: Use of an Explicit Adaptive Meshing Scheme. *SAE Int. Paper* **2005,** *1,* 1251–1256.
29. Lienert, T. J.; Stellwag, W. L., Jr.; Lehman, L. R. *Comparison of Heat Inputs: Friction Stir Welding vs. Arc Welding.* http://174.122.108.74/conferences/abstracts/2002/011.pdf (accessed 30 March 2013).
30. Frigaard, O.; Grong, O.; Midling, O. T. A Process Model for Friction Stir Welding of Age Hardening Aluminum Alloys. *Metall. Mater. Trans. A* **2001,** *32* (5), 1189–1200.

www.iran-mavad.com
مرجع مهندسی مواد و متالورژی

6.14 Bonding Technologies in Manufacturing Engineering

SM Homayouni and MR Vasili, Lenjan Branch, Islamic Azad University, Isfahan, Iran
TS Hong, Universiti Putra Malaysia, Selangor, Malaysia

© 2014 Elsevier Ltd. All rights reserved.

6.14.1	Introduction	237
6.14.2	Direct Bonding	237
6.14.3	Thermocompression Bonding	239
6.14.4	Surface Activated Bonding	241
6.14.5	Adhesive Bonding	242
6.14.6	Eutectic Bonding	243
6.14.7	Glass Frit Bonding	243
6.14.8	Concluding Remarks	244
References		244

6.14.1 Introduction

Since its invention in the 1950s, integrated circuits have been a solution for smaller size of devices. Introducing three-dimensional integrated circuits (3D IC) was a great mutation to decrease the total area of the integrated circuits. According to Lin et al. (*1*), 3D IC refers to multiple conventional device layers/chips/wafers that may be stacked vertically and electrically interconnected. They stated that improvements in 3D IC technology are expected to dramatically enhance performance, functionality, and device packaging density of microelectromechanical systems (MEMS) (also written as micro-electro-mechanical systems) applications. MEMS are composed of very small, portable, and fragile components should be packed for protection at silicon-based wafer (*2*). Among various technologies required to fabricate 3D ICs, bonding technology is the most important. Bonding process in 3D integration can be performed for structure enhancement by oxide or polymer bonding or for electrical connection by metal bonding (*1*). An integration of the electronic components (e.g., complementary metal–oxide–semiconductor (CMOS) circuitries) with the mechanical (e.g., resonators) or optical components (e.g., waveguides, mirrors) in a single, wafer-level process step is a result of using wafer bonding techniques in MEMS manufacturing (*3*). In order to maximize the advantages of both bonding techniques, hybrid bonding, metal-to-metal bonding, and oxide-to-oxide (or polymer-to-polymer) bonding, becomes a promising bonding technology in 3D IC.

Wafer bonding that can be divided into two groups, namely, direct bonding and intermediate layer bonding, is an important fabrication technique in MEMS and manufacturing of silicon-on-insulator (SOI) substrates (*4*). According to Ko and Chen (*5*), wafer bonding methods include low-temperature bonding methods and thermocompression bonding approach. They have categorized low-temperature bonding method into direct bonding, surface activated bonding (SAB), adhesive bonding, eutectic bonding, and nonmetal bonding. These methods work in room temperature up to 400 °C. Wafer bonding has found applications in MEMS to fabricate MEMS devices, to encapsulate the MEMS device in a hermetic environment, and to transfer bond a complete MEMS device to a wafer with integrated circuits. Wafer bonding has found its earliest applications for pressure sensors and accelerometers, but the applications remain boundless (*6*). In the following sections, six different techniques for wafer bonding, including direct bonding (Section 6.14.2), thermocompression bonding (Section 6.14.3), SAB (Section 6.14.4), adhesive bonding (Section 6.14.5), eutectic bonding (Section 6.14.6), and glass frit bonding (Section 6.14.7), are investigated, and a brief review of the current state of the art for each technique is described.

6.14.2 Direct Bonding

Bonding, in the strict sense of the term, is the 'glueless' joining together of two bodies/materials, and has always been considered as a high-tech process (*7*). It has consisted of various different technological options over time. In this regard, direct bonding (also referred to as glueless bonding or van der Waals bonding) is the phenomenon that occurs when two clean enantiomorphic surfaces, having complementary shapes, are brought into contact and at that very moment bond spontaneously. Flat, smooth, and clean surfaces of materials are prerequisites for direct bonding (*8*). Pretreatment of surfaces before the wafer bonding can improve the surface adhere energy to join wafers. For example, Tang et al. (*9*) stated that surface modification to increase hydrophilicity (increasing the number of hydrogen bonds via the interface) is one of the possible pretreatment methods. Moreover, they emphasized that increasing the direct contact area can improve the simplicity of direct bonding. As shown in **Figure 1**, surfaces (a) and (b) have the same root-mean-square roughness; however, surface (a) is more suitable for an easier direct bonding than surface (b).

www.iran-mavad.com
مرجع مهندسی مواد و متالورژی

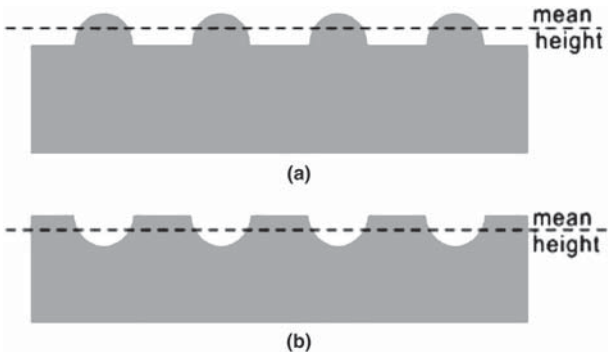

Figure 1 Two surfaces with identical root-mean-square roughness. Reproduced from Tang, Z.; Peng, P.; Shi, T.; Liao, G.; Nie, L.; Liu, S. Effect of Nanoscale Surface Topography on Low Temperature Direct Wafer Bonding Process with UV Activation. *Sens. Actuators A Phys.* **2009**, *151* (1), 81–86.

Simply defined, direct bonding consists of contacting two wafer surfaces without any adhesive or additional materials to promote the adhesion between the two surfaces. It allows different materials to be stacked together without concern for the crystalline relationship to one another (*10*). Under such circumstances, direct bonding is considered more difficult in comparison with the bonding techniques accompanied by dedicated intermediate layers between the wafers (*6*). Considering its historical evolution, direct bonding was mostly used in classical optical instruments (e.g., interferometers) in the years prior to World War II. However, subsequent to World War II, there was a rapid growth of bonding technologies in the sense that two bodies are united by additional processing of a direct bond. At this stage, direct bonding was mainly applied in semiconductor technology, optoelectronics, micromechanics, and microelectromechanics. With the advent of Si semiconductor and of SOI technologies, direct bonding was shown to have great promise for special applications in electromechanics, electro-optics, and advanced integrated circuits, so that the most well-known application of direct bonding today is the mass production of SOI bonded structures. In recent years, direct bonding has been investigated for a wide variety of materials, which has consequently resulted in significant upgrades in terms of flatness, smoothness, and cleanliness (*10*,*11*). Moreover, the latest advances in direct bonding have led to the development of low-temperature bonded structures well suited for new applications such as microtechnologies, optical devices, biotechnologies, and 3D integration (*12*). One of the important advantages of direct bonding over other techniques is that by using standard microtechnologies and microelectronics tools, most of the direct bonded structures can be subsequently processed, which is a considerable point for developing new stacked structures (*10*).

For a successful direct bonding, the two materials to be bonded have to be geometrically, mechanically, physically, chemically, and thermally compatible (see **Table 1**). This compatibility is a key concept in direct bonding. Needless to say, this does not mean that direct bonding is restricted to materials of a specific composition and of specific crystallographic property. The materials to be directly bonded may be monocrystalline, polycrystalline, amorphous, or even composite. Haisma et al. (*8*) provided some examples of the direct bonding of materials with different compositions and crystallographic properties, including monocrystalline to monocrystalline, monocrystalline to polycrystalline, monocrystalline to amorphous, polycrystalline to polycrystalline, amorphous to polycrystalline, amorphous to amorphous, and amorphous to a composite. The results provided a good impression of the wide range of possibilities of direct bonding, while the main problem was found to be how to obtain sufficiently flat, smooth, and clean surfaces. A good example of the direct bonding of monocrystalline to polycrystalline is an optimized flux rotor, which has been designed for (mini) motors. As illustrated in **Figure 2**, this rotor is an all-magnetic element. It consists of a central part of hard-magnetic material, in polycrystalline form, both sides of which are bonded to a monocrystalline soft-magnetic material, a spinel. The hard-magnetic material has been polished flat and smooth to a bondable level in its magnetized state. This has resulted in a hard-magnetic to soft-magnetic transition. Since there is no gap between the two materials, no flux losses occur across the interface.

Table 1 The compatibility requirement of two materials for a successful direct bonding

Type of compatibility	*Characteristics*
Geometrical	Related to the shape of the surfaces and also patterning at the interface. The materials' conditions have to allow surface contact on full wafer scale.
Mechanical	Related to the surface and subsurface states. The surfaces have to be free of mechanical irregularities and subsurface crystallographic defects to a level of at least a few nanometers.
Physical	Related to the defects in the material: grain boundaries, dislocations, twins, and also spikes, formed during heteroepitaxial growth.
Chemical	Related to not only the chemical surface state but also the presence of contaminants and also dopants – matters of paramount importance in semiconductor integrated circuit applications.
Thermal	Related to the expansion and/or chemical reaction of the two materials as a function of temperature.

Adapted from Haisma, J.; Spierings, G. A. C. M.; Michielsen, T. M. Frameworks for Direct Bonding. *Philips J. Res.* **1995**, *49* (1–2), 11–21.

www.iran-mavad.com
مرجع مهندسی مواد و متالورژی

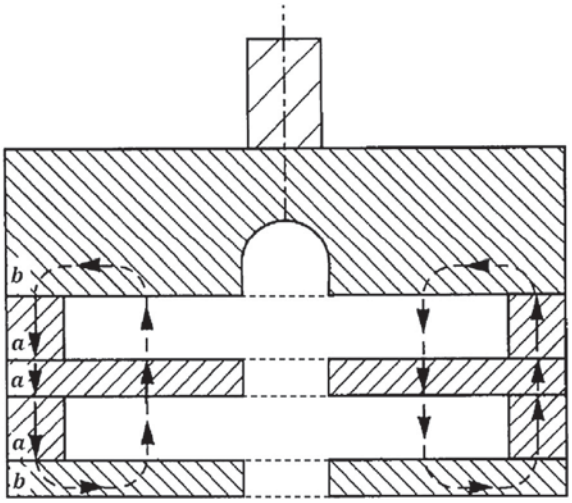

Figure 2 Schematic representation of an all-magnetic (mini) motor rotor. (a) Hard-magnetic polycrystalline material; (b) Monocrystalline soft-magnetic spinel. Reproduced from Haisma, J.; Spierings, G. A. C. M.; Michielsen, T. M. Frameworks for Direct Bonding. *Philips J. Res.* **1995**, *49* (1–2), 11–21.

Moriceau et al. (*10*) reviewed some key features of direct bonding from both experimental and practical point of views. In order to better identify the important parameters impacting the quality and reliability of the direct bonding, some indications on the physical and chemical mechanisms involved in this process were provided. They described mechanisms and report results on Si and SiO_2 bonding processes and their focus was mainly on the improvements that allow obtaining strong and high-quality bonding in low-temperature process. It was demonstrated that direct bonding can be applied as well to metal bonding, mainly to obtain conductive bonding, on the condition that an efficient process can be used for surface preparation (e.g., smoothing by chemo-mechanical polishing). It was shown that direct bonding is well suited for many heterostructures via low-temperature process, for instance.

Through investigation of all the above factors, it can be observed that direct bonding has evolved into an advanced, delicate technology and it has been used extensively for assembling materials or components in the microelectronics and microsystem industries. However, since direct bonding is more technologically dedicated than cost effective, its applications have to be selected accordingly.

6.14.3 Thermocompression Bonding

According to Fan et al. (*13*), metal-to-metal thermocompression bonding shows superior advantages in 3D IC. It enables hermetic seal, mechanical support, and electrical contact in one simultaneous step. Metal-to-metal thermocompression bonding does not require smooth surface, and there is no risk of structural degradation or electrical short. Three kinds of features would affect the quality of the thermocompression bonding method (*14*):

- Layer properties (surface roughness and surface chemistry)
- Bonding environment (bonding pressure, temperature, vacuum level, and duration of bonding)
- Instrumentation and control

Table 2 provides an overview of papers on thermocompression bonding methods. Tang et al. (*15*) stated that copper (Cu) has been proposed as a metal-level bonding medium because of its high electrical and thermal conductivity. Less cost and simpler design method attracted more and more of industry and academia efforts for researches on thermocompression of Cu wafers. Better electrical conductivity, mechanical strength, and electromigration resistance makes Cu wafers more suitable among different metal-to-metal bonding materials (*13*). The higher bonding temperature leads to higher energy for copper atoms in two bonded layers to diffuse and allows grains to grow (*16*). However, electronic devices may be destroyed under higher temperatures. Therefore, bonding temperature of Cu wafers cannot be increased unrestrictedly (*4*). A trade-off between the temperature of the thermo-compression bonding of copper layers and thus the quality of bonds and the reliability of the devices is required for further extension of Cu bonding applications.

Tsau et al. (*17*) have described a thermocompression bonding method for silicon wafers using a thin layer of gold, in which the temperature is increased to 300 °C under 7 MPa pressure. Later, Spearing et al. (*18*) modeled a thermocompression bonding method for gold in wafer level to fabricate MEMS devices. Au wafers under moderate temperature and pressure cause in a hermetic and conductive bond. They have performed finite element analysis to disclose effects of local pressure variations on the quality of wafer

www.iran-mavad.com
مرجع مهندسی مواد و متالورژی

Table 2 Main contributions in thermo-compression bonding methods

Reference	*Material*	*Main achievement*
Tang et al. (*15*)	Cu–Cu	Cu–Cu wafer surface through interdiffusion of Cu atoms
Made et al. (*14*)	Cu–Cu	Analytical model to optimize the quality of bonding method
Fan et al. (*13*)	Cu–Cu	Various bonding temperatures have been investigated
Tsau et al. (*17*), Spearing et al. (*18*)	Au–Au	Analysis of finite elements and a cohesive zone model for nonideal load displacement in wafer bonding
Tsau et al. (*19*)	Au–Au	Analysis of effects of various pressure, temperature, and time parameters on toughness of bonds
Jang et al. (*22*)	Cu–Cu	Higher adhesive energy in lower temperatures, using postannealing in N_2 for 1 h
Chen et al. (*16*)	Cu–Cu	Investigation on effects of various temperatures and bonding duration on the quality of bonds
Zhou et al. (*23*)	W–W	First applicable bonding process for tungsten to tungsten wafers
He et al. (*20*)	TiAl–steel	Discussion on the relationship of the bond parameters and tensile strength of the joints; Determination of the optimum bond parameters
Das et al. (*21*)	Alumina-Kovar	Investigation on the effects of time duration and pressure on the bonding strength

bonding. Tsau et al. (*19*) have tested effects of various pressure (30–120 MPa), temperatures (260 and 300 °C), and time (2–90 min) on the bond toughness. They concluded that higher temperature and pressure lead to higher toughness bonds. He et al. (*20*) have studied an intermetallic chemical compound (titanium aluminide, TiAl) and steel diffusion bonding method using composite barrier layers of titanium/vanadium/copper. **Figure 3** shows the microstructures of the cross section of the TiAl/titanium/vanadium/copper/steel joint diffusion bonded at 1273 K and 20 MPa for 1.2 ks. The strength of the resulting joint is 420 MPa, which is a reliable bonding method for manufacturing TiAl and steel layers. Das et al. (*21*) developed a thermocompression bonding method for alumina ceramics and Kovar (nickel–cobalt ferrous alloy composition, FerNiCo1) using aluminum interlayers. They have concluded that bonding strength increases as the bonding pressure (7.5–75 MPa) and bonding time (10–90 min) increase, under the temperature of 600 °C.

Chen et al. (*16*) have increased both temperature and bonding duration simultaneously while using the mechanical dicing, the tape, the pull, and the push tests to investigate the effects of various temperatures and bonding duration on the quality of bonds. Furthermore, they have performed thermal annealing after bonding to improve bond strength. The results reveal that increases in the bonding temperature or annealing duration result in higher bond strength. However, they concluded that postbonding annealing would improve the bond strength only if the bonding temperature is above 300 °C. Tadepalli et al. (*4*) considered the toughness of Cu–Cu thermocompression bonds, for the application of interfacial loading with mixed variable modes, using a bonded chevron specimen with layers of different thicknesses. They concluded that the asymmetric chevron test can be used to predict the yield and reliability of bonded structures that are subjected to a range of different loading conditions during fabrication and application. Zhou et al. (*23*) have proposed the thermocompression bonding method for tungsten to tungsten for the first time. This process needs very high temperature (up to 700 °C) and pressure (up to 50 MPa) for several hours. This process may result in an applicable mass fabrication of 3D tungsten structures.

Although the application of thermocompression bonding of Cu–Cu wafer joining has been emphasized in previous paragraphs, Radu et al. (*24*) have focused on nonthermocompression bonding of Cu–Cu wafers. They have reported that minimizing the

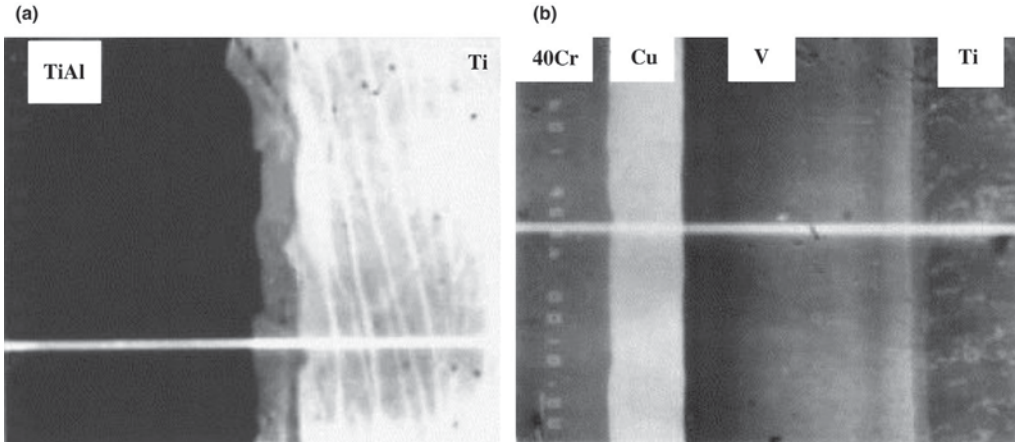

Figure 3 Interfacial microstructure of the titanium/vanadium/copper/steel joint. (a) At the TiAl/titanium interface; (b) At the titanium/vanadium/copper/steel interface. Reproduced from He, P.; Feng, J. C.; Zhang, B. G.; Qian, Y. Y. A New Technology for Diffusion Bonding Intermetallic TiAl to Steel with Composite Barrier Layers. *Mater. Charact.* **2003**, *50* (1), 87–92.

www.iran-mavad.com
مرجع مهندسی مواد و متالورژی

postbond annealing at temperatures below 400 °C can be achieved through optimization of process conditions. Moreover, the wafer-to-wafer nonthermocompression bonding allows high throughput (up to 14 wafers per hour). Nonthermocompression bonding of Cu–Cu wafers decreases the contact resistivity allowing efficient electrical conductivity. Jang et al. (*22*) have examined lower bonding temperature (300 °C) for thermocompression of Cu wafers. They recognized that although higher temperatures lead to better quality of Cu–Cu connections, diffusion of Cu atoms in other Cu layers at low bonding temperature in addition to annealing treatment after the bonding method is also effective.

In thermocompression bonding, the required adhesion for bonding of Cu films is provided by using enough force and heat. Intradiffusion of Cu atoms avoid necessity of ultraclean surface and ultrahigh vacuum. Higher bonding temperature enhances diffusion and provides higher bonding quality. However, increase in temperature is restricted by the limits of the electronic devices kept inside the wafers. This is an interesting research area to achieve higher quality of the Cu bonding method at lower temperatures. The lowest temperature for thermocompression bonding of Cu layers is 300 °C (*15*). Made et al. (*14*) described an analytical model for bonding temperature, pressure, and duration for metal–metal thermocompression bonds. This model is able to predict the parameters for quality of the bonding process. The model has been verified through experiments on Cu–Cu thermocompression bonds of electroplated Cu on diced silicon wafers with chemically/mechanically polished surfaces. Fan et al. (*13*) have analyzed effects of various bonding temperature (250, 300, and 350 °C) on wafer-level Cu-to-Cu thermocompression bonding. The best hermetical seals were reported at 350 °C; however, wafers bonded at 250 and 300 °C showed better performance than the one defined by the MIL-STD-883E standard. Lu et al. (*25*) proposed a low-temperature solid-state bonding method for two layers of Cu and Ni in 3D integrated circuits. Their microscopic observations showed a thin layer of intermetallic compound formed in the bonding surface, which is a promising solid-state bonding method for 3D integration. They stated that this joining method was carried out at 190 °C, which is much lower than the regular temperature for thermocompression bonding of Cu–Cu wafers. Reduction of energy consumption and lower reliability risks are the main achievements of their method.

6.14.4 Surface Activated Bonding

In contrast to the thermocompression wafer bonding methods, which need higher level of temperature to join layers of metals, the SAB method is an exceptional method performed at room temperature. The SAB technique provides lower thermal stress and defects in addition to strong bonding strength at room temperature without any annealing step (*5*). The SAB technique is capable of bonding various dissimilar materials without any adhesive. Two surfaces must be atomically clean, which is done by using ion beam attack or plasma activation (*26*). Among different surface treatment bonding methods, the SAB technique provides clean and activated surfaces having higher level of bonding energy (*25*). SAB techniques result in clean surfaces and incomplete chemical bonds, which are active and highly desirable to react with other atoms to form bonds (*27*). **Figure 4** provides a schematic view of the SAB bonding method.

In order to remove contaminant layers and absorbed molecules, and bring into contact at room temperature, two surfaces are activated using argon fast atom beam bombardment (*5*). Once the surface is activated, it should be kept active and clean until joining. Therefore, a high vacuum system is required for the activation and the bonding processes (*27*). Then, two unstable and reactive surfaces are mated and contacted in a small area. This contact area makes chemical bonds between the surfaces spontaneously, at room temperature and pressure-free conditions (*5,26*). According to Suga (*26*), the SAB technique has been applied to a wide variety of materials (such as silicon-to-silicon, silicon-to-ceramic, metal-to-metal, and metal-to-ceramic bonding). However, it is not effective for ionic materials such as glass, sapphire, and silicon oxide. He emphasized that the exact reason is not clear; nonetheless, it is guessed that ionic impulsively polarized materials may prevent any reduction of surface energy resulting from solid contact.

According to Taniyama et al. (*28*), the bonding possibility of Si–Si, Au–Au, and Cu–Cu wafers has been confirmed at room temperature using the SAB technique. They stated that while vacuum pressure is a vital factor for Si–Si wafer's room temperature bonding, it is not so important for the Au–Au and Cu–Cu wafer bonding. Moreover, heating at 200 °C may improve the bonding strength of Cu–Cu and Au–Au wafers up to 12.4 MPa, but it is not sensitive for the Si–Si wafer bonding and its strength reaches 16 MPa. Higurashi et al. (*29*) have proposed an SAB technique for two layers of gold at a relatively low temperature of 150 °C. They used this method to fabricate a compact and thin optical microsensor.

Figure 4 Surface activated bonding flow. Reproduced from Ko, C. -T.; Chen, K. -N. Low Temperature Bonding Technology for 3D Integration. *Microelectron. Reliab.* **2012**, *52* (2), 302–311.

www.iran-mavad.com
مرجع مهندسی مواد و متالورژی

Howlader et al. (30) have introduced an SAB technique for direct bonding of aluminum and stainless steel. They claimed that the strength of their specimens using this technique is more than 60 MPa and up to 100 MPa. Moreover, Howlader and Zhang (31) have applied SAB technique at higher temperatures on Si–Si wafer layers. They bonded the layers at room temperature and annealed it at up to 600 °C. In this technique, the bonding strength has been measured as high as 20 MPa. They have stated that the current density and amorphous layer of the interface are correlated as a function of the annealing temperature.

Colinge et al. (32) have proposed a germanium-to-silicon wafer bonding using SAB technique at low temperature, which is annealed at 200–300 °C. Kühne and Hierold (33) presented low-temperature wafer bonding for Si–SiO_2 plasma-activated surfaces hybridized by eutectic binding of ultrathin Au–Sn layers. They stated that the hybrid wafer-level bonding and interconnection technology enables the metal interconnects and multiple materials in stacked MEMS devices to be integrated. According to Ko and Chen (5), Si–Si, Au–Au, and Cu–Cu wafers have been bonded by using SAB technique in the University of Tokyo, at bonding energy of 1.95 J m^{-2} and strength of 12 MPa.

6.14.5 Adhesive Bonding

Adhesive bonding is a low-temperature technique in which a defect-free intermediate adhesive polymer layer is used for bonding in various patterns (5). Adhesive wafer bonding does not require special wafer surface treatments such as planarization and excessive cleaning. Cakmak et al. (34) stated that the most important properties of the bonding layers can be summarized as isotropic dielectric constants, good thermal stability, low Young's modulus, and good adhesion to different substrates. The main advantages of adhesive wafer bonding are as follows (35):

- Relatively low bonding temperatures (depending on the polymer material between room temperature and 350 °C)
- Insensitivity to the topology of the wafer surfaces
- Compatibility with standard CMOS wafers
- Ability to join practically any wafer material

Simplicity, robustness, and low cost are the most important characteristics of adhesive wafer bonding compared to other wafer bonding methods. However, limited temperature stability is the most important concern of adhesive wafer bonding. In addition, lower accuracy of bonding due to the shrinkage property of adhesives restricts the application of the adhesive bonding method. Thus, this bonding technique is usually applied wherever lower bonding accuracy is required, or a hybrid of adhesive bonding and other bonding methods may increase the bonding strength (5).

A polymer adhesive is used on the surfaces of the wafers to be bonded. The wafers were joined to each other under a predefined pressure to force the wafer surfaces into intimate contact and the wafer stack is heated (36). Then, the adhesive is converted from a liquid or viscoelastic state into a solid state, usually by exposing the polymer adhesive to heat or ultraviolet light. During this conversion, the adhesive film may reflow to accommodate surface topography or particles, and the adhesive is cured to form cross-link networks providing a robust bonding interface with high thermal and mechanical stability (35). Typically, thermosetting polymers (e.g., benzocyclobutene (BCB), SU-8, and Parylene) and thermoplastic polymers are used as intermediate polymer adhesive (e.g., polymethyl methacrylate, used mostly for temporary bonding requirements). Ko and Chen (5) stated that nowadays BCB and SU-8 are the most popular adhesives for precise bonding requirements under 250 °C with outstanding wafer bonding capability, chemical/thermal resistance, and bonding strength.

Niklaus et al. (37) have proposed a novel method to prevent aligned wafers from shifting relative to each other during adhesive bonding. They stated that in adhesive wafer bonding, the intermediate layer is in a liquid state to make bonds. Under bonding pressure, it is unavoidable to prevent shear forces, and thus, the wafers move relative to each other. In commercial application of adhesive wafer bonding, wafer alignment accuracy is typically 2–5 μm. Niklaus et al. (37) have invented a structure-based bonding area for adhesive wafer bonding to provide a solid-state material contact between the two wafers during the bonding process, which prevents the wafers from moving on the other surface. Oberhammer et al. (38) described an adhesive wafer-level bonding technique in which the adhesive material is structured prior to bonding. They investigated on the parameters required for the quality of bonding. Dry etch BCB and photosensitive BCB have been used as the intermediate layers for adhesive wafer bonding. While soft baking of the dry etch BCB to a polymerization degree of 50–60% is necessary for its sticky state and patterning procedure, this process is not necessary for the photosensitive BCB.

Pang et al. (39) have studied SU-8 as an intermediate layer for adhesive wafer bonding to investigate the bonding parameters required for the quality of bonding. They stated that prebake time, pumping time, and thickness of the intermediate layer are the most effective factors in the quality of the bonding. In their experiment, 90% of the area has successfully been bonded with an ultimate yield of 70% of the sensors. The measured bonding strength was 17.15 and 19.6 MPa for wafers bonded at 80 and 100 °C, respectively. Huesgen et al. (40) have optimized an adhesive wafer bonding process based on Ordyl SY300, an acrylic permanent dry-film photoresist. Their results show a bond yield of 95% and tensile bond strength of 13.36 ± 2.36 MPa for the optimized adhesive wafer bonding process tested on a structure with a feature size of 6 mm × 6 mm. They stated that the bond yield increases as the feature size decreases.

Cakmak et al. (34) have researched on SINR™ polymer materials (material from Shin-Etsu MicroSi) for adhesive bonding wafers. They used statistical analysis methods to optimize the parameters required for substrate coating process as well as wafer bonding process. The results show repeatability and reliability of coating processes. They stated that the behavior of SINR™ during the bonding

www.iran-mavad.com
مرجع مهندسی مواد و متالورژی

process makes it appropriate for applications requiring substrate planarization prior to bonding and well-defined adhesive layer thickness. Kim et al. (41) investigated on various photopatternable polymer adhesive materials for the selective wafer bonding of MEMS. They used bonding strength and residual stress and reliability tests to select the most appropriate adhesive material for the piezoresistive MEMS motion sensors. According to their bonding strength results, epoxy-based resin showed the best bonding strength of upto 42.9 MPa. Moreover, silicone-based resin showed the lowest residual stress of 3 MPa and the best reliability performance. Forsberg et al. (42) have tested the application of off stoichiometry thiolene-epoxy, OSTE(+), for adhesive wafer bonding. They stated that OSTE(+) combines a high bond energy, while still being easily removable in oxygen plasma. This makes OSTE(+) a promising candidate for heterogeneous integration technologies.

6.14.6 Eutectic Bonding

Metal eutectic wafer bonding is a popular bonding technique and a key technique for the semiconductor industry to establish strong bonds and hermetic seals (5). A eutectic alloy composition is generated in this bonding method. A eutectic alloy is a metal composition of two or more solid phases that precipitate at constant temperature from one uniform liquid phase. Those two or more phases are completely insoluble in solid state. The eutectic point of a melt is the point at which the composition of the components is exactly in a state that both constituents solidify from the melt directly (43). Usually, the eutectic point of two different metals is lower than their melting point; thus, the eutectic wafer bonding method is a low-temperature one (44). Liquid state of the interface of the metal layers results in surface planarization and provides a tolerance of surface topography and particles (5). Baum et al. (45) stated that eutectic wafer bonding gains more and more attention because of its hermetical sealing and electrical interconnection abilities within one bonding process. Lower process temperature, low resulting stress, and high bond strength are the other advantages of eutectic wafer bonding technology (45). Ko and Chen (5) stated that the eutectic wafer bonding technology does not need any ultrahigh vacuum bonding condition or postbond annealing treatment. The commonly used eutectic bonding materials include Al–Si (at temperature of 600 °C), Au–Si (at temperature of 380–400 °C), Au–Sn (at temperature of 300 °C), Au–In (at temperature of 275 °C), Cu–Sn (at temperature of 250–270 °C), Pb–Sn (at temperature of 190 °C), In–Sn (at temperature of 120 °C), etc. (5,44,46).

Kim et al. (47) have presented Au–Sn eutectic bonding for radio-frequency MEMS (RF-MEMS) application. They used an experimental process design that optimized bonding parameters and bonding temperature. Bonding can be done at a relatively low temperature below 300 °C. In a related research, Wang et al. (48) presented a low-temperature Au–Sn eutectic bonding technology wafer-level packaging scheme for RF-MEMS. The wafer bonding has been used at temperatures below 300 °C as a multilayer metallization for hermetic sealing. Moreover, Kwon and Lee (49) have used an Au–Sn eutectic wafer bonding to fabricate an MEMS condenser microphone with rigid back plate to improve acoustic characteristics.

Mitchell and Najafi (50) reported the results of encapsulation of MEMS devices using an Au–Si eutectic wafer bonding at a temperature of 390 °C. In the Au–Si eutectic bonding process, a cap wafer with Au bond rings is bonded to a device wafer with either poly-Si or gold bond rings that encircle the MEMS devices. In another related research, Lin et al. (51) have studied an Au–Si eutectic wafer-to-wafer bonding technique and tested different dimensions of Au layers to bond Si wafers. They specified that bond strength is inversely proportional to Si atom percentage. Lin et al. (51) have applied an adhesive layer of chromium and titanium with thicknesses of 10 nm and 30 nm, respectively. They stated that the Au–Si eutectic wafer bonding can be easily separated in the absence of such adhesive layer. Baum et al. (45) have investigated Au–Si and Al–Ge eutectic wafer bonding technology. They claimed that the bonding strength and the mechanical behavior of these two wafer materials are the same. However, the resistivity of the Al–Ge structure has been reported to be smaller than that of the Au–Si structure. Kühne and Hierold (52) have described that hybrid low-temperature bonding is composed of hydrophilic direct bonding of plasma-activated Si/SiO_2 surfaces and eutectic wafer bonding of the Au–Sn for the simultaneous interconnection. Thus, the proposed hybrid bonding and interconnection technology allows for the integration of metal interconnects and multiple materials in stacked MEMS devices.

Kühne and Hierold (33) have hybridized Au–Sn eutectic bonding and reflows at 300 °C and hydrophilic direct bonding of plasma-activated $Si–SiO_2$ surfaces in a test feature structure. They proposed this hybrid wafer bonding technology for the integration of metal interconnects and multiple materials in stacked MEMS devices. Gradin et al. (53) have proposed wafer-level Au–Si eutectic bonding process for TiNi to silicon integration to fabricate a novel gas microvalve. Henry and Ahlers (54) have examined the theory that platen (Pt) is a diffusion barrier for Au–Si eutectic bonding. Their results show that Pt layers of any thickness between 20 and 200 nm begin to fail at a temperature of 375 °C, which is only 12 °C above the eutectic temperature of Au–Si, and result in reductions of bond strength and hermeticity. They proposed silicon dioxide as an alternative diffusion barrier at 400 °C for Au–Si eutectic wafer bonding.

6.14.7 Glass Frit Bonding

Glass frit bonding technology is a wafer bonding method using an intermediate glass layer. This bonding technology is processed at temperatures below 450 °C. Almost all the materials used in MEMS can be bonded using glass frit (55). A low-melting-point glass that is available commercially is used to join two or more wafers (56). Typically, the intermediate layer of the wafer bonding (glass frit) is patterned on the cap wafer. Among all the wafer bonding technologies, glass frit bonding is thought to be one of the most

www.iran-mavad.com
مرجع مهندسی مواد و متالورژی

suitable technologies for MEMS packaging (2). Hermetic sealing, high process yield, less residual stress at the bonding interface, and the possibility of metallic lead through high bonding strength and good reliability are the main advantages of the glass frit bonding method (55). This bonding method is based on the low melting point of glass as the intermediate layer. In glass frit bonding technique, the material must be soft enough to wet the surface for bonding the wafers and seal the MEMS structures, but not too soft to flow into them (57). Knechtel (55) stated that maintaining soft bonding material between two bonding layers and relatively higher process costs are the most important challenge of glass frit bonding.

Dresbach et al. (58) have studied the parameters required for the long life of the glass frit bonding applied in micromachined acceleration sensors in automotive industries. These parameters include material's resistance against crack propagation, the stress situation in a micropackage, and the long-term strength behavior. Based on their results for the basic lifetime prediction of glass frit bonding, toughness, residual stress, and the linear thermal expansion coefficient of the used specimen were calculated as 0.57 MPa$\sqrt{m}$, 126 MPa, and 5.6e-6 K^{-1}, respectively. Nötzold et al. (59) have reported their experiments of the temperature-dependent fracture toughness parameters of the glass frit bonding used in microsensors. They showed that external pure tensile or combined tensile and shear loading on the bonding layer affect the fracture toughness parameter. From low temperatures to higher ones, the crack path changes from an alternating crack to a crack that grows straight through the middle of the bonding layer.

Chen et al. (2) have developed a new barrier trench technology to improve the uniformity of the dimension of glass frit during bonding process. They claimed that the proposed method provides wafer-level hermetic packaging of MEMS devices by using glass frit with the advantages of cost effectiveness, easy handling, and high performance. The shear test and water test show that the reliability in terms of shear strength and leakage fulfilled the corresponding MIL-STD. Naumann et al. (60) have studied the key parameters required to ensure functionality and reliability of a bonding seal using the glass frit bonding technology. Wu et al. (61) bonded an MEMS resonator wafer and a cap wafer together using glass frit bonding. They explained that vertical connection between the cap and the resonator wafer is provided by the silicon bumps. They also applied Au–Al eutectic bonding to ensure electrical contacts between the cap wafer and the device wafer. Cruz et al. (62) studied the formation of a hermetic bonding layer using a laser-assisted glass frit bonding technique for encapsulating devices composed of glass substrates. Excellent contact with both substrates, and no gas inclusions or voids, is the main advantage of their proposed method showing that an effective sealing was achieved.

6.14.8 Concluding Remarks

In this chapter, different aspects of various bonding techniques and their associated characteristic features were reviewed. The aim of the chapter was mainly to provide researchers and engineers with an understanding of how to choose and apply existing techniques effectively. To accomplish this, a wide range of issues that can and should be controlled in order to engineer new structures and devices using these techniques were investigated. Brief descriptions of the current state of the art in bonding technologies and discussions on future prospects were presented. One can conclude that although in recent years there has been a proliferation of bonding technologies and their applications in assembling materials or components, these technologies are still being heavily researched in order to achieve new improvements that support strong, high-quality, and high-reliability bonding.

References

1. Lin, S. L.; Huang, W. C.; Ko, C. T.; Chen, K. N. BCB-to-Oxide Bonding Technology for 3D Integration. *Microelectron. Reliab.* **2012,** *52* (2), 352–355.
2. Chen, X.; Yan, P.; Tang, J.; Xu, G.; Luo, L. Development of Wafer Level Glass Frit Bonding by Using Barrier Trench Technology and Precision Screen Printing. *Microelectron. Eng.* **2012,** *100,* 6–11.
3. Dragoi, V.; Pabo, E.; Burggraf, J.; Mittendorfer, G. CMOS: Compatible Wafer Bonding for MEMS and Wafer-level 3D Integration. *Microsyst. Technol.* **2012,** *18* (7–8), 1065–1075.
4. Tadepalli, R.; Turner, K. T.; Thompson, C. V. Mixed-mode Interface Toughness of Wafer-level Cu–Cu Bonds Using Asymmetric Chevron Test. *J. Mech. Phys. Solids* **2008,** *56* (3), 707–718.
5. Ko, C.-T.; Chen, K.-N. Low Temperature Bonding Technology for 3D Integration. *Microelectron. Reliab.* **2012,** *52* (2), 302–311.
6. Cunningham, S.; Kupnik, M. Wafer Bonding. In *MEMS Materials and Processes Handbook*, Ghodssi, R., Lin, P., Eds., Vol. 1; Springer: US, 2011; pp 817–877.
7. Haisma, J. Direct Bonding: Retrospect and Outlook. *Philips J. Res.* **1995,** *49* (1–2), 171–177.
8. Haisma, J.; Spierings, G. A. C. M.; Michielsen, T. M. Frameworks for Direct Bonding. *Philips J. Res.* **1995,** *49* (1–2), 11–21.
9. Tang, Z.; Peng, P.; Shi, T.; Liao, G.; Nie, L.; Liu, S. Effect of Nanoscale Surface Topography on Low Temperature Direct Wafer Bonding Process with UV Activation. *Sens. Actuators A Phys.* **2009,** *151* (1), 81–86.
10. Moriceau, H.; Rieutord, F.; Fournel, F.; Di Cioccio, L.; Moulet, C.; Libralesso, L.; Gueguen, P.; Taibi, R.; Deguet, C. Low Temperature Direct Bonding: An Attractive Technique for Heterostructures Build-up. *Microelectron. Reliab.* **2012,** *52* (2), 331–341.
11. Haisma, J.; Spierings, G. A. C. M. Contact Bonding, Including Direct-bonding in a Historical and Recent Context of Materials Science and Technology, Physics and Chemistry: Historical Review in a Broader Scope and Comparative Outlook. *Mater. Sci. Eng., R* **2002,** *37* (1–2), 1–60.
12. Moriceau, H.; Rieutord, F.; Fournel, F.; Tiec, Y. L.; Cioccio, L. D.; Morales, C.; Charvet, A. M.; Deguet, C. Overview of Recent Direct Wafer Bonding Advances and Applications. *Adv. Nat. Sci.: Nanosci. Nanotechnol.* **2010,** *1* (4), 043004.
13. Fan, J.; Lim, D. F.; Peng, L.; Li, K. H.; Tan, C. S. Effect of Bonding Temperature on Hermetic Seal and Mechanical Support of Wafer-level Cu-to-Cu Thermo-compression Bonding for 3D Integration. *Microsyst. Technol.* **2012,** 1–7.
14. Made, R. I.; Gan, C. L.; Yan, L.; Kor, K. H. B.; Chia, H. L.; Pey, K. L.; Thompson, C. V. Experimental Characterization and Modeling of the Mechanical Properties of Cu–Cu Thermocompression Bonds for Three-dimensional Integrated Circuits. *Acta Mater.* **2012,** *60* (2), 578–587.
15. Tang, Y.-S.; Chang, Y.-J.; Chen, K.-N. Wafer-level Cu–Cu Bonding Technology. *Microelectron. Reliab.* **2012,** *52* (2), 312–320.

www.iran-mavad.com
مرجع مهندسی مواد و متالورژی

16. Chen, K. N.; Chang, S. M.; Shen, L. C.; Reif, R. Investigations of Strength of Copper-bonded Wafers with Several Quantitative and Qualitative Tests. *J. Electron. Mater.* **2006,** *35* (5), 1082–1086.
17. Tsau, C. H.; Spearing, S. M.; Schmidt, M. A. Fabrication of Wafer-level Thermocompression Bonds. *J. Microelectromech. Syst.* **2002,** *11* (6), 641–647.
18. Spearing, S. M.; Tsau, C. H.; Schmidt, M. A. Gold Thermocompression Wafer Bonding. *Adv. Mater. Micro Nano Syst.* **2004**.
19. Tsau, C. H.; Spearing, S. M.; Schmidt, M. A. Characterization of Wafer-level Thermocompression Bonds. *J. Microelectromech. Syst.* **2004,** *13* (6), 963–971.
20. He, P.; Feng, J. C.; Zhang, B. G.; Qian, Y. Y. A New Technology for Diffusion Bonding Intermetallic TiAl to Steel with Composite Barrier Layers. *Mater. Charact.* **2003,** *50* (1), 87–92.
21. Das, S.; Tiwari, A. N.; Kulkarni, A. R. Thermo-compression Bonding of Alumina Ceramics to Metal. *J. Mater. Sci.* **2004,** *39* (10), 3345–3355.
22. Jang, E.-J.; Kim, J.-W.; Kim, B.; Matthias, T.; Park, Y.-B. Annealing Temperature Effect on the Cu-Cu Bonding Energy for 3D-IC Integration. *Met. Mater. Int.* **2011,** *17* (1), 105–109.
23. Zhou, Y.; Sridhar, S.; Mishra, K. C.; Klotzkin, D. Thermal Compression Wafer Bonding of Tungsten Applied to Fabrication of Small-period Tungsten Woodpile Structures. *Mater. Lett.* **2010,** *64* (10), 1222–1225.
24. Radu, I.; Landru, D.; Gaudin, G.; Riou, G.; Tempesta, C.; Letertre, F.; Di Cioccio, L.; Gueguen, P.; Signamarcheix, T.; Euvrard, C.; Dechamp, J.; Clavelier, L.; Sadaka, M. Recent Developments of Cu-Cu Non-thermo Compression Bonding for Wafer-to-Wafer 3D Stacking. In *IEEE International 3D Systems Integration Conference (3DIC);* Munich, 2010; pp 1–6.
25. Lu, Q.; Chen, Z.; Zhang, W.; Hu, A.; Li, M. Low-temperature Solid State Bonding Method Based on Surface Cu–Ni Alloying Microcones. *Appl. Surf. Sci.* **2013,** *268,* 368–372.
26. Suga, T. Status of Bonding Technology for Hybrid Integration – A Review of the Surface Activated Bonding (SAB). In *IEEE Photonics Conference (IPC);* Burlingame, CA, 2012; pp 749–750.
27. Lee, C.; Wang, P.; Kim, J. Advanced Bonding/Joining Techniques. In *Materials for Advanced Packaging;* Lu, D., Wong, C. P., Eds.; Springer: US, 2009; pp 51–76.
28. Taniyama, S.; Ying-Hui, W.; Fujino, M.; Suga, T. Room Temperature Wafer Bonding Using Surface Activated Bonding Method. In *IEEE 9th VLSI Packaging Workshop of Japan, (VPWJ 2008);* Kyoto, 2008; pp 141–144.
29. Higurashi, E.; Chino, D.; Suga, T.; Sawada, R. Au & Au Surface-activated Bonding and Its Application to Optical Microsensors with 3-D Structure. *IEEE J. Sel. Top. Quantum Electron.* **2009,** *15* (5), 1500–1505.
30. Howlader, M. M. R.; Kaga, T.; Suga, T. Investigation of Bonding Strength and Sealing Behavior of Aluminum/stainless Steel Bonded at Room Temperature. *Vacuum* **2010,** *84* (11), 1334–1340.
31. Howlader, M. M. R.; Zhang, F. Void-free Strong Bonding of Surface Activated Silicon Wafers from Room Temperature to Annealing at 600 °C. *Thin Solid Films* **2010,** *519* (2), 804–808.
32. Colinge, C. A.; Byun, K. Y.; Ferain, I. P.; Yu, R.; Goorsky, M. Low-temperature Fabrication of Germanium-on-insulator Using Remote Plasma Activation Bonding and Hydrogen Exfoliation. In *Semiconductor-on-insulator Materials for Nanoelectronics Applications;* Nazarov, A., Colinge, J. P., Balestra, F., Raskin, J.-P., Gamiz, F., Lysenko, V. S., Eds.; Springer: Berlin, Heidelberg, 2011; pp 31–46.
33. Kühne, S.; Hierold, C. Wafer-level Bonding and Direct Electrical Interconnection of Stacked 3D MEMS by a Hybrid Low Temperature Process. *Sens. Actuators A Phys.* **2011,** *172* (1), 341–346.
34. Cakmak, E.; Dragoi, V.; Capsuto, E.; McEwen, C.; Pabo, E. Adhesive Wafer Bonding with Photosensitive Polymers for MEMS Fabrication. *Microsyst. Technol.* **2010,** *16* (5), 799–808.
35. Lu, J.-Q.; Cale, T.; Gutmann, R. 3D Integration Based upon Dielectric Adhesive Bonding. In *Wafer Level 3-D ICs Process Technology;* Tan, C. S., Gutmann, R. J., Reif, L. R., Eds.; Springer: US, 2008; pp 1–38.
36. Niklaus, F.; Stemme, G.; Lu, J.-Q.; Gutmann, R. J. Adhesive Wafer Bonding. *J. Appl. Phys.* **2006,** *99* (3), 031101.
37. Niklaus, F.; Enoksson, P.; Kälvesten, E.; Stemme, G. A Method to Maintain Wafer Alignment Precision during Adhesive Wafer Bonding. *Sens. Actuators A Phys.* **2003,** *107* (3), 273–278.
38. Oberhammer, J.; Niklaus, F.; Stemme, G. Selective Wafer-level Adhesive Bonding with Benzocyclobutene for Fabrication of Cavities. *Sens. Actuators A Phys.* **2003,** *105* (3), 297–304.
39. Pang, C.; Zhao, Z.; Du, L.; Fang, Z. Adhesive Bonding with SU-8 in a Vacuum for Capacitive Pressure Sensors. *Sens. Actuators A Phys.* **2008,** *147* (2), 672–676.
40. Huesgen, T.; Lenk, G.; Albrecht, B.; Vulto, P.; Lemke, T.; Woias, P. Optimization and Characterization of Wafer-level Adhesive Bonding with Patterned Dry-film Photoresist for 3D MEMS Integration. *Sens. Actuators A Phys.* **2010,** *162* (1), 137–144.
41. Kim, J.; Il, K.; Choi, Y.; Paik, K.-W. Studies on the Polymer Adhesive Wafer Bonding Method Using Photo-patternable Materials for MEMS Motion Sensors Applications. *IEEE Trans. Compon., Packag., Manuf. Technol.* **2012,** *2* (7), 1118–1127.
42. Forsberg, F.; Saharil, F.; Stemme, G.; Roxhed, N.; van der Wijngaart, W.; Haraldsson, T.; Niklaus, F. Low Temperature Adhesive Wafer Bonding Using OSTE(+) for Heterogeneous 3D MEMS Integration. In *26th International Conference on IEEE Micro Electro Mechanical Systems (MEMS);* Taipei, 2013; pp 343–346.
43. Reinert, W.; Merz, P. Metallic Alloy Seal Bonding. In *Handbook of Silicon Based MEMS Materials and Technologies;* William Andrew Publishing: Boston, 2010; pp 533–542. Chapter 34.
44. Ko, C.-T.; Chen, K.-N. Wafer-level Bonding/stacking Technology for 3D Integration. *Microelectron. Reliab.* **2010,** *50* (4), 481–488.
45. Baum, M.; Chenping, J.; Haubold, M.; Wiemer, M.; Schneider, A.; Rank, H.; Trautmann, A.; Gessner, T. Eutectic Wafer Bonding for 3-D Integration. In *3rd Electronic System-integration Technology Conference (ESTC);* Berlin, 2010; pp 1–6.
46. Schneider, A.; Rank, H.; Muller-Fiedler, R.; Wittler, O.; Reichl, H. Hermeticity of Eutectic Bond Layers for Sensor Packages on Wafer-level. In *3rd Electronic System-integration Technology Conference (ESTC);* Berlin, 2010; pp 1–5.
47. Kim, W.; Wang, Q.; Jung, K.; Hwang, J.; Moon, C. Application of Au-Sn Eutectic Bonding in Hermetic RF MEMS Wafer Level Packaging. In *9th International Symposium on Advanced Packaging Materials: Processes, Properties and Interfaces;* 2004; pp 215–219.
48. Wang, Q.; Choa, S.-H.; Kim, W.; Hwang, J.; Ham, S.; Moon, C. Application of Au-Sn Eutectic Bonding in Hermetic Radio-frequency Microelectromechanical System Wafer Level Packaging. *J. Electron. Mater.* **2006,** *35* (3), 425–432.
49. Kwon, H.-S.; Lee, K.-C. Double-chip Condenser Microphone for Rigid Backplate Using DRIE and Wafer Bonding Technology. *Sens. Actuators A Phys.* **2007,** *138* (1), 81–86.
50. Mitchell, J. S.; Najafi, K. A Detailed Study of Yield and Reliability for Vacuum Packages Fabricated in a Wafer-level Au-Si Eutectic Bonding Process. In *International Solid-state Sensors, Actuators and Microsystems Conference;* 2009; pp 841–844.
51. Lin, Y. C.; Baum, M.; Haubold, M.; Fromel, J.; Wiemer, M.; Gessner, T.; Esashi, M. Development and Evaluation of AuSi Eutectic Wafer Bonding. In *International Solid-state Sensors, Actuators and Microsystems Conference;* Denver, CO, 2009; pp 244–247.
52. Kühne, S.; Hierold, C. Hybrid Low Temperature Wafer Bonding and Direct Electrical Interconnection of 3D MEMS. *Procedia Eng.* **2010,** *5,* 902–905.
53. Gradin, H.; Braun, S.; Stemme, G.; van der Wijngaart, W. SMA Microvalves for Very Large Gas Flow Control Manufactured Using Wafer-level Eutectic Bonding. *IEEE Trans. Ind. Electron.* **2012,** *59* (12), 4895–4906.
54. Henry, M. D.; Ahlers, C. R. Platinum Diffusion Barrier Breakdown in a-Si/Au Eutectic Wafer Bonding. *IEEE Trans. Compon. Packag. Manuf. Technol.* **2013,** *3* (6), 899–903.
55. Knechtel, R. Glass Frit Bonding. In *Handbook of Silicon Based MEMS Materials and Technologies;* William Andrew Publishing: Boston, 2010; pp 521–531. Chapter 33.
56. Knechtel, R.; Wiemer, M.; Frömel, J. Wafer Level Encapsulation of Microsystems Using Glass Frit Bonding. *Microsyst. Technol.* **2006,** *12* (5), 468–472.
57. Knechtel, R. Glass Frit Bonding: An Universal Technology for Wafer Level Encapsulation and Packaging. *Microsyst. Technol.* **2005,** *12* (1–2), 63–68.

www.iran-mavad.com
مرجع مهندسی مواد و متالورژی

58. Dresbach, C.; Krombholz, A.; Ebert, M.; Bagdahn, J. Mechanical Properties of Glass Frit Bonded Micro Packages. *Microsyst. Technol.* **2006,** *12* (5), 473–480.
59. Nötzold, K.; Dresbach, C.; Graf, J.; Böttge, B. Temperature Dependent Fracture Toughness of Glass Frit Bonding Layers. *Microsyst. Technol.* **2010,** *16* (7), 1243–1249.
60. Naumann, F.; Brand, S.; Bernasch, M.; Tismer, S.; Czurratis, P.; Wünsch, D.; Petzold, M. Advanced Characterization of Glass Frit Bonded Micro-chevron-test Samples Based on Scanning Acoustic Microscopy. *Microsyst. Technol.* **2012,** 1–7.
61. Wu, G.; Xu, D.; Xiong, B.; Wang, Y.; Wang, Y.; Ma, Y. Wafer-level Vacuum Packaging for MEMS Resonators Using Glass Frit Bonding. *J. Microelectromech. Syst.* **2012,** *21* (6), 1484–1491.
62. Cruz, R.; da Cruz Ranita, J. A.; Macaira, J.; Ribeiro, F.; da Silva, A. M. B.; Oliveira, J. M.; Fernandes, M. H. F. V.; Ribeiro, H. A.; Mendes, J. G.; Mendes, A. Glass-glass Laser-assisted Glass Frit Bonding. *IEEE Trans. Compon., Packag., Manuf. Technol.* **2012,** *2* (12), 1949–1956.

www.iran-mavad.com
مرجع مهندسی مواد و متالورژی